Analysing toxicity of ionic liquids based on combined targeted amino acid analysis and untargeted metabolic profiling as well as lipidomic profiling of stressed mammalian cell extracts

Dissertation

der Mathematisch-Naturwissenschaftlichen Fakultät

der Eberhard Karls Universität Tübingen

zur Erlangung des Grades eines

Doktors der Naturwissenschaften

(Dr. rer. nat.)

vorgelegt von

Corinna Tatjana Sanwald

aus Aalen

Tübingen

2021

Gedruckt mit Genehmigung der Mathematisch-Naturwissenschaftlichen Fakultät der Eberhard Karls Universität Tübingen.

Tag der mündlichen Qualifikation:	30.04.2021
Stellvertretender Dekan:	Prof. Dr. Thilo Stehle
1. Berichterstatter:	Prof. Dr. Michael Lämmerhofer
2. Berichterstatter:	Prof. Dr. Harald Groß

Dedicated to my beloved husband Dirk and my family.

“All things are poisons, for there is nothing without poisonous qualities.

It is only the dose which makes a thing poison.”

Philippus Aureolus Theophrastus Bombastus von Hohenheim - Paracelsus

Acknowledgements

At this point I would like to thank all those who have always supported me during the trip on the road to the dissertation.

First, I would like to thank Prof. Dr. Michael Lämmerhofer for being my thesis supervisor, and for the opportunity to carry out such an interesting project in a working group with many talented scientists. In particular, I would like to thank him for the inspiring discussions, his motivation, his great knowledge, which supported me in every difficult situation during this project.

Additionally, I would like to thank Prof. Dr. Harald Gross for being my second supervisor and for the evaluation of the thesis.

I also would like to thank the DAAD for the funding of my research stay in Helsinki, I really appreciated it.

Furthermore, I would like to thank Prof. Dr. Susanne Wiedmer for the opportunity of my research stay in Helsinki. Thank you for the warm welcome, your support and care. You always had an open ear for problems, be it of scientific or private nature. In addition, I would like to express my deepest gratitude to the late Prof. Dr. Juha Holopainen. It was a pleasure to meet such a great and sarcastic person, who made me laugh.

Next, I would like to thank Dr. Jeannie Horak and Dr. Stefan Neubauer for their support during my thesis. I would like to thank my former colleagues Siyao Liu, Ulrich Woiwode, Malgorzata Cebo, Ece Aydin, Mike Kaupert, Ryan Karongo, Christian Geibel, Stefan Polnick, and Heike Gerhardt for a harmonious working atmosphere, shared experiences on the road of PhD, at conferences and the exciting hiking trips. Especially, Bernhard Drotleff and Carlos Calderon are thanked for supporting me all the time in mass spectrometric and statistical related questions as well as Eveline Wachendorfer and Ingrid Straub for their tireless efforts in bureaucratic matters. Special thanks also to my former colleagues Jörg Schlotterbeck, Markus Höldrich and Alexandra Zimmermann, who made conferences unforgettable and supported me especially in the beginning.

Further thanks go to my Finnish colleagues, Antti Rantamäki, Riku Paananen, Pipsa Kulovesi, Joanna Witos and Fanny Salonen. Thank you for welcoming me so warmly

in Helsinki and integrating me into your group. I thank Suvi Ruokonen for her never-ending support far beyond my research stay. Very special thanks belong to Alexandra Robciuc. Thank you for your endless help in all cell related topics and the introduction to the world of cell culture technology. Thank you for your friendship over long distances. You made my stay in Helsinki one of the best times in my life.

Thanks to Kristina Dittrich for endless discussions in the office and finally on the phone when I was close to desperation. Thanks for coffee and cake whenever I was on the way back home and needed a break. I also would like to thank Stefanie Bäurer for her unbroken friendship and support during my doctoral studies. Thank you for many wonderful memories and light hearted hours together. A big thank you to Miriam Müller, for an unbelievable intensive friendship in the shortest time, thank you for your open ear to day and night times, for motivation and encouragement whenever it was necessary. Thanks for reviewing the thesis and for your cheerful comments.

Last but not least I would like to thank my parents, Ute and Günter, as well as my brother Michael and my sister-in-law Verena for their endless support and optimism in times where it was necessary. Thank you for always seeing more in me than I myself thought is possible. Thanks also for the encouragement to continue, especially in the last time, and not to lose courage.

Finally, from the bottom of my heart, I would like to thank my beloved husband Dirk. Thank you for going along with me on this journey, for always supporting me in all matters, for believing in me and for being my wing man, especially in the final stage.

Content

Abbreviations

$[C_{10}mim]Br$	1-decyl-3-methyimidazolium bromide
[Ch][Hex]	Choline hexanoate
[Ch][OAc]	Choline acetate
[DBNH][OAc]	1,5-Diazabicyclo(4.3.0)non-5-enium acetate
[emim][OAc]	1-Ethyl-3-methylimidazolium acetate
$[N_{4441}][OAc]$	Methyltributylammonium acetate
$[N_{4444}]Br$	Tetrabutylammonium bromide
$[omim][PF_6]$	1-methyl-3-octylimidazolium hexafluorophosphate
$[P_{14444}][OAc]$	Tributyl(tetradecyl)phosphonium acetate
$[P_{14444}]Cl$	Tributyl(tetradecyl)phosphonium chloride
$[P_{4441}][C_{13}H_{27}COO]$	Tributylmethylphosphonium tetradecanoate
$[P_{4441}][C_{15}H_{31}COO]$	Tributylmethylphosphonium hexadecanoate
$[P_{4441}][C_{17}H_{35}COO]$	Tributylmethylphosphonium octadecanoate
$[P_{4441}][C_5H_{11}COO]$	Tributylmethylphosphonium hexanoate
$[P_{4441}][C_9H_{19}COO]$	Tributylmethylphosphonium decanoate
$[P_{4441}][OAc]$	Tributylmethylphosphonium acetate
$[P_{4444}][OAc]$	Tetrabutylphosphonium acetate
$[P_{8444}][OAc]$	Tributyloctylphosphonium acetate
AA	Arachidonic acid
AC	Alternating current
ACN	Acetonitrile
AIDS	Acquired Immune Deficiency Syndrome
AIF	All-ion fragmentation
Ala	Alanine
APCI	Atmospheric pressure chemical ionisation
APPI	Atmospheric Pressure Photoionization
Arg	Arginine
Asn	Asparagine
Asp	Aspartic acid
AT	Accumulation time
BBFO	Broad Band Fluorine Observation
BCA	Bicinchoninic acid assay
BEH	Ethylene-Bridged Hybrid
BMP	Bis(monoacylglycero)phosphate

BUME	Butanol/methanol
CAC	Critical aggregation concentration
CE	Cholesteryl ester
CE	Capillary electrophoresis
Cer-NDS	(Ceramide non-hydroxyfatty acid-) dihydrosphingosines
Cer-NS	(Ceramide non-hydroxyfatty acid-) sphingosines
Cers	Ceramide
CES	Collision energy spread
cf.	Confer (compare)
$CHCl_3$	Chloroform
CHO	Chinese hamster ovary cells
Chol Ester	Cholesteryl ester
ChoP	Phosphorylcholine
CID	Collision-induced dissociation
CMC	Critical micelle concentrations
CO_2	Carbon dioxide
CoE	Collision energy
Conc.	Concentration
CSF	Cerebrospinal fluid
CT	Cycle time
CUR	Curtain gas
CV	Coefficient of variation
Cys	Cysteine
CZE	Capillary zone electrophoresis
DAG	Diacylglycerol
DC	Direct current
DDA	Data-dependent acquisition
Dec	Deconvolution
DESI	Desorption electrospray ionization
DG	Diacylglycerol
DIA	Data-independent acquisition
DLS	Dynamic light scattering
DMAPS	3-N,N-dimethylaminopropane sulfonic acid
DMEM	Dulbecco's modified Eagle's medium
DNA	Deoxyribonucleic acid

DOSY	Diffusion ordered spectroscopy
DP	Declustering potential
dpf	Days post fertilization
DPPC	Dipalmitoylphosphatidylcholine
DSC	Differential scanning calorimetry
E.coli	Escherichia coli
EC_{50}	Half maximal effective concentrations
ED_{50}	Half maximal effective dose
EDTA	Ethylene diamine tetraacetic acid
EGF	Human epidermal growth factor
eggPC	Egg phosphatidylcholine
eggPG	Egg phosphatidylglycerol
EI	Electron impact
EICs	Extracted ion chromatogram
EOF	Electroosmotic flow
EP	Extraction protocol
ESI	Electrospray ionization
ESI-MS	Electrospray ionization mass spectrometry
FA	Fatty acid, fatty acyl
FA	Formic acid
FBS	Fetal bovine serum
FDA	U.S. Food and Drug Administration
FT-ICR	Fourier-transform ion cyclotron resonance
GC	Gas chromatography
GHS	Globally harmonized system
Gln	Glutamine
Glu	Glutamic acid
Gly	Glycine
GNPS	Global Natural Product Social Molecular Networking
GS1	Nebulizer gas
GS2	Drying gas
H_2O	Water
HCD	High-energy collisional dissociation
HCE	Human corneal epithelial cells
HeLa	Henrietta Lacks cells

HexCer-NDS	(Hexosylceramide non-hydroxyfatty acid-) dihydrosphingosine
HexCer-NS	(Hexosylceramide non-hydroxyfatty acid-) sphingosine
HILIC	Hydrophilic interaction liquid chromatography
His	Histidine
HMDB	Human metabolome database
HPLC	High-pressure liquid chromatography
HPV	Human papillomavirus
HR	High resolution
HR-MS	High-resolution mass spectrometry
HSAB	Hard-soft acid-base theory
IC_{50}	Half maximal inhibitory concentration
IDA	Information-dependent-acquisition
IL	Ionic liquid
IL-8	Interleukin-8
Ile	Isoleucine
ILIS	Isotopic labelled internal standards
ILs	Ionic liquids
IMS	Ion mobility
IP_3	Inositol-1,4,5-trisphosphate
IPA75	Isopropanol 75% (25% water content v/v)
IPA90	Isopropanol 90% (10% water content v/v)
IPC	Ion Pair Chromatography
iRT	In silico retention time prediction
IS	Internal standard
ISVF	Ion-spray voltage floating
IT	Ion trap
K_2EDTA	Dipotassium ethylenediaminetetraacetic acid
keV	Kilo electron volts
LC	Liquid chromatography
LC-MS/MS	Liquid-chromatography tandem mass spectrometry
LDH	Lactate dehydrogenase
Leu	Leucine
LILY	Lipidome isotope-labelling of yeast
LIPID MAPS	LIPID Metabolites and Pathway Strategy
LLE	Liquid-liquid extraction

LLOQ	Lower limit-of-quantification
LOESS	Locally weighted scatter plot smoothing
logD	Distribution/partition coefficient
logS	Solubility
LOQ	Limit-of-quantification
LPC	Lysophosphatidylcholine
LPE	Lysophosphatidylethanolamine
LPG	Lysophosphatidylglycerol
LPI	Lysophosphatidylinositol
LUV	Large unilamellar liposomes
Lys	Lysine
m.p.	Melting point
m/z	Mass-to-charge ratio
MALDI	Matrix assisted laser desorption ionization
Max	Maximum
mbar	Millibar
MDMS-SL	Multi-dimensional MS based shotgun lipidomics
ME	Matrix effect
MEKC	Micellar electrokinetic chromatography
MeOH	Methanol
Met	Methionine
MG	Monoacylglycerol
MHz	Mega Hertz
Min	Minimum
MLVs	Multilamellar vesicles
MoNA	MassBank of North America
mpf	Month post fertilization
MRM	Multiple reaction monitoring
MRMHR	High-resolution multiple-reaction monitoring
MS	Mass spectrometry
MS^1	Mass spectrometry
MS^2	Tandem mass spectrometry
MS/MS^{ALL}	Mass Spectrometry with all ion fragmentation using unit mass precursor isolation width
MS-DIAL	Mass Spectrometry – Data Independent AnaLysis

MS^E	Mass Spectrometry Everything (All-ion fragmentation with broad precursor isolation width)
MTBE	Methyl tert-butyl ether
Na^+	Sodium ion
NaCl	Sodium chloride
NH_4^+	Ammonium ion
NIH	National Institutes of Health
NIST	National Institute of Standards and Technology
NLS	Neutral loss scans
NMMO	N-methylmorpholine-N-oxide
NMR	Nuclear-magnetic resonance
NP	Normal-phase
OPLS-DA	Orthogonal partial least squares discriminant analysis
OxPC	Oxidized phosphatidylcholine
OxPE	Oxidized phosphatidylethanolamine
OxPG	Oxidized phosphatidylglycerol
OxPS	Oxidized phosphatidylserine
PA	Phosphatidic acid
PBS	Phosphate buffered saline
PC	Principal component / Phosphatidylcholine
PCA	Principal Component Analysis
PE	Phosphatidylethanolamine
PFG	Pulsed field gradient
PG	Phosphatidylglycerol
Phe	Phenylalanine
PI	Phosphatidylinositol
PIP_2	Phosphatidylinositol-4,5-bisphosphate
PIS	Precursor ion scans
PLC	Phospholipase C
PLS	Partial least squares
PLS-DA	Partial least squares-discriminant analysis
POF	Postovulatory follicles
POPC	1-Palmitoyl-2-oleyl-phosphatidylcholine
POPG	1-Palmitoyl-2-oleoyl-sn-glycero-3-phosphatidylglycerol
PRM	Parallel reaction monitoring

Pro	Proline
PS	Phosphatidylserine
Q1	First quadrupole
Q2, q2	Second quadrupole
Q3	Third quadrupole
QC samples	Quality control samples
QTOF	Quadrupole-time-of-flight
QTRAP	Quadrupole linear ion trap
RBC	Red blood cell
rcf	Relative centrifugal force
RE	Extraction recovery
REACH	Registration, evaluation, authorization and restriction of chemicals
ReSpect	RIKEN tandem mass spectral database
RF	Radio-frequency
RM ANOVA	Repeated measures Analysis of Variance
ROS	Reactive oxygen species
RP	Reversed-phase
RSD	Relative standard deviation
RT	Retention time
RTILs	Room-temperature ILs
S/N	Signal-to-noise
SIM	Selected ion monitoring
SEM	Standard error means
Ser	Serine
SFC	Supercritical fluid chromatography
SI	Supporting information
SiIM	Single Ion Monitoring
SIMS	Secondary ion mass spectrometry
SM	Sphingomyelin
SPE	Solid-phase extraction
SPME	Solid Phase Micro Extraction
SRM	Selected reaction monitoring acquisition
SRM/MRM	Selected or multiple reaction monitoring acquisition
SV40	Simian virus 40

SWATH	Sequential window acquisition of all theoretical fragment-ion spectra
T	Temperature
TG, TAG	Triacyl-glyceride, triacylglycerol
THL	National Institute of Health and Welfare
Thr	Threonine
TIC	Total ion chromatograms
TLC	Thin layer chromatography
TOF	Time-of-flight
Trp	Tryptophan
TTBB	1,3,5-tri-tert-butylbenzene
Tyr	Tyrosine
U(H)PLC	Ultra High-Performance Liquid Chromatography
UHPLC-ESI-QqQ	Ultra High-Performance Liquid Chromatography-electrospray ionisation-triple quadrupole
ULOQ	Upper limit-of-quantification
UV	Ultraviolet
UV/VIS	Ultraviolet visible
Val	Valine
VBA	Visual basic script
VOCs	Volatile organic solvents
XIC	Extracted ion current
ZDV	Zero-dead-volume
Δm	Mass difference

Summary

Ionic Liquids are characterised by their modifiable unique properties and are used today in many different industrial processes. Their composition similar to a salt consists of an organic cation and an organic or inorganic anion. The large number of cations and anions, that can be combined with each other, makes a detailed characterisation difficult, especially with regard to their toxic effects on the environment. For this reason, a rapid analytical method was developed in the present work, which determines the toxicity of various ionic liquids based on their half maximal effective concentration (EC_{50}) and analyses their effect on the environment. EC_{50} values were determined using an AlamarBlue assay. Based on the obtained EC_{50} values, concentrations above their EC_{50} were selected and added to human corneal epithelial cells (HCE) to analyse the cause of the toxic effect by changes in the metabolome.

Amino acids are very important metabolites of an organism. They are involved in many metabolic processes, are building blocks for various metabolites and trigger various diseases. Therefore, the initial focus was placed on the development of a targeted analysis of amino acids of a cell extract after exposure to ionic liquids. Due to the large number of different ionic liquids, the development of a high-throughput method using hydrophilic interaction liquid chromatography (HILIC) coupled with high-resolution mass spectrometers, such as a quadrupole time-of-flight mass spectrometer (QTOF), was aimed to characterize potential biological effects. For this purpose, different HILIC stationary phases as well as different buffer contents of the mobile phase were compared to each other to separate amino acids with short analysis time. In order to perform a comparison, even without ultraviolet (UV) detection, 4-(dimethylamino)azobenzene was determined as an electrospray ionization mass spectrometry (ESI-MS) compatible void volume marker. An amide based neutral stationary phase provided optimal separation conditions for amino acid analysis. The use of the data-independent SWATH acquisition method (sequential window acquisition of all theoretical fragment-ion spectra) enabled the combination of a targeted amino acid analysis with an untargeted analysis of all other metabolites. Thus, optimal settings of the mass spectrometer for the amino acids could be determined and applied to achieve the highest possible sensitivity. This method was afterwards validated according to the current guidelines of the United States Food and Drug Administration (FDA). The problem of the missing blank matrix was successfully solved

by using ^{13}C,^{15}N-isotope labelled amino acid standards as surrogates. The analysis of the cell extracts after exposure to the ionic liquids showed that the concentration profiles are strongly dependent on the toxicity or EC_{50} value of the respective ionic liquid. For example, the concentration of L-alanine (L-Ala) and L-glycine (L-Gly) decreases with increasing toxicity compared to control samples. On the other hand, the ionic liquids have almost no effect on the essential aliphatic amino acids, L-leucine (L-Leu), L-isoleucine (L-Ile) and L-valine (L-Val). Furthermore, neither L-cysteine (L-Cys) or L-glutamine (L-Gln) nor L-asparagine (L-Asn) and L-aspartic acid (L-Asp) are detected in cell extracts.

Already during the EC_{50} determination, it turned out that some ionic liquids trigger the cells to build lipid droplets as a reaction. Therefore, the last project of the present work dealt with the analysis of the lipidome (lipidomics) of a cell after exposure to ionic liquids. Therefore, 4 different extraction methods were compared to each other in order to use an extraction method that extracts a wide range of lipids. Henrietta Lacks (HeLa) cells were then treated with ionic liquids for 8, 16 and 24 hours in a time-dependent study and then extracted and analysed using reversed phase high performance liquid chromatography combined with a quadrupole time-of-flight mass spectrometer with electrospray ionisation (ESI). The data processing and identification of lipids was performed with an open-source software, called Mass Spectrometry – Data Independent AnaLysis (MS-DIAL).

Due to the large number of samples, not all of them could be analysed in one sequence, which makes it necessary to correct for potential measurement differences due to equipment variations between analyses. Therefore, an Excel based macro was developed, which compares the results of the different sequences by retention time and mass-to-charge ratio (m/z). Furthermore, it is important to normalize the obtained data, as the ionic liquids cause different numbers of cells to die. Therefore, a normalization strategy based on quality control samples of each measurement sequence, on isotopically labelled lipid standards and on cell count has been developed. Finally, the ionic liquid-mixed cell extracts were compared with untreated cell extracts (control) in a statistical evaluation using t-test. This allowed some hypotheses to be made. For example, it could be shown that choline acetate ([Ch][OAc]) exerts an influence on metabolic processes, while 1-Ethyl-3-methylimidazolium acetate ([emim][OAc]) activates stress-induced metabolic

pathways. Furthermore, choline hexanoate ([Ch][Hex]) showed hardly any significant changes in the lipid profile, which means that the toxic effect cannot be explained on the basis of lipids. Tributylmethylphosphonium acetate ([P_{4441}][OAc]) on the other hand also induces stress-induced metabolic pathways and simultaneously destroys the cell membrane, whereas the most toxic ionic liquid analysed showed immediate destruction of the cell membrane.

It could be shown in this work that metabolomics and lipidomics profiling methods are suitable means to obtain information about the potential toxicity of ionic liquids, possibly also giving some insight which metabolic subnetworks are involved in toxic effects. It is becoming an established powerful tool in the field of exposomics.

Zusammenfassung

Ionische Flüssigkeiten bestechen durch ihre modifizierbaren einzigartigen Eigenschaften und werden heutzutage in vielen verschiedenen industriellen Prozessen eingesetzt. Ihre Zusammensetzung ähnlich eines Salzes besteht aus einem organischen Kation und einem organischen oder anorganischen Anion. Die große Vielzahl an miteinander kombinierbaren Kationen und Anionen erschwert eine detaillierte Charakterisierung vor allem hinsichtlich ihrer toxischen Wirkung auf die Umgebung. Aus diesem Grund wurde in der vorliegenden Arbeit eine schnelle Analysenmethode entwickelt, welche die Toxizität verschiedenster ionischer Flüssigkeiten anhand ihrer mittleren effektiven Konzentration (EC_{50}) bestimmt und ihre Wirkung auf die Umgebung analysiert. Die EC_{50} Werte wurden mittels eines AlamarBlue Assays bestimmt. Basierend auf den ermittelten EC_{50} Werten wurden Konzentrationen oberhalb ihrer EC_{50} ausgewählt und menschliche Hornhautepithelzellen (HCE) damit versetzt, um die Ursache der toxischen Wirkung anhand Veränderungen im Metabolom zu analysieren.

Aminosäuren sind sehr wichtige Metaboliten eines Organismus. Sie sind an vielen metabolischen Prozessen beteiligt, sind Baustein für verschiedene Metabolite und Auslöser verschiedenster Krankheiten. Deshalb lag der Fokus zunächst auf der Entwicklung einer gezielten (engl.: targeted) Analyse der Aminosäuren eines Zellextrakts nach Einwirkung der ionischen Flüssigkeiten. Aufgrund der großen Anzahl verschiedenster ionischer Flüssigkeiten zielte die Entwicklung einer Hochdurchsatzmethode mittels Hydrophiler Interaktions-Flüssigchromatographie (HILIC) gekoppelt an hochauflösende Massenspektrometer, wie zum Beispiel ein Quadrupol-Flugzeitmassenspektrometer (QTOF), auf die Charakterisierung möglicher biologischer Effekte ab. Hierzu wurden verschiedene HILIC stationäre Phasen, als auch verschiedene Pufferanteile der Mobilen Phase miteinander verglichen, um Aminosäuren schnell aufzutrennen. Um einen Vergleich auch ohne Ultraviolett (UV)-Detektor realisieren zu können, wurde 4-(Dimethylamino)azobenzol als ESI-MS kompatibler Totzeitmarker ermittelt. Eine Amid-basierte neutrale stationäre Phase zeigte optimale Trennbedingungen für die Aminosäureanalytik. Die Verwendung der Datenunabhängigen SWATH Akquisitionsmethode (engl.: sequential window acquisition of all theoretical fragment-ion spectra) ermöglichte die Kombination einer gezielten Aminosäureanalytik mit einer nicht-gezielten (engl.: untargeted) Analyse aller

weiteren Metabolite. Dadurch konnten für die Aminosäuren optimale Einstellungen des Massenspektrometers ermittelt und angewendet werden, um eine höchstmögliche Empfindlichkeit zu erreichen. Diese Methode wurde im Anschluss gemäß den aktuellen Richtlinien der US-Behörde für Lebens- und Arzneimittel validiert. Dabei konnte die Problematik der fehlenden Blankmatrix durch den Einsatz von ^{13}C,^{15}N-isotopen markierten Aminosäurestandards als Ersatz-Analyten (engl.: Surrogate) erfolgreich gelöst werden. Die Analyse der Zellextrakte nach Einwirkung der ionischen Flüssigkeiten zeigte, dass die Konzentrationsprofile stark abhängig sind von der Toxizität bzw. des EC_{50} Wertes der jeweiligen ionischen Flüssigkeit. So nimmt zum Beispiel die Konzentration an L-Alanine (L-Ala) und L-Glycin (L-Gly) im Vergleich zu Kontrollproben mit steigender Toxizität ab. Auf der anderen Seite haben die ionischen Flüssigkeiten nahezu keinen Einfluss auf die essentiellen aliphatischen Aminosäuren, L-Leucine (L-Leu), L-Isoleucin (L-Ile) und L-Valin (L-Val). Des Weiteren werden weder L-Cystein (L-Cys) oder L-Glutamin (L-Gln) noch L-Asparagin (L-Asn) und L-Asparaginsäure (L-Asp) in Zellextrakten detektiert.

Bereits während der EC_{50} Bestimmung kristallisierte sich heraus, dass manche ionische Flüssigkeiten die Zellen dazu veranlassen Lipidtröpfchen als Reaktion zu bilden. Deshalb fokussierte sich das letzte Projekt der vorliegenden Arbeit auf die Analyse des Lipidoms (engl.: Lipidomics) einer Zelle nach Einwirkung von ionischen Flüssigkeiten. Dafür wurden zunächst 4 verschiedene Extraktionsmethoden miteinander verglichen, um eine Extraktionsmethode zu verwenden, welche eine möglichst große Bandbreite an Lipiden extrahiert. Anschließend wurden Henrietta Lacks (HeLa) Zellen in einer zeitabhängigen Studie für 8, 16 und 24h mit ionischen Flüssigkeiten versetzt und anschließend extrahiert und mittels einer Umkehrphasen-Hochleistungsflüssigchromatographie verbunden mit einem Quadrupol-Flugzeitmassenspektrometer mit Elektrospray-Ionisation (ESI) analysiert. Die Datenverarbeitung und Identifizierung der Lipide erfolgte mit einer frei verfügbaren Software, MS-DIAL.

Aufgrund der großen Probenanzahl konnten nicht alle in einer Sequenz analysiert werden, wodurch eine Korrektur potentieller Messunterschiede durch Geräteschwankungen zwischen den Analysen erforderlich ist. Deshalb wurde ein Excel-basiertes Makro entwickelt, welches die Ergebnisse der verschiedenen Sequenzen, anhand der Retentionszeit und des Masse-zu-Ladungs Verhältnisses

(m/z) miteinander vergleicht. Des Weiteren ist es wichtig die erhaltenen Daten zu normalisieren, da durch das Einwirken der ionischen Flüssigkeiten unterschiedlich viele Zellen sterben. Daher wurde eine Normalisierungsstrategie, basierend auf Qualitätskontrollproben einer jeden Messsequenz, auf isotopenmarkierten Lipidstandards und auf der Zellanzahl, entwickelt. Letztendlich wurden die mit ionischen Flüssigkeiten versetzten Zellextrakte mit unbehandelten Zellextrakten (Kontrolle) in einer statistischen Auswertung mittels t-test miteinander verglichen. Dadurch konnten einige Hypothesen aufgestellt werden. Zum Beispiel konnte gezeigt werden, dass Cholin Acetat ([Ch][OAc]) einen Einfluss auf metabolische Prozesse ausübt, während 1-Ethyl-3-methylimidazolium acetat ([emim][OAc]) eher stress-induzierte Stoffwechselwege aktiviert. Des Weiteren zeigte Cholin Hexanoat ([Ch][Hex]) kaum signifikante Veränderungen im Lipidprofil, wodurch die toxische Wirkung nicht anhand der Lipide erklärt werden kann. Tributylmethylphosphonium acetat ([P_{4441}][OAc]) auf der anderen Seite induziert auch stress-basierte Stoffwechselwege und zerstört gleichzeitig die Zellmembran, wohingegen die giftigste analysierte ionische Flüssigkeit sofortige Zerstörung der Zellmembran zeigte.

In dieser Arbeit konnte gezeigt werden, dass Metabolomics- und Lipidomics-Methoden geeignete Mittel sind, um Informationen über die potenzielle Toxizität ionischer Flüssigkeiten zu erhalten, und möglicherweise auch einen Einblick zu geben, welche metabolischen Subnetzwerke an toxischen Wirkungen beteiligt sind. Es entwickeln sich diese zu einem etablierten leistungsstarken Werkzeug auf dem Gebiet der Exposomik.

List of publications

a) Accepted manuscripts

Publication I

S.-K. Ruokonen, C. Sanwald, M. Sundvik, S. Polnick, K. Vyavaharkar, F. Duša, A. J. Holding, A. W. T. King, I. Kilpeläinen, M. Lämmerhofer, P. Panula, and S. K. Wiedmer, Effect of Ionic Liquids on Zebrafish (Danio rerio) Viability, Behavior, and Histology; Correlation between Toxicity and Ionic Liquid Aggregation
Environ. Sci. Technol. **2016**, 50:7116-7125, DOI: 10.1021/acs.est.5b06107

Publication II

S.-K. Ruokonen, C. Sanwald, A. Robciuc, S. Hietala, A.H. Rantamäki, J. Witos, A.W.T. King, M. Lämmerhofer, S.K. Wiedmer, Correlation between ionic liquid cytotoxicity and liposome-ionic liquid interactions, *Chem. Eur. J.* **2017**, 24:2669-2680, DOI:10.1002/chem.201704924

Publication III

C. Sanwald, A. Robciuc, S.-K. Ruokonen, S.K. Wiedmer, M. Lämmerhofer, A combined targeted/untargeted LC-MS/MS-based screening approach for mammalian cell lines treated with ionic liquids: Toxicity correlates with metabolic profile, *Talanta* **2019**, 197:472–481, DOI: 10.1016/j.talanta.2019.01.054.

Publication IV

C. Calderón, C. Sanwald, J. Schlotterbeck, B. Drotleff, M. Lämmerhofer, Comparison of simple monophasic versus classical biphasic extraction protocols for comprehensive UHPLC-MS/MS lipidomic analysis of Hela cells, *Anal. Chim. Acta* **2018**, 1048:66–74, DOI: 10.1016/j.aca.2018.10.035.

b) Not yet submitted manuscripts

Publication V

C. Sanwald, S. Bäurer, A. Sievers-Engler, M. Lämmerhofer, Electrospray ionization-compatible t-zero markers for hydrophilic interaction liquid chromatography

Publication VI

C. Sanwald, A. Robciuc, K. Dittrich, C. Calderón, J. Moilanen, S. K. Wiedmer, M. Lämmerhofer, Lipid profiling of HeLa cells under ionic liquid stress

c) Accepted manuscripts, not included in the thesis

Publication VII

A. Zimmermann, J. Horak, A. Sievers-Engler, C. Sanwald, W. Lindner, M. Kramer, M. Lämmerhofer, Surface-crosslinked poly(3-mercaptopropyl)methylsiloxane-coatings on silica as new platform for low-bleed mass spectrometry-compatible functionalized stationary phases synthesized via thiol-ene click reaction, *J Chromatogr A* **2016**, 1436:73-83, DOI: 10.1016/j.chroma.2016.01.058.

Author Contribution

Publication I

Effect of Ionic Liquids on Zebrafish (Danio rerio) Viability, Behavior, and Histology; Correlation between Toxicity and Ionic Liquid Aggregation

Suvi-Katriina Ruokonen:

Idea generation

Viability, behaviour, and histology analysis on the Zebrafish (Danio rerio)

CMC measurements

Sample processing, analysis and statistical analysis

Data evaluation and interpretation

Writing of the main part

Corinna Sanwald:

Toxicity analysis on CHO cells

Review of the manuscript

Maria Sundvik:

Supervision of the Zebrafish (Danio rerio) studies

Review of the manuscript

Stefan Polnick:

Toxicity analysis on CHO cells

Kashmira Vyavaharkar:

Synthesis of ILs

NMR testing for ILs

Filip Duša:

Supporting CMC measurements

Ashley. J. Holding:

Synthesis of ILs

NMR testing for ILs

Alistair W. T. King:

Synthesis and characterisation of the ionic liquids

Review of the manuscript

Prof. Ilkka Kilpeläinen:

Sponsoring and planning of the project

Review of the manuscript

Prof. Dr. Michael Lämmerhofer:

Discussion of the research

Review of the manuscript

Prof. Pertti Panula:

Planning of the project

Revision of the manuscript

Prof. Dr. Susanne K. Wiedmer:

Idea generation, initiating, managing and sponsoring of the project

Review and approval of the manuscript

Corresponding author

Publication II

Correlation between ionic liquid cytotoxicity and liposome-ionic liquid interactions

Suvi-Katriina Ruokonen:

NMR and zeta sizer analysis

CMC measurements, DSC and DLS analysis

Data evaluation and writing of the manuscript

Corinna Sanwald:

Toxicity analysis on HCE cells

Review of the manuscript

Alexandra Robciuc:

Toxicity analysis on HCE cells

Performance of RBC hemolysis test

Review of the manuscript

Sami Hietala:

Planning and supporting NMR analysis

Review of the manuscript

Antti H. Rantamäki:

Toxicity analysis on the Vibrio fischeri cells

Review of the manuscript

Joana Witos:

zeta sizer analysis

Review of the manuscript

Alistair W.T. King:

Synthesis and characterisation of the ionic liquids

Review of the manuscript

Prof. Dr. Michael Lämmerhofer:

Discussion of the research

Review of the manuscript

Prof. Dr. Susanne K. Wiedmer:

Idea generation, initiating, managing and sponsoring of the project

Interpretation of results

Review and approval of the manuscript

Corresponding author

Publication III

A combined targeted/untargeted LC-MS/MS-based screening approach for mammalian cell lines treated with ionic liquids: Toxicity correlates with metabolic profile

Corinna Sanwald:

Idea generation

Sample processing and analysis

Data evaluation and interpretation

Writing of the main part

Alexandra Robciuc:

Support in cell culturing

Development of toxicity assay

Data evaluation

Partial writing and review of the manuscript

Suvi-Katriina Ruokonen:

Support using the ionic liquids

Providing the ionic liquids

Review of the manuscript

Prof. Dr. Susanne K. Wiedmer:

Managing and sponsoring of the project

Review of the manuscript

Prof. Dr. Michael Lämmerhofer:

Idea generation, initiating, managing and sponsoring of the project

Interpretation of results

Review and approval of the manuscript

Corresponding author

Publication IV

Comparison of simple monophasic versus classical biphasic extraction protocols for comprehensive UHPLC-MS/MS lipidomic analysis of Hela cells

Carlos Calderón:

Idea generation

Sample processing and analysis

Data evaluation

Writing of the main part

Corinna Sanwald:

Cultivation of the HeLa cells

Review of the manuscript

Jörg Schlotterbeck:

Support of mass spectrometer maintenance

Review of the manuscript

Bernhard Drotleff:

Consulting on lipidomics profiling using SWATH-MS/MS

Support of mass spectrometer maintenance

Review of the manuscript

Prof. Dr. Michael Lämmerhofer:

Idea generation, initiating, managing and sponsoring of the project

Interpretation of results

Review and approval of the manuscript

Corresponding author

Publication V

Electrospray ionization-compatible t-zero markers for hydrophilic interaction liquid chromatography

Corinna Sanwald:

Idea generation

Sample processing and analysis

Data evaluation and interpretation

Writing of the main part

Stefanie Bäurer:

Data evaluation

Partial writing and review of the manuscript

Adrian Sievers-Engler:

Data evaluation

Partial writing and review of the manuscript

Prof. Dr. Michael Lämmerhofer

Idea generation, initiating, managing and sponsoring of the project

Interpretation of results

Review and approval of the manuscript

Corresponding author

Publication VI

Lipid profiling of HeLa cells under ionic liquid stress

Corinna Sanwald:

Idea generation

Cell cultivation

Sample processing and analysis

Data evaluation and interpretation

Writing of the main part

Alexandra Robciuc:

Sample processing and analysis of EC_{50} values

Partial writing and review of the manuscript

Kristina Dittrich:

Development of the alignment tool

Partial writing and review of the manuscript

Carlos Calderón:

Support in sample extraction

Review of the manuscript

Jukka Moilanen:

Review of the manuscript

Susanne K. Wiedmer:

Review of the manuscript

Prof. Dr. Michael Lämmerhofer:

Idea generation, initiating, managing and sponsoring of the project

Interpretation of results

Review and approval of the manuscript

Corresponding author

Publication VII

Surface-crosslinked poly(3-mercaptopropyl)methylsiloxane-coatings on silica as new platform for low-bleed mass spectrometry-compatible functionalized stationary phases synthesized via thiol-ene click reaction

Aleksandra Zimmermann:

Idea generation
Development of synthesis method
Chromatographic characterization
Data evaluation and interpretation
Writing of the main part

Jeannie Horak:

Supporting the synthesis method development
Performance of MS-measurements
Proofreading, discussing and approving of the manuscript

Adrian Sievers-Engler:

Performance of MS-measurements
Proofreading and approving of the manuscript

Corinna Sanwald:

Performance of MS-measurements
Proofreading of the manuscript

Wolfgang Lindner

Approval of the manuscript

Markus Kramer:

Approval of the manuscript

Prof. Dr. Michael Lämmerhofer

Idea generation, initiating, managing and sponsoring of the project

Interpretation and discussion of results

Review and approval of the manuscript

Corresponding author

List of poster presentations

HPLC, 2015, Geneva, Swiss, June 21st – 25th
HPLC-ESI-QTOF-MS/MS based Metabolic Profiling of Mammalian Cell Lines
Corinna Sanwald, Michael Lämmerhofer

ITP/NoSSS, 2015, Helsinki, Finland, August 30th – September 3rd
Comparison of different acquisition modes for LC-MS/MS- based Metabolic Profiling of Mammalian Cell Lines
Corinna Sanwald, Michael Lämmerhofer

ISCC, 2016, Riva del Garda, Italy, May 31st – June 3rd
HPLC-ESI-QTOF-MS/MS based Metabolic Profiling of Mammalian Cell Lines with Data-Independent SWATH Acquisition
Corinna Sanwald, Jörg Schlotterbeck, Susanne K. Wiedmer, Michael Lämmerhofer

ANAKON, 2017, Tübingen, Germany, April 3rd – 6th
HPLC-ESI-QTOF-MS/MS based Metabolic Profiling of Stressed Human Corneal Epithelial Cells with Data-Independent SWATH Acquisition
Corinna Sanwald, Susanne K. Wiedmer, Michael Lämmerhofer

HPLC, 2017, Prague, Czech Republic, June 18th – 22nd
HPLC-ESI-QTOF-MS/MS based Quantitative Amino Acid Analysis and Simultaneous Metabolic Profiling of Stressed Human Corneal Epithelial Cells with Data-Independent SWATH Acquisition
Corinna Sanwald, Michael Lämmerhofer

1. Introduction

1.1. Ionic liquids

Ionic liquids (ILs) are described as class of liquid organic salts, containing a relatively large organic cation and a corresponding inorganic or organic anion [1–3]. They have melting points (m.p.) below or equal to 100 °C. Nowadays scientists developed a sub-class, which is called room-temperature ILs (RTILs), containing ILs, which are liquid at room temperature (approx. 25 °C) [4,5]. The most common ILs have organic cations like imidazolium, pyridinium, pyrrolidinium, phosphonium, ammonium and choline and inorganic anions like Cl^-, PF_6^-, BF_4^-or organic anions, including trifluoromethyl sulfonate $[CF_3SO_3]$-, bis[(trifluoromethyl)sulfonyl]imide $[(CF_3SO_2)_2N]^-$, trifluoro ethanoate $[CF_3COO]^-$ [4], bromide, tetrafluoroborate, hexafluorophosphate [2], acetate $[CH_3COO]^-$ and hexanoate [Hex] (Figure 1).

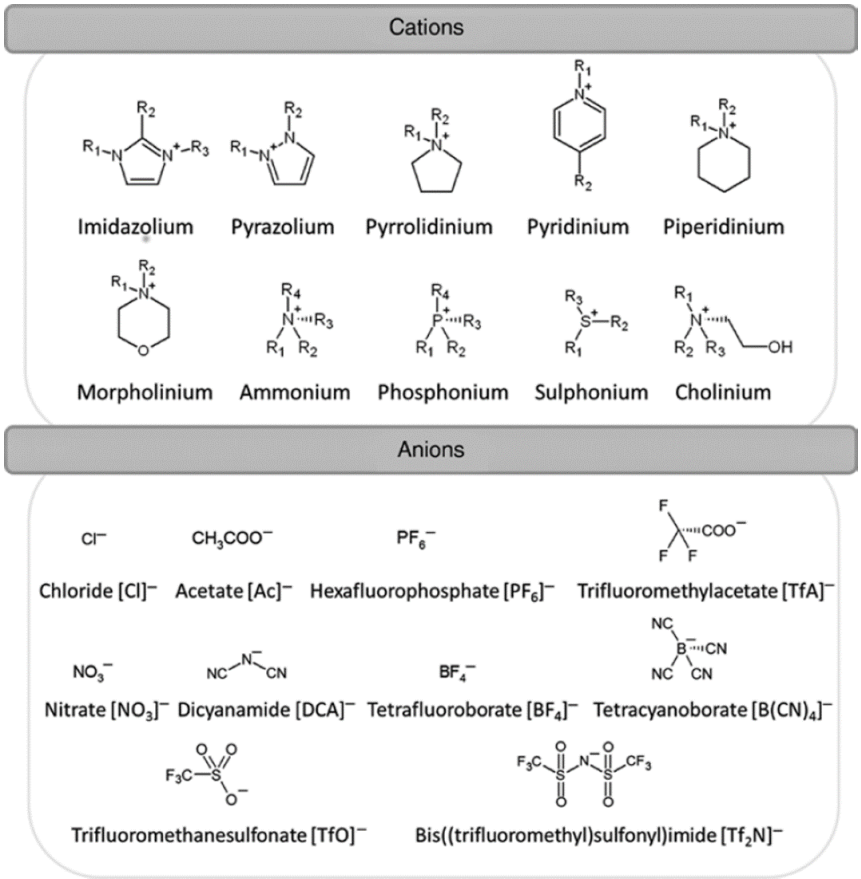

Figure 1: Overview of the main ionic liquids: Mainly imidazolium, pyrazolium, pyrrolidinium, pyridinium, piperidinium, morpholinium, ammonium, phosphonium, sulphonium and cholinium cations are used during the synthesis of ionic liquids in combination with the following anions: chloride, acetate, hexafluorophosphate, trifluoromethylacetate, nitrate, dicyanamide, tretrafluoroborate, tetracyanoborate, trifluoromethanesulfonate and bis((trifluoromethyl)sulfonyl)imide. Reprinted with permission from Rynkowska *et al.* [6]

The first ionic liquid (IL), ethanolammonium nitrate (m.p. 52-55°C), was found by Gabriel and Weiner in 1888 even though it was not called IL at that moment. Therefore, the “first” official IL, ethylammonium nitrate [$EtNH_3$] [NO_3], with a melting point of 12°C was discovered in 1914. A new class of IL, called dialkylimidazolium chloraluminate, was reported in 1982 by Wilkes *et al.* The chloraluminate containing ILs were reactive with moisture and many chemicals and therefore couldn’t receive the interest from other scientists. Considerable interest for ILs occurred in 1992 with the development of the first air- and moisture stable imidazolium IL [4].

ILs are similar to metallic salts, like sodium chloride [NaCl] and therefore often called “molten salts”. The cations and anions of metallic salts fit perfectly together building several layers and finally a crystal (Figure 2).

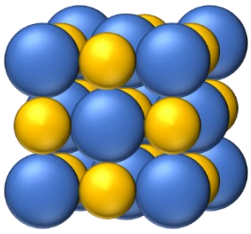

Figure 2: Sodium chloride salt: Lattice structure of a sodium chloride crystal showing the densest spherical packing

This behaviour results in high lattice energy and solid compounds. Compared to metallic salts, the ILs have, due to the relatively bulky organic cations and the weakly organized inorganic or organic anions [4], very low symmetries, unable to form layers and crystals, which causes low lattice energies. Therefore, their structure totally composed of ions result in unique properties [4]. They are colourless liquids in a wide range, have low volatilities, are thermal, chemical and electrochemical stable, have electrolytic conductivity, are viscous over a wide range, can be reused, are mostly not biodegradable, are non-flammable, non-explosive and the miscibility with solvents is adjustable [2–4,6–8]. The properties of ILs are dependent on the cation and anion [4,6], therefore, ILs are sometimes noted as designer solvents, because the cations and anions can be selected based on the desired properties [1,5]. In consequence, combinations of different cations and anions end up in around 1018 different ILs [4].

Based on their low volatility and non-flammable character, the ILs are often quoted as “green” solvents [1,5]. Although, the evaporation into the atmosphere is negligible, many ILs are water soluble and can enter the environment via the aquatic ecosystem. Most of the ILs

are not biodegradable, so once the ILs have entered the aquatic ecosystem, they can accumulate there in small aquatic organisms and thus reach higher organisms in the food chain, so even humans can be affected [1,5,7]. Additionally, hydrophobic ILs can due to accidental spills sediment into the ground and thus remain persistently in the environment [9]. The huge variability of ILs causes the fact, that the mechanism of toxicity or toxicity itself is only poorly known [1,5,7]. Therefore, the understanding of toxicity, environmental impact, effects on plants, bacteria, fungi, and mammalians deserve more attention [5]. Sometimes, the toxicity of certain ILs is higher compared to the most conventional used organic solvents, like benzene, methanol (MeOH), dimethylformamide or propan-2-ol by two to four orders of magnitude [9]. In general, the toxicity itself is mainly influenced by the molecular size of the cation [10]. Therefore, aromatic cations such as imidazolium and pyridinium seem to be more toxic than non-aromatic cations such as pyrrolidinium, piperidinium, phosphonium and ammonium, so that imidazolium-based ILs are currently the most studied and phosphonium-based ILs the least studied ILs.

Especially, the length of the cationic side chain is decisive [11]. In addition to hydrophobicity, lipophilicity also has a considerable influence on toxicity [12]. The more hydrophobic/lipophilic the ILs are, the higher toxic effects can be expected [9]. This means, among other things, that for example imidazole IL with C_{14} or C_{16} side chains are very lipophilic and can therefore attach themselves very well to the lipid bilayer of the cell membrane, for example [12]. However, ILs with branched side chains show significantly lower toxicities. Normally, the positions of side chains on the cation have only minor effects on the toxicity [13]. The length of the alkyl side chain of the cation is crucial for the toxicity of ILs. The longer the side chain, the more toxic the IL [5,11,12,14]. ILs with long side chains are mainly attached to the membrane or diffuse with the side chain into the bilayer [9,12]. One could now assume that the membrane destruction caused by the attachment of IL increases more and more the longer the side chain, i.e. the more lipophilic the IL becomes. However, a kind of plateau has been found in various research projects [15–20] and during this work. This means that the toxic effect of the IL does not increase any further after a certain chain length, called "cut-off" effect. A possible explanation is a slowed down diffusion into the cells by steric hindrance of the long side chains [12] and due to the lack of solubility [19]. Even though, the toxicity mechanism of ILs is not yet fully understood, it is known that their toxicity is usually based on the disruption and destruction of cell membranes

and that ILs can even accumulate in organisms [9]. Therefore, ILs are under investigation to act in a similar way as detergents, pesticides and antibiotics [9].

In summary, this means that an IL cation can be described similar to a lipid. Thus, the side chain, so-called "IL tail" [21–23], inserts itself into the hydrophobic regions of the lipid bilayer and even accumulates there [9]. This causes a permeable membrane. The insertion of the IL “tail” into the membrane limits the stretching of lipid and IL “tails” perpendicular to the membrane, resulting in a thinner membrane [24] of about 1Å. Additionally, the area per lipid is increased [25]. The longer the side chain length, the deeper the insertion, the more toxic is the IL [26]. This process is supported by coulomb forces of the positively charged cation of the ILs and the negatively charged headgroup of the lipids in the membrane. Normally, only the side chains are incorporated in the lipid bilayer, stabilized by the dispersion forces of the IL cation and the lipid. The cation as "IL head" on the other side, rather interacts with the head groups of the lipids [27] (Figure 3).

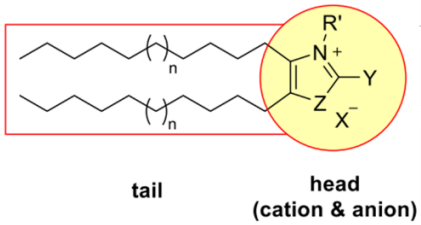

Figure 3: Scheme of ionic liquid structure: Ionic liquids with long side chains attached to the cation behave similar to lipids. The cation and anion represent the “IL head” corresponding to the headgroup of a lipid. The long side chains are called “IL tail”, equal to the fatty acids attached to the headgroup of a lipid, called lipid tail. Adapted with permission from Rakers *et al*. [28]

Most likely they also interact with hydrophobic areas of the membrane enzymes [9] and enter the nucleus causing an increased production of reactive oxygen species (ROS) resulting in damaging the DNA [29–31]. Mostly, after 24h of IL exposure, the nuclei downsize in elliptical structures [30]. Further investigations showed that for example lipophilic phosphonium cations with increased side chain length are selectively incorporated into mitochondrial membranes [32,33]. Nevertheless, the mitochondrial membrane seems not to be the first target of ILs as ROS production and DNA damage occurs first [30]. As described above, the first instance is the roughening of the cell membrane, following disturbance, disruption and destruction in the worst case [27], which leads to cell death [34]. Even amphiphilic ILs are toxic and perform disruption of cellular membranes [34].

On the other hand, short alkyl chains leave "holes" in the membrane due to the insertion, which is filled by curling lipid tails from the lipids (Figure 4).

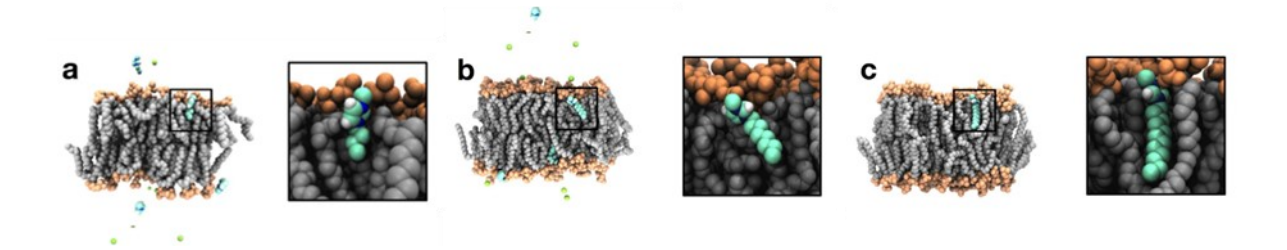

Figure 4: Insertion of different sized ionic liquids into a lipid bilayer: a) represents the insertion of an ionic liquid with a short cationic side chain, creating “holes” in the membrane. b) shows the integration of an ionic liquid with a semi long side chain and c) displays the alignment of an ionic liquid carrying a long side chain, which causes straight insertion of the side chain parallel to the lipid tails of the bilayer. Adapted with permission from Yoo *et al.* [35]

However, this leads to a significantly increased disorder of the membrane, causing a thinner membrane bilayer, as both lipid layers move closer together [24]. Longer amphiphilic ILs on the other side have no influence on the thickness [34]. Experiments using Liposomes showed the insertion of long side chains into the membrane without disruption [36]. Middle long side chains are also incorporated into the membrane, but cause destabilization of the membrane due to disturbance of the lipid bilayer ordering based on the mismatch of the long lipid tail and the middle long side chain [36]. Short side chains crossed the membrane without any major damages of the cell membrane [36] (Figure 5).

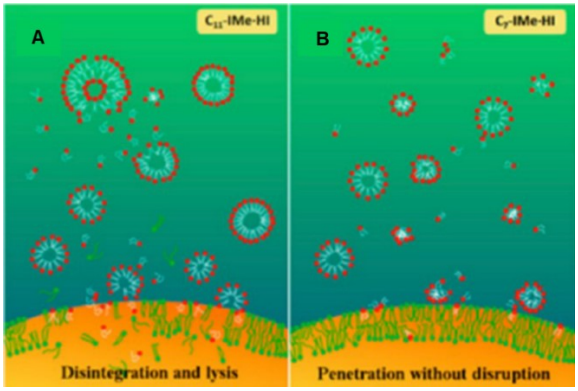

Figure 5: Insertion of different sized ionic liquids, causing different responses of the cell: A) shows the insertion of an ionic liquid with a long side chain, resulting in the disordering of the membrane, followed by disruption. B) represents the integration of a short chain ionic liquid, which enters the lipid bilayer without disruption. Adapted with permission from Benedetto *et al.* [36] (https://pubs.acs.org/doi/10.1021/acs.langmuir.7b04361, further permissions related to the material excerpted should be directed to the ACS)

Besides the length of the side chain, the selection of the anion also controls the toxicity [12], but is more or less only important for the toxic effect when comparing ILs with the same cation and side chain lengths [11,37]. For example, tetrafluoroborate anion causes the highest toxicity with regard to anions [5]. Close by, the anions bromide and chloride are

located on the scale of anion toxicity [5], although chloride [23] tends to remain in the aqueous phase. Additional, tetrafluoroborate and hexafluorophosphate are less toxic than bis(trifluoromethylsulfonyl)imide or octylsulfate, which are considered as the most toxic anions at the moment [19]. Even if ILs carry long side chains as anion, they are most likely rejected by the negative charge of the phospholipid head group and their own negative charge [21]. But in some cases, the chain length of for example alkanoate anions are long enough for inserting into the membrane, as the negative charge at the end of the chain can be kept far away, avoiding repulsion [38]. Also the insertion of hydroxyl groups into the carbon chain of the anion leads to more polar ILs, which can build hydrogen bridges to the membrane or enzymes [26]. That means, that no general answer regarding toxicity is available. In the case ILs are combined with very hydrophobic anions, like (trifluoromethanesulfonyl)-imide ($[NTf_2]^-$) not only the cation owns the ability to insert into the membrane, but also the anion can interact with the membrane [34]. In addition to the side chain length, nitrogen in the ring of aromatic cations, polar head groups, molecular size and the branching of the side chains play an important role [9]. The more nitrogen atoms are located in the aromatic ring of the cation, the more toxic is the behaviour of the IL, whereas, methylation decreases the toxicity [12]. In general, membrane rupture/destruction/perforation by ILs starts due to electrostatic forces with the attachment of the cation of the IL flatly to the membrane like a layer and covers it completely depending on the concentration [21–23] (Figure 6).

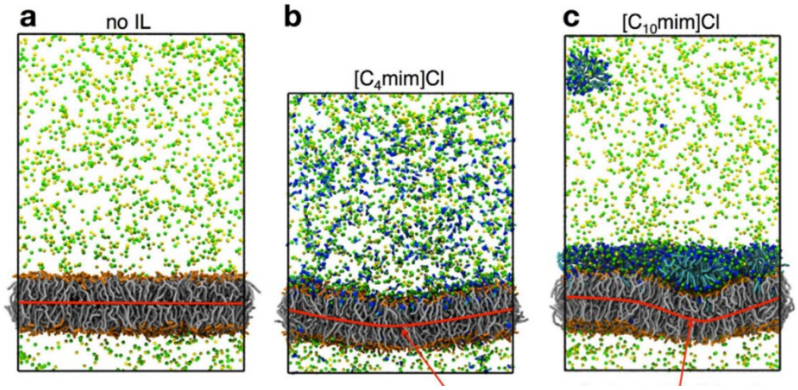

Figure 6: Attachment of ionic liquids onto the cell membrane: a) shows the cell membrane without ionic liquid treatment. b) represents a treatment with a short chain ionic liquid and c) displays the alignment of a long chain ionic liquid as ionic liquid layer on top of the lipid bilayer. Adapted with permission from Yoo *et al.* [35]

That means, the cation interacts with one or maximum two lipids [24]. In some cases, the interaction of the side chains with the lipid bilayer, results in a thicker membrane, which is increased with increasing concentrations of the ILs [27]. The analysis of cytoplasm

separated from the cell membrane underlined the hypothesis, that the cations are inserted into the membrane, as no IL could be obtained in the cytoplasm fraction [23,39]. On the other side, the toxicity is decreased, if a carboxyl group is implemented at the end of a C_{10} alkyl chain, for example [14]. If an ester was present instead of the carboxyl group, the toxicity was not increased excessively, but similar to the occurrence of an amide function, the biodegradability of the IL is increased [24]. Additionally, ILs with for example two long alkyl side chains are more toxic than the same IL with only one long side chain [14]. Analysis, using vesicles ended up in micelles out of a mixture of IL and lipid [40] (Figure 7), causing a decreased lysosomal membrane integrity and phagocytosis activity due to ILs [41].

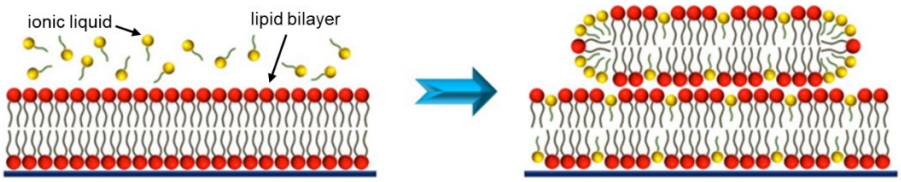

Figure 7: Formation of micelles: The ionic liquids insert themselves with their IL tail into the cell membrane, resulting in the creation of micelles out of ionic liquids and lipids. Adapted with permission from Jing *et al.* [34] (Copyright© 2016, American Chemical Society)

Two long side chains lead also to a behaviour similar to lipids, forming micelles. ILs, which behave like a lipid cause also less perturbations in the membrane compared to other ILs [24]. In some cases, the cells survive the roughening of the membrane long enough to activate stress-pathways, resulting in secretion of interleukin-8 (IL-8) for example before they die [22].

Since the last 30 years, the number of publications about ILs increased significantly (Figure 8), displaying the increased interest on ILs as novel solvents and reporting the tremendous potential of ILs for chemical analysis [4–6].

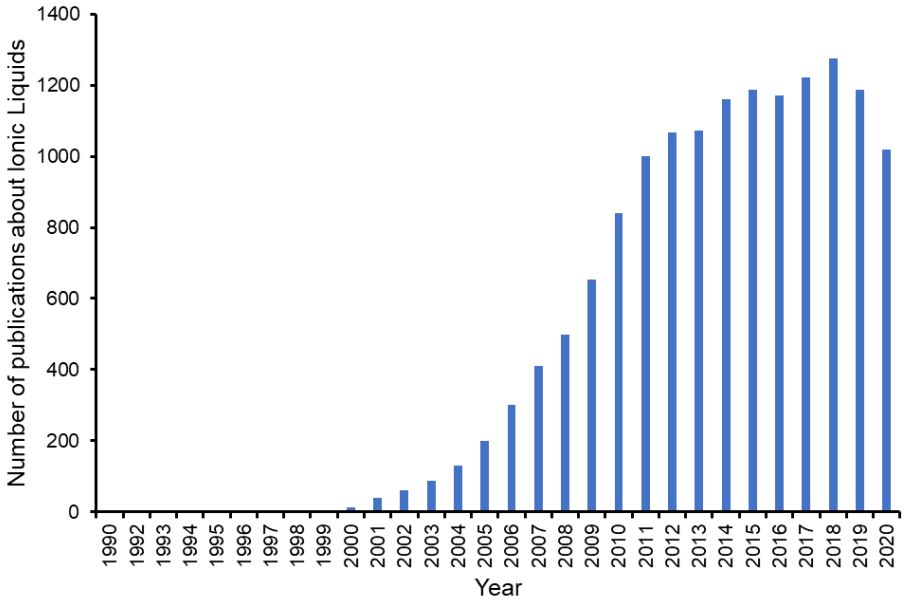

Figure 8: Number of publications about ionic liquids: The interest in ionic liquids has grown steadily over the last 30 years, which is reflected in the increasing number of publications on ionic liquids (PubMed, 21.11.2020)

Regarding the environment, the longest-standing problems of using large amounts of toxic, hazardous, flammable and environmentally damaging organic solvents called volatile organic solvents (VOCs) in industry and academia could be overcome by exchanging VOCs with ILs [3,6].

Even if the ILs at certain concentrations are toxic for various organisms, they can be useful in lower concentrations [42]. From this point of view, ILs can be designed for usage as therapeutic agents [42]. Especially, choline and ammonium containing ILs might be interesting for investigations in the area of antimicrobial, anti-cancer and anti-tumour activities [5]. In response, the National Cancer Institute has already demonstrated the anti-cancer effect and cytotoxicity of some ILs with imidazolium, ammonium and phosphonium as cation, making them potential therapeutics [9]. Additionally, ILs are widely used in industrial, commercial and pharmaceutical applications, in organic synthesis, catalysis and in analytical chemistry [1,4]. The application in analytical chemistry is divided into eight sections: i) extraction, ii) gas chromatography (GC), iii) liquid chromatography (LC), iv) capillary electrophoresis (CE), v) mass spectrometry (MS), vi) electrochemistry, vii) sensors and viii) spectroscopy [2,4,6] (Figure 9).

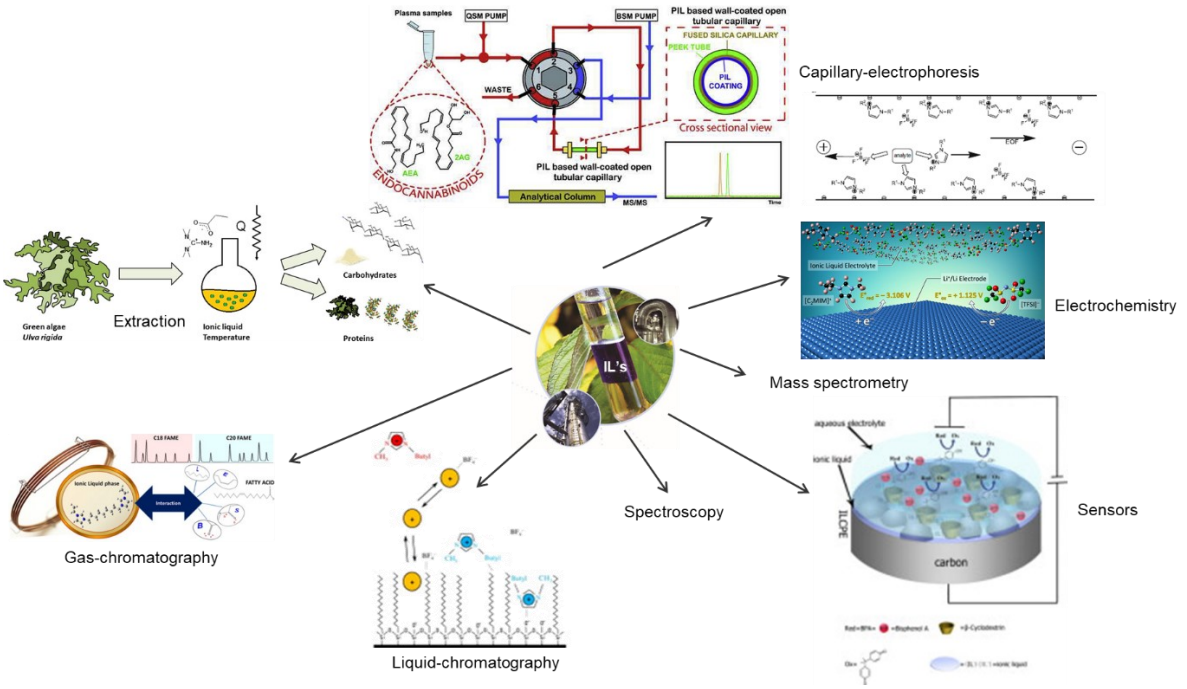

Figure 9: Ionic liquid applications: The applications of ionic liquids [43] in analytical chemistry can be divided into eight fields: i) extraction [44], ii) gas chromatography (GC) [45], iii) liquid chromatography (LC) [46], iv) capillary electrophoresis (CE) [47,48], v) mass spectrometry (MS), vi) electrochemistry [49], vii) sensors [50] and viii) spectroscopy. Reprinted with the permissions of the corresponding authors

Nowadays, ILs are broadly used as solvents and reaction media during drug processing in medicine and pharmaceutical technology [51]. However, it should be mentioned that, ILs are only starting materials and don't remain liquid in several applications. For example, the preparation of Solid Phase Micro Extraction (SPME) fibres or stationary phases in the liquid chromatography needs to bind the IL to a solid silica surface. In other applications, the ILs are used as additive, for example in CE running buffers, mobile phases for LC and as complexing agent in MS detection [4].

The toxic effect of the ILs on the organisms are not only controlled by the IL itself, but also by the properties of the membrane [36]. Therefore, the ILs can be designed, especially to interact with certain cellular membranes [36]. For example, cell membranes of healthy eukaryotic cells are mostly contained of palmitoyl-oleoyl phosphatidylcholine (POPC), resulting in a more or less neutral charged cellular surface, whereby cell membranes of bacteria and cancer cells are mainly contained of phosphatidylglycerol and phosphatidic acid (bacteria cells) and phosphatidylserine (cancer cells), respectively [36]. That means, the property of the ILs could be designed due to the choice of the side chains and anion to specifically interact with the negative cellular surface of bacteria and cancer cells but not with the neutral charged surface of healthy cells, resulting in a milestone in cancer treatment [36]. Additionally, not only cellular membranes are affected from ILs in general,

but also the membrane of the mitochondria, leading to mitochondrial dysfunction followed by cell death [52]. The aim is to improve the produced drugs, since ILs can not only influence cell membranes, but can also inhibit enzymes. For example, the enzymes alcohol dehydrogenase, AMP-deaminase, anti-oxidant enzymes and acetylcholinesterase are inhibited in their function. The latter leads to distortion of various neurological processes, followed by heart disease [51]. On the other hand, the inhibition of anti-oxidant enzymes lead to cellular stress and therefore increased production of ROS, resulting in DNA damage due to accumulation of ROS [13]. No matter which process, they are all time and concentration dependent [13]. In order to be able to make the most accurate statements for humans during cytotoxicity studies, it is advisable to use human cell lines, such as Henrietta Lacks (HeLa) cells [7]. Furthermore, epithelial cells are also the first instance of exposure to toxic substances [51]. Mostly, half maximal effective concentrations (EC_{50}) values are determined for comparisons of different ILs (see chapter 1.2). Nevertheless, due to the high variability of the ILs, the experimental evaluation of toxicities is very time consuming, causes very high costs [10,53] and suffers from standardization of the measurement process [12] and therefore, seems impossible [10,53]. Additionally, the toxicity cannot be estimated by summation of individually determined toxic effects of the cation and anion [12]. Nevertheless, a toxicity ranking exist [10]. So far, imidazolium, pyridinium, phosphonium and ammonium ILs are the main categories and therefore, most analysed [54]. The imidazolium ILs were long time the most toxic ILs, followed by pyridinium, pyrrolidinium and piperidinium [12]. Choline based ILs are still considered as harmless [12].

In any case, the toxicity of the ILs has to be monitored and decreased if necessary. One approach is to replace existing synthetic cations, like ammonium, imidazolium and pyridinium with naturally present cations, such as choline. In addition, fluorinated anions, like tetrafluoroborate and hexafluorophosphate are also exchanged by naturally occurring anions, as amino acids or other organic acids. This type is called natural ILs and gain at the moment great popularity, especially due to the lower price compared to the current synthetic ILs [23]. To summarize, for future synthesis of new “greener” ILs the structure of the cation has to be chosen carefully and afterwards analysed for the toxicity effect by using different anions to select the best combination.

1.1.1. Room-temperature Ionic Liquids (RTILs)

Room-temperature ILs are ILs contained of an organic cation and an inorganic or organic anion (Figure 10) with melting temperatures below approximately 25 °C.

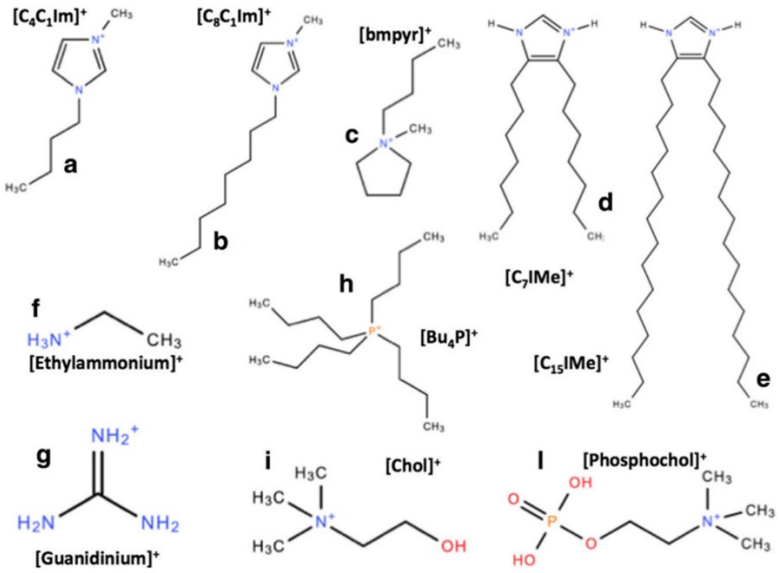

Figure 10: Room-temperature ionic liquids: a)-c) represent imidazolium and pyridinium RTIL cations; d) and e) are imidazolium RTIL cations showing an equal behaviour to lipids with their two long side chains; f) and g) display ethylammonium and guanidinium RTIL cations, which support the avoidance of amyloidogenesis [55–57]; h) shows a phosphonium RTIL cation; i) and l) represent choline and phosphocholine RTIL cations. Reprinted with the permission from Benedetto *et al.* [25]

Therefore, most RTILs are liquid at room temperature, but not necessarily, as some of them are more like waxes. The main characteristics of RTILs are described in the abilities to kill bacteria [25,58], to extract, purify and to operate as solvent for DNA storage [25,59,60], to stabilize proteins and enzymes, respectively [25,61,62], to avoid protein amyloidogenesis and to bring amyloid fibres back into a functional protein structure [25,55–57], to enter, building wholes and to destroy the cell membrane [25,27,35,63–69] and to dissolve cellulose and other polysaccharides [25,70–74]. In some cases, RTILs with long side chains build micelles out of themselves and adsorb to the lipid bilayer, resulting in a first membrane layer out of RTILs [25]. RTIL can be used as solvents instead of water or volatile organic compounds, respectively, or as additives to support the behaviour of proteins in an aqueous solution [75]. The first characteristic named here are actually very interesting in future, as the RTILs already destroy specifically the cell membrane of cancer cells nearly without disturbing healthy cells [25]. RTILs are popular since their anti-tumour activity is known. A higher anti-tumour activity can be achieved by imidazolium based ILs with alkyl side chains at position 4 and 5 [12,76].

1.1.2. Imidazolium Ionic liquids

This group of IL was the first used for industrial purposes [12,77] and target for most of toxicological studies using ILs [12]. For a long time, imidazolium ILs have been considered the most toxic group par excellence [12]. Compared to most toxic organic solvents, like dichloromethane, phenol and xylene, imidazolium ILs have same effects, but at concentrations four to five times lower [7]. Regarding the toxicity of tetrachloromethane and tri-chloromethane, similar concentrations of imidazolium ILs result in similar effects. Benzene, methanol and acetonitrile (ACN) are less hazardous in similar concentrations compared to imidazolium ILs [29]. Imidazolium ionic liquids are contained of cationic imidazole core substituted with different sized alkyl chains, whereas one of the side chains are mostly a methyl or ethyl residue [54] and inorganic or organic anions [12]. Imidazolium ILs induce changes in the metabolism even in semi-lethal concentrations. The IL with ethyl side chain is the most toxic, effective and non-biodegradable IL [12]. Gathergood *et al.* found a drastic reduction in toxicity once an oxygen and chlorine atom are present within the side chain [11,12,51]. In addition, the biodegradability is increased. The same effect can be achieved by terminal hydroxyl or nitrile groups [12]. In general, polar functional groups included in the alkyl side chain as well as hydrogen in 1-position instead of alkyl side chain decrease the toxic effect of imidazole ILs [37]. The presence of an ethoxy group in the side chain of imidazolium ILs decreased the biological effects [9]. Already an ethyl residue at the imidazolium core increases the production of ROS and intracellular calcium concentration enormously. In addition, the destruction of the cell membrane itself leads to programmed cell death in most cells, known as apoptosis (Figure 11).

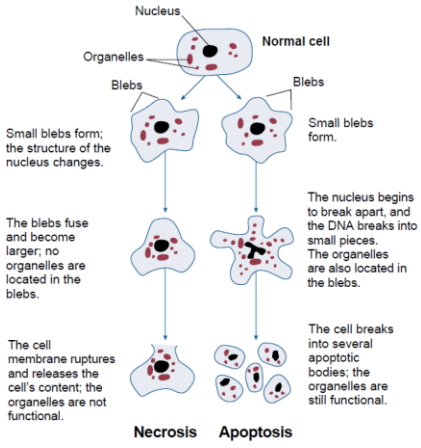

Figure 11: Cell death: Apoptosis as well as necrosis are mechanisms resulting in the death of the cell. Apoptosis is thereby the programmed cell death and necrosis describes the cell death due to cell injury, for example chemical, mechanical or physical damage. Both cell death mechanisms follow own pathways. Reprinted with permission from Goodlett *et al.* [78]

The membrane potential of the mitochondria is also reduced by the attachment of IL, which additionally forces apoptosis [12,52]. Beside the above mentioned increased production of ROS, superoxide dismutase and catalase enzymes are inhibited, causing reduction of glutathione concentration and increase of cellular malondialdehyde concentrations, which induces also apoptosis of the cells [52]. Therefore, ROS is considered an early sign of apoptosis due to imidazolium ILs. Additionally, caspases initiate apoptosis of cells and thus play a major role in this process [52]. Negatively charged phospholipids in the lipid bilayer promote the accumulation of the imidazolium ILs at the membrane [21]. For example, $[C_8mim]^+$ ILs introduce their C_8 hydrophobic side chain in the lipid bilayer mainly contained of phospholipids. The introduction is thermodynamically supported, since the enthalpy change is negative [27,79]. The charged core interacts additionally with the headgroups of the phospholipids, phosphocholine or phosphoserine, respectively [21].

Imidazolium ILs with shorter more aliphatic side chains first attach to the membrane with their imidazolium cation. The ILs then switch over so that the alkyl side chain is completely embedded in the membrane (Figure 12). However, the switching of the ILs takes more time than the direct attachment of the side chain to the membrane. In this case, the different methods are dependent on the length of the side chain [27].

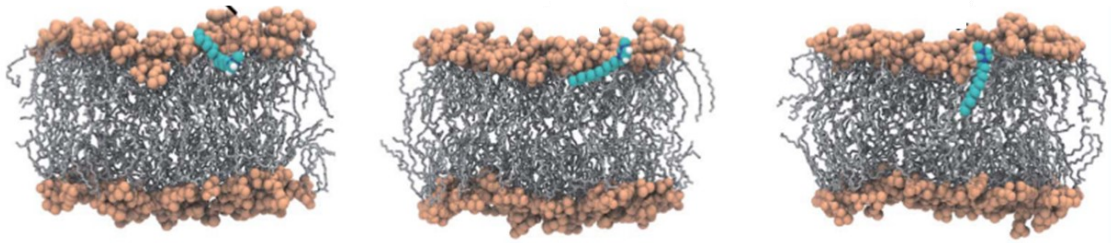

Figure 12: **Flipping of the ILs:** The ionic liquid first attaches itself with the "IL head" (cation) to the cell membrane and then inserts the "IL tail" (side chain of the cation) into the membrane by flipping it over. Adapted with permission from Yoo *et al.* [27]

At certain concentrations below the critical concentration, the long lipophilic and hydrophobic side chains are aligned to the cell membrane. Afterwards they are inserted in the cell membrane lipid bilayer, resulting in a swelling of the membrane [27,34,80]. The structure in general is similar to the structure of available cationic surfactants, therefore ILs have the ability to affect biomembranes and increase their permeability [30]. On the other side, if a C_8 alkyl chain is present as anion of an imidazolium ILs, the alkyl chain inserts also into the lipid bilayer, but instead of staying in the membrane, destabilization and disruption of the membrane occurred [21]. This means, an imidazolium IL with a hydrophobic/lipophilic anion can insert into the membrane with both functionalities, the side chain and the anion [27].

Thus, the order of the lipid bilayer is disturbed, the membrane is more roughened with increasing IL concentrations and afterwards destroyed [12,27]. Initially, a few cells are in a kind of shock state due to the destruction of the membrane order, resulting in cell death. This is called necrosis [12] (Figure 11). That means, the cell membrane was disturbed due to direct chemical, mechanical or physical damages, resulting in non-regulated and irreversible morphologic changes [23] causing instantly cell death before a survival program could be started [23]. Over the years, various research groups have observed an antimicrobial effect, which should enable ILs to serve as a substitute for antibiotics in the future. The antimicrobial effect can also be controlled by the side chain. For example, the antimicrobial effect is reduced if the side chain is lengthened at position R1 or if symmetrical side chains are present in position R1 and R3 [12]. However, the introduction of methyl or hydroxyethyl group in the imidazolium ring increases the antimicrobial activity [37]. The steric hindrance is one of the possible explanations causing decreased interaction with the cell membranes of the pathogens [12]. Therefore, the position of the incorporation of the polar functionalities strongly affects the toxicity [37]. The larger the distance to the imidazolium ring, the less toxic the ILs [16,37]. In cytotoxicity tests using cell cultures, the acceptance of the cells for ILs is strongly depending on the composition of the culture medium. The higher the nutrients or salt content, the lower the toxic effect of ILs. Another indication of membrane permeability is the analysis of lactate dehydrogenase (LDH) in the extracellular space, since this enzyme is released relatively quickly into the medium as soon as the cell membrane is disrupted [30]. In the group of ILs, imidazolium ILs have the biggest effect on the activity of enzymes [51]. For example, the lactic dehydrogenase was inhibited due to the presence of imidazolium ILs [23]. Imidazolium heterocyclic ring was more toxic than ILs with morpholinium or pyridinium ring [23]. Already, the imidazolium ILs with only one long side chain are highly toxic to different species, but imidazolium ILs with two long side chains own in comparison three orders of magnitude higher anti-tumour activity [76]. Therefore, it is very important in cell experiments to be as close as possible to the real conditions [12]. In general, during cytotoxicity experiments using cell cultures, the cell viability monitoring is recommended as main factor to determine toxicities [52].

1.1.3. Ammonium salt Ionic liquids

In general, ammonium salt ionic liquids are contained of a cationic ammonium core coupled to different residues and inorganic or organic anions. Most of the time ammonium salt ILs are based on a quaternary ammonium cation, sometimes called simply “quats”, which are

very well analysed as surfactants carrying antiseptic effects [24,81] and are more toxic than other ammonium salt ILs [11]. Therefore, it was not surprising that ammonium salt ILs own antimicrobial properties [24,81]. Further, quats are broadly used as disinfectant and for the preservation of wood, in particular with nitrites, nitrates, lactates, acesulfamates and saccharinates as anion [12]. As true for all ILs, the toxicity is strongly dependent from the length of the residues connected to the cation. A special type of quaternary ammonium salt ILs is presented by choline based ILs.

1.1.4. Choline Ionic liquids

Choline based ILs are a special sub-category of quaternary ammonium based ILs [53]. They are always contained of choline as cationic part and different inorganic and even organic anions. For a long time, these ILs were assumed to be the less toxic in comparison to all other ILs. Nowadays, choline is described as essential vitamin related to the vitamin B category (pseudo-vitamin) [53]. Therefore, choline is often used as food additive. Based on that, choline based ILs were considered harmless and additionally registered as non-toxic to the environment unless the ecotoxicological profile is sparely known [53]. Especially, the combination of choline and chloride are completely harmless for different organisms [9]. Additionally, Choline ILs are particularly popular because it is a substance that is already part of the body and is expected to be biocompatible [75]. Additionally, they are biodegradable [9,12,82–85]. Due to the highly ionic properties, most choline-based ILs are water-soluble [53,86,87] and can therefore be released into the environment via the aqueous ecosystem [15,53].

In the case of choline based ILs the length of the alkyl chains connected to the cation is fixed. Therefore, the toxicity is controlled by the length of the carbon chain of the anion or, respectively, the structure of the anions. However, the correlation of increased toxicity the higher the hydrophobicity and lipophilicity are, is still valid [53]. Thus, the mechanism of toxicity is most likely a different one than the accumulation of the cationic side chains at or in the cell membrane, respectively. This assumption is proven, when comparing the toxicity of choline cation with other quaternary ammonium or other cations, because it is higher for choline ILs [53]. Nevertheless, talking about choline ILs with alkylated anions, the positively charged choline is perfectly attracted to the negatively charged membrane [26] and the alkyl chain of the anions inserts into the lipid bilayer. However, if the alkyl chain of an alkanoate anion becomes too short, the repulsion of two negatively charged groups (membrane and carboxyl group of the anion) predominates [21]. Therefore, choline alkanoates with short

carbon chains are even at lethal concentrations, not able to penetrate the membrane by insertion [21]. Although they are considered harmless, some choline ILs show higher toxicities [21], which is due to the influence, following alteration of the metabolism of the respective organism. However, the toxicity is still significantly lower compared to imidazolium ILs, for example. That means, imidazolium ILs with same chain length are still more toxic than choline ILs with alkyl anion [21]. The toxicity is only based on disordering of the membrane without a total damaging. As a result, the ILs choline hexanoate and choline acetate, for example, are divided into different categories, which describe the toxicity mechanisms. Accordingly, choline hexanoate is in the group of ILs that influence the metabolism but also disturb the membrane order. Choline acetate, on the other hand, is classified in the category of ILs that only affect the metabolism. In summary, choline based ILs remain less toxic than imidazolium, pyrrolidinium and piperidinium ILs [38], but should not be underestimated during ecotoxicity testing.

1.1.5. Pyridinium Ionic liquids

Pyridinium based ILs are contained of a cationic pyridine core with different side chains and residues. A morpholinium core with only a methyl group as side chain is highly recommended, assuming low toxicity [16]. On the other side, for example, dimethylaminopyridinium as core cation resulted in very strong effects on aquatic organisms and is therefore, considered as harmful IL [16]. The toxicity is mostly based on the inhibition of enzymes. However, in this area, phosphonium based ILs as well as imidazolium ILs achieve the biggest influences of enzyme inhibition [51].

1.1.6. Phosphonium Ionic liquids

For a long time, imidazolium ILs were ranked as one of the most toxic ILs ever. Nowadays, phosphonium-based ILs are considered the most toxic ILs [5,13,19]. In comparison to quaternary ammonium and imidazolium ILs, phosphonium ILs are thermally and chemically more stable due to lower electronegativity [88]. Phosphonium based ILs rupture and destroy the cell membrane direct in a completely non-specific way, regardless of the exposure time. The membrane disruption/destruction leads to loss of membrane integrity, release of intracellular metabolites, followed by immediate cell death [88]. In some cases, interleukin-8 secretion can be obtained, which means the cells survive the attack of the ILs long enough for activating certain stress pathways. However, in most cases interleukin-8 concentrations cannot be detected, either due to immediate cell death or too less survived cells [22]. In

general, phosphonium ILs are much more toxic than ammonium ILs, for example [32]. Successful studies in HeLa cells, which compare phosphonium ILs with cisplatin, describe the more toxic ILs as possible anti-cancer agents within a targeted therapy [32]. Additionally, antimicrobial activity is also obtained in phosphonium based ILs [9,12].

1.2. Half maximal effective concentration (EC_{50})

During drug [89], antibody or development of other compounds, the effect on the population or the toxicity have to be evaluated before the compound will undergo the way of all clinical phases before the approval to sell the drug or antibody. Especially, the toxicity of the mostly uncharacterized ILs have to be determined, before they are used wide spread in industrial processes. There are different values to describe the effect of a certain compound. One possibility is the half maximal inhibitory concentration (IC_{50}) [89]. This concentration describes the value, the compound shows 50% inhibitory activity. Nevertheless, the IC_{50} value is normally mainly used for competition binding assays and functional antagonist assays [90]. Another possibility to describe the effect of a certain compound is the half maximal effective dose (ED_{50}). But mostly, the potency of such a compound is described by the EC_{50} value [89,90]. EC_{50} is closely related to IC_{50} and represents the concentration of the drug, antibody or toxin halfway between the minimum (baseline) and the maximum (maximum effect of the compound) after a certain time of exposure [91]. A small change in the concentration of the compound causes fast effects on the biological system. Usually, this kind of dose-response curve follows a sigmoidal curve [91]. The halfway value indicates the concentration when 50% of the maximal effect within a concentration gradient of the compound are achieved. This means in detail, the EC_{50} value is located at the bending point of the sigmoidal curve [91], when the increase of the concentration of the compound causes slowly decreasing reaction of the compound on the population. In general, the EC_{50} value is estimated by the derivative of the best-fit line of the sigmoidal curve. For the EC_{50} estimation, the two terms are established: i) relative EC_{50} and ii) absolute EC_{50} values [89]. This is also valid for the IC_{50} values as they are closely related. Nevertheless, the further discussion will focus on the EC_{50} determination, as the toxicity of the ILs as antagonist are analysed. The National Institutes of Health (NIH) Chemical Genomics Center proposed the following definitions (see Figure 13) [89].

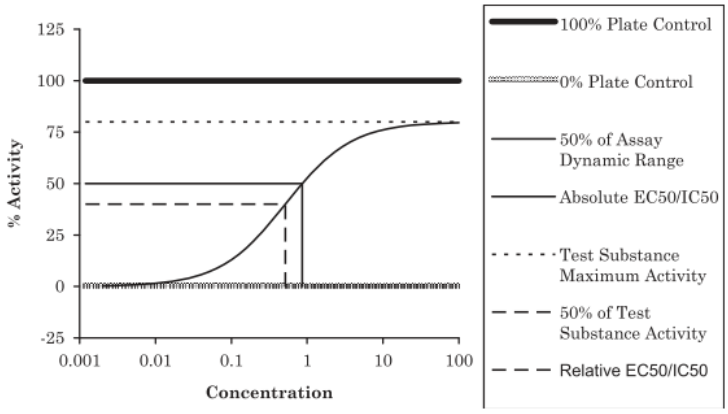

Figure 13: Illustration of two ways defining EC_{50}/IC_{50}: Relative EC_{50}/IC_{50} are described as variable c in the below explained 4-parameter logistic model and displays the concentration equivalent to a value halfway between the predicted lower and upper level and absolute EC_{50}/IC_{50} are defined as reaction corresponding to the 50% control (mean value of the 0% and 100% assay controls). Reprinted with permission from Sebaugh *et al.* [89]

The relative EC_{50} estimation uses a 4-parameter logistic model [89,91], with parameter c as the EC_{50} value, describing the concentration which corresponds to the response half way the lower and upper plateau. This model describes a sigmoidal curve, which can be calculated with the following equation (Equation 1) and is mainly used to calculate the EC_{50} value [89,92]:

$$Y = \frac{a-d}{1+(X/c)^b} + d$$

Equation 1: Equation for 4-parameter logistic model: The model describes a sigmoidal curve with y as response and x as concentration of the analysed compound. The variable a describes the baseline (minimum) and d the upper limit (maximum) of the sigmoidal curve. The slope of the curve is displayed with the variable b and the concentration equivalent to a value halfway between the predicted lower and upper level by the variable c. Reprinted with permission from Sebaugh *et al.* [89]

With y as the response, x as the concentration, a = minimum of the curve (baseline), d = upper asymptote (maximum), b = slope of the curve and c as the halfway concentration between the maximum and minimum [89].

The absolute EC_{50} value is estimated as the mean of control samples without compound, but treated in the same way as samples containing compound (0% controls) and control samples containing for example no stimulation, no enzymes or a high amount of a compound, which is known for a maximum effect on the population (100% control). It is important to note that the 100% control does not always correspond to the maximum effect of the substance and that the maximum effect varies for different substances. The estimation of the absolute EC_{50} value is based on the following equation (Equation 2) [89]:

$$\mathrm{EC50/IC50} = c\left(\frac{a - 50\%\mathrm{response}}{50\%\mathrm{response} - d}\right)^{1/b}$$

Equation 2: Equation for estimation of the absolute EC_{50} value: The variable a displays as mentioned for the 4-parameter logistic model the baseline (minimum), d the upper limit (maximum) of the sigmoidal curve, the slope of the curve is described with the variable b and variable c describes the halfway value between a and d. Reprinted with permission from Sebaugh *et al.* [89]

With a = baseline, b = slope, c = halfway value between minimum and maximum and d = maximum [89].

For both determinations two assumptions are made: i) there is a monotopic relationship between the concentration and the assay response and ii) there is a consistent definition of the response at 50% of the curve [89]. Therefore, the estimation of c (EC_{50} value) is strongly dependent of the precise determination of the minimum and maximum of the curve. This is affected by two different factors, first by the total number of different concentrations covering the sigmoidal curve and second, by the precision of the response at same concentrations. The latter is dependent from the type of assay chosen for the determination. An assay using cells for example varies more than other assay forms [89]. Nevertheless, the cell assay is the most convenient assay to use. Regarding the different concentrations covering the curve, for absolute EC_{50} value estimation at least two concentration levels below and above the 50% response are sufficient to achieve accurate calculations [89]. For all assays without stable 100% control samples, only relative EC_{50} values can be calculated. Therefore, the relative estimation is most accurate by at least two concentration levels beyond the lower and upper bending point, which is sufficient for the maximum accuracy. Higher numbers do not achieve higher accuracies [89]. Additionally, for better accuracy of the relative EC_{50} determination, the lower and upper bend point can be calculated using the following equations (Equation 3 and Equation 4) [89]:

$$c * (k) * \frac{1}{b}$$

Equation 3: Equation for the calculation of the bend points: The bend points are described as the coordinates of the minimum and the maximum of the linear portion and calculated with the above explained variables c (halfway concentration) and b (slope) and the additional constant k = 4.6805. Reprinted with permission from Sebaugh *et al.* [89]

$$c * \left(\frac{1}{k}\right) * \frac{1}{b}$$

Equation 4: Equation for the calculation of the bend points: The bend points are described as the coordinates of the minimum and the maximum of the linear portion and calculated with the above explained variables c (halfway concentration) and b (slope) and the additional constant k = 4.6805. Reprinted with permission from Sebaugh *et al.* [89]

With c as the halfway concentration, b as slope and k as a constant value k = 4.6805 [89]. Based on these equations, computational software systems can quickly produce numerical estimation of EC_{50} values. Nevertheless, the values are most of the time not very accurate [89]. Even the graphical EC_{50} determination based on experimentally acquired curves often provides inaccurate results. Therefore, Verschuren *et al.* [93] combined both methods, by using the computational software system "solver" implemented in Windows Excel and experimentally acquired data of sigmoidal curves. Based on the equation developed from Verschuren *et al*., the following equation (Equation 5) was adjusted and used for the estimation of all EC_{50} values determined within the below described projects:

$$y = \frac{a_3}{(1 + e^{(a_2 * (x - a_1))})}$$

Equation 5: Equation of the sigmoidal curve: The equation was modified according to Verschuren *et al.* and contains the following variables; a_1 as the EC_{50} value, a_2 describes the slope, x displays the concentration of the compound and a_3 is a constant variable

With y as the response, a_3 as a constant coefficient, a_2 as the slope, a_1 as the EC_{50} value and x as the concentration of the compound.

The experimental data of the EC_{50} estimation within all described projects was achieved by growing adherent cells in deep-well plates until confluence, starved for 8h in fetal bovine serum (FBS) free media, before different concentration levels of the ILs dissolved in FBS free media were added and incubated for 24h. Two hours before ending of the treatment time, the redox sensitive dye alamarBlue was added to the cells. The alamarBlue dye contains the organic compound resazurin, which is a non-toxic blue dye, does not show fluorescence and interacts within a redox reaction with the intracellular $NADH/H^+$ of the cells after diffusion into the cells, resulting in the pink coloured compound resorufin, which is fluorescence active [94] (see Figure 14).

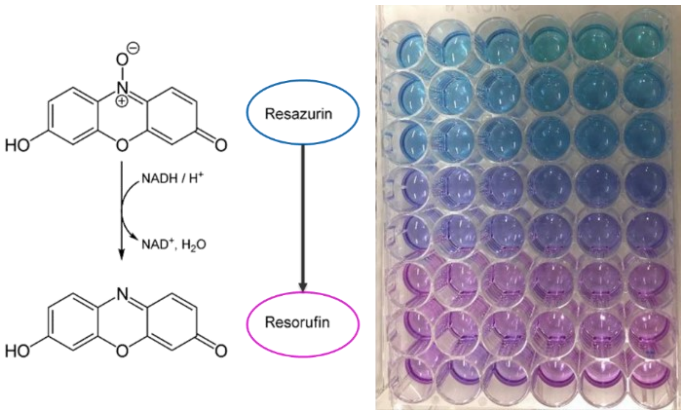

Figure 14: AlamarBlue redox dye: On the left side of the picture, the reaction of the alamarBlue dye with the NADH/H^+ of the cells is shown. On the right side of the figure, a 48-well plate, used for the EC_{50} determination in all projects, is shown after the incubation with alamarBlue dye

That means blue wells indicate dead cells and pink wells contain living cells. The small differences in the colours are determined by using a fluorescence detector implemented in a plate reader. As a positive control, cells were incubated with FBS free media and alamarBlue but without any dissolved IL and as a negative control, only FBS free media was incubated with alamarBlue. That means fluorescence units are nonlinearly linked to a certain viable cell number. Therefore, a serial dilution of known cell densities in FBS free media were incubated with the alamarBlue dye to correlate the fluorescence units with the cell number (see Figure 15).

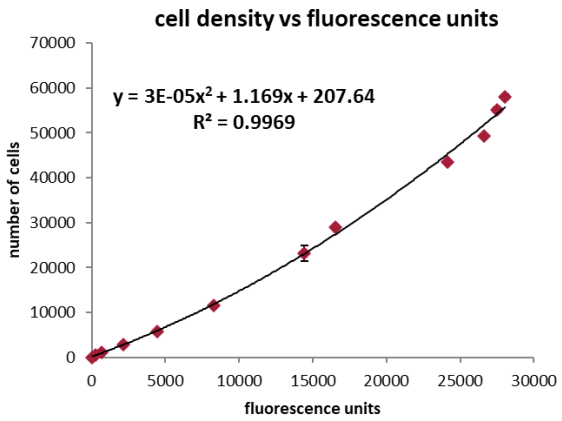

Figure 15: Polynomial function: Known cell densities as serial dilution were incubated with alamarBlue for correlation of fluorescence units with cell numbers

The achieved fluorescence units were corrected for the background noise by subtraction of the negative control, before the cell number was calculated based on the polynomial curve function, describing the correlation of the fluorescence units and the viable cell number. Afterwards, the positive control was used to normalize the mean of the calculated cell numbers [95]. The sigmoidal curve was calculated using the above developed equation (see Figure 15), resulting in predicted values and a predicted sigmoidal curve, which

describes the obtained values the best. Based on the predicted values the sum of least squares was calculated each. These values were used for the iterative curve fitting using the add-in of excel, called solver [93]. The tool is mathematically determining the minimum sum of least squares, by varying the EC_{50} value and the slope as a_3 of the equation is constant (see Figure 16).

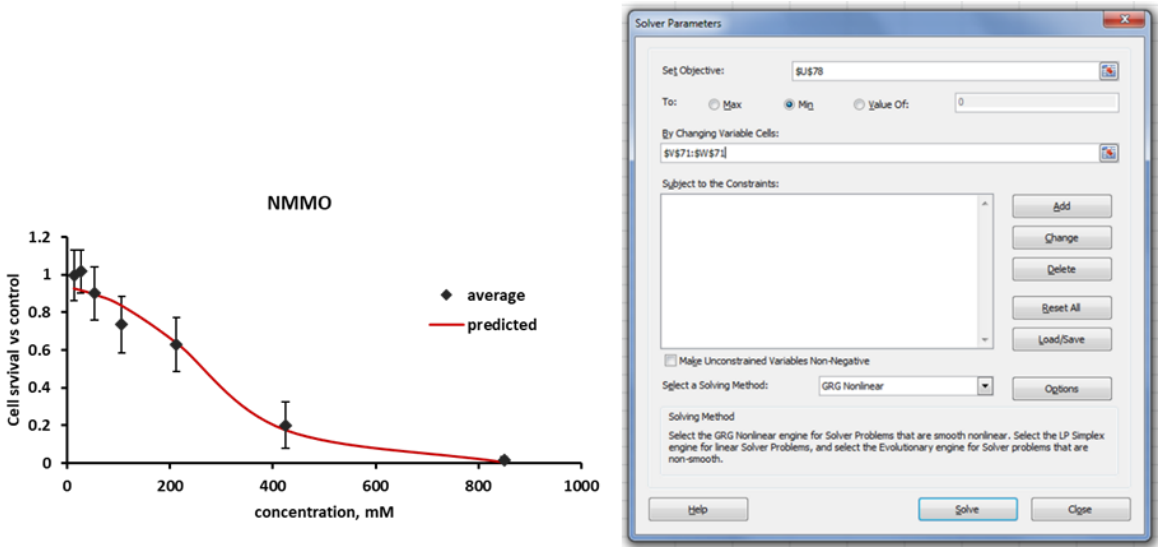

Figure 16: Prediction of EC_{50} values: On the left side of the figure shows a sigmoidal curve from one of the EC_{50} determinations, which were performed within all described projects and the corresponding input mask of the excel add-on, solver

To summarize, the EC_{50} value is finally determined based on the experimentally obtained cell numbers and the iterative curve fitting combining experimental data with computerized software systems to achieve the most accurate estimation of the EC_{50} value. In the present work different cell lines were used for the determination of the EC_{50} values of various analysed ionic liquids and will therefore be described in the following chapters.

1.3. Mammalian Cell Line

During the projects, different mammalian cell lines were used for the investigation of the toxicity of various ILs. In total three cell lines, human corneal epithelial cells (HCE), Chinese hamster ovary cells (CHO) and HeLa cells, were used for different reasons, described below.

1.3.1. Human Corneal Epithelial Cells (HCE-cells)

The eye as one of several human organs is permanently exposed to environmental influences. Therefore, the eye is composed of the cornea, which contains five different layers, the epithelium, Bowman's layer, stroma and the Descemet's membrane [96]. The epithelium builds after the tear film layer the first mechanical barrier against the external

environment and is comprised of HCE-cells [97] (Figure 17).

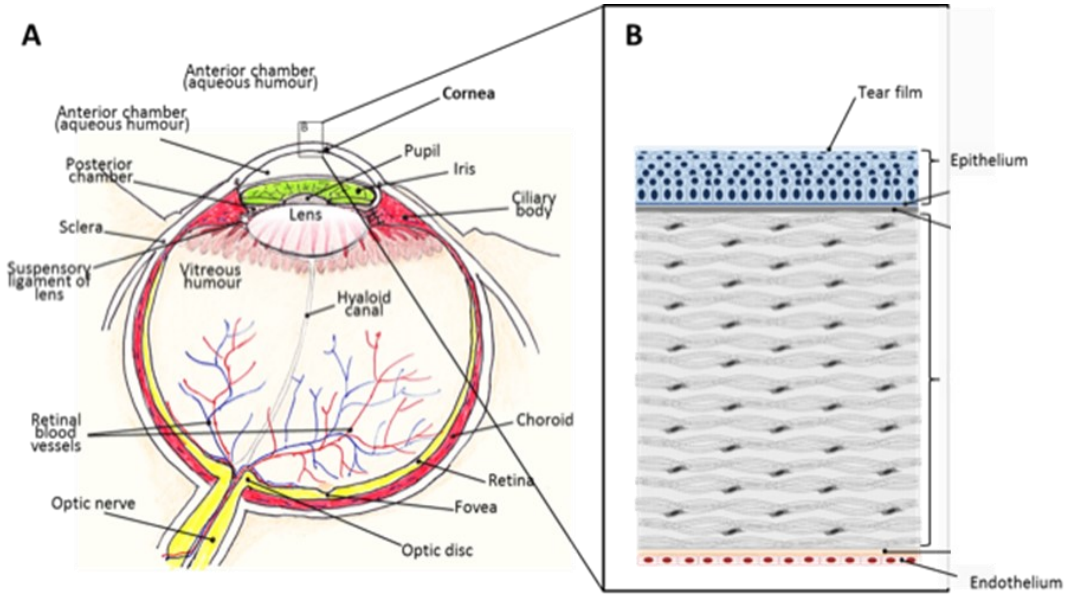

Figure 17: Structure of the eye and cornea: (A) shows the structure of an eye. (B) represents a zoomed cut-out of the cornea with the tear film layer and the epithelium, containing HCE cells as first barrier against all environmental effects, followed by additional parts of the cornea, basements membrane, Bowman's layer, stroma, Descemet's membrane and the endothelium. Adapted with permission from A. Robciuc [98]

The HCE-cells, which are used for the following work, are treated with an simian virus 40 (sv40)-adenovirus vector [99,100] to achieve an immortalized corneal epithelial cell line and to enable the possibility to grow a stable and reproducible cell culture [100]. Nowadays, HCE-cells are used as model cornea and replace donor cornea in the research of eye diseases [101]. The corneal epithelial cells can be damaged by several corneal injuries, which can lead to total loss of sight [101]. Additionally, an injured corneal epithelium may play an important role as inflammatory mediators [97]. On the other side, the HCE-cells are beneficial for physiologic, toxicologic and viral studies [102]. Therefore, and for the reason of the first mechanical barrier, the HCE-cells were chosen as model cell line in the following toxicologic and metabolomics studies.

1.3.2. Henrietta Lacks Cells (HeLa-cells)

This cell line has become the most applied human cell line and was involved in the characterization of important molecular and human cellular processes, 60.000 publications and several Nobel prizes [103]. The HeLa cell line is so far the most widely spread, immortalized human cell line [104,105].

The HeLa cell line is named after the initials of Henrietta Lacks [105,106]. She was present with cervical carcinoma at the John Hopkins Hospital in Baltimore 1951 [105,107]. During

cancer treatment, the surgeon collected tissue samples from Henrietta. Dr. George Gey, which concerns was the healing of cancer, isolated together with his wife, a trained surgical nurse, a single cell from the tissue of Henrietta and tried to grow a cell culture [106,108]. They were successful, established the roller-tube cell culture technique and the HeLa cell line became the first immortalized human cultured cell line [105–107,109]. They further recognized three differences to normal cells [106]:

1. the fast growth, even considering their cancerous character
2. the higher number of chromosomes
3. the cells are immortal and will divide infinitely

Immortalized cell lines are mainly tumorous cells which doesn't stop division or they are cells which are by hand manipulated to indefinitely grow [110]. HeLa cells are tumorous cells with a highly active telomerase, which rebuilds the telomeres after each division. Therefore, the cells are protected against cellular aging and can proliferate indefinitely. As a result, the cells avoid reaching the Hayflick limit. This limit describes the number of cell division a normal cell can pass until cell death. HeLa cells have a doubling time of 24h and a hypertriploid chromosome number (3n+) of 76 to 80 chromosomes. A normal cell is contained of 46 chromosomes as comparison. 22 to 25 chromosomes of the HeLa cells are clonally abnormal and therefore so called HeLa signature chromosomes [105,106]. These cells were used in many different laboratories and are well described [111]. Especially, they are theoretically homogenous and grow in genetically identical populations [110]. Additionally, there are only slight changes in the Golgi apparatus, the lysosomes, the endoplasmic reticulum, the mitochondria and on intranuclear structures [112].

The genome of HeLa cells are noticeable stable after years of cell growth, which suggests the assumption the genetic alterations observed in HeLa cells were already present in the original tumour and might be responsible for the cervical cancer [105]. Because of the stable genomic growth, this cell line became also the first ever sold biological human material. Additionally, the separation of a cell aggregate is easily done and the cell number can be obtained precisely because of less interstitial material.

The HeLa cells are also epithelial cells like the HCE-cells [113] and were spread around the world by Dr. Gey. The usage in many different laboratories, the property of floating on dust particles and unwashed hands led to the major problem by using HeLa cell culture beside other cell cultures in the same laboratory. Due to the rapid growth of HeLa cells, they easily

overgrow other cell cultures without recognition [104–107]. Nowadays, it is known, that the HeLa cells are not a cervical carcinoma, but are contained of a human papillomavirus (HPV) 18, which is linked to a highly aggressive adenocarcinoma class. This explains the very fast growth of the HeLa cells, whereof Dr. Gey was surprised [104,105,107].

In general, the characteristics of the cell line leads to consistent and reproducible results using HeLa cells as a model cell line for experiments. For instance, they were used for studying the cell adherence and mitosis, for the assay of toxic substances and for the investigation of bio-synthetic processes [114]. On the other side HeLa cells were used for the development of the vaccine against the polio virus as one of the earliest use of HeLa cells and the first ever mass production of cells in a cell production factory [105,115]. Additionally, HeLa cells were the first cells on a space mission to analyse the influence of zero gravity. So this cells were used already for many scientific landmarks, like gene mapping, in vitro fertilization, for the first ever cloning, Acquired Immune Deficiency Syndrome (AIDS) and studies for the effects of radiation and toxic substances [104–106].

Based on these facts, the HeLa cell line turned out to be the perfect cell line to study metabolism [108] and was therefore chosen for the following lipidomic studies.

1.3.3. Chinese Hamster Ovary Cells (CHO-cells)

Already in 1919, the Chinese Hamster was used for the characterization of pneumococci. The first CHO cell line was established by Puck *et al.* in 1957 (only a couple of years after he cloned the HeLa cell line for the first time [116,117]. During the years different CHO cell lines were developed, but all CHO cell lines lacking the synthesis of the amino acid proline. This is caused by the original cell culture, which is the origin of all further developed CHO cell lines [118]. CHO cells are the main host cells for the production of therapeutic proteins [119,120] due to their robustness [118] and unique geno- and phenotypes [116]. Additionally, the glycan structures of the recombinant proteins produced in CHO cells are similar to the glycan pattern isolated from humans [121]. Nevertheless, the glycosylation pattern is not exactly the same compared to human patterns causing in some cases immunogenic proteins [118]. Mostly eukaryotic cells are used due to the possibility of post-translational modifications [120]. Therefore, it is desired to grow CHO cells in a huge amount, so called fed-batch cultures [119,120], to achieve a high cell density and productivity of the recombinant proteins. Therefore, it is necessary to choose a CHO cell line which is adapted to grow in suspension, as the original CHO cells are adherent growing epithelial cells.

Suspension CHO cell lines need to be grown in a chemically defined medium supplemented with different carbon sources to achieve a stable metabolism over a long period of cultivation [122]. The advantage using CHO cells for the production of therapeutic proteins are their unique glycosylation properties. But they are also known to require large amounts of nutrients. Most of the nutrients are converted to by-products, like lactate or ammonium, which are released in large quantities into the medium. These by-products are also known as cytotoxic compounds, which leads to the death of the cells. Therefore, it is of most importance to constantly monitor the glucose content and consequently minimize the lactate and ammonium concentrations in the medium. An increased lactate content inhibits cell growth and productivity, not only in CHO cells, but in many different mammalian cell lines [119,123,124]. However, the increase in concentration of ammonium is far worse, as it inhibits growth and productivity, but also affects the glycosylation pattern of the produced recombinant therapeutic proteins. Therefore, the pH value in the medium is constantly monitored by using a pH probe within an industrial reactor approach. The pH value changes due to the release of lactate and ammonium into the media. Correspondingly glucose is added to the media as needed [119]. Since in 2011, the entire genome of a CHO cell line was sequenced for the first time, the development of the optimized conditions for the maximum growth rate and productivity was accelerated [118] and therefore, the cells were used for the first EC_{50} determination of the ILs during the here described work. However, the overall goal of this dissertation was to develop an analytical workflow to study the toxic effects on mammalian cells by metabolic fingerprinting.

1.3.4. Extraction and quenching strategies for cell samples

One of the most crucial steps in metabolic fingerprinting of cells are the quenching and the extraction strategies. Thereby, the strategy depends strongly on which part of the cell culture the analysis should be performed, because metabolic fingerprinting of mammalian cells can be subdivided into two sub-groups: i) extracellular metabolites and ii) intracellular metabolites [125,126]. The analysis of extracellular metabolites is of most convenience performed by using adherent growing cells. That means the cell culture media has to be taken for analysis. Nevertheless, it is quite difficult to establish a direct link from the concentration of the exometabolome to the actual state of the cell culture [125]. Therefore, mostly the intracellular metabolites are analysed, because they build up a more precise picture of the real-time status of the cells [125]. Nevertheless, the analysis of endometabolites is challenging due to concentration ranges of several orders of magnitude.

One of the most important topics to consider when analysing endometabolites is the quenching of the metabolism of the cells [125,127–129]. Due to the fact that some metabolites (for example ATP, etc.) metabolize quite fast or have a fast turn over number, respectively, it is necessary to quench the cellular metabolism as fast as possible to be able to analyse the real-time status of the cells [125,127,130]. Especially mammalian cells will need the quenching step before extraction. Normally, the quenching process is performed using dramatic changes of temperature or buffer solutions with a specific pH value [125,129,131]. The most critical point is, that the cells tend to burst due to drop in temperature or increasing/deceasing of the salt concentration surrounding the cells. That would cause loss of metabolites before the extraction. A good alternative to temperature and pH will be organic solvents. Using organic solvents for quenching, the cells will be placed immediately after removal of the media on ice [125]. The further steps will be carried out as fast as possible to be able to analyse the real-time status of the cells. Another important issue to consider is the separation of the cells from the media. For adherent cells, the separation is the easiest step during extraction [132,133]. The media can be simply poured away, but for the extraction, the cells have to be detached from the cell wall. Usually trypsin/ ethylene diamine tetraacetic acid (EDTA) solution is used for detachment [129]. Nevertheless, studies showed metabolite loss and changes in the metabolome due to treatment with trypsin/EDTA [131,132,134]. The changes in the metabolome already occurred after seconds. The detachment process is time consuming, as it depends on the cell line how long the trypsinization should be performed. Additionally, that would mean that the quenching can only be performed after detachment, which causes that the real-time status of the cells cannot be analysed by using adherent cells. Therefore, the cell detachment can also be performed by using so called cell scraper, but it causes delay in quenching of the metabolism, metabolite loss and is as well time consuming as the trypsinization [131,132,134]. The best method would be the combination of the quenching and extraction step, skipping the detachment of the cells, by pouring directly cold aqueous methanol (MeOH) solution to the cells and scrape them off the flask wall with a cell scraper [125,131,132]. The biggest advantage is, that the metabolites, which would be lost using only the scrapers, are directly released into the extraction solvent. Additionally, the quenching is performed at the earliest timepoint [118]. Total different difficulties occur by using cells, which grow in suspension. The most crucial step is the separation of the cells from the surrounding medium. There are various different methods to apply: i) centrifugation,

which is time consuming and the effect of centrifugal forces on the cells has to be taken into account, ii) fast filtration using specific sized filters. Fast filtration can only be used for small quantities as the cell number is limited due to the possibility of blocking the filter [125,130]. Another important step to prevent mixing up extracellular and intracellular metabolites is the washing with for example buffer before the extraction. However, Dietmair *et al.* showed growing cell damage during washing steps [130,132].

For the analysis of intracellular metabolites, the metabolites have to be released from the sample to a solution which is compatible with the desired analytical method. Independent of the analytical platform, the removal of proteins is always necessary, which can be achieved using organic solvents, like described above. Methanol causes that the cells burst [125,130]. Therefore, the quenching step and the extraction step will be combined to avoid losing metabolites. Nevertheless, there is no universal extraction method which covers the whole metabolome and is suitable for all cell lines [125,127]. Several publications in literature showed that intracellular metabolites were extracted the best using pure organic solvents or an aqueous mixture. Mostly aqueous MeOH, aqueous acetonitrile (ACN) or pure MeOH showed best results [125,130,132,135–137]. A second important fact is the complete rupture of all cell membranes. Therefore, the use of ultrasonication or liquid nitrogen for freeze/thaw cycles are used. To summarize, the use of aqueous MeOH solution (20:80, v/v) or aqueous ACN (20:80, v/v) can combine quenching and extraction step [125,129,131,132]. Nevertheless, there are beside extraction using organic solvents several other methods, like deproteinization using heat or inorganic acids. This leads to lower metabolite coverage [138,139]. Additionally, some metabolites only occur in very small quantities in the cells, which rases the need to concentrate the metabolites [125]. One possibility is the biphasic liquid-liquid extraction (LLE), which combines extraction and enrichment of metabolites in the corresponding liquid phase in one step [125,128]. The biggest advantage using LLE would be that at least two different solvents are used, which lead to a broad coverage of extracted metabolites, as the metabolites are already separated in the aqueous and the organic phase. They can be directly analysed by using different analytical techniques [128,138]. Nevertheless, high amounts of solvents are used, it is very time consuming and can hardly be automated, which is a big disadvantage for high throughput analytics needed for example in clinical studies [128,138]. Additionally, the transfer of the two phases to different vials are not easy, as the proteins are precipitated in the middle at the phase border, which means that the protein precipitate have to be punctured to reach

the lower phase with metabolites. A more selective and convenient extraction can be achieved using solid-phase extraction (SPE). For example, high abundant metabolites can be removed, leading to reduced matrix effects [129,138]. The selectivity can be controlled by using different solid sorbents. Therefore, monolithic silica can be used to provide a very high ratio of surface-area to volume solvent. Thus, carbon nanotubes can be used as SPE sorbent, which leads to a large specific surface area, a strong adsorption capacity and a high chemical and mechanical stability. However, extraction with SPE is time consuming and only a part of the metabolites will be extracted based on the selectivity of the sorbent material. Therefore, the extraction using pure organic solvents or aqueous mixtures would be most probably the best extraction method for cells in combination with untargeted metabolomics [138] and LLE and/or SPE is more suitable for targeted analysis [125]. In general, the most errors, resulting in metabolite loss, occur during sample processing. Therefore, only minimal sample pre-treatment is recommended [140]. Especially, samples extracted from cell culture need a good sample processing strategy. The cell density, for example, highly affects the intracellular and extracellular metabolite concentration [125]. Additionally, one single extraction method is not sufficient to cover the whole metabolome and depends strongly on the desired metabolites. Therefore, in any further metabolomics studies using cells, the following aspects need to be considered: i) standard cultivation conditions necessary to use, to prevent variations in metabolism due to external influences, ii) usage of standardized sample preparation to produce results that are as reproducible and reliable as possible, iii) develop new sample preparation strategies, covering a broader range of metabolites extracted within a single sample preparation step, and iv) usage of adequate quality control strategies, controlling the robustness of the single steps during metabolomics [125]. Therefore, normalization of the cell extracts is of utmost importance, because the raw data is most likely not reflecting the changes in concentration. For example, isotopic labelled internal standards (ILIS) used for normalization are highly recommended even though they are not always available [125].

1.3.5. Normalization of metabolomics samples

Compared to other omics analysis, like proteomics or genomics, the normalization of metabolomics analysis is much more challenging due to its wide variety of concentrations and characteristics of metabolites [134]. Nevertheless, the variability in cultured cells is relatively small compared to body fluids, like human plasma or urine. The metabolome from body fluids is additionally influenced by diet, age, gender, body weight and so on [134]. This

renders a precise study design essential. Metabolomics using cells contains the risk, that the results are not reproducible or vary strongly. For example, in aliquot 1, different metabolites are detected than in aliquot 2, caused by the fact that different numbers of cells died during the same treatment in the different aliquots [125]. For this reason, it is crucial to perform a normalization of the data. The normalization can be performed pre-analysis or post-analysis [134]. One possibility of pre-analysis normalization would be adjusting the sample volume or concentration for example before the analysis of body fluids. In clinical studies sometimes, the normalization is performed by adjusting the volume as described above based on the concentration of a specific metabolite [125,134], for example creatinine for the analysis of urine samples [134]. Another version is the normalization based on protein concentration [125,134] determined by a Bradford or bicinchoninic acid assay (BCA) [134]. But for metabolomics of cell samples no metabolite, which is present in every cell line and is directly linked to the concentration of the other metabolites is available. That means, for every cell line the development of normalization process has to be repeated. On the other side, the assays are well established and convenient. However, Silva *et al.* showed that the correlation of the protein concentration and the cell number failed due to poor recovery of the proteins and incomplete re-solubilization of proteins from the cell pellets [134]. A major advantage of pre-acquisition normalization is that for every sample similar signal response occur. Additionally, intra-group variations due to biological variations are reduced. Nevertheless, an additional aliquot per sample has to be taken and an additional experimental step hast to be performed, which is time consuming and not suitable for high throughput analysis [134]. Therefore, the normalization based on the cell number [125,134] shows one possibility. Suspension cell cultures are more convenient for this additional step. Adherent growing cells have to be detached first [134], and the influence to the intracellular metabolic homeostasis is not yet analysed [125]. Additionally, the detachment causes further problems as described above [134]. For adherent growing cells the determination of the dry weight of the cell debris can be performed alternatively, but also on the expense of time and relatively large errors [134]. In general, the normalization based on cell counting lacks high accuracy as inhomogeneity of the taken cell sample is a big issue, especially for cell lines which are famous for agglomeration [134]. In particular adherent growing cells stick to tubes, pipette tips and agglomerate after detachment, causing necessarily repeating of cell counts [132]. Nevertheless, cell counting was used as one of several normalization steps during the present work, because the cell numbers were highly different due to the treatment

with ILs and the usage of mainly suspension cells reduced the risk of agglomeration during cell counting. Additionally, it was more convenient than dry weight or protein assays.

Another more convenient possibility is described by post-acquisition normalization. For example, in the case of liquid-chromatography tandem mass spectrometry (LC-MS/MS) analysis of cell extracts an additional ultraviolet (UV) detector could be implemented, which enables a normalization based on the UV signal without performing neither any additional experimental steps nor needing additional aliquots [134]. Even more convenient is the normalization using the total metabolite intensity. Nevertheless, this method is only suitable for comparison of samples, which concentrations differ by less than 2-fold [134]. Otherwise, the false-positive rate would be too high. Therefore, a better way of normalization is based on the peak areas [141], as there is a linear correlation between the sum of all peak areas and corresponding cell counts. That means, the normalization of each peak area based on the sum of all peak areas are a good alternative compared with normalization based on cell counts, especially for cells growing in suspension [132]. Another post-acquisition normalization approach uses stable isotopically labelled internal standards, which are highly recommended at least one for every subclass of metabolite [138]. This would correct potential errors occurred during sample processing as well as sample acquisition [138]. The internal standard (IS) should be therefore carefully selected. Otherwise, the IS corrects only for analytical errors and not for possible ion suppression occurred in the mass analyser [128]. As stable isotopically labelled IS are not always available, the desired cells can be grown using media supplemented for example with ^{13}C-labeled glucose. Most cell lines are using glucose as nutrition to build all essential building blocks, for example nucleic acid, amino acids and so forth. Therefore, the extraction of this cells leads to a ^{13}C-labeled internal standard for all metabolites, which are present in the cells [138]. A major drawback of this method is, that the total labelling of the metabolites as well as the extraction of the full metabolite profile cannot be ensured. Therefore, so called quality control samples (QC samples) can be used for normalization [127] based on the locally weighted scatter plot smoothing (LOESS) algorithm. QC samples can be a pool of all analysed samples or a commercially available standard sample [128] like human plasma standard reference material SRM® 1950 [142], for example. QC samples are normally placed at the beginning and end of the analysis and randomly distributed during the analysis of the samples. The QC samples at the beginning of the analytical sequence are used for equilibration purposes and for system suitability testing. In general, they are used to track possible variances during

the sample analysis [127], to evaluate intermediate precision within different analytical sequence of similar samples and for post-acquisition normalization of the data within a sequence or between different sequences [128].

Even, pre-acquisition normalization is preferred [134], this normalization will not compensate the errors which occurred during sample preparation [132]. But, as the main variations of metabolite concentration occur during sample processing, sample analysing and data processing, it is highly recommended to implement additionally post-acquisition normalization to correct for these kind of errors [134].

1.4. Metabolomics

The term metabolomics and the analysis of molecules in this form was first used and performed in the mid-1990s [125]. Metabolomics is mainly used in cancer research, with the general interest of medicine in discovering new biomarkers and investigating the effects of drugs [127], since most health disorders or diseases are due to altered metabolism or accompanied by changes in metabolism [142]. There are mainly three levels describing a biological system: i) genomics/ transcriptomics analyses methods which were developed in the 80s ii) proteomics, which has its beginnings in the 90s and iii) metabolomics which started around 15 years ago and is still developing [127]. All three levels are part of the so called “omics” technology [140,143–146]. The term “genomics” describes the analysis of DNA. The analysis of mRNA is called transcriptomics and proteomics describes the analytics of proteins (Figure 18).

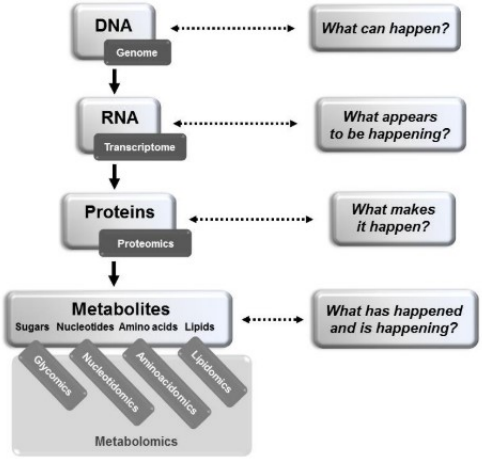

Figure 18: The order of the omics technologies: Genomics is the beginning of the cascade and contains the analysis of the DNA of a system and therefore, the possible effects on the metabolome. Transcriptomics describes the analysis of mRNA and the most likely effect on the system, whereas the analysis of proteins is called proteomics and shows the reason for the effects on the system before, metabolomics at the end of the omics cascade describes the real-time response to effects in a biological system due to one of the other omic areas. Reprinted with permission of Jurowski *et al.* [147]

The metabolome compared to genome/transcriptome or proteome is therefore a direct downstream product of a biological system and is directly linked to the real-time situation of a biological system. It shows reaction of the system to environmental stress and is described as a global unbiased qualitative and quantitative insight into a biological system [140,143–146]. In addition, the analysis offers great potential to build a bridge between genotype, which describes all heritable genes and phenotype, which describes the characteristics of an organism [148]. Therefore, metabolic profiling is one of the most promising fields for early diagnostics or discovering potential biomarkers [149]. Toxicity of certain drugs can also be monitored using metabolomics analysis [127]. That means, that metabolomics covers a broad range of small compounds known as metabolites, like lipids, amino acids, peptides, nucleic acids, organic acids, vitamins, thiols and carbohydrates [126]. The advantage of the metabolism is that it is only slightly changed from animal to human. This means that studies in animals can be almost completely transferred to humans [150].

Within a metabolome there are all metabolic intermediates, hormones, signalling molecules and primary molecules. Already, the primary metabolites, like amino acids, carbohydrates, peptides, lipids, nucleic acids, organic acids, ketones, amines, steroids, vitamins, etc. only, are a huge number of compounds [140,145,151–153]. Additionally, they are involved in various pathways [154] and processes essential for live [127], which underlines the importance of their analysis. Therefore, the study design is one of the most important considerations within a metabolomics study. Any external influence can have an impact on the analysis result. For example, nutrition plays a major role, as well as genetic predisposition, etc. [127]. Another point that should be considered during the design of the study is the time needed to take the samples [155]. Large-scale studies remain a challenge because a large number of samples must be prepared for analysis [128] and one strategy never covers the entire metabolome, so several different strategies have to be applied in series [156]. Attention should be paid to the fact, that the sample preparation as well as the following analysis should be randomized in order not to influence the analysis results by possible systematic errors, for example, if the samples of a time profile are processed in chronological order and thus an actually non-existent profile is erroneously generated [129]. Initially metabolomics analyses were performed with biofluid and cell samples and later used for tissue and biopsy analyses [127,138]. Primary cells are rarely available for metabolomics experiments, so the use of cell cultures offers a good alternative [125]. The chemical and physical diversity of the metabolome is very large and the concentrations range from pmol

to mmol [127,142]. Due to their huge diversity, it is still difficult to estimate the whole number of metabolites within a given metabolome [140,153]. Right now, there are 114.260 entrances in the human metabolome database (HMDB; 21.11.2020). Nevertheless, the analysis of metabolites has a great potential to discover new biomarkers, also in early diagnosis states, so-called diagnostic markers in case of medicinal studies [154]. Additionally, metabolomics analysis is also quite interesting for predicting drug efficacy (pharmacometabonomics) and drug toxicity for safety assessments. It is also an essential tool in medicine to develop an individual prevention of diseases or a personalized treatment [128]. Talking about the analysis of the metabolome, there are two basic terms i) metabolomics and ii) metabonomics. The latter describes more the comparison of test and control group [154]. Already in 1940, Roger William found out that every individuum owns his own metabolic profile for example in body fluids [128]. Therefore, the concentration dynamic range of the metabolite´s concentration spans nine orders of magnitude [140] and the metabolites have additionally different characteristics in terms of volatility and polarity [140,154,157–159]. Therefore, it was very difficult to develop an analytical method to analyse metabolites.

1.4.1. Analytical techniques in Metabolomics

Since the 80s, Nuclear-magnetic resonance (NMR) is the first choice for analysing metabolites [140]. NMR is a fast and non-destructive analytical technique, which does not need a specific sample preparation and is therefore suitable for high-throughput analysis and for structural elucidation [127,160]. A normal NMR spectrum of a metabolomic analysis contains 2-3000 peaks/signals [160] (Figure 19). The area is directly linked to the concentration of the metabolite [128].

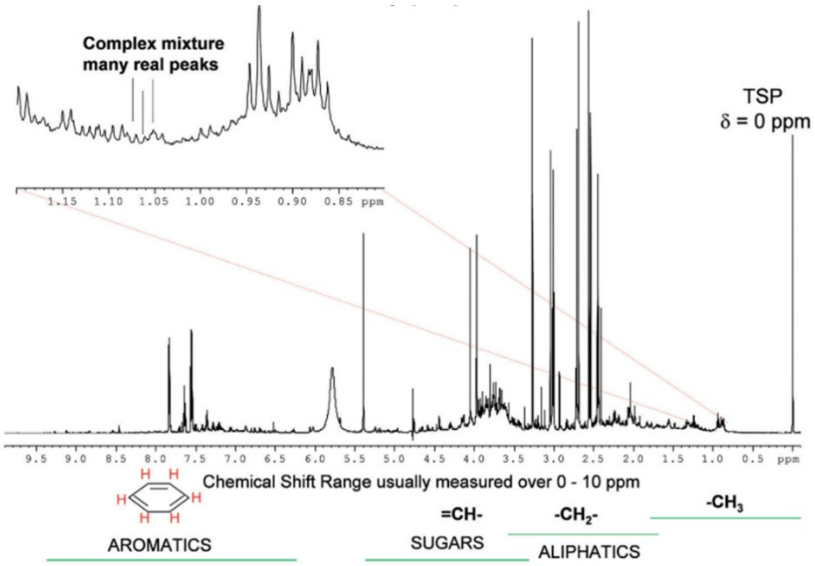

Figure 19: NMR spectrum: The analysis of the global metabolome using a NMR results in very crowded and spectra, which are difficult to interpret. Reprinted with permission from Clarke *et al.* [160]

That means, NMR analysis combines qualitative and quantitative analysis within one analysis [140]. The spectra itself are very reproducible but very crowded and already metabolites lower than 1µM will be most probably below the detection limit of NMR analysers [126,128]. To overcome the problem of crowded spectra and detection limits, the analysis of the metabolome using mass analysers coupled with a separation technique in front was developed.

The beginning of MS-based metabolomics analysis was performed from Dalgliesh *et al.* already long before the terms metabolome and metabolomics were introduced, which was 30 years later [128]. They used the gas chromatography technique hyphenated to a mass analyser [128]. One of the biggest advantages, is the ionization with electron impact (EI), because this kind of ionization technique is very reproducible [127,128,140,155,161]. That means the spectra are reproducible also in comparison of different laboratories [140]. Therefore, metabolite identification using GC-MS benefits from the spectral data base, developed from the National Institute of Standards and Technology and therefore called NIST [127,128,161,162]. Nevertheless, GC-MS can only analyse volatile compounds [127,156,161,163,164]. That means, the metabolites has to be derivatized to change their characteristics from involatile to volatile metabolites [126,127,154,156,161,164–166]. This additional step costs a lot of time and cannot guarantee for 100% derivatisation, which causes loss of metabolites [140]. Additional, thermolabile metabolites can be lost [128]. Ion Pair Chromatography (IPC) is the most suitable option for hydrophilic and charged metabolites, but the equilibration of the

column takes quite a long time and a switch of the ionization is not possible, because the reagent in the mobile phase would cause ion suppression and it is almost impossible to flush it out of the column without leaving residues [161]. However, capillary zone electrophoresis (CZE) and micellar electrokinetic chromatography (MEKC) are often used for ionic metabolites in a targeted analysis [161]. Besides CZE and MEKC, CE-MS is also often used for polar ionizable analytes [154]. CE-MS with its high analyte resolution is a powerful and promising tool [126]. In comparison with LC, CE impresses with fast analysis times, low sample volume and small amounts of solvent [126,161]. Nevertheless, it requires additional know-how in practical handling compared to GC or LC to achieve a stable MS signal [128]. Furthermore, the inner wall of the capillary has to be modified in order to prevent interferences from the sample binding irreversibly to the inner wall, which would result in poor reproducibility and a low throughput [154,161]. In addition, an analysis using CE-MS is not very robust [154]. For the analysis of the metabolome with LC-MS, derivatisation is usually not needed, resulting in LC-MS as the major analytical technique used for metabolomics [154].

LC impresses with higher selectivity due to interactions of the metabolites with the respective stationary phase of the LC column [128]. The development of smaller column particles, respectively the core-shell technology and the resulting possibility of Ultra High-Performance Liquid Chromatography (U(H)PLC) increases the peak capacity and separation selectivity, whereby significantly more metabolites can be detected within one analysis. The most significant advantage of using U(H)PLC is the improved separation performance, but without increasing the analysis time [156]. However, for some analytes, derivatisation is necessary to improve the detectability and to be able to analyse polar metabolites by reversed-phase (RP) chromatography [161]. However, due to the high diversity and broad dynamic range of the metabolites, it is still not possible to detect all metabolites with only one analytical technique. Therefore, different separation techniques, like Hydrophilic interaction liquid chromatography (HILIC) with various stationary phases and RP chromatography should be taken into account for the analysis of the global metabolome.

1.4.2. Hydrophilic interaction liquid chromatography (HILIC)

Hydrophilic interaction (liquid) chromatography is a chromatography technique with a polar stationary phase and an organic mobile phase (almost always acetonitrile-based) containing at least 2-3% water [167–169]. This technique was already used in the early 1940s by Martin and Synge to separate amino acids on a silica column with water-saturated chloroform as

the mobile phase, although it was not yet called HILIC [170]. Linden *et al.* also used this type of chromatography technique to separate sugars in the 1970s [127]. But it was Alpert *et al.* who first introduced the term HILIC in the early 90s [168,170,172–179]. Previously, similar chromatographic applications had been referred to as aqueous normal-phase (NP) chromatography [170,175,180], since HILIC uses stationary phases of NP chromatography. However, HILIC shows some advantages over NP chromatography as well as over RP chromatography, for which HILIC is now considered the most useful complementary separation technique. In contrast to normal phase chromatography, the mobile phase of a HILIC separation contains at least 2-3% water [167–169], making even very polar analytes soluble. In addition, the high organic content ensures that, for example, samples can be injected directly after a liquid-liquid extraction, protein precipitation or even after a solid phase separation without further sample evaporation and reconstitution [167,176,179]. Probably the most important advantage is the possibility to hyphenate HILIC separation with electro spray ionization mass spectrometry (ESI-MS) detection. The high content of organic solvent as mobile phase improves the ionization efficiency and sensitivity by a factor of four to six compared to RP-LC [167,171]. A further advantage of the high organic content in the mobile phase is the low viscosity, which leads to low back pressure in the column and therefore, high flow rates and a faster and more efficient separation [167,169,170,173,176,179]. HILIC was initially developed only for the analysis of carbohydrates [171,175]. Alpert *et al.* were the first to develop a theory of the separation mechanism. They stated that the separation takes place due to the distribution of the analyte between the organic part of the mobile phase and a water-saturated layer on the surface of the stationary phase [172,173,176,179] (Figure 20).

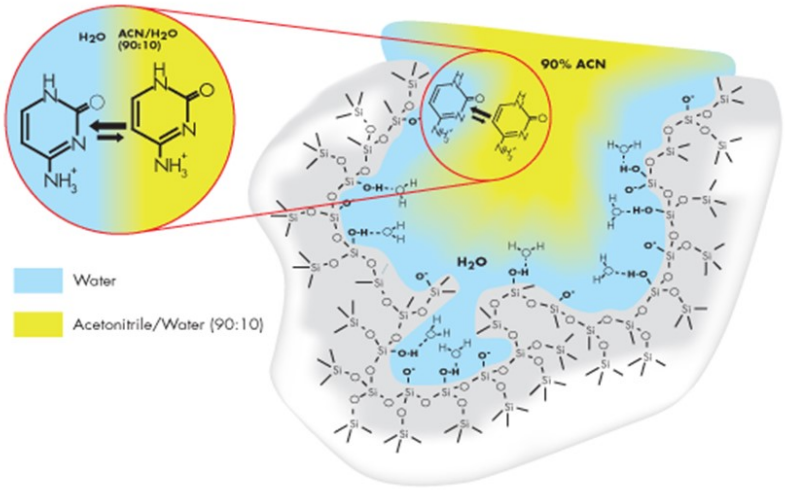

Figure 20: Scheme of HILIC chromatography: The silanol groups of the stationary phase of the HILIC column are surrounded by a water layer. The thickness of the layer is dependent on the amount of water in the mobile phase of the HILIC chromatography. The organic part of the mobile phase is located above the water layer and the compounds, which are analysed with HILIC chromatography are distributed within the water and organic phase according to their properties [181]

The polar stationary phases used for HILIC bind water from the aqueous mobile phase at their surface. This creates a gradient from an organic layer to a water-rich layer on the column surface. Accordingly, HILIC could be described as a liquid-liquid separation [169,171]. This means that polar, hydrophilic analytes prefer to stay in the water-rich layer, or are dissolved and thus retarded. In the early days of HILIC chromatography, mainly only silica columns were used. It soon became apparent that the separation mechanism is far more complex than Alpert *et al.* had thought and that separation by distribution does not describe the entire separation process. In addition to the distribution of the analytes between the organic and water-rich layer, ionic interactions (electrostatic interactions) and the direct adsorption of the analytes to the stationary phase by means of hydrogen bonding and dipole-dipole interaction were involved in the separation [168,169,171,172,175,176,182,183]. This allows certain separation properties to be controlled by the type of stationary phase of a HILIC column. Column manufacturers started to couple silica particles with different molecules. Today, HILIC stationary phases are divided into groups according to their structure. These include a) neutral stationary phases in which, for example, amide, cyano or diol compounds are coupled to silica gel, b) positively charged column surfaces, amino, imidazole or triazole functionalities are attached to silica gel, c) negatively charged column surfaces, polyaspartic acid coupled to silica gel or only pure silica gel and d) zwitterionic column surfaces, sulfobetaine combined with silica gel particles [167,169–171,173,175,178]. The latter is used today as the standard column in HILIC analysis. Depending on the nature of the stationary phase of a HILIC

column, other interactions occur in addition to the distribution and affect the separation of the analytes. Accordingly, the thickness of the water-rich layer also depends on the chemistry of the stationary phase [168,169,173]. The more polar the stationary phase, the more water is bound and the thicker the water-rich layer. Additionally, the thickness is influenced by the content of organic solvent in the mobile phase [172]. An organic solvent can be used as the mobile phase of a HILIC separation based on the following conditions: The solvent should be miscible with water, but should not have hydrogen acceptor or donor properties [167–169,171,179]. Acetonitrile meets all these requirements and is therefore used as the standard mobile phase for HILIC separations. However, alcohols (for example methanol) can also be used as mobile phase [168,169,171,184]. The higher the acetonitrile content, the thinner the water-rich layer that is formed. Therefore, the mobile phase should contain at least 2-3% water [167–169], but already with 5% water, a monolayer is completely formed [173]. Often the aqueous part of the mobile phase is replaced by aqueous buffer solutions. Mainly the volatile salts ammonium acetate and formate are used [168]. Nevertheless, other non-volatile salts can also be used, but can prohibit the detection by MS. Of course, the salt concentration and the pH value of the mobile phase also affect the separation mechanism [167,171,173,176]. For example, the pH value of the mobile phase will be adjusted that the analytes are charged, as they are more hydrophilic in a charged state than in an uncharged state [169]. The effect of the pH value on the stationary phase is infinitesimally small, however, polymer-based or hybrid (e.g. ethylene-bridged hybrid, BEH) columns achieve a better pH stability compared to silica particles [167,169]. The stationary phase is rather impacted by the concentration of ionic strength in the mobile phase [169]. Accordingly, electrostatic interactions of the analyte with the stationary phase are more likely to be suppressed the higher the salt content in the mobile phase. The HILIC separation is hardly controlled by changing the temperature. A decrease in retention can be observed by increasing the temperature [169,173]. To summarize, the chemistry of the stationary phase is the most important influencing factor, followed by the water/organic content, the pH value and the ionic strength of the mobile phase. All these independent parameters make a prediction of retention almost impossible. In addition, the separation mechanism of HILIC has not yet been fully understood to date, despite many research efforts to clarify it. To better understand and improve predictability, one should start by checking the function and task of the water-rich layer. In the following section different stationary phases, used during the projects, will be presented.

1.4.3. Zwitterionic Stationary Phases

Zwitterionic stationary phases were initially developed for ion exchange chromatography. Nowadays, however, they are most frequently used in HILIC analyses [167,170,175]. In general, these are silica gel particles or polymer beads to which equal amounts of oppositely charged groups are bound. In most cases, these are strongly acidic and basic functionalities, which are connected to the particles by alkyl groups [169–171,175]. One of the most common representatives is sulfoalkyl betaine with strongly acidic sulfonic acid groups and strongly basic quaternary ammonium groups separated by a short alkyl spacer (see Figure 21).

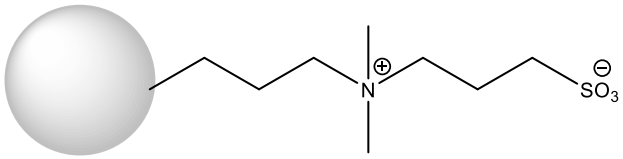

Figure 21: Sulfoalkylbetaine stationary phase: Zwitterionic stationary phases are characterised by oppositely charged groups, which are attached via spacers on silica gel particles resulting in a zero-net charge. The sulfoalkylbetaine stationary phase always contains a quaternary amine and a sulfonic acid group [185].

Both oppositely charged groups are used 1:1, so that in sum, theoretically the net charge is zero. However, in reality, the stationary phase surface is slightly negatively charged [169,173,175,186]. Sulfoalkyl betaine based stationary phases are known for their strong water-binding properties [169,171,175]. Another type of a zwitterionic stationary phase immobilize phosphorylcholine (ChoP) groups on silica particles [175,178]. Therefore, the stationary phase consists of a negatively charged phosphoryl group and a positively charged quaternary ammonium group at the end of the linker (Figure 22).

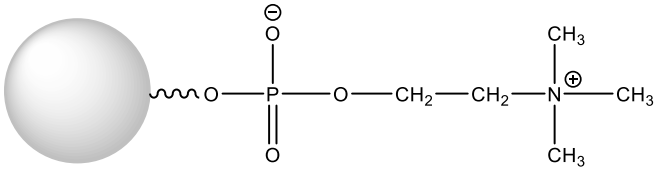

Figure 22: Phosphorylcholine stationary phase: Oppositely charged groups are attached via spacers on silica gel particles resulting in a zero-net charge. The phosphorylcholine stationary phase always contains a quaternary amine and a phosphonic acid group

In addition to the distribution of the analytes in the water-rich layer during a HILIC separation, polar interactions, such as hydrogen bridge binding and dipole-dipole interactions are in the focus [168,169,171,172,175,176,182,183]. Nevertheless, electrostatic interactions between either positively or negatively charged analytes and the sulfonic acid, phosphorylcholine or quaternary ammonium groups of the stationary phase also take place [169,171,172,175,176]. These properties qualify this type of stationary phase for the

analysis of small polar analytes, metabolites, glucosinolates, aminoglycosides, peptides and glycopeptides, among others [175]. Fast and efficient separation is becoming increasingly important in this context. For this reason, core-shell silica particles are now used as basic material, instead of fully porous silica gel particles [167,175]. Core-shell particles consist of an impermeable solid core coated with porous silica gel material. In general, effective distances for diffusive mass transfer are usually shorter for core shell (typically 0.2 to 0.5 µm shell thickness) than fully porous particles (>1.6 µm diameters), which reduces the diffusional peak dispersion due to smaller C-term regarding the Van-Deemter equation [167]. The Van-Deemter equation describes the performance of a column in terms of separation efficiency (Figure 23). The variable A is referred to as eddy diffusion and describes the path of the analyte through the column during an analytical separation. The variable B is named longitudinal diffusion and represents the distribution of the analyte within the mobile phase to the longitudinal axis of the column. Mass transfer indicates the interaction of the analyte with the stationary phase and the mobile phase in the horizontal axis of the column and is labelled as C term [147]. Another benefit of core-shell particles in comparison to fully porous particles is the reduced A-term, as particle size distribution is narrower, resulting in more homogenously packed column beds. The analyte cannot enter the particle as deeply as into the porous particle [167], therefore can be faster released again into the mobile phase, resulting in more narrow peaks (shorter diffusion paths as mentioned above).

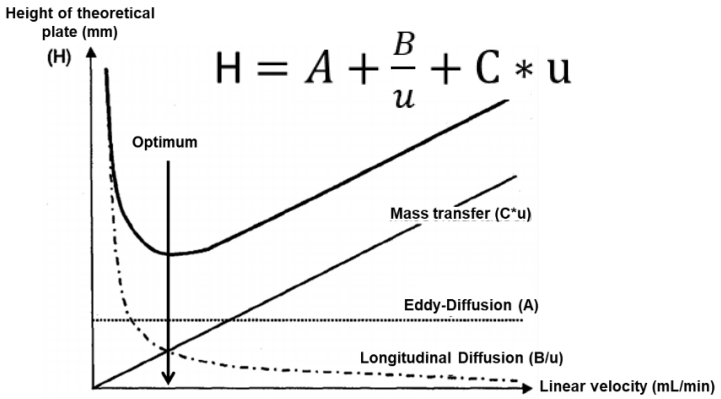

Figure 23: Van-Deemter: The Van-Deemter equation describes the optimal settings of a chromatographical separation. The variable H shows the height of theoretical plate of the chromatography column. The variable A is called Eddy-diffusion and is explained by the way of a compound through the column. The longitudinal diffusion, variable B, represents the diffusion of the analyte in the mobile phase of a chromatographic separation to the longitudinal axis and C, the mass transfer shows the interaction of the analyte with the stationary phase and the mobile phase in the horizontal axis of the column adapted with permission from Will *et al.* [187]

One of the popular core-shell stationary phases in HILIC links 3-N,N-dimethylaminopropane sulfonic acid (DMAPS) to the core-shell silica gel particle and carries therefore a neutral net-

charge with positively and negatively charged compounds as well as the other zwitterionic stationary phases (Figure 21).

The difference to DMAPS stationary phase lies not only in different negatively charged groups, but also in the order of the charges within the linker. The DMAPS stationary phase carries the negative charge externally compared to the positive charge in the ChoP stationary phase. This can affect the selectivity of the separation as well as the elution order of the analytes, thus selecting the optimal column based on the application. For example, acidic analytes retard more on the ChoP stationary phase and basic analytes more on the DMAPS stationary phase [169,189]. Another advantage of the DMAPS stationary phase is that, compared to the ChoP phase, the ionic interactions are mainly applied and the distribution of the analytes in the water-rich layer on the stationary phase only has a moderate influence on the separation of the analytes [182].

1.4.4. Neutral Stationary Phases

Neutral stationary phases usually have polar functionalities bound to silica gel particles, which are normally uncharged at a pH value of three to eight [169]. It should be noted that any free silanol groups of the particles are negatively charged at a pH above 4-5 [169]. As a result, increased electrostatic interactions between analyte and stationary phase can occur and affect the separation [169]. Most HILIC stationary phases belong to this category, which consists of a broad range of polar functionalities (e.g. amides, aspartamides, diols, cyano groups, cyclodextrins and saccharides) [169] (Figure 24).

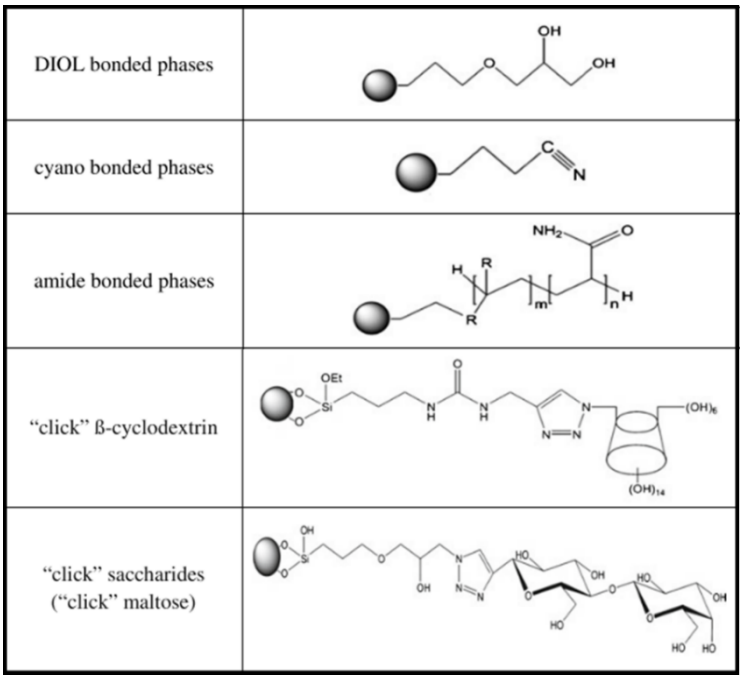

Figure 24: Neutral stationary phases: Neutral stationary phases mainly used in HILIC chromatography adapted with permission from Buszewski *et al.* [171]

Amide-based stationary phases contain carbamoyl groups attached to silica gel particles via alkyl spacers and are recommended for efficient and rapid analysis of strongly polar analytes [175]. For example, the stationary phase of a column especially designed for the separation of water-soluble vitamins and carbohydrates such as mono-, di-, oligo- and polysaccharides connects the silanol backbone via ethylene bridge linkers to gain stability. Due to the fact that this phase does not contain any charged groups, ionic interactions are not significant compared to zwitterionic phases [175]. Additionally, in comparison to amino stationary phases, no Schiff base can be formed with reducing sugars or other carbonyl compounds because primary amino groups are missing [179]. This is advantageous as irreversible binding of analytes is hardly possible. Therefore, it shows a higher stability in retention and selectivity over a longer period of time [182]. Additionally, mobile phases containing salt are no longer needed with this surface chemistry and therefore, the connection to a mass analyser is possible [175].

1.4.5. Reversed Phase Stationary Phase

Most of the time talking about LC-MS/MS, using a RP stationary phase for liquid chromatography is meant. RP stationary phases are mainly contained of C_{18} chains linked to silica particles or polymer beads [128,161]. Also, shorter hydrocarbon chains like C_8 or C_4 are used in RP [190]. Due to steric hindrance of the long hydrocarbon chains, not all silanol groups are occupied by a hydrocarbon chain. The free silanol groups of the silica

particles give the stationary phases a polar character. Therefore, they are mostly shielded by the process of end-capping. The stationary phases themselves are mostly non-polar and therefore retain non-polar to semi-polar analytes [129] mainly by hydrophobic interactions and by the action of van der Waals forces. The best results can be achieved by gradient elution. Therefore, the gradient starts with a high amount of polar mobile phase and reduces partly the polar content by non-polar organic mobile phase. Polar analytes elute thereby nearly unretained at first, which leads to the limitation of RP analytics [154,171]. This means, that the more non-polar the analyte, the longer it remains on the column and is only eluted later in the gradient with a higher proportion of organic mobile phase. Therefore, RP stationary phases are only suitable for the analysis of non-polar or semi polar analytes. Nevertheless, RP is a robust, most reliable and sophisticated stationary phase [154]. In contrast to HILIC chromatography, the analytes dissolved in water are suitable for RP approaches, which ensures the need in the field of metabolomics [161]. Additionally, RP chromatography covers the analysis of a wide range of hydrophobic up to semi-polar analytes [161]. Mostly the mobile phases are consisted of organic solvents, like acetonitrile or methanol in a mixture with water and at least 0.1% formic acid. Sometimes additives, as ammonium acetate, ammonium formate or others are added [161]. Even polar analytes can be analysed after derivatisation using RP stationary phases, as a hydrophobic derivatisation reagent is attached to the metabolite or blocks the polar functionality of the metabolite. For example, aldehydes or ketones are retained on a RP column after derivatisation to decrease the polar properties of the analytes [161]. However, derivatisation is an additional sample preparation step, combined with possible loss of analytes, because the reaction efficiency is not always 100%, depending on the reactive group. Additionally, by-products can be produced due to more than one reactive group of the metabolites and in case of the introduction of a hydrophobic functionality by the derivatisation reagent, all metabolites own the same retention properties [179]. Therefore, RP is nowadays mostly used for the analysis of lipids as a sub-omics category of metabolomics. However, the combination of RP and HILIC in 2D-chromatography would be the breakthrough in the field of metabolomics [142].

1.5. Targeted Metabolomics

In general, metabolomics can be divided in two different categories: i) targeted and ii) untargeted metabolomics [140]. No matter which one, for both strategies the sample preparation is the most problematic, requires the most time and consumes the most resources [154]. However, both strategies may have different requirements for sample

preparation [138]. Due to high sensitivity and selectivity, targeted metabolomics is mostly performed by LC-MS/MS analysis using a triple quadrupole mass analyser or a trapping instrument [128]. Nowadays, there is a new classification in the field of metabolomics, which describes 3 categories: i) targeted metabolomics, ii) metabolic profiling and iii) metabolic fingerprinting (Figure 25).

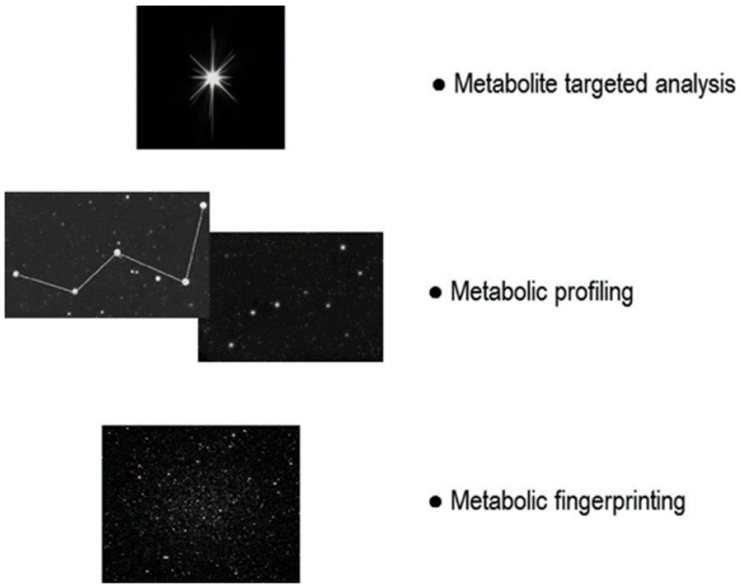

Figure 25: Different terms of Metabolomics: Targeted metabolomics is defined by the analysis of a few chosen metabolites, like the observation of a single star in the whole universe. Metabolic profiling analyses all metabolites of one class comparable to the monitoring of a star image and metabolic fingerprinting screens the whole metabolites contained in an organism, similar to all stars in the universe. Reprinted with permission from Courant *et al.* [127]

A targeted analysis detects and quantifies targeted metabolites. Metabolic profiling has developed as a subcategory of targeted metabolomics and analyses targeted metabolite classes or metabolites of certain pathways etc. instead of single targeted metabolites. Only metabolic fingerprinting is considered to be an untargeted metabolomics approach, since this type of analysis is used to compare entire metabolomes [127,161]. The major challenge of developing a targeted metabolomics method arises when no commercially available standards are present. In addition, a true “blank matrix” without containing the targeted metabolites is often missing. Therefore, most method validations are prepared using a surrogate matrix, authentic matrix with surrogate metabolites or a commercially available plasma/serum, which contains only low concentrations of the analytes [161]. Unfortunately, all approaches, however, use standard addition, which requires relatively high numbers of additional measurements for statistical evaluation in triplicates. Therefore, the best strategy is to use labelled internal standards in water or organic solvents as calibration lines for quantification [161]. Additionally, in contrast to untargeted metabolomics, targeted

metabolomics requires prior knowledge of the desired metabolites, for example the exact mass and fragments, as well as characteristic properties, so that optimal settings can be selected during method development to quantify the targeted metabolites in a specific sample [154]. This means that in a targeted analysis, hypotheses about certain metabolites already exist, which should be confirmed by this analysis, whereas an untargeted method generates hypotheses [140]. As mentioned above, most targeted metabolomics approaches use LC-MS/MS methods, mostly coupled to a triple quadrupole or a trapping system, like ion trap (IT). For example, by using a triple quadrupole, there are different scan modes, which will be described in more detail below, depending on the knowledge about the analytes and the desired analysis (Figure 26).

Although these mass analysers have a lower resolution, they are highly sensitive and selective [156]. Selected ion monitoring (SIM) with respective mass-to-charge ratio (m/z) of the targets selected in the first quadrupole (Q1) can be used for quantification [156]. However, this type of quantification is not as popular as selected or multiple reaction monitoring acquisition (SRM/MRM) in the field of targeted metabolomics, especially when it comes to the analysis of complex matrices [156], because MRM filters not only the precursor mass but also specific, previously defined fragment masses of each precursor analyte or all fragment masses of a single pre-selected precursor (see Figure 26, top and middle), which simplifies the analysis of a complex matrix through the unique assignment of precursor and specific fragment. However, ionization of low abundant metabolites in the presence of high abundant metabolites leads to ion suppression and is a limiting factor during quantification [142]. For large scale studies, relative quantification is often used instead of absolute quantification due to lack of time, simplicity [156] and the cost intensive need of isotopic labelled internal standards for every single metabolite [156]. Today, targeted metabolomics in combination with triple quadrupole using MRM acquisition is widely used to determine and verify biomarkers in clinical research, especially in the fight against cancer, infectious diseases, cardiovascular diseases etc. [161]. Therefore, the MRM acquisition appears as one of the most important acquisition techniques in the field of targeted metabolomics and is described in the following chapter.

1.5.1. Multiple Reaction Monitoring (MRM)

Since many years, LC hyphenated with a mass analyser using SRM/MRM acquisition is well established for quantification of compounds within drug development, environmental and forensic studies [191,192]. In general, MRM is a targeted acquisition mode, in which the

selection of the precursor and product ions is performed before the acquisition by programming different ion transitions (pairs of m/z in Q1 and third quadrupole, Q3) [191]. For targeted analysis triple quadrupoles or linear IT (QTRAP) instruments are mainly used, because of high sensitivity, high specificity and fast scan speed due to three different scan modes (Figure 26) [191].

During the product-ion scan, the Q1 is set as a filter for one specific precursor ion mass and Q3 scans all produced product ions of this specific mass (see Figure 26; top). The neutral-loss scan operates the Q1 in radio-frequency (RF) mode scanning all precursor ions in the desired mass range. Q3 is also used in scan mode in a synchronized manner and detects afterwards all fragments with a specific mass difference (Δm) between Q1 and Q3 (see Figure 26; bottom).

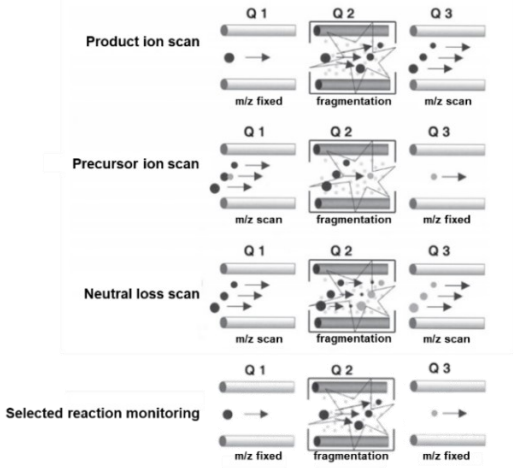

Figure 26: Different acquisition modes of targeted analysis: During the product ion scan, one precursor mass is selected, fragmented in the second quadrupole and all fragment masses (products) are scanned. The precursor ion scan acquisition scans all precursor masses, which are fragmented and filters only one fragment mass afterwards. While the acquisition, neutral loss scan, all precursor masses are scanned, fragmented and all fragment masses are scanned based on a defined mass loss. During Selected reaction monitoring a specific mass is selected, fragmented in the second quadrupole and a specific fragment mass is filtered afterwards. Adapted with permission from Gross *et al.* [193]

However, the classical SRM/MRM acquisition is normally performed on a triple quadrupole analyser with Q1 and Q3 at unit mass resolution [192]. That means, selection of the specific precursor ions in Q1, fragmentation in the collision cell (q2) and selection of one or mostly two specific fragment ions in Q3 (see Figure 26) [156]. The fragment ions are already selected as most abundant fragment ions during method development. Therefore, at least one in most cases two transitions are programmed within SRM/MRM acquisition. The second fragment ion is mostly used as qualifier of the analysis based on the comparison of the ratio of both fragments [194]. During the MRM acquisition only one precursor ion is selected at a time with a narrow m/z (unit mass) providing high selectivity. Even, if a second

precursor ion is selected in the same unit mass window due to similar masses, the fragments do not interfere with the other fragments from the first precursor as long as they are not the same. Nevertheless, selection of another fragment for one of both precursor ions detected in the same window can avoid misleading quantification [192]. Nevertheless, this is always based on loss of sensitivity as this fragment is no longer the most abundant fragment [192]. Therefore, the MRM acquisition is limited in the number of selected precursor ions due to the needed time for switching between different masses, cycle time, settling time (equilibration of the electronics after switching to new parameter settings) and width of the chromatographic peak [191,192].

Additionally, during method development of MRM methods, standards of the targeted analytes are necessary for optimization of the chromatographic separation, the collision energy (CoE), the declustering potential (DP) [156] and to select at least the two most abundant fragment masses [156,195]. Standards are used to find the optimal analytical conditions for the selected analyte without the influence of analytes with similar masses or properties. Furthermore, the sensitivity can be increased by optimized DP and CoE. DP is a voltage applied to the orifice which ensures that clusters of target ions are dissociated and the target enter the ion path as single monomeric gas-phase ions. The voltage supports the desolvation process up to free analyte ions and controls the acceleration of the ions into the orifice. On the way, the ions collide with the residual gas molecules, reducing undesired adducts or solvent clusters. However, if the voltage is too high, a so-called in-source decay may occur, especially for labile compounds, and the precursor ion yield is reduced. The fragmentation process is controlled by the CoE. By selecting the optimal CoE, the specific fragment masses of an analyte are generated as the highest abundant fragment masses. The selection of two high abundant fragments enables a precise assignment of the precursor to the fragments or identification of the analyte. At the same time, the bottleneck of method development in MRM, as in many cases, is the unavailability of the cost intensive standards of the desired analytes [156,161].

MRM acquisition can be further improved by including the retention time in so-called scheduled MRM acquisition [192]. In scheduled MRM acquisition the selection of a specific precursor mass is only performed within the corresponding retention time window [192]. In the next retention time window, the next precursor is selected and so on, resulting in increased collection time of certain precursor ions and therefore, better MS and MS/MS data, which are used for quantification. Another modified MRM like acquisition is called

parallel reaction monitoring (PRM) and is mostly used in combination with trapping (e.g. orbitrap) or time-of-flight (TOF) instruments [191]. In PRM acquisition, precursor ions are selected in unit mass windows in Q1, fragmented in high-energy collisional dissociation (HCD) / collision-induced dissociation (CID) and afterwards all existing fragments are detected [191] resulting in a powerful tool for targeted analysis [191]. Screening a variety of fragments can increase the selectivity and response due to the unpredictable intensity of any fragment within one analysis and existence of potential interferences [192]. Therefore, MRM analysis is often used for amino acid analysis, as one of the most important building blocks for further metabolites, like enzymes, proteins and nucleic acids [149].

1.5.2. Amino acids as biomarkers

Various studies suggested that amino acids can potentially be used as indicators of cancer. Therefore, the metabolic profiling of amino acids is becoming more and more interesting. Amino acids have important roles in human organisms, for example as building blocks for all proteins [196]. Additionally, amino acids are involved in neurotransmission, energy metabolism and detoxification [196,197] (Figure 27).

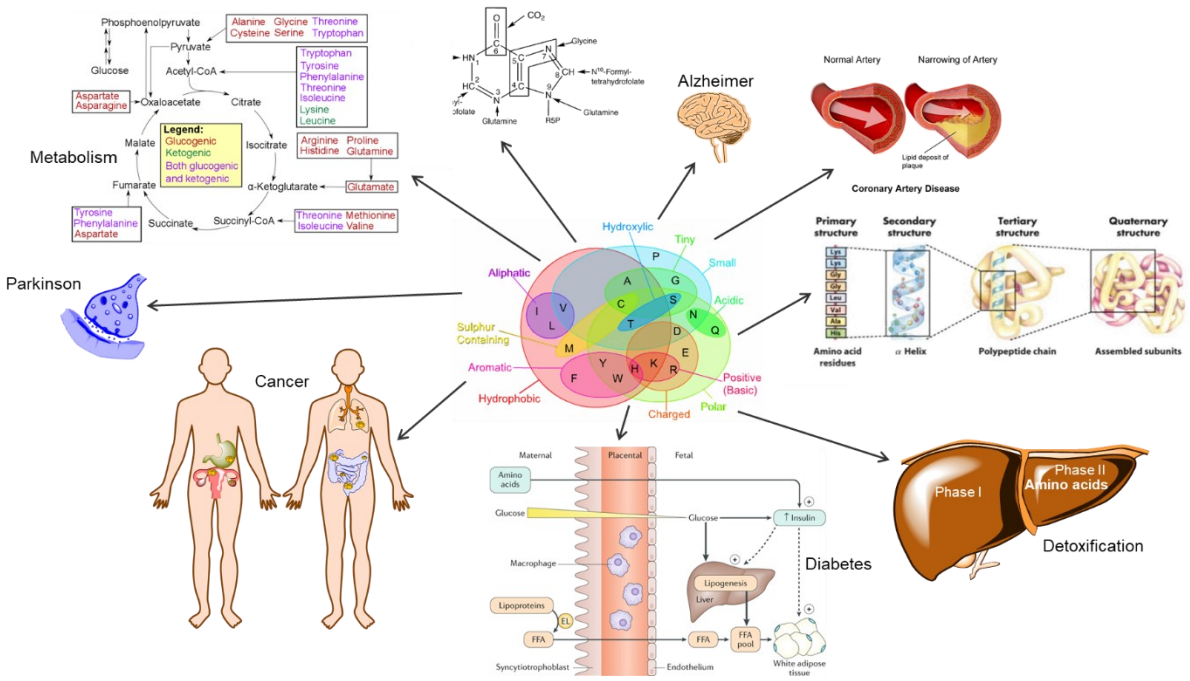

Figure 27: Amino acid applications: Amino acids are part of various metabolic pathways (energy metabolism) [198], are involved in detoxification processes and serve as building blocks for example for proteins [199,200] and purines [201]. The absence or excess of different amino acids trigger a huge number of diseases: i) cancer [202,203], ii) neurotransmission (Parkinson), iii) diabetes [204,205] and vi) coronary artery disease [206]. Reprinted with permission from the corresponding authors

Since 1996, the concentrations of amino acids have been analysed to detect inborn defects in the metabolism and was one of the milestones in diagnostics at the time [196]. Glutamine alone accounts for 20% of the total amino acid content. Glutamine is mainly involved in energy metabolism and maintains the nitrogen balance in the body [196,197]. Defects in the synthesis pathway for non-essential amino acids usually trigger defects in the central nervous system [196]. For example, HeLa cells need 13 amino acids for survival and growth (Figure 28).

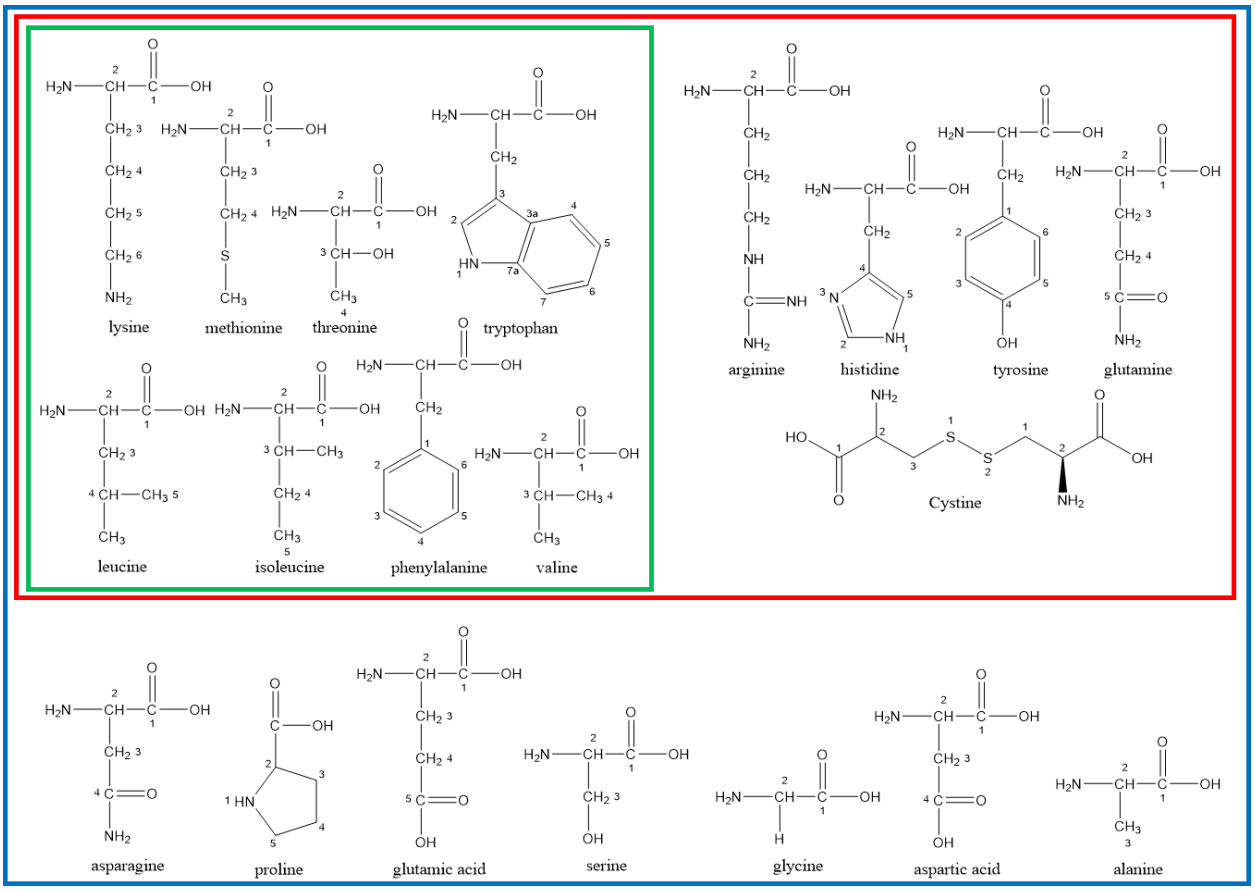

Figure 28: Amino acids: The green rectangle contains all 8 essential amino acids, which are needed for the nitrogen balance [207]; the red rectangle shows the 13 amino acids necessary for growth and survival of HeLa cells [208] and the blue rectangle contains all "natural" occurring amino acids of an organism

Absence of cystine, arginine (Arg), glutamine, histidine (His), isoleucine, leucine, lysine (Lys), methionine (Met), phenylalanine, threonine, tyrosine or valine resulted in the death of the cell [208]. The absence of only one amino acid at a time resulted in death after a couple of days, but if they lack a couple of amino acids at the same time, the cells started to grow as much as 2-3-fold for 6-13 days before they started to die [208]. One of these amino acids is tryptophan. Some differences were shown in malignant cells compared to healthy cells, for cystine, glutamine, isoleucine, lysine, phenylalanine and valine [208]. Cells need the amino acids to build the non-essential amino acids, purines and pyrimidines together with

glucose. Therefore, huge amounts of glutamine were required [208]. The addition of non-essential amino acids did not change the cell's need for these amino acids, but had a glutamine saving effect [208]. Nevertheless, glutamine remains an essential amino acid. However, an extremely high concentration of glutamic acid (Glu) can compensate for the glutamine deficit [208]. Normally only eight amino acids are considered essential [208] (Figure 28, green rectangle). However, Eagle *et al.* claimed that there are 13 essential amino acids instead of eight, which could be due to the fact that the cells have altered during proliferation [208]. Alternatively, these five additional amino acids are only important for tissue cells because they grow particularly fast [208].

Most researchers, like Maeda *et al.*, Miyagi *et al.*, Kim *et al.*, Leichtle *et al.*, Stover and MacFarlane, Qiu *et al.*, Budczies *et al.*, Gu *et al.* and Shingyoji *et al.* [209–217] claim that amino acids should be analysed as potential markers for cancer [149]. Based on the still increasing number of new cases of cancer every year, the demand for a new and fast method of analysis for amino acids is rising. The method should be as specific and sensitive as possible. The first studies already showed differences in amino acid concentrations between healthy and cancer patients [209]. Since malignant cells multiply much faster, they need higher concentrations of amino acids to form nucleic acids and proteins. Serine (Ser) and Glycine, for example, play an important role in folic acid metabolism [149,218]. Alanine could also be used as a biomarker for breast cancer, where studies have already shown that alanine increases the proliferation of breast cancer cells [149,216]. Significant changes in the amino acid profile could already detect cancer, although the usual markers that are currently used to diagnose cancer were still at a normal level [149]. Thus, cancer could be detected earlier based on the analysis of amino acid concentration. Furthermore, it was found that certain amino acids are specifically linked to a specific type of cancer, which enables detection of the species at an early stage [149]. This in turn leads to a very early therapy specially adapted to the type of cancer and hopefully also to better chances of recovery for the respective patient.

As described above MRM acquisition is the golden standard in targeted analysis, nevertheless, the low metabolite coverage, time and cost intensive method development and the need of analysing also unknown metabolites fast, limits this acquisition type. Therefore, further development regarding selection of higher numbers of precursors without a lot of method development and knowledge is highly driven resulting in “pseudo”-targeted and untargeted analysis by using data-dependent and data-independent acquisition [192].

1.6. Untargeted metabolomics

The need for a measurement method for hypothesis generation, such as untargeted metabolomics, has increased enormously in recent years [140], since targeted metabolomics relates to the verification of already existing hypotheses only. Especially in the medical field, the interest in developing untargeted methods is increasing, for example, when it comes to the research of unknown diseases, finding biomarkers and developing personalized drugs to prevent certain diseases [127,138,150,154]. Necessarily, untargeted methods based on targeted methods have been developed. So-called "pseudo"-targeted methods represent an intermediate stage [129,161,191]. Compared to targeted approaches, “pseudo”-targeted metabolomics is no longer limited to known metabolites [129,219]. For example, all metabolite ion pairs are detected by means of a quadrupole-time-of-flight (QTOF) mass spectrometer in full scan mode. Afterwards, the obtained MS/MS spectra are used to extract precursor ions and associated fragments for a targeted analysis using a triple quadrupole [129]. Therefore, “pseudo”-targeted metabolomics is the pre-stage to untargeted metabolomics. The higher sensitivity, good linearity and good data quality, characteristics of targeted metabolomics, is preserved [129]. Only the scan speed limits the number of spectra that can be acquired [156]. Therefore, the further development and technical improvements of the mass spectrometers enabled untargeted metabolomics [156]. The most popular combination in untargeted metabolomics is LC hyphenated with high resolution (HR) mass analysers [140]. The complex samples, containing metabolites with a variety of different structures and properties, especially if the global metabolome is analysed, require mass analysers with the highest resolution [154]. Therefore, untargeted metabolomics is mostly applied on QTOF instruments or orbitraps. A QTOF mass analyser has a high mass resolution (30 000-60 000), accuracy (< 5 ppm) and fast scan speed (50-100 Hz) [128]. Talking about untargeted metabolomics usually means an analysis in full scan mode between 50-1000amu [154]. Additionally, untargeted metabolomics can be divided in two sub-classes: i) data-dependent and ii) data-independent acquisition. Data-dependent acquisition screens the entire mass range during a full scan and afterwards the most abundant precursor masses are fragmented. In comparison, data-independent acquisition first prepares also a full scan and afterwards fragments any precursor mass included in the sample, regardless of the concentration [148,220]. In most cases, an untargeted metabolomics approach is used to discover new biomarkers. This leads to potential hypotheses and first metabolites may be identified. Even though an unknown metabolite is

identified, a targeted method including the newly identified metabolite as standard is needed for confirmation [154]. In general, the identification of the metabolites is done via MS^1 or MS/MS spectra [156]. The high-class specific diversity requires mass analysers in both modes, positive and negative mode [161]. However, the biological interpretation remains difficult and can only be achieved in combination with other "omics" technologies, such as genomics, transcriptomics, etc. In combination, significant changes in pathways and biomolecular mechanisms can be detected [128]. Nevertheless, the entire metabolome can still not be completely detected with only one sample preparation method and one type of analysis used [154,155].

More and more samples have to be analysed in a shorter time, which makes a fast acquisition technique essential [221]. A high resolution mass spectrometer (HR-MS), such as an Orbitrap, provides high quality measurements by reducing the interference of noise and co-eluting substances [129]. Metabolic fingerprinting is performed, for example, with the mass analyser in full scan [127]. The most important factors for choosing the right mass analyser are coverage, selectivity, dynamic range, detection limits, accuracy and precision [155]. Usually triple quadrupoles or QTOFs are used as mass analysers [140], because they are characterized by high mass accuracy (less than 5 ppm), excellent sensitivity and high resolution [126,154]. The resolving power of a QTOF is independent of the acquisition speed and a fixed value and good results can be achieved even with an acquisition speed at the lower end, like 10msec [192].

1.6.1. TripleTOF

LC-MS/MS is nowadays irreplaceable in the field of metabolomics. Throughout this work a QTOF from Sciex coupled to a U(H)PLC was used. A QTOF always consists of at least two quadrupoles and a TOF analyser at the end (Figure 29) [222].

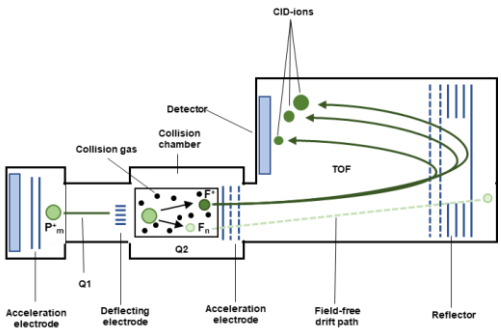

Figure 29: QTOF mass analyser: Scheme of a reflector quadrupole time-of-flight mass analyser with first quadrupole (Q1) as mass filter, second quadrupole (Q2) as collision cell and the time-of-flight mass (TOF) analyser for scanning and detecting the fragments

In addition, each mass spectrometer has an ion source in which ionisation takes place and, if necessary, further quadrupoles for ion transport. Mass analysers coupled to an LC usually use soft ionization, for example atmospheric pressure chemical ionisation (APCI), which is contained of a corona discharge needle, transferring the liquid stream into a plasma and afterwards into ions. For polar compounds, ESI is the most common ionization principle, which converts the liquid stream into gas phase ions due to a spray [193,223,224]. The latter was used during the present work. Both types of ionization take place at atmospheric pressure. The resulting ion stream passes through the orifice, a transfer capillary and sometimes various numbers of quadrupoles used as ion guides into the Q1. A quadrupole is composed of four cylindrical or hyperbolically shaped metal rods, to which on an alternating basis alternating current (AC) and direct current (DC) voltage is applied (Figure 30) [193,225].

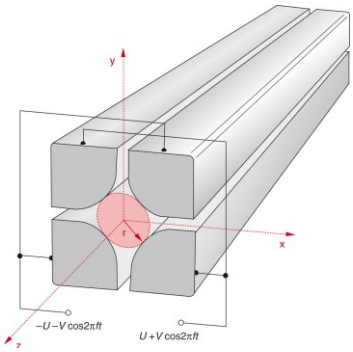

Figure 30: Quadrupole: Shape of the metal rods (electrodes) and their arrangement in a quadrupole mass filter. Reprinted with permission from Springer publisher [225]

The opposite metal rods are connected in the same way. That means one pair has an attracting effect and the other a repelling effect [225]. These opposing forces effect each type of ion differently. A periodic voltage is applied to the rods, resulting in alternating attraction and repulsion forces in the x and y directions [193]. The applied voltages focus the ions with defined m/z on stable oscillating paths. All other ions move on unstable orbits and are discharged by collision with the metal rods [225]. The electric field along the asymptotes is zero. It is therefore possible for ions with a certain m/z ratio to pass through the quadrupole without colliding with electrodes. It is necessary that the movement in z-direction is stable with a limited amplitude in x- and y-direction. Such conditions can be derived using the Mathieu equations (Figure 31) [193].

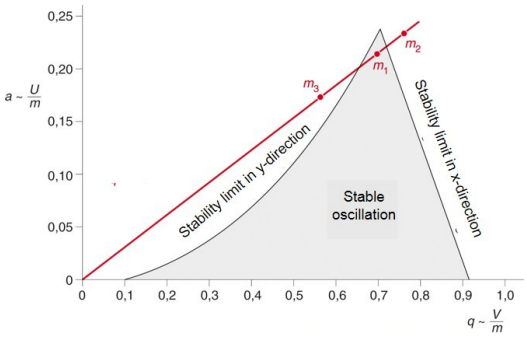

$$\frac{d^2x}{d\tau^2} + (a_x + 2q_x \cos 2\tau)x = 0$$

$$\frac{d^2y}{d\tau^2} + (a_y + 2q_y \cos 2\tau)y = 0$$

$$a_x = -a_y = \frac{4eU}{m_i {r_0}^2 \omega^2}, \quad q_x = -q_y = \frac{2eV}{m_i {r_0}^2 \omega^2}, \quad \tau = \frac{\omega t}{2}$$

Figure 31: Mathieu equations: On the right side, the Mathieu equations are shown and on the left side of the picture the corresponding stability diagram for the two-dimensional quadrupole field in x and y direction is shown. Adapted with permission from Springer publisher [225]

The Mathieu equations can be solved in two different ways: One solution leads to finite oscillation amplitudes, which results in a stable motion through the quadrupole. Another solution leads to increasing amplitudes in x or y direction [207]. When scanning the mass range, the DC voltage and the amplitude of the alternating field are simultaneously increased, which results in sequentially entering of the ions into the stable range [193,225] (Figure 32).

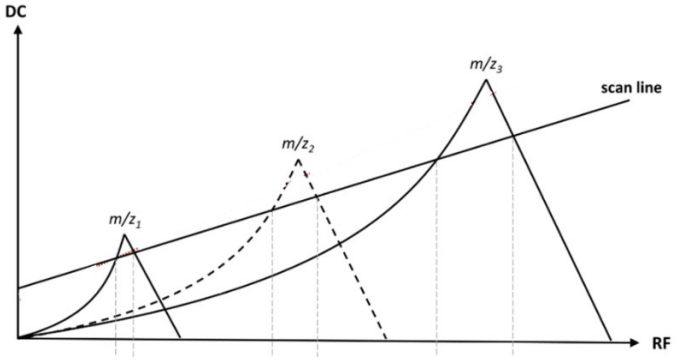

Figure 32: Stability diagram of a quadrupole: During the scan of a certain mass range, the DC voltage and the amplitude of the alternating field are simultaneously increased. As a result, different ions will enter stepwise the stable range. Adapted with permission from B. Drotleff [222]

Therefore, the step size and the measurement time of each step is very important during scanning, because the step size influences the accuracy and the measuring time determines the sensitivity [225]. When only a small m/z range remains stable, the sufficient resolution is reached [193]. With MRM acquisition, on the other hand, the Q1 already acts selectively and filters out masses in the quadrupole in a targeted manner, whereby a higher sensitivity can be achieved. Often also described as Single Ion Monitoring (SIM) [225]. A quadrupole can reach a mass range up to m/z of 2000, but in general is mostly only used as a mass filter. However, the quadrupole provides high transmission, low ion acceleration voltage and a high possible sampling rate [193]. In the second quadrupole (q2), on the other hand, voltages are specifically applied to produce fragments. This voltage is called collision energy

and can be significantly different for different analytes, which further complicates the analysis of the entire metabolic profile in one analysis. To determine the optimal CoE settings, a mixture of the analytes is injected by direct infusion into the mass analyser and the different CoE in the range between 0eV and 50eV are applied stepwise to generate product ion spectra [192]. The fragments are then analysed in the TOF mass analyser for mass accuracy below 5 ppm.

The first TOF mass analyser was designed by W. E. Stephens in 1946 [193]. Initially in the middle of the 50ies, the first TOF-analysers were developed from the company Bendix in combination with gas chromatography instruments, but were shortly replaced by linear quadrupole analysers [193]. 30-years later, TOF analysers started to boom again, after the development of pulsed ionization in form of matrix assisted laser desorption ionization (MALDI), which is essential for TOF analysers [193]. Later on, the development of orthogonal ion extraction enabled the coupling of TOF analysers with an ESI source (Figure 8) [225]. Before the ion beam, which is continuously released from the collision cell enters the TOF analyser, an orthogonally oriented pulsed electric field, in so-called ion bunches, is applied (Figure 33) [193]. The most important benefits of a TOF analyser are thereby, resolution up to 60 000 [225], the ability to separate ions with small mass differences and the mass accuracy, which describes the accurateness of the determination of an ion mass.

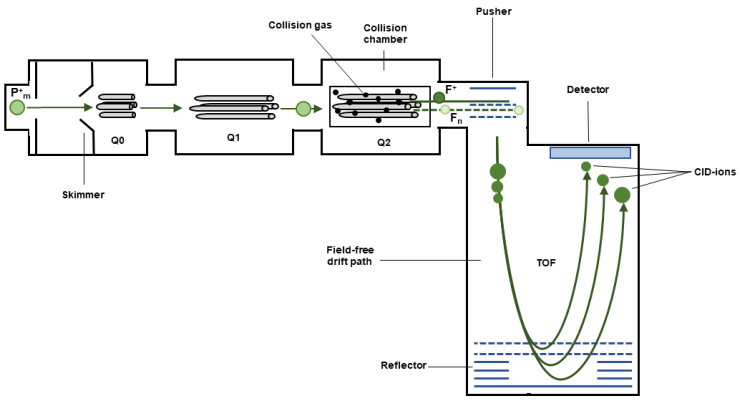

Figure 33: Orthogonal quadrupole time-of-flight mass analyser: Theoretical structure of a quadrupole time-of-flight mass spectrometer. Precursor ions of a defined m/z ratio are filtered in Q1, fragmented in Q2 and the fragment ions are afterwards analysed and detected in the reflector-TOF analyser, which is arranged orthogonal to the quadrupoles

The time, which is needed by the ion to reach the detector, starting from the source, is essential. This is electronically measured as the time of flight [225]. Therefore, a kinetic energy of a few kilo electron volts (keV) is applied to the ions within an electrostatic field in the accelerator (pusher), causing an acceleration of the ions in the direction of the TOF

analyser. The ions are separated based on their m/z ratio after they are released from the pusher and enter the field-free drift path of defined length [225]. During the drift path from the electrodes to the detector, ions with different m/z ratios will be exited to different velocities containing the same kinetic energy. This means, heavier ions enter the detector later, although they started at the same time as the lighter ions (Figure 34) [225].

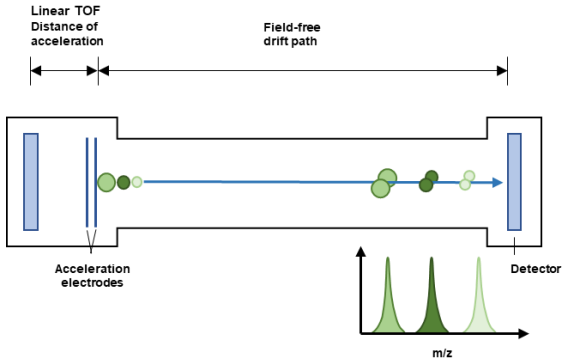

Figure 34: Linear TOF-analyser: Scheme of a linear time-of-flight mass spectrometer. The ions with different m/z values, but same charge have different speeds. Lighter ions with low m/z values reach the detector earlier than heavy ions

The m/z ratio of an ion is determined by measuring the flight time at a defined acceleration voltage and trajectory. For calibration, reference standards are used [225]. However, after passing through the accelerator zone, not all ions with the same m/z value also have the same kinetic energy [225], resulting in different times the detector is reached, even if ions from the same type have the same starting point. Therefore, in 1994, Mamyrin further developed the TOF analyser to the so-called reflector (Figure 35) [193,226].

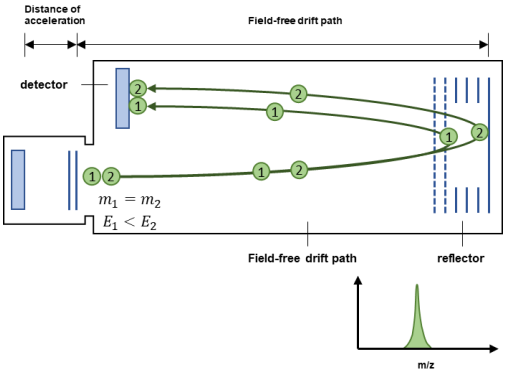

Figure 35: Reflector-TOF analyser: Scheme of a reflector time-of-flight mass spectrometer. The ions with different m/z values, same charge but different speeds are decelerated due to an electric field. Heavier ions with higher m/z values enter further into the reflector and stay there longer than lighter ions, before they are accelerated in the opposite direction

The reflector can be considered as a mirror that focuses ions with different kinetic energies. The reason for this is a decelerating electric field, which is part of the reflector and is located opposite the ion source, behind the field-free drift region [193]. A series of ring-shaped electrodes with increasing electrode potential generate the decelerating electric field. The

ions enter the reflector until they lose their kinetic energy. This means that ions with higher kinetic energy enter further into the decelerating field and stay longer in the reflector before they are accelerated in the opposite direction [193]. This adjusts the time-of-flight of each ion accordingly, which significantly improves the resolving power (Figure 35). However, due to their altered kinetic energy, ions will be lost, if metastable fragmentation occurs (Figure 36) [193].

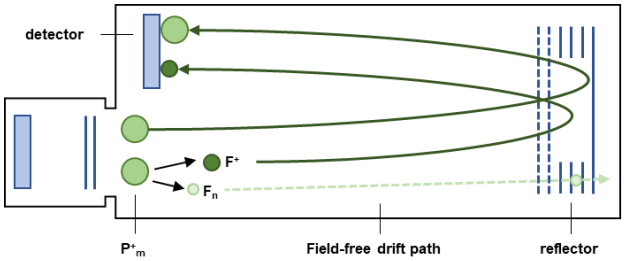

Figure 36: Reflector-TOF analyser: Scheme of metastable fragmentation of instable molecule ions (P_m^+) resulting in a charged fragment (F^+) and a neutral fragment (F_n). The neutral fragment is due to the lack of charge not reflected by the reflector and therefore not detected and lost

The risk of such collisions can be lowered by applying a higher vacuum, which increases the mean free path length of the ions. The advantages of a TOF are unlimited m/z range, very fast measurement, high sensitivity, exact mass determination and the possibility of tandem MS analysis [193]. Nevertheless, all benefits of a TOF analyser are always dependent from the ionization source, in the case of the projects performed during the dissertation, the ESI source was used.

1.6.2. Electrospray Ionisation (ESI)

In most cases, liquid chromatography is connected to a mass analyser via an electrospray interface [127,128,227]. The electrospray interface is a soft ionization [193,223,224]. ESI is ideally used for the analysis of large, non-volatile and easily charge-accepting molecules such as proteins or nucleic acids [193,228–231], but is also often used for the analysis of small, polar molecules in the m/z 50-1500 range, e.g. in metabolomics [127,128,227]. The principles behind ESI ionization were already described by Zeleny in 1917 [232] and by Taylor in 1964 [193,233]. At that time, however, it was not possible to detect ionized molecules by ESI with any mass analyser because ionization takes place at atmospheric pressure and a high vacuum dominates in the mass spectrometer, causing the freeze out of ions when passing from atmospheric pressure to high vacuum [193]. Due to research work by Fenn *et al.* at the end of the 1980s molecules with a molecular weight of up to 2000 u could be analysed by ESI ionization and a quadrupole [234–236]. This was possible by a

special designed interface, with which Fenn *et al.* revolutionized ESI ionization coupled to mass spectrometers (Figure 37) [234,236–238].

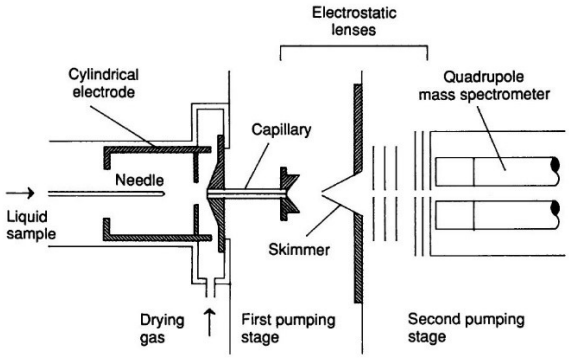

Figure 37: ESI-source interface: Scheme of the ESI-source interface with the spray capillary (Needle in the graphic), the capillary, which bridges the spray chamber under atmospheric pressure and the first pumping stage of the high vacuum and the skimmer. Reprinted with permission from Fenn *et al.* [234]

A sufficient energy supply was the major factor. The energy is introduced either via a counter gas flow, often called curtain gas, or via a heated capillary [193]. In contrast to electron impact ionization, mostly used in combination with gas chromatography, the ESI interface coupled to an MS can only be used to analyse molecules that already carry a charge in mobile phases due to corresponding pH values or additives [193]. An ESI interface consists of a spray capillary, a capillary and a skimmer [225]. After chromatographic separation, the molecules are transferred to the spray capillary in a continuous flow. Between the spray capillary and the orifice of the mass spectrometer a potential of about 3-4 kV is applied [193]. As a result, the continuous liquid flow is exposed to an electric field at the capillary tip, which leads to charge separation within the flow and a deformation towards the cone, the so-called Taylor cone (Figure 38 and Figure 37) [193,233].

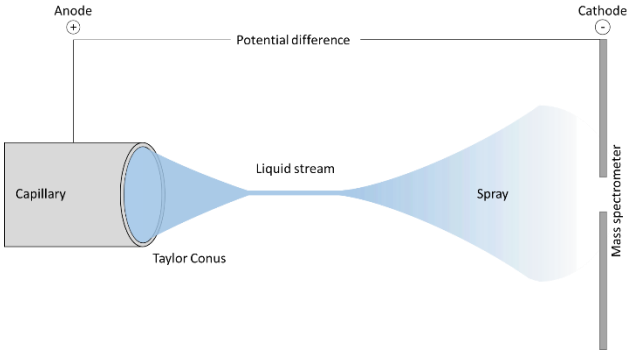

Figure 38: ESI-source: Principle of the formation of the Taylor cone followed by a fine aerosol spray contained of small droplets

Once the surface tension of the cone is exceeded, a fine stream flows from its tip to the counter electrode (orifice) [239]. The highest charge density is located at the tip of the cone, i.e. either almost exclusively positive ions or negative ions [193,240]. The oppositely charged

ions are neutralized by electrons resulting from the oxidation of anions (positive mode) or reduction of cations (negative mode) [193,241]. Nevertheless, this stream is not very stable and disperses into many small droplets (spray) (Figure 39) [193,242].

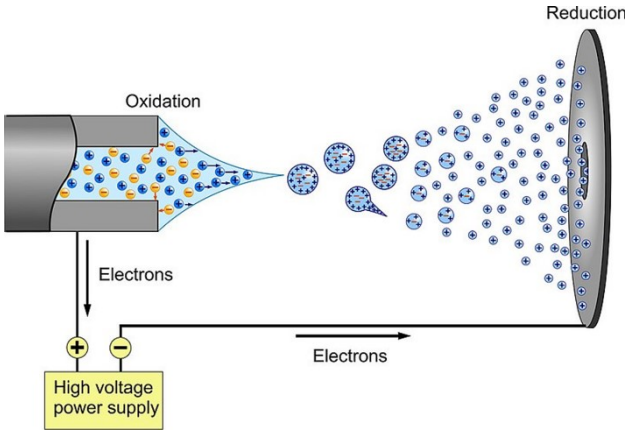

Figure 39: ESI process: Formation of the Taylor cone, followed by the fine aerosol spray, the desolvation of the droplets and the release of desolvated ions. Reprinted with permission from A. Dahlin [243]

Today this process is supported by the so-called nebulizer gas, which flows along the outside of the spray capillary [193,244,245]. The counter-heated gas flow, usually nitrogen, provides the evaporation of the solvent that surrounds the molecules [193,246]. This ensures that uncharged molecules and impurities do not enter the orifice and that the small droplets of the spray continue to shrink, while the charge density at the surface continues to increase [193]. At a certain point the electrostatic repulsion exceeds the surface tension, called Rayleigh limit [247], and the droplet disperses. This process is repeated over and over again until a single desolvated and charged ion is present (Figure 40) [193].

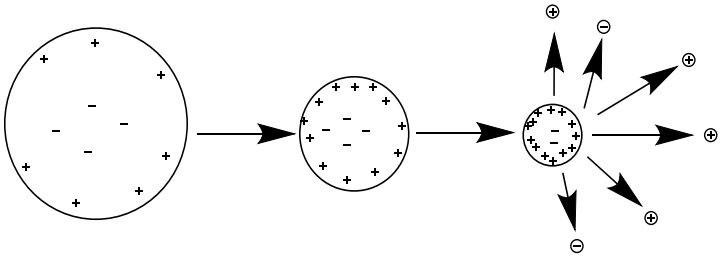

Figure 40: Coulomb explosion: The size of the charged droplet of the aerosol spray is continuously decreased due to evaporation of the surrounding liquid, while the charge density is increased until the Rayleigh limit is reached and the droplet is dispersed

Initially it was assumed that the droplets would burst due to the Coulomb explosion (repulsion of identical charges) [193]. Recently, however, we know that the droplets do not explode but deform into ellipses, releasing many small droplets at the conical end, similar to the Taylor cone, called “Droplet Jet Fission” [193,248–250].

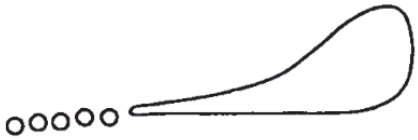

Figure 41: Droplet Jet Fission: Scheme of the dispersion of a droplet after the Rayleigh limit is reached. Adapted with permission from Gross *et al.* [193]

These small droplets shrink until gas phase ions are obtained which then pass through the orifice into a heated capillary that forms a connection between the spray chamber at atmospheric pressure and the first pumping stage of the high vacuum (10^2 Pa). The ions then pass through the skimmer into the high vacuum range of the mass spectrometer (10^{-3} – 10^{-4} Pa) [193]. However, there are other models described for ionization, such as the charged-residue model, which postulates that the droplets successively lose solvent molecules until only one analyte molecule is left [193,251,252]. A further model is the so-called ion evaporation [193,253,254], in which desolvated ions are produced by direct evaporation from the surface of the droplets [193,255]. However, the exact mechanism of ionization by means of an ESI interface has not yet been fully determined [193]. In general, ESI ionization can produce ions, solvent adducts, ion clusters and multiple charged ions. Nowadays the linear arrangement of the spray capillary has been replaced by an orthogonal arrangement [193]. This leads to less contamination and allows a wide opening of the orifice, resulting in a higher robustness and sensitivity of the mass spectrometer [256]. In addition, ESI can be used for analysis over a relatively wide range, from small to higher molecular masses and from almost non-polar to ionic analytes [193].

1.6.3. Data dependent acquisition (DDA)

Data-dependent acquisition (DDA) can be applied in combination with trapping mass analysers and with analysers using a collision cell, like quadrupoles, QTOF and Orbitrap [192]. DDA workflow is similar to MRM acquisition [257]. Compared to MRM, during DDA continuously survey scans followed by target precursor ion selection and fragmentation are performed [192] (Figure 42). The selection of the precursor is therefore performed during the acquisition and not before the acquisition by the operator.

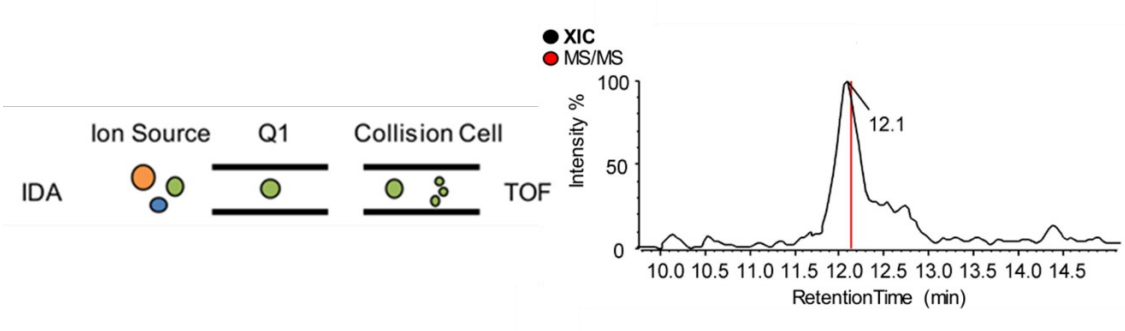

Figure 42: Data-dependent workflow: One of the main used data-dependent acquisition workflows was the information-dependent-acquisition, called IDA (synonymous to DDA). The IDA acquisition performs a survey scan in Q1 and if the masses reach the pre-defined threshold (right side of the figure), they are selected and fragmented in the collision cell. Adapted with permission from J. Schlotterbeck [258]

During DDA workflow, the precursors are selected only if they reach a certain predefined threshold [257]. The selection based on a threshold is only one possibility, as it can be also based on isotope pattern (characteristic intensity pattern of the masses of different isotopes of a molecule [259]), mass defect (difference between exact mass and nominal mass of a molecule [260]), presence of diagnostic ion and based on characteristic neutral loss within MS^2 spectra [257]. Afterwards, the mass spectrometer switches to MS/MS mode for fragmentation [257]. That means the precursor is selected as soon as for example the threshold is reached, which is in most cases not the inflection point of the peak, causing low quality MS spectra [192]. Therefore, the survey scan is repeated during one analytical run to overcome the possible loss of precursor ions, but leads to limited numbers of collected precursor ions [192]. Precursor ions are only selected if they pass the criteria [257]. Therefore, it might be that other interesting precursor ions are not selected, because they coelute with high abundant compounds [257]. Additionally, the selection of precursor ions is not very reproducible, as the signal intensity changes even if the same sample is reinjected [257]. Some DDA approaches using dynamic exclusion, listing all m/z masses which are already occurred during the analysis, preventing the reselection of the same precursor ion [221]. Therefore, in theory only one spectrum is acquired for each selected precursor ion [221], but practically all coeluting additional ions are acquired beside the targeted fragment, resulting in crowded MS^2 spectra, difficult to evaluate [221,257]. Additionally, the noisy MS^2 spectra prevent the identification of the many unknown metabolites by library search [257]. Nevertheless, DDA is used for quantification based on precursor MS^1 spectra [192] in the field of metabolomics, but not as wide spread applied as in proteomics [257]. Therefore, data-independent acquisition workflows are developed and gained fast attraction in the field of metabolomics, as fragments for all precursor ions can be

detected simultaneously to the precursor ions itself [257] and the quantification is performed using either MS^1 or MS^2 spectra [192].

1.6.4. Data independent acquisition (DIA)

The improvements of the mass analyser technique led to the hyphenation with data-independent acquisition (DIA) modes, benefiting acquired data which is not controlled by the acquisition. This is of utmost importance, especially for the analysis of small molecules [192]. In metabolic fingerprinting, the main problems are to analyse a wide range of different metabolites, with different characteristics in a broad concentration range within one analytical run. Therefore, it is necessary to develop a fast analysis technique to detect as many metabolites as possible in one analysis. The rising interest in identifying and, in the best case, quantifying global metabolome, drastically increases the need for MS/MS analysis using DIA [221]. All DIA techniques cover the certain mass range through repeated stepwise analysis of smaller mass ranges within the entire mass range. Additionally, all detected precursor ions are fragmented [192]. As a result, all fragments of each precursor are detected [221] and contained in composite spectra [192] to obtain further information about the metabolite, but at the expense of selectivity and sensitivity [221]. Either IT or TOF mass analyser [192] are used for DIA. Considering, that the number of trapped ions (trapping time), precursor as well as fragments are the limiting factor for sufficient resolution and mass accuracy, the IT analysers are not very suitable for metabolic fingerprinting [192].

In most cases the selection of the precursor ion is performed by a quadrupole, as they are able to switch the selected masses fast, including good transmissions [192]. Therefore, one of the favorite used mass analysers is the quadrupole combined with time-of-flight mass analyser. Optimally, the product ions are selected by stepping along 1 Da units and at every step a product ion is selected. But the acquisition covering a mass range of 1000 Da would take 20 msec per step, resulting in 20 seconds total cycle time, which is not feasible using liquid-chromatography, as the peaks are to narrow [192]. To overcome the problematic of peak width a better option is setting the first quadrupole to RF mode, which means that every precursor ion mass is transferred to the collision cell without any selection. In the collision cell two different collision energies are applied in this acquisition model. One energy in the lower range for detection of the precursor mass and one in the upper range for fragmentation [192]. This kind of acquisition mode which skips the precursor selection is called MS Everything (MS^E) or MS All (MS^{ALL}) and is per definition no MS^2 acquisition method [192] (Figure 43).

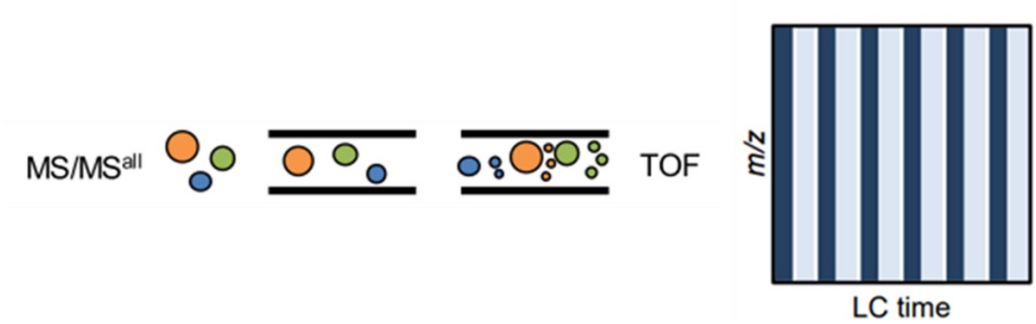

Figure 43: Data-independent acquisition MS^E/MS^{ALL}: MS^E/MS^{ALL} acquisition detects all precursor masses, which enter the quadrupole within the entire chromatographic analysis. Adapted with permission from J. Schlotterbeck and Raetz *et al.* [258,261]

Nevertheless, MS^E was the first applied DIA method in metabolomics analysis [257] and steps alternately through high and low fragmentation settings [192]. Therefore, a very good separation of the analytes by previous chromatography is extremely important to be able to assign the corresponding fragments to the precursor. Additionally, a method described as MS/MS^{ALL} is used for analysing lipids with flow injection [192].

In 2012, the vendor Sciex developed a special acquisition technique called sequential window acquisition of all theoretical fragment-ion spectra (SWATH) [221] which was described for the first time by Gillet *et al.* [220]. SWATH was established by Venable *et al.* [220] first only for proteomics to acquire all peptides contained in the sample within one analytical run but over the years it has gained a strong interest in the analysis of drug metabolism and small analytes. It is related to MS^{ALL} and MS^E, but has several benefits [221]. SWATH is a data-independent acquisition technique and consists of different Q1 precursor isolation windows with a fixed size, mostly of 25 Da [220,221]. Every window overlaps at least with 1 Da [258]. That means for example window one ranges from 50 to 75 Da and window two starts with 74 to 100 Da. First of all, during the analytical run, a survey scan is performed following the screening of the different windows [221]. Within these windows every precursor with a mass corresponding to the 25 Da range is detected and further fragmented in the collision cell. After fragmentation all created fragments are detected [221]. The Q1 is therefore used as mass filter in the fixed window width mass range [192] (Figure 44). All programmed windows are screened within one cycle, limited by the cycle time and the cycles are repeated several times within the retention time frame.

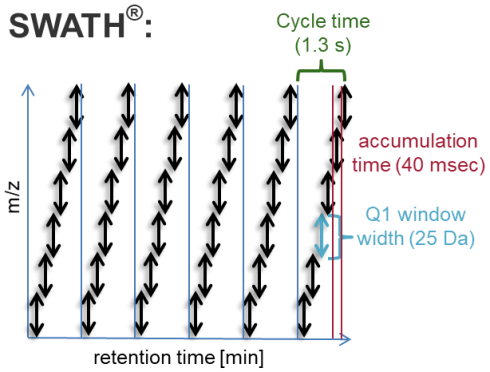

Figure 44: SWATH acquisition: Scheme of SWATH acquisition mode with fixed Q1 window width of 25 Da, scanning the complete mass range divided in packages (windows) over the entire retention time

The advantage is that fragments can be helpful in analysing the structure of a metabolite and works additionally as further criteria during library search [192]. In addition, data of a particular compound class can be evaluated and even years later data of another compound class can be evaluated without further knowledge, the need of a new sample and reanalysis. Nevertheless, the assignment of the fragments to the precursors is often difficult, because with SWATH acquisition all precursor ions are detected in the corresponding window. Simultaneously, the fragments are also acquired in the same windows [221]. Therefore, the relationship of precursor and fragment is missing [192]. If the windows are relatively large, it is even more difficult to link precursors with corresponding fragments during data evaluation [192], especially if there are precursors with similar masses and similar fragments. Therefore, SWATH was further developed to the next generation, called SWATH 2.0 acquisition using windows with variable width [192] (Figure 45).

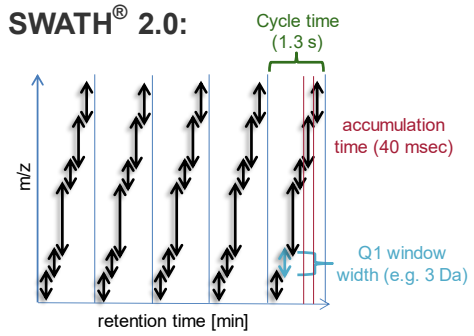

Figure 45: SWATH 2.0 acquisition: Scheme of SWATH 2.0 acquisition with variable Q1 window width, which enables the combination of targeted analysis by programming narrow windows of for example 3 Da and untargeted analysis by setting bigger windows

That enables the combination of targeted and untargeted analysis, by setting the window sizes as small as possible in the mass range of the targeted analytes and keeping the windows in the remaining mass range wide [221]. In these narrow windows, it is also possible to optimize parameters such as CoE and DP to achieve the highest possible

sensitivity. Thus, SWATH 2.0 acquisition with variable window width offers the flexibility to detect interesting target metabolites and all other metabolites within a sample and one analysis [221].

In general, SWATH acquisition was developed as quantification method, as data is acquired over the whole peak which enables the possibility to use also the fragment for quantification [221], increasing in some cases the specificity. However, it can be used as qualitative acquisition method as well. The only problem of qualitative analysis using SWATH is the missing relationship of the precursor and fragment ion [192]. Correlation of chromatographic peaks during data evaluation, like in MS^E, can overcome this problem, as long as there are not many precursor ions, coeluting compounds with similar masses and good peak shapes [192].

Additionally, MS^3 analysis can be performed using SWATH acquisition and precursor ions which are fragmented already in the source before the first mass selection occurs [192]. Therefore, the fragment is selected in the corresponding SWATH window instead of the precursor, is fragmented in the collision cell to further fragments and all are detected [192]. Generally speaking, the analysis of samples with DIA methods result in relative quantification of the analytes performed post-acquisition, as absolute quantification necessarily requires a calibration for the correlation of the MS response and the concentration of the analyte. Nevertheless, with SWATH acquisition generic standards can be mixed with the sample, preparing the calibration curve post-acquisition to achieve absolute quantification [192]. Of course, it is of utmost importance to choose the optimal SWATH window sizes. Therefore, Bonner *et al.* programmed the software SWATH Tuner [262]. This software generates the window width based on three different approaches: i) SWATH windows based on equally divided mass ranges, which results in fixed window sizes, ii) SWATH window sizes based on the total number of precursor ions divided by the number of windows and iii) SWATH window sizes based on the total ion current generated by all precursor ions divided also by the number of windows [192]. It turned out that the latter is the best choice for identifying metabolites [192].

Comparing SWATH with MS^{ALL} acquisition it is clear to achieve better spectra quality using SWATH acquisition [192] as MS^{ALL} deals with higher background noise due to its detection of everything every time and therefore limited sensitivity for identification in addition to the lower dynamic range for quantification [192]. SWATH acquisition offers various methods of data analysis. The metabolites can be analysed based on predicted behaviour, based on

quantification of high-resolution spectra either from precursor or fragment ions and due to mass defect filtering [192]. This means data-independent acquisition techniques acquire reproducible MS/MS spectra of any ionized substance entering the MS source. Even fragments related to low abundant precursor masses can be acquired [221].

However, with SWATH acquisition, it is not possible to cover the entire mass range within one analytical run, as the cycle time must be large enough [192,221] to include at least 10 data points per peak for quantification [156]. If, for example, many SWATH windows are created to cover the entire mass range, the cycle time will be too small, or the scan rate of the mass spectrometer will be not sufficient, causing improper quantification of the analytes [192,221]. A solution to this problem is to divide the windows into different analyses. In analysis 1, for example, a mass range of 50-500 Da is covered and in analysis 2, a mass range of 500-1000 Da is covered. However, the data evaluation afterwards is quite complex, time-consuming and sufficient sample volumes for 2 analytical runs are needed. Therefore, the mass range is usually set to a smaller range, as not all metabolites can be determined with a single analytical setup [126,127,131]. The identification using SWATH acquisition benefits from the detection of the entire isotope pattern of one precursor due to the selection based on SWATH windows [192]. Therefore, SWATH 2.0 acquisition revolutionizes all existing workflows from selecting the proper acquisition mode for the desired output to the selection of the data evaluation strategy afterwards and is nowadays highly accepted in metabolomics area. Also, because it is not necessary to perform a time-consuming method development and additionally, there are no further adjustments to be performed in order to analyse additional analytes [192]. The combination of qualitative and quantitative measurements combined with re-interpretation at any time post-acquisition, a good data processing, interpretation and visualization strategy is highly recommended. Another problem hereby is that every metabolomics team develops own workflows as this might be the most challenging part nowadays in metabolomic analysis. To overcome the problem of identification of the huge number of detected unknowns in the sample, a library containing as many metabolites as possible together with their retention times are of most interest [221]. Nevertheless, the lack of a standardized workflow like in proteomics and the lack of a computerized system makes subsequent data processing very difficult, time-consuming and complex [192]. To summarize, the bottleneck of the data evaluation of DIA analyses are a standardized workflow, computational software programs, which

mathematically deconvolute precursor and fragment masses [192,257,263] and a library including retention times.

1.6.5. Data evaluation

DIA modes generate MS spectra, which are convoluted, very complex and hard to identify by the operator, even after a separation technique such as LC was used. Each LC data file represents more or less a 3D structure based on thousands of panes. Each pane contains a 2D full scan mass spectrum [154,264], which makes interpretation of the data time-consuming and difficult. In addition, there are also some sources of error during the analysis, which complicate the interpretation and require further actions and additional time [154]. For example, it is very important to ensure a stable chromatography. Furthermore, especially with TOF mass analysers, changes in mass accuracy due to external influences are quite common. However, the bottleneck of metabolomic analysis changed nowadays from the lack of appropriate mass analyser technique to the missing computational software for the identification of unknowns and adequate libraries as every research group uses own in-house generated libraries [125,192]. At the moment there are numerous, sometimes open source, databases of different research groups. However, the non-standardized nomenclature of metabolites [148] makes it often difficult to use the various databases. Additionally, the databases contain so far only limited numbers of metabolites, which results in higher numbers of unknown features during untargeted metabolomics, than identified metabolites [160]. In some cases, only 30% of the total MS signals are identified regarding their structures, resulting in 70% of unknown features [127]. As long as there is no uniform evaluation strategy, as for example in proteomics, or uniform database, as for GC-MS analytics, the data evaluation remains the bottleneck in the field of metabolomics and biomarker detection [127,154]. Thus, a unique workflow like in the field of proteomics is highly desired. However, nearly every mass analyser vendor offers its own data evaluation software, for example PeakView, MasterView and MultiQuant from Sciex and every research group develops their own workflow, which delays further development of data processing dramatically. For this reason, in 2012, Tsugawa *et al.* [265] developed an open source software called Mass Spectrometry – Data Independent AnaLysis (MS-DIAL) especially for the data evaluation of untargeted metabolomics [192]. MS-DIAL is thereby directly linked to an analytical method, containing a specific column and a fixed gradient, as retention time is an additional identification criterion [192]. Acquired precursor ions are

connected to their retention time and accurate mass and plotted as single spots in a diagram, with m/z as y- and retention time as x-axis (see Figure 46) [192].

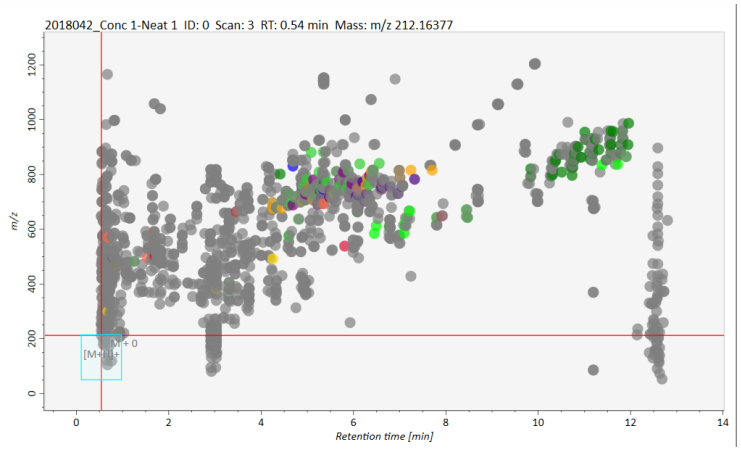

Figure 46: Peak spotting: Every spot describes a metabolite by the corresponding mass-charge ratio and retention time. The grey spots are unknown metabolites and the coloured spots are identified metabolites, categorized in classes. One colour symbolizes one specific class

In untargeted DIA approaches, like SWATH, the precursor ion is not linked to the corresponding fragment ions, therefore the MS peaks need to be aligned to the corresponding MS/MS peaks. MS-DIAL is using an own developed MS^2 Dec algorithm for alignment [192], resulting in deconvoluted spectra (Figure 47 and Figure 48,) and an alignment plot with retention time and m/z (Figure 49 and Figure 50).

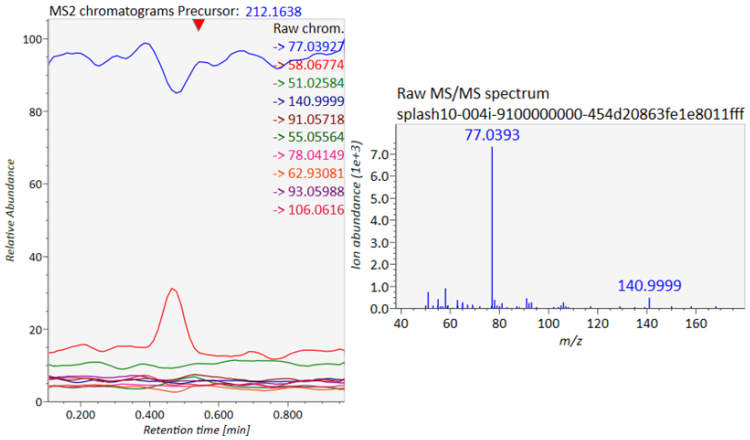

Figure 47: Raw MS/MS chromatogram: The raw MS/MS chromatogram displays all detected fragment masses detected in the window of the selected precursor mass

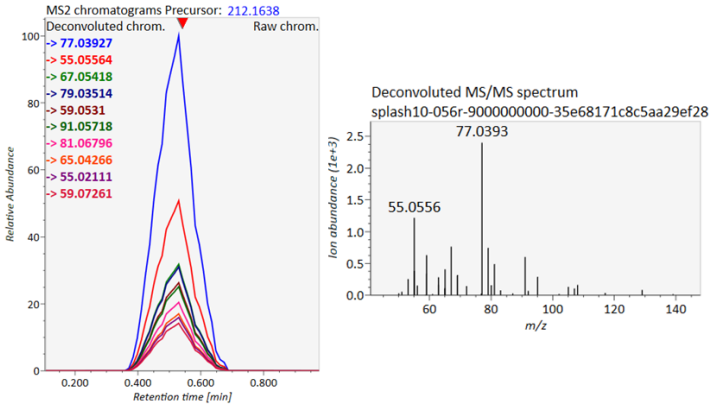

Figure 48: Deconvoluted MS/MS chromatogram: The deconvoluted MS/MS chromatogram shows only the fragment masses which could be aligned to the selected precursor mass

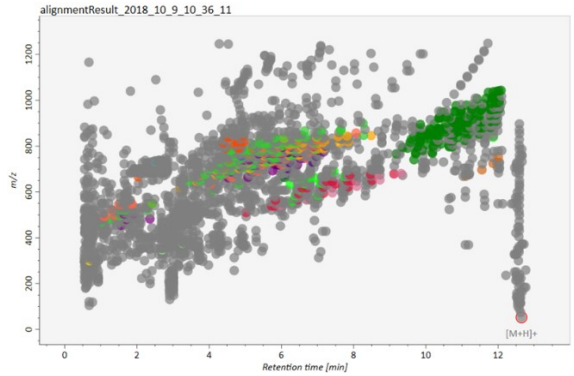

Figure 49: Alignment plot: Every spot represents an aligned feature, which is visualised in the alignment plot according to the m/z value and the corresponding retention time

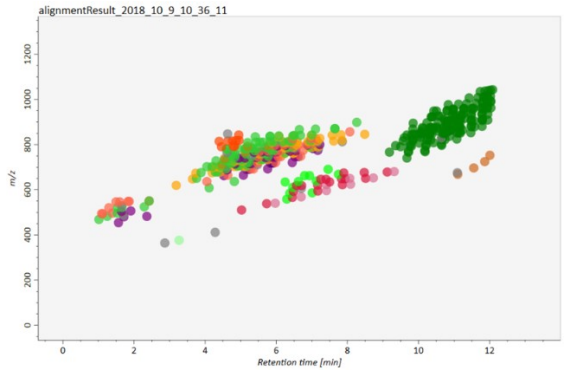

Figure 50: Alignment plot of identified features: This alignment plot shows only identified features, which could be aligned during the Dec^2 algorithm of MS-DIAL. The present alignment plot was prepared during a lipid analysis and the spots are additionally coloured based on their lipid class. For example, the pink spots represent ceramides and the green spots triacyl-glycerides

The alignment is contained of 4 steps. First a reference table is created based on a representative sample, e.g. a QC sample. Next, a peak table is created for each sample and linked to the reference table in the appropriate place. The aligned peaks are screened for missing values in the second last step and in a last step these missing values are filled up based on the mean m/z and retention time of the corresponding feature [258].

The comparison of peak shapes of extracted ion current chromatograms for identification of the features is not suitable, as the peaks can change their shape during the chromatographical run due to fronting, tailing or peak splitting [192]. Afterwards, MS^1, MS^2 spectra and libraries containing MS^2 reference spectra either experimentally obtained or in silico are used for the identification of the features [192]. Additionally, the features are quantified based on either height or area of the precursor peak after preparation of extracted ion current (XIC) chromatograms [192] (Figure 51).

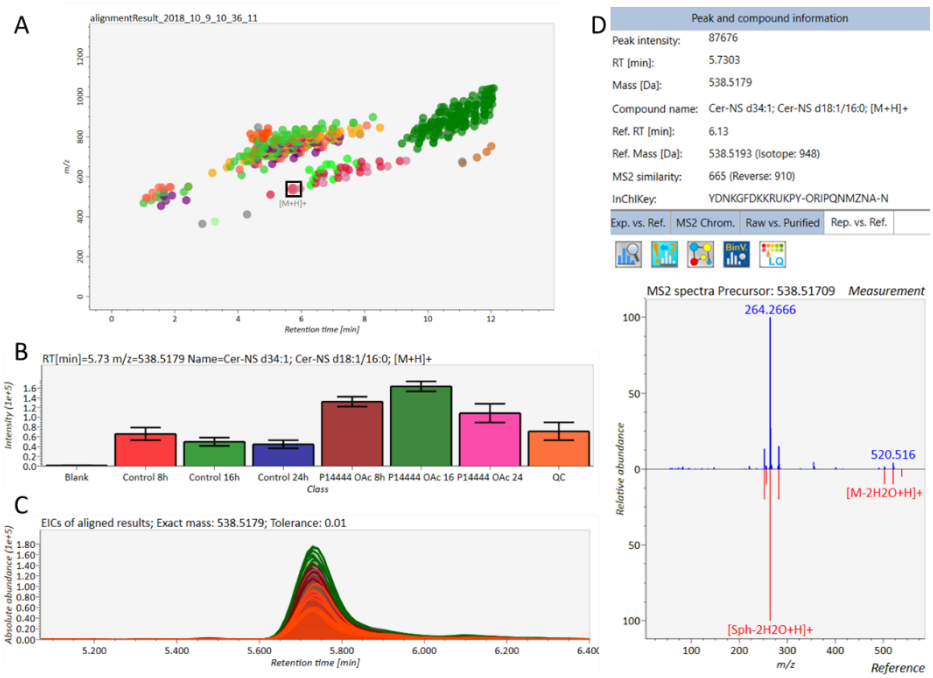

Figure 51: MS-DIAL workflow: A) shows an alignment plot of identified lipids and the spot in the black rectangle is chosen as example. B) displays the distribution of the concentration in the different samples, which clearly visualizes the increasing concentration in the treated samples compared to the control samples. C) represents ion current chromatograms of the selected feature in all analysed samples. D) displays the peak and compound information based on the database as well as the MS^2 similarity (top) and the MS/MS spectra compared with the spectra from the database (bottom)

Other metabolomic research groups developed a R based metabolomics package, called MetDIA [192,257]. MetDIA selects targeted compounds out of the complex MS^2 spectra following five steps [192]. First, precursor ions are monitored and aligned, followed by extraction of desired chromatograms in step two. Pseudo MS^2 spectra and peak-groups are created in step three, before the identification of the metabolites is performed in step four. Last, the results are generated including a statistical evaluation [192] (Figure 52).

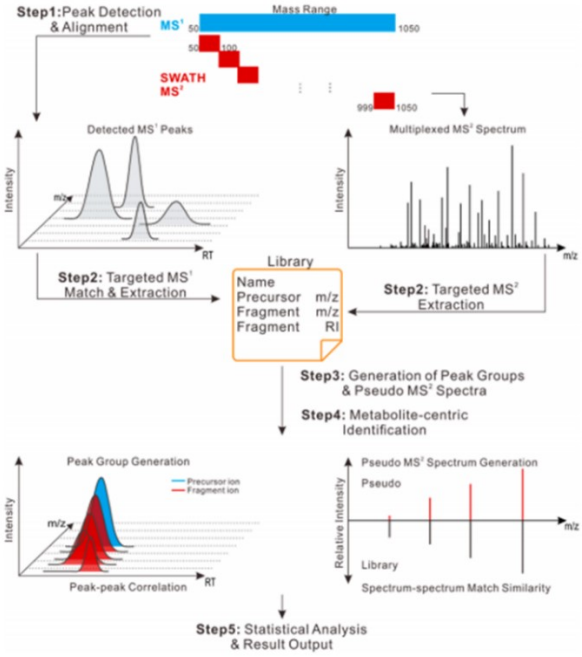

Figure 52: MetDIA workflow: In step 1 precursor ions are detected and aligned, followed by extraction in step two. Additionally, targeted MS^2 spectra are also extracted in step two. During step 3 pseudo MS^2 spectra and peak-groups are generated. Step four describes the identification of the metabolites. In step 5, statistical analysis is performed as well as the results table is produced. Reprinted with permission from Li *et al.* [266]

For the deconvolution using the MetDIA approach, two orthogonal evaluation criteria are used, the peak-peak correlation and the spectrum-spectrum match [192]. Data evaluation using MetDIA is comparable with MS-DIAL. Nevertheless, with MetDIA 20 to 75% more features could be identified analysing biological samples [192]. However, the main challenge in data processing of metabolomics remains the lack of a unique workflow, containing one library, standardized compound names and corresponding retention times, which offers the possibility of retention time adjustment, like the in silico retention time prediction (iRT) of peptides in proteomics [192].

Summarized, good strategies of data evaluation, including databases, software tools and multivariate statistics, are essential [154]. The high diversity and the fact that one sample preparation strategy and one analysis strategy is not sufficient to cover the entire metabolome also led to the division into so-called sub-omic areas, such as metabolomics and lipidomics [142]. Through the lipid map project [267] and the development of an in silico mass spectrometry database, called LipidBlast [268], the situation for lipidomics analysis already appears slightly better compared to the analysis of the global metabolome.

1.6.6. Lipidomics

Lipidomics describes the analysis of the entire lipidome of an organism, which contains all lipids of an organism [269]. Lipids fulfil several important functions in an organism. On the one hand, they serve as the main component of the hydrophobic cell membrane to protect the cell of an organism from its hydrophilic environment [270], on the other hand they serve as an energy source [270] and signal molecule in various metabolic pathways [270]. The lipidome itself, like the entire metabolome, is in fact a very complicated system, which is probably the reason why, the NIH founded the consortium LIPID Metabolites and Pathway Strategy (LIPID MAPS) at the beginning of the increasing interest. The lipids are divided into 8 categories. 1) fatty acyls, 2) glycerolipids, 3) glycerophospholipids, 4) sphingolipids, 5) sterol lipids, 6) prenol lipids, 7) saccharolipids and 8) polyketides [270–272]. Moreover, the different categories are further divided into lipid classes and subclasses [270] (Figure 53).

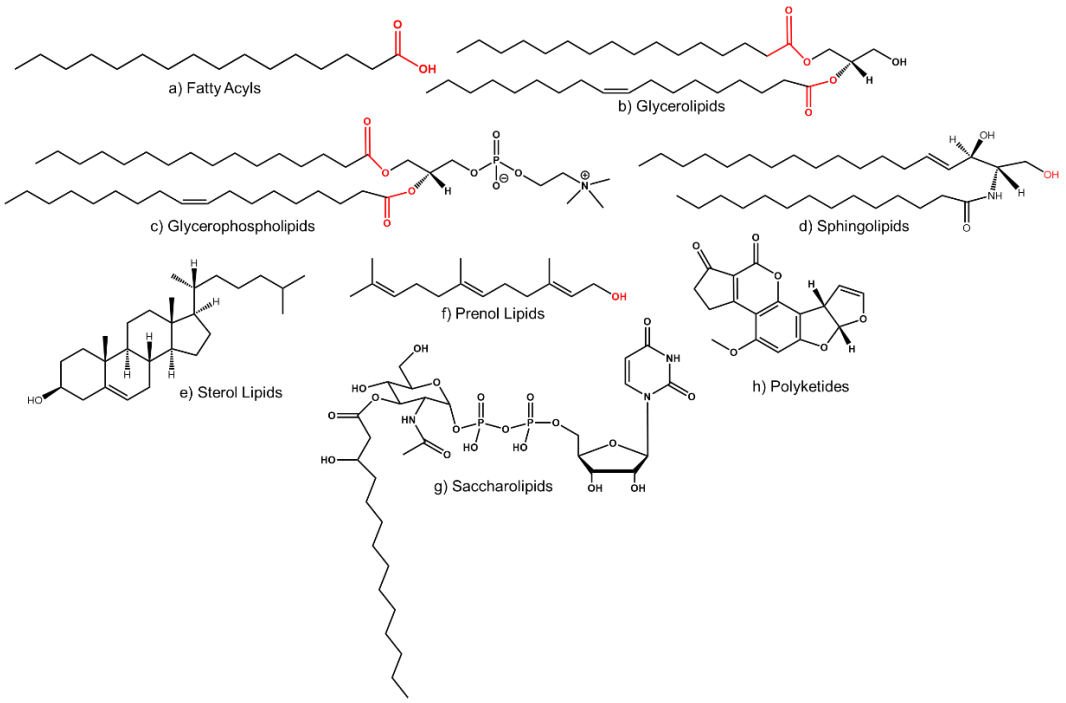

Figure 53: Lipid classes: The lipids of the entire lipidome are currently divided into 8 lipid categories: a) fatty acyls, b) glycerolipids, c) glycerophospholipids, d) sphingolipids, e) sterol lipids, f) prenol lipids, g) saccharolipids and h) polyketides. All categories can be further divided into classes and sub-classes. Adapted according to [273]

For a long time, it was not possible to analyse lipids or metabolites in general, but the further development of mass analysers led to an increased interest in analysing lipids from 2003 onwards (Figure 54). Thus Han and Gross described the concept of "lipidomics" for the first time in 2003 [269]. The interest in this field of analysis increased, among other things,

because they might be potential biomarkers or prognosis indicators for various diseases. For example, it is nowadays known that lipids are involved in diseases such as atherosclerosis, diabetes, Alzheimer, tumorigenesis, chronic inflammation, cardiovascular and neurodegenerative disorders and cancer [270,274–277]. Mainly classic biological samples like blood, plasma, urine and excrement are used for lipid analysis [147]. In the meantime, however, analyses with unconventional samples such as saliva, cerebral spinal fluid (CSF), tissue, tears and nails are also being conducted [147].

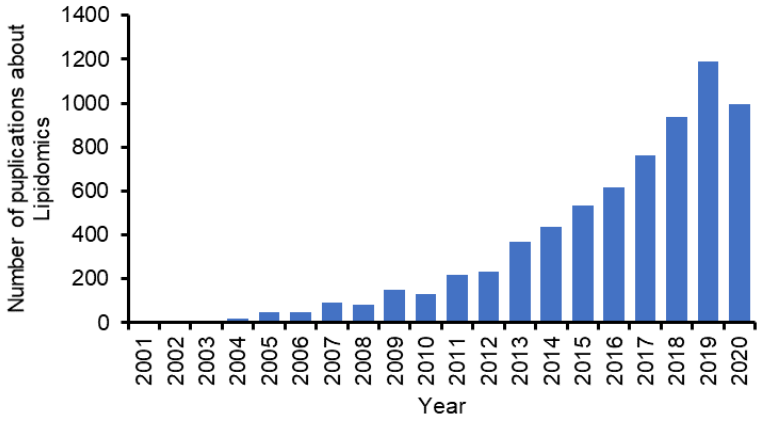

Figure 54: Number of Publications about Lipidomics: The interest in lipidomics analysis steadily increases since the term lipidomics was first coined in 2003 until now, which can be seen in an increase of publications about lipidomics since the beginning (PubMed 27.08.2020)

Already in 1994, lipids were analysed, but instead of using chromatography, the lipids were analysed by direct infusion, nowadays also known as shotgun lipidomics [278,279]. Currently there are three different types of shotgun analysis: i) tandem MS (MS/MS) based shotgun lipidomics; ii) high-mass accuracy-based shotgun lipidomics and iii) multi-dimensional MS based shotgun lipidomics (MDMS-SL) [269]. The big advantage of shotgun lipidomics is the fast analysis of lipids. However, all lipids are simultaneously injected into the source of the mass spectrometer and ionized, which can lead to strong ion suppression effects. Therefore, low abundant lipids or lipids that cannot ionize easily are not analysed.

One way to overcome this problem, is to prepare the sample prior to analysis by LLE or SPE to separate all other metabolites from the lipids [278,280–283]. However, SPE is not suitable for high-throughput analyses or for analyses containing large numbers of samples. Furthermore, SPE is only used to extract certain lipid classes, which makes it unsuitable for the analysis of the whole lipidome [278]. However, selection of LLE type, can also separate certain lipid groups from each other [278,280]. In the beginning of the lipidomics analysis, the method according to Bligh-and-Dyer, respectively, a modified form according to Folch

was widely used [269,278,280,282,284–286]. Both extraction methods added chloroform and water as the main components. The lipids are thus enriched in the organic layer on the bottom of the vessel. On the phase boundary in the middle, a layer of accumulated proteins is formed, which has to be penetrated to collect the dissolved lipids in the organic layer on the bottom. This often leads to contamination with polar analytes from the aqueous phase [282]. As a result, Matyash developed an extraction method based on methyl tert-butyl ether (MTBE) and water [278,287]. MTBE is less dangerous than chloroform and as a further advantage the organic phase with the dissolved lipids is on top and can be easily collected [278,282]. Nevertheless, water-soluble substances could also be carried into the organic phase [282] and in addition there is no option for automation, which would be an important benefit for high-throughput analysis. The problem of carry-over of water-soluble compounds into the organic phase can be circumvented [282,288] by using butanol/methanol (BUME) (3:1; v/v) followed by heptane/ethylacetate (3:1; v/v) as extraction solvent and acetic acid in the last step for phase separation [278,289,290]. The BUME method requires only small amounts of solvent, which offers the possibility of automation with a pipetting robot [278,288,290]. However, it is difficult to evaporate butanol to concentrate the lipids prior to analysis [282]. Extraction methods are constantly further developed, because one technique alone is usually not sufficient to extract all lipids, especially when it comes to low abundant lipids [147]. Therefore, several extraction methods are performed one after the other. This led to the development of a 3-phase extraction system consisting of hexane, methyl acetate, ACN and water. The aqueous phase is located at the bottom, in the middle is the organic layer with the most polar lipids and at the top are the neutral lipids like triacylglycerols in another organic layer [278] (Figure 55).

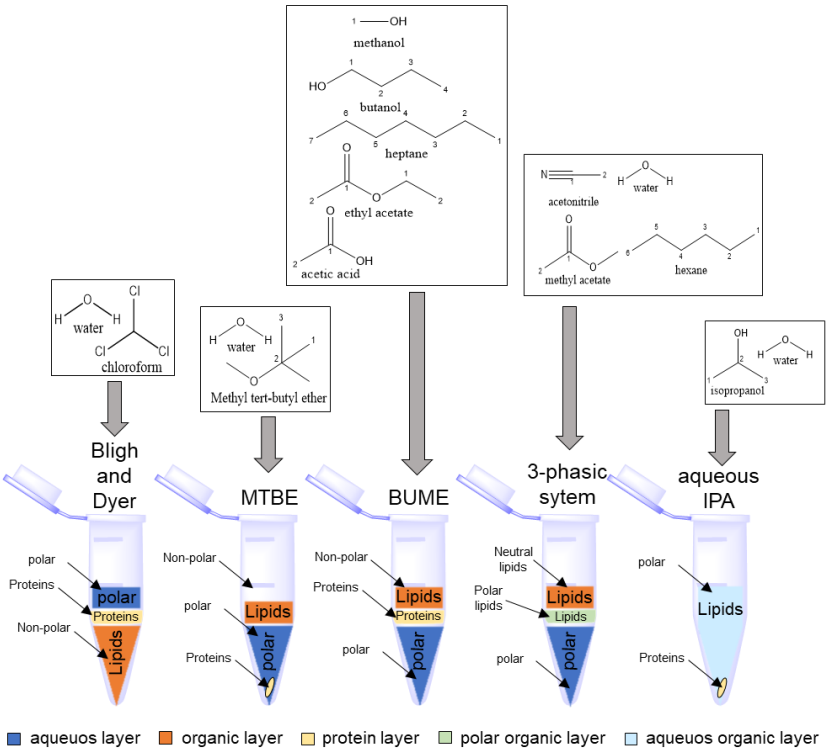

Figure 55: Comparison of different lipid extraction protocols: The Bligh-and-Dyer extraction method as well as the Folch method use mixtures of chloroform/water as extraction solvent, resulting in an organic layer containing the lipids at the bottom and the aqueous layer on top, separated by a protein layer. The MTBE extraction method uses a mixture of methyl-tert-butyl-ether/water as extraction solvent, ending up with the aqueous phase at the bottom as well as a protein pellet and the organic layer with the dissolved lipids on top, easy to remove. BUME uses sequentially mixtures of methanol/butanol and heptane/ethyl acetate followed by acetic acid for phase separation. The polar phase is located at the bottom and the non-polar phase on top, also separated by a protein layer in the middle. The 3-phasic system uses mixtures of acetonitrile/water/methyl acetate/hexane as extraction solvent, resulting in a polar phase at the bottom, an organic phase in the middle containing polar lipids and another organic phase on top with dissolved neutral lipids. One possible one-phasic extraction protocol uses a mixture of isopropanol (IPA) and water as extraction solvent. The proteins are pelleted at the bottom surrounded by the dissolved compound in the extraction solvent

So, it is possible to separate certain lipid groups from each other during the extraction process. However, this is also time-consuming and the use of hexane should be avoided for the protection of the environment. Of course, the extraction method depends on the lipid classes to be analysed. In order to further simplify the extraction process, to extract as many lipids as possible and to fulfil today's requirements of high-throughput analysis, numerous single-phase extraction methods have been developed [280,291]. One of them, using an isopropanol/water mixture (90:10, v/v) was used as extraction solvent for lipids in this work.

Another way to circumvent the problem of very complex data sets after shotgun analysis, is the so-called intra-source separation. In this process, certain lipids are selectively ionized, controlled by different conditions of the surrounding solvent [269,292,293]. Additionally, individual lipid classes can be isolated from a mixture by specific neutral loss scans (NLS) or precursor ion scans (PIS) [269,292]. Ionisation can be improved by derivatising the lipids

or by adding certain additives to the solvent [269,294–296]. Derivatisation can also be helpful if the desired lipid would normally be unstable, if certain fragmentation patterns have to be generated during the analysis or if characteristics for ionization are missing [278,281]. A switch to high-resolution mass spectrometers, such as orbitrap or Fourier-transform ion cyclotron resonance (FT-ICR), can also help in the separation of isobars [127]. High-resolution mass analysers analyse all product ions in narrow "bins" within the entire mass range and achieve a lower rate of false-positively identified lipids with accurate acquisition of m/z ratios and high resolution [269].

In addition to sample pre-treatment and MS/MS analysis of lipids, other separation techniques can also be used. For example, non-volatile lipids are separated by thin layer chromatography (TLC) with the great advantage of a simple and inexpensive setup and fast analysis. However, with TLC only a low resolution is achieved and real-time separation for coupling to a mass spectrometer is impossible [269]. The use of GC chromatography would also be feasible for thermally stable and volatile lipids or, after prior derivatisation, also for non-volatile lipids, as it has an extremely high separation accuracy. However, derivatisation is time-consuming and in general the EI ionisation associated with GC is too hard, resulting in excessive fragmentation of the lipids, loss of all structural information and eventual assembling into new molecules, which increases the probability of misinterpretation. In addition, high source temperatures lead to the degradation of certain lipids to other lipids, which further increases the misinterpretation [269,297]. GC-MS is nowadays mainly used for fatty acid analysis. Supercritical fluid chromatography (SFC), which is a high-resolution separation technique, holds a small position in lipid analysis. SFC is based on supercritical carbon dioxide as solvent, which leads to faster and better analysis compared to classical high-pressure liquid chromatography (HPLC), due to its high diffusion coefficients and low viscosity [147]. Until now, NMR was considered the gold standard for the identification of metabolites/lipids. However, NMR is not really well suited for the analysis of lipids due to in chapter 1.4.1 mentioned reasons. Additionally, because lipids are usually only present in low concentrations, which cannot be detected by NMR.

Therefore HPLC-MS analysis is mostly used in the field of lipidomics, because it shows good reproducibility and high resolution and works efficiently and selectively [147]. Mainly RP chromatography is used prior to MS analysis. Even if carry-over effects, which are common in lipid analysis, are observed with C_{18} or C_{30} column materials [270], RP or LC in general has the following advantages over shotgun lipidomics: Matrix effects, due to complex

samples and thus ion suppression are reduced, isomers can be separated, which allows a more accurate quantification and low abundant lipids can be analysed with higher probability [147,269,270,278,297].

Not only other analytical techniques can be used, nowadays also different ionization methods are applied: a) ESI, b) MALDI; c) APCI/ Atmospheric Pressure Photoionization (APPI); d) secondary ion mass spectrometry (SIMS) and e) Desorption electrospray ionization (DESI) [269]. ESI is the most frequently used ionization, but MALDI-MS also has its place in the field of lipidomics analysis. MALDI is an ionization method that can ionize a wide range of biomolecules and also identify unknown molecules using MS. The main advantages of MALDI are its tolerance to impurities such as buffers and salts and the ability to analyse large arrays of complex samples [147]. The most important aspect is the optimal selection of the matrix. This also leads to a major disadvantage because the spectra are very much affected by background noise from the matrix and therefore only simple lipid mixtures can be analysed, since the separation prior to MS is missing or has to be carried out offline, which is time-consuming [147]. Furthermore, a fragmentation unit is missing, unless a MALDI ionization is coupled to a TOF/TOF mass spectrometer. Nevertheless, MALDI-MS has its place in the imaging analysis of tissue samples [147]. A concentration profile of the lipids within a piece of tissue can be generated by exact scanning of the tissue. For example, this technique can be used in surgery during tumour removal, so that the lipid profile can be analysed while cutting, whether the tissue is already healthy or not [280].

Nevertheless, the analysis of lipids is nowadays mostly performed by U(H)PLC-MS coupled to high resolution mass spectrometers, such as QTOF, Orbitrap or FT-ICR. The most commonly used separation techniques are RP and HILIC [270,298]. RP columns separate the lipids according to their fatty acyl chain composition. Lipids are retarded longer on an RP column, the longer the fatty acid chains are. In contrast, lipids elute earlier the higher the number of double bonds is [278,299]. Whereas HILIC separates the lipids according to their head group, so that a 2D LCxLC chromatography consisting of HILIC in the first dimension and RP in the second dimension might have some advantages [147,270,278]. One of the major advantages of the 2D-LC is the significantly increased peak capacity [269]. However, the setup is very complex, the analysis times would be very long and due to the dilution of the sample in the second dimension selectivity could be lost [147]. Furthermore, the constantly increasing speed of chromatography means that peaks become narrower and narrower as the stationary phases improve in order to achieve higher peak capacities. The

limiting factor here is the speed of the mass spectrometer or its duty cycle, since a sufficient number of measuring points should cover the chromatographic peak for quantification [258,278]. A further development of the lipidomic workflow including data processing, especially for the identification of unknown lipids and the investigation of the functions in different pathways, is therefore extremely important [278,300]. In addition, the retention time in databases is a further identification feature, as lipids can be identified on the basis of retention time (chromatography) and spectral data (precursor and fragment masses) [282]. However, the retention time in the database is linked to a specific setup. A large coverage enables the monitoring of as many metabolic pathways as possible, in which lipid classes/subclasses are involved, whereby connections of the different pathways and the whole system can be better understood [282].

In general, the analysis of lipids can be divided into two categories, targeted and non-targeted lipidomics [300], whereas a targeted approach mainly uses SRM or MRM [281]. SRM/MRM is characterized by high specificity and a stable wide dynamic range [269], which makes both methods highly suitable for quantification [269]. A preliminary stage to untargeted lipidomics involves several successively acquired SIM analyses of 20-50 m/z mass ranges, which are then combined into a full scan spectrum using software tools. The untargeted analysis can be further divided into data-dependent and data-independent analysis. With untargeted approaches using data-dependent acquisition, the problem is that only a limited number of high abundant lipids are selected and fragmented after the first scan, so that low abundant lipids cannot be analysed easily [269]. Therefore, nowadays the untargeted lipidomics analysis is mainly performed with data-independent approaches such as SWATH or MS^{ALL}. Untargeted lipidomics is mostly used for hypothesis development, pre-selection of potential biomarkers or characterization of new lipids, which later have to be confirmed with a targeted approach. The disadvantage of untargeted approaches, however, is the resulting complex spectra and the difficulty of correctly characterizing the lipids down to their fatty acids, which is the reason why the development and application of bioinformatic software tools for data analysis are essential [269]. The consortium LIPID MAPS therefore developed a virtual lipid database, which is steadily growing. This enables the comparison of spectra and the identification of unknown lipids. Both databases of the METLIN Metabolomics Database and the Human Metabolome Database also contain lipids for comparison and pathway analysis [269].

The main problem is that the identification depends strongly on the complexity of the measured sample, the ionizability, the concentration and the algorithm used during data evaluation [270]. The difference to metabolomics or proteomics lies in the chemical structure of the lipids contained of polar head group and acyl chains. Whereby the similarity of the fragment ions is defined by specific scoring factors in a comparison with corresponding databases [270]. To identify a lipid, five important properties must be described: a) lipid category and lipid class; b) number of carbons, rings, double bonds and oxygen of fatty acids; c) position of functional groups; d) geometry of double bonds; and e) stereochemistry of chiral centres [300]. Lipids are one of the most difficult types to identify compared to other metabolites, since a mass in MS can theoretically be assigned to many different molecules, so-called isomers [281,300,301]. Therefore, it is extremely important to separate the [M+2] peak of a lipid from the lipid of the same lipid class with only one double bond less [270]. Nevertheless, the identification of lipids remains difficult because stereoisomers, sn1, sn2, enantiomeric or double bond positions cannot be analysed with MS/MS. In addition, the exact length and number of double bonds of the lipids cannot be determined precisely because the specific MS/MS spectra are usually not sufficient for a clear assignment [270]. Furthermore, the signal response of the fragments of two species within a lipid class is not always the same, making accurate quantification often difficult [269]. In addition, similar to metabolomics, each research group follows its own workflow and create their own nomenclature of lipids.

Therefore, the LIPID MAPS consortium is aimed at developing a uniform nomenclature and standardization of the whole process. In general, a normal lipidomics workflow always includes the following steps: a) sample collection; b) sample storage; c) sample preparation/extraction; d) analysis; e) data processing and identification of unknowns [147,269]. LIPID MAPS provides therefore, lipid-drawing tools, data deposition and lipidomics informatic tools.

However, another problem remains, the sampling. Clinical studies usually extend over longer periods of time, up to years [280]. This means a very long storage of the samples. In order to avoid data corruption due to performance fluctuations, all samples should be measured in one batch if possible [280]. However, lipids are very sensitive to oxidation and long storage periods, which would affect the results [280]. Therefore, the better option is to measure the samples in smaller batches as soon as possible after sampling [280]. The inter-batch variations due to drift of instrument sensitivity, changes of eluent over the time,

temperature fluctuations, performance fluctuations or stopped analysis due to instrument error can be normalized in two different ways [270,278,280]. On the one hand, a normalization based on LOESS regression, using quality control samples, which are measured at least every ten, in the present work every three samples and are usually composed of a pool of all samples or a certified reference material is possible [270,278,280]. On the other hand, a normalization based on internal standards spread over the entire retention time range is possible [270,278,280]. For this purpose, software programs already exist, which search for the appropriate internal standard for each lipid. Due to the fact that internal standards are often very expensive or difficult to obtain, in most cases one standard per lipid class is sufficient [270]. It is recommended to use isotopically labelled lipids as internal standards, as they elute simultaneously and have the same properties [280].

For shotgun lipidomics also one internal standard per lipid class is sufficient, since no chromatographic separation has been performed before, which could have an influence on the lipids due to changing the composition etc. of the mobile phase and therefore only the polar head group is decisive for ionization. However, the selection of the appropriate internal standards is still a great challenge and an expensive issue, so that in metabolomics and lipidomics studies a relative quantification is usually preferred instead of an absolute quantification. Relative quantification is based on the relationship between the lipid and its internal standard between two samples without knowing the exact content [269]. In this context, the use of LC chromatography offers the advantage that individual lipids elute within their lipid class, just like the corresponding internal standard of the corresponding lipid class [270,278,280]. In contrast to shotgun analysis, which uses ion peak intensities for quantification, LC-MS analysis mainly uses chromatographic data, such as peak areas, so that a more accurate quantification is possible [282]. An interesting approach to avoid the cost of isotopically labelled internal standards is the lipidome isotope-labelling of yeast (LILY) approach, which grows yeast in ^{13}C-labelled medium so that the whole yeast lipidome is ^{13}C-labelled [270,278,302]. The main advantage of this approach is the existence of a labelled standard for each individual lipid as long as it is the same organism. However, in order to quantify ^{13}C-labelled lipids accurately, they must be compared once with known concentrations of unlabelled equivalents. This means that unlabelled standards have to be commercially purchased once, which makes this method less feasible [278]. The normalization in the present work was a combination of different strategies. First of all, the MS-DIAL alignment algorithm was used, before the aligned data set was normalized based

on a QC sample and the LOESS algorithm. In a next step an in-house developed R based script was applied for the calculation of the best fit of used internal standard and detected feature. This output list was implemented into MS-DIAL, normalizing the raw data with a combination of LOESS algorithm and internal standard. In a final step, the cell counts of every sample were taken into account, resulting in a LOESS, IS and cell count normalized data set (Figure 56).

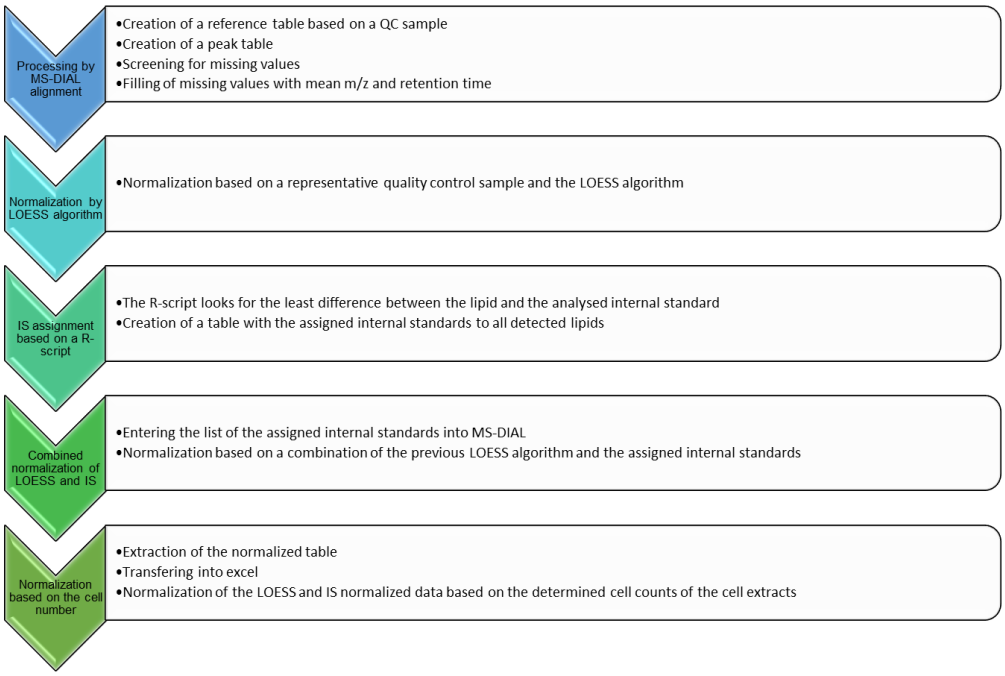

Figure 56: Workflow of the normalization process: In the first step, the data was evaluated using MS-DIAL. The second step normalized the aligned data with LOESS algorithm, based on a QC sample. An in-house created R script determined the best fit of internal standard and detected feature in step three, followed by a combined normalization of LOESS and internal standards in step four. Finally, the data set was corrected for the cell counts of each sample as step five

Nevertheless, we still do not know the exact number of lipids in an organism and we do not know whether we will ever detect all of them. It is estimated that 50% of the features of an untargeted analysis are previously unknown lipids and identification is more than time consuming and difficult due to the high diversity of lipids. Therefore, bioinformatic software tools are absolutely essential for data evaluation as well as statistical analysis, such as multivariate analysis, like Principal Component Analysis (PCA) [281,297,303], Partial least squares-discriminant analysis (PLS-DA) or Orthogonal partial least squares discriminant analysis (OPLS-DA) [281,303], because univariate statistics only consider single lipids and not the complex interactions [297]. A first step in the right direction is definitely the standardization of processes, starting with the nomenclature and classification developed by LIPID MAPS [271,272,297,300] and continuing with the standardization of the whole lipidomic workflow through guidelines and data quality assessment by the Lipidomics

standards initiative (LSI) [278,300]. Once all problems of annotation, standardization, automation and quantification are solved, Lipidomics will be a powerful analysis tool for clinical studies, personalized medicine, etc. [278].

1.7. Future

Of course, the goal should be to interpret both sub-omic areas, lipidomics and metabolomics together, but it should not be ignored that both analyses provide two different and complex data sets [142], which means that identification still remains a challenge and are thus the bottleneck of metabolomics [127]. A step in the right direction would be the development of a sample preparation which is not only automated and fast for high-throughput analysis, but also quantitative and standardized, which would make it easier to create the missing databases across research groups [138]. In addition, large scale data sets also require an excellent chemometric and statistical evaluation strategy [125]. In future research, the implementation of a further separation dimension, such as ion mobility spectrometry (IMS), should also be considered to increase the identification of unknown metabolites [154,257].

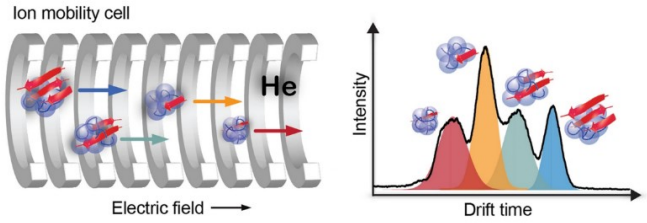

Figure 57: Ion mobility mass spectrometry: The ion mobility separates different compounds based on their shape and size, which enables even the separation of isobars and offers a further separation dimension. Reprinted with permission from Hoffmann *et al.* [304]

IMS brings a further separating dimension [270,282,305], as molecules are separated on the basis of their shape and size [278,297,306,307], including isobaric analysis [300] (Figure 57). This is important for the analysis of triacyl-glycerides (TAGs), for example, because many of them have identical masses [300]. Both techniques, shotgun and LC-MS are compatible with IMS. Nevertheless, the dynamic range of a mass analyser is smaller than the concentration range to be analysed [155].

2. Aim of the work

Ionic liquids are widely used in industry as green solvents, even though the toxicity of them to the environment is not fully known and the mechanisms behind are not understood. Therefore, the aim of the study was to investigate the toxicity of selected common ionic liquids or respectively the mechanisms, which can explain the toxic effects on mammalian cells as a correlation to humans. The first step was to determine the EC_{50} values of various mammalian cell lines, HCE, CHO and HeLa cells, as indicator of the toxicity. A colorimetric cell assay with a redox reactive dye was used for the evaluation of the EC_{50} values by fluorescence measurement. Based on these results, the fluorescence units were correlated with the cell number. The corresponding EC_{50} value was calculated by a computerised iteration of the least squares of measured and predicted values.

To gain a deeper understanding of the mechanisms describing the toxic effects, the objective in a second study was the development of a fast and highly sensitive LC-MS/MS method for the analysis of the metabolic profile of mammalian cells. For this purpose, the optimal stationary phase for the liquid-chromatography separation of metabolites was needed to be defined. As the analysis of the metabolome was initially focused on the substance group of amino acids, as one of the most important substance group of an organism, different stationary phases for HILIC chromatography were investigated. By the reason of the comparison of different sized columns with different stationary phases based on their performance using a QTOF mass analyser, a compound used as void volume marker compatible with MS detection was evaluated to establish the best suited HILIC column for amino acid analysis in terms of retention time, peak shape and sensitivity. The amino acids were chosen as target metabolites for the metabolic profile. They are involved in a huge number of metabolic pathways, are part of various compounds and are building blocks of proteins within an organism. On the contrary, other metabolites could also be part of the toxic effect of ionic liquids. Hence, the aim was to develop a LC-MS/MS method that would combine targeted and non-targeted analysis of the metabolome in one analysis to achieve the best sensitivity for the amino acids, but gaining also some knowledge about the concentrations of other metabolites in treated cells compared to control samples. MS^E or MS^{ALL} would have been an alternative to reach this goal. However, the correlation of precursor and fragment masses are quite difficult with these approaches. Therefore, SWATH acquisition in combination with a QTOF mass analyser was used for combining targeted and untargeted analysis. In comparison to MS^E and MS^{ALL} the SWATH acquisition

divides the entire mass range into so called precursor isolation windows (for MS^2), with fixed mass ranges of for example 25 Da. This allows better alignment of precursor and fragment masses, due to a limited mass range within one window. In particular the second generation of SWATH acquisition, SWATH 2.0, with variable window sizes offered the possibility to set the window sizes as small as possible, that only one amino acid will be scanned and wide windows for the remaining metabolites. That means, for the amino acids optimal measuring conditions and the highest sensitivity can be achieved. Further, the precursor masses can easier be aligned to the fragment masses. Nevertheless, all other metabolites of the cell metabolome are still detected with good sensitivity regarding their precursor and fragment masses. Even though, we were focused on the amino acids, we could look into the profile of carbohydrates for example even after months/years the analysis was performed without the need of taking and analysing a new sample.

First results within the EC_{50} determination leads to the perception that some ionic liquids cause formation of intracellular lipid droplets in HCE cells (Figure 58).

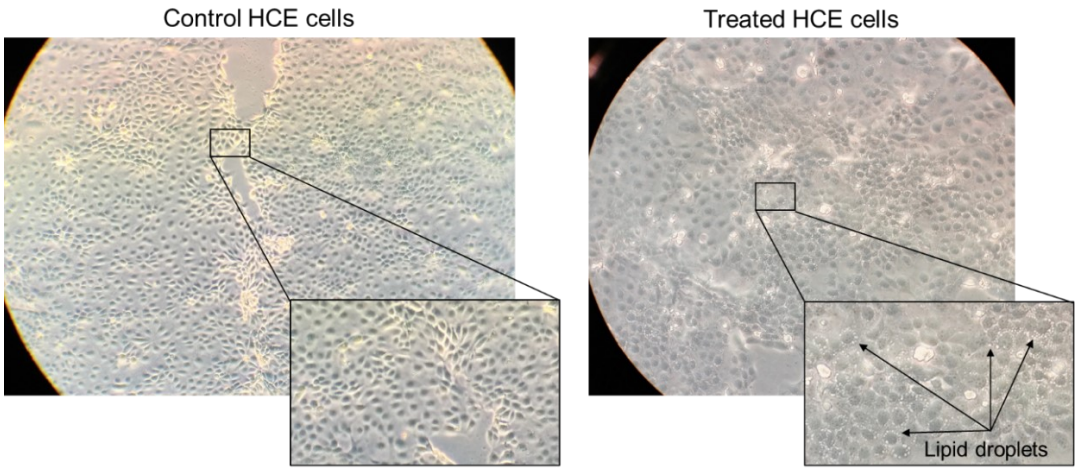

Figure 58: Formation of lipid droplets: HCE cells showed formation of lipid droplets within the cells during ionic liquid treatment

Further investigations on these findings were started in a new project, which was focused on the lipid profiling of HeLa cells. As the lipidome contains a huge number of lipids with different characteristics, a new approach for the best suited extraction solvent and protocol to extract the highest number of lipids was developed and finally a one-phasic extraction protocol was applied. The most interesting point was to find out why in previous experiments only some ILs formed lipid droplets and what could be the mechanism behind. Therefore, a LC-MS/MS lipidomics study was arranged as time-dependent study, where HeLa cells were treated with different ionic liquids and concentrations above their EC_{50} concentrations, for 8,

16 and 24 hours. Afterwards, the cells were extracted and analysed using an adapted already published LC-MS/MS method with SWATH 2.0 acquisition. The biggest challenge of this project was to process and align the large data sets, measured on different days, using one internal standard per lipid class instead of one per lipid. In addition, the data sets need to be compared with databases to identify unknown lipids and to form initial hypotheses about the toxicity mechanisms. Therefore, a strategy for data evaluation needed to be developed. Regarding different factors, which impact the results due to above mentioned circumstances, renders a carefully planned normalization strategy of the data necessary. For example, different numbers of cells die during the toxic effect of the ionic liquids during the treatment of the cells. Also, sample preparation time does not allow the analysis of all samples at the same time, but as the lipids are sensitive to oxidation, they need to be analysed immediately after sample collection. Therefore, the analysis in different batches on different days were unavoidable, dramatically increasing the need for an alignment workflow as part of data evaluation in form of a visual basic script (VBA). This alignment strategy correlates m/z values and retention times of compounds detected in different batches to compensate inter-batch variations caused by external influences such as temperature changes or changes in the composition of the mobile phase, etc. during the different LC-MS/MS analyses.

At the end, the normalization strategy was implemented into the data evaluation workflow for data base comparison and identification of unknown lipids using MS-DIAL and the data was afterwards aligned.

In summary, within the present work, an analytical setup was established to determine EC_{50} toxicities values of various ionic liquids evaluated in three different cell lines, as well as to investigate toxicity mechanisms of the ionic liquids by a metabolic fingerprinting method, combining targeted metabolomics of amino acids and untargeted metabolomics. Furthermore, the first hints of toxic mechanisms could be studied by lipidomic profiling of HeLa cells using a developed data evaluation process linking normalization and alignment of the data sets for hypotheses generation and identification.

3. Results and Discussion

3.1. Effect of ionic liquids on zebrafish (Danio rerio) viability, behaviour, and histology; correlation between toxicity and ionic liquid aggregation

3.1.1. Abstract

The effect of eleven common amidinium, imidazolium, and phosphonium based ionic liquids (ILs) on zebrafish (Danio rerio) and Chinese hamster ovary cells (CHO) was investigated with specific emphasis on the effect of anion and cation chain length and aggregation of phosphonium based ILs. Viability and behavioural alteration in the locomotor activity and place preference, after IL treatment of 5 days postfertilization larvae, was recorded. Behaviour and histological damage evaluation was performed for adult fish in order to get insight into the long-term effects of two potential biomass-dissolving ILs, [DBNH][OAc] and [P_{4441}][OAc]. To get an understanding of how IL aggregation is linked to the toxicity of ILs, median effective concentrations (EC_{50}) and critical micelle concentrations (CMC) were determined. The long-chain ILs were significantly more toxic than the short-chain ones, and the anion chain length was shown to be less significant than the cation chain length when assessing the impact of ILs on the viability of the organisms. Furthermore, most of the ILs were as monomers when the EC_{50} was reached. In addition, the ILs used in the long-term tests showed no significant effect on the zebrafish behaviour, breeding, or histology, within the used concentration range.

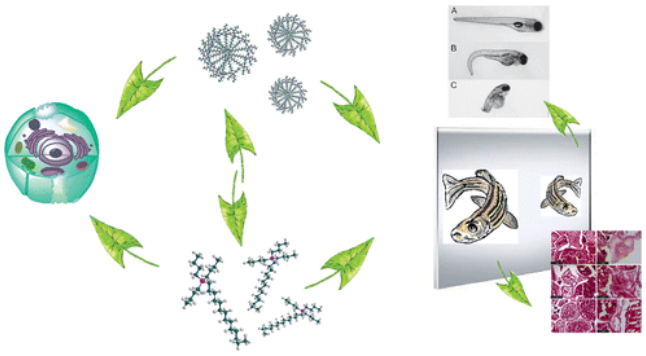

Figure 59: Graphical Abstract: Effect of ionic liquids on zebrafish (Danio rerio) viability, behaviour, and histology; correlation between toxicity and ionic liquid aggregation

3.1.2. Introduction

Ionic liquids (ILs, Figure 60) are composed solely of cations and anions and are defined as salts with melting points below 100 °C.

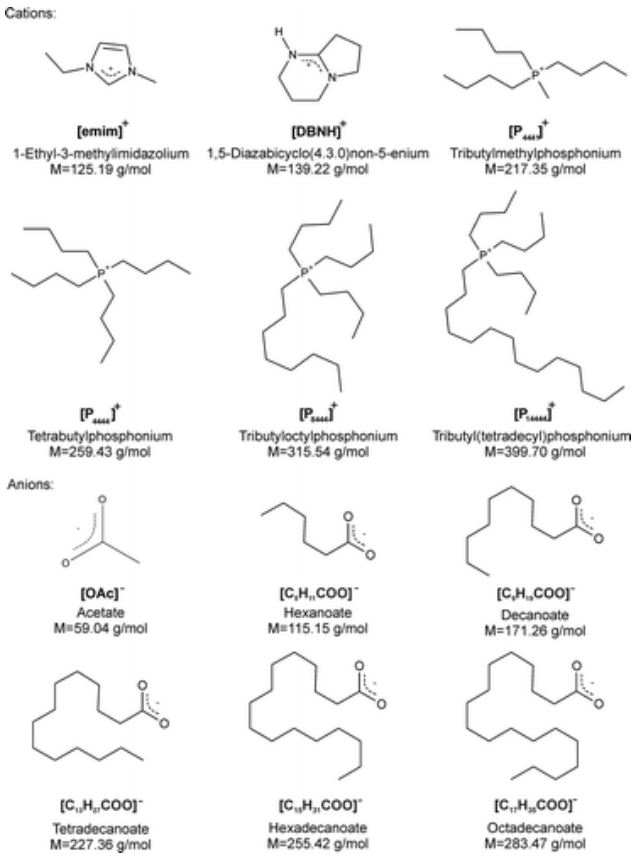

Figure 60: Ionic liquids: Chemical structures of ionic liquid cations and anions

They have received much attention due to their unique chemical and physical properties. ILs are often quoted as having low vapor pressures, low flammabilities and they are thermally and chemically stable, therefore they are widely used in various pharmaceutical and industrial applications, such as catalysis, organic synthesis, extractions, electroseparations, hydrometallurgy [4,308,309],and importantly for cellulose dissolution and in wood extraction [310]. Despite the fact that their low vapor pressures minimize the impact of ILs on the atmosphere, their effect on water ecosystems and furthermore towards different aquatic organisms cannot be ignored or underestimated. Depending on the lipophilicity and alkyl chain length, the direct interaction between ILs and biological membranes might lead to bioaccumulation, induce disruption and leakage, and eventually even lead to cell death [311]. Imidazolium based ILs have been under investigation in many studies [8] but recently amidinium and guanidinium based ILs are becoming more widely used due to their recyclable structures for cellulose and hemicellulose

processing [312–314]. Despite many studies regarding IL cation effects toward various systems, there are only a few studies concerning the IL anion and especially the anion chain length. Muhammad *et al.* have shown that the cytotoxicity slightly increases when the anion chain length is increased using cholinium carboxylate ILs [38] while the group of Hartmann has shown that cholinium carboxylates were unable to cause serious cell damage to fungal plasma membrane, even at concentrations leading to cell death [21]. Yang *et al.* have shown that $[P_{4444}]^+$ carboxylate ILs (C < 20) can have strong hydrogen-bond basicities and relatively low viscosities and are therefore a good option for various extractions [315]. Moreover, Abe and co-workers have recently focused on ILs with tetraalkylphosphonium cations together with carboxylate anions and their ability to dissolve cellulose [316]. By increasing the anion chain length instead of the cation chain length, the unique biomass dissolving capabilities of IL could possibly be maintained while decreasing the toxicity of the IL. In recent years there have been studies on the toxicity of ILs on different cells, aquatic organisms, and other biological systems. These are extensively reviewed in reviews by Bubalo *et al.* [9], Egorova *et al.* [13], Kudłak *et al.* [51], and Amde *et al.* [37]. Most of the ILs are water-soluble and therefore the ILs can potentially cause health risks to the environment due to accidental leakage. Different organisms are affected differently and one compound being toxic to one organism can be harmful or nontoxic to another [26]. Fish are one of the most widely populated species in the aquatic food chain. Therefore, it is relevant to assess the toxicity of ILs also to fish when evaluating the toxicity of ILs on the aquatic ecosystem. Zebrafish are one of the most used test animals among vertebrates due to their easy maintenance, low cost, and rapid development of transparent embryos, however there are only few studies concerning the impact of ILs on fish. Pretti *et al.* have studied the impact of 15 ammonium based ILs [317] and 18 ammonium, morpholinium, thiophenium, and sulfonium based ILs [11] on zebrafish. In addition, the toxicity of tetrabutylammonium bromide ($[N_{4444}]Br$) on 4 days old zebrafish [318], the effect of 1-methyl-3-octylimidazolium hexafluorophosphate ($[omim][PF_6]$) on the reactive oxygen species and on DNA damage in zebrafish [31], and the effect of 1-decyl-3-methyimidazolium bromide ($[C_{10}mim]Br$) on the antioxidant enzyme system and DNA in zebrafish [319] have been assessed. Furthermore, some immunomarkers of three-spined stickleback after treatment of four phosphonium based ILs have been determined [41] and the toxicity of two aromatic phosphonium based ILs on guppy fish have been studied [320].

Eleven different ILs with varying cation (hereafter called cationic ILs) or anion (hereafter called anionic ILs) structures and alkyl chain lengths were chosen based on our previous studies [22]. The zebrafish embryos were treated with ILs for five days and the effect of ILs on the viability of the embryos was determined. In order to evaluate long-term impact of two interesting biomass-dissolving ILs, i.e. [DBNH][OAc] and $[P_{4441}][OAc]$, on the zebrafish, the fish development and behavioural alterations (locomotor activity, boldness, and aggressiveness) were monitored. Furthermore, histological examination was performed on liver, gills, intestines, and gonads.

In order to get a further insight into the impact of the ILs on the fish the median effective concentrations (EC_{50}) of the ILs were determined using Chinese hamster ovary (CHO) cells. CHO cells are ideal models for mammalian cells and they are commonly used in biological and medical applications, especially in EC_{50} determinations, due to their rapid growth, low chromosome number, and clear karyotype. Furthermore, they are frequently used as a host cells for therapeutic proteins [321].

For gaining a deeper understanding of how the chain length and aggregation of the ILs are related to their toxicity, the critical micelle concentrations (CMCs), were determined for the ILs capable to form aggregates.

3.1.3. Experimental Section

Detailed information on the chemicals used and on the preparation of ionic liquid samples and used buffers can be found in Supporting Information (SI) on page 105-106. 1-Ethyl-3-methylimidazolium acetate [emim][OAc] (purity > 98%) and tributylmethylphosphonium methyl carbonate solution (purity >95%, 80% w/v in methanol) were purchased from IoLiTec GmbH (Heilbronn, Germany). 1,5-Diazabicyclo(4.3.0)non-5-enium acetate [DBNH][OAc] was synthesized according to our previous article [314]. Tetrabutylphosphonium acetate $[P_{4444}][OAc]$, tributyloctylphosphonium acetate $[P_{8444}][OAc]$ and tributyl(tetradecyl)phosphonium acetate $[P_{14444}][OAc]$ were synthesized by anion metathesis described in previous articles [22,310]. Tributylmethylphosphonium acetate $[P_{4441}][OAc]$, tributylmethylphosphonium hexanoate $[P_{4441}][C_5H_{11}COO]$, tributylmethylphosphonium decanoate $[P_{4441}][C_9H_{19}COO]$, tributylmethylphosphonium tetradecanoate $[P_{4441}][C_{13}H_{27}COO]$, tributylmethylphosphonium hexadecanoate $[P_{4441}][C_{15}H_{31}COO]$, and tributylmethylphosphonium octadecanoate $[P_{4441}][C_{17}H_{35}COO]$, were synthesized from tributylmethylphosphonium methyl carbonate.

The appropriate Brønsted acid (1.0 equiv) was added to the starting material at room temperature to yield the corresponding anion exchange salt. The mixture was stirred overnight, rotary evaporated to remove methanol and kept under vacuum for 2 hours at 40 ºC for removal of trace solvent impurities. Metathesis was determined to be complete and the purity was assessed using 1H NMR (300 MHz Varian spectrometer) as shown in Supporting Information (SI Figure S1 -Figure S6). The synthesized ILs were stored at room temperature.

3.1.3.1. Animals

Zebrafish of the Turku line [322–324] were fed, bred, and maintained according to an established protocol [325]. Fish were used right after fertilization (n = 2250), 2.5 months post fertilization (mpf, n = 48), and 5 mpf (n = 48). The permits for the experiments were obtained from the Office of the Regional Government of Southern Finland in agreement with the ethical guidelines of the European convention.

3.1.3.2. Toxicity Analysis of Zebrafish

Zebrafish embryos from at least four different fish pairs per batch were collected right after fertilization and transferred in groups of 30 to 6-well plates with IL solutions. Two concentrations were chosen of all ILs based on some commonly used toxicity ranges (United Nations globally harmonized system of classification and labelling of chemicals; acute toxicity toward aquatic environment) [326]. ILs were added as follows: 1 and 100 $mg \cdot L^{-1}$ of [emim][OAc], [DBNH][OAc], $[P_{4441}][OAc]$, $[P_{4444}][OAc]$, $[P_{8444}][OAc]$, $[P_{14444}][OAc]$, $[P_{4441}][C_5H_{11}COO]$, and $[P_{4441}][C_9H_{19}COO]$ in 3 mL of E3 medium and 1 and 10 $mg \cdot L^{-1}$ of $[P_{4441}][C_{13}H_{27}COO]$, $[P_{4441}][C_{15}H_{31}COO]$, and $[P_{4441}][C_{17}H_{35}COO]$ in 3 mL of E3 medium. Different concentrations were used for ILs containing tetradecanoate, hexadecanoate, and octadecanoate anions due to precipitation of ILs at concentrations above 10 $mg \cdot L^{-1}$. Each well plate contained a control group and the plates were incubated at 28 °C and illuminated for 14 hours per day. ILs were changed daily and dead fish were removed from the plates. The phenotypic malformations and mortality of the embryos were noted 10 min after IL addition and after 24, 48, 72, 96, and 120 hours after IL addition. All measurements were performed as triplicates (90 embryos per one IL concentration).

3.1.3.3. Behavioural Assay

In order to get an insight into the behavioural alteration of the zebrafish, the locomotor activity of 5 dpf larvae (n>16) was recorded for 10 min. In addition, long-term impact of

[DBNH][OAc] and [P_{4441}][OAc] ILs on the behaviour of 2.5 mpf zebrafish (n=16 per IL group) was estimated by assessing differences in locomotor activity (1 – 11 min after fish addition), aggressiveness (1 – 11 min and 30 – 40 min after novel object addition), and boldness (1 – 11 min and 30 – 40 min after fish addition) of zebrafish. All data were analysed with the EthoVision software (Noldus Information Technologies) as described earlier [327]. Detailed information can be found in the SI, page 108-109.

3.1.3.4. Histological Examination

To reveal possible effects of ILs on reproductive organs, liver, gills, and intestines, a histological examination was conducted for [DBNH][OAc]- and [P_{4441}][OAc]- treated IL groups and for a control group. An invert light microscope, Leica DM IRB, with Leica Application Suite, Multifocus option (Leica Microsystems GmbH) was used to visualize and acquire pictures of the zebrafish organs. See SI for details (page 109-110).

3.1.3.5. Cell Culture Preparation

CHO-K1 cells were grown in T-flask with Ham's F12 containing 10% of FBS. More details can be found in the SI on page 110.

3.1.3.6. Determination of Critical Micelle Concentration

The CMC determinations in water, in sodium phosphate buffer, and in E3 medium, were performed with a contact angle meter (CAM 200 Optical Contact Angle Meter, Biolin Scientific, KSV Instruments, Finland) using an optical pendant drop method. In comparison, the CMCs for the anionic ILs in water were determined by capillary electrophoresis (CE) using a Hewlett-Packard ^{3D}CE system (Agilent, Waldbronn, Germany). More details can be found in SI, page 111. The methods are described in more detailed in our previous articles [22,328].

3.1.4. Results and Discussion

3.1.4.1. Viability of Zebrafish Embryos

The impact of cationic and anionic ILs on the viability of zebrafish embryos and larvae was assessed by growing the fish in IL solutions for 5 days post fertilization, shown in SI Figure S7. All measurements were repeated three times and the errors are given as standard error means (SEM). Two-way RM ANOVA with Dunnett's multiple comparison test was used to assess the significance of the IL treatment on fish viability (time × treatment interaction, 2-way RM ANOVA, $p < 0.0001$, Figure 61A, B, and D).

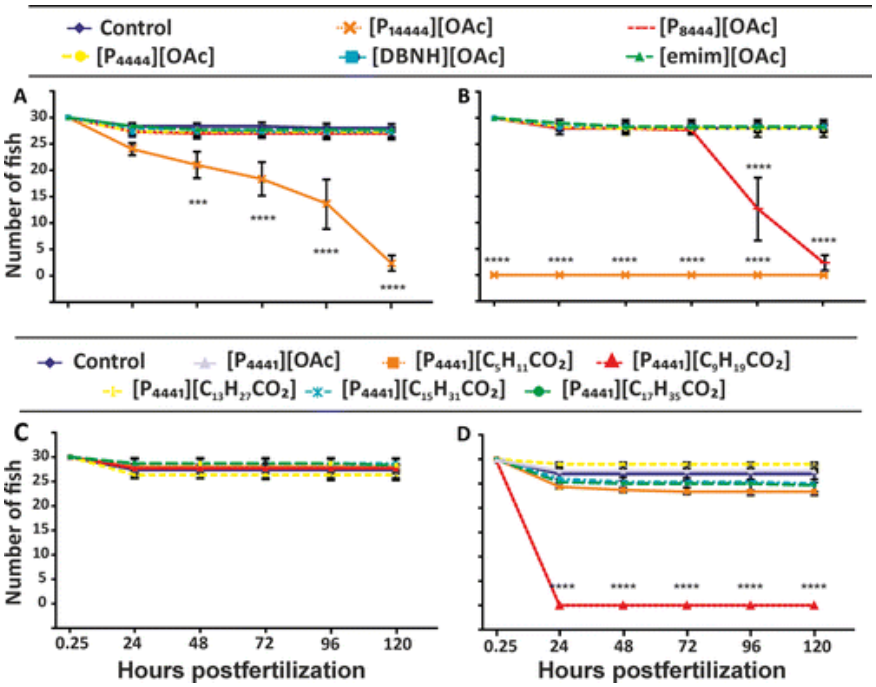

Figure 61: Viability of zebrafish embryos: Two-way RM ANOVA with Dunnett's multiple comparison test. Time × treatment interaction, $p < 0.0001$, n = 30 at initial time point. Results are presented as mean ± SEM. ***$p < 0.001$ and ****$p < 0.0001$. A) Effect of 1 mg·L^{-1} cationic ILs. B) Effect of 100 mg·L^{-1} cationic ILs. C) Effect of 1 mg·L^{-1} anionic ILs, and D) effect of 100 mg·L^{-1} ([P_{4441}][C_n H_{2n+1}COO]; n ≤ 9) and 10 mg·L^{-1} ([P_{4441}][C_n H_{2n+1}COO]; n ≥ 13) anionic ILs on the viability of zebrafish embryos and larvae during 5 days postfertilization

Results for cationic ILs are shown in Figure 61A (1 mg·L^{-1}) and Figure 61B (100 mg·L^{-1}) and results for anionic ILs are shown in Figure 61C (1 mg·L^{-1}) and Figure 61D (10 mg·L^{-1} for ([P_{4441}][C_nH_{2n+1}COO]; n ≥ 13 and 100 mg·L-1 for [P_{4441}][C_nH_{2n+1}COO]; n ≤ 9). In addition, the results are summarized in Table 1.

Table 1: Critical micelle concentrations and EC_{50} values: Of ILs, and significance of ILs on zebrafish malformation

	CMC ($mg \cdot L^{-1}$) [mM]				EC_{50} ($mg \cdot L^{-1}$) [mM]		Significant malformation[c]		
	Optical pendant drop method			CE	Zebrafish[a]	CHO cells[b]			
	water	Sodium phosphate buffer	E3 medium	water			1 $mg \cdot L^{-1}$	10 $mg \cdot L^{-1}$	100 $mg \cdot L^{-1}$
$[P_{14444}][OAc]$	408 ± 3 (0.89 ± 0.01)	148 ± 14 (0.32 ± 0.03)	131 ± 7 (0.29 ± 0.02)	nd	< 1	2.54 ± 0.85 (0.0055 ± 0.0019)	mild*	nd	dead
$[P_{8444}][OAc]$	29196 ± 753 (77.94 ± 2.01)	31225 ± 2776 (83.36 ± 7.41)	28968 ± 1106 (77.33 ± 2.95)	nd	< 100	54 ± 2 (0.14 ± 0.01)	No	nd	mild*
$[P_{4444}][OAc]$	91073 ± 3793 (292 ± 12)	nd	nd	nd	> 100	1399 ± 498 (4.48 ± 1.59)	No	nd	No
[DBNH][OAc]	nd	nd	nd	nd	> 100	13356 ± 858 (72.51 ± 4.66)	No	nd	No
[emim][OAc]	nd	nd	nd	nd	> 100	16717 ± 1379 (98.22 ± 8.10)	No	nd	No
$[P_{4441}][OAc]$	82214 ± 2966 (297 ± 11)	nd	nd	nd	> 100	982 ± 220 (3.55 ± 0.80)	No	nd	No
$[P_{4441}][C_5H_{11}COO]$	108889 ± 2382 (327 ± 7)	nd	nd	nd	> 100	3209 ± 355 (9.65 ± 1.07)	No	nd	severe**
$[P_{4441}][C_9H_{19}COO]$	1494 ±45 (3.85 ± 0.12)	3093 ± 65 (7.96 ± 0.17)	n/a	1889 (4.86)	< 100	201 ± 35 (0.52 ± 0.09)	No	nd	dead
$[P_{4441}][C_{13}H_{27}COO]$	830 ± 116 (1.87 ± 0.26)	536 ± 42 (1.21 ± 0.09)	n/a	1014 (2.28)	> 10	173 ± 98 (0.39 ± 0.22)	No	No	nd
$[P_{4441}][C_{15}H_{31}COO]$	332 ± 40 (0.70 ± 0.08)	n/a	n/a	662 (1.40)	> 10	461 ± 257 (0.97 ± 0.54)	No	No	nd
$[P_{4441}][C_{17}H_{37}COO]$	394 ± 54 (0.79 ± 0.11)	n/a	n/a	301 (0.60)	> 10	673 ± 48 (1.34 ± 0.10)	No	No	nd

nd – not determined; n/a – determined, but no data obtained

[a]after 5 days of IL treatment

[b]after 24 hours of incubation with ILs

[c]two-way ANOVA with Dunnett's multiple comparison test (*$p<0.05$ and **$p<0.01$)

100 mg·L^{-1} of [P_{14444}][OAc] was lethal to all embryos within 10 min (Figure 61B) and after 48 hours a concentration of 1 mg·L^{-1} of the IL had a significant effect (***p < 0.001) on the fish, decreasing the fish number to 21 (Figure 61A). Furthermore, only 0 - 5 fish were alive after 120 hours of treatment with 1 mg·L^{-1} of [P_{14444}][OAc], indicating that the median effective concentration (EC_{50}) value, after 5 days of treatment, was < 1 mg·L^{-1}. The EC_{50} is defined as a concentration which causes 50% of the desired effect on the test group. Due to the low EC_{50}, [P_{14444}][OAc] can be assigned to category Acute 1 of the united nations globally harmonized system (GHS) of classification and labelling of chemicals [326], indicating high acute toxicity. After 96 hours post treatment 100 mg·L^{-1} of [P_{4441}][C_9H_{19}COO] and [P_{8444}][OAc] were lethal to all the embryos (****p < 0.0001) (Figure 61B and D) but not toxic at all when embryos were treated with a 1 mg·L^{-1} concentration of the ILs (Figure 61A and C). In addition, referring to the GHS, [P_{4441}][C_9H_{19}COO] and [P_{8444}][OAc] are hazardous to the aquatic environment, and belong to category Acute 2 (1 mg·L^{-1} < EC_{50} ≤ 10 mg·L^{-1}) or 3 (10 mg·L^{-1} < EC_{50} ≤ 100 mg·L^{-1}) [326]. The lethal effect of [P_{4441}][C_9H_{19}COO] and [P_{8444}][OAc] occurred after 24 hours and after 72 hours post treatment, respectively, indicating that [P_{4441}][C_9H_{19}COO] is penetrating faster into the embryo chorions killing the embryos. Therefore, [P_{4441}][C_9H_{19}COO] can be considered to be more toxic than [P_{8444}][OAc], which initializes larvae mortality after the larvae are hatched from their protecting chorions. Most of the zebrafish embryos hatch from their chorions during the third day postfertilization [329], causing the embryos to be in direct contact with their environment. It has been shown that e.g. cationic polymers of high molar weights [330] are blocked by the chorions, which delay their toxic impact. It is inevitable that the long alkyl chain with increasing hydrophobicity is affecting the toxicity of the ILs by making the substances more penetrable to the larvae. Even though it is known that the cation structure is more relevant than the anion moiety when assessing the toxicity of ILs [10], hydrophobic anions with long alkyl chain lengths can in addition penetrate into the organism. This can furthermore cause cell damage and death. Long anionic ILs ([P_{4441}][C_nH_{2n+1}COO] n ≥ 13) did not have any significant effect on the viability of the zebrafish embryos and larvae during 5 dpf, which is due to the low concentrations used (precipitation occurred at concentrations above 10 mg L^{-1}). The rest of the ILs did not have any significant effect on the viability of the zebrafish during 5 dpf at the tested concentrations, indicating that the EC_{50} values of the long alkyl chained anionic (C ≥ 14) ILs were above 10 mg·L^{-1} and above 100 mg·L^{-1} for rest of the anionic ILs.

3.1.4.2. Effect of ILs on Zebrafish Larval Malformations

The effect of ILs on the malformation in the fish phenotype was assessed by dividing all the 5 dpf fish into three groups by their phenotypic malformations (SI Table S1): no malformations, mild malformations, and severe malformations (SI Figure S8A, B, and C, respectively). The group exhibiting mild malformations had bent tail, short trunk, mild deformation in the head area, yolk sac edema, and pericardium edema, while the group with severe malformation had severely defective (short and curved) trunk development, truncated tail, small eyes, deformations in the head area, and yolk sac edema. The effect on the phenotype of the 5 dpf larvae could not be assessed for the most toxic ILs (100 $mg \cdot L^{-1}$ of $[P_{14444}][OAc]$ and 100 $mg \cdot L^{-1}$ of $[P_{4441}][C_9H_{19}COO]$) due to their lethal impact. Two-way ANOVA with Dunnett's multiple comparison test was used to assess the significance of the IL treatment on the fish phenotype. The total number of fish (n) included into the assay after 5 days of IL treatment is given in the brackets. Long alkyl chained $[P_{14444}][OAc]$ at 1 $mg \cdot L^{-1}$ and $[P_{8444}][OAc]$ at 100 $mg \cdot L^{-1}$ caused mild malformation on the larvae (two-way ANOVA $*p < 0.05$; n = 10 and $**p < 0.01$; n = 7, respectively) and 100 $mg \cdot L^{-1}$ of $[P_{4441}][C_5H_{11}COO]$, which had the highest concentration of the anionic ILs, was the sole IL causing severe malformation on the zebrafish larvae ($*p < 0.05$; n = 120). Furthermore, long alkyl chained ILs ($[P_{4441}][C_{15}H_{31}COO]$ and $[P_{4441}][C_{17}H_{35}COO]$) caused mild and severe malformations on the fish, however the results were statistically insignificant and they can as well be caused by biological variance in addition to the effect of ILs. The results are summarized in Table 1. The ILs causing malformations were also the most lethal ones towards zebrafish, thus explaining the low amount of fish included in the assay.

3.1.4.3. Behavioural Analysis

Different species exhibit several syndromes, which maintain individual differences in behaviour as an outcome of natural selection [331]. These differences reflect heritable, fundamentally different alternative strategies to cope with environmental changes. Aggressive individuals show an active response to an external stimulus, whereas non-aggressive individuals adopt a passive strategy. However, different external alterations may have an impact on the behaviour of individuals. Aggression-boldness syndrome has been described in many animals, such as mammals [332], birds [333], and fish [334–337]. According to aggressive-boldness syndrome, animals that are more aggressive will, in addition, be bolder and more explorative in novel environments. Zebrafish possess also this correlation between aggressiveness and boldness and is exhibited by both sexes [337]. In

this study the effect of ILs on the behaviour of zebrafish was assessed. First the effect of ILs on the locomotor activity of zebrafish was tested using 5 dpf larvae and secondly 2.5 mpf fish, treated 5 days post fertilization with [DBNH][OAc] and $[P_{4441}][OAc]$ in concentration of 100 $mg \cdot L^{-1}$, were chosen for further studies. [DBNH][OAc] and $[P_{4441}][OAc]$ were chosen to the long-term tests due to their excellent biomass dissolving potential. [DBNH][OAc] has been shown to dissolve high concentrations of cellulose at moderate temperatures. Moreover, the cellulose could be afterwards spun into fibres with excellent mechanical properties, thus making them suitable as a reinforcing material in composite structures and for textile applications [314,338,339]. The $[P_{4441}]^+$ cation, on the other hand, is promising for wood dissolution and $[P_{4441}][MeSO_4]$ has been shown to dissolve lignin efficiently [340]. In addition, to locomotor activity measurements, aggressiveness, and boldness were assessed using different measurement protocols.

3.1.4.3.1. 5 dpf larvae

Fish treated with 100 and 1 $mg \cdot L^{-1}$ of $[P_{14444}][OAc]$, 100 $mg \cdot L^{-1}$ of $[P_{8444}][OAc]$, and 100 $mg \cdot L^{-1}$ of $[P_{4441}][C_9H_{19}COO]$ were not included in this study because they were dead or dying. From the swimming patterns, total and maximum distance moved, turn angle, angular velocity, and turns per distance (meander) were measured. All errors are given as SEM and all measurements were repeated three times. IL-treated zebrafish larvae did not experience any major effects after the IL treatment. However, larvae, grown in 100 $mg \cdot L^{-1}$ of $[P_{4441}][OAc]$ solution, swam 30 % shorter distance in total (38.38 ± 11.11 cm, n = 23 – 78, $^{**}p < 0.01$, SI Figure S9, top right graph) than the control fish. Larvae grown in 10 $mg \cdot L^{-1}$ of $[P_{4441}][C_{13}H_{27}COO]$ solution swam 23 % longer continuous distance (0.14 ± 0.05 cm, n = 21 – 73, $^{*}p < 0.05$) than the control larvae (SI Figure S9, bottom right graph). However, there were no significant effect on the other behavioural tests (turn angle, angular velocity, and meander) indicating that the ILs did not have any significant impact on the locomotor activity of zebrafish larvae.

3.1.4.3.2. 2.5 mpf fish

In all behavioural analysis frequency (how many times fish initialize movement), total duration at the zone, total and maximum distance moved, and latency of first occurrence at the zone were recorded for 10 minutes.

In the locomotor activity analysis (Figure 62Ai) the tanks were divided into three different zones and the swimming patterns were recorded 2 minutes after fish addition. All fish spent

most of the time at the outer zone near the tank wall, due to their natural survival instinct, and there were no significant differences between the IL-treated groups and the control groups (Figure 62B). Boldness of the zebrafish was assessed measuring time spent close to novel object using a protocol from Wright *et al.* [341]. In the novel object analysis the fish activity was measured from two different zones (seen in Figure 62Aii), right after the novel object was added (15 minutes after fish addition) and after 30 minutes of novel object addition. Fish spent more time in the zone away from the novel object, as expected, indicating a cautious approach towards new objects but no signs of aggressive behaviour. Furthermore, there were no significant differences in the fish behaviour between the IL treated groups and control group (Figure 62C).

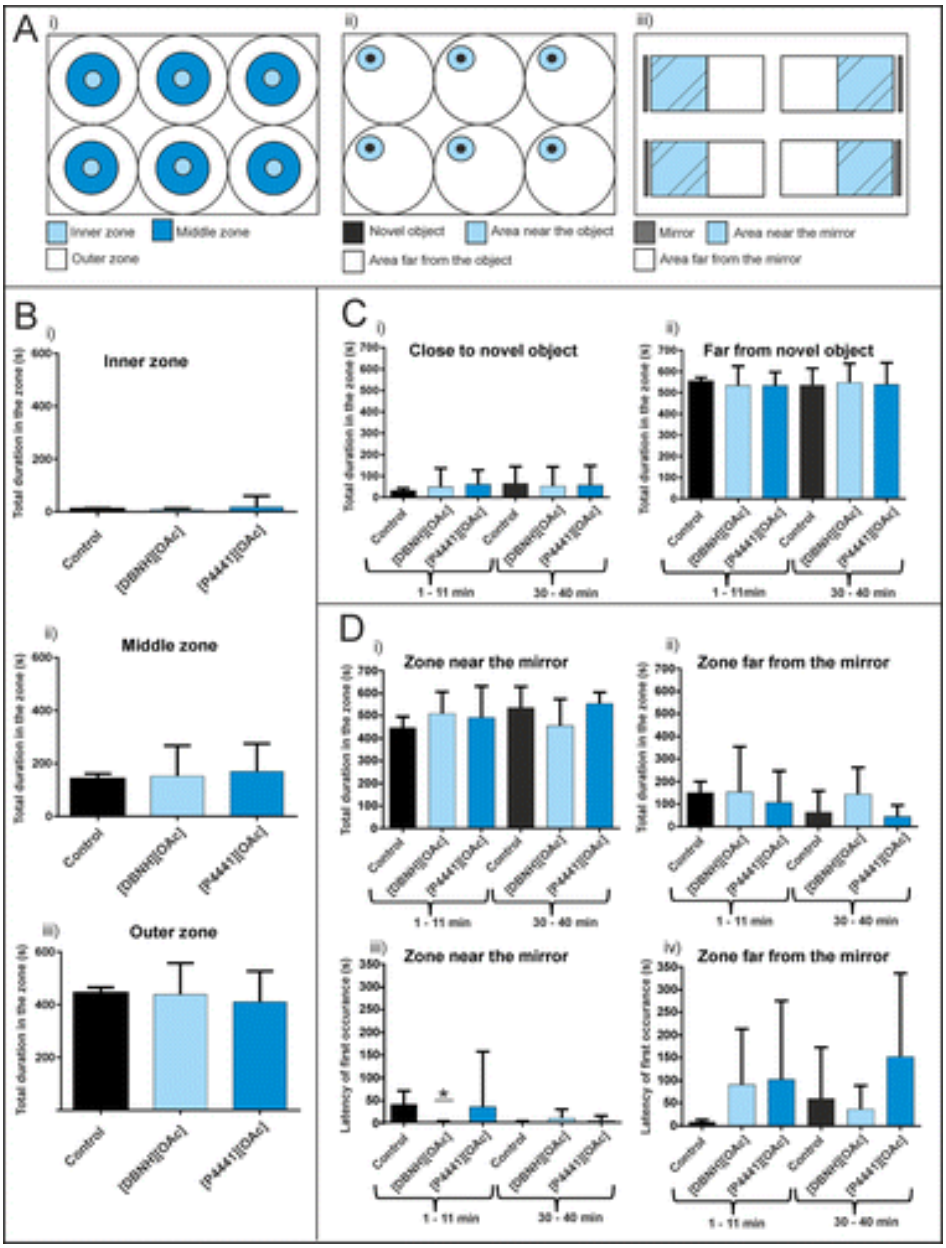

Figure 62: Assessing the aggressive-boldness syndrome of 2.5 mpf zebrafish: Graphed values are means ± SEM. A) Schematics of tanks used to measure IL effect on fish i) locomotor activity, ii) novel object boldness, and iii) aggressive behaviour. B) Total duration spent in different zones when assessing the locomotor activity. One-way ANOVA test with Dunnett's multiple comparison test, n = 15 wild-type, n = 8 [DBNH][OAc], and n = 13 [P_{4441}][OAc]. C) Total duration spent near the novel object when assessing the novel object boldness. One-way ANOVA test with Dunnett's multiple comparison test, n = 12 wild-type, n = 9 [DBNH][OAc] and n = 12 [P_{4441}][OAc] (1 – 11 min. period); n = 14 wild-type, n = 10 [DBNH][OAc] and n = 13 [P_{4441}][OAc] (30 – 40 min. period). D) Total duration spent and latency of first occurrence near and far from the mirror when assessing the zebrafish aggressiveness. Kruskal-Wallis test with Dunn's multiple comparison test, n = 12 wild-type, n = 7 [DBNH][OAc] and n = 13 [P_{4441}][OAc] (1 – 11 min. period); n = 8, n = 9 [DBNH][OAc], and n = 11 [P_{4441}][OAc] (30 – 40 min. period)

To assess the aggressiveness of the zebrafish a protocol from Norton *et al.* was applied [335,342]. Fish are unable to recognize their own mirror reflection and therefore they attack the mirror as if they would recognize an intruder [343]. In the mirror assay (Figure 62Aiii) the swimming patterns were measured after 1 and 30 minutes of

familiarization. All fish spent more time in the mirror zone and no significant changes were seen in the behaviour, except for fish treated with [DBNH][OAc]. The latency of first occurrence in the mirror zone was significantly lower for [DBNH][OAc]-treated fish than with control fish (Figure 62Diii, $p^*<0.05$), however, the total duration of [DBNH][OAc]-treated fish spent in the mirror zone was not different than with the control fish, indicating that the total effect of [DBNH][OAc] on the zebrafish was insignificant. In addition, control fish occurred more likely in the mirror zone after fish addition than the rest of the groups.

3.1.4.4. Histological Examination

Due to the small amount or the lack of spawning with IL-treated fish (see SI, page 113-114), the histological examination was concentrated on gonads. In previous works, ILs have been shown to effect skin, gill, and intestine of gold fish at various developmental stages [344,345]. Therefore, gills, intestines, and liver were photographed and examined. The stages of the whole ovaries were assessed and postovulatory follicles (POF) were searched. At the post spawning state (female fish has ovulated) POFs appear. POFs are remains of the ovarian follicles, shown in SI Figure S10, that occur in fish ovaries after spawning. All zebrafish have similar spawning stages indicating that their ovaries should be in similar stages when they are killed at the same time. All the control fish were at mid- or latevitollegenic stage and all of them had POFs in the ovaries, indicating reproductive capability.

The ovaries of $[P_{4441}][OAc]$-treated fish were in the midvitellogenic stage and all contained POFs. The ovaries of [DBNH][OAc]-treated fish contained slightly less matured oocytes but all of them also contained POFs. There were no significant differences between the ovaries of the control fish and the IL-treated fish. In addition, there was no change in the liver, gill, or intestine tissue.

3.1.4.5. Cytotoxicity of Ionic Liquids toward Chinese Hamster Ovary Cells

In order to evaluate the extent of IL toxicity, the EC_{50} values were determined using CHO cells. CHO cells are epithelial cells which grow as an adherent monolayer in culture. The cell cultures were treated with various concentrations of ILs and the viability was measured using an alamarBlue assay. The results are shown in Figure 63 and summarized in Table 1.

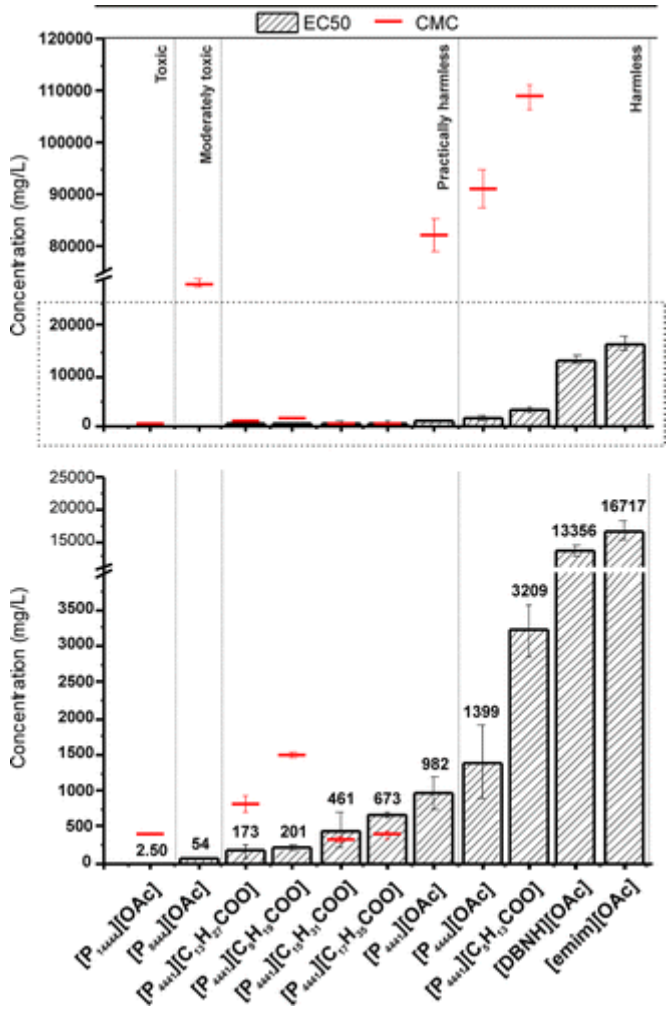

Figure 63: Cellular toxicity of ILs on CHO cells – EC_{50} values and CMCs: The cells were incubated for 24 hours with the selected ILs at various concentrations, and the cytotoxicity was assessed by an alamarBlue assay after 2 hours of the alamarBlue addition. The marked area in the upper figure is enlarged in the lower figure

Based on the GHS classification system [326] and the recently proposed classification by Ventura *et al.* [53], the IL toxicity was classified into 5 categories: 1 “highly toxic” (< 1 mg L^{-1}), 2 “toxic” (1–10 mg·L^{-1}), 3 “moderately toxic” (10–100 mg·L^{-1}), 4 “practically harmless” (100-1000 mg·L^{-1}), and 5 “harmless” (>1000 mg·L^{-1}). The most toxic ILs in this study were cationic $[P_{14444}][OAc]$ and $[P_{8444}][OAc]$ (EC_{50} = 2.5 ± 0.85 mg·L^{-1} and 54 ± 2 mg·L^{-1}, respectively) and they can be classified as “toxic” and “moderately toxic”, respectively. When the longest alkyl chain length was reduced to 4 ($[P_{4444}][OAc]$ and $[P_{4441}][OAc]$) the EC_{50} increased significantly making the ILs less toxic (“practically harmless” or “harmless”). This indicates that even a small increase in the alkyl chain length of the IL cation increases the cell mortality and toxicity of the ILs. The results are in accordance with our previous study when assessing the cytotoxicity of ILs on human corneal epithelial cells (HCE) and *Escherichia coli* (E.coli) cells [22]. Anionic $[P_{4441}][C_{13}H_{19}COO]$ with same number of carbons

in its longest alkyl chain as the most toxic [P_{14444}][OAc] had over 70 times higher EC_{50} value (173 ± 98 mg L^{-1}) and could be classified as “practically harmless”. Moreover, longer chained [P_{4441}][$C_{15}H_{31}COO$] and [P_{4441}][$C_{17}H_{35}COO$] had even higher EC_{50} values (461 ± 257 mg L^{-1} and 673 ± 48 mg L^{-1}), indicating that elongation of the alkyl chain length in the IL anion has considerably less impact on the toxicity of ILs than elongation of the alkyl chain length in the IL cation. This, therefore, highlights the importance of the location of the hydrophobic chain when assessing the toxicity of ILs. Moreover, increasing the anion chain length instead of the cation chain length might help to maintain the unique extraction properties of ILs without increasing the ILs’ toxicity significantly. When comparing the toxicity results, some ILs (i.e. [P_{14444}][OAc] and [P_{4441}][$C_9H_{19}COO$]) were noticed to be more toxic towards zebrafish embryos than towards CHO cells. This can be explained by the difference of the tested organisms. Even though, zebrafish embryos are used as a simple mammalian model, they are much more complex than bare cells. The cytotoxicity of anionic ILs did not increase as a function of alkyl chain length elongation. In order to figure out whether the aggregation behaviour of the ILs affects their cytotoxicity, the CMC values of the ILs were determined.

3.1.4.6. Critical Micelle Concentration

Addition of a surfactant above the CMC value leads to the formation of micelles of various sizes depending on the used concentration. Due to the fact that ILs may have different properties and interactions with lipid bilayers depending whether they are occurring as monomers or aggregates, the CMC values were determined to all ILs that were able to form aggregates (more information in SI, page 115). The CMC values for the anionic ILs (i.e. [P_{4441}][$C_9H_{19}COO$], [P_{4441}][$C_{13}H_{27}COO$], [P_{4441}][$C_{15}H_{31}COO$], and [P_{4441}][$C_{17}H_{35}COO$]) were determined in water and in phosphate buffer using a contact angle meter (the pendant drop method), as well as in water using a CE instrument. Furthermore, in order to get information on whether the long anion alkyl chained ILs adsorb on the fused silica capillary wall, the electroosmotic flow was measured using different concentrations of the ILs in phosphate buffer (see SI, pages 116 – 117). The CMC values for the cationic ILs, excluding [emim][OAc] and [DBNH][OAc], which do not aggregate or the aggregation cannot be determined by the methods used in this study, were determined in water (and in sodium phosphate buffer and in E3 medium, in some cases) using the pendant drop method. The CMCs are presented in Figure 63 and summarized in Table 1.

The CMC values of anionic ILs ([P_{4441}][$C_nH_{2n+1}COO$], n ≥ 9) in E3 medium and long alkyl chained anionic ILs ([P_{4441}][$C_nH_{2n+1}COO$], n ≥ 15) in sodium phosphate buffer could not be determined because of precipitation in the solvent. ILs with long alkyl chain lengths (C ≥ 10) aggregated fast (see SI Figure S11A), while ILs with relatively short alkyl chain lengths (C ≤ 8, SI Figure S11B) did not show any abrupt decrease in their surface tension, which indicates that, in addition of assembling at the surface of the drop, the additional monomers aggregate to unspecified oligomers as shown before [328,346]. The aggregation of these ILs seem to contain several different steps and therefore the term critical aggregation concentration (CAC) describes the aggregation behaviour better than critical micelle concentration. However, to simplify the text all critical aggregation values are called CMCs. Moreover, the CMCs for ILs given in Table 1 are concentrations after which no change occurs in the surface tension i.e. all additional monomers are aggregating or are included in preformed aggregates.

CMC values obtained using CE were in good agreement with the values obtained by the optical pendant drop method. However, the change in the current caused by the aggregation is hardly distinguishable, especially with ILs having high CMC values and therefore the optical pendant drop method is preferred.

The lower CMCs of the ILs in sodium phosphate buffer and in the E3 medium than in water are caused by the increasing concentration of salt ions, which compress the electric double layer surrounding the IL micelles reducing the repulsion between polar head groups and stabilizing the aggregates [347,348]. The only exception is [P_{4441}][[$C_9H_{19}COO$] which has a slightly lower CMC in water than in sodium phosphate buffer. [P_{4441}][[$C_9H_{19}COO$] and [P_{4441}][[$C_{13}H_{27}COO$] both precipitated in the sodium phosphate buffer, which causes uncertainty in the surface tension determination.

All ILs, except [P_{4441}][$C_{15}H_{31}COO$] and [P_{4441}][$C_{17}H_{35}COO$], had their EC_{50} values below their CMC values, indicating a direct sorption of ILs onto/into the CHO cells and zebrafish already in their monomeric form. This is expected due to the fact that hydrophobic moiety of the IL prefers a hydrophobic environment and is therefore easily penetrated into the lipid bilayer. However, in the case of [P_{4441}][$C_{15}H_{31}COO$] and [P_{4441}][$C_{17}H_{35}COO$] the CMCs were lower than the EC_{50} values, indicating that the ILs, with chain lengths [P_{4441}][$C_nH_{2n+1}COO$] n ≥ 15, prefer self-aggregation over interaction with the cell walls, thus biasing the EC_{50} towards higher values making them less toxic.

The results show the effect of various ILs, with varying cation and anion structures, on zebrafish and Chinese hamster ovary cells. Cationic ILs with long alkyl chains, i.e. $[P_{14444}][OAc]$ and $[P_{8444}][OAc]$ and an anionic ILs $[P_{4441}][C_{13}H_{27}CO_2]$ and $[P_{4441}][C_9H_{19}CO_2]$ were the most toxic ILs. $[P_{14444}][OAc]$ and $[P_{8444}][OAc]$ caused mild malformations and $[P_{4441}][C_5H_{11}COO]$ at the highest concentration caused severe malformation on zebrafish phenotype, indicating that they cannot be considered safe to the aquatic environment. Most of the phosphonium based ILs can be classified as “practically harmless” and [DBNH][OAc] and [emim][OAc] can be classified as “harmless”.

There was no significant change in the behaviour of the 5 dpf zebrafish after IL treatment and there were no significant alterations in the behaviour of [DBNH][OAc] and $[P_{4441}][OAc]$ treated 2.5 mpf fish, indicating that the ILs did not reinforce aggressive or bold behaviour. In addition, there was no significant impact of the ILs on the breeding capability or on the histology of the 2.5 mpf fish when the applied concentrations and protocols were used. CMCs were determined for ILs able to aggregate, using CE and contact angle meter and both techniques were in good agreement with each other. Moreover, the optical pendant drop method was found to be the most suitable technique for the IL aggregation studies in a variety of solvents. Most of the ILs interacted with the tested organisms in their monomeric form inducing mortality. The elongation of the anion moiety ($[P_{4441}][CnH_{2n+1}COO]$ $n \geq 15$) increased the viability of the cells by self-aggregation of the ILs. Therefore, by increasing the anion alkyl chain length, instead of cation alkyl chain length, it is possible to increase IL hydrophobicity without significantly increasing the IL toxicity. In general, elongation of the anion moiety caused less impact on the zebrafish and CHO cells than elongation of the cation moiety.

Regarding the extensive synthesis and utilization of ILs in various applications the information of IL toxicity is essential. The proposed experiments offer crucial information about the acute toxicity of ILs and furthermore they offer a convenient way to assess information about long-term exposure effects of ILs in aquatic environments.

3.1.5. Supporting information

Effect of ionic liquids on zebrafish (Danio rerio) viability, behaviour, and histology; correlation between toxicity and ionic liquid aggregation

3.1.5.1. Chemicals

CHO-K1 cells, Ham's F12, and Ham's F12 media supplement with 10% fetal bovine serum (FBS) were from CLS cell line services GmbH (Eppelheim, Germany). Trypsin/EDTA and Trypan blue (T8154) were purchased from Sigma-Aldrich (Steinheim, Germany), alamarBlue was purchased from Invitrogen and phosphate buffered saline (PBS) was from Life Technologies (Paisley, United Kingdom). Cell culture ware was purchased from Greiner BioOne (Frickenhausen, Germany). Sodium dihydrogen phosphate was from Mallinckrodt Baker (Deventer, The Netherlands) and sodium hydrogen phosphate was purchased from Sigma (Darmstadt, Germany). The pH solutions (7 and 10) used for calibrating the pH meter were purchased from Merck (Darmstadt, Germany). Paraformaldehyde (PFA; 4%) was purchased from Sigma and Mayer's Hemalum solution (hematoxylin) and Eosin G dye was purchased from (Merck). Fish growing medium, E3 medium, comprised 5.00 mM of sodium chloride (Riedel-de Haën), 0.17 mM of potassium chloride (Sigma), 0.44 mM of calcium chloride dehydrate (Sigma), and 0.33 mM of magnesium sulfate heptahydrate (Merck). Phosphate-buffered saline (PBS) (pH 7.4, I = 0.1 M) containing 8.0 g of sodium chloride, 0.2 g of potassium chloride, 1.4 g of disodium hydrogen phosphate dihydrate (Merck), and 0.2 g of potassium dihydrogen phosphate (J. T. Baker) in 1 L was prepared in the laboratory. The Brønsted acids hexanoic acid, tetradecanoic acid, and stearic acid were purchased from Fluka AG (Buchs, Switzerland), while decanoic acid was from Sigma-Aldrich and tetradecanoic acid was from Riedel-de Haën.

3.1.5.2. Ionic liquid sample and buffer preparations

All the diluted IL samples were prepared as w/v by adding appropriate amount of E3 medium, water, Ham's F12 medium or sodium phosphate buffer. For the EC_{50} determinations eight concentrations, prepared as binary dilutions with eight repetitions, were chosen for all ILs above and below the EC_{50} values. All measurements were repeated at least two times. Anionic ILs with chain lengths $[P_{4441}][C_nH_{2n+1}COO]$ $n \geq 13$, did not dissolve totally in the cell medium and required heating and sonication when dilution series were prepared. Sodium phosphate buffer (pH 7.4, I = 10 mM) was prepared by mixing sodium hydrogen phosphate and sodium dihydrogen phosphate to yield an ionic strength of 10 mM

and a pH of 7.4. The buffer solution was filtered through a 0.45-µm syringe filter (Gelman Sciences, Ann Arbor, MI, USA) before use. Sodium phosphate buffer was used as a background electrolyte solution for all the CE runs and as a solvent in the CMC determinations.

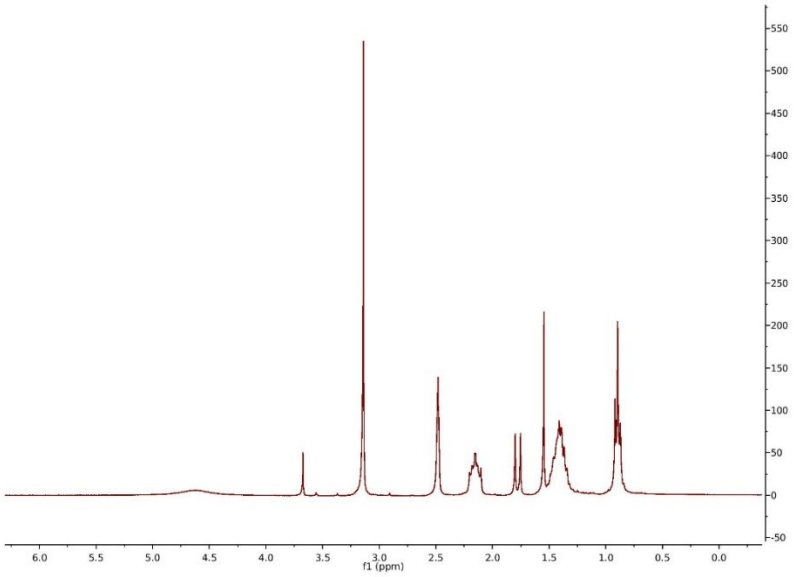

Figure S1: ^{1}H NMR spectrum of [P_{4441}][OAc]: (300MHz, DMSO) δ0.89 (9H, t, CH3), δ1.5- δ 1.3 (12H, m), δ1.55 (3H, s), δ1.8 (3H, d), δ 2.15 (6H, q)

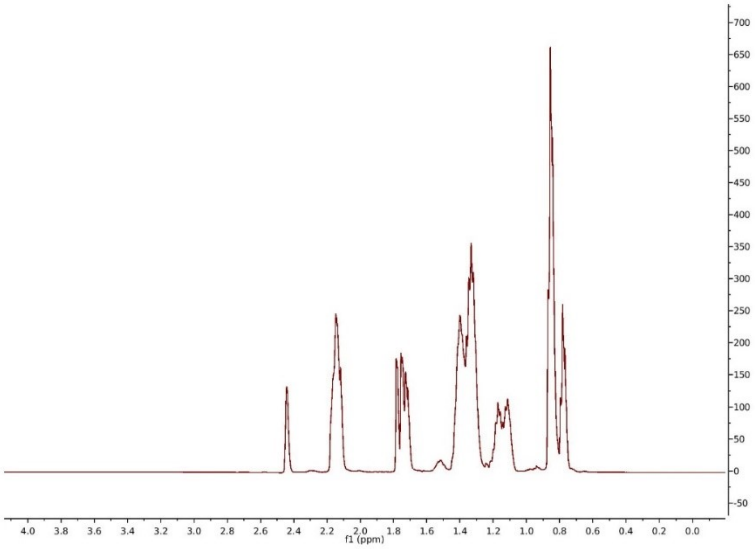

Figure S2: ^{1}H NMR spectrum of [P_{4441}][$C_5H_{11}COO$]: (300MHz, DMSO) δ0.82 (3H, t), δ 0.89 (9H, t), δ 1.28- δ 1.1 (6H, m), δ 1.55- δ 1.28 (12H, m), δ 1.74 (2H, t), δ 1.8 (3H, d), δ 2.08- δ 2.25 (6H, m)

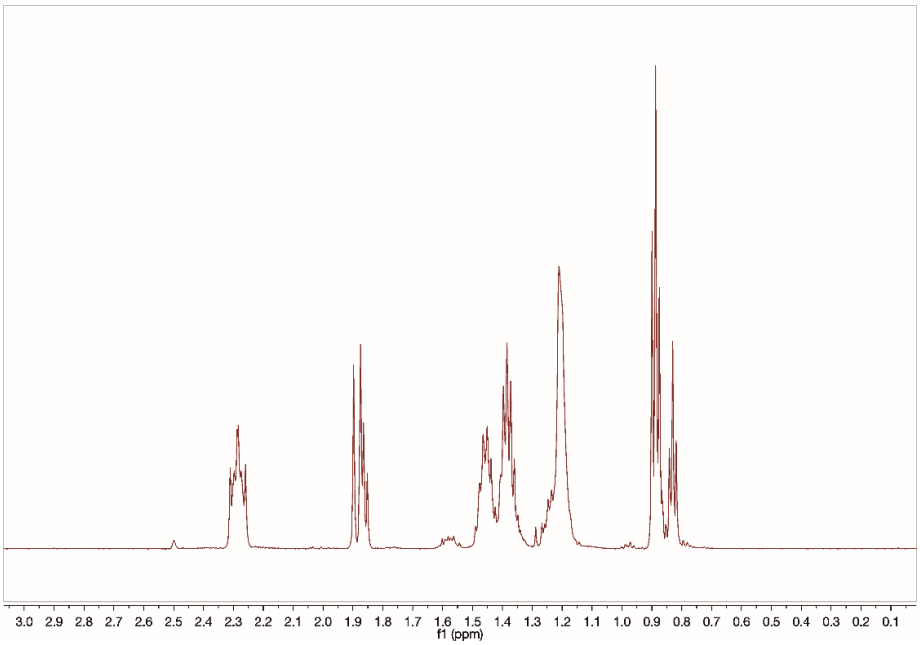

Figure S3: ^{1}H NMR spectrum of [P_{4441}][$C_9H_{19}COO$]: (300MHz, DMSO) δ0.83 (3H, t), δ 0.89 (9H, t), δ 1.22 (14H, s), δ 1.29- δ 1.6 (12H, m), δ1.85 (2H, t), δ 1.92 (3H, d), δ 2.26- δ 2.33 (6H, m)

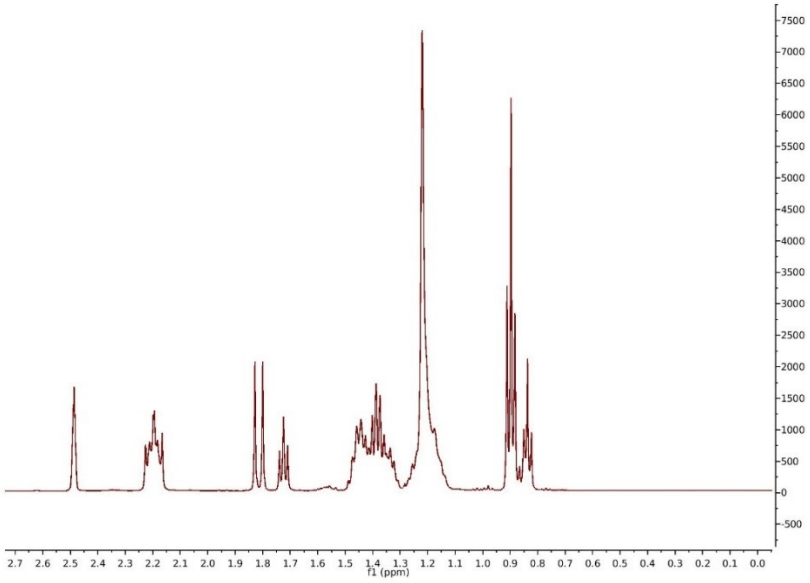

Figure S4: ^{1}H NMR spectrum of [P_{4441}][$C_{13}H_{27}COO$]: (300MHz, DMSO) δ 0.83 (3H, t), δ 0.89 (9H, t), δ 1.22 (22H, s), δ 1.3- δ 1.65 (12H, m), δ 1.71 (2H, t), δ 1.78 (3H, d), δ 2.34- δ 2.05 (6H, m)

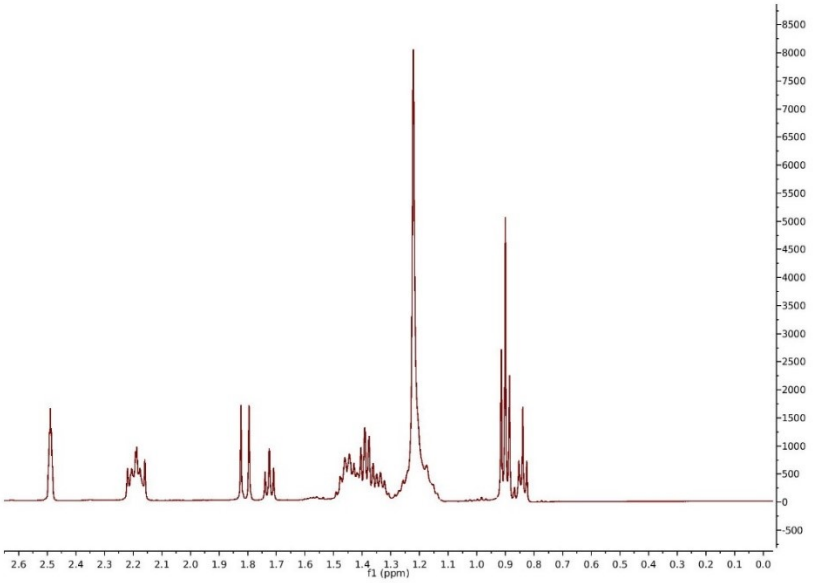

Figure S5: ^{1}H NMR spectrum of [P_{4441}][$C_{15}H_{31}COO$]: (300MHz, DMSO) δ 0.84 (3H, t), δ 0.9 (9H, t), δ 1.22(12H, m), δ 1.72 (2H, d), δ 2.09- δ 2.3 (6H, m)

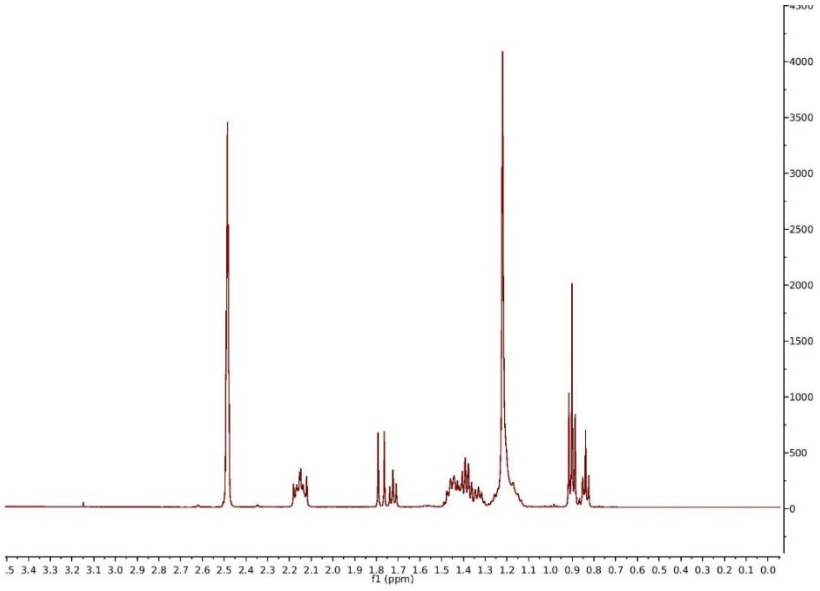

Figure S6: ^{1}H NMR spectrum of [P_{4441}][$C_{17}H_{37}COO$]: (300MHz, DMSO) δ 0.84 (3H, t), δ 0.9 (9H, t), δ 1.22 (30H, s), δ 1.29- δ 1.59 (12H, m), δ 1.72 (2H, t), δ 1.77 (3H, t), δ2.05- δ2.33 (6H, m)

3.1.5.3. Behavioural assay

For assessing the locomotor behaviour of the IL-treated 5 dpf larvae the IL-E3 solutions were disposed and the wells were washed gently three times with 3 mL of E3 medium. At least sixteen larvae of each group were transferred to a 48-well plate, each well containing 1 mL of fresh E3 medium. The plate was placed under the camera and the locomotor activity was recorded for 10 min. Measurements were repeated three times and the following parameters were analysed: total distance moved (cm), maximum distance moved (cm), turn angle (degrees), angular velocity (degrees/s), and meander (degrees/cm). One-way

ANOVA with Bartlett's test and Dunnett's multiple comparison test were assessed when the data followed Gaussian distribution, while a non-parametric Kruskal-Wallis test with Dunn's multiple comparison test was applied when the data did not follow Gaussian distribution. Sixteen larvae of both sexes were selected to further studies from [DBNH][OAc] and [P_{4441}][OAc] treated groups and from the control group. They were transferred and kept in 1.5 L tanks and when reaching adulthood, they were transferred to 10 L tanks.

Three behavioural assays were used for 2.5 mpf zebrafish to assess the long-term impact of [DBNH][OAc] and [P_{4441}][OAc] on the more complex behaviour of zebrafish to detect possible modest toxic effects not detectable at earlier stages. White round tanks were used to assess changes in the locomotor activity and aggressiveness of zebrafish. First, the locomotor activity of the zebrafish was measured between 1 – 11 min after fish addition. Secondly, a brown Eppendorf vial was used as a novel object and the change in the fish behaviour was recorded. After addition of the novel object the swimming patterns were recorded between 1 – 11 min and 30 – 40 min to assess the boldness of the zebrafish. Mirror-induced aggression protocol was conducted by transferring 4 fish at a time to 4 rectangular tanks. Both long sides and the short side were covered with white paper to avoid visual contact of the fish assessed in different tanks. The fourth side was covered with a mirror placed at a ~20° angle. The behavioural response to the presence of the mirror was recorded between 1 – 11 min and between 30 – 40 min after fish addition. All tanks were divided into different sections and GraphPad Prism (GraphPad Software) and Microsoft office Excel 2013 were used for statistical analysis when assessing the differences between the control group and the IL-treated fish. One-way ANOVA and Dunnett's or Sidak's multiple comparison test was applied to assess the significance of the IL treatment on the locomotor activity of zebrafish in different environments. Non-parametric Kruskal-Wallis test with Dunn's multiple comparison test was used when the data was not normally distributed.

3.1.5.4. Histological examination

To reveal possible effects of ILs on reproductive organs, liver, gills and intestines six fish, three of both sexes, from each three examined groups ([DBNH][OAc], [P_{4441}][OAc], and a control group) were killed by adding the fish to ice cold water. The fish were retained in PFA for 1 night, washed 3 times with PBS and retained for 30 h in a solution containing 20% sucrose in PBS. After removal of sucrose the fish were frozen with carbon dioxide ice. The whole fish were cut sagittally to 10 µm sections and every tenth section was stained with

hematoxylin and eosin (HE) stain to study the morphology of liver, gills, intestines, and gonads.

3.1.5.5. Cell culture preparation

CHO cells were incubated (CO-150, CO_2 incubator, New Brunswick Scientific, Germany) in Ham's F12 cell culture medium supplemented with 10 % FBS at 37 °C with 5% CO_2. When 80% confluence was reached the media was discarded and the cells were washed with pre-warmed phosphate buffered saline (PBS). The cells were detached from the T75-flask with trypsin/EDTA and fresh medium was added after 7 min in order to inactivate the Trypsin/EDTA. The suspension was centrifuged (Varifuge 3.0, Heraeus Sepatech, Hanau, Germany) at 700 rcf for 3 min. After supernatant removal the cells were resuspended with fresh medium and declumped manually using a 10 mL pipette in order to separate the cells and avoid cell clumps. The viability of the cells was inspected by staining the cell sample with trypan blue and counting the cells using Neubauer's counting chamber. Rest of the cells were seeded into 96-well plates and they were incubated until confluence. After the confluence serum free medium was added and the cells were serum starved for 7-8 hours before the treatment with ILs.

3.1.5.6. Cytotoxicity assay

The cells were incubated for 24 h with the IL solutions, which were dissolved in the serum-free medium. Cells incubated with medium and dye were used as positive control and medium with dye was used as negative control. Redox sensitive alamarBlue reagent was added (1:10 v:v) to the wells 2 h before the incubation time expired. Aliquot of each well was transferred to a black 96-well plate and the fluorescence was determined using a multilabel counter plate reader (Viktor^3 – PerkinElmer, Waltham, MA) at excitation/emission wavelengths of 535/595 nm. The alamarBlue assay is used as a fluorometric/colorimetric cell viability indicator, based on the detection of metabolic activity of the cells. The alamarBlue reagent shifts from non-fluorescent state (blue) to fluorescent state (red) in the presence of intracellular reducing agents. The number of viable cells is nonlinearly proportional to the fluorescence shift of alamarBlue reagent. Therefore, a binary dilution series of cells was prepared in serum free medium together with alamarBlue and mathematical correlation between the fluorescence and number of cells was determined after 2 hours of incubation.

Negative control was subtracted and the number of cells was calculated from the second order polynomial function. These values were normalized to positive controls and logistic sigmoidal fits were applied to determine the EC_{50} values.

3.1.5.7. CMC measurements using capillary electrophoresis

Uncoated fused silica capillaries were purchased from Polymicro Technologies (Phoenix, AZ, USA) with 50 µm I.D and 375 µm outer diameter. The total capillary length was 47 cm and the length to the detector was 38.5 cm. New capillaries were conditioned for the measurements by rinsing for 10 min with 0.1 M sodium hydroxide, for 10 min with water, and for 2 min with the anionic ILs in sodium phosphate buffer or in water at a pressure of 930-950 mbar. A new capillary was taken into use when changing the type of phosphonium IL. A voltage of +25 kV was applied between the sample vials for 1.5 min and the current was recorded. The runs were performed at least three times for each sample concentration.

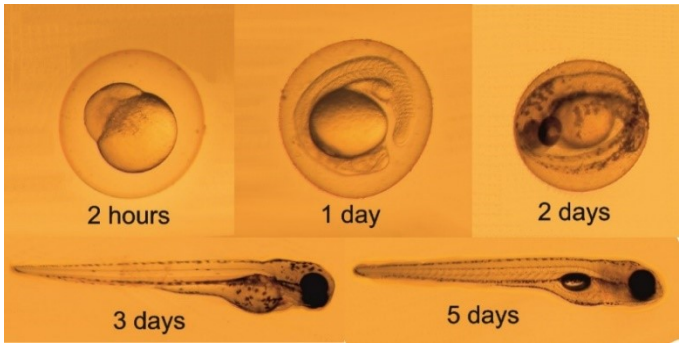

Figure S7: Growth performance of a Zebrafish: Zebrafish growth during 5 days postfertilization

Table S1: Amount of malformed fish: After 5 days of IL treatment

	Control		$[P_{144444}][OAc]$				$[P_{8444}][OAc]$				$[P_{4444}][OAc]$				[DBNH][OAc]				[emim][OAc]			
			100 mg·L^{-1}		1 mg·L^{-1}		100 mg·L^{-1}		1 mg·L^{-1}		100 mg·L^{-1}		1 mg·L^{-1}		100 mg·L^{-1}		1 mg·L^{-1}		100 mg·L^{-1}		1 mg·L^{-1}	
Repetition	M[a]	S[b]	M	S	M	S	M	S	M	S	M	S	M	S	M	S	M	S	M	S	M	S
1	[c]0/[d]25	0/25	N/A	N/A	N/A	N/A	N/A	N/A	-/26	-/26	-/27	-/27	-/25	-/25	-/29	-/29	-/26	-/26	1/26	-/26	-/25	-/25
2	0/25	0/25	N/A	N/A	5/5	-/5	5/5	-/5	-/27	-/27	-/28	-/28	-/28	-/28	-/27	-/27	-/28	-/28	-/29	-/29	-/28	-/28
3	0/29	0/29	N/A	N/A	-/5	-/5	1/2	-/2	-/28	-/28	-/29	-/29	-/29	-/29	1/29	-/29	-/28	-/28	-/30	-/30	-/30	-/30
4	0/25	0/25																				
5	0/30	0/30																				
6	0/30	0/30																				

	Control		$[P_{4441}][OAc]$		$[P_{4441}][C_5H_{11}COO]$				$[P_{4441}][C_9H_{19}COO]$				$[P_{4441}][C_{13}H_{27}COO]$				$[P_{4441}][C_{15}H_{31}COO]$				$[P_{4441}][C_{17}H_{35}COO]$			
			100 mg·L^{-1}		100 mg·L^{-1}		1 mg·L^{-1}		100 mg·L^{-1}		1 mg·L^{-1}		10 mg·L^{-1}		1 mg·L^{-1}		10 mg·L^{-1}		1 mg·L^{-1}		10 mg·L^{-1}		1 mg·L^{-1}	
Repetition	M	S	M	S	M	S	M	S	M	S	M	S	M	S	M	S	M	S	M	S	M	S	M	S
1	1/29	-/29	1/28	-/28	-/27	-/27	-/29	-/29	N/A	N/A	-/27	-/27	-/28	-/28	-/25	-/25	1/24	1/24	1/28	3/28	1/21	-/21	-/26	-/26
2	-/25	-/25	-/27	-/27	2/15	5/15	-/25	-/25	N/A	N/A	-/27	-/27	1/29	-/29	-/26	-/26	-/21	2/21	1/28	-/28	1/25	3/25	-/29	-/29
3	-/26	-/26	-/28	-/28	-/28	-/28	-/30	-/30	N/A	N/A	-/29	-/29	-/30	-/30	-/28	-/28	-/30	-/30	-/30	-/30	-/28	-/28	-/30	-/30
4	-/25	-/25			3/26	3/26			N/A	N/A			-/26	-/26			1/28	-/28			-/27	-/27		
5	-/28	-/28			3/24	1/24			N/A	N/A			-/25	-/25			-/19	-/19			-/27	1/27		
6	-/30	-/30																						
7	-/26	-/26																						
8	-/20	-/20																						

[a]Mild malformation
[b]Severe malformation
[c]amount of malformed fish
[d]total amount of fish after 5 days post treatment
N/A No alive fish after 5 days post treatment

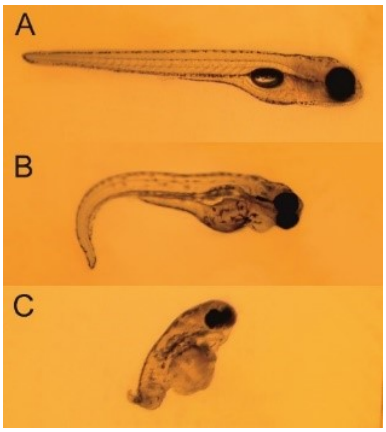

Figure S8: Malformation on the phenotype of 5 dpf zebrafish induced by ILs: A) Control larvae, larvae with B) mild malformations (fish treated with 10 mg·L^{-1} [P_{4441}][$C_{15}H_{31}COO$]), and C) serious malformations (fish treated with 10 mg·L^{-1} [P_{4441}][$C_{17}H_{35}COO$])

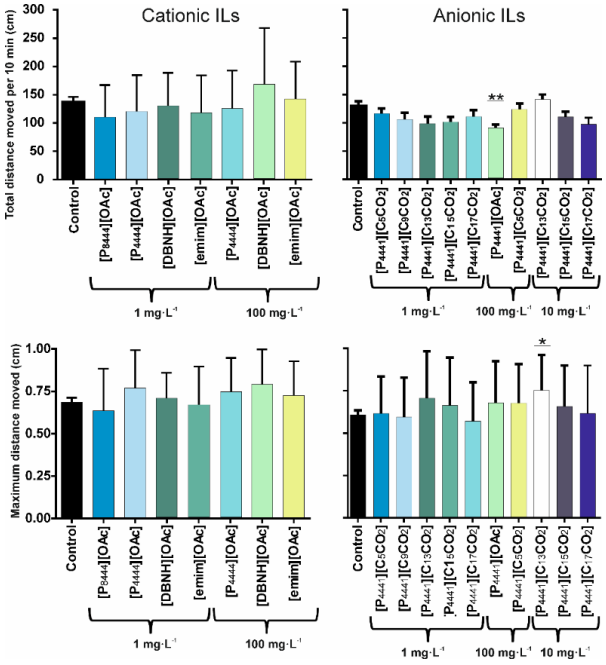

Figure S9: Effect of IL treatment on the total and maximum distance moved at 5 dpf during 10 mins: n = 75 wild-type and n = 39, 35, 31, 39, 40, 37, and 35 per IL group of cationic ILs, respectively and n = 78 wild-type and n = 32, 34, 23, 31, 30, 43, 30, 39, 32, and 22 per IL group of anionic ILs respectively. **p < 0.01 and *p < 0.05, One-way ANOVA. Graphed values are means ± SEM

3.1.5.8. Breeding analysis

Experimental. To detect possible effects of ILs on reproduction, three 5 to 6 mpf fish pairs of both sexes from both IL groups ([DBNH][OAc] and [P_{4441}] [OAc]) and from the control group were transferred into breeding tanks, containing two compartments divided by a plastic wall. Fish were kept in the tanks for one night and the plastic walls were removed the next morning at the onset of lights. After approximately one hour

the possible fertilized eggs were collected and counted. The breeding experiments were repeated 8 times.

Results. Fish used in the study were treated 5 days post fertilization with [DBNH][OAc] or [P_{4441}][OAc] at concentrations of 100 mg·L^{-1}. Three control fish groups were able to spawn in the controlled environment, producing 78, 94, and 103 embryos. The reason for the relatively small numbers of fertilized eggs can be due to the fact that the fish were young and had no previous experience of spawning. [DBNH][OAc]-treated fish did not spawn at all. [P_{4441}][OAc]-treated fish spawned once and produced 243 embryos, which is almost three times higher than the number produced by the average control group. However, because only one pair spawned, the large number of embryos might not be due to the effect of the IL. Because of the small amount of spawning couples, no statistical analysis could be performed. Embryos were grown for 1 week and there were no significant differences between the control group and the [P_{4441}][OAc]-treated larvae offspring.

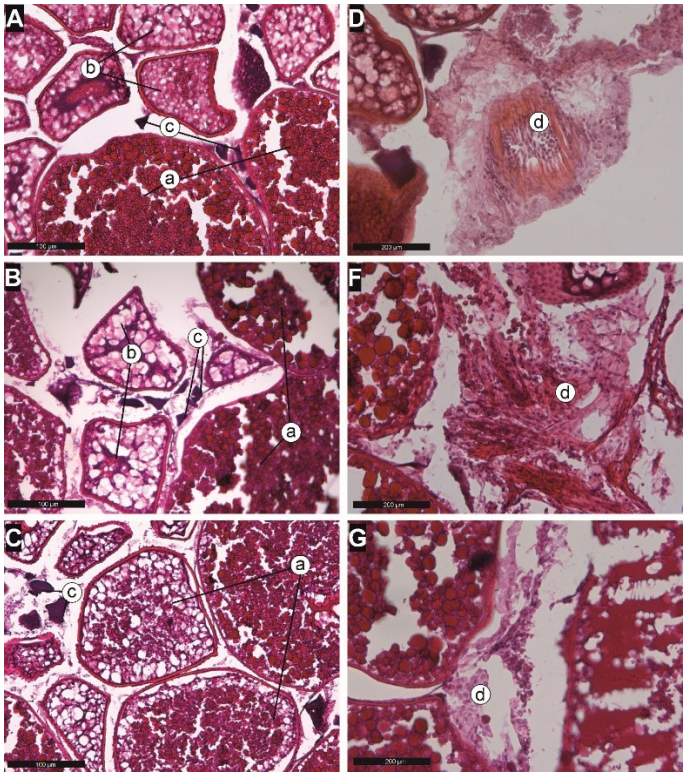

Figure S10: Histological 10 µm sagittal section of zebrafish ovary: 20x zoom of A) wild-type, B) [DBNH][OAc], and C) [P_{4441}][OAc] ovary; n = 3 per group. 10x zoom of D) wild-type, F) [DBNH][OAc], and G) [P_{4441}][OAc] ovary including post ovulatory follicles; n = 3 per group. a) vitellogenic oocyte, b) pre-vitellogenic oocytes, c) oogonium and d) postovulatory follicle

3.1.5.9. Critical micelle concentrations

CMC is often defined as a concentration of a surface-active compound (surfactant) at and above which micelles are formed in a solution [349]. However, the transition from monomeric form to aggregated surfactant does not occur at a sharply defined concentration. The more accepted definition of CMC is that it corresponds to the concentration range where the maximum change in its physical property appears [350,351].

With increasing IL concentrations a liposome bilayer surface becomes rough, which can eventually lead to bilayer disruption [27]. Furthermore, some charged molecular aggregates, especially cations, have been shown to form pores or channels into the lipid bilayer causing structural damages [352–354]. In addition, bioanalytical analyses have shown that ILs exhibiting the strongest micellization effect have the most pronounced binding and disruption effect on membrane bilayers [311].

The CMCs were determined using CE in a fused silica capillary by measuring the electric current, which is linearly dependent on the conductivity of the electrolyte solution at constant voltage, for various concentrations of ILs. This modification of a conventional conductivity method is based on the difference in the mobility of the surfactant, occurring either as single monomers or in an aggregated form. The average electric current was calculated and plotted against the increasing concentration of the IL. Applying a fitting function reported before [355], the CMC could be obtained from an intersection point of two smoothly connected trend lines. In comparison, the CMCs of both cationic and anionic ILs were determined by the optical pendant drop method, where the surface tensions of ILs at various concentrations were measured. The CMC was derived from the intersection point of two trend lines, when the surface tension, γ was plotted as a function of logarithm of the IL concentration. The surface tension of the IL solution decreases when the IL concentration is increased due to monomer orientation at the surface of the drop until the CMC is reached, after which it becomes almost constant due to aggregation of additional IL monomers [356].

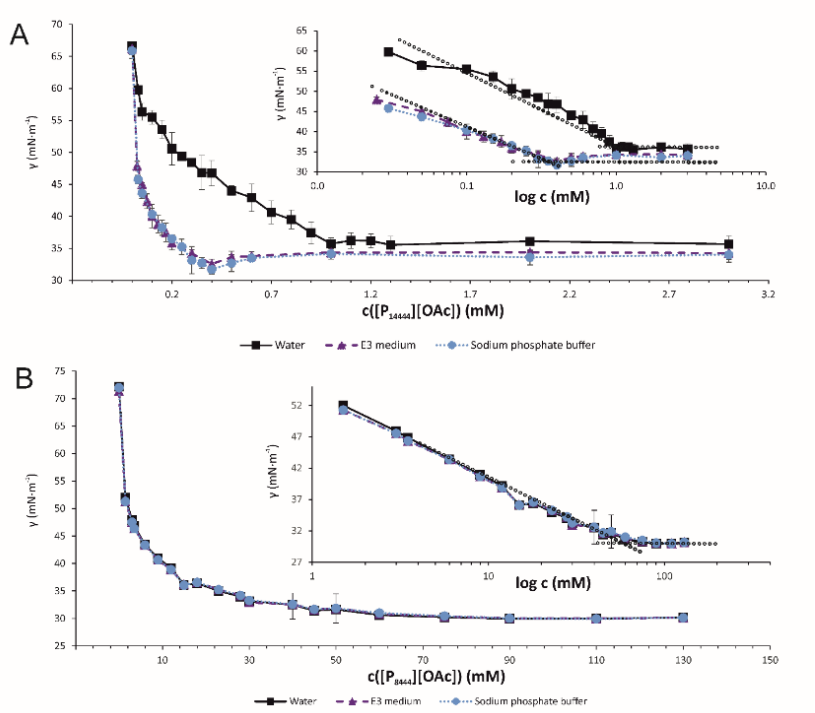

Figure S11: Determination of critical micelle concentrations using optical contact angle meter: Surface tension as a function of increasing concentration of A) $[P_{14444}][OAc]$ and B) $[P_{8444}][OAc]$

3.1.5.10. Effect of ionic liquids on the electroosmotic flow

Experimental. The same capillary electrophoresis system with the same parameters was used as in the CMC measurements. The separation conditions were as follows: voltage +25 kV; temperature of the cassette 25 °C. Sample injection was at 10 mbar for 10 s and 0.5 mM of thiourea in sodium phosphate buffer was used as an electroosmotic flow (EOF) mobility marker in all runs. The runs were performed at least three times for each sample concentration.

Results. To be able to determine the CMCs of the anionic ILs using CE, the interactions between the ILs and the silica capillary wall had to be determined (SI Figure S12). Adsorption of ILs on the silica wall results in a decrease of free ion concentration in the solution which might lead into a decrease of the conductivity of the solution. Therefore, the EOF mobility was measured in background electrolyte solutions with various IL concentrations. The EOF mobility in pure silica capillary was measured before IL addition to assess the capillary condition. The reproducibility of the EOF mobility varied slightly due to a different capillary used for each IL, however the repeatability was good and therefore all concentrations of each IL were measured using the same system within one day. $[P_{4441}][OAc]$ reversed the EOF when the IL

concentration exceeded 10 000 mg·L^{-1} indicating the strongest interaction with the negatively charged fused silica capillary wall. ILs with long anion chain lengths decreased the EOF less than 23% when the IL concentrations were 1000 mg·L^{-1} or below, indicating minor interactions between the fused silica wall and the IL. The EOF mobility reduction was increased to 38- 54% when the IL concentration was 10 000 mg·L^{-1}. Phosphonium ILs have previously been shown to suppress the mobility of EOF [357–360]. Moreover, in our previous study we showed that [P_{14444}]Cl reverses the EOF already at a concentration of 20 mg·L^{-1}. The decrease or even reversal of the EOF is highly dependent on the chain length of the cation; longer chain length being more effective. The results indicate that the long anion alkyl chain shields the cation, thus preventing interactions between the negatively charged silica capillary wall and the positively charged [P_{4441}]$^+$ cation. Furthermore, even a small increase in the anion chain length (C=5) helps to decrease the interactions between the silica wall and the IL cation by 10 – 80%, depending on the used IL concentration.

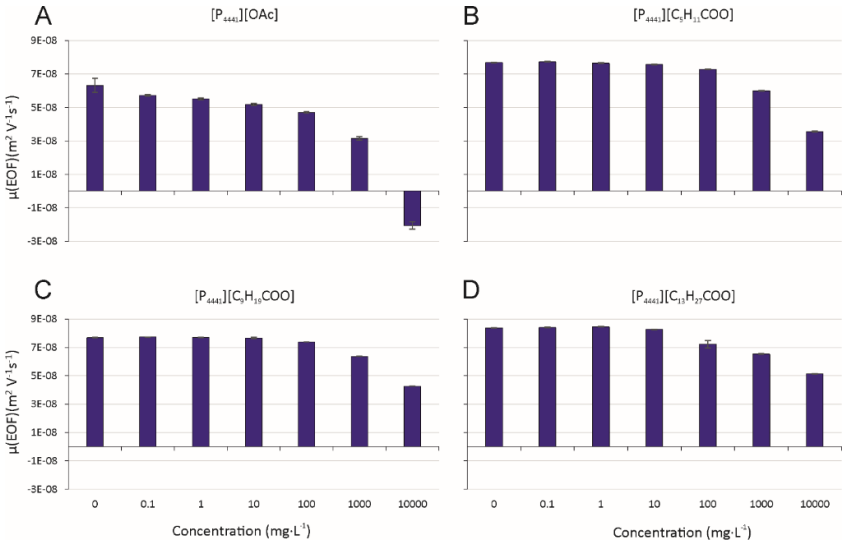

Figure S12: Electroosmotic flow mobility in the fused silica capillary in the presence of various concentrations of ILs: (A) [P_{4441}][OAc], (B) [P_{4441}][C_5H_{11}COO], (C) [P_{4441}][C_9H_{19}COO], and (D) [P_{4441}][$C_{13}H_{27}$COO] in sodium phosphate buffer at pH 7.4 (I = 10 mM). Separation conditions were as follows: capillary length 38.5/47 cm; capillary diameter I.D. 50 µm, outer diameter 375 µm; separation voltage 25 kV; capillary cassette temperature 25 °C; sample injection 10 s 10 mbar; UV-detection 200, 238, 254, and 280 nm; current 7.5 – 10 µA. 0.5 mM thiourea in buffer was used as an EOF mobility marker

3.2. Correlation between ionic liquid cytotoxicity and liposome-ionic liquid interactions

3.2.1. Abstract

This study aims at extending the understanding of the toxicity mechanism of ionic liquids (ILs) using various analytical methods and cytotoxicity assays. The cytotoxicity of eight ILs and one zwitterionic compound was determined using mammalian and bacterial cells. The time dependency of the IL toxicity was assessed using human corneal epithelial cells. Hemolysis was performed using human red blood cells and the results were compared with destabilization data of synthetic liposomes upon addition of ILs. The effect of the ILs on the size and zeta potential of liposomes revealed information on changes in the lipid bilayer. Differential scanning calorimetry was used to study the penetration of the ILs into the lipid bilayer. Pulsed field gradient nuclear magnetic resonance spectroscopy was used to determine whether the ILs occurred as unimers, micelles, or if they were bound to liposomes. The results show that the investigated ILs can be divided into three groups based on the cytotoxicity mechanism: cell wall disrupting ILs, ILs exerting toxicity through both cell wall penetration and metabolic alteration, and ILs affecting solely cell metabolism.

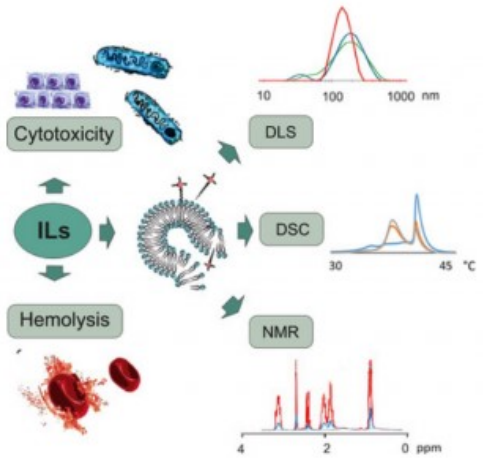

Figure 64: Graphical Abstract: The toxicity of ionic liquids is predicted using biomimicking liposomes instead of living organisms and the results are in a good agreement with the cytotoxicity results obtained using various cell lines

3.2.2. Introduction

Ionic liquids (ILs; Figure 65) are commonly defined as liquid organic salts, consisting of an anion and a cation and having melting points below 100 °C. ILs are often quoted as designer solvents because the selection of an appropriate IL cation and anion pair

allows the generation of ILs with a diversity of physical and chemical properties. Owing to their unique properties, ILs are a commonly used organic salt group in various industrial, commercial, and pharmaceutical applications. Several of these applications such as their usage in pharmaceutical [361], environmental [37], and in food [362] related applications, in organic synthesis and catalysis [308], and in analytical chemistry [4] have been reviewed previously.

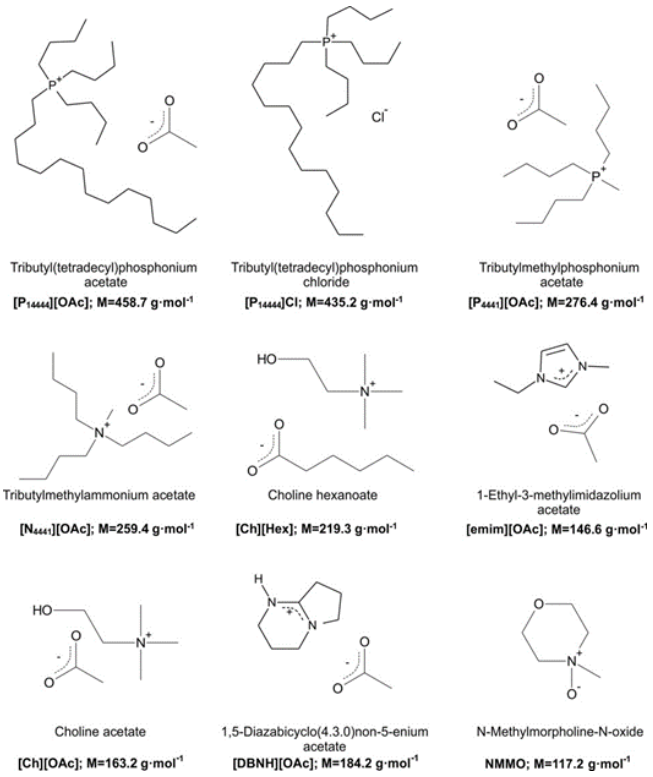

Figure 65: Ionic liquids: Structures of the studied compounds

ILs are often claimed as “green” due to their “nonflammable” nature and low vapor pressure. Hence, their evaporation into the atmosphere is miniscule and requires a vast amount of energy. However, many classes of ILs are water-soluble and they can end up into the aqueous ecosystem through accidental spills and drains. Moreover, due to the high variety of possible IL combinations not all ILs are biodegradable and they can bioaccumulate into small aquatic organisms and furthermore be transferred to animals in higher trophic levels in a food chain, and eventually even to humans.

There are a myriad of studies regarding IL toxicity [9,13,363–365], yet, due to the structural variety of ILs, the mechanism of toxicity is still poorly known. The cation and anion selection, alkyl chain length, and the oxygenated functional groups are few properties known to affect the toxicity of ILs. In addition to the IL properties, the test organism and the IL environment (solvent, pH, temperature etc.) influence the

observed results. Toxicity measurements, which best describe the harmfulness to humans, such as animal tests using rats, fish etc. are usually expensive, time consuming, and ethically dubious. Herein, the purpose was to gain more information on the IL cytotoxicity. In addition, we wanted to investigate if it is possible to obtain similar information with novel analytical methodologies without the use of living organisms. Because the plasma membrane is the first cellular constituent encountered by an external toxicant, *i.e.* the IL, biomimetic phospholipid membranes (liposomes) were used as target objects for this purpose. Large unilamellar liposomes (LUV), consisting of phospholipid bilayers enclosing an aqueous compartment, are excellent models for the cell membranes. The possibility to modify the amount and quality of the membrane building blocks (phospholipids, cholesterol, sugars, proteins etc.) is also a great advantage of using liposomes.

The intercalation properties of surface-active ILs into cell membranes are known to affect the toxicity of ILs and hence, the IL-cell membrane interactions are widely studied by utilizing liposomes [22,366–368]. The interdependency of hydrophobicity and toxicity of ILs is generally supported in many such publications [34,311,369,370]. The toxicity of surface-active ILs is speculated to be due to a facilitated uptake of a compound into an organism, leading to an increased internal toxicant concentration and to an altered metabolism. Another hypothesis is that IL-induced perturbation and increase of the membrane fluidity might result in alterations of the ion and/or molecule transport through the membrane [15]. Yet, it is clear that the toxicity increases when adsorbed or absorbed hydrophobic ILs compromise the membrane integrity. Surface-active ILs have been speculated to permeate into the membrane inducing roughening [27] and/or swelling [34] of the membrane prior to membrane leakage and/or even membrane disruption. Lipids, disengaged from the disrupted liposomes, have further been shown to aggregate with surface-active imidazolium based ILs forming IL-lipid micelles [34], as seen also with other surfactants [371]. In addition, imidazolium and cholinium based ILs with lactate anion [372] and imidazolium, pyrrolidinium, and pyridinium based ILs [366] have been shown to even induce liposome fusion.

In this study, our aim was to deepen the knowledge of the IL toxicity mechanism utilizing various analytical methods and comparing these results with data obtained from cytotoxicity measurements.

3.2.3. Results and Discussion

3.2.3.1. Cytotoxicity of ILS toward human corneal epithelial and Vibrio fischeri cells

To evaluate the toxicity of the ILs, the median effective concentration (EC_{50}) were determined using human corneal epithelial (HCE) cells and *Vibrio fischeri* (*V. fischeri)* bacteria. Moreover, the EC_{50} values shown in Figure 66 and summarized in Table 2 were utilized in the selection of appropriate IL concentrations for the liposome studies. Tributyl(tetradecyl)phosphonium acetate ($[P_{14444}][OAc]$) and tributyl(tetradecyl)phosphonium chloride ($[P_{14444}]Cl$) were the most toxic ILs and based on a classification system introduced in our previous study [95], they were classified as "toxic". Methyltributylphosphonium acetate ($[P_{4441}][OAc]$) and methyltributylammonium acetate ($[N_{4441}][OAc]$) were classified as "practically harmless" or "harmless" and the rest of the compounds, *i.e.,* 1-ethyl-3-methylimidazolium acetate ([emim][OAc]), 1,5-diazabicyclo(4.3.0)non-5-enium acetate ([DBNH][OAc]), choline hexanoate ([Ch][Hex]), choline acetate ([Ch][OAc]), and *N*-methylmorpholine-*N*-oxide (NMMO) were classified as "harmless".

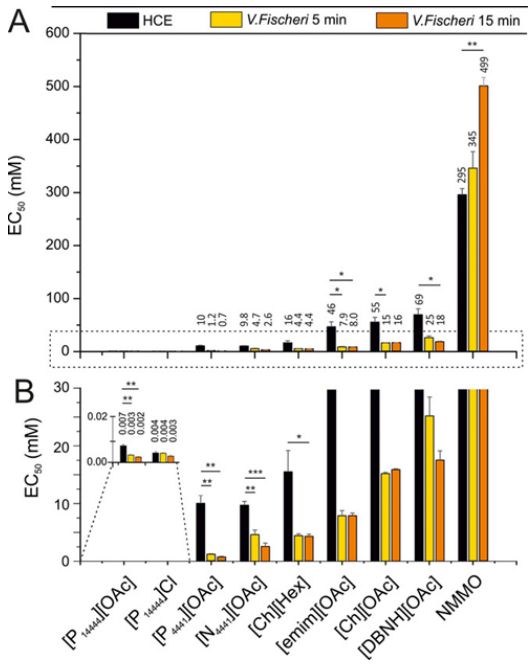

Figure 66: EC_{50} values: A) Median effective concentrations (EC_{50}) of ILs and NMMO determined using HCE and V. fischeri cells. B) Magnification of Figure A. One-way ANOVA with Tukey HSD post-hoc test, ***p<0.001, **p<0.01, and *p<0.05. n=5,2,2; 5,2,2; 3,2,2; 3,6,5; 3,2,3; 3,2,2; 4,2,2; 3,2,2; and 3,3,2 for the compounds from left to right

Table 2: Summary of results: EC_{50} values and effect of time on cytotoxicity. Effect of analytes on hemolysis and on size, zeta potential, and transition temperature of liposomes. Diffusion constants with liposomes

	Cytotoxicity (EC_{50} in mM)			Time dependency	Hemolysis	Zetasizer		DSC	NMR			
					Concentration range [effective concentration] (mM)							
	HCE cells	*V.Fischeri* 5 min	*V.Fischeri* 15 min	Cell death reached (hours) [Cell death %]	[Lysis]	Size [disruption of liposomes]	zeta potential [potential conversion]	[T_m change]	Concentration range (mM)	D_{Cation} (10^{-10} $m^2 \cdot s^{-1}$)	D_{Anion} (10^{-10} $m^2 \cdot s^{-1}$)	CMC in water (mM)
[P_{14444}][OAc]	0.0071 ± 0.0005	0.0031 ± 0.0002	0.0022 ± 0.0002	≤2 [40]	0.0007-0.044 [0.011]	0-1 [1]	0-0.8 [0.015]	0-5 [0.01]	0.5 - 5	0.1 - 0.6	5.8 - 7.1	0.89 ± 0.01
[P_{14444}][Cl]	0.0041 ± 0.0006	0.0039 ± 0.0000	0.0027 ± 0.0004	≤2 [40]	0.0007-0.046 [0.0115]	0-1 [1]	0-0.8 [0.015]	0-5 [0.01]	0.5-6	0.1 - 0.6	5.8 - 7.1	1
[P_{4441}][OAc]	10 ± 1.3	1.2 ± 0.1	0.67 ± 0.12	8–24 [40]	0.7-45 [n/a]	0-30	0-25	0-180 [10]	Jan 30	3.5 - 3.6	6.5 - 6.7	297 ± 11
[N_{4441}][OAc]	9.8 ± 0.7	4.7 ± 0.8	2.6 ± 0.6	8–24 [15]	0.75-48 [n/a]	0-30	0-25	0-180 [100]	Mrz 40	3.4 - 3.7	6.5 - 6.8	
[Ch][Hex]	16 ± 3.7	4.4 ± 0.3	4.3 ± 0.4	8–24 [25]	3.6-228 [n/a]	0-50	0-50	0-200 [15]	Jan 50	6.2 -6.4	4.5 - 4.8	673 ± 2
[emim][OAc]	46 ± 9.3	7.9 ± 0.9	8.0 ± 0.5	8–24 [25]	2.3-147 [n/a]	0-120	0-60	0-300 [n/a]	Jan 70	6.2 - 6.3	6.6 - 6.9	nd
[Ch][OAc]	55 ± 9.0	15 ± 0.2	16 ± 0.2	8–24 [25]	4.8-306 [n/a]	0-100	0-50	0-300 [n/a]	3 - 150	6.2 - 6.5	6.5 - 6.9	nd
[DBNH][OAc]	69 ± 11	25 ± 3.3	18 ± 1.6	8–24 [25]	4.2-271 [n/a]	0-100	0-40	0-400 [n/a]	1 - 200	5.2 - 5.5	6.2 - 6.6	nd
NMMO	295 ± 11	345 ± 31	499 ± 16	8–24 [40]	13.3-850 [n/a]	0-420	0-420	0-800 [200]	5 - 500	4.7 - 5.2		nd

n/a no effect; D diffusion constant; nd not detected

The results are in a good agreement with the afore mentioned study where the EC_{50} values of $[P_{14444}][OAc]$, $[P_{4441}][OAc]$, [emim][OAc], and [DBNH][OAc] were determined [95]. All compounds, excluding $[P_{14444}]Cl$ and NMMO, were significantly ($p < 0.05$, One-way ANOVA with Tukey HSD post-hoc test) more toxic toward the bacteria than toward the HCE cells, which is consistent with previous studies where cytotoxicities of ILs [13] and energetic compounds [373] were assessed using different mammalian and bacterial cell lines. This and the difference in the incubation times of HCE and *V. fischeri* cells (24 hours and 15 minutes, respectively) indicate that the mammalian cells were more resistant toward the external toxicants. The difference can be explained by the variation in the cell structure and metabolism of the prokaryotic and eukaryotic cells. Another plausible explanation is the difference in the EC_{50} determination methods of the assays. Whereas the metabolically active alamarBlue dye is reduced in the presence of living HCE cells, the decay in the bioluminescence of the *V. fischeri* bacteria is recorded. In short, the bioluminescence arises when luciferin is oxidized with a help of luciferase enzyme. Therefore, the bioluminescence inhibition is not necessarily solely affected by cell death, but can occur when the gene expression or energy transfer processes *etc.* of the bacteria are altered [374]. Mariscal *et al.* have shown that the bioluminescence of *Vibrio harveyi* increased when they were exposed to organic solvents, known to permeate the bacteria membrane, at concentrations below their toxic ranges [375]. The bioluminescence might therefore even increase after the bacteria have adjusted to the external permeating substance, *i.e.* NMMO. This seems especially likely for substances which are only slightly toxic or non-toxic, *i.e.,* are not lethal to the bacteria within the time period the bioluminescence is recorded. For instance, the EC_{50} value of NMMO was lower when HCE cells were used instead of *V. fischeri* bacteria indicating that after the initial 'shock' caused by the addition of NMMO to the bacteria the bioluminescence increased as a function of time. In order to gain more information on the time dependency of the toxicity of ILs, a real-time cytotoxicity assay was performed.

3.2.3.2. Real-time cytotoxicity assay

The EC_{50} value measurements showed that the ILs are cytotoxic over a relatively wide range of concentrations. To gain more insight into this process, a CellTox™ assay was used to determine the time range of the toxic effects of the ILs. Using a continuous monitoring of cytotoxicity, we were able to determine how soon after the addition of the

ILs the first signs of toxicity appeared. For this assay we used HCE cells and treated them with the ILs at their EC_{50} concentrations for a maximum of 24 h, therefore, the maximum toxicity was expected to be 50%. Most ILs behaved in a similar manner, with moderate cell death apparent after a lag period of 8–10 h (Figure 67, Table 2). Noticeable exceptions were the long chained phosphonium ILs, $[P_{14444}]Cl$ and $[P_{14444}][OAc]$, which reached their maximum toxicity levels in less than 2 h of incubation.

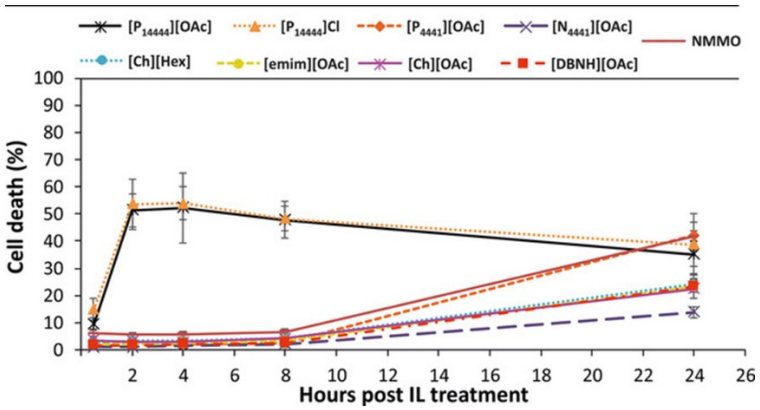

Figure 67: Real-time measurement of the cytotoxicity of ILs: HCE cells were treated with the compounds at the following concentrations: $[P_{14444}][OAc]$ 8 µM, $[P_{14444}]Cl$ 8 µM, $[P_{4441}][OAc]$ 12 mM, [emim][OAc] 46 mM, [Ch][OAc] 72 mM, [Ch][Hex] 15 mM, $[N_{4441}][OAc]$ 12 mM, [DBNH][OAc] 70 mM, and NMMO 270 mM. Data was collected at 2, 4, 8, and 24 hours post treatment

Not all ILs could induce a 50% cell death measurable by the assay. The two assays for HCE cells (EC_{50} determination and real-time cytotoxicity assay) used to measure cell toxicity employ different methods of detection: the alamarBlue uses a membrane permeable dye and highlights the metabolic activity while the CellTox™ assay utilizes a non-permeant fluorescent dye that highlights cell breakage. This suggests that $[P_{14444}]Cl$ and $[P_{14444}][OAc]$ are the most efficient at destabilizing the plasma membrane. They affect significantly the integrity of the cellular membrane and the cells are lysed, while the other compounds induced cell death more slowly, showing a noticeable change in the cell viability after incubation of 24 hours. Using both methods, we obtained information about the cytotoxicity of ILs from different perspectives. For example, $[N_{4441}][OAc]$ at its EC_{50} concentration kills 50% of the HCE cells by affecting the metabolism but the cell death is only 15% in the real-time cytotoxicity test after 24 hours, indicating that the plasma membrane integrity is not significantly altered. On the other hand, for $[P_{4441}][OAc]$ a similar concentration affects equally the metabolism and the permeability of the plasma membrane. To assess the effect of ILs on the membrane breakage a red blood cell (RBC) hemolysis test was performed.

3.2.3.3. Hemolysis

The different mechanism of toxicity of the ILs was validated by a hemolysis assay, in which the ability of the ILs to lyse RBCs was tested (Figure 68, Table 2).

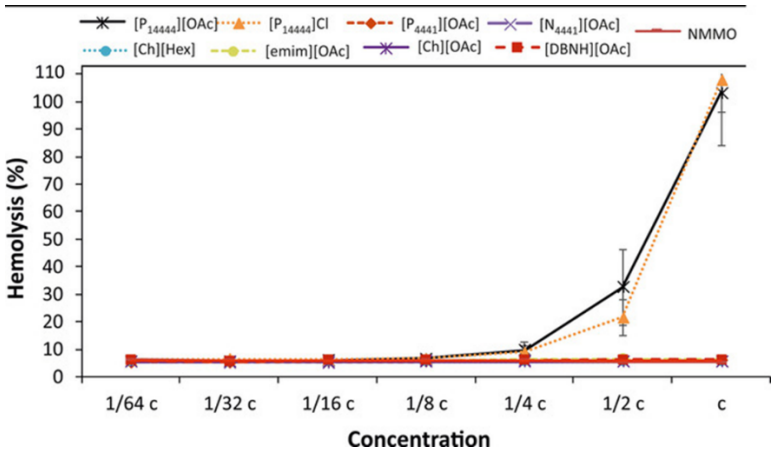

Figure 68: Hemolysis of red blood cells: Hemolysis was assessed using binary dilutions. Initial concentrations (c) were as follows: $[P_{14444}][OAc]$ 44 µM, $[P_{14444}]Cl$ 46 µM, $[P_{4441}][OAc]$ 45 mM, [emim][OAc] 147 mM, [Ch][OAc] 306 mM, [Ch][Hex] 228 mM, $[N_{4441}][OAc]$ 48 mM, [DBNH][OAc] 271 mM, and NMMO 850 mM. The red line indicates the negative control level of hemolysis

Of all tested ILs only $[P_{14444}]Cl$ and $[P_{14444}][OAc]$ were able to lyse the RBCs. The lysis occurred when the IL concentrations exceeded their EC_{50} values. The hemolysis was tested at the same concentration ranges that were used for the EC_{50} calculation with the intention of understanding the most likely cause of cell death at the EC_{50} levels. In this particular assay the ILs were in contact with the cells for ca. 20 min, indicating that the time required for membrane perturbation is essential. IL-membrane interaction is time-dependent, as seen in Figure 67. However, it seems that prior to the time point when the compound penetration is initiated the compound concentration is insignificant, thus, the penetration is independent on the concentration. Figure 68 shows that ILs causing cell mortality after 24 hours (Figure 67) do not cause any effect on the RBCs within 20 min. For example, $[P_{4441}][OAc]$ could not induce cell lysis even at 45 mM - a concentration that is four times higher than the EC_{50} value. These experiments suggest that there is a clear difference between the mechanism of toxicity of the ILs, with $[P_{14444}]Cl$ and $[P_{14444}][OAc]$ affecting cell viability from the outside by disrupting the membrane integrity. In contrast, the other ILs require more time and/or their toxicity is most likely manifested intracellularly, affecting the cell metabolism. In order to gain more information on the mechanism of IL toxicity, several analytical methods were used for studying interactions between ILs and biomimicking liposomes.

3.2.3.4. Dynamic light scattering

Dynamic light scattering (DLS) was utilized to see if the ILs had an effect on the liposome size and zeta potential. The zeta potential describes the potential around the liposomes caused by the negatively charged phosphate groups of the lipids on the liposome surface. Figure 69 and Table 2 show that the sizes of the liposomes did not change remarkably upon addition of the ILs.

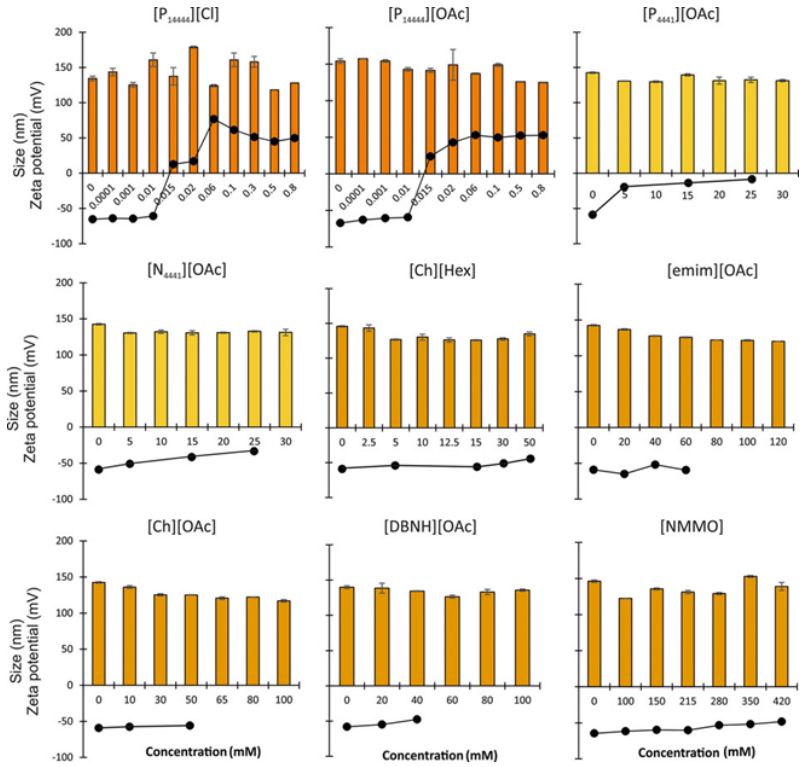

Figure 69: Zeta potential measurements: The effect of ILs and NMMO on size (z-average; marked as bars) and surface charge (zeta potential; marked as dots) of 0.15 mM eggPC/eggPG (80/20 mol%) liposomes

The effect of [emim][OAc], [Ch][OAc], and [DBNH][OAc] ILs on the zeta potential of the liposomes could not be determined at concentrations near and above their EC_{50} values due to high conductivity and, thus, oxidation of the electrodes. However, it seems that the zeta potential is not changing significantly at concentrations below the EC_{50} values. This indicates that the small IL cations are not adsorbed on the liposome surface, hence, not changing the surface charge (ca. -60 mV) of the liposomes. The same behaviour was also seen with [Ch][Hex] and zwitterionic NMMO. [Ch][Hex] has a lipophilic component in the anion moiety causing an electrostatic repulsion between the hexanoate and liposome surface, and therefore possible sorption of the IL is not clearly observable with this technique. On the other hand, the effect caused by $[P_{4441}][OAc]$ and $[N_{4441}][OAc]$ on the liposomes was more substantial. These IL cations

interact with the liposomes nearly neutralizing the liposome surface and resulting in only a slightly negative zeta potential. $[P_{4441}][OAc]$ decreased the zero potential more than $[N_{4441}][OAc]$ indicating a stronger interaction with the liposomes, seen in Figure 69. However, because the zeta potential was not converted from negative to positive, the cations seem to be loosely adsorbed on the surface of the liposomes and not penetrated into the membrane within the short incubation time used in this study.

The most toxic ILs, $[P_{14444}][OAc]$ and $[P_{14444}]Cl$, on the other hand, switched the zeta potential of the liposomes from negative to positive at a concentration of 0.015 mM, evidencing a strong, possibly irreversible, sorption of the ILs into/onto the liposome. The concentrations at which the zeta potentials turned positive were relatively close to the EC_{50} values (0.004-0.007 mM) of these ILs. In order to evaluate the compatibility of the results obtained using the two biomembrane sources (liposomes and HCE cells), the liposome amount and surface area as well as the concentration of lipids in HCE cells were estimated (SI page 142 and 143). The concentration of lipids used in the zeta potential measurements was 0.15 mM, which is equivalent to approximately 300 billion liposomes, while the concentration of lipids in HCE cells was estimated to be 0.34 mM corresponding to 340 000 cells. Cells have bigger diameters than liposomes (8200 – 51 700 vs. 150 nm, respectively) hence, the surface area of liposomes, which is the first cellular constituent encountered of external toxicant, is also larger (15 000 vs. 67 – 2100 μm^2). However, because the concentrations and the surface areas of both biomembranes are in good agreement, the effect of toxicants were comparable and in a good agreement with each other.

It seems that the mechanism of toxicity of the $[P_{14444}]^+$ ILs is primarily related to a strong IL-biomembrane interaction of the cation: the same concentration of the IL caused a response of the biomembrane, *i.e.*, the IL penetrated into the membrane bilayer causing a cell mortality or conversion of the surface charge.

The sizes of the liposomes could not be measured reliably when the concentrations of $[P_{14444}]^+$ ILs exceeded 1 mM due to occurance of different sized IL-lipid aggregates (SI page 143) and overall, the size distributions varied with time upon addition of $[P_{14444}]^+$ ILs. $[P_{14444}]^+$ cations seem to penetrate into the liposome, destabilizing the bilayer, and eventually rupturing the membrane and forming varying sized IL-lipid aggregates. This was already noticed in our previous study [22] when L-*α*-phosphatidylcholine/ 1-palmitoyl-2-oleoyl-*sn*-glycero-3-phosphocholine

(eggPC/POPG; 75/25 mol%) liposomes were used. However, in that work the breakage occurred already at 0.2 mM instead of 1 mM as seen in the current study. As seen from the real-time toxicity results, the incubation time of the sample has a noteworthy impact on the IL-cell interactions, and therefore we can assume that increasing the incubation time before the size measurement could have decreased the concentration rupturing the liposomes. To study the effect of ILs on the processes occurring inside the lipid bilayer, main phase transition temperature changes of dipalmitoylphosphatidylcholine (DPPC) liposomes were measured by differential scanning calorimetry (DSC).

3.2.3.5. Differential scanning calorimetry

DSC measures thermodynamic properties of phase transitions or conformational changes, which require or release energy. In liposomes, a phase transition occurs when a lipid bilayer undergoes a gradual transformation from an ordered gel phase into a disordered fluidic phase or vice versa within a short temperature range. When the lipid bilayer is perturbed with an external surface-active compound, the lipid order is reduced and its phase transition temperature is decreased. The effect of various concentrations of ILs and NMMO below and above their EC_{50} values on the DPPC phase transition temperature are shown in Figure 70 and summarized in Table 2.

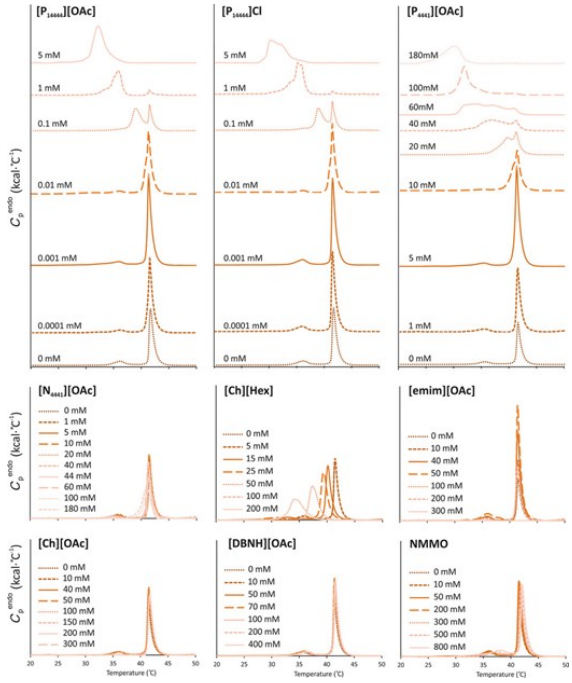

Figure 70: DSC measurements of the DPPC phase transition temperature: Effect of ILs and NMMO on the phase transition temperatures of 0.4 mM DPPC liposomes. Second endotherms are shown in the figure except the first endotherm is shown for $[P_{14444}]OAc$ and $[P_{14444}]Cl$ at concentration of 5 mM

In the case of [emim][OAc], [Ch][OAc], and [DBNH][OAc] the T_m of DPPC did not change at all, when concentrations six times higher than the EC_{50} were added to the lipid dispersion. This confirms that these ILs do not disturb at all the bilayer but, more likely, the small ILs passed through the membrane without compromising the ordered structure of the lipids in the bilayer. ILs are relatively small (<500-600 g/mol) and despite their charge they might be absorbed through the plasma membrane without causing any effect to the membrane itself (*transcellular permeability*). On the other hand, the smallest ILs (<150 g/mol) might also enter tissues via *paracellular permeability* using intercellular aqueducts for transportation or via suitable transporters. However, all ILs are charged and thus, it is plausible that they do not cross the plasma membrane at all but bind to receptors which induce subcellular responses inside the cell that elicit tissue dysfunction [376,377]. The external toxicant can be harmful itself or it can undergo metabolism and become toxic [378]. If the mechanism of toxicity is considered according to the hard-soft acid-base theory (HSAB theory) [379] the imidazolium and amidinium IL cations can be considered to be soft electrophiles, which prefer to interact with soft nucleophiles, *i.e.,* proteins, and can cause organ damage. Phosphonium and cholinium based IL, instead, can be considered as hard electrophiles and prefer to interact with DNA and RNA and are therefore prone to cause cancer. It has been suggested before that imidazolium based ILs can inhibit trypsin activity [380], acetylcholinesterase enzymes [381], and AMP deaminase activity [382], which supports the HSAB hypothesis. However, because of many possible IL combinations it is impossible to say what is the exact mechanism of toxicity of these ILs.

Instead of making the bilayer more disordered, zwitterionic NMMO seemed to stabilize the order of the lipids resulting in a slight increase of the T_m at concentrations above 200 mM. Interestingly [Ch][Hex], the only compound having a relatively long alkyl chain length in the anion, started to permeate into the liposome bilayer at concentration between 5 and 15 mM, causing the endotherm to shift to a lower temperature. The concentration corresponds to the EC_{50} value, meaning that the toxicity of [Ch][Hex] is caused by the penetration of the IL into the bilayer, compromising the integrity of the plasma membrane, in addition of altering the organism metabolism as seen from the cytotoxicity assays.

[N_{4441}][OAc] increased the zeta potential of the liposomes by adsorbing onto their surface. However, the DSC data show that the IL does not permeate into the bilayer at its EC_{50} concentration. The shift in the endotherm, at a concentration 10 times higher than the EC_{50}, is only minor, suggesting that the penetration is not extensive. This confirms that the mechanism of toxicity of [N_{4441}][OAc] is an alteration in the metabolic activity of the cell and not related to the penetration of the IL into the plasma membrane. In contrast, the phosphonium based ILs [P_{14444}][OAc], [P_{14444}]Cl, and [P_{4441}][OAc] were able to permeate into the liposomes causing a decrease of the T_m. The effect of [P_{4441}][OAc] was not as strong and immediate as with the longer chained ILs seen from the hemolysis test and from the zeta potential data. With all the phosphonium-based ILs the destabilization of the lipid bilayer occurred at concentrations in close proximity of their EC_{50} values. For [P_{14444}][OAc] and [P_{14444}]Cl at concentrations in the range of 0.001-0.01 mM (EC_{50} values are 0.007 and 0.004 mM, respectively) and for [P_{4441}][OAc] at 5-10 mM (EC_{50} 10 mM). Therefore, it seems that the toxicity can be estimated utilizing DSC for these liposome permeating ILs, without the use of living organisms. An increase in the concentration decreased the T_m gradually and another endothermic peak appeared in the thermogram, proving an existence of two species in the system. Based on our earlier results [367] we assume that the main endotherm corresponds to the pure lipid bilayer without a remarkable amount of surfactants included, and the second endotherm at a lower temperature corresponds to newly formed mixed lipid-surfactant vesicles or a heterogeneous lipid-surfactant area in the otherwise pure liposome. In our previous study [383] we have shown that the lamellar distances of 1-palmitoyl-2-oleyl-phosphatidylcholine (POPC) multilamellar vesicles (MLVs) decrease and the lamellar disorder increases when [P_{14444}][OAc] was added to the dispersion. The IL at a concentration of 0.4 mM caused also uneven lamellar spacing in the MLVs, suggesting that the effect of the IL is possibly different on the outer and inner lamellae. Due to the fact that we used MLVs in the DSC studies instead of unilamellar vesicles, it is also possible that the heterogeneous outermost bilayer gives the signal at lower phase transition and the remains of the original signal at 41.3 °C is caused by the unaffected lipid lamellae close to the core of the liposome.

Lopez *et al.* [371] have shown that a gradual increase of Triton-X (a non-ionic surfactant) concentration caused the surfactants to penetrate into the studied egg

phosphatidylcholine liposome membrane until a saturation point was reached, followed by aggregation of surfactants and lipids, and a subsequent appearance of mixed vesicles and mixed micelles. This phenomenon is characteristic for lipids and surface-active compounds shown many times before [384–386]. The mixed micelles lack the ordered structure of a lipid bilayer and, thus, no phase transition takes place. It is plausible that during this process from pure liposomes to mixed vesicles and further to mixed micelles, a stage where heterogeneous vesicles with different sizes coexist. This was seen by DLS for $[P_{14444}]^+$; a wider size distribution was observed when the $[P_{14444}]^+$ concentration was increased, until a liposome breakage point was reached. The coexistence of mixed vesicles and mixed micelles is seen from the DSC scans as a decrease in the endothermic peak area upon increasing IL concentration. A constant concentration of 0.4 mM of DPPC liposomes was used in all measurements and all the thermograms were normalized to the DPPC concentration, omitting the impact of surfactant concentration. In order to normalize the needed energy for the phase transition to the amount of substance, the total concentration of unimers involved in the phase transition (all unimers in mixed vesicles) would have to be known. When the surfactant concentration is much below the DPPC concentration the impact of the normalization on the peak area is insignificant ($c[P_{14444}]^+$ ILs ≤ 0.1). However, at high concentrations ($c_{IL} >> c_{DPPC}$) the number of unimers in the vesicles ($c_{total\ unimers} - (c_{mixed\ micelles} + c_{free\ unimers})$) becomes significant and this might result in oversized peak areas. Yet, with all liposome penetrating ILs ($[P_{14444}][OAc]$, $[P_{14444}]Cl$, $[P_{4441}][OAc]$, and [Ch][Hex]) the peaks became smaller, proving that the number of bilayers undergoing phase transition is gradually decreasing. Moreover, when $[P_{14444}]^+$ ILs at a concentration of 5 mM were added to the liposome dispersion, only peaks in the first heat scans were observable (shown in Figure 70), whereas the second and third heat scans as well as all three cooling scans were flat. This indicates a total disruption of the bilayer structure in the vesicles at the mentioned concentration.

From the DLS measurements we observed that there was more than one species (lipid and/or surfactant aggregate) existing when the concentration exceeded 1 mM. Therefore, it seems that $[P_{14444}]^+$ ILs initiate the permeation into the lipid bilayer at 0.001-0.1 mM concentration, gradually removing phospholipids from the liposomes when the IL concentration is further increased above 0.1 mM. It has been shown in our previous study [387] that at 1 mM $[P_{14444}][OAc]$ concentration the ILs are forming

IL-lipid aggregates, yet the whole liposome integrity was not compromised. Raising the concentration of the ILs to 5 mM eventually irreversibly disrupt the remaining mixed vesicles and all the lipids and ILs are organized in aggregates without structures able to undergo phase transition at the temperature range used. However, it has been shown by Majhi *et al.* that a transition from mixed micelles to mixed vesicles can be detected at higher temperatures (40 to 70 °C) for a mixed surfactant/lipid system containing sodium dodecylsulfate and dimyristoyl phosphatidylcholine [386]. In order to monitor the location of the IL unimers in the presence of liposomes pulsed field gradient (PFG) NMR was further utilized.

3.2.3.6. Nuclear magnetic resonance spectroscopy

As diffusion coefficients decrease upon aggregation of surfactants, PFG NMR is a valuable tool for CMC determinations, especially for CMC_1 and CMC_2 detection [388] as well as probing interactions between solution components. The diffusion coefficients of the IL cations and anions (Table 2) did not change significantly when $[N_{4441}]$[OAc], [DBNH][OAc], [emim][OAc], or [Ch][OAc] ILs were added to the LUV dispersions at any concentration compared to their diffusion coefficient in pure solvent. Interestingly, no significant change was observed even when mixing the membrane-interacting ILs $[P_{4441}]$[OAc] and [Ch][Hex] with the liposomes. It seems that the interactions of these ILs were too weak for detection with this technique. Furthermore, the neat ILs did not show changes in their diffusion coefficients, because the measurements were performed below the CMCs of the IL (CMCs are shown in Table 2). The diffusion coefficients of neat $[P_{14444}]$Cl and $[P_{14444}]$[OAc] in D_2O decreased when the concentrations of the ILs increased from 0.8 to 5 mM (Figure 71), indicating an aggregation of the cations.

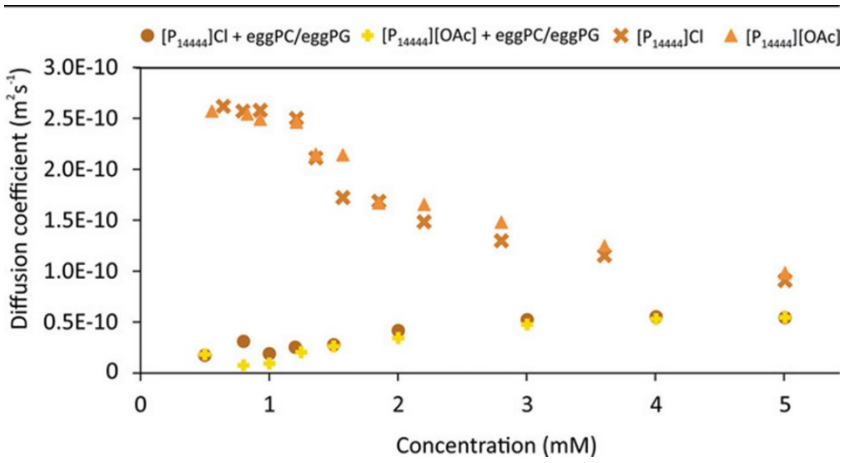

Figure 71: Diffusion coefficients: Diffusion coefficients of $[P_{14444}][OAc]$ and $[P_{14444}]Cl$ with and without the presence of 1 mM eggPC/eggPG (80/20 mol%) liposomes

The most abrupt change was observed at 1.2 mM (CMC_1), which correlates with the CMC values previously determined by our group (0.9 mM for $[P_{14444}][OAc]$ [95] and 1 mM for the $[P_{14444}]Cl$ [22] in water) by surface tension measurements. We have earlier confirmed that the aggregation of $[P_{14444}]^+$ occurs in a narrow concentration range. Therefore, the observed NMR diffusion coefficient above the CMC was considered as the diffusion coefficient of the sole aggregate, even though the fast exchange kinetics between the free and aggregated ILs and the longer timescale of the NMR experiment may lead to a signal averaged from both species [81,388]. Above the CMC_1, the diffusion coefficients kept decreasing upon increasing concentration of ILs, indicating a continuation of aggregation. One plausible explanation is that $[P_{14444}]^+$ ILs initially form micelles around their CMC due to their long alkyl chains and they are then able to aggregate further when the concentration is increased. However, a clear breaking point was absent and a value representing a CMC_2 above 1.2 mM concentration could not be determined. Using the Stokes-Einstein equation (Equation 7) estimations of the sizes of diffusing species were done: the size of $[P_{14444}]^+$ below the CMC_1 value (<1.2 mM) varies between 1.3 – 1.4 nm. The size of a single $[P_{14444}]^+$ molecule using a simple 3D model yields a largest distance of 2.3 nm, assuming that the angles between the carbon bonds in the alkyl chains are constant (109.5°). However, the hydrophobic chains of the molecules are not fully extended in water solution, and therefore the size of an average molecule correlates well with the experimentally observed size from PFG NMR measurements. The results show that the size of the IL aggregates increases to 2.1 nm above the CMC_1 (1.2 – 2 mM), indicating aggregation of the ILs. When exceeding 2 mM IL

concentration the aggregate size increases further to 3.5–3.8 nm, evidencing the formation of larger aggregates.

The diffusion coefficient of pure liposomes was approximately $3 \cdot 10^{-12}$ $m^2 \cdot s^{-1}$, which corresponds to a size of 120 nm and agrees well with the DLS data. When $[P_{14444}][OAc]$ and $[P_{14444}]Cl$ were introduced to the liposome dispersion, the diffusion coefficients of the ILs were over eight times smaller than in the absence of liposomes, Figure 7. This is a clear indication that these ILs interact with the liposomes making them diffuse slower. The diffusion coefficients of the ILs started to increase above 1 mM concentration, showing that some of the ILs were disengaged from the liposomes. Because, neat IL molecules are known to aggregate at 1 mM concentration (cmcs for $[P_{14444}][OAc]$ and $[P_{14444}]Cl$ are 0.9 and 1.0 mM, respectively; Table 2) it is not likely that free unimers occur above 1 mM concentration. DSC measurements show that $[P_{14444}]^+$ ILs disrupt liposomes, thus, it is likely that the ILs aggregate with the disrupted lipids forming IL-lipid aggregates. It has previously been shown that amphiphilic long alkyl chained imidazolium based ILs rupture liposomes, resulting in the formation of IL-lipid micelles in aqueous suspensions [34]. Above 2 mM concentration, the diffusion coefficients increased but did not reach the values of the neat IL micelles, indicating a balance between the smaller IL aggregates and bigger IL-lipid aggregates.

3.2.4. Conclusions

Toxicities of a set of ionic liquids with different surface-active properties were evaluated using two different cell lines and correlated to changes observed by DLS, DSC, and NMR. All ILs were more toxic towards *V. fischeri* bacteria than towards HCE cells. This is assumed to be due to a different detection method or/and due to a different cell structure and metabolism. The toxicity was shown to be highly dependent on time. While long alkyl chained phosphonium ILs ($[P_{14444}][OAc]$ and $[P_{14444}]Cl$) exerted toxicity within 2 hours post treatment, it took 24 hours to see the same response with the other studied compounds ($[P_{4441}][OAc]$, $[N_{4441}][OAc]$, [Ch][Hex], [emim][OAc], [Ch][OAc], [DBNH][OAc], and NMMO). In addition, it was shown that within a short period of time (20 min) only $[P_{14444}][OAc]$ and $[P_{14444}]Cl$ could induce cell lysis, even at concentrations 3 to 14 times higher than the EC_{50} values. $[P_{4441}][OAc]$ and [Ch][Hex] were shown to permeate the cell membrane, however, hemolysis did not take place. This indicates that the cell lysis is independent on the toxicant concentration prior to the threshold time point at which the cell penetration is initiated. In addition, the time and

concentration dependencies are determined by the IL structure and the mechanism of toxicity.

According to DLS, the liposome sizes did not change remarkably upon addition of [P_{4441}][OAc], [N_{4441}][OAc], [Ch][Hex], [emim][OAc], [Ch][OAc], [DBNH][OAc], or NMMO. For [P_{14444}][OAc] and [P_{14444}]Cl the sizes were relatively stable prior to the liposome breakage point, whereas multiple aggregate sizes appeared after the liposomes had ruptured. Changes in the zeta potential of the liposomes were negligible for [Ch][Hex], [emim][OAc], [Ch][OAc], [DBNH][OAc], and NMMO, whereas the values increased for [P_{4441}][OAc], [N_{4441}][OAc] but remained negative. However, upon addition of [P_{14444}][OAc] and [P_{14444}]Cl positive zeta potential values were observed above 0.01 mM IL concentration. This indicates that the long alkyl chain ILs have permanent irreversible interactions with the liposomes while the other compounds have lesser or no interactions at all with the membranes. DSC data revealed that in addition to [P_{14444}][OAc] and [P_{14444}]Cl ILs, also [P_{4441}][OAc] and [Ch][Hex] penetrate into the liposome membranes. The membrane penetration is initiated at concentrations equivalent to the EC_{50} values. NMR data verified that [P_{14444}][OAc] and [P_{14444}]Cl were the only ILs having resilient interactions with the studied liposomes. In addition, the formation of novel IL-lipid micelles after liposome breakage was observed. The results show that the cytotoxicity of ILs is highly dependent on the used cell line and the time of the IL exposure. When the time of the effect (threshold) is exceeded, the toxicity is also dependent on the concentration. Furthermore, the dependency itself is determined by the IL structure. Based on the data shown in this study, we can divide the ILs into three categories: cell membrane rupturing ILs ([P_{14444}][OAc] and [P_{14444}]Cl,) partially cell membrane rupturing ILs ([P_{4441}][OAc] and [Ch][Hex]), and compounds that affect the cell metabolism ([N_{4441}][OAc], [emim][OAc], [Ch][OAc], [DBNH][OAc], and NMMO).

3.2.5. Experimental Section

3.2.5.1. Chemicals

All the lipid stocks eggPC (Egg, Chicken) L-α-phosphatidylglycerol (eggPG; Egg, Chicken; sodium salt), and DPPC in chloroform were purchased from Avanti Polar Lipids (Alabaster, Alabama, USA). Deuterated water (99.9%), used for all IL and

IL-liposome dilutions in NMR measurements was purchased from Euriso-Top (France). Methanol was from Sigma (Steinheim, Germany).

3.2.5.2. Cells

HCE are epithelial cells that occupy the outermost layer of cornea and grow as adherent monolayers in cultures. They represent a well defined cell line for drug toxicity studies.[28] Ham's F12/Dulbecco's modified eagle medium (DMEM), fetal bovine serum (FBS), human epidermal growth factor (EGF), insulin, gentamicin, alamarBlue, and cell culture ware were purchased from Thermo Fischer Scientific (Grand Island, NY). Cholera toxin was purchased from Sigma-Aldrich-Merck (St. Louis, MO). *V. fischeri* marine bacteria, reconstitution solution, and osmotic adjustment solution for running the Microtox assay were purchased form Modern Water (New Castle, DE, USA).

3.2.5.3. Ionic liquids

[emim][OAc] was purchased from IoLiTec GmbH (Heilbronn, Germany) and NMMO was from Sigma (Schnelldorf, Germany). [P_{14444}]Cl was provided by Cytec Industries (Woodland Park, NJ). Synthesis and characterization of [Ch][OAc], [Ch][Hex], and [N_{4441}][OAc] are shown in SI (Pages 143-145). [DBNH][OAc] was synthesized according to a previously published method [314]. [P_{14444}][OAc] was synthesized by anion metathesis described in previous articles [22,310] and HCE[P_{4441}][OAc] was synthesized from tributylmethylphosphonium methyl carbonate according to our previous article [95].

3.2.5.4. Liposome preparation

Phosphatidylcholine is the main component of the cell membrane and therefore eggPC was used as a main lipid for preparing the biomimicking liposomes. In order to gain a negative surface charge, naturally occurring in eukaryotic cells, 20 mol% of eggPG was added to the lipid dispersion. The lipid stocks in chloroform were mixed in suitable proportions and chloroform was evaporated using air. The lipid film was further dried under reduced pressure over night to ensure the removal of chloroform traces. Next, the lipids were suspended in water by heating the dispersion at 60 °C for 1 hour in a thermoshaker. Finally, the lipid MLV dispersion was extruded 19 times through a 100 nm polycarbonate membrane in order to obtain large unilamellar vesicles. Instead of eggPC, multilamellar DPPC was used in DSC studies. DPPC has a well-defined phase transition temperature at 41.3 °C [389], whereas the phase transition of eggPC

occurs in a wider temperature region due to its high content of different fatty acid moieties with a varying degree of saturated chains [390]. Therefore, a temperature range of 10–60 °C was applied in the DSC studies.

3.2.5.5. Cytotoxicity assays

Vibrio fischeri

Microtox® M500 luminometer/thermostate (Modern Water, USA) was used to measure the EC_{50} values for the ILs using bioluminescencing *V. fischeri* marine bacteria. The instructions of the manufacturer for aqueous samples were followed. In short, bioluminescence was measured before and after the exposure to at least four IL dilutions and the decay in the bioluminescence of the bacteria was recorded. The EC_{50} values were determined after 5 and 15 minutes post IL treatment using the Modern Water MicrotoxOmni 4.2 software. Measurements were performed for each IL at least two individual times as duplicates and the error bars are given as standard deviations.

Human corneal epithelial cells

An alamarBlue assay (Invitrogen) was used as a fluorometric/colorimetric cell viability indicator to determine the EC_{50} values of the ILs. The alamarBlue reagent is reduced from a non-fluorescent state (blue) to a fluorescent state (red) in the presence of metabolically active cells (live cells). The SV-40 immortalized HCE cells [100] were grown in 48-well plates in a cell culture mixture containing DMEM/Ham's F12 medium supplemented with 15% FBS, 5 $\mu g \cdot mL^{-1}$ insulin, 10 $ng \cdot mL^{-1}$ human EGF, 1 $\mu g \cdot mL^{-1}$ glutamine, 0.1 $\mu g \cdot mL^{-1}$ cholera toxin, and 40 $\mu g \cdot mL^{-1}$ gentamycin. After confluence, they were serum-starved over-night. The serum-starved cells were incubated in serum-free medium at 37°C in atmosphere containing 5% CO_2 for 24 h. Each plate contained at least 7 different IL concentrations as triplicates. AlamarBlue solution was added to every well (1:10 v:v) 90 min before the incubation time expired. An aliquot of each well was transferred to a black 96-well plate and fluorescence was determined with a multimodal plate reader (EnSpire – PerkinElmer, Waltham, MA) at excitation/emission wavelengths of 570/590 nm. Cells incubated with media and dye were used as a positive control and media with dye was used as a blank sample on each plate.

In order to determine the correlation between the number of cells and fluorescence a calibration curve was prepared. A dilution series of the cells was made in serum free media and the fluorescence was determined after 90 minutes incubation with

alamarBlue. The number of cells in the IL treated samples were calculated from a second order polynomial equation obtained from the calibration curve and the values were normalized to the positive control. Finally, a logistic sigmoid function was applied to determine the EC_{50} values for each IL. All measurements were repeated three times and the error bars were given as standard deviations.

Real-time cytotoxicity assay

CellTox™ Green cytotoxicity assay (Promega, Madison, WI) was used to determine the time line of the IL-induced changes in the membrane integrity of the HCE cells. The assay uses a cyanine dye that is not attached to viable cells but stains the DNA strands of the dead cells once the integrity of the plasma membrane has been compromised. Upon binding to DNA from non-viable cells, the dye becomes fluorescent, and the fluorescence is directly proportional to the level of cell death. By adding the dye in the cell culture media together with the IL we were able to monitor the changes in fluorescence/cell viability in real time and construct a kinetic curve of IL cytotoxicity. The HCE cells were seeded on a 96-well plate at 20 000 cells/well and allowed to attach for two hours. The ILs were dissolved in the cell culture media at concentrations in close proximity to their EC_{50} values and they were added to the attached cells together with the CellTox™ Green dye. Changes in the fluorescence signal were measured after 30 min, 2 h, 4 h, 8 h, and 24 h by reading the plate at excitation/emission wavelengths of 485/520 nm. Cells incubated with media and dye were used as a negative control. Cells lysed with the lysis solution, provided with the kit, were considered as the positive control and determined the upper limit of the fluorescence reading (100% cell death reached). In order to calculate the number of dead cells at each time point, a scale of cytotoxicity was created by mixing live and dead cells in determined proportions. For this, the cells were divided in two, and one half was kept untouched, while the other half was sonicated to simulate a 100% dead population of the cells. These two populations of cells were then mixed in different proportions to cover the entire scale of toxicity – from 0% to 100% dead cells. A second order polynomial function was used to link the fluorescence units to the number of cells. Each plate contained three repetitions of each IL concentration and the experiments were repeated twice. The error bars are standard deviations.

Red blood cell hemolysis

The capacity of the ILs to induce cell lysis was measured using RBCs in a hemolysis assay [391]. Blood collected in dipotassium ethylenediaminetetraacetic acid (K_2EDTA) spray-coated tubes was centrifuged (750 g) at room temperature for 5 min and plasma was discarded. The resultant RBC pellet was re-suspended in isotonic phosphate buffer (pH 7.4, PBS), and centrifuged three more times. The washed RBC pellet was diluted with PBS 3:11 (v/v) to constitute the RBC stock dispersion. The IL dilution series containing 8 different concentrations below and above the EC_{50} values, were prepared in PBS and mixed with the RBC stock dispersion 1:10 (v:v). All samples and controls were incubated for 5 min at room temperature with shaking and centrifuged at 3000 rpm for 3 min to pellet unbroken RBC. 25 µL of the resultant supernatant was mixed with 500 µL of 99.7% ethanol and 37% HCl mixture (39:1; v/v) and the absorbance was measured with a multimodal plate reader at 398 nm. 100% hemolysis was obtained by mixing the RBC stock dispersion with distilled water 1:10 (v:v) and PBS alone was used as a negative control. The relative hemolysis was calculated as A_{398}sample/A_{398}positive control × 100%, where A_{398} represents the absorbance measured at 398 nm. Each sample was run in triplicate or as quadruplicate and the error bars were calculated as standard deviations.

Dynamic light scattering

DLS measurements were performed using a Malvern Zetasizer Nano ZS (Malvern Instruments Ltd, Worcestershire, UK) in order to determine the effect of the ILs on the size and zeta potential (surface charge) of unilamellar eggPC/eggPG (80/20 mol%) liposomes in water. Size and zeta potential determinations were performed employing a helium/neon laser at 633 nm and using laser Doppler micro-electrophoresis, respectively. The liposome dispersion concentration was kept constant at 0.15 mM and IL concentrations were chosen to vary below and above their EC_{50} values. All measurements were conducted at constant temperature of 20 ˚C using disposable cuvettes and disposable folded capillary cells for size and zeta potential measurements, respectively. All samples were measured three times – one run consisting of a minimum of ten individual measurements and the error bars were calculated as standard deviations. The ILs were mixed with liposomes 10–15 minutes before each measurement.

Differential scanning calorimetry

Microcalorimetry (DSC) measurements were conducted with a VP-DSC MicroCalorimeter (MicroCal LLC, MA, USA) to determine the effect of ILs on the main phase transition temperature (T_m) of DPPC liposomes. A heating rate of 60 ˚C·h^{-1} was used within a temperature range from 10 to 60 ˚C. Multilamellar DPPC liposome dispersions (0.4 mM) with and without ILs were degassed under vacuum for ca. 5 min prior to the DSC measurements. The concentrations of the ILs varied below and above their EC_{50} values and all samples were diluted in Milli-Q water. Three heating and three cooling scans were recorded and the samples were kept at 10 ˚C for 30 min prior to the heating scans.

Nuclear magnetic resonance spectroscopy

^{1}H and PFG NMR measurements were performed on a 500 MHz Bruker Avance III spectrometer equipped with a 5 mm BBFO probe with Z-axis gradient. All PFG NMR measurements were conducted on ^{1}H nuclei with diffusion ordered spectroscopy (DOSY) using a stimulated echo pulse sequence (longitudinal eddy delay and bipolar gradient pulses). The gradient strength (G) of the pulses varied from 2 to 95% of the maximum gradient strength (0.47 T·m^{-1}) in 32 steps. The durations of the gradient pulses (δ, 2 ms), the delay time (Δ, 150 ms), and the temperature (T, 21 ˚C) were kept constant. The signal attenuation (S) of probe molecules with gradient strength variation were recorded and analysed using Top Spin software to extract the translational diffusion coefficients (D). When probe molecules are in unhindered motion, the signal is attenuated with respect to the signal in the absence of a gradient (S_0) as

$$\frac{I}{I_0} = \exp\left(-\gamma^2\delta^2G^2D(\Delta - \frac{\delta}{3}\right)$$

Equation 6: Stejskal Tanner Equation: With γ as gyromagnetic ratio, δ as duration of the gradient pulses, G as gradient strength, D as diffusion coefficient and Δ as delay time

where the gyromagnetic ratio (γ) is 42.6 MHz·T^{-1} for ^{1}H nuclei. Furthermore, the hydrodynamic radius (R_h) of the diffusing aggregates were estimated from the Stokes-Einstein equation

$$D = \frac{k_BT}{6\pi\eta R_h}$$

Equation 7: Stokes-Einstein equation: With k_B as Boltzmann constant, D as diffusion coefficient, T as temperature, and η as viscosity

where k_B is the Boltzmann constant, T is the temperature, and η is the viscosity.

Critical micelle concentration determinations

The critical micelle concentration (CMC) determinations of [Ch][Hex] and [N_{4441}][OAc] in water were performed using a contact angle meter (CAM 200 Optical Contact Angle Meter, Biolin Scientific, KSV Instruments, Finland) measuring the surface tension of a drop upon an increasing concentration of the IL (optical pendant drop method). The method is described in more detailed in our previous articles [22,328].

3.2.6. Supporting information

Correlation between ionic liquid cytotoxicity and liposome-ionic liquid interactions

3.2.6.1. Calculation of liposome amount and surface area, HCE lipid concentrations

In order to evaluate the impact of ILs towards different biomembranes i.e. liposomes and HCE cells the liposome amount and surface area as well as the concentration of lipids in HCE cells was estimated from Equation 8, Equation 9, and Equation 10. All values for the calculations and the calculated values are shown in Table 2. The calculated values are marked in bold. First the lipid amount (N_{lipids}) was estimated for all biomembranes using Equation 8 summing the surface areas of both lipid bilayers and dividing the sum with the surface area of a single lipid.

$$N_{lipids} = \frac{4\pi\left[\left(\frac{d}{2}\right)^2 + \left(\frac{d}{2} - h\right)^2\right]}{A}$$

Equation 8: Calculation of lipid amount (N_{lipids}): With d as diameter, h as bilayer thickness and A as surface area per lipid

The diameters (d), bilayer thicknesses (h), and the surface areas per lipid (A) are shown in Table 3. The lipid concentration (c_{lipids}) in HCE cells could be estimated by combining Equation 9 and Equation 10.

$$N_{tot} = c_{lipids} * V_{solution} * N_A$$

Equation 9: Calculation of total amount of unimers (N_{tot}): With c_{lipids} as lipid concentration in HECE cells, $V_{solution}$ as volume of the solution and N_A as Avogadro's number

N_{tot} is total amount of unimers, $V_{solution}$ is the volume of the solution and N_A is the Avogadro's number. The amount of units (N_{unit}) for liposomes were calculated from Equation 10.

$$N_{unit} = \frac{N_{tot}}{N_{lipids}}$$

Equation 10: Calculation of amount of units (N_{unit}): With N_{lipids} as lipid amount and N_{tot} as total amount of unimers

Finally, the total surface area of liposomes was calculated by multiplying the surface area of one liposome ($4\pi r^2$) with the number of units.

Table 3: Number of HCE cells and the amount and surface area of the liposomes

	eggPC/eggPG (80/20 mol%)*	DPPC	HCE cells
Unit diameter (nm)	150	150	8 210 - 51 690
Surface area/lipid (nm^2)	0.63[392]	0.63[393]	0.63
Bilayer thickness (nm)	3.4[394]	3.9[394]	3.6[395]
Volume (µL)	700	500	110
Number of lipids/unit (N_{lipid})	**214 000**	**213 000**	**0.067 - 2.7E+10**
Number of unit (N_{unit})	**3.0E+11**	**5.7E+11**	3.4E+05
Total surface area ($µm^2$)	**15000**	**15000**	67 - 2100[396]
Lipid concentration (mM)	0.15	0.4	**0.34**

*Calculations done for the eggPC/eggPG mixture used in zeta potential measurement

3.2.6.2. Size distribution of eggPC/eggPG (80/20 mol%) liposomes with and without 1 mM and 3 mM [P_{14444}][OAc]

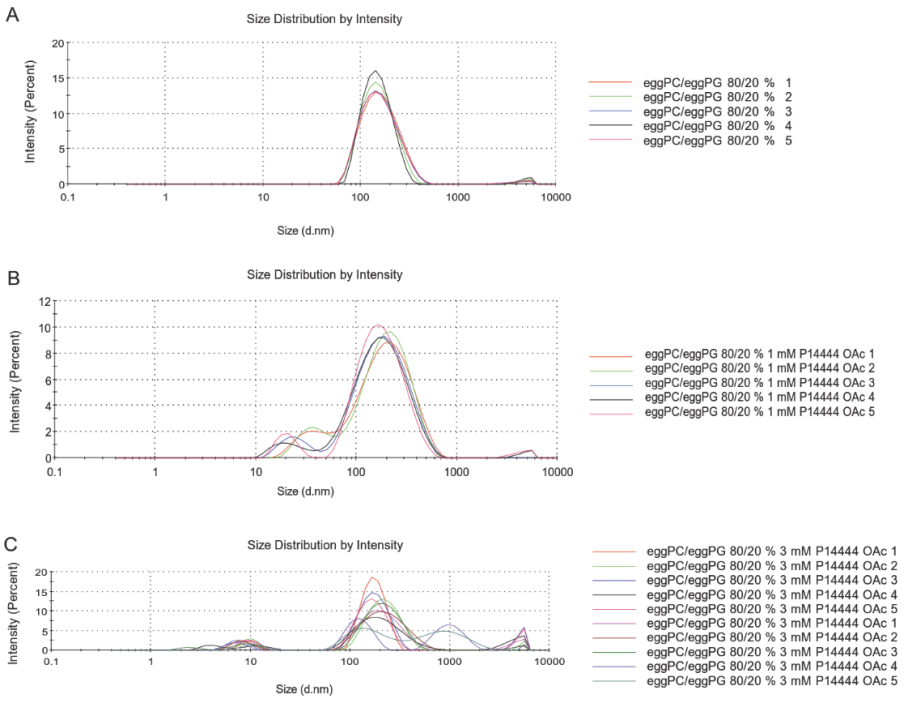

Figure S13: Size distribution of eggPC/eggPG (80/20 mol%) liposomes with and without 1 mM and 3 mM [P_{14444}][OAc]: A) 0.15 mM eggPC/eggPG (80/20 mol%) with B) 1 mM [P_{14444}][OAc] and C) 3 mM [P_{14444}][OAc].

3.2.6.3. Synthesis and characterization of [Ch][OAc]

Choline bicarbonate (191.49 g, 0.91 mol, 80 wt% in water) was weighed into a round bottom flask and diluted to about double the total volume with distilled water. Glacial acetic acid (55.69 g, 0.91 mol) was slowly added to the mixture while stirring. The progress of the reaction was monitored using ^{1}H NMR (SI Figure S14 to ensure that there was a 1:1 mol ratio of cholinium cation to acetate anion.

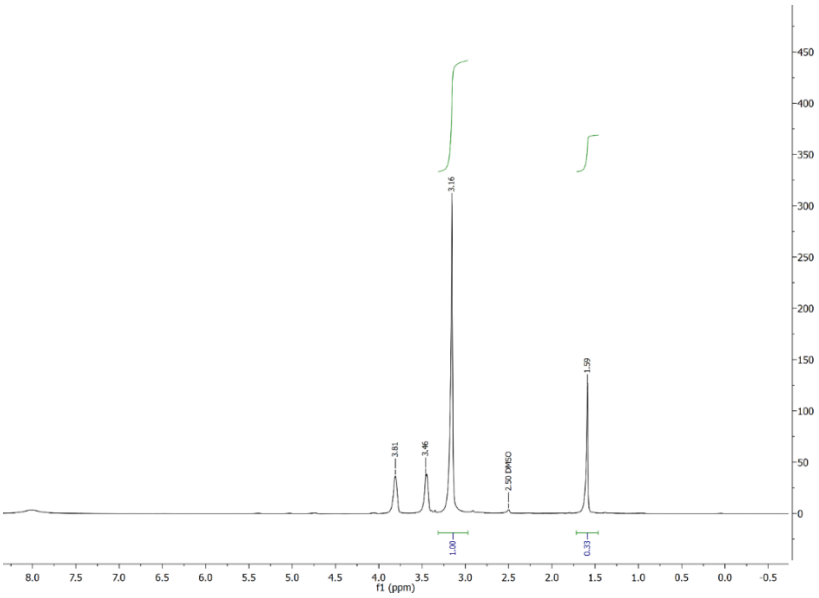

Figure S14: ^{1}H NMR spectrum of [Chol][OAc] in DMSO-d6: ^{1}H NMR (300 MHz, DMSO-d6) δ 3.81 (s, 2H), 3.46 (s, 2H), 3.16 (s, 9H), 1.59 (s, 3H)

3.2.6.4. Synthesis and characterization of [Ch][OAc]

Choline bicarbonate (191.49 g, 0.91 mol, 80 wt% in water) was weighed into a round bottom flask and diluted to about double the total volume with distilled water. Hexanoic acid (105.71 g, 0.91 mol) was slowly added to the mixture while stirring. The progress of the reaction was monitored using ^{1}H NMR (SI Figure S15) to ensure that there was a 1:1 mol ratio of cholinium cation to hexanoate anion.

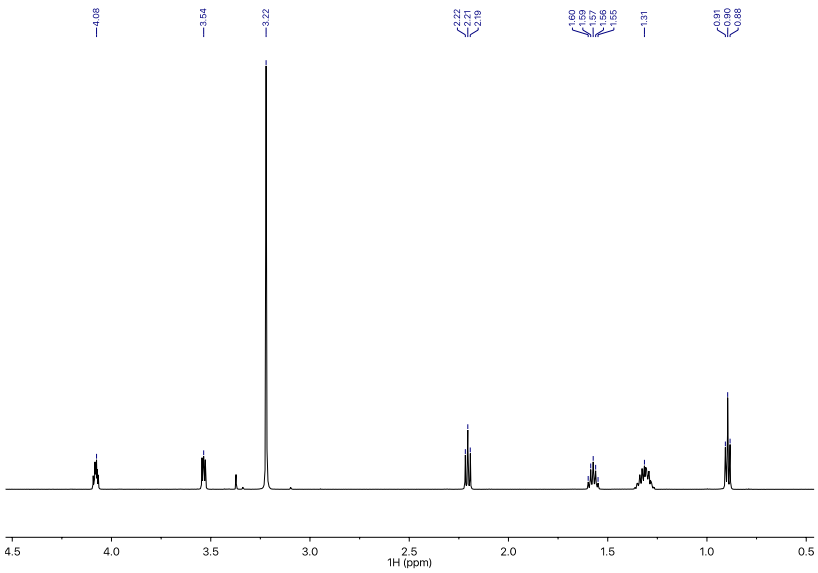

Figure S15: ^{1}H NMR spectrum of [Chol][Hex] in D_2O: ^{1}H NMR (600 MHz, D2O) δ 0.90 (t, J 7.2 Hz, 3H), 1.31 (m, 2H), 1.57 (m, 2H), 2.21 (t, J 7.5 Hz, 2H), 3.22 (s, 9H), 3.54 (m, 2H), 4.08 (m, 2H)

3.2.6.5. Synthesis and characterization of [N_{4441}][OAc]

[N_{4441}]Cl (75 wt% aq, TCI Europe: T2873) was evaporated to dryness in a rotary evaporator. Isopropyl alcohol (500 ml) was added to the dry [N_{4441}]Cl (100.0 g, 0.424 mol) and the mixture was heated to 80 °C to dissolve the sample. Potassium acetate (43.7 g, 0.445 mol) was added to the solution and the resulting mixture was left to stir at 80 °C overnight (18 hr). The solution was allowed to cool to room temperature and sit for 2 hr. The precipitated chloride salt was removed by filtration through celite. Isopropyl alcohol was removed using a rotor evaporator. Acetone (500 ml) was added and the sample was left in the fridge overnight (18 hr). The mixture was re-filtered through celite and the acetone evaporated to give a light orange solid. SI Figure S16 shows the ^{1}H NMR spectrum of [N_{4441}][OAc] in D_2O.

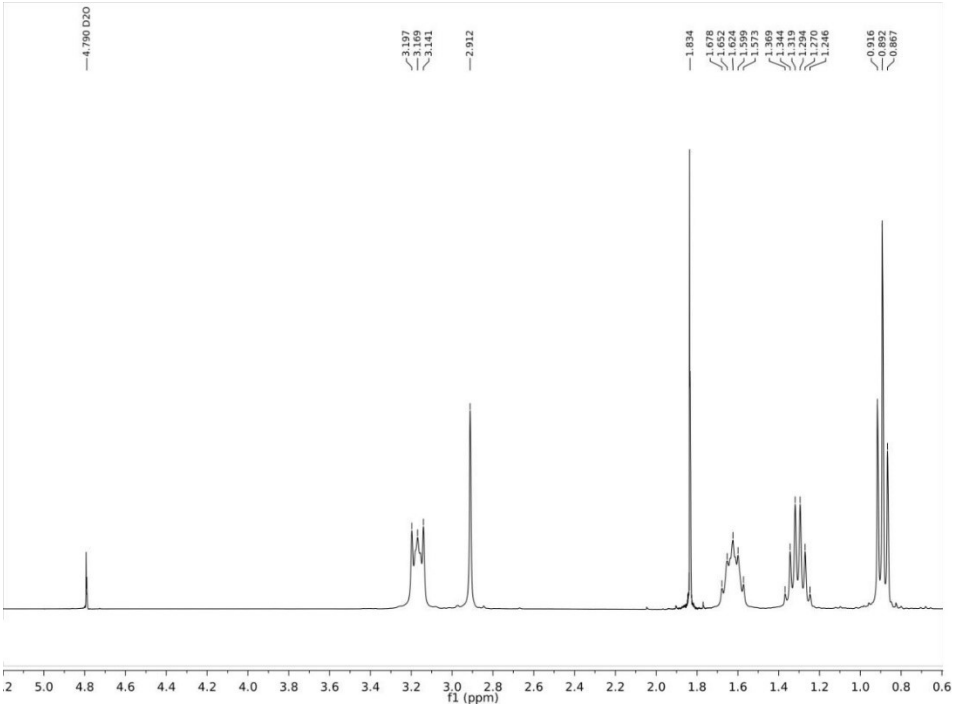

Figure S16: ^{1}H NMR spectrum of [N_{4441}][OAc] in D_2O (doped with acetonitrile - 2.9 ppm): ^{1}H NMR (300 MHz, D_2O) δ 0.89 (t, J 7.2 Hz, 3H), 1.30 (m, 6H), 1.62 (m, 6H), 1.83 (s, 3H), 3.17 (m, 6H)

3.3. Electrospray ionization-compatible t-zero markers for hydrophilic interaction liquid chromatography

3.3.1. Abstract

Commonly used void volume markers widely applied for different hydrophilic interaction liquid chromatography (HILIC) such as toluene, do not ionize in electrospray ion sources. Hence, alternatives are urgently needed. Thus, a comparative study of 5 potential void volume markers (dimethylaniline, diethylaniline, diphenylamine, 1,3,5- *tri*-tert-butylbenzene and (4-dimethylamino)-azobenzene) was performed on 4 different HILIC columns (SeQuant ZIC-cHILIC, Nucleoshell HILIC, Acquity UPLC BEH Amide and SiELC Corsep SB), by using 6 different mobile phases with regard to different buffer strengths and pH with ultraviolet (UV)- and mass spectrometry (MS) detection. For comparison, toluene was utilized as benchmark for an accepted void volume marker in combination with UV-detection. The results indicate, that the behaviour of the tested potential void volume markers is slightly different depending on the column stationary phase. It was also found that 1,3,5-*tri*-tert-butyl-benzene elutes earlier than toluene on zwitterionic stationary phases, caused by exclusion from particle pores. Therefore, dimethylaniline is most suitable as void volume marker on zwitterionic phases, whereas (4-dimethylamino)-azobenzene is recommended as void volume marker on neutral amide phases. In the end, there is no universal void volume marker for all HILIC stationary phases, like uracil for reversed phase chromatography. Therefore, the selection of tested potential void volume marker depends on the stationary phase characteristic.

3.3.2. Introduction

Research interest in hydrophilic interaction liquid chromatography (HILIC) has increased strongly for various applications in the past decade [171,185,397–400]. Especially for the commonly encountered analytes in bioanalysis, i.e. water soluble natural products, metabolites, peptides and nucleic acids, HILIC represents a useful option for chromatographic separation [168,169,171,175,176,178]. Moreover, comprehensive analysis of the metabolome requires besides reversed-phase chromatography (RP) a complementary separation for polar metabolites, like HILIC, in order to achieve maximal coverage of the metabolome. For both modes, detectability

by mass spectrometry is a requirement to allow reliable identification and accurate quantitative analysis of the metabolome [154].

During the development and optimization process of such methods, column comparisons are needed to identify the best suitable separation system. Retention time normalization considering column length and mobile phase flow rate is of great importance. The retention factor represents the ratio of the residence times of the analyte in the stationary and mobile phases. Its calculation is based on the knowledge of the void volume or t_0 [401]. In general, the void volume is described as total volume of a mobile phase in the column [402,403]. There are several commonly used methods, like pycnometry, minor disturbance method and tracer pulse method. For the pycnometry method the column will be filled with two different solvents with unique densities and the column will be weighted. That means, the column has to be removed from the system several times, which is inconvenient. Additionally, no sorption of the mobile phase to the stationary phase is supposed. For this reason, tracer pulse method is also not recommended for the void volume determination. Often the results gaining from minor disturbance method are difficult to interpret, because the void volume calculation is based on the injection peak of a pure solvent, which is most of the time only slightly visible [401,404]. Therefore, the most common method of void volume determination of a particular column is to perform an isocratic experiment with unretained compound [401]. In reversed-phase chromatography non-ionizable small molecules, like acetone, uracil and urea are commonly used [190,403,405]. For HILIC chromatography, an apolar neutral compound without retention has to be found. When using UV/VIS detection, this is mostly accomplished by the use of toluene as void volume marker [406,407], as this compound provides good UV absorbance and lack of polar molecular moieties, like amine-, hydroxy-, carbonyl- or carboxy-functional groups.

Due to its apolar neutral and volatile nature, devoid of any polar moieties toluene is not suitable as t_0 marker when electrospray ionization (ESI) is used. The only detectability of toluene in ESI arises from electrochemical modification on the surface of the ESI capillary emitter tip or as a by-product of an undesired corona discharge emerging from said tip. Aforementioned processes, however, require rather large injection volumes in order to yield suitable signals. Current void volume detection methods applied to HILIC-ESI-MS use either a void volume estimation with a HPLC-UV system, before analysing

the compounds with HPLC-MS [408,409], by using split flow techniques [410–413] diverting a portion of the eluent into a separate UV/VIS detector or by UV-detection in series with MS detection. However, the former extends the analysis time, which should be avoided especially in high-throughput analysis, and the latter has to take the extra tubing contribution into account which needs to be considered and subtracted, respectively.

However, as the addition of a void volume marker to every chromatographic analysis is of utmost importance to detect differences in flow rates due to pumping errors or changing mobile phase contents, it is important to develop a void volume marker suitable for the measurement setup [404]. Therefore, this study is focused on the development of an HILIC-ESI-MS compatible void volume marker for metabolomics.

3.3.3. Experimental

3.3.3.1. Materials

Ultra-LC-MS grade acetonitrile and formic acid was purchased from Carl Roth (Karlsruhe, Germany). Demineralized water was purified with an Elga PurLab Ultra purification system (Celle, Germany). Ammonium formate, ≥99.995% trace metals basis, was purchased from Sigma Aldrich (Steinheim, Germany). Toluene, HPLC grade, was from Sigma Aldrich (Steinheim, Germany). Dimethylaniline and diethylaniline were in-house synthesized, 4-dimethylaminoazobenzene-solution was from Merck (Steinheim, Germany) and diphenylamine was supplied by Stierand GmbH (Waldstetten, Germany).

3.3.3.2. Instrumentation

LC-MS experiments were conducted on a Sciex TripleTOF 5600+ mass spectrometer coupled via duospray ion source (Sciex, Concord, Ontario; Canada) to an Agilent 1290 Infinity Series UHPLC instrument (Agilent, Waldbronn, Germany) with Pal HTC-XS autosampler from CTC (Zwingen, Switzerland). Liquid chromatography with UV/VIS detection was performed on an Agilent 1100 Series HPLC instrument equipped with a degasser, quaternary pump, autosampler, thermostated column compartment and a DAD-detector. The extra column volume UV-measurements were performed using a zero-dead-volume (ZDV) union from Agilent (Waldbronn, Germany).

All MS measurements were controlled by AnalystTF Software 1.7 (Sciex) and the data were evaluated by PeakView 2.1 (Sciex). The calibration data were processed by MultiQuant (Sciex). The UV-measurements were controlled by Open Lab CDS ChemStation – Edition for LC & LC/MS System (Rev. B.04.03.16). The solubility and distribution coefficients were calculated using a calculation module developed by ChemAxon, implemented in MarvinSketch, version 14.12.15.0 (ChemAxon).

3.3.3.3. Stationary phases

The following columns (Figure 75) were included in the comparison: zwitterionic Nucleoshell HILIC column (4.6 x 50 mm; 2.7 µm particle size; 90 Å) from Macherey and Nagel (Düren, Germany), the zwitterionic SeQuant ZIC-cHILIC column (2.1 x 100 mm; 3 µm particle size; 100 Å) from Merck (Steinheim, Germany), the neutral Acquity UPLC BEH Amide column (2.1 x 50 mm; 1.7 µm particle size; 130 Å) from Waters (Eschborn, Germany) and the Coresep SB mixed-mode column (4.6 x 50 mm; 2.7 µm particle size; 90 Å) combining alkyl ligand with a strongly basic ion-pairing group from SiELC Technologies (Wheeling, IL, USA).

3.3.3.4. LC-MS/MS conditions

The six measured mobile phases were composed of A: 10 or 20 mM ammonium formate in Ultra-MS-Grade water adjusted with formic acid to pH 4, 3.5 and 3 and B: 10 or 20 mM ammonium formate in ACN/water (98:2; v/v) adjusted to pH 4, 3.5 and 3. The isocratic conditions were 90% B and 10% A (v/v) with a flow rate of 300 µL/min for 5 min. The column temperature was set to 25 °C and the injection volume was 2 µL.

The following mass spectrometer (MS)-settings were used for all experiments: Curtain gas (CUR) 30 psi, nebulizer gas (GS1) 50 psi, drying gas (GS2) 40 psi, source voltage (ISVF) +5500 V, source temperature (T) 400°C and scan window (SW) m/z =30 to 1000.

High resolution MS as well as MS/MS data were acquired in information-dependent (IDA) acquisition mode. The IDA mode consists of a TOF MS scan, accumulation time (AT) 250 ms, cycle time (CT) 700 ms, collision energy (CoE) 10 V and declustering potential (DP) 100 V, RF transmission (RF) m/z = 20 33%, m/z = 70 33% and m/z 270 34%) with 4 product ion scans (SW m/z 30 – 300, AT 100 ms, CoE 30 V, collision energy spread (CES) 10 V, RF m/z 20 50% and m/z 50 50%).

3.3.3.5. Preparation of test substances

Analytes (Figure 72) were dissolved in mobile phase (90 % B and 10 % A, v/v). First, stock solutions of diphenylamine and 1,3,5-*tri*-tert-butylbenzene in MilliQ water were prepared at a concentration of 1 mg/mL and afterwards diluted 1:1000 (v:v) (diphenylamine) and 1:2 (v:v) (1,3,5-*tri*-tert-butylbenzene) with the mobile phase. Dimethylaniline and diethylaniline were diluted 1:1000 (v:v), 4-dimethylaminoazobenzene was diluted 1:100 (v:v) with mobile phase. Additionally, toluene was diluted 1:1000 (v:v) with mobile phase for the UV-measurements.

3.3.4. Results and discussion

The aim of this study was to find a void volume marker suitable for HILIC-ESI-MS. Successful candidate substances had to meet somewhat antagonistic requirements: First, a molecular moiety suited to be charged during ESI process, i.e. having functional groups that can be protonated or deprotonated. Second, said moiety must remain in its uncharged state at typical HILIC conditions and preferably shielded in order not to interact with functional groups of the stationary phase [404]. Additionally, no interactions with the water layer on the surface of HILIC phases should occur, which means high positive partition coefficients (logD) and high negative solubility (logS).

Toluene is widely used as inert substance for defining void volumes [406,407]. However, this is only possible for UV-measurements, because toluene does not possess any polar groups, which are ionizable in the ESI-source. Being a standard void volume marker, we employed toluene as reference compound, and referred its elution behaviour in form of the column volume to that of candidate substances via UV-detection. The UV-measurements of the void volume marker were performed at pH 3 containing 10% mobile phase A (10 mM ammonium formate in water) and 90% mobile phase B (10 mM ammonium formate in ACN/H_2O; 98:2, v/v). The column volume (V_0) was calculated based on the following equation (Equation 11).

$$V_0 = (t_0 - t_{extra\ column\ volume}) * flow\ rate$$

Equation 11: Calculation of the column volume (V_0): With t_0 as retention time of the injected test compound, $t_{extra\ column\ volume}$ as the volume, which is needed from injector to detector without a column and flow rate as the flow rate of the mobile phase

The retention time of the tested compound is described by the variable t_0 and subtracted by the extra column volume, which was determined for all tested compounds by UV-measurements without an installed column. Therefore, the injector

was directly connected with the UV-detector using a zero-dead-volume union. For the calculations, the mean of all measured extra column volumes was used. Subsequently, the ESI-compatibility was demonstrated.

3.3.4.1. General observations

Void volume markers are compounds not interacting with the stationary phase. Ideally, composition of mobile phases does not have an effect on interaction potential and thus retention time and column volumes. Therefore, suitable HILIC void volume markers selected via UV-measurements were examined regarding their electrospray compatibility using six different mobile phases, covering the prospective working conditions on the HILIC-type columns.

Surprisingly, standard void volume marker toluene did not exert the lowest column volume (Table 4, column volume of HPLC-UV measurements). Instead, 1,3,5-*tri*-tert-butyl-benzene showed on both zwitterionic tested columns, the lowest retention time. Zwitterionic stationary phases are known to adsorb more water from the mobile phase into the pores of the silica gel particles compared to amide phases [414]. That means, compounds with a higher aqueous solubility (logS) as well as a lower distribution coefficient (logD) interact with the aqueous phase and therefore are more retarded.

Consequently, the ability of an analyte to enter the aqueous surface layer of the HILIC stationary phase seems influential to retention. SI Table S2 shows aqueous solubility and distribution coefficients of all tested potential void volume markers at the three different pH values (3; 3.5 and 4). For 1,3,5-*tri*-tert-butyl-benzene, a lower logS (-5.79) [415], as well as a higher logD (5.71) [415] is predicted than for toluene (logS = -1.85; logP = 2.49) [415]. Hence, it is most likely, that toluene interacts with the water layer in the pores of the silica particles, which causes higher retention in comparison to 1,3,5-*tri*-tert-butyl-benzene. Furthermore, it could be argued that 1,3,5-*tri*-tert-butyl-benzene is excluded from the pores due to steric hindrances of the bulky structure (Figure 72). The only exception from this hypothesis was dimethylaniline. Albeit significantly more soluble and showing a low distribution coefficient at pH 3 (SI Table S2) compared to all other tested compounds, it still eluted shortly after or with toluene. This retention behaviour could not be explained by a facile solubility or distribution model.

Table 4: Column volumes (V_0): Column Volumes of the measurements of 5 - 6 compounds with six different mobile phase compositions and 4 different columns

	UPLC-QTOF												HPLC-UV	
	20mM, pH 3		**20mM, pH 3.5**		**20mM, pH 4**		**10mM, pH 3**		**10mM, pH 3.5**		**10mM, pH 4**		**10mM, pH 3**	
	V_0 [mL]	rel. STD	V_0 [mL]	rel. STD	V_0 [mL]	rel. STD	V_0 [mL]	rel. STD	V_0 [mL]	rel. STD	V_0 [mL]	rel. STD	V_0 [mL]	rel. STD
Nucleoshell														
Toluene	-	-	-	-	-	-	-	-	-	-	-	-	0.510	0.0043
Tri-tert-butylbenzene	0.479	0.0047	0.482	0.0054	0.49	0.0228	0.48	0.0118	0.481	0.0082	0.483	0.0068	0.493	0.0058
(4-dimethylamino)-azobenzene	0.51	0.0547	0.477	0.0038	0.478	0.0029	0.474	0.0097	0.476	0.0060	0.51[a]	0.0538	0.517	0.0021
Diphenylamine	0.476	0.0010	0.477	0.0052	0.477	0.0027	0.471	0.0023	0.472	0.0034	0.475	0.0054	0.515	0.0044
Diethylaniline	0.521	0.0017	0.476	0.0013	0.4546	0.0001	0.507	0.0012	0.486	0.0004	0.477	0.0012	0.526	0.0038
Dimethylaniline	0.4806	0.0004	0.457	0.0008	0.4543	0.0002	0.479	0.0012	0.478	0.0008	0.4782	0.0006	0.512	0.0034
Acquity UPLC BEH Amide														
Toluene	-	-	-	-	-	-	-	-	-	-	-	-	0.144	0.0095
Tri-tert-butylbenzene	0.112	0.0056	0.113	0.0053	0.115	0.0059	0.113	0.0091	0.115	0.0079	0.115	0.0030	0.14	0.0166
(4-dimethylamino)-azobenzene	0.114	0.0056	0.114	0.0013	0.114	0.0057	0.113	0.0035	0.113	0.0073	0.113	0.0047	0.14	0.0100
Diphenylamine	0.115	0.0097	0.115	0.0033	0.115	0.0035	0.114	0.0096	0.114	0.0079	0.114	0.0055	0.140	0.0043
Diethylaniline	0.122	0.0019	0.1087	0.0005	0.104	0.0030	0.120	0.0011	0.116	0.0027	0.113	0.0035	0.157	0.0077
Dimethylaniline	0.113	0.0019	0.114	0.0029	0.105	0.0043	0.114	0.0073	0.114	0.0029	0.114	0.0035	0.148	0.0042
Sequant ZIC-cHILIC														
Toluene	-	-	-	-	-	-	-	-	-	-	-	-	0.251	0.0070
Tri-tert-butylbenzene	0.213	0.0030	0.215	0.0051	0.218	0.0045	0.213	0.0059	0.218	0.0039	0.216	0.0037	0.238	0.0032
(4-dimethylamino)-azobenzene	0.215	0.0012	0.195	0.0030	0.195	0.0012	0.219	0.0017	0.220	0.0010	0.219	0.0017	0.243	0.0093
Diphenylamine	0.22	0.0169	0.198	0.0027	0.198	0.0078	0.221	0.0018	0.223	0.0035	0.222	0.0089	0.248	0.0021
Diethylaniline	0.238	0.0023	0.2129	0.0009	0.203	0.0013	0.237	0.0028	0.232	0.0021	0.226	0.0010	0.2702	0.0006
Dimethylaniline	0.226	0.0015	0.2067	0.0002	0.206	0.0030	0.230	0.0020	0.230	0.0023	0.2284	0.0008	0.255	0.0036
Coresep SB														
Toluene	-	-	-	-	-	-	-	-	-	-	-	-	0.470	0.0055
Tri-tert-butylbenzene	0.43	0.0100	0.429	0.0064	0.430	0.0022	0.430	0.0047	0.431	0.0015	0.432	0.0055	0.4660	0.0010
(4-dimethylamino)-azobenzene	0.4304	0.0001	0.430	0.0028	0.429	0.0012	0.4318	0.0002	0.4332	0.0008	0.434	0.0010	0.4821	0.0006
Diphenylamine	0.416	0.0094	0.41	0.0387	0.42	0.0325	0.41	0.0377	0.419	0.0076	0.42	0.0186	0.4677	0.0006
Diethylaniline	0.497	0.0019	0.455	0.0017	0.4298	0.0007	0.478[a]	0.0025	0.4570	0.0005	0.440	0.0052	0.566[a]	0.0014
Dimethylaniline	0.434	0.0022	0.427	0.0028	0.425	0.0024	0.433	0.0011	0.431	0.0037	0.431	0.0014	0.4871	0.0007

a: declared as outlier

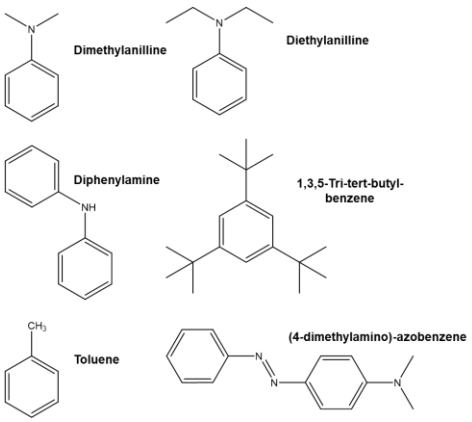

Figure 72: Void volume marker: Structure of potential void volume markers

The summarized column volumes are shown in Table 4. The corresponding chromatograms of all potential void volume markers and one mobile phase composition (mobile phase A: 10 mM ammonium formate, pH 3 and mobile phase B: 10 mM ammonium formate in ACN/H_2O (98:2, v/v) are shown in Figure 73 (UV measurements) and Figure 74 (MS measurements).

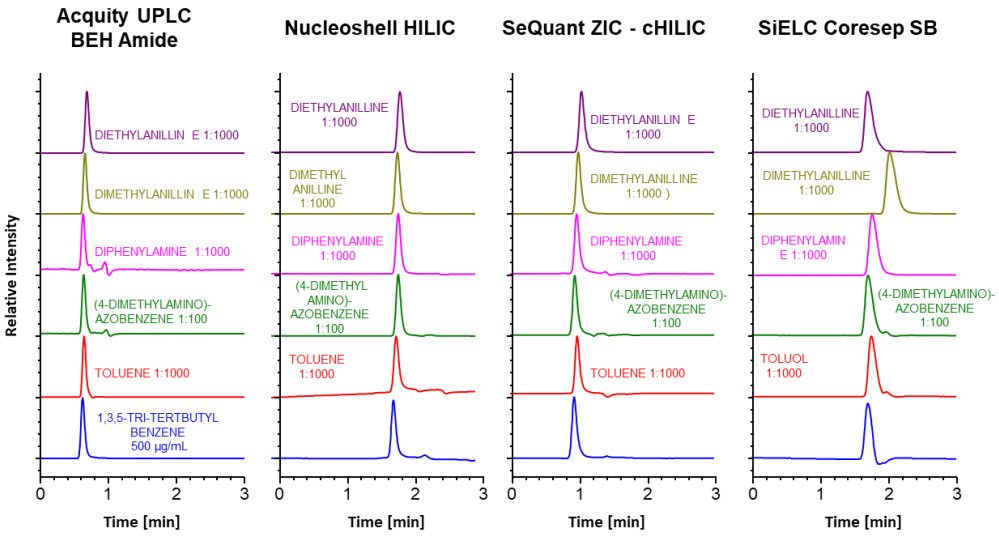

Figure 73: Chromatograms of all tested potential void volume markers detected by UV/VIS detection: Agilent 1100 Series, Mobile Phase A: 10 mM NH_4FA pH 3 adjusted with FA; B: ACN/H_2O (98:2, v/v) containing 10 mM NH_4FA; Isocratic conditions: 90% B for 5 min; flow rate: 0.3 mL/min; Sample: 0.1 % Toluene; 1% (4-dimethylamino)-azobenzene; 0.1 % Diphenylamine; 0.1 % Dimethylaniline; 0.1 % Diethylaniline; all dissolved in 90:10, v/v mobile phase B; injection volume: 2 µL; T=25 °C, λ=280 nm (Diphenylamine, Diethylaniline, Dimethylaniline); λ=254 nm (Toluene, Tri-tert-butylbenzene); λ=395 nm (4-dimethylamino)-azobenzene)

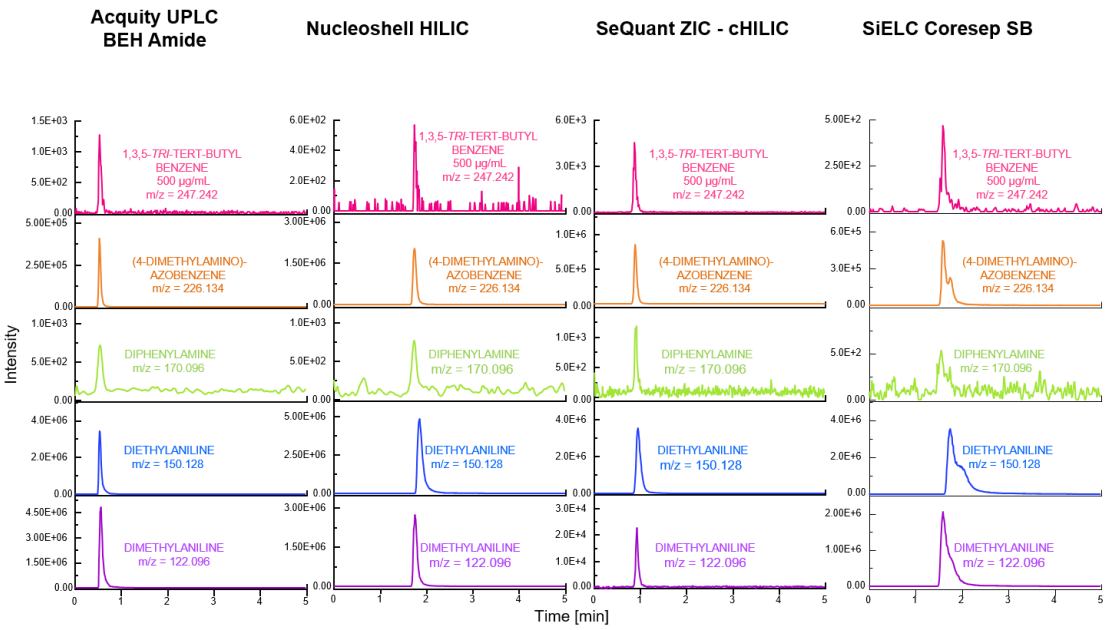

Figure 74: Comparison of the extracted ion chromatograms (MS-measurement) of investigated potential void volume markers on the utilized columns: Agilent 1290 Series, Mobile Phase A: 10 mM NH_4FA pH 3 adjusted with FA; B: ACN/H_2O (98:2, v/v) containing 10 mM NH_4FA; Isocratic conditions: 90% B for 5 min; flow rate: 0.3 mL/min; Sample: 1% (4-dimethylamino)-azobenzene; 0.1 % Diphenylamine; 0.1 % Dimethylaniline; 0.1 % Diethylaniline; all dissolved in 90:10, v/v mobile phase B; injection volume: 2 µL; T=25 °C

3.3.4.2. Zwitterionic stationary phase

In this study, two stationary phases with zwitterionic selectors were investigated, Nucleoshell HILIC from Macherey and Nagel and SeQuant ZIC-cHILIC from Merck. Both stationary phases employ quaternary nitrogen as cationic moiety and a sulfonic acid (Nucleoshell HILIC) or phosphoryl group (ZIC-cHILIC) as negatively charged functionalities (Figure 75A and B), resulting in a relatively broad pH range (2 – 8.5 for Nucleoshell HILIC [416] and 2 - 8 for ZIC-cHILIC [417]) of net neutral zwitterionic state (SI Figure S17). Besides HILIC mode, both ligands can be employed for separation in ion-exchange mode (see Figure 75). They are widely used in HILIC applications [418–422]. It is additionally important to point out that the sulfobetaine structure of Nucleoshell HILIC as well as the phosphorylcholine structure of the ZIC-cHILIC strongly adsorbs water on the surface [414], the latter interacting predominantly with small polar compounds, such as metabolites, glucosinolates and aminoglycosides [175].

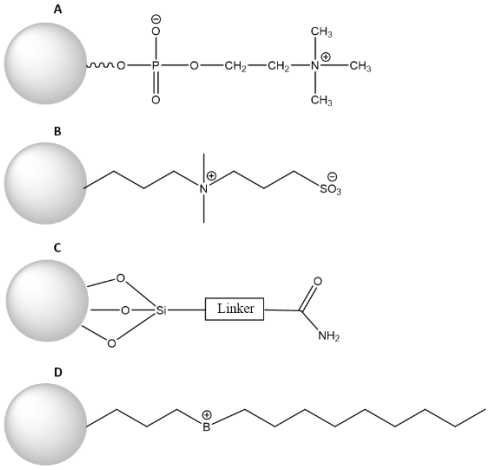

Figure 75: Surface conditions of the investigated stationary phases: A) SeQuant ZIC – cHILIC; B) Nucleoshell HILIC; C) Acquity UPLC BEH Amide and D) SiELC Coresep SB

Nucleoshell HILIC

The UV-chromatograms shown in Figure 73 reveal small differences in elution times for the tested compounds. Respective column volumes are summarized in Table 4. Overall, column volume data of UV measurement revealed dimethylaniline and diphenylamine as retention wise equivalent to toluene (Table 4). However, UPLC-ESI-QTOF measurements for dimethylaniline show significant differences in column volume as a function of ionic strength and pH value (Table 4). Due to the fact that at pH 3 99% of dimethylaniline is protonated (SI Figure S17), there might be ionic interactions with the zwitterionic form of the stationary phase, resulting in retention. Already at pH 4, only 90% of the protonated form is present, which reduces the ionic interactions and the retention. But it seems, that the distribution in the water layer plays a more important role, since a change in the pH value with 10mM ammonium formate in the mobile phase compared to 20mM has no effect on the column volume of dimethylaniline (Table 4). This is due to the fact that the thickness of the water layer increases with increasing ionic strength [169], which makes differences in the distribution coefficients (logD) and solubilities (logS) more noticeable. Therefore, dimethylaniline interacts most with the water layer at 20mM ammonium formate and pH 3, since solubility is decreasing and distribution coefficient is increasing with rising pH (SI Table S2), causing less interaction and retention (Table 4). Diphenylamine on the other side is not affected by the ionic strength or pH as the solubility as well as the distribution coefficient are not influenced in the tested pH and buffer concentration range (SI Table S2). All other substances, except 1,3,5-*tri*-tert-butylbenzene (TTBB)

(already discussed above in section 3.3.4.1), are retained longer with regard to UV measurements (Table 4). Due to the least solubility in water (logS = -5.79) [415], the highest hydrophobicity (logD = 5.71) [415] (SI Table S2) and the non-ionizable bulky structure of TTBB (Figure 75) compared to the other tested compounds, there are less interactions with the water layer of the stationary phase as well as no ionic interactions with the zwitterionic stationary phase. Therefore, the elution is not affected by pH or ionic strength of the mobile phase (Table 4). The most retained substance was diethylaniline (Table 4), showing the same behaviour as dimethylaniline (explained above), except that the differences in solubility and increasing distribution coefficients (SI Table S2) are obtained with 10mM ammonium formate as well.

(4-Dimethylamino)-azobenzene is also less retarded with increasing pH due to decreasing interaction with the water layer (Table 4) caused by decreasing solubility and increasing distribution coefficients (SI Table S2). However, (4-dimethylamino)-azobenzene is 80% protonated at pH 3 and only 30% at pH 4 (SI Figure S17), so a stronger differentiation of the column volumes due to decreasing ionic interactions would be more likely. Therefore, the assumption, that the separation by distribution is dominant compared to ionic interactions with the stationary phase is more suitable. Especially, as zwitterionic stationary phases are known to adsorb the water of the mobile phases exceptionally strong [414]. To summarize, dimethylaniline performed well and was therefore chosen as void volume marker.

SeQuant ZIC-cHILIC

Column volumes (Table 4; UV-measurements) reveal also diphenylamine and dimethylaniline as toluene equivalent void volume markers for the SeQuant ZIC-cHILIC column. However, the results of the other tested compounds differ somewhat from the zwitterionic Nucleoshell HILIC column. Therefore, not only 1,3,5-*tri*-tert-butylbenzene eluted before toluene but also (4-dimethylamino)-azobenzene (Table 4). The UV measurements were conducted at pH 3 with 7% protonated and 93% zwitterionic surface of ZIC-cHILIC (SI Figure S18). Due to the fact that a higher ionic strength increases the thickness of the water layer and the compound is more retarded in the case of electrostatic repulsion [169], it can be assumed that with 10mM ammonium formate the repulsion of the two positive charges of stationary phase and (4-dimethylamino)-azobenzene is reflected in an earlier elution (Table 4). However, with regard to the MS measurements, the same behaviour as described above (Chapter

Nucleoshell HILIC) was obtained. The same is true for diethylaniline, except, that in comparison, the decreased retention with increasing pH at 10mM ionic strength is not as obvious. Also, diphenylamine showed almost unchanged behaviour in comparison (Table 4). Unfortunately, diphenylamine exerted poor signal intensity in subsequent ESI-MS experiments (Figure 76). Nevertheless, dimethylaniline was therefore chosen as void volume marker as the column volume was unaffected by the pH with 10mM ammonium formate buffer and showed only small differences between pH 3 and 3.5/4 with 20mM ionic strength (Table 4).

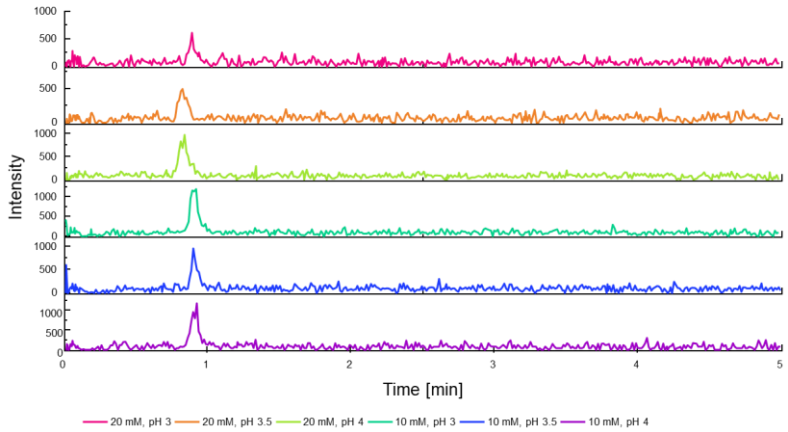

Figure 76: Comparison of the elution of diphenylamine (m/z = 170.096) using different buffer concentrations and pH values on SeQuant ZIC-cHILIC column detected by mass spectrometry (QTOF): Agilent 1290 Series, Mobile Phase A: 10 mM NH_4FA pH 3 adjusted with FA; B: ACN/H_2O (98:2, v/v) containing 10 mM NH_4FA; Isocratic conditions: 90% B for 5 min; flow rate: 0.3 mL/min; Sample: 0.1 % Diphenylamine dissolved in 90:10, v/v mobile phase B; injection volume: 2 µL

3.3.4.3. Neutral amide stationary phase

The Acquity UPLC BEH Amide column has surface carbamoyl groups immobilized on ethylene bridge hybrid organic-inorganic silica particles 1.7 µm (Figure 75C). The benefit of the amide group against the amino group is less reactivity and basicity. Based on these characteristics and the fact, that therefore the formation of a Schiff's base with aldehydes (such as carbohydrates) is prevented, the column was specifically engineered for separating water soluble vitamins and carbohydrates, like mono-, di-, oligo- and polysaccharides [423–428]. Another advantage in separating polar analytes in HILIC mode with this stationary phase is absence of ion-exchange interactions. Hence, this surface chemistry does not require high salt concentrations in the mobile phases, which makes them compatible for hyphenation to mass spectrometry [175].

Comparing the column volumes (Table 4; UV-measurements) obtained on Acquity UPLC BEH Amide column, (4-dimethylamino)-azobenzene, 1,3,5-*tri*-tert-butylbenzene

and diphenylamine were revealed as equivalent replacements of toluene as void volume marker and both *N*-alkylated aniline derivatives showed significant retention relative to toluene. In comparison, both N-alkylated anilines have positive logS values (SI Table S2), thus interactions with the water layer are more realistic than for the other tested molecules. A closer look at the MS measurements also shows that 1,3,5-*tri*-tert-butylbenzene, (4-dimethylamino)-azobenzene and diphenylamine are completely unaffected by changing pH values and ionic strengths (Table 4). Due to the neutral stationary phase no ionic interactions can occur and only interactions with the water layer can cause retention. However, the differences in the solubilities or in the distribution coefficients in the selected pH range are not as big (SI Table S2) that significant differences in retention can be noticed. Although, dimethylaniline shows the best solubility and biggest increase of distribution coefficients with increased pH values (SI Table S2), no significant differences are obtained by differing pH and ionic strength (Table 4). The only differences in column volume can be observed for diethylaniline (Table 4). Since the distribution coefficient increases with increasing pH value (SI Table S2) the interactions with the water layer gradually decreases, resulting in less retention. However, the differences are not as clear as observed with zwitterionic columns due to the missing ionic interactions. Therefore, (4-dimethylamino)-azobenzene was chosen as void volume marker for neutral amide stationary phases.

3.3.4.4. Mixed-mode stationary phase with alkyl and basic ion-pairing moieties

According to the manufacturer, Coresep SB possesses C18 carbon chains and a basic group with pKa 14. More comprehensive information was not disclosed.

UV measurement results for column Coresep SB (Table 4) reveal diphenylamine and 1,3,5-*tri*-tert-butylbenzene as toluene equivalent void volume markers. As already mentioned above for the SeQuant ZIC-cHILIC column, diphenylamine exerted poor signal intensity in subsequent ESI-MS experiments (Figure 77). A more detailed examination of the MS measurements shows that different column volumes due to changes in ionic strength and/or pH value can only be observed for diethylaniline (Table 4). All other tested substances show no influence on their retention behaviour by changing pH values and ionic strengths (Table 4).

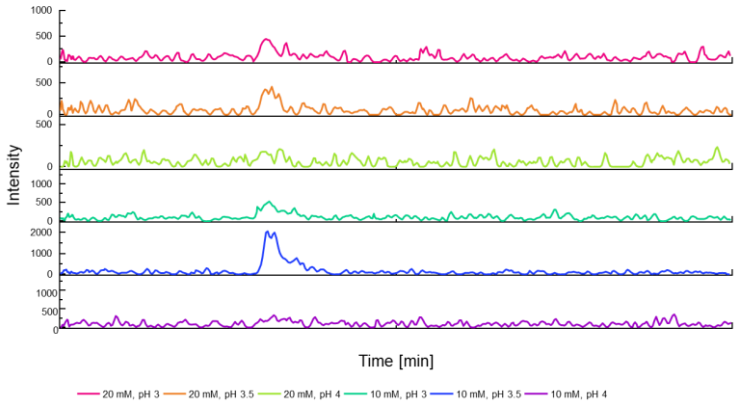

Figure 77: Comparison of the elution of diphenylamine (m/z = 170.096) using different buffer concentrations and pH values on Coresep SB column detected by mass spectrometry (QTOF): Agilent 1290 Series, Mobile Phase A: 10 mM NH4FA pH 3 adjusted with FA; B: ACN/H2O (98:2, v/v) containing 10 mM NH4FA; Isocratic conditions: 90% B for 5 min; flow rate: 0.3 mL/min; Sample: 0.1 % Diphenylamine dissolved in 90:10, v/v mobile phase B; injection volume: 2 µL

3.3.5. Conclusion

This study presents MS-compatible alternatives to toluene for use as void volume marker in HILIC-ESI-MS, summarized in Table 5. Therefore, diphenylamine and dimethylaniline performed well as void volume marker on zwitterionic stationary phases, like Nucleoshell HILIC and SeQuant ZIC-cHILIC. But unfortunately, diphenylamine displayed only a weak signal intensity in subsequent ESI-MS experiments, resulting in dimethylaniline as preferred void volume marker for zwitterionic stationary phases. The mixed-mode stationary phase, CoresepSB, showed for the tested conditions bad peak shapes during HILIC-ESI-MS measurements, which renders a selection of optimal void volume marker nearly impossible. An electrospray compatible void volume marker for neutral stationary phases, for example Acquity UPLC BEH Amide was identified by (4-dimethylamino)-azobenzene, which performed well and exerted good signal intensity in ESI-QTOF mass spectrometry. However, the paper demonstrates, that there is not only one universal void volume marker in HILIC-ESI-MS.

Table 5: Utility matrix for tested compounds: X marks toluene equivalent or faster elution, asterix (*) marks ESI-incompatibility

Compound	Nucleoshell HILIC	Acquity UPLC BEH-Amid	SeQuant ZIC-cHILIC	Coresep SB
1,3,5-*tri*-tert-butyl-benzene	x*	x*	x*	x*
Diphenylamine	x	x	x*	x*
(4-Dimethylamino)-azobenzene		x	x	
Toluene	x*	x*	x*	x*
Diethylaniline				
Dimethylaniline	x		x	

3.3.6. Supporting Information

Electrospray ionization-compatible t-zero markers for hydrophilic interaction liquid chromatography

Table S2: Aqueous solubility (logS) and distribution coefficients (logD): Calculated logS and logD values of all tested potential void volume markers

	Distribution coefficient (logD)			Aqueous solubility (logS)		
Compound	**pH 3.0**	**pH 3.5**	**pH 4.0**	**pH 3.0**	**pH 3.5**	**pH 4.0**
Tri-tert-butylbenzene	5.71	5.71	5.71	-5.79	-5.79	-5.79
Diphenylamine	3.41	3.41	3.41	-3.17	-3.17	-3.17
(4-dimethylamino)-azobenzene	3.80	4.14	4.35	-2.28	-2.62	-2.83
Toluene	2.49	2.49	2.49	-1.85	-1.85	-1.85
Diethylaniline	0.14	0.51	0.95	0.04	0.04	-0.10
Dimethylaniline	0.09	0.56	1.02	0.74	0.28	-0.20

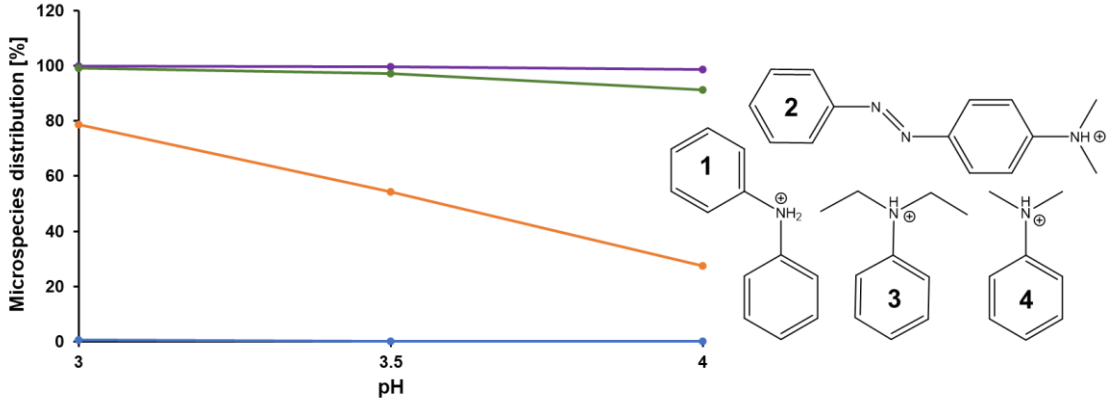

Figure S17: Relationship between pH value and amount of charged void volume marker: diphenylamine (1: blue); (4-dimethylamino)-azobenzene (2: red); diethylaniline (3: purple) and dimethylaniline (4: green)

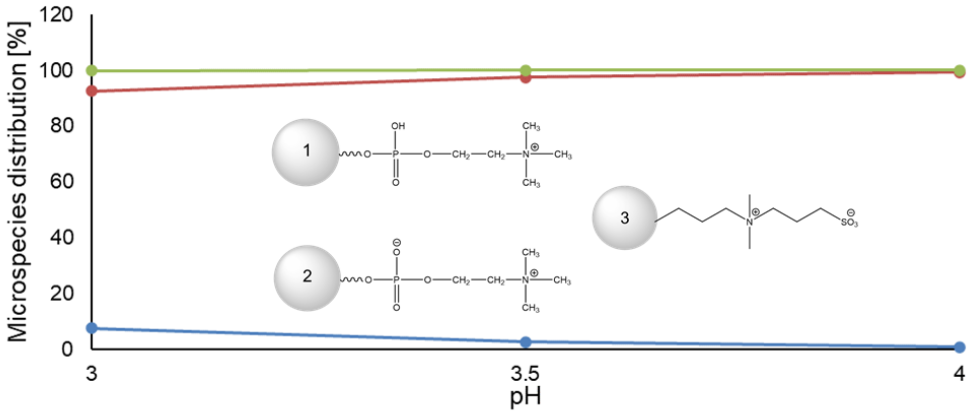

Figure S18: Relationship between pH value and charge state of column surface: ZIC-cHILIC stationary phase; 1: positively charged, blue; 2: zwitterionic structure, red and Nucleoshell HILIC stationary phase; 3: zwitterionic structure, green

3.4. A combined Targeted/Untargeted LC-MS/MS-based Screening Approach for Mammalian Cell Lines Treated with Ionic Liquids: Toxicity Correlates with Metabolic Profile

3.4.1. Abstract

This work presents the development and validation of a quantitative HILIC UHPLC-ESI-QTOF-MS/MS method for amino acids combined with untargeted metabolic profiling of human corneal epithelial (HCE) cells after treatment with ionic liquids. The work included a preliminary metabotoxicity screening of 14 different ionic liquids, of which 9 carefully selected ionic liquids were chosen for a metabolomics study. This study is focused on the correlation between the toxicity of the ionic liquids and their metabolic profiles. The method development included the comparison of different MS/MS acquisition modes. A sequential window acquisition of all theoretical fragment ion mass spectra (SWATH) method with variable Q1 window widths and narrow Q1 target windows of 5 Da for most of the amino acids was selected as the optimal acquisition mode. Due to the absence of a true blank matrix, 13C,15N-isotopically labelled amino acids were utilized as surrogate calibrants, instead of proteinogenic amino acids. Partial least squares (PLS) analysis of the median effective concentrations (EC_{50}) of 9 selected ionic liquids showed a correlation with their metabolic profile measured by the untargeted screening.

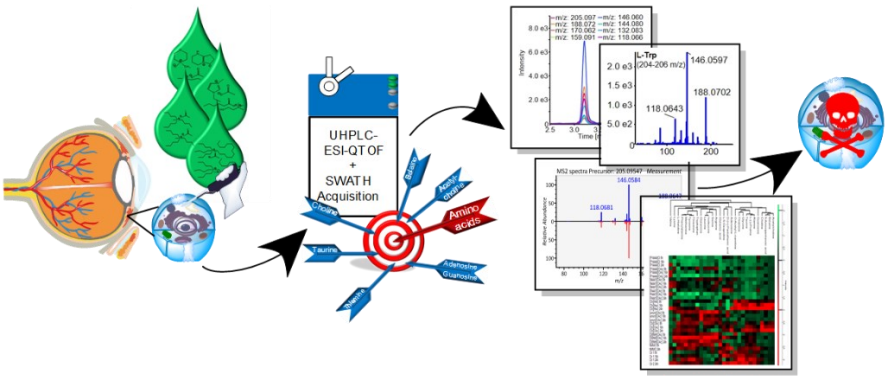

Figure 78: Graphical Abstract: A combined Targeted/Untargeted LC-MS/MS-based Screening Approach for Mammalian Cell Lines Treated with Ionic Liquids: Toxicity Correlates with Metabolic Profile

3.4.2. Introduction

The industrial use of ionic liquids (ILs) as environmentally friendly solvents is steadily increasing [4,429]. Because of their structure, ILs are also called “molten salts” [9]. They have many unique characteristics, such as i) wide temperature range (incl. room temperature) of liquid state, ii) thermal, chemical and electrochemical stability, iii) high electrochemical conductivity. Since they are non-flammable, non-explosive, and non-volatile, they are used in many applications, also owing to their large range of solubilities and miscibilities. Their lack of biodegradability, however, renders toxicity studies imperative [1,5]. This matter is complicated because of the high structural variability and large number of existing ILs, requiring a differentiated picture of toxic effects of ILs [6,429,430]. One important future aspect is the structural design and development of environmentally friendly ILs. For this purpose, the understanding of toxic effects is of high importance, and effects of ILs on metabolic profiles might well serve as an indicator for their toxicity. Along this line, toxicometabolomics and toxicolipidomics could shed some light on effects of ILs [431,432].

Such metabolomics studies could be either devised as targeted or untargeted assays. The former make typically use of UHPLC hyphenated to triple quadrupole instruments with electrospray ionization (UHPLC-ESI-QqQ) which has advantages in terms of sensitivity and linear range [432,433]. The latter use high-resolution mass spectrometry (HR-MS) hyphenated to UHPLC and allow comprehensive recording of all detectable metabolites. However, the new generation of high-resolution mass spectrometers (QTOF and quadrupole-orbitraps) show improved performance for quantitative analysis [221,434]. Hence, there is an increasing interest in performing qualitative and quantitative analysis in a single run [221,435–438]. In general, HR-MS-based untargeted metabolomics is typically performed by data-dependent acquisition (DDA) (also called information-dependent acquisition, IDA). DDA methods use information from an MS scan for selection of the most abundant precursors for fragmentation being able to identify metabolites based on MS/MS spectra. Unfortunately, low abundant metabolites are not triggered for fragmentation [221,262,435,439–441]. Relative quantification is exclusively based on MS data which may be less sensitive. To overcome this shortcoming, data-independent acquisition (DIA) such as all-ion fragmentation (AIF), MS^E, or MS/MS^{ALL} has been proposed as an alternative [192,441]. This acquisition mode selects all

precursor ions for simultaneous co-fragmentation. The resultant MS/MS spectra may be relatively complex composite spectra, if many compounds coelute [192,221]. Consequently, qualitative analysis of unknowns may be quite challenging by these classical DIA methods [433,441]. It has been shown that a better spectral quality data can be obtained with a DIA method called sequential window acquisition of all theoretical fragment ion mass spectra (SWATH) [262,440], an acquisition approach first proposed for linear ion trap [442]. In DIA with SWATH, a sequence of MS/MS experiments with intermediate wide Q1 precursor ion selection windows (SWATH windows) (typically 20-30 Da wide) are consecutively stepped through the targeted m/z range [221,433]. The resultant MS/MS spectra are less complex than in AIF or MS^E, which facilitates identification. A broader metabolite coverage compared to DDA was reported [265,443]. Since MS/MS data have been collected comprehensively throughout the chromatogram, quantitative analysis can be performed on the MS/MS level as well, potentially leading to better sensitivity [442].

Amino acids are central cellular metabolites. For instance, they are important for protein synthesis, cell signalling, and redox balance [444]. Major perturbations may indicate problems with cellular homeostasis. Thus, in the current study amino acids were selected as surrogate biomarkers of cellular toxicity of ILs. Numerous HPLC-MS assays for targeted analysis of amino acids have been reported [194,445,446]. Many times, amino acids were derivatized prior to their analysis to improve detection sensitivity [447]. In the present work, the aim was to develop a fast and straightforward UHPLC-ESI-QTOF-MS/MS method which combines targeted analysis of amino acids without any derivatization and simultaneously allow untargeted profiling of alterations in the metabolome. DIA with SWATH was used as the acquisition mode to realize this combined qualitative/quantitative assay. Human corneal epithelial (HCE) cells were employed as representative model cells. A wide variety of ILs were selected and the metabolic profiles measured after incubation of the HCE cells with ILs at concentration levels corresponding to their median effective concentration (EC_{50}) values [1]. Here we will demonstrate that there is a correlation between the changes in the metabolic profiles and the toxicity of the ILs.

3.4.3. Materials and methods

3.4.3.1. Materials and instruments

Ultra-LC-MS grade acetonitrile was purchased from Carl Roth (Karlsruhe, Germany), MilliQ water was purified with an Elga PurLab Ultra purification system (Celle, Germany), ammonium formate was purchased from Sigma Aldrich (Munich, Germany), cell free amino acid mix (20AA, U-13C, 97-99%+; U-15N, 97-99%) and Metabolomics Amino Acid Mix Standard was purchased from Cambridge Isotope Laboratories (Tewksbury, MA, USA). $^{13}C_2$-maleic acid and $^{13}C_6$-glucose were purchased from Santa Cruz Biotechnology (Heidelberg, Germany), d8-L-valine, ring-d4-L-tyrosine, 3,3,4,4,5,5,6,6-d8-L-lysine·2HCl were purchased from Eurisotop (Saarbrücken, Germany). Phosphate buffered saline (PBS) was made “in-house” by the National Institute of Health and Welfare (THL), Helsinki, Finland. Ham’s F12/Dulbecco’s modified eagle medium (DMEM), fetal bovine serum (FBS), human epidermal growth factor (EGF), insulin, and gentamicin were all purchased from Thermo-Fisher Scientific (Waltham, MA, USA). Methanol and cholera toxin were purchased from Sigma (St. Louis, MO, USA). Cell incubator and centrifuges were from Thermo-Fisher Scientific (Waltham, MA, USA). Samples were ultrasonicated using Soniprep 150 from MSE (London, UK). Standard solutions were prepared as described in Supporting Information.

3.4.3.2. Cell culture and metabolite extraction

The SV-40 immortalized HCE cells [100] were grown in a 10cm petri dish until confluence (8.8 x 10^6 cells) in Ham’s F12/DMEM supplemented with 15% FBS and EGF, insulin, cholera toxin and gentamicin. Before IL treatment, the cells were starved for 18 hours in serum free Ham’s F12/DMEM supplemented with EGF, insulin, cholera toxin, and gentamicin to achieve serum free conditions, eliminate serum growth factor and nutrient activities on the surface of the cells, and equalize all cells to the same cell cycle phase by stopping the cell growth. After starvation, the cells were incubated with different ILs (Figure 79) dissolved in serum free media to achieve concentrations around their EC_{50} values, determined by Ruokonen *et al.* [1].

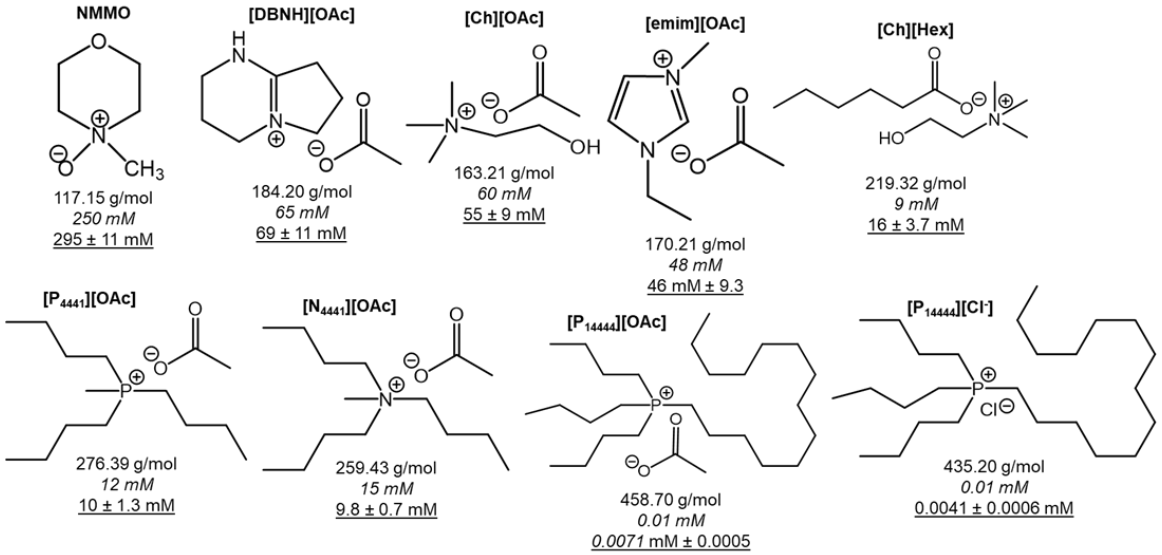

Figure 79: Used ionic liquids (ILs): With corresponding *concentrations used for IL treatment*; Molar mass of the IL and EC_{50}-value ± STD

After 8, 16, and 24h the petri dishes were placed directly on ice for quenching the enzyme activity immediately. The cell monolayer was washed twice with 5 to 7 mL cold PBS buffer before 600 µL of ice-cold extraction mix was added. The extraction mix composed of 258 µL of MeOH, 300 µL of cell free amino acid mix (1 mg/mL), and 42 µL of ACN:H_2O (1:1 v/v). Next, the cells were scraped from the petri dish wall into the extraction mixture and the suspension of the cells was transferred into an Eppendorf tube. The suspension was ultrasonicated with a MSE Soniprep 150 probe ultrasonicator (10 sec, 23 MHz, pulse of 5-7 microns) and centrifuged at 10 000 g for 5 minutes, and the supernatant separated from the cell pellet was stored at -80 °C until further analysis.

3.4.3.3. LC-MS/MS instrumentation

All analyses were performed on a Sciex TripleTOF 5600+ equipped with a Duospray ion source (Sciex, Concord, Ontario; Canada) and carried out with electrospray ionization (ESI) in positive ion mode. The mass spectrometer was coupled to an Agilent 1290 Series UHPLC instrument (Agilent, Waldbronn, Germany) with a Pal HTC-XS autosampler from CTC (Zwingen, Switzerland).

The chromatographic HILIC separation was performed on an Acquity UPLC BEH Amide column (2.1 x 50 mm) packed with 1.7 µm particles (Waters, Eschborn) equipped with an Acquity UPLC BEH Amide 1.7 µm Van-guard column. The mobile phase composed of A) 10 mM ammonium formate in MilliQ water with 0.15 % (v/v) formic acid adjusted to pH 3 and B) 2 mM ammonium formate in ACN with 0.15 % (v/v)

formic acid. The following mobile phase gradient was used: 0.00 – 0.50 min, 95 % B; 0.50 – 0.51 min, 95 – 90 % B; 0.51 – 8.00 min, 90 – 70 % B; 8.00 – 10.00 min, 70 % B; 10.00 – 10.01 min, 70 – 95 % B; 10.01 – 12.00 min, 95 % B. The flow rate was 300 µL/min and the column temperature was set at 40 °C. The injection volume was 2 µL for all measurements.

The following MS settings of the mass spectrometer were identical for all four investigated acquisition modes: Curtain gas (CUR) 20 psi, nebulizer gas (GS1) 60 psi, drying gas (GS2) 60 psi, ion-spray voltage floating (ISVF) +4000 V and source temperature (T) 500 °C. Nitrogen was used as curtain gas, nebulizer gas and drying gas.

High-resolution MS and high-sensitivity MS/MS data for the amino acid mixture containing all 20 proteinogenic amino acids, were acquired by three different acquisition modes: MRM^{HR}, SWATH with fixed Q1 window widths and SWATH with variable Q1 window widths (SWATH 2.0) (for details see Supporting Information). An external calibration was performed every five samples.

For the finally used method, SWATH acquisition mode with variable window widths was utilized. It consisted of a TOF-MS scan (collision energy CoE 10 V, declustering potential DP 30 V, cycle time CT 1.3 s, accumulation time AT 200 ms, SW m/z 30–1000 and RF m/z 20 33 %, m/z 70 33 %, m/z 270 34 %) and several different product ion scans with individual CoE and DP settings (Table 1). The product ion scans consisted of 27 Q1 windows with different window widths in the mass range of 30–300 m/z (Table 1).

3.4.3.4. Calibration and validation

3.4.3.4.1. Matrix effect

The matrix effect (ME) can be determined by calculating the ratios of slopes of calibration functions in presence and absence of matrix components, i.e. post-extraction spike of surrogate calibrants and neat standard solution of surrogate calibrants, according to Equation 12.

$$ME = \frac{slope_{HCE\ extract}}{slope_{neat\ solution}} * 100$$

Equation 12: Calculation of matrix effect (ME): Serial dilutions of $^{13}C,^{15}N$-isotopically labelled amino acids in HCE cell extracts as well as in ACN:MilliQ water (1:1; v:v) were measured, resulting in different calibration functions. The $slope_{HCE\ extract}$ describes the slope of calibration function of serial dilutions in HCE cell extracts and $slope_{neat\ solution}$ in ACN:MilliQ water (1:1; v:v)

Therefore, the $^{13}C,^{15}N$-isotopically labelled amino acids were diluted with ACN:MilliQ water (1:1; v:v) to achieve the same dilutions as described in SI chapter 3.4.6.4. Response factors. The same serial dilutions were prepared in a HCE cell extract (not treated with ILs). Deuterated amino acids were used as internal standards.

3.4.3.4.2. Calibration

$^{13}C,^{15}N$-L-amino acids were used as surrogate calibrants for calibration and validation. The surrogate calibration was prepared in a matrix-matched manner. Different amounts of $^{13}C,^{15}N$-amino acid standard mixture were spiked into an untreated HCE cell extract to prepare dilutions of 1:10; 1:20; 1:40; 1:160; 1:640; 1:1000; 1:4000; 1:16 000; 1:64 000 and 1:250 000. The HCE extract itself was finally diluted by a factor of 10 with ACN:MilliQ water (1:1; v:v) in all calibration solutions. Deuterated amino acids were used as internal standards. The dilution series in cell extract matrix was measured four times. The calibration functions were obtained by plotting peak area ratios versus concentrations of the $^{13}C,^{15}N$-isotopically labelled amino acids. Based on these functions, unweighted linear regression functions were constructed using the MultiQuant software. These calibration functions were used for the quantification of amino acids in treated HCE cell extracts taking the response factors (RF; see SI for details) into account according to Equation 13 where a is the slope and b is the intercept of the calibration function of the $^{13}C,^{15}N$-isotopically labelled amino acids.

$$concentration_{Analyte} = \frac{[area_{Analyte}/area_{internal\ standard}] * RF - b}{a}$$

Equation 13: Calculation of amount analyte ($concentration_{Analyte}$): With a as slope and b as intercept of calibration functions of $^{13}C,^{15}N$-isotopically labelled amino acids. RF describes the response factor and $area_{Analyte}/area_{internal\ standard}$ displays the ratio of the areas of the analyte and the corresponding internal standard

3.4.3.4.3. Validation

The validation process comprising intra-day and inter-day precision and accuracy as well as freeze-thaw stability measurements was carried out by measuring quality control (QC) samples. These were prepared by spiking different amounts of $^{13}C,^{15}N$-isotopically labelled amino acid mixture to untreated HCE cell extracts at different

levels across the entire range. The deuterated amino acids 3,3,4,4,5,5,6,6-d8-L-Lys 2HCl (5 µg/mL), ring-d4-L-Tyr (250 ng/mL), and d8-L-Val (16 ng/mL) were used as internal standards. Eight different QC samples were prepared by dilution (1:12.5; 1:25; 1:100; 1:400; 1:800; 1:2000; 1:10 000 and 1:100 000) of the $^{13}C,^{15}N$-isotopically labelled amino acids spiked HCE cell extracts with ACN:MilliQ water (1:1, v:v). The HCE cell extracts were finally diluted to 1:10 (% v/v) in all QC samples. The inter-day precision and accuracy were determined with n=8 at three different days within a week (day 1, 3, and 4) with a calibration series at the beginning and the end of the measurement sequence. Intra-day precisions and accuracies were calculated separately every single day.

The QC samples for the freeze-thaw stability test were frozen and thawed according to recommendations by the U.S. Food and Drug Administration (FDA) guidelines on bioanalytical method validation. The samples were measured four times and autosampler stability was verified on day four of the validation by measuring the calibration calibrants according to the FDA guidelines.

3.4.3.4.4. Data processing of untargeted analysis

Raw data (.wiff) files were converted to .abf files for using MS-Dial (version 2.80) with a combination of MassBank, MoNA, ReSpect, and GNPS databases. The MS-Dial software was used for peak alignment, peak detection, peak identification, and deconvolution [265,443]. The used parameters for MS-Dial are listed in detail in SI Table S4. Multivariate statistical evaluation of the pre-processed metabolic profiling data was performed with SIMCA-P+ (version12) (Umetrics, Umeå, Sweden). The signal intensity data were log transformed, scaled (Pareto), and finally a Partial least squares (PLS) analysis was carried out using log EC_{50} values as the dependent (Y) variables and all the molecular features as X-variables. The heatmap was generated with Perseus and the data were scaled to z-score.

3.4.4. Results and discussion

3.4.4.1. Chromatographic conditions

Several common HILIC columns were screened initially and BEH Amide (1.7 µm) was finally selected for further optimization of the gradient profile, column temperature (30-60 °C), and flow rate (250-700 µL/min). The prime focus of these experiments was to achieve a separation of the amino acid pairs Leu/Ile, Asn/Asp, and Gln/Glu.

Furthermore, the aim was to keep run times short at sufficient resolution of metabolites to reduce ion suppression (matrix) effects. A temperature of 40 °C and a flow rate of 300 µL/min were selected as a best compromise between a reasonable separation of the amino acids and good sensitivities (*i.e.*, better signal-to-noise, S/N). Figure 80 shows the MS/MS chromatograms (MS chromatogram in case of Gly) of the 20 proteinogenic amino acids obtained the with optimized HILIC method. The amino acids were widely spread over the chromatogram between 3 and 9 min. The isomeric amino acids leucine and isoleucine were fully separated, like the critical amino acid pairs Glu/Gln and Asn/Asp. Some peak tailing was observed for amino acids with basic side chains and aspartic acid. Such peak tailing can be reduced by using higher buffer concentrations at expense of signal intensity loss which was therefore not implemented.

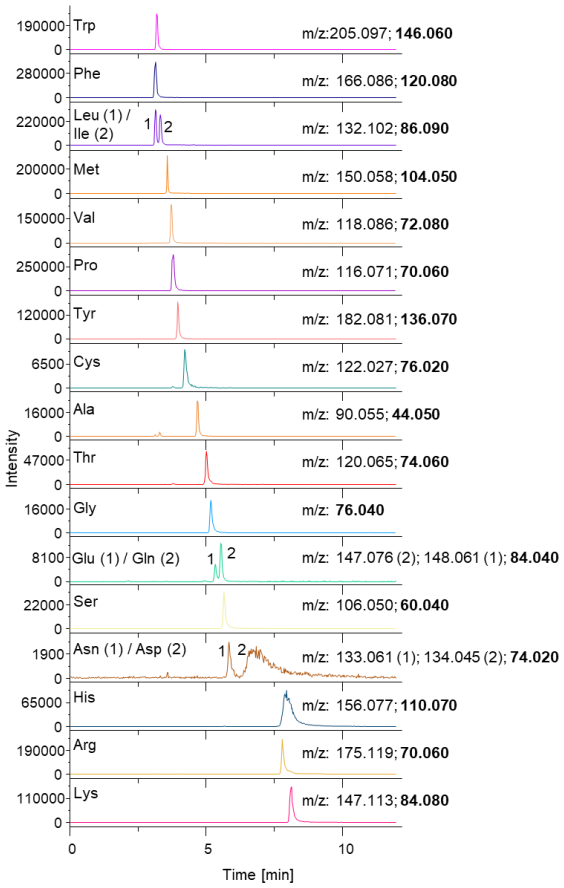

Figure 80: Chromatographic separation: Chromatographic separation of a standard solution of 20 proteinogenic amino acids (10 µg/mL) in HILIC mode using a BEH Amide column and the optimized SWATH 2.0 method. The m/z values of precursor and fragment ions (**bold**) are listed on the right side. For the EIC chromatograms fragment masses were used

3.4.4.2. Mass spectrometry settings and acquisition mode

The adopted acquisition mode should allow sensitive detection of the targeted compounds and, on the other hand, a molecular profiling without prior knowledge of the molecular structure of sample components. One option is to utilize product ion scans (termed MRM^{HR}) with unit mass Q1 precursor selection for fragmentation and HR-MS/MS spectra readout by the TOF mass analyser. It allows comprehensive untargeted profiling in MS mode while additionally for preselected targets MS/MS spectra are recorded throughout the chromatogram. Therefore, MS/MS chromatograms (EICs) can be generated for the targeted compounds. These EICs are benefiting from the effective filtering of the background noise and the narrow isolation windows (usually 5-10 mDa wide). Unfortunately, for untargeted molecules no MS/MS data are available if this acquisition mode is selected. This limits identification and metabolite coverage. Since DDA provides MS/MS spectra for the most abundant precursors only and does not allow to extract MS/MS-chromatograms, we decided to evaluate DIA with SWATH in comparison to MRM^{HR} (parameters see SI Table S3) as data acquisition mode.

SWATH combines features of targeted and untargeted profiling assays. Each MS cycle in this acquisition mode consisted of a TOF MS scan over a predefined *m/z*, herein *m/z* 30-300, followed by a series of MS/MS experiments covering the entire m/z range by a set of sequential intermediate-sized Q1 precursor isolation windows (SWATH windows). Two distinct SWATH methods were compared: One with fixed SWATH windows which consisted of 27 MS/MS experiments each with 10 Da Q1 isolation width (SWATH with fixed Q1 windows; see SI Table S4 and SI Figure S19). A second method made use of variable Q1 precursor isolation windows which were narrower for the targeted precursors (*e.g.* 2-5 Da wide; one to four amino acids per SWATH window) and wider for other m/z ranges (SWATH with variable window approach; SWATH 2.0, see Table 6 and SI Figure S19). Co-eluting compounds which are co-isolated in the same SWATH window for fragmentation yield composite spectra. Hence, MS/MS spectra quality may be worse than in DDA, but deconvolution may remove contaminating ions leading to reasonable spectral quality. In the variable SWATH window approach, assay specificity can be adjusted by selection of narrow Q1 windows for targets. The great benefit of these SWATH methods is that MS/MS data are acquired comprehensively across the peak, over the entire chromatogram and across

all samples. This enables post acquisition selection of the most suitable ion (precursor from MS^1, precursor from MS^2 if available, or any fragment ion from MS^2) for signal processing and data evaluation whichever is more selective and/or more sensitive. In this combined targeted/untargeted assay, ion source and fragmentation parameters were optimized for the targeted amino acids (for MRM^{HR} method see SI Table S3, for SWATH with fixed Q1 windows approach see SI Table S4 and for the finally selected SWATH with variable Q1 windows approach, denoted SWATH 2.0, see Table 6). For each SWATH window CoE and DP can be set individually to achieve the highest sensitivity for the target masses of interest.

Table 6: Overview of the MS-settings: Used for SWATH acquisition mode with variable Q1 window widths; in bold are the "targeted" Q1 windows

Experiment number	Q1 window range [m/z]	target amino acid; precursor mass [m/z]; fragment mass [m/z]	Collision energy [V]	Declustering potential [V]
SWATH with variable Q1 window width				
0	30 - 1000	TOF MS	10	30
1	30 - 75		10	20
2	**75 - 80**	Gly; 76.0393; -	5	20
3	80 - 89		10	20
4	**89 - 95**	Ala;90.0547;44.0533	21	10
5	95 - 105		10	20
6	**105 - 111**	Ser;106.0499;60.0462	20	10
7	111 - 115		10	30
8	**115 - 117**	Pro;116.0706;70.0685	20	20
9	**117 - 119**	Val;118.0863;72.0833	16	20
10	**119 - 121**	Thr;120.0655;74.0618	17	30
11	**121 - 123**	Cys;122.0270;76.0236	20	20
12	123 - 131		17	30
13	**131 - 135**	Leu/Ile;132.1019;86.0979 Asn;133.0608;74.0258 Asp;134.0448;74.0260	12	30
14	135 - 146		14	30
15	**146 - 149**	Gln;147.0764;84.0457 Lys;147.1128;84.0822 Glu;148.0613;84.0450	23	15
16	**149 - 151**	Met;150.0583;104.0530	15	60
17	151 - 155		25	20
18	**155 - 157**	His;156.0768;110.0710	21	40
19	157 - 164		10	30
20	**164 - 167**	Phe;166.0863;120.0810	23	15
21	167 - 174		23	15
22	**174 - 177**	Arg;175.1190;70.0679	35	50
23	177 - 181		21	10
24	**181 - 183**	Tyr;182.0812;136.0752	22	20
25	183 - 204		30	30
26	**204 - 206**	Trp;205.0972;146.0598	25	10
27	206 - 300		25	10

The three acquisition modes mentioned above were compared to each other. The relative peak areas of the amino acid fragment masses having the same concentration were evaluated with MultiQuant software. The measured concentrations of the neat amino acid standard mixtures are listed in SI Table S5. The comparison in SI Figure S20, however, is based on the lowest measured concentration of each amino acid (*i.e.* concentration level 8), except for L-Cys (640 ng/mL), L-Asp (400 ng/mL), and L-Met (6.4 ng/mL). SI Figure S20 shows the results normalized to the peak areas of MRM^{HR}. The column chart clearly visualizes the sensitivity improvement of SWATH 2.0 (SWATH with variable Q1 windows) compared to SWATH (SWATH with fixed Q1 windows) and MRM^{HR}. Since most of the SWATH 2.0 windows contained only one target amino acid, the target-optimized CoEs and DPs could be transferred from MRM^{HR} to the respective SWATH windows. In this context, it is interesting to note that, in spite of identical CoE, DP, and accumulation times, the sensitivities of the SWATH method with variable windows was better than with MRM^{HR}. With fixed SWATH windows of 10 Da, a compromise in CoE/DP had to be accepted for many amino acids because several of these targets were isolated in the same SWATH window (see SI Table S4) causing lower sensitivity. SWATH with variable Q1 windows was therefore selected as acquisition mode for the further work and MS settings optimized for each window.

With the optimized SWATH method (Table 6) peak group chromatograms, *i.e.,* series of overlapping MS/MS chromatograms as exemplified in Figure 81A, can be obtained for both targeted as well as untargeted metabolites due to comprehensive MS/MS data. The corresponding MS/MS spectra as measured in standard solution, HCE cell extract, and the deconvoluted MS/MS spectra with database match are shown in Figure 81B, C, and D, respectively. MS/MS spectra and peak group chromatograms of all the other target amino acids are shown in SI Figure S21 and Figure S22, respectively. MRM^{HR} offers this possibility only for the previously selected targets, but not for the untargeted metabolites. Examples of MS/MS chromatograms of untargeted metabolites are depicted in Figure 82A and Figure 82B along with corresponding MS/MS spectra in standard solution, HCE extract and deconvoluted ones from HCE extract (Figure 82C, D and E).

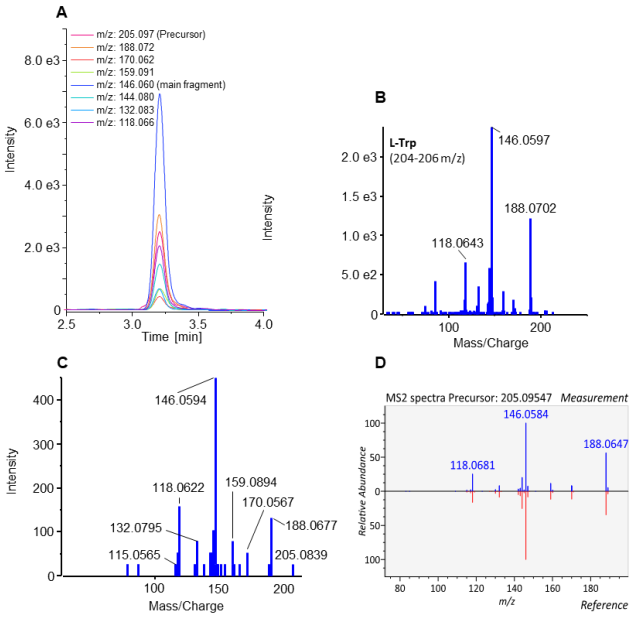

Figure 81: Targeted analysis of Tryptophan (precursor: m/z 205.097 and main fragment: m/z 146.060) in HCE cell extracts (QC sample): (A) Peak group chromatograms measured by SWATH 2.0, the extracted fragment mass was m/z 146.06 with an extraction window of +/- 5 mDa; (B) MS/MS spectrum by SWATH 2.0 measured in HCE cell extracts; (C) MS/MS spectrum of tryptophan in neat standard solution measured by MRM^{HR}; (D) deconvoluted MS/MS spectrum (blue) matched against database spectrum (red)

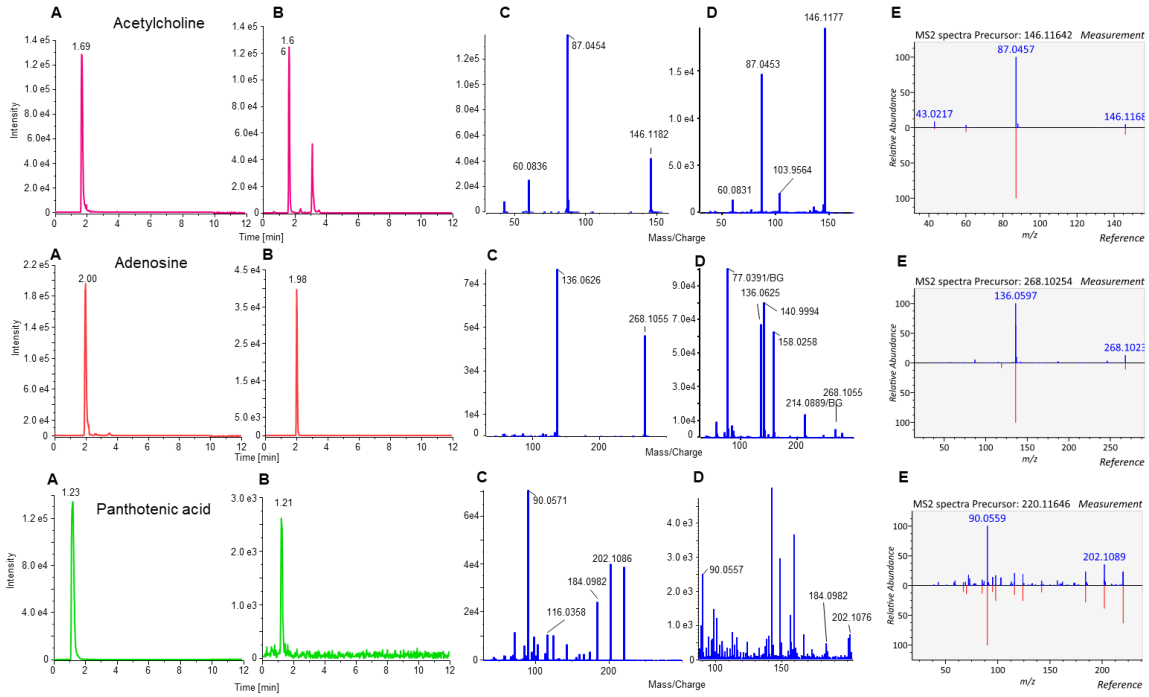

Figure 82: Examples of identified metabolites from untargeted analysis of HCE cell extracts: (A) EIC MS/MS chromatogram (Acetylcholine: m/z 146.1153, Adenosine: m/z 268.1030 and Pantothenic acid: m/z 220.1168; m/z values were used for EIC generation in A and B) of standard solution with an extraction window of +/- 5 mDa; (B) EIC MS/MS chromatogram of HCE extract with an extraction window of +/- 5 mDa; (C) MS/MS spectrum from standard solution; (D) MS/MS spectrum from HCE extract; (E) deconvoluted MS/MS spectrum from the HCE extract (blue) matched against database spectrum (red)

The most intensive signal (and/or the one with suitable assay specificity) was then selected post-acquisition for quantitative analysis of the targets (Table 7) while other signals were used as qualifiers for verification. Table 7 shows S/N ratios (calculated by PeakView software) for distinct EICs from a HCE cell extract measured using SWATH 2.0 (with variable Q1 windows). The S/N ratios are based on EICs for either the precursor ion in MS or MS/MS experiment or the fragment ion in the MS/MS experiment. As can be seen, the MS/MS signals are by far more sensitive (best S/N always obtained with fragment ion in the corresponding SWATH window except for Gly and Pro for which the precursor ion in the corresponding SWATH window gave higher S/N) (Table 7).

Table 7: Comparison of S/N ratios (as calculated with PeakView): For EICs of precursor ions from TOF-MS scans, of precursor ions from MS/MS experiment (i.e. corresponding SWATH window), and of fragment ions from MS/MS experiment (SWATH window) as measured in HCE cell extract (QC sample)

				Signal-to-noise		
Amino acid	Precursor ion [m/z]	Fragment ion [m/z]	Internal standard[b]	S/N Precursor TOF-MS	S/N Precursor SWATH window	S/N Fragment SWATH window
Gly	76.0393	-	d-Tyr	43	**1407**	-
L-Ala	90.0547	44.0533	d-Tyr	175	13	**418**
L-Ser	106.0499	60.0462	d-Tyr	33	10	**184**
L-Pro[c]	116.0706	70.0685	d-Tyr	2962	**5286**	3439
L-Val	118.0863	72.0800	d-Val	224	336	**1069**
L-Thr	120.0655	74.0618	d-Tyr	379	215	**1819**
L-Cys	122.0270	76.0236	d-Tyr	-[a]	-[a]	-[a]
L-Leu	132.1019	86.0979	d-Val	133	114	**1232**
L-Ile	132.1019	86.0979/(69.0727)	d-Val	122	140	**2671/(111)**
L-Asn	133.0608	88.0395	d-Tyr	-[a]	-[a]	-[a]
L-Asp	134.0448	88.0394	d-Lys	-[a]	-[a]	-[a]
L-Gln	147.0764	84.0457	d-Tyr	-[a]	-[a]	-[a]
L-Lys	147.1128	84.0822	d-Lys	46	6	**297**
L-Glu	148.0613	84.0450	d-Tyr	246	36	**1017**
L-Met	150.0583	104.0527	d-Val	297	292	**971**
L-His	156.0768	110.0714	d-Lys	111	90	**849**
L-Phe	166.0863	120.0814	d-Val	592	96	**6762**
L-Arg	175.1190	70.0679	d-Lys	200	-	**1108**
L-Tyr	182.0812	136.0752	d-Tyr	318	41	**1579**
L-Trp	205.0972	146.0598	d-Val	43	-	**645**

[a] not detected in HCE cell extract samples

[b] assignment based on retention times of the amino acid and the corresponding internal standard

[c] very high abundant in HCE cell extracts, therefore end of linear range (ULOQ) is easily reached

in bold: most sensitive signal with highest S/N ratio used for quantitation (except Pro for which also the fragment ion was used)

3.4.4.3. Method calibration and validation

Due to significant endogenic amino acid levels in HCE cells, no blank matrix was available for calibration and validation. Working with an artificial matrix or standard addition were ruled out as options. To ensure an accurate quantification, a surrogate calibration method was chosen [448]. In this approach, isotope-labelled standards were used as external calibrants instead of the authentic reference compounds. However, the detector response of the surrogate calibrant had to be the same as for the respective target analyte (parallelism of calibration lines). If a significant deviation occurs, as in this work for the target amino acids, a response factor correction (see SI, Equation S1) has to be applied. Response factors of uniformly-^{13}C,^{15}N-labelled amino acids were determined in comparison to authentic amino acids by their respective slope ratios (see SI Table S7) and applied to obtain corrected calibration functions (Equation 13) (SI Figure S23).

Matrix effects are a prime source for inaccurate results in quantitative LC-MS analysis with ESI and represent always a considerable challenge, especially in metabolomics [449]. Due to sample complexity and elimination of dedicated sample preparation to avoid metabolite losses, the accuracy of the results can be negatively influenced by the matrix effects. Therefore, matrix effects were estimated by establishing calibration series of surrogate calibrants (^{13}C,^{15}N-labelled amino acids) in matrix (HCE cell extract) and in matrix-free (neat) solutions using Equation 12. Table 8 summarizes the results for the determined matrix effects. For a majority of targeted amino acids, matrix effects are in an acceptable range. However, for a small number of targets, there is a significant matrix effect. Hence, it is advisable to perform matrix-matched calibration and for this reason a surrogate calibrant approach was selected.

Table 8: Summary of validation: Calibration, method sensitivity and estimation of matrix effects (n = 4)

Compound Name	M [g/mol]	t_R [min]	Product ion (m/z)	Slope	S_e (slope)	Intercept	S_e (intercept)	Linearity (R^2)	LLOQ [ng/mL]	ULOQ [µg/mL]	Absolute matrix effect [%]
Glycine	79.0	5.24	79.04	0.00442	0.00010	-0.05	0.72	0.9943	47	19	122
L-Alanine	94.1	4.74	47.05	0.00527	0.00005	-0.11	0.26	0.9990	56	11	107
L-Serine	110.1	5.72	63.05	0.00449	0.00005	-0.30	0.28	0.9989	66	13	99
L-Proline	122.1	3.83	75.08	0.15950	0.00105	0.14	0.22	0.9996	1	0.5	72
L-Valine	124.1	3.78	77.09	0.04902	0.00049	0.08	0.33	0.9988	1	1.8	76
L-Threonine	125.1	5.09	78.07	0.00852	0.00008	0.00	0.26	0.9991	19	7.5	100
L-Cysteine [a]	126.0	9.11	124.02	0.00027	0.00000	0.20	0.03	0.9998	600	60	145
L-Leucine	139.1	3.18	92.11	0.07897	0.00103	-0.12	0.94	0.9983	5	2	90
L-Isoleucine	139.1	3.36	92.11	0.09605	0.00054	-0.03	0.46	0.9997	5	2	105
L-Aspartic acid	139.1	6.85	92.05	0.00071	0.00001	0.02	0.08	0.9995	333	33	152
L-Lysine	155.1	8.15	90.10	0.00580	0.00003	0.09	0.03	0.9998	6	2.3	105
L-Glutamic acid	154.1	5.63	89.06	0.00942	0.00016	-0.32	1.31	0.9971	92	18.4	134
L-Methionine	156.1	3.60	109.06	0.01078	0.00021	-0.07	0.76	0.9968	23	9.3	78
L-Histidine	165.1	8.12	118.08	0.02213	0.00034	0.57	0.40	0.9980	24	2.4	110
L-Phenylalanine	176.1	3.15	129.11	0.04264	0.00056	0.03	0.62	0.9982	2	2.6	80
L-Arginine	185.1	7.86	75.08	0.01401	0.00010	0.16	0.14	0.9995	2	3.3	120
L-Tyrosine	192.1	4.00	145.10	0.00572	0.00005	0.09	0.41	0.9992	28	22.7	85

$^{13}C,^{15}N$ isotopically labelled amino acids (Eurisotop Std) were used as surrogate calibrants

The linear range is from LLOQ to ULOQ

The amino acids Trp, Asn and Gln were not included in the $^{13}C,^{15}N$ isotopically labelled amino acid standard mixture. Asn and Gln were therefore not calibrated but were also not detected in the HCE cell extracts at all. Trp was calibrated based on $^{13}C,^{15}N$-Lys as surrogate calibrant (see SI Table S7)

[a] Cysteine was detected as the dimer cystine with m/z 124.02 in the SWATH window of m/z 206 - 300

Deuterated amino acids were used as internal standards (see Table 7). The calibration series consisted of 10 different concentrations of $^{13}C,^{15}N$-amino acids spiked into untreated HCE cell extract samples. The linear range, lower-limit-of-quantification (LLOQ) and upper-limit-of-quantification (ULOQ) were determined according to FDA guidelines and these are summarized in Table 8 along with slope, intercept, and linearity values for each amino acid. These guidelines set the following criteria: the S/N ratio should be equal to 10 or higher with a precision of 20% and an accuracy of 100 ± 20% for the LLOQ and the ULOQ. The concentration levels should be in between the LLOQ and ULOQ and an accuracy of 100 ± 15% is needed. The linear range should cover two to three orders of magnitude with an R^2 of >0.99 for all analytes.

During the validation process intra-day and inter-day precision were determined with eight different QC samples, which were composed of $^{13}C,^{15}N$-amino acids spiked into untreated HCE cell extract samples with deuterated amino acids as internal standards. Nevertheless, only three QC samples (QC_{low}, QC_{middle}, QC_{high}; for concentrations see SI Table S8) were taken into consideration for assessment. Accuracies (as % recoveries) and precisions (as coefficients of variation CV in %) were determined on three different days. All results were evaluated based on FDA guidelines with the following criteria: the QC samples should show an accuracy of 100 ± 15 %. Every QC sample was measured eight times and according to the guidelines four out of the eight should be within 15% CV. Additionally, the freeze/thaw stability of the cell extracts was examined by preparing the same QC samples according to FDA guidelines.

The results of the validation and stability study are summarized in SI Table S8. Since accuracies were between 88 and 115% and precisions <13% CV, the targeted assay was found to be suitable for quantitative analysis of amino acids in HCE cell extracts.

3.4.4.4. Application to Human Corneal Epithelial Cell Extracts

The validity and applicability of the targeted assay was verified by measuring several HCE cell extracts (controls and IL treated ones) after 1:10 dilution. The sample injection order was randomized and is shown in SI Table S9. The corresponding quantitative results for amino acids are summarized in SI Table S10. The calculations of the concentrations were based on linear calibration functions of $^{13}C,^{15}N$-isotopically labelled amino acids, taking the response factor correction into account (Table 8).

Except for Cys, Gln, Asn, and Asp all proteinogenic amino acids were detected in the cell extracts.

A closer look at the amino acid concentrations as a function of the treatment with different ionic liquids (see SI Table S10) reveals clear trends for the classification of the amino acids into the same chemical group. For example, the essential aliphatic amino acids Leu, Ile, and Val are not much affected by the addition of ionic liquids. Alanine concentrations in the IL-treated cells, on the other hand, decrease in comparison to the control samples depending on the toxicity of the IL. Similar to alanine, the concentration of glycine decreases the more toxic the IL is, except for the two choline containing ILs. Altered concentrations are found for other amino acids as well. This supports the hypothesis of Ruokonen *et al.* that ILs, *e.g.* [Ch][Hex], interact with the cell membrane and affect the cell metabolism [1].

Additional information was provided by the untargeted metabolic profiling data. The data pre-processing was done with MS-Dial comprising peak spotting, deisotoping, adduct annotation, alignment, deconvolution, and identification based on metabolomics data bases described in detail above [265]. Successful identification of several metabolites in HCE cell extracts by spectral match in various databases was verified with authentic standards (Table 9). The tentative metabolites were injected as a standard mixture dissolved in MilliQ water and product ion scans were acquired. Retention times and MS/MS spectra of the tentative metabolites acquired in the standard solution were compared with the corresponding data measured in the HCE cell extracts (SI Figure S24) and some representative results are shown in Figure 82. In case of acetylcholine and oxo-proline more than one peak with the same precursor mass was detected in the HCE extract, but the right peak was easily identified using the MS/MS spectra. Raw MS/MS spectra of SWATH acquisition often have poor spectral quality because they represent composite spectra of several precursors isolated in the same Q1 (SWATH) window which are fragmented simultaneously. The composite MS/MS spectra of the TOF-MS read out may be difficult to interpret in some cases. However, MS-DIAL has implemented a deconvolution tool which provides deconvoluted MS/MS spectra of good quality and matches them against database spectra. For example, the raw MS/MS spectrum of acetylcholine in the HCE extract (Figure 82D; top panel) is of relatively good quality and shows the three main fragments found in the reference spectrum of the standard solution (Figure 82C; top panel).

Table 9: Identified metabolites: Identified metabolites from untargeted profiling in HCE extracts (other than amino acids)

Compound	sum formula	t_R in neat solution [min]	t_R in HCE extracts [min]	Δt_R [min]	Precursor m/z (experimental)	Precursor m/z (calculated)	error [ppm]	Fragment masses [m/z]
Acetylcholine	$C_7H_{16}NO_2$	1.69	1.66	0.03	146.1177	146.1176	0.7	87.0454; 60.0836
Adenosine	$C_{10}H_{13}N_5O_4$	2.00	1.98	0.02	268.1041	268.1040	0.4	136.0626
Betaine	$C_5H_{11}NO_2$	3.33	3.31	0.02	118.0866	118.0863	2.5	59.0756; 58.0679
Choline	$C_5H_{14}NO$	2.26	2.18	0.08	104.1071	104.1070	1.0	60.0837
D-(+)-Pantothenic acid	$C_9H_{17}NO_5$	1.23	1.21	0.02	220.1178	220.1180	0.9	202.1086; 184.0982; 116.0358; 90.0571
Guanosine	$C_{10}H_{13}N_5O_5$	3.32	3.31	0.01	284.1006	284.0990	5.6	152.057
L-5-Oxoproline	$C_5H_7NO_3$	2.80	2.75	0.05	130.0497	130.0499	1.5	84.0463; 56.0531
O-Acetyl-L-carnitine	$C_9H_{17}NO_4$	2.92	2.94	-0.02	204.1229	204.1230	0.5	145.0496; 85.0295; 60.0832
Taurine	$C_2H_7NO_3S$	3.91	3.86	0.05	126.0212	126.0219	5.6	108.0125; 44.0551
Thiamine	$C_{12}H_{17}N_4OS$	3.59	3.51	0.08	265.1115	265.1118	1.1	144.0479; 122.0722; 81.0465
Norvaline	$C_5H_{11}NO_2$	3.29	3.31	-0.02	118.0858	118.0863	4.2	101.0609; 100.0770; 83.0508; 59.0755; 58.0684; 56.0530; 55.0579
5-Aminopentanoic acid	$C_5H_{11}NO_2$	3.29	3.31	-0.02	118.0858	118.0863	4.2	101.0609; 100.0770; 83.0508; 59.0755; 58.0684; 56.0530; 55.0579

[HMDB]: Human metabolome database

Only a minor contaminating ion (m/z 103.9564) is present, which was, however, removed in the deconvoluted MS/MS spectrum (Figure 82E; top panel). On the other hand, the MS/MS spectrum of adenosine measured in the HCE extract shows poor quality (Figure 82D; middle panel). However, the deconvoluted spectrum perfectly matches with the MS/MS spectrum of the standard solution and database. The co-fragmented ions were successfully removed by the deconvolution approach. Hence, efficient deconvolution can overcome limited spectral quality of SWATH acquisition. Similarly, the MS/MS spectrum of pantothenic acid measured in the cell extract is not a good match with the spectrum obtained from the standard solution (Figure 82, bottom; *cf.* D and C). Again, the deconvolution process re-establishes an MS/MS spectrum of sufficient quality for spectral matching with standard solutions and MS/MS databases (Figure 82E, bottom).

PLS analysis was performed with EC_{50} values as dependent variables to explore whether there is a correlation between the metabolic profiles in IL-treated HCE cells and the toxicity of the ILs. Both data sets (Y and X-matrices) were log transformed prior to PLS. Figure 83 shows the resultant score plot of the first two principal components.

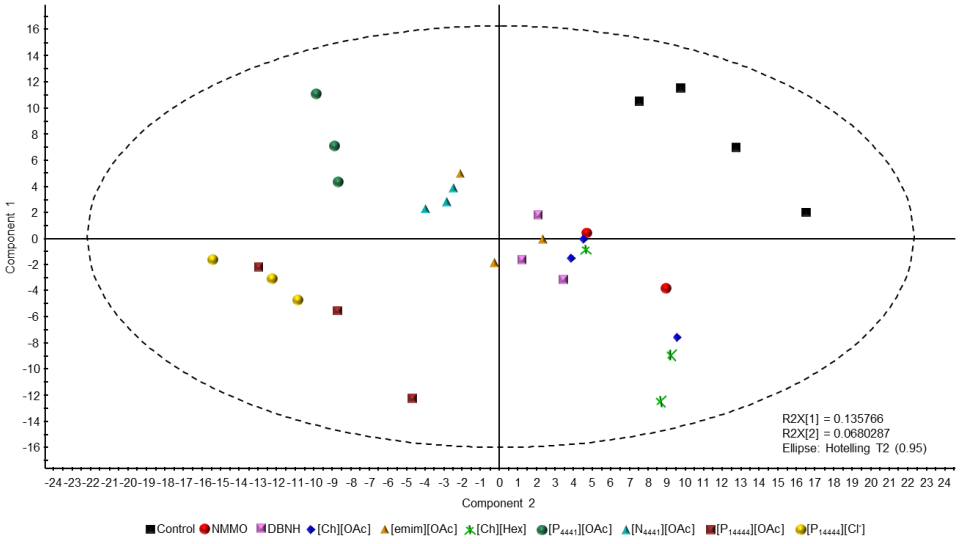

Figure 83: Multivariate data analysis: PLS analysis showing the correlation of toxicity data (log EC_{50} as dependent variable) and metabolic profile (all molecular features log transformed as independent variables): Score plot of 1st and 2nd principal component (for statistical parameters see SI Table S11)

The full statistical data of the PLS model is given in SI Table S11. The PLS model shows a good model fit ($R^2Y_{(cum)}$ = 0.997 with 4 principal components PCs) and yields a satisfactory predictive power ($Q^2_{(cum)}$ = 0.884 with 4 PCs). In the score plot the most toxic ionic liquids tributyl(tetradecyl)phosphonium acetate ([P_{14444}][OAc]) and

tributyl(tetradecyl)phosphonium chloride ([P_{14444}]Cl) are grouped together in a cluster that is most distant from the controls. The second most toxic ILs tributylmethylphosphonium acetate ([P_{4441}][OAc]) and tributylmethylammonium acetate ([N_{4441}][OAc]) are also farther away from the controls than the least toxic IL 1,5-diazabicyclo(4.3.0)non-5-enium acetates ([DBNH][OAc]) and the reference compound *N*-methylmorpholine N-oxide (NMMO). The results are confirmed by the heatmap shown in Figure 84.

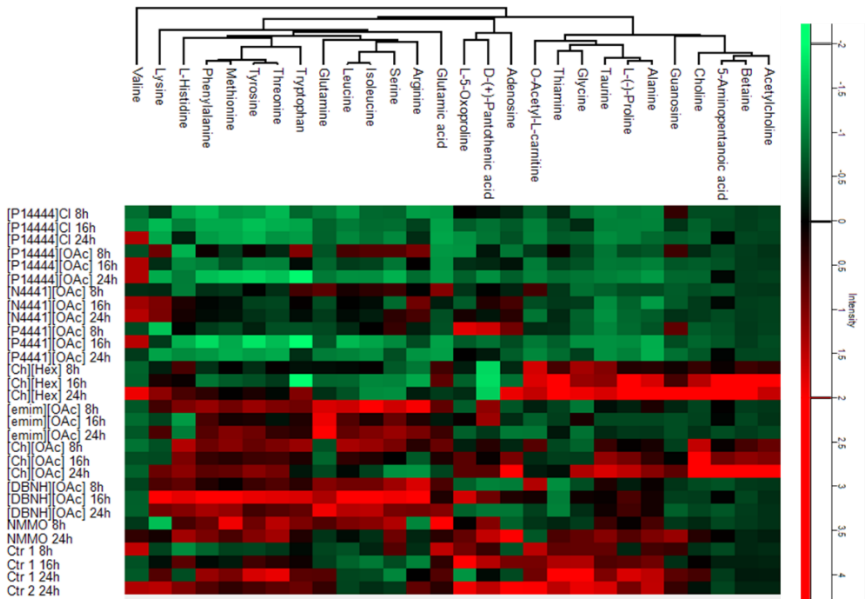

Figure 84: Heatmap: Showing perturbations of identified features by ILs as compared to untreated controls of HCE cells; intensities were z-score normalized and the samples (treated with IL) are sorted by EC_{50} values (from low on top to high at the bottom)

It visualizes the relative concentration profiles of target amino acids and other identified metabolites according to the IL used for the treatment. Z-score normalization of the data was applied. The most significant perturbations can be seen for the two ILs with the highest toxicity ([P_{14444}][OAc] and [P_{14444}]Cl). Additionally, [P_{4441}][OAc] shows also significantly altered metabolite concentrations. This was partly expected regarding its EC_{50} value.

In general, our data suggest that cellular toxicometabolomics profiling of ILs can be a useful strategy to classify ILs for their toxicity potential. Already Ruokonen *et al.* pointed out that the used ILs can be separated into three groups based on their toxicity mechanism [1]. ILs, which exert toxicity by penetrating into the cell membrane ([P_{14444}][OAc], and [P_{14444}]Cl), ILs which affect both the cell membrane and the cell metabolism ([P_{4441}][OAc], and [Ch][Hexanoate]), and ILs which only influence cell

metabolism ([N_{4441}][OAc], [emim][OAc], [DBNH][OAc], [Ch][OAc], and the reference compound NMMO) [1]. The different groups are also clearly seen in the LC-MS analysis results in form of grouped ILs in the PLS score plot (Figure 83). Therefore, the most harmful ILs are [P_{4441}][OAc], [P_{14444}][OAc], and [P_{14444}]Cl, however, there are two different toxicity mechanisms involved [1].

3.4.5. Conclusions

A targeted UHPLC-ESI-MS/MS method for amino acids combined with untargeted metabolic profiling in cells after IL treatment was developed and utilized for a preliminary toxicometabolomics study. Data independent acquisition using SWATH with variable Q1 window sizes (narrow Q1 precursor isolation windows for the target amino acids and wider Q1 windows for other metabolites) provided comprehensive MS and MS/MS data for quantification in either MS or MS/MS mode. The latter was shown to be more sensitive. Uniformly ^{13}C,^{15}N-labelled amino acids were used as surrogate calibrants for accurate quantification of the target metabolites. PLS analysis revealed a significant correlation between the toxicity (as measured by EC_{50} values) and the metabolic profiles in IL-treated HCE cells.

The results of the targeted and untargeted analysis support the data of Ruokonen *et al.* [1]. The most toxic ILs ([P_{14444}][OAc] and [P_{14444}]Cl) result in different heatmap profiles compared to the practically harmless ILs (*e.g.* [emim][OAc]). Therefore, LC-MS based metabolic profiling is a useful strategy in the future for screening the toxicity of ILs. A full toxicometabolomics study will be carried out with selected ILs implementing a sufficient number of biological replicates and focusing on a wider metabolite coverage (positive and negative ion mode; hydrophilic and lipophilic metabolites) to allow derivation of meaningful interpretation of the toxicometabolic regulations.

3.4.6. Supporting Information

A combined Targeted/Untargeted LC-MS/MS-based Screening Approach for Mammalian Cell Lines Treated with Ionic Liquids: Toxicity Correlates with Metabolic Profile

3.4.6.1. Sample preparation

3.4.6.1.1. Amino acid standard mixture

The amino acid standard mixture contained all 20 proteinogenic amino acids, prepared from single amino acid stock solutions of 1 mg/mL dissolved in ACN/MilliQ water (v/v; 1:1), except L-Cys, L-Tyr, L-Glu, L-Asn and L-Asp, which were dissolved in ACN/MilliQ water (v/v; 1:4) containing 0.45% (v/v) trifluoroacetic acid. From each single amino acid stock solution, equal amounts were mixed to obtain a mixed amino acid stock solution with a concentration of 50 µg/mL of each amino acid. A second amino acid standard mixture contained 20 proteinogenic amino acids with a final concentration of 2.5 mM and was prepared from the 20 single amino acid standard solutions (50 mM) which were dissolved in 0.1 M HCl.

3.4.6.1.2. Internal standards

As internal standards d8-L-valine (40 ng/mL), ring-d4-L-tyrosine (5 µg/mL), 3,3,4,4,5,5,6,6-d8-L-lysine 2HCl (25 µg/mL) dissolved in ACN/MilliQ water (v/v; 1:1) were used for all calibrations and the validation process. Cell free amino acid mix (20AA, U-13C, 97-99%+; U-15N, 97-99%) (500µg/mL) were additionally used as an internal standard in all cell extract samples.

3.4.6.2. Optimization of mass spectrometry settings

3.4.6.2.1. Optimization of source settings

Different source temperatures between 150 °C and 500 °C were investigated in steps of 50 °C. A temperature of 500 °C showed the best signal-to-noise (S/N) ratio combined with the optimized gradient, the optimized flow rate (300 µL/min), and the optimized column temperature (40 °C).

The nebulizing gas was screened in the range of 0 to 90 psi in intervals of 10 psi by direct infusion of the standard amino acid mixture (10 µg/mL). Standard settings were chosen for the remaining MS parameters: GS2 40 psi; CUR 30 psi and ISVF 5500 V.

Without any nebulizing gas the MS spectrum appeared empty, *i.e*. the ESI process was highly ineffective. A nebulizing gas pressure at 60 psi gave the best results. Since the nebulizing gas and the drying gas are closely linked to each other, the drying gas was subsequently optimized. Similar to the nebulizing gas, a range between 0 and 90 psi was investigated also in steps of 10 psi, keeping the other settings constant and the nebulizing gas at 60 psi. There were no big differences in the MS spectra, but the intensities were a bit higher with a stronger flow of the drying gas. The optimal pressure for the drying gas was 60 psi. The third optimized gas flow was the curtain gas. It was varied between 20 to 50 psi in steps of 10 psi. The best results were achieved with the curtain gas at 20 psi. As a last step, the ISVF voltage was optimized. It turned out that a voltage of 5500 V, which corresponds to the possible maximum, is not necessary for an optimal result. Above 4000 V, no improvement of the result could be achieved.

3.4.6.2.2. Optimization of fragment mass detection

For the best limit-of-quantification (LOQ) values optimized collision energy (CoE) values for every single amino acid are very important, which clearly emerged during method development. The CoE was finally adjusted based on the highest possible intensity of particular main fragment masses shown in Table 6 of the main document. The screening was performed by direct infusion of single amino acid standards (1 mg/mL). In a further study, it became clear that not only the CoE plays an important role for optimal results but also the declustering potential (DP) significantly influences the intensity of the detected fragments. Therefore, the DP was also optimized for the same fragment masses. The optimized CoE and DP values for the final method are shown in Table 6 of the main document.

3.4.6.3. Comparison of acquisition modes

Different acquisition modes were compared based on the relative peak areas of the amino acids. For this purpose, a dilution series with different concentrations of distinct amino acids was prepared. The above described single amino acid standard solutions were mixed together in three different groups. Group I comprised L-Phe, L-Leu, L-Ile, L-Met, L-Pro, L-Tyr, and L-Arg, 5 µL each (5 µg/mL), L-Trp, and L-Val, 12.5 µL each (12.5 µg/mL) and 25 µL of L-Lys (25 µg/mL) dissolved in 915 µL solvent (ACN:MilliQ water, 1:1; v:v). Group II comprised 20 µL of L-Gln, L- Glu and L-His (20 µg/mL), 50 µL of L-Ser and Gly (50 µg/mL), 200 µL of L-Asn (200 µg/mL), and 100 µL of L-Ala and

L-Thr (100 µg/mL). Group III comprised 500 µL of each remaining amino acid L-Asp and L-Cys (500 µg/mL). These group stock solutions (I-III) were diluted by a factor of 20 to give final stock solution concentrations of 250 ng/mL, 625 ng/mL and 1.25 µg/mL (group I), 10 µg/mL, 5 µg/mL, 2.5 µg/mL, and 1 µg/mL (group II) and 25 µg/mL (group III). The final stock solutions were mixed together to prepare different concentrations according to SI Table S5. A volume of 5 µL of the diluting solvent was replaced by U-^{13}C,^{15}N “cell free” amino acid mix (1 mg/mL).

3.4.6.3.1. Multiple reaction monitoring acquisition mode

The high-resolution (HR) multiple reaction monitoring (MRM^{HR}) mode consisted of a TOF-MS scan in high-resolution mode with the following parameters: accumulation time (AT) 200 ms, cycle time (CT) 1.3 s, collision energy (CoE) 10 V, declustering potential (DP) 30 V, scan window (SW) m/z 30–1000 and RF transmission (RF) m/z 20 33 %, m/z 70 33 %, m/z 270 34 %, and 27 characteristic product ion scans in the mass range of m/z 30–300 and RF m/z 20 50 %, m/z 50 50 % with the settings shown in SI Table S3.

3.4.6.3.2. SWATH with fixed window width

The SWATH mode with a fixed window width consisted of a TOF-MS scan in high-resolution mode (CoE 10 V, DP 30 V, CT 1.3 s, AT 200 ms, SW m/z 30–1000 and RF m/z 20 33 %, m/z 70 33 %, m/z 270 34 %) and several different product ion scans (CoE 20 V, CES 10 V, DP 30, CT 1.3 s, AT 40 ms and RF m/z 20 50 %, m/z 50 50 %). The product ion scans consisted of 27 consecutive Q1 windows with 30 Da each in the mass range of 30–300 m/z to achieve comparable MS settings within different acquisition modes. All Q1 windows were overlapped by 1 Da on each side (SI Table S4).

3.4.6.3.3. SWATH with variable window width

The SWATH mode with variable window widths consisted of a TOF-MS scan (CoE 10 V, DP 30 V, CT 1.3 s, AT 200 ms, SW m/z 30–1000 and RF m/z 20 33 %, m/z 70 33 %, m/z 270 34 %) and several different product ion scans with individual CoE and DP settings (Table 6). The product ion scans consisted of 27 Q1 windows with different window widths in the mass range of 30–300 m/z (Table 6).

3.4.6.4. Response factor

Due to the lack of a true blank matrix, $^{13}C,^{15}N$ isotopically labelled standards were used as surrogate analytes. This surrogate calibrant approach requires parallelism of the calibration functions of the surrogate calibrants and the corresponding unlabelled analytes. In case of deviations a correction factor for different detector response has to be considered. Thus, detector responses of surrogate calibrants and amino acid analytes have been investigated by a dilution series. Therefore, standard solutions of $^{13}C,^{15}N$ isotopically labelled and unlabelled amino acids were mixed together at same concentrations in neat solution before measurement. To do so, a commercially available metabolomics amino acid standard mix containing 17 $^{13}C,^{15}N$-isotopically labelled amino acids of 2.5 mM in 0.1 M HCl was used. Additionally, single unlabelled amino acid standards at 50mM in 0.1 M HCl were prepared and mixed together to a final concentration of 2.5 mM. Both standard mixtures were combined in equal amounts. To achieve 10 different concentration levels, the mixture was dissolved in ACN/MilliQ water (1:1; v:v) 1:10; 1:50; 1:100; 1:250; 1:500; 1:1000; 1:5000; 1:10 000; 1:50 000 and 1:100 000. Deuterated amino acids of ring-d4-L-Tyr (250 ng/mL), d8-L-Val (16 ng/mL), and 3,3,4,4,5,5,6,6-d8-L-Lys 2HCl (5 µg/mL) were added as internal standards.

The comparison of the detector responses of unlabelled amino acids and $^{13}C,^{15}N$-isotopically labelled amino acids was based on the peak areas, which were determined with the MultiQuant™ software from Sciex. The response factors (RF) were calculated using SI Equation S1:

$$\boldsymbol{RF = area_{surrogate\ analyte} / area_{analyte}}$$

Equation S1: Calculation of Response factor (RF): Calculated as ratio of the area of analyte and corresponding surrogate analyte

Table S3: Overview of MS-settings: Used for high resolution multiple reaction monitoring acquisition mode (MRM^{HR})

			Potential parameters [V]			
Amino acid	M [g/mol]	precursor ion m/z [M + H]	CE	DP	CES	Main fragment [m/z]
Glycine	75.07	76.04	5	20	0	76.0393
L-Alanine	89.10	90.05	21	10	0	44.0533
L-Serine	105.09	106.05	20	10	0	60.0462
L-Proline	115.13	116.07	20	20	0	70.0685
L-Valine	117.15	118.09	16	20	0	72.0833
L-Threonine	119.12	120.07	17	30	0	74.0618
L-Cysteine	121.16	122.03	20	60	0	76.0236
L-Leucine	131.18	132.10	13	30	0	86.0979
L-Isoleucine	131.17	132.10	14	30	0	86.0986
L-Asparagine	132.12	133.06	11	40	0	74.0258
L-Aspartic acid	133.10	134.04	14	20	0	74.0260
L-Glutamine	146.15	147.07	25	10	0	84.0457
L-Lysine	146.19	147.11	27	20	0	84.0822
L-Glutamic acid	147.13	148.05	22	20	0	84.0450
L-Methionine	149.21	150.06	15	60	0	104.0527
L-Histidine	155.16	156.07	27	20	0	110.0714
L-Phenylalanine	165.19	166.09	21	10	0	120.0814
L-Arginine	174.20	175.11	35	50	0	70.0679
L-Tyrosine	181.19	182.08	22	20	0	136.0752
L-Tryptophan	204.23	205.09	25	10	0	146.0598
- [a]	- [a]	241.03	20	30	10	-
- [a]	- [a]	78.00	20	30	10	-
- [a]	- [a]	103.00	20	30	10	-
- [a]	- [a]	123.00	20	30	10	-
- [a]	- [a]	127.00	20	30	10	-
- [a]	- [a]	136.00	20	30	10	-
- [a]	- [a]	167.00	20	30	10	-

[a] Space holder for comparable accumulation and cycle times

Table S4: Overview of the MS-settings: Used for SWATH acquisition mode with fixed Q1 window widths

Experiment number	Q1 window range [m/z]	target amino acid; retention time [min]	Collision energy [V]	Declustering potential [V]	Collision energy spread [V]
SWATH with fixed Q1 window width					
0	30 - 1000	TOF MS	10	30	-
1	30 - 40		20	30	10
2	39 - 50		20	30	10
3	49 - 60		20	30	10
4	59 - 70		20	30	10
5	69 - 80	Gly; 5.26	20	30	10
6	79 - 90		20	30	10
7	89 - 100	Ala; 4.78	20	30	10
8	99 - 110	Ser; 5.75	20	30	10
9	109 - 120	Pro; 3.88 / Val; 3.82	20	30	10
10	119 - 130	Thr; 5.10 / Cys; 4.26	20	30	10
11	129 - 140	Leu; 3.21 / Ile; 3.40 / Asn; 5.72 / Asp; 6.07	20	30	10
12	139 - 150	Glu; 5.34 / Gln; 5.54 / Lys; 8.08	20	30	10
13	149 - 160	Met; 3.65 / His; 7.76	20	30	10
14	159 - 170	Phe; 3.17	20	30	10
15	169 - 180	Arg; 7.72	20	30	10
16	179 - 190	Tyr; 4.01	20	30	10
17	189 - 200		20	30	10
18	199 - 210	Trp; 3.22	20	30	10
19	209 - 220		20	30	10
20	219 - 230		20	30	10
21	229 - 240		20	30	10
22	239 - 250		20	30	10
23	249 - 260		20	30	10
24	259 - 270		20	30	10
25	269 - 280		20	30	10
26	279 - 290		20	30	10
27	289 - 300		20	30	10

Table S5: Amino acid concentrations: Used for the acquisition mode comparison and linear range measurements

		ng/mL								Stock [ng/mL]	Group Stocks
Group	Amino acid	8	7	6	5	4	3	2	1		
1	L-Phe	2.50	4.00	6.40	8.00	12.8	16.0	20.0	25.0	250	I
	L-Leu	2.50	4.00	6.40	8.00	12.8	16.0	20.0	25.0		
	L-Ile	2.50	4.00	6.40	8.00	12.8	16.0	20.0	25.0		
	L-Met	2.50	4.00	6.40	8.00	12.8	16.0	20.0	25.0		
	L-Pro	2.50	4.00	6.40	8.00	12.8	16.0	20.0	25.0		
	L-Tyr	2.50	4.00	6.40	8.00	12.8	16.0	20.0	25.0		
	L-Arg	2.50	4.00	6.40	8.00	12.8	16.0	20.0	25.0		
2	L-Trp	6.25	10.0	16.0	20.0	32.0	40.0	50.0	62.5	625	
	L-Val	6.25	10.0	16.0	20.0	32.0	40.0	50.0	62.5		
3	L-Lys	12.5	20.0	32.0	40.0	64.0	80.0	100	125	1250	
4	L-Gln	10.0	16.0	25.6	32.0	51.2	64.0	80.0	100	1000	II
	L-Glu	10.0	16.0	25.6	32.0	51.2	64.0	80.0	100		
	L-His	10.0	16.0	25.6	32.0	51.2	64.0	80.0	100		
5	L-Ser	25.0	40.0	64.0	80.0	128	160	200	250	2500	
	Gly	25.0	40.0	64.0	80.0	128	160	200	250		
6	L-Ala	50.0	80.0	128	160	256	320	400	500	5000	
	L-Thr	50.0	80.0	128	160	256	320	400	500		
7	L-Asn	100	160	256	320	512	640	800	1000	10000	
8	L-Asp	250	400	640	800	1280	1600	2000	2500	25000	III
	L-Cys	250	400	640	800	1280	1600	2000	2500		

Table S6: MS-DIAL Parameters: Used for processing the untargeted profiling data with MS-DIAL software

Data collection parameters	
Retention time begin	0.5
Retention time end	10
Mass range begin	30
Mass range end	1000
Centroid parameters	
MS1 tolerance	0.01
MS2 tolerance	0.05
Peak detection-based	TRUE
Peak detection parameters	
Smoothing method	Linear Weighted Moving Average
Smoothing level	3
Minimum peak width	5
Minimum peak height	1000
Peak spotting parameters	
Mass slice width	0.1
Exclusion mass list (mass & tolerance)	
Deconvolution parameters	
Peak consideration	Both
Sigma window value	0.5
Exclude after precursor	TRUE
MSP file and MS/MS identification setting	
MSP file	MSMS-MassBank-Curated-Pos.msp
Retention time tolerance	100
Accurate mass tolerance (MS1)	0.01
Accurate mass tolerance (MS2)	0.05
Identification score cut off	80
Text file and post identification (retention time and accurate mass based) setting	
Text file	Mass list isotopic labelled amino acids.txt
Retention time tolerance	0.2
Accurate mass tolerance	0.01
Identification score cut off	85
Advanced setting for identification	
Relative abundance cut off	0
Top candidate report	TRUE
Adduct ion setting	
$[M+H]^+$	
$[M+NH_4]^+$	
$[M+Na]^+$	
$[M+2H]^{2+}$	
Alignment parameters setting	
Reference file	HCE cell extract QC 5.abf
Retention time tolerance	0.1
MS1 tolerance	0.025
Retention time factor	0.5
MS1 factor	0.5
Peak count filter	5
QC at least filter	FALSE
Tracking of isotope labels	
Tracking of isotopic labels	FALSE

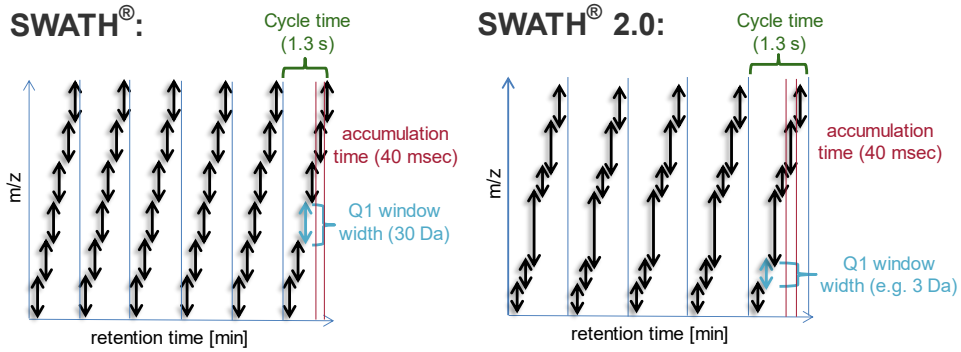

Figure S19: Scheme of SWATH acquisition mode: SWATH with fixed Q1 window width of 30 Da and SWATH 2.0 with variable Q1 window width combining narrow windows of 3 Da for amino acids and bigger windows for the remaining metabolites in the cell extract

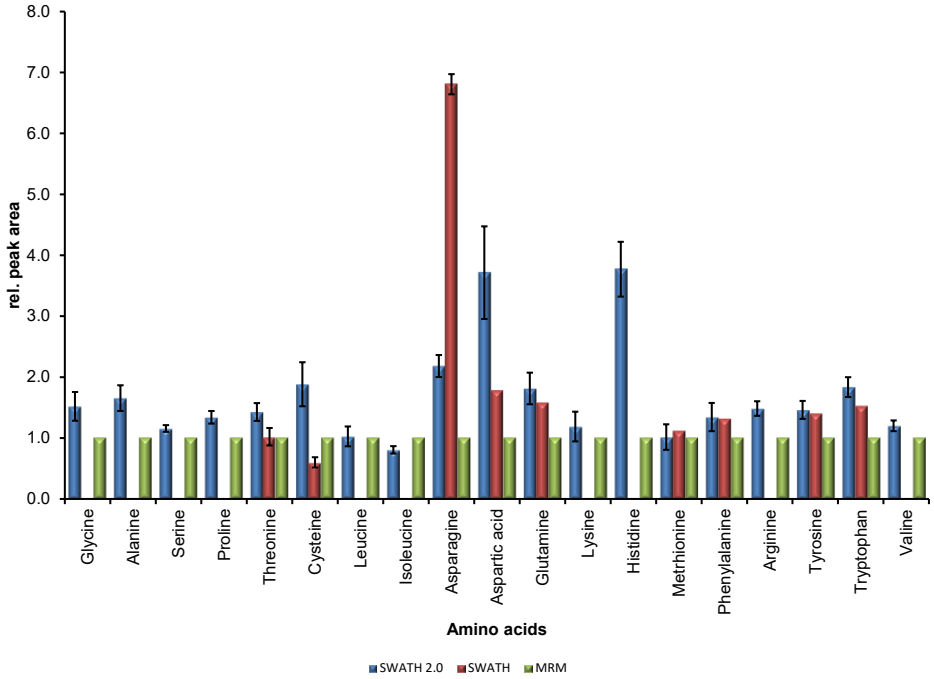

Figure S20: Comparison of relative intensities of all 3 acquisition modes: MRM^{HR}, SWATH (with fixed window widths) and SWATH 2.0 (with variable window widths) based on measurements of amino acid mixture in neat solution at different concentrations (n = 4). The relative peak areas are normalized to MRM^{HR} and only the lowest measured concentration was taken into account for the comparison, except in the case of L-Cys, L-Asp and L-Met

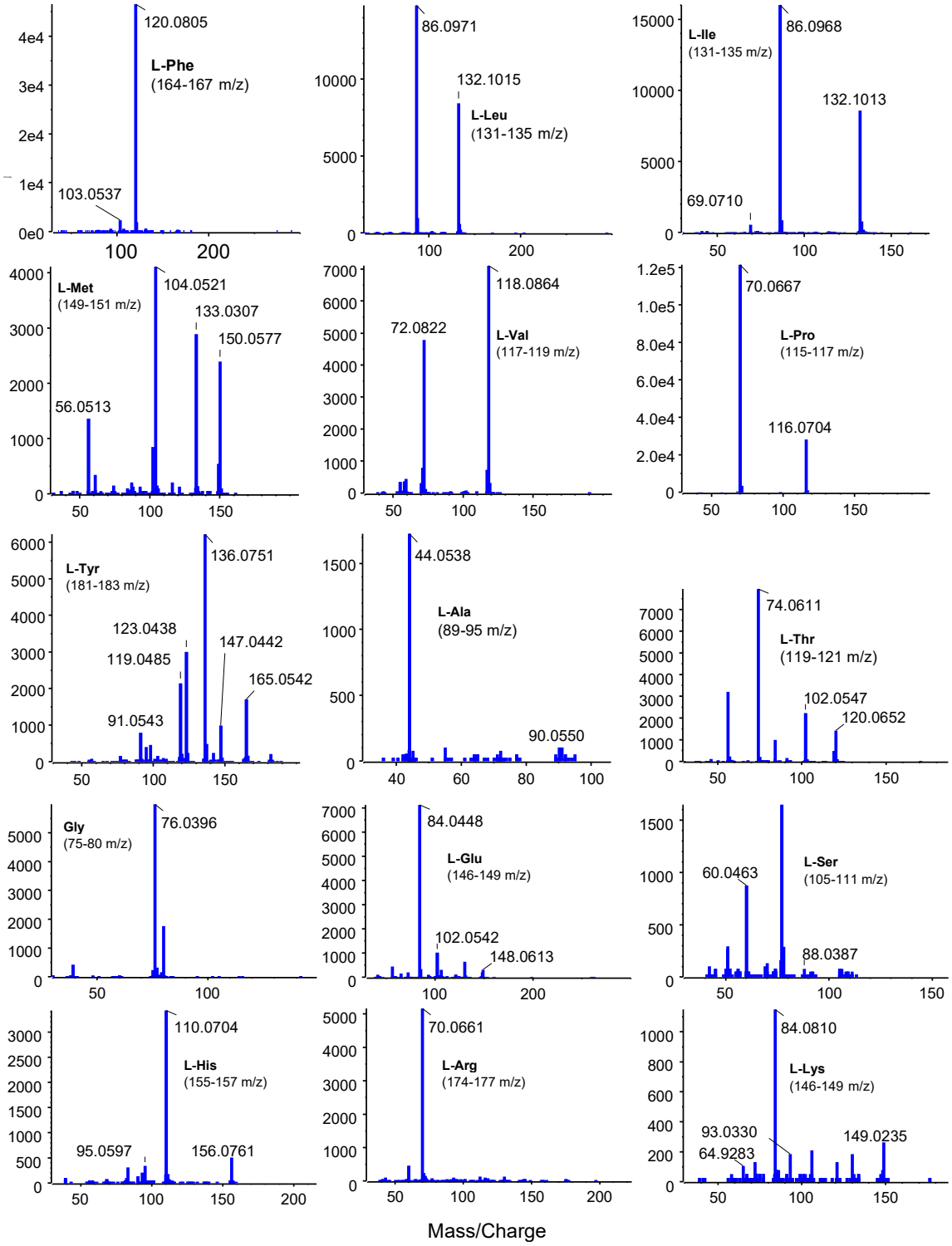

Figure S21: MS/MS spectra of targeted amino acids: MS/MS spectra from SWATH measured in cell extract (m/z range indicates SWATH window for precursor of corresponding amino acid)

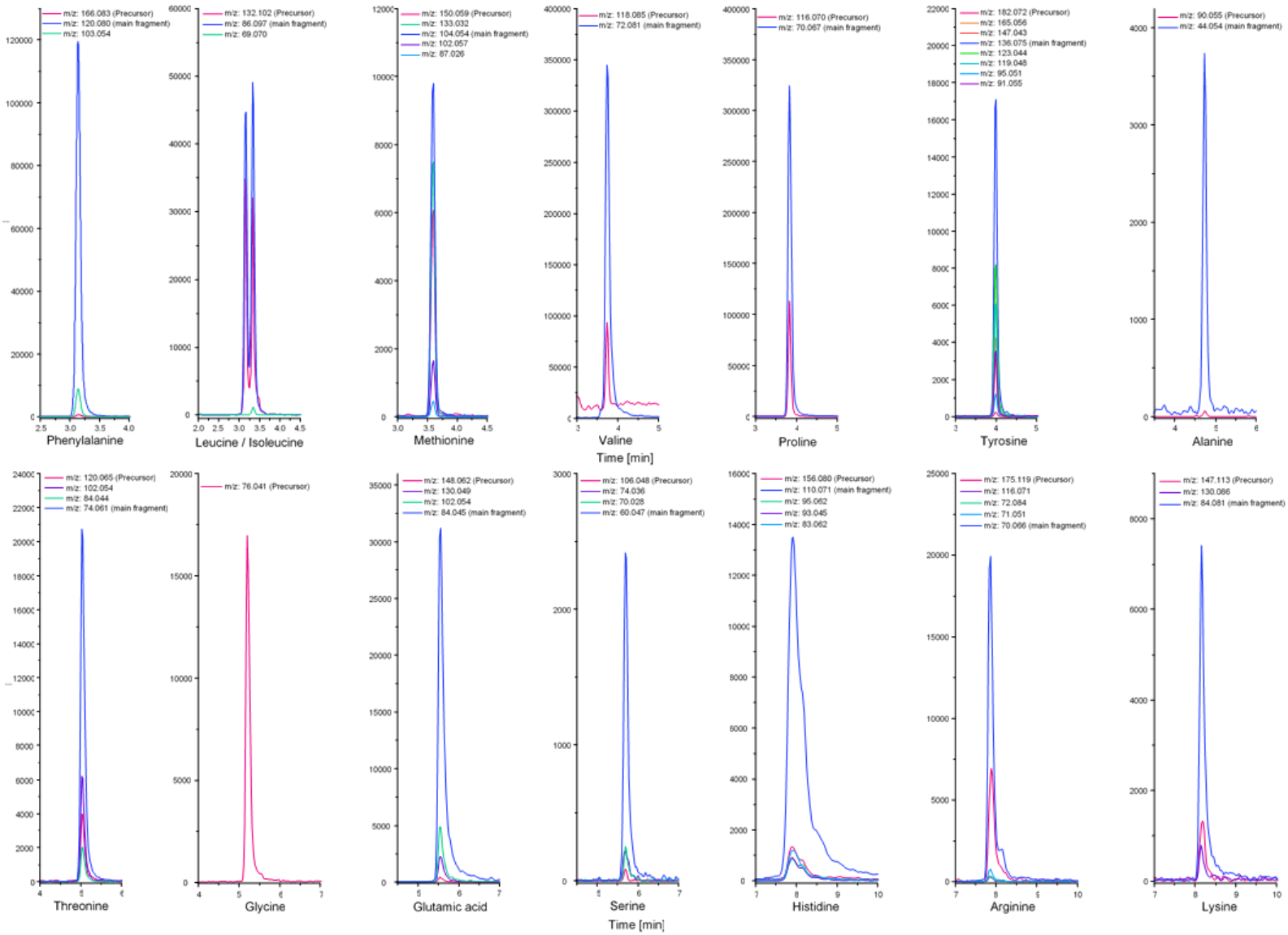

Figure S22: EIC chromatograms from HCE cell extract (QC) measured with SWATH 2.0 method: Main fragment indicates the fragment mass used for quantification

Table S7: Linear functions: Used for recalculation of amino acid peak areas after taking response factors into account (n = 4)

	RF	STD (RF)	slope surrogate analyte	s_e (slope)	intercept surrogate analytes	s_e (intercept)	R^2
Gly	1.2	0.3	0.00417	9.27E-09	0.03315	0.00007	0.99950
Ala	1.5	0.3	0.00399	2.34E-08	-0.00206	0.00012	0.99960
Ser	1.3	0.3	0.00472	1.86E-08	0.04847	0.00011	0.99980
Pro	1.1	0.2	0.13840	4.94E-07	0.08939	0.00011	0.99960
Val	1.2	0.1	0.05045	1.22E-07	0.05538	0.00009	0.99970
Thr	1.3	0.3	0.00681	3.10E-08	-0.01049	0.00010	0.99990
Leu	1.5	0.1	0.08257	1.11E-07	0.18588	0.00010	0.99990
Ile	1.4	0.1	0.10586	1.37E-07	0.11736	0.00012	0.99980
Asp	1.3	0.3	0.00074	5.98E-09	0.23217	0.00009	0.99999
Glu	0.6	0.2	0.00852	1.34E-08	0.46138	0.00011	0.99970
Lys	0.9	0.4	0.00592	1.12E-07	0.20993	0.00011	0.99996
Met	0.6	0.1	0.01108	1.88E-08	-0.01642	0.00007	0.99998
His	1.2	0.4	0.01765	1.23E-07	0.63205	0.00014	0.99999
Phe	0.4	0.1	0.04676	1.00E-07	0.03672	0.00011	0.99980
Arg	1.0	0.4	0.01454	6.14E-08	0.71982	0.00009	0.99967
Tyr	0.7	0.3	0.00431	9.48E-09	0.15642	0.00009	0.99940

Calculations for tryptophan are based on the response factor and linear function of lysine because tryptophan was not included in the ^{13}C, ^{15}N- isotopic labelled amino acid mixture. Both unlabelled amino acids showed similar slopes in neat solution (y=0.00565x + 0.01229 for Trp and y=0.00637x + 0.16536 for Lys). The verification of the calculations is based on the comparison of unlabelled and isotopically labelled amino acids: Gly (y=0.00285x + 0.01936), Ser (y=0.00285x + 0.6632), ^{13}C, ^{15}N-Gly (y=0.00367x – 0.04699), and ^{13}C, ^{15}N-L-Ser (y=0.00390x – 0.07786).

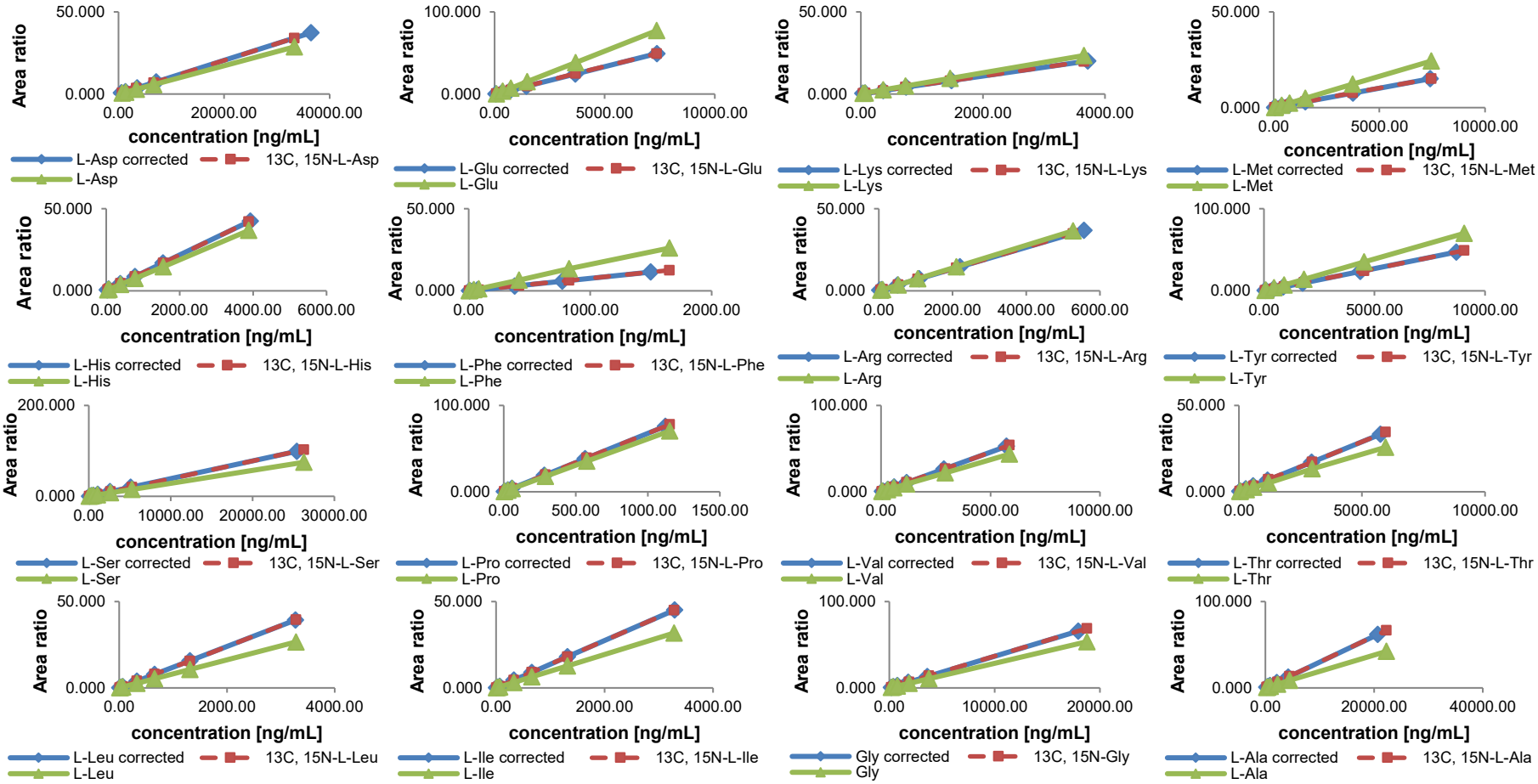

Figure S23: Calibration curves: $^{13}C,^{15}N$-labelled amino acids (red) and unlabelled amino acids before (green) and after (blue) the correction by different response factors (RF). Parallelism of calibration functions between labelled and unlabelled amino acids was required to make this surrogate calibrant approach valid. Labelled and unlabelled amino acids had the same concentrations in the mixture (n = 4)

Table S8: Validation data: Inter-day, intra-day accuracy and precision as well as freeze / thaw stability of HCE cell extracts spiked with $^{13}C,^{15}N$ - isotopically labelled amino acids (Eurisotop), n = 8

Name	QC $_{low}$										
	Day 1			Day 3		Day 4		Mean	Mean	Freeze / thaw stability	
	Concentration [ng/mL]	Accuracy [%]	Coefficient of variation (CV) [%]	Accuracy [%]	Coefficient of variation (CV) [%]	Accuracy [%]	Coefficient of variation (CV) [%]	Inter-day precision [%]	Inter-day accuracy [%]	Accuracy [%]	Coefficient of variation (CV) [%]
Gly	93.8	114.8	3.3	104.8	1.4	97.7	2.2	7.3	105.8	103.3	1.4
L-Ala	111.4	109.6	7.9	89.7	8.6	108.9	6.0	11.4	102.7	112.7	2.5
L-Ser	131.4	105.3	4.6	96.8	5.0	104.0	2.9	5.5	102.0	93.3	3.8
L-Pro	2.9	101.4	2.6	104.7	1.2	98.7	9.4	8.6	101.6	103.3	3.7
L-Val	2.9	109.7	1.9	101.0	6.9	109.2	3.8	5.8	106.6	97.5	1.7
L-Thr	29.8	97.0	5.1	104.1	6.7	99.7	4.6	6.0	100.2	100.8	6.5
L-Cystine	750.9	102.0	4.9	97.5	3.3	97.3	2.5	4.2	98.9	110.5	0.9
L-Leu	32.8	110.1	7.4	111.9	4.1	114.2	6.4	6.0	112.1	107.7	3.6
L-Ile	32.8	106.2	2.8	109.1	4.3	104.1	4.0	4.1	106.5	105.6	3.0
L-Asp	415.9	113.8	6.4	101.7	3.4	96.8	2.4	8.3	104.1	100.7	2.4
L-Glu	183.9	114.5	2.3	94.2	5.2	106.2	2.3	8.5	105.0	101.7	1.9
L-Lys	36.6	98.5	4.9	110.6	5.9	104.9	2.4	6.4	104.7	104.0	0.8
L-Met	37.3	111.3	3.0	102.3	1.9	113.8	3.2	5.3	109.1	96.0	2.0
L-His	38.8	107.2	5.7	103.2	4.1	104.4	2.0	4.3	104.9	102.9	4.6
L-Phe	4.1	108.5	11.9	101.4	2.3	95.3	9.0	10.5	101.7	96.3	2.4
L-Arg	5.3	110.7	4.5	102.6	8.8	97.7	13.1	9.5	103.7	107.9	8.5
L-Tyr	45.3	98.2	9.0	89.2	9.2	93.9	6.2	8.5	93.8	107.8	3.7

Table S8: Validation Data: Inter-day, intra-day accuracy and precision as well as freeze / thaw stability of HCE cell extracts spiked with $^{13}C,^{15}N$ - isotopically labelled amino acids (Eurisotop), n = 8 (Continuation)

Name	QC middle										
	Day 1			Day 3		Day 4		Mean	Mean	Freeze / thaw stability	
	Concentration [ng/mL]	Accuracy [%]	Coefficient of variation (CV) [%]	Accuracy [%]	Coefficient of variation (CV) [%]	Accuracy [%]	Coefficient of variation (CV) [%]	Inter-day precision [%]	Inter-day accuracy [%]	Accuracy [%]	Coefficient of variation (CV) [%]
Gly	1876.8	98.8	3.5	102.8	2.2	97.5	2.6	3.5	99.7	99.1	1.5
L-Ala	556.9	100.0	5.9	99.3	3.9	102.0	1.2	4.1	100.4	101.6	8.0
L-Ser	656.8	104.4	5.5	107.25	2.4	103.9	5.9	4.8	105.2	102.3	0.6
L-Pro	28.8	99.0	6.3	99.4	2.9	98.7	2.0	4.1	99.0	94.2	7.4
L-Val	146.4	105.6	7.3	102.1	7.2	99.0	5.7	7.1	102.2	100.7	0.7
L-Thr	372.3	93.0	6.7	102.0	1.8	90.6	4.7	6.9	95.2	96.4	6.0
L-Cystine	6007.5	104.4	2.4	101.5	1.7	103.0	1.6	2.2	103.0	106.2	1.6
L-Leu	164.0	102.2	3.1	100.8	3.4	99.7	6.9	4.7	100.9	98.2	1.8
L-Ile	164.0	104.9	9.4	96.7	9.2	100.2	4.4	8.4	100.6	98.2	2.6
L-Asp	3327.5	105.2	1.5	101.7	1.0	101.1	1.4	2.2	102.7	100.7	1.1
L-Glu	919.6	105.5	3.8	101.0	0.9	98.3	2.3	3.9	101.6	101.5	2.1
L-Lys	182.7	105.1	3.3	103.1	3.4	105.3	1.0	2.8	104.5	100.9	1.3
L-Met	466.3	88.4	4.2	98.7	3.4	90.7	4.2	6.2	92.6	-[a]	-[a]
L-His	194.0	104.1	3.1	100.5	0.6	101.8	1.9	2.5	102.1	100.5	1.3
L-Phe	206.5	101.4	2.3	99.8	3.9	101.7	2.9	3.0	101.0	101.4	3.7
L-Arg	263.3	105.0	4.3	99.9	5.4	107.1	2.8	4.8	104.0	99.9	4.2
L-Tyr	1132.4	101.7	2.8	102.8	1.5	105.1	1.6	2.4	103.2	104.8	0.8

Table S8: Validation Data: Inter-day, intra-day accuracy and precision as well as freeze / thaw stability of HCE cell extracts spiked with $^{13}C,^{15}N$ - isotopically labelled amino acids (Eurisotop), n = 8 (Continuation)

Name	QC high										
	Day 1			Day 3		Day 4		Mean	Mean	Freeze / thaw stability	
	Concentration [ng/mL]	Accuracy [%]	Coefficient of variation (CV) [%]	Accuracy [%]	Coefficient of variation (CV) [%]	Accuracy [%]	Coefficient of variation (CV) [%]	Inter-day precision [%]	Inter-day accuracy [%]	Accuracy [%]	Coefficient of variation (CV) [%]
Gly	15014.0	99.8	3.6	100.1	2.6	99.4	2.4	2.7	99.8	100.1	1.9
L-Ala	8910.0	100.0	5.3	100.0	4.8	100.1	2.5	4.2	100.0	100.1	3.0
L-Ser	10509.0	100.1	6.0	100.2	5.4	100.1	1.4	4.5	100.1	100.0	2.3
L-Pro	359.8	100.0	2.8	100.0	3.7	99.9	2.1	2.8	100.0	99.8	1.2
L-Val	732.2	100.8	4.6	100.0	5.7	99.9	1.7	4.2	100.2	100.0	3.0
L-Thr	2978.0	99.9	4.2	100.0	2.4	99.8	3.0	3.1	99.9	99.9	4.4
L-Cystine	48060.0	100.7	1.7	100.3	1.5	100.3	1.6	1.5	100.4	101.0	3.0
L-Leu	819.9	100.7	1.9	100.6	3.3	100.6	5.1	3.4	100.7	100.1	2.8
L-Ile	819.8	100.9	7.7	99.9	3.5	100.2	3.5	5.1	100.4	100.1	7.5
L-Asp	26620.0	101.3	2.9	100.3	0.9	99.9	6.5	4.0	100.5	100.1	3.1
L-Glu	14713.0	100.2	3.7	100.0	2.3	100.0	2.1	2.6	100.0	100.0	1.6
L-Lys	913.7	100.6	1.7	100.7	1.2	100.8	2.7	1.9	100.7	100.2	2.1
L-Met	3730.3	99.7	2.8	99.9	2.0	99.8	3.9	2.9	99.8	99.9	0.4
L-His	969.8	100.8	2.1	100.2	1.2	100.4	1.6	1.6	100.4	100.2	0.9
L-Phe	1032.4	99.7	7.2	99.7	2.3	99.8	3.2	4.4	99.8	100.0	1.0
L-Arg	1316.6	101.4	2.9	100.2	1.9	100.3	3.2	2.6	100.7	100.0	4.0
L-Tyr	18119.0	100.0	7.6	100.2	4.8	100.1	2.6	5.2	100.1	100.2	2.8

[a]: rejected as outlier

Table S9: Sample sequence table: Showing randomized injection order of the samples between calibrants (Cal concentration level_replicate) and quality control samples (QC concentration level_replicate)

Injection no.	sample	Injection no.	sample	Injection no.	sample
1	Cal 10_1	29	QC 8_2	57	Control 24h
2	Cal 9_1	30	QC 7_2	58	$[P_{14444}][OAc]$ 8h
3	Cal 8_1	31	QC 6_2	59	$[P_{14444}]Cl$ 8h
4	Cal 7_1	32	QC 5_2	60	$[N_{4441}][OAc]$ 16h
5	Cal 6_1	33	QC 4_2	61	NMMO 24h
6	Cal 5_1	34	QC 3_2	62	[Ch][OAc] 8h
7	Cal 4_1	35	QC 2_2	63	Control 24h
8	Cal 3_1	36	QC 1_2	64	$[N_{4441}][OAc]$ 8h
9	Cal 2_1	37	$[N_{4441}][OAc]$ 24h	65	QC 8_4
10	Cal 1_1	38	[Ch][Hex] 8h	66	QC 7_4
11	QC 8_1	39	[emim][OAc] 8h	67	QC 6_4
12	QC 7_1	40	[DBNH][OAc] 8h	68	QC 5_4
13	QC 6_1	41	$[P_{4441}][OAc]$ 24h	69	QC 4_4
14	QC 5_1	42	$[P_{14444}][OAc]$ 16h	70	QC 3_4
15	QC 4_1	43	[Ch][Hex] 24h	71	QC 2_4
16	QC 3_1	44	[Ch][OAc] 16h	72	QC 1_4
17	QC 2_1	45	[Ch][Hex] 16h	73	Cal 10_2
18	QC 1_1	46	[DBNH][OAc] 16h	74	Cal 9_2
19	Control 16h	47	QC 8_3	75	Cal 8_2
20	$[P_{14444}]Cl$ 16h	48	QC 7_3	76	Cal 7_2
21	NMMO 8h	49	QC 6_3	77	Cal 6_2
22	[DBNH][OAc] 24h	50	QC 5_3	78	Cal 5_2
23	$[P_{4441}][OAc]$ 16h	51	QC 4_3	79	Cal 4_2
24	Control 8h	52	QC 3_3	80	Cal 3_2
25	$[P_{4441}][OAc]$ 8h	53	QC 2_3	81	Cal 2_2
26	$[P_{14444}]Cl$ 24h	54	QC 1_3	82	Cal 1_2
27	[emim][OAc] 24h	55	[Ch][OAc] 24h		
28	$[P_{14444}][OAc]$ 24h	56	[emim][OAc] 16h		

Table S10: Concentrations of amino acids: In treated and untreated HCE cell extracts

Amino acid	Glycine	Alanine	Serine	Proline	Valine	Threonine
Cell extract	Calculated concentrations [ng/mL]*					
Ctr 1 8h	1763.1 ± 46.7	409.0 ± 10.5	667.3 ± 12.8	802.1 ± 44.4	194.2 ± 9.2	1182.5 ± 27.5
Ctr 1 16h	2917.5 ± 77.1	553.0 ± 14.2	476.8 ± 9.2	1148.8 ± 63.6	207.9 ± 9.8	1575.6 ± 36.6
Ctr 1 24h	3028.1 ± 80.1	817.5 ± 20.9	358.2 ± 6.9	1131.0 ± 62.6	217.1 ± 10.3	1938.5 ± 45.0
Ctr 2 24h	2799.3 ± 74.0	584.5 ± 15.0	385.1 ± 7.4	1291.4 ± 71.5	240.1 ± 11.4	1970.8 ± 45.8
NMMO 8h	1431.8 ± 37.9	1050.5 ± 26.9	1211.2 ± 23.2	943.7 ± 52.2	357.0 ± 16.9	2293.1 ± 53.3
NMMO 24h	1920.0 ± 50.8	783.4 ± 20.1	693.9 ± 13.3	1053.4 ± 58.3	262.4 ± 12.4	2020.1 ± 46.9
[Ch][OAc] 8h	2125.7 ± 56.2	507.5 ± 13.0	1098.5 ± 21.0	1125.2 ± 62.3	451.3 ± 21.3	2155.4 ± 50.1
[Ch][OAc] 16h	2504.2 ± 66.2	567.3 ± 14.5	573.6 ± 11.0	1457.1 ± 80.6	297.5 ± 14.1	1978.4 ± 46.0
[Ch][OAc] 24h	2721.5 ± 72.0	549.3 ± 14.1	406.9 ± 7.8	1190.9 ± 65.9	310.6 ± 14.7	1721.9 ± 40.0
[Ch][Hex] 8h	1929.7 ± 51.1	154.0 ± 3.9	546.2 ± 10.5	942.6 ± 52.2	229.1 ± 10.8	1096.3 ± 25.5
[Ch][Hex] 16h	2168.5 ± 57.4	130.9 ± 3.3	238.7 ± 4.6	1146.9 ± 63.5	139.3 ± 6.6	771.2 ± 17.9
[Ch][Hex] 24h	3200.8 ± 84.6	297.6 ± 7.6	520.5 ± 10.0	1457.7 ± 80.7	258.7 ± 12.2	1419.4 ± 33.0
[emim][OAc] 8h	1071.9 ± 28.4	632.8 ± 16.2	1223.5 ± 23.4	828.1 ± 45.8	487.2 ± 23.0	1901.1 ± 44.2
[emim][OAc] 16h	668.0 ± 17.7	535.0 ± 13.7	850.9 ± 16.3	668.9 ± 37.0	342.4 ± 16.2	1332.5 ± 30.9
[emim][OAc] 24h	632.9 ± 16.8	663.2 ± 17.0	913.0 ± 17.5	656.6 ± 36.4	356.3 ± 16.8	1472.7 ± 34.2
[DBNH][OAc] 8h	1002.6 ± 26.6	547.5 ± 14.0	847.2 ± 16.2	792.4 ± 43.9	295.4 ± 14.0	1586.8 ± 36.9
[DBNH][OAc] 16h	1560.0 ± 41.3	1116.4 ± 28.6	1178.8 ± 22.5	1039.7 ± 57.6	514.5 ± 24.3	2406.6 ± 55.9
[DBNH][OAc] 24h	1272.0 ± 33.7	1068.8 ± 27.4	752.7 ± 14.4	977.4 ± 54.1	364.8 ± 17.2	1707.3 ± 39.7
$[P_{4441}]$[OAc] 8h	293.0 ± 7.8	280.0 ± 7.2	594.3 ± 11.4	420.5 ± 23.3	273.6 ± 12.9	987.0 ± 22.9
$[P_{4441}]$[OAc] 16h	142.7 ± 3.9	84.4 ± 2.2	191.2 ± 3.7	132.8 ± 7.4	142.9 ± 6.8	311.3 ± 7.2
$[P_{4441}]$[OAc] 24h	192.5 ± 5.2	218.1 ± 5.6	306.4 ± 5.9	229.1 ± 12.7	165.8 ± 7.9	590.1 ± 13.7
$[N_{4441}]$[OAc] 8h	657.7 ± 17.5	467.2 ± 12.0	546.8 ± 10.5	569.5 ± 31.5	311.0 ± 14.7	1118.9 ± 26.0
$[N_{4441}]$[OAc] 16h	654.4 ± 17.4	405.7 ± 10.4	476.8 ± 9.2	550.8 ± 30.5	260.6 ± 12.3	1006.6 ± 23.4
$[N_{4441}]$[OAc] 24h	527.4 ± 14.0	578.2 ± 14.8	488.0 ± 9.4	530.5 ± 29.4	309.6 ± 14.6	1109.8 ± 25.8
$[P_{14444}]$[OAc] 8h	505.0 ± 13.4	252.2 ± 6.5	665.1 ± 12.8	538.5 ± 29.8	298.4 ± 14.1	1018.1 ± 23.6
$[P_{14444}]$[OAc] 16h	354.1 ± 9.5	163.5 ± 4.2	390.6 ± 7.5	311.2 ± 17.2	245.2 ± 11.6	672.9 ± 15.6
$[P_{14444}]$[OAc] 24h	176.6 ± 4.8	140.8 ± 3.6	244.3 ± 4.7	189.7 ± 10.5	142.3 ± 6.7	379.4 ± 8.8
$[P_{14444}]$Cl 8h	275.0 ± 7.4	93.6 ± 2.4	331.6 ± 6.4	263.3 ± 14.6	146.6 ± 6.9	537.7 ± 12.5
$[P_{14444}]$Cl 16h	230.2 ± 6.2	114.5 ± 2.9	273.7 ± 5.3	219.5 ± 12.2	134.3 ± 6.4	517.2 ± 12.0
$[P_{14444}]$Cl 24h	186.9 ± 5.0	81.1 ± 2.1	270.3 ± 5.2	182.4 ± 10.1	140.7 ± 6.7	437.0 ± 10.1

Table S10: Concentrations of amino acids: In treated and untreated HCE cell extracts (Continuation)

amino acid	Leucine	Isoleucine	Glutamic acid	Lysine	Methionine
cell extract	calculated concentration [ng/mL] *				
Ctr 1 8h	571.1 ± 19.6	444.0 ± 20.6	1117.5 ± 43.7	203.4 ± 12.2	195.7 ± 6.4
Ctr 1 16h	494.0 ± 17.0	341.0 ± 15.9	673.7 ± 26.7	299.0 ± 17.6	244.1 ± 7.9
Ctr 1 24h	499.8 ± 17.2	347.1 ± 16.1	768.0 ± 30.3	271.8 ± 16.1	284.2 ± 9.2
Ctr 2 24h	602.6 ± 20.7	455.0 ± 21.1	868.2 ± 34.2	335.6 ± 19.6	256.3 ± 8.3
NMMO 8h	1013.6 ± 34.8	796.8 ± 37.0	1820.0 ± 70.5	224.1 ± 13.4	360.3 ± 11.7
NMMO 24h	705.9 ± 24.3	493.3 ± 22.9	653.6 ± 26.0	263.5 ± 15.6	323.8 ± 10.5
[Ch][OAc] 8h	1321.7 ± 45.4	977.9 ± 45.4	1147.5 ± 44.8	259.0 ± 15.3	413.9 ± 13.5
[Ch][OAc] 16h	901.3 ± 31.0	654.6 ± 30.4	808.2 ± 31.9	299.7 ± 17.6	338.3 ± 11.0
[Ch][OAc] 24h	857.8 ± 29.5	524.0 ± 24.3	330.1 ± 13.6	323.6 ± 18.9	348.7 ± 11.3
[Ch][Hex] 8h	616.9 ± 21.2	494.1 ± 23.0	771.9 ± 30.5	208.3 ± 12.5	197.3 ± 6.4
[Ch][Hex] 16h	374.2 ± 12.9	245.1 ± 11.4	624.3 ± 24.8	155.3 ± 9.6	119.7 ± 3.9
[Ch][Hex] 24h	560.1 ± 19.3	311.3 ± 14.5	337.7 ± 13.9	360.7 ± 21.0	250.7 ± 8.2
[emim][OAc] 8h	1476.1 ± 50.7	1065.1 ± 49.5	1103.5 ± 43.1	337.7 ± 19.7	375.2 ± 12.2
[emim][OAc] 16h	1057.1 ± 36.3	734.9 ± 34.1	654.4 ± 26.0	238.4 ± 14.2	335.9 ± 10.9
[emim][OAc] 24h	972.5 ± 33.4	723.8 ± 33.6	1017.7 ± 39.9	217.0 ± 13.0	345.7 ± 11.2
[DBNH][OAc] 8h	840.3 ± 28.9	678.2 ± 31.5	947.3 ± 37.2	357.4 ± 20.8	271.6 ± 8.8
[DBNH][OAc] 16h	1678.5 ± 57.6	1227.4 ± 57.0	874.0 ± 34.4	552.0 ± 31.6	449.9 ± 14.6
[DBNH][OAc] 24h	1118.6 ± 38.4	803.7 ± 37.3	1187.0 ± 46.3	414.4 ± 24.0	342.8 ± 11.2
$[P_{4441}]$[OAc] 8h	831.5 ± 28.6	583.5 ± 27.1	393.0 ± 16.0	189.9 ± 11.5	225.9 ± 7.3
$[P_{4441}]$[OAc] 16h	381.2 ± 13.1	281.5 ± 13.1	48.6 ± 2.7	173.8 ± 10.6	106.0 ± 3.4
$[P_{4441}]$[OAc] 24h	455.9 ± 15.7	302.7 ± 14.1	68.4 ± 3.5	212.1 ± 12.7	139.5 ± 4.5
$[N_{4441}]$[OAc] 8h	857.3 ± 29.5	668.1 ± 31.0	1210.2 ± 47.2	278.3 ± 16.4	238.8 ± 7.8
$[N_{4441}]$[OAc] 16h	705.5 ± 24.2	491.8 ± 22.9	509.9 ± 20.5	382.9 ± 22.2	244.2 ± 7.9
$[N_{4441}]$[OAc] 24h	741.4 ± 25.5	557.8 ± 25.9	450.4 ± 18.2	404.6 ± 23.4	251.2 ± 8.2
$[P_{14444}]$[OAc] 8h	820.7 ± 28.2	652.3 ± 30.3	120.8 ± 5.5	252.1 ± 15.0	233.6 ± 7.6
$[P_{14444}]$[OAc] 16h	642.7 ± 22.1	510.1 ± 23.7	47.9 ± 2.7	252.8 ± 15.0	180.7 ± 5.9
$[P_{14444}]$[OAc] 24h	390.5 ± 13.4	324.8 ± 15.1	8.2 ± 0.9	130.0 ± 8.1	117.4 ± 3.8
$[P_{14444}]$Cl 8h	441.6 ± 15.2	352.4 ± 16.4	38.9 ± 2.3	145.3 ± 9.0	120.5 ± 3.9
$[P_{14444}]$Cl 16h	428.9 ± 14.8	312.8 ± 14.5	30.4 ± 1.9	165.3 ± 10.1	108.3 ± 3.5
$[P_{14444}]$Cl 24h	402.0 ± 13.8	307.2 ± 14.3	13.0 ± 1.1	131.1 ± 8.2	110.1 ± 3.6

Table S10: Concentrations of amino acids: In treated and untreated HCE cell extracts (Continuation)

amino acid	Histidine	Phenylalanine	Arginine	Tyrosine	Tryptophan
cell extract	calculated concentration [ng/mL] *				
Ctr 1 8h	297.9 ± 6.2	380.2 ± 15.2	367.2 ± 16.5	679.0 ± 36.1	576.7 ± 33.0
Ctr 1 16h	426.7 ± 8.7	540.8 ± 21.6	306.8 ± 14.0	924.7 ± 48.8	604.8 ± 34.6
Ctr 1 24h	525.0 ± 10.7	671.4 ± 26.8	299.8 ± 13.7	1099.3 ± 57.8	793.1 ± 45.0
Ctr 2 24h	466.5 ± 9.5	661.1 ± 26.4	440.7 ± 19.6	1230.3 ± 64.6	874.2 ± 49.6
NMMO 8h	489.9 ± 10.0	665.5 ± 26.6	282.1 ± 12.9	1084.1 ± 57.0	954.9 ± 54.0
NMMO 24h	521.9 ± 10.6	689.4 ± 27.5	315.3 ± 14.3	1074.5 ± 56.5	1000.5 ± 56.6
[Ch][OAc] 8h	602.5 ± 12.2	862.1 ± 34.4	466.3 ± 20.7	1343.6 ± 70.5	1158.4 ± 65.4
[Ch][OAc] 16h	555.5 ± 11.3	650.4 ± 26.0	341.7 ± 15.4	1277.5 ± 67.0	941.4 ± 53.3
[Ch][OAc] 24h	540.4 ± 11.0	742.6 ± 29.6	229.7 ± 10.7	1058.8 ± 55.7	942.0 ± 53.3
[Ch][Hex] 8h	324.8 ± 6.7	421.2 ± 16.8	310.0 ± 14.1	694.3 ± 36.9	570.6 ± 32.7
[Ch][Hex] 16h	163.0 ± 3.5	250.4 ± 10.0	89.5 ± 4.7	457.7 ± 24.6	325.2 ± 19.0
[Ch][Hex] 24h	358.5 ± 7.4	532.9 ± 21.3	294.2 ± 13.4	916.1 ± 48.3	651.8 ± 37.2
[emim][OAc] 8h	548.7 ± 11.1	929.7 ± 37.1	677.9 ± 29.6	1297.5 ± 68.1	1204.4 ± 67.9
[emim][OAc] 16h	399.0 ± 8.2	700.9 ± 28.0	445.0 ± 19.8	916.3 ± 48.3	1111.3 ± 62.7
[emim][OAc] 24h	347.7 ± 7.2	791.4 ± 31.6	397.5 ± 17.8	945.8 ± 49.9	1019.9 ± 57.7
[DBNH][OAc] 8h	431.9 ± 8.8	508.3 ± 20.3	649.6 ± 28.4	909.5 ± 48.0	676.9 ± 38.6
[DBNH][OAc] 16h	638.8 ± 12.9	1077.5 ± 43.0	728.9 ± 31.8	1366.1 ± 71.6	1272.2 ± 71.7
[DBNH][OAc] 24h	487.1 ± 9.9	650.7 ± 26.0	492.3 ± 21.8	1062.3 ± 55.9	955.3 ± 54.1
$[P_{4441}]$[OAc] 8h	323.0 ± 6.7	460.6 ± 18.4	405.5 ± 18.1	784.8 ± 41.5	788.7 ± 44.8
$[P_{4441}]$[OAc] 16h	110.0 ± 2.5	242.3 ± 9.7	324.9 ± 14.7	256.2 ± 14.2	356.6 ± 20.8
$[P_{4441}]$[OAc] 24h	191.0 ± 4.1	296.2 ± 11.8	289.2 ± 13.2	457.5 ± 24.6	416.6 ± 24.1
$[N_{4441}]$[OAc] 8h	381.4 ± 7.8	544.2 ± 21.7	448.5 ± 19.9	699.2 ± 37.1	792.0 ± 45.0
$[N_{4441}]$[OAc] 16h	330.8 ± 6.8	503.8 ± 20.1	572.9 ± 25.2	817.8 ± 43.2	790.2 ± 44.9
$[N_{4441}]$[OAc] 24h	405.6 ± 8.3	578.6 ± 23.1	570.7 ± 25.1	945.3 ± 49.8	871.0 ± 49.4
$[P_{14444}]$[OAc] 8h	298.8 ± 6.2	463.7 ± 18.5	462.9 ± 20.6	727.8 ± 38.6	677.3 ± 38.6
$[P_{14444}]$[OAc] 16h	242.1 ± 5.1	395.2 ± 15.8	505.1 ± 22.3	589.7 ± 31.4	604.6 ± 34.6
$[P_{14444}]$[OAc] 24h	119.7 ± 2.7	246.3 ± 9.8	270.9 ± 12.4	345.7 ± 18.8	348.4 ± 20.3
$[P_{14444}]$Cl 8h	150.4 ± 3.3	254.5 ± 10.2	284.5 ± 13.0	427.2 ± 23.0	359.5 ± 20.9
$[P_{14444}]$Cl 16h	149.3 ± 3.3	249.1 ± 9.9	296.3 ± 13.5	410.6 ± 22.2	365.5 ± 21.3
$[P_{14444}]$Cl 24h	141.7 ± 3.1	230.6 ± 9.2	287.5 ± 13.1	344.3 ± 18.7	356.6 ± 20.8

* the calculation of the error was based on SI Equation S2

$$\frac{\Delta x}{x} = \sqrt{\left(\frac{\sqrt{\left(A * RF * \sqrt{(\Delta y)^2 + \left(\frac{\Delta RF}{RF}\right)^2}\right)^2 + (\Delta b)^2}}{A * RF - b}\right) + (\frac{\Delta a}{a})^2}$$

Equation S2: Error calculation: Where a is the slope and b is the intercept of the respective ^{13}C,^{15}N- amino acid calibration function y = a * x + b. For the relative error of y ($\frac{\Delta y}{y}$), the average relative standard deviation of each concentration in the corresponding QC sample implemented into the measurement sequence of the samples was used. Integration of $\left(\frac{\Delta RF}{RF}\right)$ was used as error of the response factor.

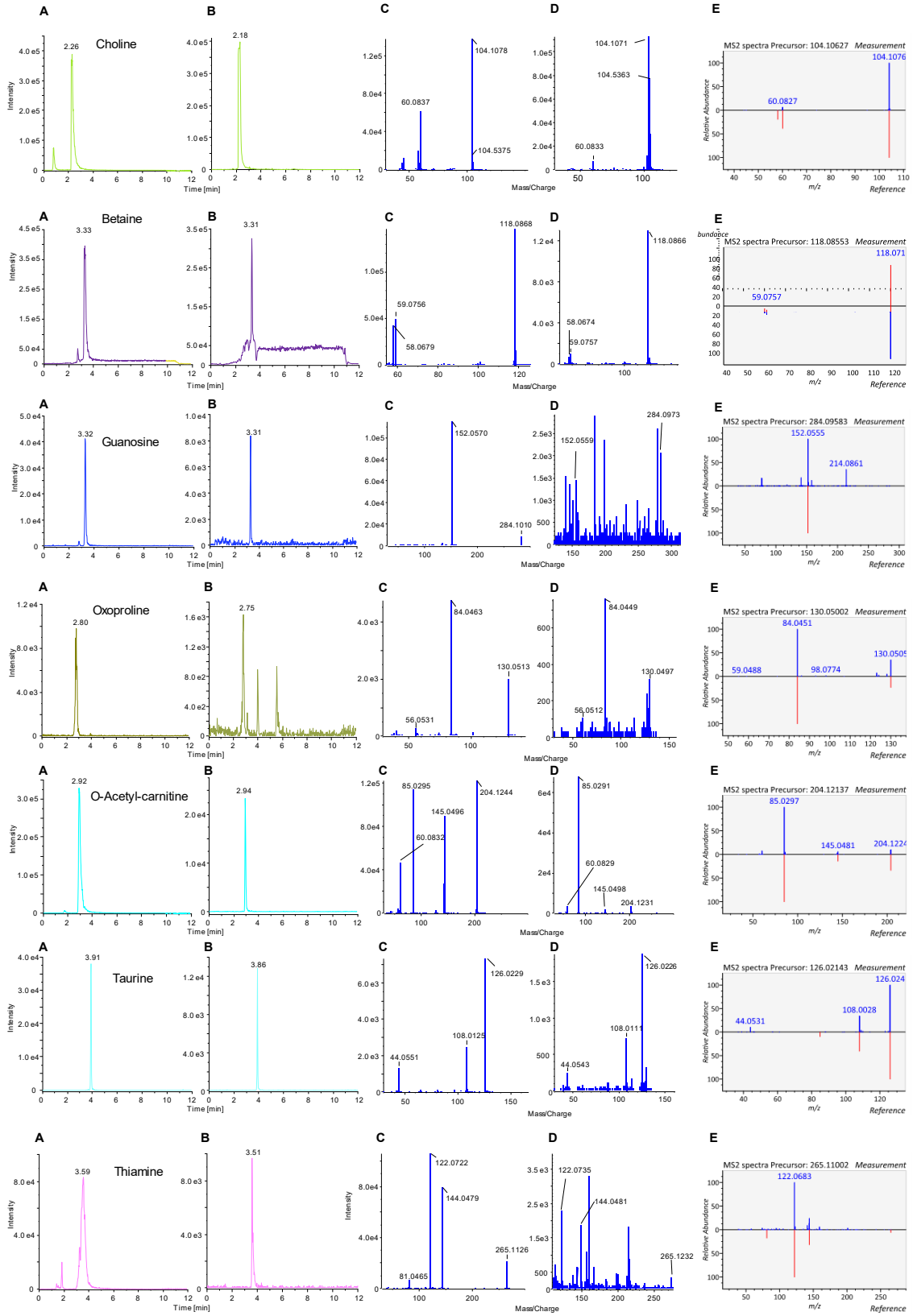

Figure S24: Identified metabolites of untargeted analysis in HCE cell extracts: (A) EIC MS/MS chromatogram of standard solution with an extraction window of +/- 5 mDa; (B) EIC MS/MS chromatogram of HCE extract with an extraction window of +/- 5 mDa; (C) MS/MS spectrum from standard solution; (D) MS/MS spectrum from HCE extract; (E) deconvoluted MS/MS spectrum from the HCE extract (blue) matched against database spectrum (red)

Table S11: Model statistics for PLS analysis: All detected features measured in HCE cell extracts treated with different ILs. Toxicity data was used as dependent variable (Y = log EC_{50}) (X data log transformed; data Pareto scaled)

A	R^2X	$R^2X_{(cum)}$	Eigenvalue	R^2Y	$R^2Y_{(cum)}$	Q^2	$Q^2_{(cum)}$
0	Cent			Cent			
1	0.136	0.136	4.07	0.625	0.625	0.300	0.300
2	0.068	0.204	2.04	0.312	0.937	0.449	0.614
3	0.102	0.305	3.05	0.0433	0.98	0.398	0.768
4	0.058	0.363	1.73	0.0172	0.997	0.502	0.884

3.5. Comparison of simple monophasic versus classical biphasic extraction protocols for comprehensive UHPLC-MS/MS lipidomic analysis of Hela cells

3.5.1. Abstract

In this study, two monophasic isopropanol-water mixtures (IPA:H_2O 75:25 v/v and IPA:H_2O 90:10 v/v) were compared with traditionally employed biphasic methods of Bligh & Dyer and Matyash *et al.* as extraction systems for lipidomics analysis in Hela cells. Samples were analysed by UHPLC-ESI-QTOF-MS/MS in positive and negative mode using sequential window acquisition of all theoretical fragment ion spectra (SWATH) and a relatively new software (MS-DIAL) was employed for the processing of the data which includes detection of peaks, MS/MS spectra deconvolution, identification of detected lipids and alignment of peaks through the analysed samples.

The studied performance parameters such as precision, recoveries of isotopically labelled internal standards and endogenous lipids, number of extracted lipids, and complexity of employed procedure showed that extraction with IPA:H_2O 90:10 v/v performs similar to the Matyash protocol and better than Bligh & Dyer as well as IPA:H_2O 75:25 v/v. However, less complex monophasic protocol which is simpler to implement and can be executed in plastic rather than glass, make the monophasic IPA:H_2O 90:10 v/v protocol an excellent alternative to the classical biphasic protocols for reversed phase LC-MS lipidomics studies.

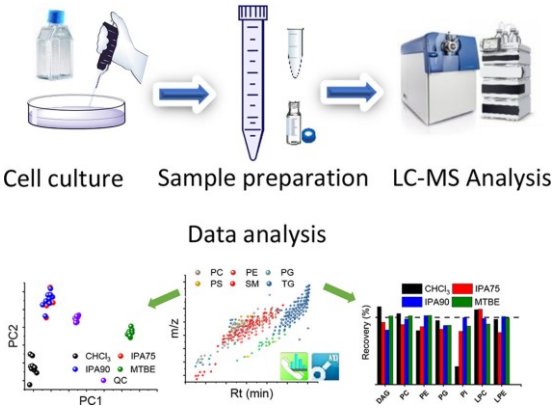

Figure 85: Graphical Abstract: Comparison of simple monophasic versus classical biphasic extraction protocols for comprehensive UHPLC-MS/MS lipidomic analysis of Hela cells

3.5.2. Introduction

Liquid chromatography-mass spectrometry (LC-MS) has become the most widely used analytical tool for lipidomics analysis in the last few years [299,450–452]. Despite many

reported publications on this topic, there is no consensus about the most adequate protocol to follow. One of the most critical points is the sample preparation and therefore the choice of a solvent or solvent mixture for the lipid extraction, since this will determine which lipid classes are mostly recovered from the sample [453]. Extractions with the system chloroform-methanol-water ($CHCl_3$-MeOH-H_2O), at specific ratios, were introduced more than six decades ago, with the pioneering works of Folch [286] and Bligh & Dyer [284], and have frequently been described as “gold standards” [287,299,454–458]. Hexane-isopropanol-water (Hexane-IPA-H_2O) was proposed in 1978 by Hara *et al*. as a less toxic option [459]. However, its performance in terms of wide coverage of distinct lipid classes is modest [460–462]. Recently, two methods using methyl *tert*-butyl ether-methanol-water (MTBE-MeOH-H_2O) [287] and butanol-MeOH-H_2O [290] were introduced and they have become popular because of their similar or even better performance, less tedious procedure for preparing the samples and less toxicity with respect to the chloroform mixtures.

Solvent mixtures have been suggested for lipid extraction after considering that most of the biological samples are composed of some amount of water and that the lipids are mainly soluble in organic solvents. Thus, the strategy for extractions of lipids has traditionally been based on two steps, a first one where a miscible solvent mixture (considering the water present in the sample) is added to the sample, which allows good interaction between solvent and sample matrix, and a second one where more aqueous or organic solvent or both are added to the original mixture in order to create a biphasic system which separates the extracted lipids, in the organic layer, from the rest of the sample, in the aqueous layer. However, considering that nowadays many workflows for lipidomics analysis include a reversed phase liquid chromatographic separation and polar interferences elute in the first minutes of the separation, the use of a biphasic system is not strictly required [463]. In 2017 Jurowski *et al.* [463] reviewed the use of some monophasic mixtures for lipidomics studies. Among the cited examples are $CHCl_3$:MeOH (2:1 v/v) [464,465], 1-butanol/methanol (1:1 v/v) [466] for plasma samples, $CHCl_3$:MeOH (1:2 v/v) for sphingolipids analysis in mammalian cells [467,468] and aqueous isopropanol for extraction of lipids on microalgae [469]. In 2014, Sarafian *et al*. [470] published a study showing a monophasic mixture IPA-H_2O as a good choice for lipid extraction of plasma samples with good recoveries for most of the lipid classes.

In this study, we evaluated the performance of monophasic isopropanol extraction in comparison to biphasic extraction protocols in detail for lipid extraction from Hela Cells. No information about the suitability of this monophasic extraction protocol for mammalian cells and how it compares to classical extraction protocols was available. Thus, two IPA-H_2O mixtures (75:25 v/v and 90:10 v/v) were compared with the biphasic extraction systems: $CHCl_3$-MeOH-H_2O (2:2:1.8 v/v/v, Bligh & Dyer) [284] and MTBE:MeOH:H_2O (10:3:2.5, v/v/v, Matyash) [287], which currently are two of the most widely employed protocols for lipid analysis [454,456,461,462,471–474].

3.5.3. Materials and Methods

3.5.3.1. Materials

Mobile phases were prepared with solvents of LC-MS grade. Methanol (MeOH), acetonitrile (ACN) and isopropanol (IPA) were supplied by Roth (Karlsruhe, Germany). As additive, formic acid (FA, 98%) was obtained by Carl Roth (Karlsruhe, Germany) and ammonium formate was purchased from Sigma–Aldrich (Steinheim, Germany). Water was purified by a water filtration system from Elga (High Wycombe, United Kingdom).

Solvents for extraction were of HPLC grade: chloroform ($CHCl_3$, ≥ 99.8%) and tert-butyl methyl ether (MTBE, anhydrous, 99.8%) from Sigma-Aldrich.

SPLASH™ Lipidomix® solution containing the following isotopically labelled internal standards (ILIS): 15:0-18:1(d7) PC, 15:0-18:1(d7) PE, 15:0-18:1(d7) PS, 15:0-18:1(d7) PG, 15:0-18:1(d7) PI, 15:0-18:1(d7) PA, 18:1(d7) LPC, 18:1(d7) LPE, 18:1(d7) Chol Ester, 18:1(d7) MG, 15:0-18:1(d7) DG, 15:0-18:1(d7)-15:0 TG, 18:1(d9) SM, Cholesterol (d7) was obtained from Avanti Polar Lipids (Alabama, USA) (See SI Table S12 for more information about internal standards).

3.5.3.2. Cell culture

The human cervical cancer HeLa cells adapted to serum free conditions (AC free, ECACC 08011102) were grown in T75-flask and EX-CELL HeLa serum free media (Sigma Aldrich) supplemented with 2 mM L-glutamine (Sigma Aldrich), until they reached a density of around 2-3 x 10^6 cells/mL. Afterwards they were transferred to 50 mL falcon tubes and centrifuged for 5 min at 700 rcf, before the supernatant was discarded. The cell pellet was resuspended in 15 mL ice-cold Dulbecco's Phosphate

Buffered Saline (PBS, Sigma Aldrich) for washing and centrifuged again for 5 min at 700 rcf. The washing was repeated twice and after the last resuspension cells were counted in triplicate with a hemocytometer. According to the mean of the counted cells, aliquots containing approximately 8 x 10^5 cells were transferred randomly to 15 mL falcon tubes (for extraction with isopropanol mixtures) and 15 mL glass tubes (for extractions with $CHCl_3$ and MTBE). Samples were centrifuged at 700 rcf for 5 min and the pellets were stored at -80 ºC until extraction.

3.5.3.3. Extraction protocols

Extraction solvents were kept on ice before their addition to the samples. For each extraction protocol, 10 samples (pellets containing 8 x 10^5 cells) were extracted. In order to estimate the recovery of some lipid classes, 5 of these samples were spiked before the extraction with 100 µL of 5 % v/v SPLASH Lipidomix solution in methanol and were resuspended with 100 µL MeOH before the LC-MS measurement (pre-extraction spiking). For the other 5 samples 100 µL of MeOH were added before the extraction and they were resuspended with 100 µL of 5 % v/v SPLASH Lipidomix solution before the LC-MS measurement (post-extraction spiking). Recoveries were calculated as ratio of average intensities for internal standards in the pre-extraction and post extraction spiked samples.

3.5.3.3.1. Extraction with MTBE:MeOH:H_2O (10:3:2.5, v/v/v, “MTBE”)

This EP was based on Matyash *et al.* [287]. Either methanol or solution of 5% SPLASH Lipidomix in MeOH (100 µL) was added to the pellet. Then 1.4 mL of methanol and 5 mL of MTBE were added. Vortexing (30 s), ultrasonication (2 min) and vortexing (30 s) cycle was applied to disrupt the pellet. Samples were incubated on ice while shaking (500 rpm, 60 min). After the extraction, 1.25 mL of H_2O was added and samples were incubated on ice for another 10 min. Afterwards, centrifugation at 3500 rcf for 10 min was applied and the upper layer was transferred to a glass tube. Samples were dried in an evaporator (Genevac EZ-2; Warminster, Pennsylvania, USA) for 10 hours under nitrogen protection. The lipid extract was resuspended in 100 µL of either methanol or solution of 5% SPLASH Lipidomix while sonication (2 min) and vortexing (30 s) were applied. Centrifugation at 3500 rcf for 10 min was applied and the supernatant was transferred to vials for MS-measurements. During the last

step, 10 µL aliquot of each sample were transferred to a separate vial to prepare a pooled QC sample.

3.5.3.3.2. Extraction with IPA:H_2O (75:25 v/v, "IPA75")

Either methanol or solution of 5% SPLASH Lipidomix in MeOH (100 µL) was added to the pellet. Then 5.0 mL of IPA:H_2O (75:25 v/v) were added. Vortexing (30 s), ultrasonication (2 min) and vortexing (30 s) cycle was applied to disrupt the pellet. Samples were incubated on ice while shaking (500 rpm, 60 min). After the extraction, centrifugation at 3500 rcf for 10 min was applied and supernatant was transferred to a 15 mL falcon tube. Samples were dried in an evaporator for 10 hours under nitrogen protection. The lipid extract was resuspended in 100 µL of either methanol or solution of 5% SPLASH Lipidomix while sonication (2 min) and vortexing (30 s) were applied. Centrifugation at 3500 rcf for 10 min was applied and the supernatant was transferred to vials for MS-measurements. During the last step, 10 µL aliquot of each sample were transferred to a separate vial to prepare a pooled QC sample.

3.5.3.3.3. Extraction with IPA:H_2O (90:10 v/v, "IPA90")

As described before for extraction with IPA75, only that IPA:H_2O (90:10 v/v) was used instead of IPA:H_2O (75:25 v/v).

3.5.3.3.4. Extraction with $CHCl_3$-MeOH-H_2O (2:2:1.8 v/v/v, "$CHCl_3$")

This EP was based on Bligh & Dyer [284]. Either methanol or solution of 5% SPLASH Lipidomix in MeOH (100 µL) was added to the pellet. Then, 0.8 mL of H_2O, 1.90 mL of MeOH and 1.0 mL of $CHCl_3$ were added. Vortexing (30 s), ultrasonication (2 min) and vortexing (30 s) cycle was applied to disrupt the pellet. Samples were incubated on ice while shaking (500 rpm, 60 min). After the extraction 1.0 mL $CHCl_3$ and 1.0 mL of H_2O were added and samples were incubated on ice for another 10 min. Afterwards, centrifugation at 3500 rcf for 10 min was applied and the upper layer was transferred to a glass tube. Samples were dried in an evaporator for 10 hours under nitrogen protection. The lipid extract was resuspended in 100 µL of either methanol or solution of 5% SPLASH Lipidomix while sonication (2 min) and vortexing (30 s) were applied. Centrifugation at 3500 rcf for 10 min was applied and the supernatant was transferred to vials for MS-measurements. During the last step, 10 µL aliquot of each sample were transferred to a separate vial to prepare a pooled QC sample.

3.5.3.3.5. Blank extractions for all extraction protocols

Seven blank extraction replicates for each extraction protocol were performed following the same steps indicated above, only that extraction solvents were added to empty falcon or glass tubes. For further analysis, an additional IPA90 blank extraction protocol (also 7 replicates) was performed replacing plasticware with glassware. The results from these blank samples were used to correct the result from the cell extractions.

3.5.3.3.6. Extractions without internal standards

One cell extract for each EP was prepared following the same steps described before, but no ILIS were added. These samples were used to validate assay specificity for internal standards i.e. to check that no significant signals are present at m/z and retention times corresponding to the ILIS. For all EPs no signals i.e., no interferences were found.

3.5.3.4. LC-MS measurements

All analyses were performed on an Agilent 1290 Series UHPLC instrument (Agilent, Waldbronn, Germany) coupled to a Sciex TripleTOF 5600+ mass spectrometer (Sciex, Concord, Ontario; Canada). Duospray ion source for ESI in positive and negative ion mode was used. Sample injections were done in randomized order with a Pal HTC-XS autosampler from CTC (Zwingen, Switzerland). QC samples were run at the beginning of the sequence, during the sequence (every five samples) and at the end of the sequence.

Chromatographic separation was performed according to conditions published by Tsugawa *et al.* [265] in order to enable retention time scoring for peak identification with MS-Dial software. Briefly an Acquity UPLC CSH C18 Column, 130Å, 1.7 µm, 2.1 mm X 100 mm with an Acquity UPLC CSH C18 VanGuard Pre-column, 130Å, 1.7 µm, 2.1 mm X 5 mm (Waters, Eschborn, Germany) was used. The mobile phase was composed of 10 mM ammonium formate and 0.1 % formic acid in A) 60:40 ACN:H_2O (v/v) and B) 90:10 (v/v) IPA:ACN. The following gradient profile was used: 0.00 min, 15 % B; 2.00 min, 30 % B; 2.50 min, 48 % B; 11.00 min, 82 % B; 11.50 min, 99 % B; 12.00 min, 99 % B; 12.10 min, 15 % B, 15.00 min, 15 % B. Flow rate was 600 µL/min and column temperature was 65 °C. The injection volumes were 3 µL and 5 µL for positive and negative mode, respectively.

The following MS-settings of the mass spectrometer were used: Curtain gas (CUR) 35 psi, nebulizer gas (GS1) 60 psi, drying gas (GS2) 60 psi, ion-spray voltage floating (ISVF) +5500 V in positive and -4500 V in negative mode, source temperature (T) 350°C, collision energy 45 V, collision energy spread 15 V, declustering potential (DP) 80 V, mass range m/z 50 – 1250 in ESI (+) and 50 – 1050 in ESI (-), and RF Transmission (RF) m/z 40: 50 % and m/z 120: 50 %. An external mass calibration was performed every five samples (see SI Table S13).

MS data was obtained by using sequential window acquisition of all theoretical fragment ion spectra (SWATH) [433,475], after optimizing Q1 windows size (See SI Table S14) with Swath Tuner software [262].

3.5.3.5. MS data processing

MS-Dial software (RIKEN, version 3.06) [265] was used to process the MS data (see parameters in SI Table S15). This included detection of peaks, MS^2 data deconvolution, compound identification and alignment of peaks through all the samples. For identification a cut off value of 80% was selected: This value is based on 6 different similarity scores: 1 for retention time, 1 for m/z, 1 for isotopic pattern and 3 for MS/MS (dot product, dot product reversed and presence). An important condition established in MS-Dial was that a peak was selected for alignment only when it was present in at least 51% of the samples of one extraction protocol. Features which were relatively close (m/z difference less than 0.03 Da and retention time difference less than 0.1 min) in the alignment file of MS-Dial were visually inspected in order to determine if they are effectively corresponding to more than one feature, otherwise the repeated feature was removed. List of aligned peaks from MS-Dial were further evaluated with Multiquant 3.0 (Sciex). Intensities were processed for principal component analysis (PCA) with MarkerView (Sciex) and exported to Excel for statistical analysis. A feature was considered for comparison between the different extraction protocols when it was present in at least 90 % of the samples of one extraction protocol having a CV less than 30% for the 10 extraction replicates of that protocol. Furthermore, blank extraction samples were used to exclude features that have m/z difference less than 0.01 Da, retention time difference less than 0.5 min and fold change less than 5 between the cell extraction and blank extraction replicates (List of detected features in extraction blanks are in Appendix D, shown in the online version of the publication, not shown in the thesis).

Peaks corresponding to internal standards were removed from MS-Dial detected features and were analysed directly with Multiquant to evaluate the recoveries.

3.5.4. Results and discussion

In order to compare the different EPs some modifications were introduced to the originally published protocols. Thus, extraction volumes were modified to be as similar as possible for all EPs while keeping the solvent ratios for each EP as they were published. Variables like temperature, vortexing time, vortexing intensity, centrifugation time and centrifugation speed were kept the same for all extraction protocols. For the same reason no re-extractions were done for any of the extraction protocols. The solvent evaporation step was performed overnight to save time and it was kept at 10 hours even when the time required for the evaporation of each solvent ranges from less than 3 hours, in the case for $CHCl_3$ and MTBE, to approximately 6 hours, in the case of IPA75. Thus, all the extracts were kept under nitrogen atmosphere until resuspension to minimize possible oxidation of lipids.

3.5.4.1. Chromatograms and principal component analysis (PCA)

Total ion chromatograms (TICs) in positive and negative mode for extracted samples with different EPs (Figure 86) show a very similar profile with only some slight differences, especially during the first minutes. After processing the data with MS-Dial and Multiquant, peak intensities for detected features were analysed by PCA (Figure 87). Score plots with the first two principal components, in both ESI (+) and ESI (-) mode (Figure 87A and C), show a clear separation between the samples extracted with each protocol, except for extractions with isopropanol 75% and isopropanol 90%, which are overlapped. This result indicates that the detected features and their corresponding intensities show significant alterations between the different extraction protocols. Loadings plots, with the first two principal components, are shown in Figure 87B and D, for positive and negative mode respectively (for a better visualization, unknown features and lipid classes with less than five identified features were excluded from each loadings plot). In Figure 87B it is possible to note influences of some lipid classes to the shown differentiation of EPs in Figure 87A, for example LPE are oriented in the direction of $CHCl_3$ and PGs are oriented in the direction of the EPs IPA75 and IPA90, which means that those lipid classes are better extracted with the mentioned EPs. In the same manner, in Figure 87D, LPCs and LPEs are oriented

in the same direction of the EP $CHCl_3$ and Cers are oriented in the direction of the EPs IPA75 and IPA90.

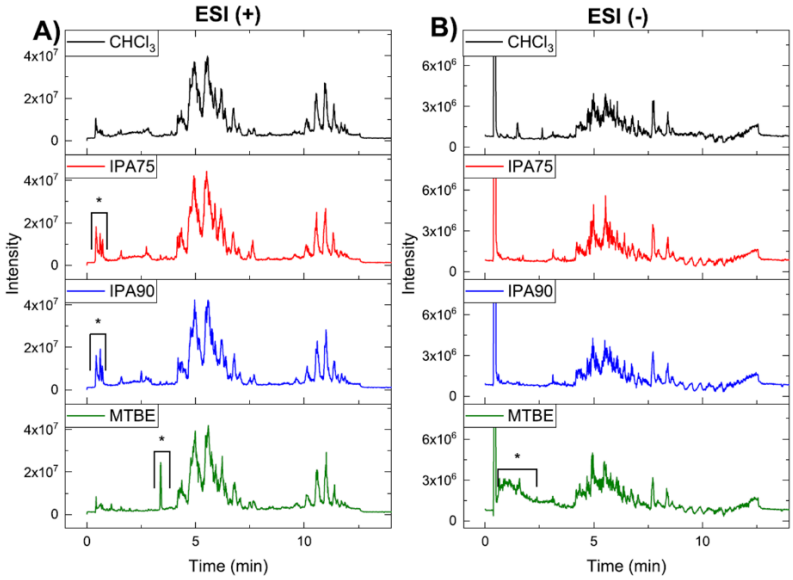

Figure 86: Representative TICs for samples extracted with four different Eps: Using A) ESI (+) and B) ESI (-) mode. Asterixes indicate major differences between the chromatograms

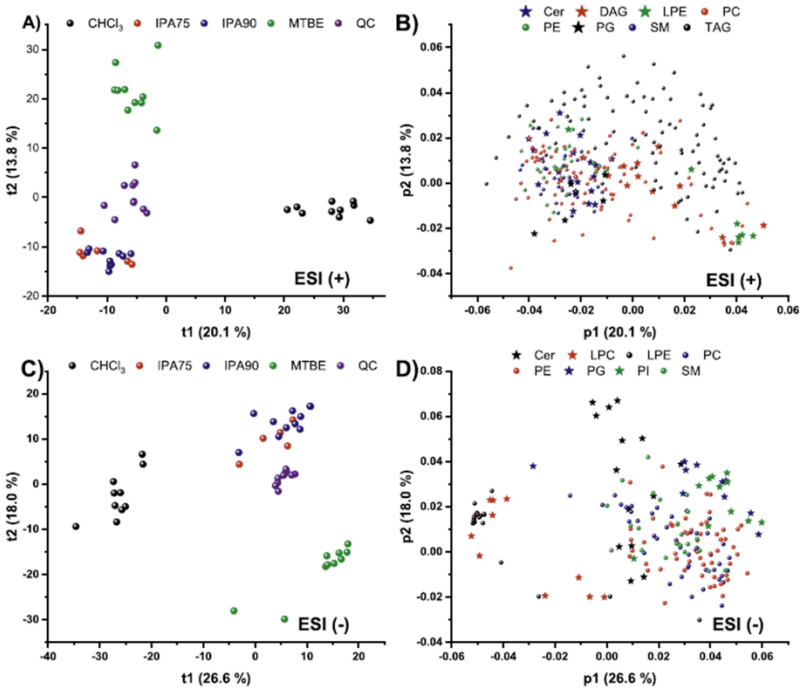

Figure 87: PCA plots for intensities of detected features: A) Scores plot in ESI (+), B) Loadings plot including only lipid classes with more than 5 identified features ESI (+) C) Scores plot in ESI (-), D) Loadings plot including only lipid classes with more than 5 identified features ESI (-)

3.5.4.2. Number of detected features

Table 10 and Figure 88 show the numbers and distribution of features detected in ESI (+) and ESI (-) for the EPs (Specific data about detected features can be observed in Appendix B, shown in the online version of the publication, not shown in the thesis).

Table 10: Description of processed features: With MS-Dial and Multiquant software

	ESI (+)					ESI (-)				
Description	**Total**	**$CHCl_3$**	**IPA75**	**IPA90**	**MTBE**	**Total**	**$CHCl_3$**	**IPA75**	**IPA90**	**MTBE**
Detected features in MS-Dial [1]	**1872**	904	893	928	1038	**1541**	708	674	718	1015
Detected features after processing with Multiquant[2]	**1382**	1110	1054	1118	1183	**1074**	824	759	771	906
Detected features after correction with blanks	**1167**	991 (85%)	955 (82%)	1003 (86%)	985 (84%)	**842**	777 (92%)	713 (85%)	725 (86%)	701 (83%)
Identified features	292	289 (99%)	285 (97.6%)	290 (99.3%)	291 (99.7%)	206	205 (99.5%)	201 (97.6%)	205 (99.5%)	200 (97.1%)
SM	**29**	29	28	29	29	**22**	22	22	22	22
PG	**6**	6	5	6	6	**10**	10	10	10	10
PE	**29**	29	29	29	29	**55**	55	54	55	55
PC	**88**	88	88	87	87	**43**	43	43	43	43
LPE	**7**	7	7	7	7	**22**	22	20	22	20
LPC	**4**	4	4	4	4	**11**	11	11	11	10
Cer-NS	**12**	12	10	12	12	**6**	6	6	6	6
Cer-NDS	**5**	5	5	5	5	**2**	2	2	2	2
TG	**92**	89	89	91	92					
HexCer-NS	**3**	3	3	3	3	**1**	1	1	1	1
DG	**12**	12	12	12	12					
CE	**2**	2	2	2	2					
BMP	**3**	3	3	3	3					
PS	**-**	-	-	-	-	**1**	1	1	1	1
PI	**-**	-	-	-	-	**11**	11	10	11	11
OxPS	**-**	-	-	-	-	**1**	1	1	1	1
OxPG	**-**	-	-	-	-	**1**	1	1	1	1
OxPE	**-**	-	-	-	-	**6**	6	5	5	5
OxPC	**-**	-	-	-	-	**3**	3	3	3	3
LPI	**-**	-	-	-	-	**2**	2	2	2	2
LPG	**-**	-	-	-	-	**2**	2	2	2	2
HexCer-NDS	**-**	-	-	-	-	**5**	5	5	5	5
FA	**-**	-	-	-	-	**2**	1	2	2	0

[1] present in at least 51 % of samples of one group [2] present in at least 90 % of samples of one EP having a CV < 30%

Features list obtained after processing with MS-Dial was reprocessed with Multiquant. In this manner we are combining the capabilities of MS-Dial for recognizing features and the identification of approximately 15 % of them with the capabilities of Multiquant for a more controlled integration, making it easier to determine whether a feature is present or not in a group of samples. After the processing with Multiquant and the feature filtration (only those features which are present in at least 90 % of the samples of one EP and have a CV less than 30 % for the replicates of that EP were selected) the number of features was reduced from 1872 to 1382 in ESI (+) and from 1541 to

1024 in ESI (-) but the number of features which were found with each EP was higher (See Table 10).

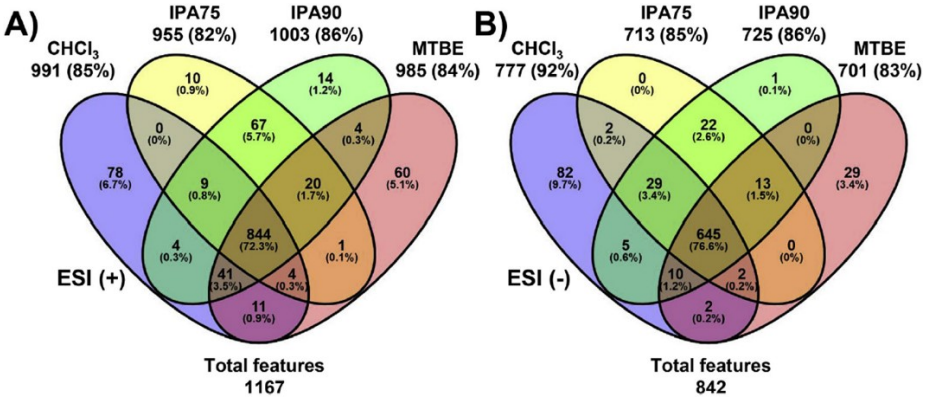

Figure 88: Venn diagrams: Showing the distribution of detected features with each EP and their overlapping selectivities. A) Results from ESI (+) and B) ESI (-) modes

Similar procedures with MS-Dial and Multiquant were applied to blank extraction replicates and peak exclusion lists were used to filter only the features coming from the cell pellets (1167 features in ESI (+) and 842 features in ESI (-)). In terms of the total number of detected features, all extractions protocols show similar performance in ESI (+) (maximum difference is 4 % between IPA90 and IPA75) and a slight greater amount is obtained with $CHCl_3$ in ESI (-) (difference of 9 % respect to the MTBE protocol). Venn diagrams in Figure 88 show the distribution of detected features in ESI (+) and ESI (-) modes. It is possible to see that 72 % of the features in ESI (+) and 77% in negative mode were detected with all EPs. In ESI (+) the amount of features that can be exclusively extracted with each extraction protocol is very similar (6.7 % with $CHCl_3$, 5.7 % in common with IPA75 and IPA90 and 5.1% with MTBE).

In ESI (-), $CHCl_3$ protocol extracts exclusively 9.7 % of total detected features in comparison to 3.4 % of MTBE and 2.6 % of IPA75 and IPA90 (in common). These features detected with only one of the specific EP (or two of them in the case of IPA75 and IPA90) correspond to not identified features which are spread through the whole studied range of m/z and retention time and for this reason no specific lipid class can be assigned to them.

3.5.4.3. Identified lipids and relative recovery of endogenous lipids

Table 10 also shows the distribution of lipids identified with each EP (Specific data about identified features can be observed in Appendix C, shown in the online version of the publication, not shown in the thesis). Only IPA75 and MTBE extraction allowed the identification of a few less features (2% less in each mode for IPA75 and 2% less

in negative mode for MTBE), it means that in terms of the number of identified features the four studied EPs have similar performance. However, Figure 87B and D, already showed that even when similar number of lipids where detected with each EP, their intensities were significantly different for some lipid classes.

In order to describe the relative ability of each EP to extract a particular lipid class, a relative recovery of endogenous extracted lipids was calculated using IPA90 as a reference. Thus, the average intensity of each identified lipid extracted with $CHCl_3$, IPA75 and MTBE was normalized with respect to the average intensity of the same lipid after extraction with IPA90. Afterwards, the normalized values were averaged for the lipids belonging to the same lipid class (Figure 89, SI Table S16).

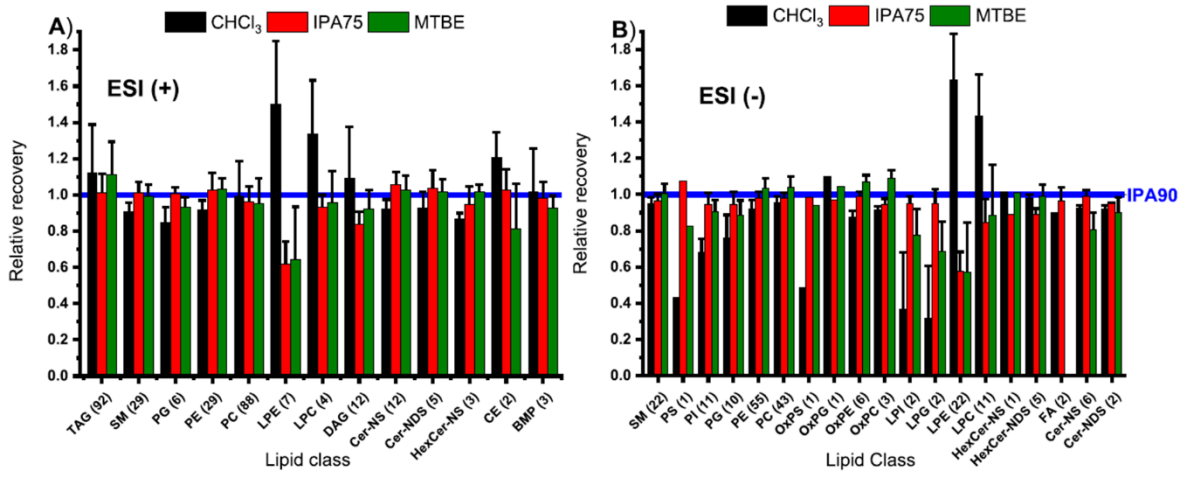

Figure 89: Relative lipid class recoveries of endogenous lipids obtained with different EPs and using IPA90 as a reference: A) Results from ESI (+) and B) ESI (-) modes. Numbers in parenthesis indicate the number of identified lipids from each lipid class that were normalized and averaged

The results show similar intensities for some lipid classes independently of which protocol was employed. However, in some other cases significant differences are noted. In ESI (-) mode, for example, significantly lower intensities were obtained for polar lipids LPG, LPI, PG, PI, PS and FA when $CHCl_3$ and MTBE extractions were employed. Also, higher intensities are achieved for LPE and LPC with $CHCl_3$ protocol while lower ones are obtained with IPA75 and MTBE. This higher recovery for LPC and LPE with $CHCl_3$ has to be further investigated considering that these are two of the most polar lipid classes and it is expected that polar mixtures IPA:H_2O can extract better these substances, as it has been indicated previously [470].

3.5.4.4. Lipid recovery of internal standards

To determine the absolute recovery of lipid classes with each EP, pre-extraction and post-extraction spiking of the samples with a mixture of ILIS was performed. Figure 90 and SI Table S17 show the % recovery for each ILIS. As an average MTBE and IPA90 have the best performance. In the case of $CHCl_3$, its performance is significantly higher than other protocols for the recovery of TG. IPA75 shows recoveries in most of the cases lower than the ones that can be reached with IPA90. $CHCl_3$ protocols shows significantly lower recoveries for polar lipid classes PA, PI and PS.

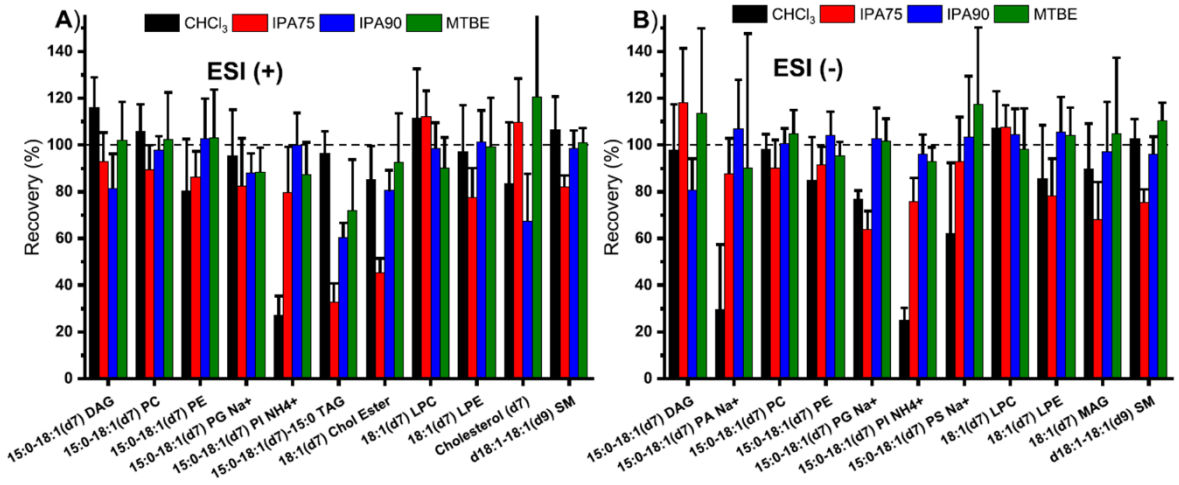

Figure 90: **Recoveries of isotopically labelled internal standards after pre- and post-extraction spiking:** A) Results from ESI (+) and B) ESI (-) modes

Here, it is important to highlight that beside the fact that ILIS were added to the pellet just before the addition of extraction solvent, which means they have less interaction with cellular matrix and more direct contact with extraction solvent than endogenous lipids, a good correlation was observed for the recoveries that were calculated with the ILIS in comparison with the relative recoveries of endogenous lipids described in section 3.5.4.3. Only exception for this finding was the anomalous mentioned case of LPEs and LPCs.

Also, good correlation was observed between the obtained recoveries and reported results by Sarafian *et al.* [470] in plasma samples after extraction with isopropanol and relative comparison with protocols based on MTBE (Matyash) and $CHCl_3$ (Bligh and Dyer, Folch). However, only recovery of odd-chained internal standards was reported at that moment and no comparison with endogenous lipids was done.

Higher recoveries obtained with IPA90 respect to IPA75, especially for the most abundant lipid classes are also in good concordance with comparison done by

Yao *et al.* [469] in microalgae and soybeans, where aqueous isopropanol mixtures with 88 % and 95 % of isopropanol yielded higher oil extraction efficiency than mixtures with 50 % and 70 % isopropanol.

3.5.4.5. Precision

For a comparison of precisions obtained with the EPs, CV % for each detected feature was calculated. A profile of the CVs for the features that were found with each EP (1167 features in ESI (+) and 842 features in ESI (-), see Figure 88) is shown in Figure 91 and SI Table S18. For features detected in ESI (+), CV profiles show to be very similar having a maximum CV % bin from 10 to 15% and around 80 % of the features with CV less than 30 % independently of the employed EP. For features detected with ESI (-), IPA75 and IPA90 have a maximum CV bin from 5 to 10 %, while $CHCl_3$ and MTBE have a maximum CV bin from 10 to 15 %. All EPs have more than 90% of detected features with a CV below 30%.

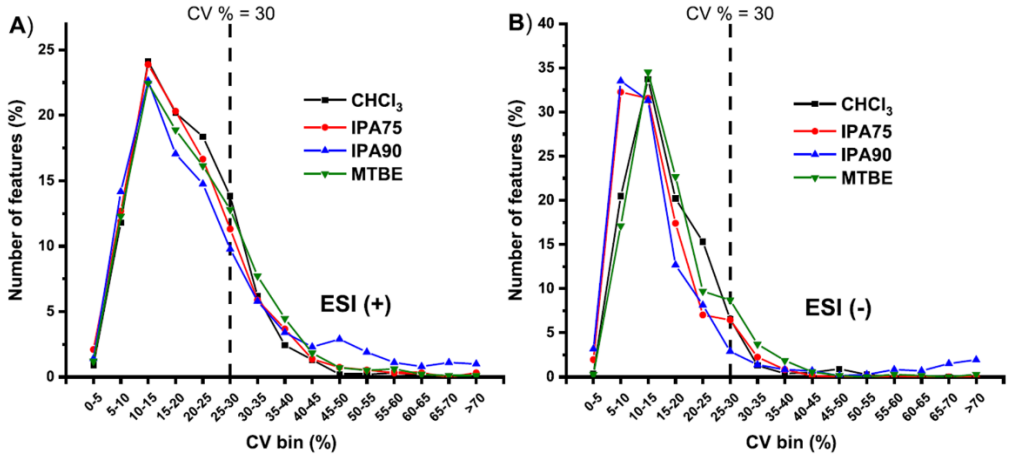

Figure 91: Distribution of CVs (%) obtained for precision evaluation of peak intensities of features detected in all four Eps: A) Results from ESI (+) (1167 analysed features) and B) ESI (-) modes (842 analysed features)

3.5.4.6. Protocol complexity

Many publications have already made emphasis about the advantage of using extraction protocols where the organic layer is the upper phase (as in MTBE protocol) and not the lower one (as in $CHCl_3$ protocol) of a two-phase partitioning system. The reason for this is the more tedious removal of the lipid containing organic phase when this one is in the bottom, especially because a layer of protein is located between the organic and aqueous layer. In the case of tested EPs IPA75 and IPA90, the fact of having a monophasic mixture makes this process even easier because only a separation of the supernatant from the solid residue is required. A possible

disadvantage of employing monophasic mixtures for extraction rely on the presence of salts as part of the extract. However, in reversed phase LC-MS this is not necessarily a problem because these salts elute during the first minutes of chromatographic run. As part of this research, QC samples run at the beginning, in between and at the end of measured sequences in ESI (+) and ESI (-), did not show significant differences in terms of intensity (see SI Figure S25).

Another advantage for IPA75 and IPA90 extractions, is that they are compatible with plasticware, which does not happen with MTBE and $CHCl_3$. In our study, extraction blanks were performed to remove those features which are not coming from cell pellets (lists of features detected in extractions blanks are in Appendix D, shown in the online version of the publication, not shown in the thesis). Additionally, an extra extraction blank for IPA90 using glassware, yielded a higher amount of detected features than the corresponding one using plasticware (See SI Figure S26 and Figure S27). This higher amount of detected features could be related with the cleaning process employed for the glass tubes. Therefore, in the case that glassware is employed for these extractions, either new glassware has to be utilized for each new extraction, which is very expensive or a very strict cleaning protocol has to be employed, which will demand extra time and make the process more tedious. Consequently, it can be said that the extraction protocols IPA75 and IPA90, employing plasticware, are less time consuming, cheaper and easy to automatize.

3.5.5. Concluding remarks

After comparison of the performance for extraction of lipids, it is possible to conclude that there was no significant difference with the number of identified lipids with each EP. In terms of recoveries for different lipid classes, extraction with IPA90 showed similar results as MTBE for most of the lipid classes, better results than $CHCl_3$ for the more polar lipid classes and better results than IPA75 for the less polar lipid classes. Precision with IPA mixtures showed to be slightly better in ESI (-) and similar in ESI (+) than the precision obtained with MTBE and $CHCl_3$. In terms of complexity, monophasic extractions with IPA offered a simpler, less time consuming and cheaper protocol. Also, MS signal intensities did not show any decrease after samples extracted with IPA:H_2O mixtures were measured, which could be corroborated with the reproducibility of measured intensities for QC samples through the whole study. Considering all these

aspects, extraction with IPA90 represents an excellent alternative as a solvent for developing reversed-phase LC-MS lipidomics studies.

3.5.6. Supporting information

Comparison of simple monophasic versus classical biphasic extraction protocols for comprehensive UHPLC-MS/MS lipidomic analysis of Hela cells

Table S12: Internal standard: Information about internal standards of the SPLASH™ Lipidomix® Mass Spec Standard (in MeOH)

Mixture Components	Target Conc. (µg/mL)
15:0-18:1(d7) PC	160
15:0-18:1(d7) PE	5
15:0-18:1(d7) PS	5
15:0-18:1(d7) PG	30
15:0-18:1(d7) PI	10
15:0-18:1(d7) PA	7
18:1(d7) LPC	25
18:1(d7) LPE	5
18:1(d7) Chol Ester	350
18:1(d7) MG	2
15:0-18:1(d7) DG	10
15:0-18:1(d7)-15:0 TG	55
18:1(d9) SM	30
Cholesterol (d7)	100

Table S13: Acetate cluster masses: m/z values of sodium acetate clusters used for external calibration of QTOF

ESI+ (m/z)	ESI- (m/z)
104.99230	141.01693
351.00152	223.02000
433.00459	305.02307
515.00767	387.02615
597.01074	469.02922
679.01381	551.03230
761.01689	633.03537
843.01996	715.03844
1007.02611	797.04152
1089.02918	879.04459
	961.04767
	1043.05074

Table S14: MS windows: Information about design of MS experiments

Experiment	MS Type	Accumulation time (ms)	Pos mode		Neg mode	
			Min m/z	Max m/z	Min m/z	Max m/z
MS	SCAN	80	50	1250	50	1050
MS/MS	SWATH 1	31	50.0	214.6	50.0	342.2
MS/MS	SWATH 2	31	213.6	281.8	341.2	453.6
MS/MS	SWATH 3	31	280.8	390.7	452.6	480.8
MS/MS	SWATH 4	31	389.7	480.4	479.8	507.8
MS/MS	SWATH 5	31	479.4	509	506.8	532.3
MS/MS	SWATH 6	31	508	536.5	531.3	566.8
MS/MS	SWATH 7	31	535.5	610.6	565.8	617.4
MS/MS	SWATH 8	31	609.6	677.1	616.4	687.1
MS/MS	SWATH 9	31	676.1	709.0	686.1	715.0
MS/MS	SWATH 10	31	708.0	735.1	714.0	744.1
MS/MS	SWATH 11	31	734.1	759.1	743.1	755.1
MS/MS	SWATH 12	31	758.1	773.1	754.1	776.0
MS/MS	SWATH 13	31	772.1	790.2	775.0	794.6
MS/MS	SWATH 14	31	789.2	811.2	793.6	807.6
MS/MS	SWATH 15	31	810.2	827.2	806.6	830.3
MS/MS	SWATH 16	31	826.2	856.2	829.3	840.1
MS/MS	SWATH 17	31	855.2	884.3	839.1	859.2
MS/MS	SWATH 18	31	883.3	915.9	858.2	889.1
MS/MS	SWATH 19	31	914.9	983.7	888.1	924.6
MS/MS	SWATH 20	31	982.7	1250.0	923.6	1050.0

Table S15: MS-DIAL parameters: Used for processing of data with MS-Dial in negative and positive mode

Mode	POSITIVE	NEGATIVE
Data collection parameters		
Retention time begin	0.5	0.5
Retention time end	13	13
Mass range begin	50	50
Mass range end	1250	1050
Centroid parameters		
MS1 tolerance	0.01	0.01
MS2 tolerance	0.025	0.025
Peak detection-based	TRUE	TRUE
Isotope recognition		
Maximum charged number	2	2
Data processing		
Number of threads	4	3
Peak detection parameters		
Smoothing method	Linear Weighted Moving Average	Linear Weighted Moving Average
Smoothing level	3	3
Minimum peak width	5	5
Minimum peak height	3000	1000
Peak spotting parameters		
Mass slice width	0.1	0.1
Exclusion mass list (mass & tolerance)		
Deconvolution parameters		
Peak consideration	Both	Both
Sigma window value	0.5	0.5
Exclude after precursor	TRUE	TRUE
MSP file and MS/MS identification setting		
MSP file	MSDIAL-LipidDBs-VS35-FiehnO.lbm	MSDIAL-LipidDBs-VS35-FiehnO.lbm
Retention time tolerance	0.5	0.5
Accurate mass tolerance (MS1)	0.01	0.01
Accurate mass tolerance (MS2)	0.05	0.05
Identification score cut off	80	80
Text file and post identification (retention time and accurate mass based) setting		
Text file	IS_PostIdentification_Pos.txt	IS_PostIdentification_Neg.txt
Retention time tolerance	0.1	0.1
Accurate mass tolerance	0.01	0.01
Identification score cut off	85	85
Advanced setting for identification		
Relative abundance cut off	0	0
Top candidate report	TRUE	TRUE
Adduct ion setting		
	$[M+H]^+$, $[M+NH4]^+$, $[M+Na]^+$	$[M-H]^-$, $[M-H2O-H]^-$, $[M+Cl]^-$, $[M+FA-H]^-$
Alignment parameters setting		
Reference file	QC-5.abf	QC-05.abf
Retention time tolerance	0.05	0.05
MS1 tolerance	0.015	0.015
Retention time factor	0.5	0.5
MS1 factor	0.5	0.5
Peak count filter	0	0
N% detected in at least one group	51	51
QC at least filter	FALSE	FALSE
Tracking of isotope labels		
Tracking of isotopic labels	FALSE	FALSE

Table S16: Relative recoveries: Of endogenous lipids extracted with $CHCl_3$, IPA75 and MTBE EPs respect to IPA90 EP. Each identified lipid was normalized with the corresponding intensity detected by using IPA90 EP. Then all the values from lipids belonging to the same lipid class were averaged and their standard deviation was calculated

ESI (+)				ESI (-)			
Lipid class[1]	**$CHCl_3$[2]**	**IPA75[2]**	**MTBE[2]**	**Lipid class[1]**	**$CHCl_3$[2]**	**IPA75[2]**	**MTBE[2]**
TAG (92)	1.12 (0.13)	1.01 (0.05)	1.11 (0.09)	**SM (22)**	0.95 (0.02)	0.97 (0.02)	1 (0.03)
SM (29)	0.91 (0.03)	1.01 (0.03)	0.99 (0.03)	**PS (1)**	0.43	1.07	0.82
PG (6)	0.85 (0.04)	1.01 (0.02)	0.93 (0.03)	**PI (11)**	0.68 (0.04)	0.94 (0.03)	0.9 (0.03)
PE (29)	0.92 (0.03)	1.03 (0.05)	1.03 (0.03)	**PG (10)**	0.76 (0.06)	0.94 (0.04)	0.88 (0.04)
PC (88)	0.99 (0.1)	0.96 (0.04)	0.95 (0.07)	**PE (55)**	0.92 (0.03)	0.98 (0.02)	1.04 (0.03)
LPE (7)	1.5 (0.18)	0.62 (0.06)	0.64 (0.15)	**PC (43)**	0.95 (0.02)	0.98 (0.02)	1.04 (0.03)
LPC (4)	1.34 (0.15)	0.93 (0.03)	0.96 (0.09)	**OxPS (1)**	0.49	0.98	0.94
HexCer-NS (3)	0.87 (0.02)	0.95 (0.05)	1.02 (0.02)	**OxPG (1)**	1.1	0.97	1.05
DAG (12)	1.09 (0.14)	0.84 (0.03)	0.92 (0.05)	**OxPE (6)**	0.88 (0.02)	0.99 (0.01)	1.07 (0.02)
Cer-NS (12)	0.92 (0.03)	1.06 (0.03)	1.02 (0.04)	**OxPC (3)**	0.91 (0.01)	0.94 (0.02)	1.09 (0.02)
Cer-NDS (5)	0.93 (0.04)	1.04 (0.05)	1.02 (0.03)	**LPI (2)**	0.37 (0.16)	0.95 (0.02)	0.77 (0.07)
CE (2)	1.21 (0.07)	1.03 (0.06)	0.81 (0.13)	**LPG (2)**	0.32 (0.14)	0.95 (0.04)	0.69 (0.08)
BMP (3)	1.02 (0.12)	0.98 (0.05)	0.93 (0.03)	**LPE (22)**	1.63 (0.13)	0.58 (0.05)	0.57 (0.14)
				LPC (11)	1.43 (0.11)	0.84 (0.07)	0.88 (0.14)
				HexCer-NS (1)	1.02	0.89	1.01
				HexCer-NDS (5)	0.98 (0.01)	0.89 (0.02)	0.99 (0.03)
				FA (2)	0.9	0.96 (0.04)	
				Cer-NS (6)	0.92 (0.01)	0.99 (0.02)	0.8 (0.05)
				Cer-NDS (2)	0.92 (0.01)	0.95	0.9 (0.04)
Average	**1.05**	**0.96**	**0.95**	**Average**	**0.87**	**0.93**	**0.87**

[1]In parenthesis it is indicated the number of lipids identified in each lipid class
[2]Values in parenthesis are standard deviations for relative recoveries of lipids belonging to the same lipid class

Table S17: Recoveries of isotopically labelled internal standards: After pre-extraction and post-extraction spiking

Mode	**ESI (+)**				**ESI (-)**			
Isotopically labelled internal standard	**$CHCl_3$**	**IPA75**	**IPA90**	**MTBE**	**$CHCl_3$**	**IPA75**	**IPA90**	**MTBE**
15:0-18:1(d7) DAG	116 (13)	93 (12)	81 (15)	102 (16)	98 (20)	118 (23)	81 (13)	113 (36)
15:0-18:1(d7) PA Na+					30 (28)	88 (15)	107 (21)	90 (58)
15:0-18:1(d7) PC	106 (12)	89 (10)	98 (6)	102 (20)	98 (6)	90 (12)	100 (7)	105 (10)
15:0-18:1(d7) PE	80 (22)	86 (11)	103 (17)	103 (21)	85 (18)	92 (8)	104 (10)	95 (6)
15:0-18:1(d7) PG Na+	95 (20)	82 (20)	88 (8)	88 (11)	77 (4)	64 (8)	103 (13)	102 (10)
15:0-18:1(d7) PI NH4+	27 (8)	79 (20)	100 (14)	87 (14)	25 (5)	76 (10)	96 (8)	93 (6)
15:0-18:1(d7) PS Na+					62 (30)	93 (19)	103 (26)	118 (33)
15:0-18:1(d7)-15:0 TAG	96 (10)	33 (8)	60 (6)	72 (22)				
18:1(d7) Chol Ester	85 (14)	45 (6)	80 (9)	92 (21)				
18:1(d7) LPC	112 (21)	112 (11)	99 (11)	90 (13)	107 (16)	107 (10)	104 (11)	98 (17)
18:1(d7) LPE	97 (20)	78 (12)	101 (13)	99 (21)	85 (23)	78 (16)	105 (15)	104 (12)
18:1(d7) MAG	83 (96)	86 (37)	91 (32)	85 (66)	90 (19)	68 (16)	97 (21)	105 (33)
Cholesterol (d7)	83 (26)	110 (19)	67 (20)	121 (58)				
d18:1-18:1(d9) SM	107 (14)	82 (5)	99 (8)	101 (6)	103 (8)	75 (6)	96 (8)	110 (8)
Average	**88**	**80**	**90**	**95**	**78**	**86**	**100**	**103**

Table S18: Distribution of CVs (%): Obtained for precision evaluation of peak intensities of features detected in all four EPs

	% of features falling in the respective category							
	ESI (+)				ESI (-)			
CV bin(%)	$CHCl_3$	IPA75	IPA90	MTBE	$CHCl_3$	IPA75	IPA90	MTBE
0-5	0.9	2.1	1.4	1.2	0.4	2.0	3.2	0.3
5-10	11.8	12.7	14.2	12.3	20.5	32.3	33.5	17.1
10-15	24.1	23.9	22.6	22.4	33.7	31.6	31.3	34.5
15-20	20.2	20.3	17.0	18.9	20.2	17.4	12.7	22.7
20-25	18.4	16.6	14.8	16.1	15.3	7.0	8.1	9.7
25-30	13.8	11.3	9.8	12.8	6.6	6.5	2.9	8.7
30-35	6.2	5.9	5.8	7.7	1.3	2.2	1.4	3.7
35-40	2.4	3.7	3.4	4.5	0.4	0.8	0.8	1.9
40-45	1.3	1.4	2.3	1.8	0.5	0.1	0.7	0.6
45-50	0.2	0.7	2.9	0.7	0.9	0.0	0.1	0.1
50-55	0.2	0.5	1.9	0.5	0.3	0.1	0.3	0.0
55-60	0.3	0.3	1.1	0.6	0.0	0.0	0.8	0.3
60-65	0.1	0.3	0.8	0.2	0.0	0.0	0.7	0.1
65-70	0.0	0.0	1.1	0.1	0.0	0.0	1.5	0.0
>70	0.1	0.3	1.0	0.1	0.0	0.0	1.9	0.3
Total	100.0	100.0	100.0	100.0	100.0	100.0	100.0	100.0

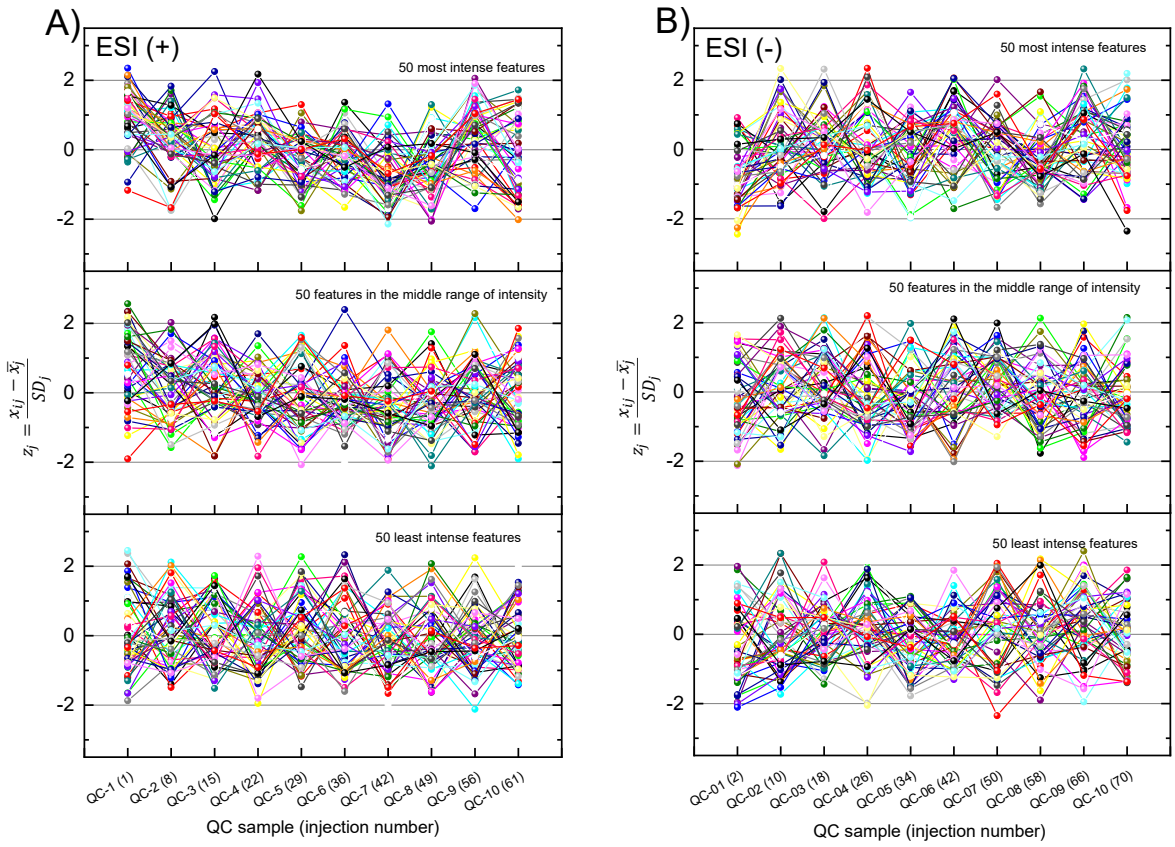

Figure S25: Z values for selected features (based on their intensity) in QC samples through the run sequence in A) ESI (+) and B) ESI (-): The number in parenthesis for each QC sample is the position of that QC in the sequence of injected samples. SD means standard deviation

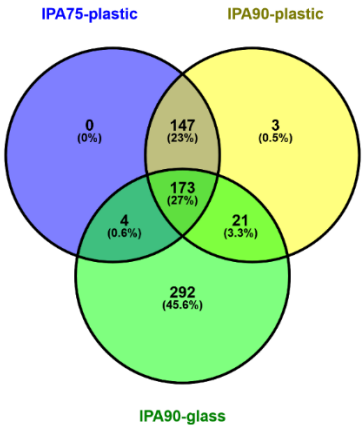

Figure S26: Venn diagram: Showing the distribution of detected features with blanks for EPs of IPA75 using plasticware, IPA90 using plasticware and IPA 90 using glassware in ESI (+)

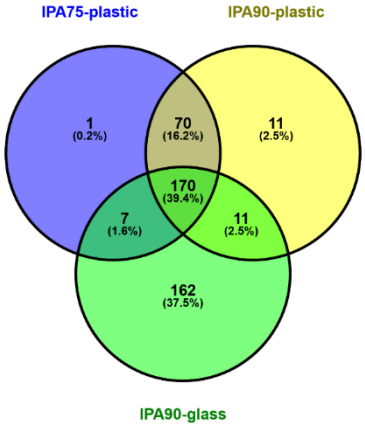

Figure S27: Venn diagram: Showing the distribution of detected features with blanks for EPs of IPA75 using plasticware, IPA90 using plasticware and IPA 90 using glassware in ESI (-)

3.6. Lipid profiling of HeLa cells under ionic liquid stress

3.6.1. Abstract

The present work describes the development and validation of a lipid profiling workflow using a reversed phase (RP) UHPLC-ESI-QTOF-MS/MS method and HeLa cell extracts after treatment with five different ionic liquids (ILs). As ILs are widely used as green solvents without detailed knowledge about toxicity, the study includes determination of the EC_{50} values on human epithelial cells with the help of a redox dye. We observed that during the IL treatment the cells accumulated lipid droplets, therefore, the following work is focused on lipid profiling. The cell extracts were prepared using a monophasic extraction protocol and analysed using RP UHLPC-ESI-QTOF-MS/MS analysis linked with several combined normalization strategies (LOESS normalization, normalization based on internal standards and cell counts). Additionally, the data of the single ILs were aligned with each other based on a comparison of retention time and m/z values by an in-house developed visual basic script to analyse the differences in the lipid profile between the different ILs. Finally, the data of all ILs was evaluated in one batch for hypothesis generation regarding the different toxicity mechanisms and activated stress pathways. The results show, that toxicity is time-dependent for most of the investigated ILs. Additionally, differences in activated pathways are visible, as [Ch][OAc] affect metabolic processes involving phospholipids whereas [emim][OAc] influences sphingolipid pathways. A combination of activating sphingolipid pathways as well as other metabolic processes, resulting in highly toxic effects is shown by $[P_{4441}][OAc]$. Clear differences are evident between $[P_{4441}][OAc]$ and [Ch][Hex], whereby the latter shows almost no significantly altered lipids. Hence, the toxicity of [Ch][Hex] is not based on metabolic processes containing lipids. However, $[P_{14444}][OAc]$ causes rapid disturbance of the sphingolipid pathway with subsequent membrane fusion due to membrane destruction by the IL.

3.6.2. Introduction

The first imidazolium based ionic liquid (IL) was developed in 1982 by Wilkes *et al.* [476] and is nowadays one of the most used IL class in industry [12]. Ionic liquids (ILs) in general are composed of an organic cation [51], for example imidazolium, pyridinium, quaternary phosphonium or ammonium [14,51,54] and an organic or inorganic anion like chloride, bromide, acetate, tetrafluoroborate,

hexafluorophosphate, bis(trifluoromethylsulfonyl)imide or dicyanamide [14]. They are also called “molten salts”, because their structure leads to special characteristics. They are i) liquid in a broad temperature range, room temperature included; ii) thermally, chemically and electrochemically stable and iii) have high electrochemical conductivity [88]. In industry, they are mostly used as “green solvents”, because they are non-inflammable, non-explosive, non-volatile and soluble in a large range. Their lack of biodegradability causes accumulation in the environment, in soil or aquatic organisms, and this makes the analysis of their toxicity imperative [8,9,14,22,53]. The high structural variability of ILs challenges, however, this endeavour. There are up to 1018 different ILs [4], that are used for a) dissolving polysaccharides and cellulose for spinning fibres afterwards, b) stabilization of proteins and enzymes, c) extraction, purification and preservation of DNA, d) killing bacteria and cancerous cells, without affecting healthy eukaryotic cells, e) supporting or preserving the aggregation of proteins in amyloids, or f) penetration and possibly disruption of biomembranes [76,477]. Among other applications, ILs are especially designed to show anti-tumour or anti-viral effects [9,24,25,32,36,42,76,477,478]. For example, the linkage of peptides with antibiotic effects with ILs ease the cell membrane penetration or enables a targeted cell recognition of altered cells [75]. Thus, ILs are important compounds for the development of new therapeutic strategies in pharmaceutical industry. Nonetheless, since the new European chemical legislation REACH (registration, evaluation, authorization and restriction of chemicals) is introduced, the manufacturer itself is responsible for the safety of the manufactured chemicals and products [16]. Initially, simple tests of cellular viability after contact with ILs were considered to represent reasonably well the degree of toxicity [52]. Several papers in the past have shown, however, that ILs increase the production of reactive oxygen species (ROS), thereby triggering mitochondrial dysfunction, which is considered the major cause of DNA damage followed by cell apoptosis [5,12,23,31,52,479]. Due to the huge variety of ILs, it is of utmost importance to develop simple and rapid analytical techniques, which enable the detailed analysis of the toxicity and thus assure environmental safety.

For this reason, we present in this work a lipidomics workflow for the profiling of the cellular lipid changes caused by ILs. Numerous publications showed already the toxicity of various ILs. Most of the publications describe the interactions of ILs with the

cell membrane of different organisms [5,9,88,13,21,22,24,27,34,37,75]. However, the mechanisms which cause toxicity or are responsible for the antimicrobial effect of ILs remain unclear [9]. With the aim to gain some insight in metabolic pathways perturbed by ILs, we performed a metabolic profiling study of human corneal epithelial cells incubated with various ILs in a previous work [480]. During this preliminary study, we observed that some of the tested toxic ILs were accumulated in lipid droplets in the cells. Epithelial cells were used in these studies as they are usually first barriers that come in contact with the environment and exogenic agents such as ILs [7,51]. As an extension towards the lipophilic metabolites, the present work focused on the lipidomic profiling of HeLa cells treated with five different ILs (choline acetate ([Ch][OAc]), 1-ethyl-3-methylimidazolium acetate ([emim][OAc]), choline hexanoate ([Ch][Hex]), tributylmethylphosphonium acetate ([P_{4441}][OAc]) and tributyl(tetradecyl) phosphonium acetate ([P_{14444}][OAc])). The HeLa cell line is a widely used epithelial cell culture model of human origin that can offer valuable insight into ILs effects, especially on the complex human organism [7]. Numerous reports presented the time and dose-dependency of the toxicity of ILs [13,22,30–32,479]. It is typically given as EC_{50} values. Based on these former results of EC_{50} value determination of the currently investigated ILs, the cells were treated herein with ILs in concentrations below the EC_{50} for 8, 16 and 24h. For the analysis of the lipid profiles with and without ILs, a previously reported UHPLC-ESI-QTOF-MS/MS assay using data-independent acquisition with SWATH (sequential window acquisition of all theoretical fragment ion mass spectra) was adjusted [265,291,481]. For cellular lipid profiling and in particular sphingolipid analysis, as one of the most important lipid classes among the stress pathways, MS/MS is the only technique that provides the required sensitivity for lipid species identification [468]. Another advantage is the possibility of high throughput analysis which is of importance for large sample sizes.

3.6.3. Materials and methods

3.6.3.1. Materials and instruments

Ultra-LC-MS grade acetonitrile, methanol, 2-propanol, and formic acid was purchased from Carl Roth (Karlsruhe, Germany). MilliQ water was obtained by water purification with an Elga PurLab Ultra purification system (Celle, Germany). EX CELL HeLa serum free medium, L-Glutamine and Ammonium formate were supplied by Sigma Aldrich (Steinheim, Germany). Phosphate buffered saline was obtained from Thermo-Fisher

Scientific (Waltham, MA). SPLASH™ Lipidomix Mass Spec Standard was purchased from Avanti Polar Lipids (Alabama, USA). Cellcounter Cellometer Auto T4 was purchased from Nexcelom Bioscience (Lawrence, MA). Cell incubator Hera cell, centrifuges Varifuge 3.0 and IEC Micromax RF were from Thermo-Fisher Scientific.

3.6.3.2. Internal standards

As internal standard SPLASH™ Lipidomix Mass Spec Standard dissolved in methanol, containing 14 isotopically labelled lipid standards (ILIS) was used. In the validation process, the ILIS was further diluted with methanol to 10, 5 and 2.5% (v/v) of the original standard solution and to a 5 % (v/v) solution in all extraction samples (see Supplementary information (SI) Table S19 for detailed information).

3.6.3.3. Cell culture samples for validation

The human cervical cancer HeLa cells adapted to serum free conditions (AC free, ECACC 08011102) were grown in T75-flask and EX-CELL HeLa serum free media, supplemented with 2 mM L-Glutamine, until they reached a density of 10 x 10^7 cells. Afterwards they were transferred to a 50 mL falcon tube and centrifuged at 700 rcf for 3 min and the supernatant was discarded. The cell pellet was washed with 10 mL ice-cold PBS buffer and centrifuged again for 3 min at 700 rcf. The washing step was repeated twice but in the last wash three aliquots of 50 µL were each mixed with 50 µL TrypanBlue (0.2% solution; v/v) for cell counting with the Cellometer Auto T4. Aliquots of approximately 1 million cells per mL were then transferred to 15 mL falcon tubes and centrifuged for 5 min at 700 rcf. The supernatant was discarded, and the cell pellet was stored at -80 °C until lipid extraction.

The above described procedure was repeated with [emim][OAc] treated cells. Therefore, the HeLa cells were grown until they reached a density of 10 x 10^7 cells. The cell suspension was transferred to a 50 mL falcon tube and centrifuged for 3 min at 700 rcf. Afterwards the supernatant was discarded, the pellet was resuspended in media supplemented with 10 mM [emim][OAc], transferred back into a T75-flask and then the cells were incubated for 24 h at 37 °C, 5% CO_2 and 120 rpm stirring. After 24 h the cells were washed and counted as described above.

3.6.3.4. Incubation of cell culture samples with ILs

Before IL treatment, the cells were grown in 12 wells of a 24-well plate until they reached approximately 2 million cells per well. The media in 6 wells was exchanged by HeLa serum free media supplemented with different IL concentrations below the EC_{50} values (see SI 3.6.6.1.1 for detailed information about EC_{50} determination). The concentrations used for EC_{50} determination and IL treatment are listed in SI Table S20 and S3. HeLa serum free media without IL was used for control samples, 6 for each IL and time point. The cells were incubated for 8, 16 and 24 hours with the different ILs. Afterwards, the 24-well plate was centrifuged for 3 min at 1720 rpm in a pre-cooled (-5 °C) centrifuge. The supernatant was discarded, and the cells were resuspended and washed in 2 mL ice-cold PBS buffer and centrifuged again for 3 min at 1720 rpm. The washing cycle was repeated twice, but after the last resuspension, the cell suspension was transferred to 15 mL falcon tubes and aliquots of 50 µL were taken for cell counting according to the procedure mentioned above. Afterwards, the falcon tubes were centrifuged for 5 min at 700 rcf, the supernatant was discarded, and the cell pellets were stored at -80 °C until extraction.

3.6.3.5. Extraction protocol of cell samples

All samples were extracted following the monophasic extraction protocol with 2-propranol/water (90:10; v/v) (IPA90) from Calderón *et al.* [291]. In total, three different concentrations of ILIS were used for validation, concentration 1 (conc 1; 10% related to original Lipidomix, v/v; corresponding to 1:10 dilution of Lipidomix as supplied), concentration 2 (conc 2; 5%, v/v; 1:20 dilution) and concentration 3 (conc 3; 2.5%, v/v; 1:40 dilution). Thus, 30 aliquots of [emim][OAc] treated cell suspension were transferred into 15 mL falcon tubes, washed and centrifuged as described above. To each of 5 cell pellets, either 4.9 mL of pre-cooled 2-propanol/water solution (90:10; v/v) and 100 µL of ILIS (conc 1) (pre-spike) or 5 mL of pre-cooled 2-propanol/water solution (90:10; v/v) (post-spike) were added. This was repeated for conc 2 and conc 3. All cell pellets were vortexed (30 s) and ultrasonicated (2 min). This was repeated until the cell pellet was completely disrupted. The samples were then incubated on ice on an orbital shaker (500 rpm) for 1 h, and then centrifuged for 10 min at 3500 rcf. The supernatants were transferred to new falcon tubes and dried overnight in a centrifugal evaporator. Next, the residues were resuspended in 100 µL of pre-cooled methanol (pre-spike samples) or in 100 µL of ILIS in methanol (10, 5 or 2.5 %; v/v) (post-spike samples),

vortexed (30 s) and centrifuged afterwards for 5 min at 3500 rcf, before the extracts were transferred into HPLC-Vials for measurement.

The extraction procedure for the cell samples used for lipid profiling was performed as described above, except, that the cells were grown in 24-well plates and the cell pellets were prepared as described in chapter 3.6.3.4. Additionally, ILIS solution was only added post-extraction and only one concentration of ILIS, the 5% (v/v) solution, was used for the reconstitution of the dried lipid extract. In both cases an aliquot each was pooled to a quality control (QC) sample.

3.6.3.6. LC-MS/MS method

All analyses were performed on a Sciex TripleTOF 5600+ equipped with a Duospray ion source (Sciex, Concord, Ontario, Canada) and carried out with ESI interface in positive and negative ion mode. The mass spectrometer was coupled to an Agilent 1290 Infinity Series UHPLC instrument (Agilent, Waldbronn, Germany) with a Pal HTC-XS autosampler from CTC (Zwingen, Switzerland).

The chromatographic separation was performed on an Acquity UPLC charged-surface hybrid (CSH) C18 column (2.1 x 100 mm) packed with 1.7 µm particles (Waters, Eschborn) equipped with an Acquity CSH C18 Van-guard pre-column (2.1 x 5 mm; 1.7 µm). The mobile phase was composed of A) 10 mM ammonium formate in 60:40 (v:v) acetonitrile:water and 0.1% (v:v) formic acid and B) 10 mM ammonium formate in 90:10 (v:v) 2-propanol:acetonitrile and 0.1% (v:v) formic acid [265]. The following gradient profile according to Tsugawa *et al.* was used to allow retention time scoring for peak identification during data evaluation: 0.00 min, 15 % B; 2.00 min, 30 % B; 2.50 min, 48 % B; 11.00 min, 82 % B; 11.50 min, 99 % B; 12.00 min, 99 % B; 12.10 min, 15 % B, 15.00 min, 15 % B. The flow rate was 600 µL/min and the column temperature set to 65 °C. The injection volume was 3 µL for measurements in positive and 5 µL in negative mode.

The following MS-settings of the mass spectrometer were used: Curtain gas (CUR) 35 psi, nebulizer gas (GS1) 60 psi, drying gas (GS2) 60 psi, ion-spray voltage floating (ISVF) +5500 V in positive and -4500 V in negative mode, source temperature (T) 350°C, collision energy (CoE) 45 V, collision energy spread 15 V, declustering potential (DP) 80 V, mass range m/z 100 - 1250 and RF Transmission (RF) m/z 80: 50% and m/z 200: 50%. The samples were injected in a randomized order with QC samples at

the beginning of the sequence, during the sequence (every three samples) and at the end of the sequence. At first the validation sequence was measured following by various sequences contained of extraction samples, one sequence per IL (see SI Table S22-Table S27). An external mass calibration was performed every five samples. Data-independent acquisition (DIA) by sequential window acquisition of all theoretical fragment ion mass spectra (SWATH) was used for data acquisition. The size of the individual Q1 precursor isolation windows were optimized using Swath Tuner software (see SI Table S28).

3.6.3.7. Data Processing

Data processing comprising peak detection, compound identification, peak alignment, deconvolution and normalization was performed using the MS-Dial software (RIKEN, version 3.08) [265]. The used parameters are listed in SI Table S29. The data was normalized by LOESS before an R based script was run to determine the optimal internal lipid class standard for every single detected compound [482]. The optimum internal standard for each lipid feature was chosen based on minimum relative standard deviation (RSD) values in QC samples after normalization with every internal standard. Based on these minima an assignment table for normalization within MS-Dial was created and entered into MS-Dial. The LOESS and internal standard normalized data were afterwards normalized by the cell number, before another R script was run for statistical analysis.

3.6.3.7.1. Statistical analysis

As a first step, mean, standard deviation and RSD of the normalized areas were calculated. The data of pooled QC (pooled cell extract samples, one set for each IL), control and treated cell extract samples for one IL per analysis were grouped into 7 different classes. Classes 1-3 represented treated cell extracts after 8, 16 and 24h; classes 4-6 were non-treated control cell extracts after 8, 16 and 24h and class 7 comprised all QC samples, from the specific IL. Afterwards, the classes were checked for equal variances between all possible binary combinations. As a last step, a t-test was run for every possible combination. In order to highlight alterations between the individual classes, fold changes were calculated. The selection of significantly altered features in binary class comparisons (i.e. treated cell extracts after 8, 16, and 24 h versus the corresponding control samples) was based on q-values, i.e. p-values

corrected for multiple hypothesis testing calculated with the R-based Bioconductor q-value package [483]. For a better visualization of the alterations of control samples compared to treated samples, Boxplots of the significant features were created (see an example in SI Figure S29). For the statistical analysis of all ILs, independent of the time-points, new classes were defined. Class 1: Control samples of all ILs, class 2: [Ch][OAc], class 3: [Ch][Hex], class 4: [emim][OAc], class 5: $[P_{4441}][OAc]$, class 6: $[P_{14444}][OAc]$ and class 7: QC samples of all ILs.

3.6.3.7.2. Feature alignment for time-dependent and IL-dependent lipid profiling

For the comparison of the different ILs based on their lipid profile, between-batch feature alignment was performed using an „in-house“ alignment tool (based on Visual Basic (VBA) implemented in Excel) as the data had to be acquired in multiple analysis batches. For feature alignment, only significantly altered features from each IL ($q \leq 0.05$, see section statistical analysis) were used. The alignment was based on the similarity of the m/z value and the retention time (RT) within tight ranges (delta m/z: 0.01 u, delta RT: 0.05 min) of features from two tables. When two features were identical, they were written as one feature in a new table with the mean of m/z and RT values. On contrary, features which could not be aligned were written in separate tables. Since the alignment tool works only pairwise, the whole feature alignment was a multiple step procedure (see SI chapter 3.6.6.1.2 and SI Figure S30A-C).

3.6.3.8. Validation

Validation of extraction recoveries was performed according to the protocol of Matuszewski *et al.* [484]. Thus, the response of the 14 isotopically labelled lipid standards, spiked before the extraction (pre-extraction spike) and after the extraction (post-extraction spike) were compared. Therefore, batches of five aliquots of cell pellets, treated with emim acetate ([emim][OAc]) for 24h, were spiked before extraction (pre-extraction spike samples) and after extraction (post-extraction spike samples) as described above (section 3.6.3.5).

The comparison of the detector response of lipids contained in ILIS listed in SI Table S19 was based on the peak areas, which were determined by MultiQuant software from Sciex.

Extraction recoveries (RE) were calculated according to Matuszewski *et al.* [484] by using the following equation (Equation 14).

$$RE = \frac{mean\ peak\ area\ of\ pre-extraction\ spike\ samples}{mean\ peak\ area\ of\ post-extraction\ spike\ samples} * 100$$

Equation 14: Calculation of extraction recoveries (RE): With mean peak areas of pre-and post-extraction spiked samples

Additionally, precisions (coefficients of variation; %CV) and accuracies, calculated from the corresponding concentrations by MultiQuant, were determined and are summarized in SI Table S30 (ESI+) and Table S31 (ESI-).

3.6.4. Results and discussion

3.6.4.1. EC_{50} Determination

Imidazolium-based ILs are the most frequently studied group [12,19], were first used in industrial applications [12,77] and were considered to be the most toxic IL in the group of pyridinium, pyrrolidinium, and piperidinium ionic liquids [12] . Numerous recent publications rank quaternary phosphonium based ILs as even more toxic [5,13,14,19,32]. Since imidazolium and quaternary phosphonium ILs are less biodegradable, the focus was directed on choline-based ILs. They are considered to be harmless to the environment and to humans because, for example, choline chloride is an endogenic substance [5,9,12,21,26,37,38,53,75] and often considered as pseudo-vitamin [53].

In this work, ILs of all three groups were used and compared with each other (Figure 92). It is known that the toxicity of ILs is dependent on the cation and the length of their attached side chains and is less influenced by the type of anion [485,486]. For this reason, and for better comparability, all of the tested ILs are composed of the same anion, namely acetate, except for a second choline-based IL which carries hexanoate as the anion. It was additionally selected because it was found that the toxicity of choline-based ILs increase with increasing hydrophobicity of the anion [21,26]. Ruokonen *et al.* proposed previously that the five tested ILs (Figure 92) can be divided into three different groups [1], based on how they affect the cells. The first group has an effect on cell metabolism without disturbing the cell membrane and is composed of choline acetate ([Ch][OAc]) and emim acetate ([emim][OAc]). ILs of the second group affect cell metabolism and partially rupture the cell membrane. This group is composed

of choline hexanoate ([Ch][Hex]) and tributylmethylphosphonium acetate ([P_{4441}][OAc]). The third and last group completely rupture and destroy the cell membrane, and includes tributyl(tetradecyl) phosphonium acetate ([P_{14444}][OAc]) (Figure 92).

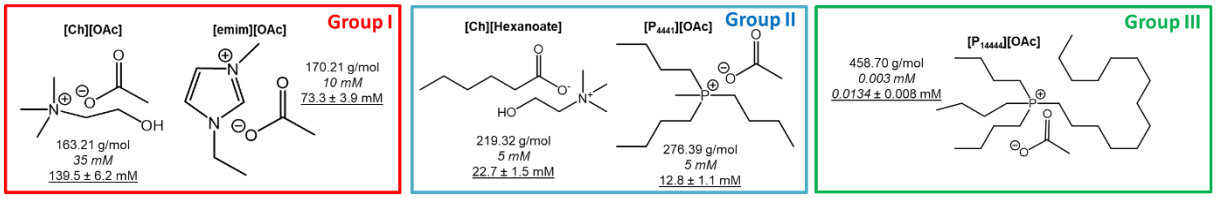

Figure 92: **Used Ionic Liquids (ILs):** With corresponding *concentrations used for IL treatment*; Molar mass of the IL and EC_{50}-value ± SD

First of all, the toxicity of the five chosen ILs was determined by alamarBlue assay enabling the calculation of EC_{50} values (see SI chapter 3.6.6.1.1 and SI Figure S28). The thus obtained EC_{50} values were in good agreement with already published data and were therefore considered to be good indicators of toxicity (SI Table S20) [1,95]. [Ch][OAc] is the most harmless IL, followed by the slightly more toxic IL [emim][OAc] from the same group. Surprisingly, since choline-based ILs are considered harmless [5,9,12,21,26,37,38,53,75], [Ch][Hex] and [P_{4441}][OAc] have similar EC_{50} values (SI Table S20). Although the cation usually determines the level of toxicity, the anion is of relevance in the comparison of two ILs with the same cation [21,26]. Accordingly, the toxicity of [Ch][Hex] is higher compared to [Ch][OAc], because of its longer side chain in the anionic part of the IL [37]. As expected, the highest toxicity was associated with [P_{14444}][OAc], because it has the longest side chain at the cation, making the molecule more hydrophobic and therefore more disruptive for cellular membranes [9,11,38,41,42,369,487–490,12–14,20,22,25,30,37]. However, this is limited to some extent by the so-called "cut-off" effect, which means that a further increase of the chain length does not necessarily result in a corresponding increase in toxicity. It was explained by steric effects through very long side chains leading to a lower binding affinity to the lipid bilayer [16,19,24,36].

3.6.4.2. Untargeted lipidomics profiling method

In a previous study, we compared different lipid extraction protocols for HeLa cells as well as different extraction solvents [291]. Based on the recovery and other factors, the best suited lipid extraction protocol for lipids from HeLa cells was the monophasic extraction with 2-propanol:H_20 (90:10, v / v). This lipid extraction protocol was adopted

for the current study. The lipid extracts were analysed by reversed-phase LC-MS/MS with an Acquity UPLC CSH C18 column hyphenated to a Sciex TripleTOF 5600+ operated in positive and negative ESI mode. The separation of the lipid species was achieved by running a 2-propanol-acetonitrile-water gradient [265]

Aliquots of a batch of cells treated with [emim][OAc] were used for the validation during this work. Three different concentration levels of ILIS mixture (Lipidomix) were spiked pre- and post-extraction to five treated cell pellets each. In order to control the quality of the measurements and analytical performance, various QCs (pool of all pre- and post-extraction validation samples) were included in the analytical sequence (see SI Table S22). For evaluation of extraction recoveries respective pre- and post-extraction spiked samples were compared. Table S30 and Table S31 in SI shows the validation results for ESI^+ and ESI^-, respectively. Extraction recoveries (in %) for each lipid in the ILIS mixture (Lipidomix) were > 80%, except 15:0-18:1(d7)-15:0 TAG and 18:1(d7)-Cholesteryl ester (both around 40%). The significantly lower recovery for these lipids in relation to other lipids was also observed by Calderón *et al*. [291]. Overall, however, the extraction protocol with 2-propanol/H_20 (90:10, v/v) was found to be suitable for HeLa cells after treatment with ILs because all lipids tested could be extracted with high precision (coefficient of variation < 10%).

3.6.4.3. Lipid profile alteration depending on IL treatment and incubation time

Like the transcriptome and proteome, the cellular lipidome is remodelled by stimuli and various cellular stress conditions. Thus, comprehensive lipidomic analysis of whole cell lysates of cell culture models is deemed to be an appropriate method to capture metabolic changes induced by ILs.

In our preliminary study, addition of imidazolium-based IL showed, under the optical microscope, increased formation of intracellular lipid droplets as a general response to toxic compounds (stress) [491,492]. Wang *et al.* observed also formation of vesicles after exposure to imidazolium IL of HeLa cells, resulting in apoptosis [5]. Therefore, this work focused on the elucidation of changes in the lipid metabolism of IL-treated cells compared to untreated control cells. For this purpose, the HeLa cells were incubated with ILs at concentrations below their EC_{50} values (see SI Table S21). A first

look at the number of significantly altered lipids compared to the control (Table 11) displays very clearly the time-dependency of the cytotoxicity.

Table 11: Significantly altered features: All significantly altered features (q < 0.05) upon treatment with specified ILs

all significant			Number of significantly altered features in ESI+			Number of significantly altered features in ESI-		
Group	Ionic liquid	EC_{50} concentration [mM]	8h	16h	24h	8h	16h	24h
I	[Ch][OAc]	139.5	88	379	120	186	(67)	(81)
	[emim][OAc]	73.3	28	239	321	108	280	275
II	[Ch][Hex]	22.7	(128)	157	646	(43)	40	189
	$[P_{4441}][OAc]$	12.8	1220	975	988	520	479	413
III	$[P_{14444}][OAc]$	0.0134	175	625	833	196	295	339

() numbers in brackets show features only significant based on p-value <= 0.05

For most of the ILs, the total number of significantly altered lipids measured in ESI positive (ESI+) mode increases over the duration of the treatment, for example [emim][OAc], [Ch][Hex], and $[P_{14444}][OAc]$. Nevertheless, this is not the case for all ILs. For example, choline acetate ([Ch][OAc]) shows a significant increase of altered lipids between 8 and 16h, but the number of significantly altered lipids after 24h is similar to the number after 8h of IL treatment. A different profile is demonstrated by $[P_{4441}][OAc]$, the impact on the lipid metabolism is higher after 8h, than after 16 or 24h, where the total number of significantly altered lipids is stable. This means a longer exposer time does not always result in higher toxicity.

For the most ILs, the total number of significantly altered features measured by LC-MS/MS operating in ESI negative (ESI-) mode is significantly lower compared to the ESI positive (ESI+) mode (Table 11). The profile of significantly altered feature number within the experimental time range seen in ESI+ is verified by similar profiles of features with ESI- ionization. However, the differences in total number of significantly altered features obtained with ESI- mode at different time points, are not as clear as with ESI+ mode. A grouping into Venn-diagrams of significantly altered lipids at a certain time point intensifies this observation (Figure 93). The choline and imidazolium based ILs share up to 10% of the altered lipids with all time points in ESI+ and ESI-, except [emim][OAc] in ESI- mode, which shows nearly 30% of shared lipids of all time points. Approximately 50% of the total number of altered lipids are present in all 3 time points

for the phosphonium based IL [P_{4441}][OAc]. This might be a first hint, that [P_{4441}][OAc] are more toxically aggressive than choline and imidazolium based ILs. Additionally, [Ch][OAc], [Ch][Hex] and [emim][OAc] might activate different pathways within the investigated time range. Additionally, the time-dependent effect of the toxicity is clearly visible, as the number of shared features increases from 8h/16h to 16h/24h (Figure 93).

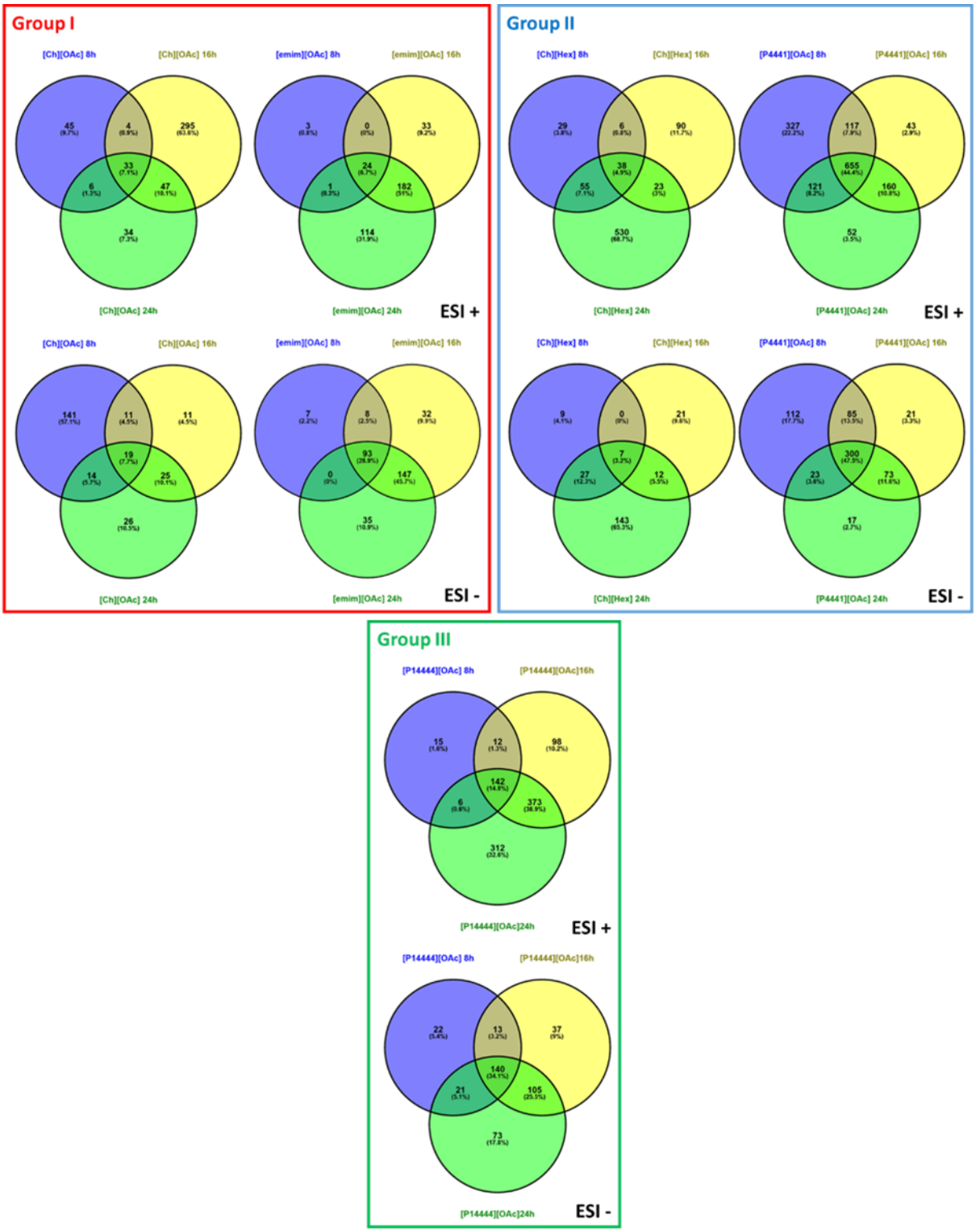

Figure 93: **Venn-diagram:** Showing significant altered lipids at a specific time point of the IL treatment

3.6.4.4. Evaluation of shared and unique altered features of all ILs

To clarify whether the various ionic liquids have shared biomarkers for possible metabolic disorders, all significantly altered lipids caused by one IL were aligned with significantly altered lipids of other IL treatments and visualized in a bar chart (Figure 94).

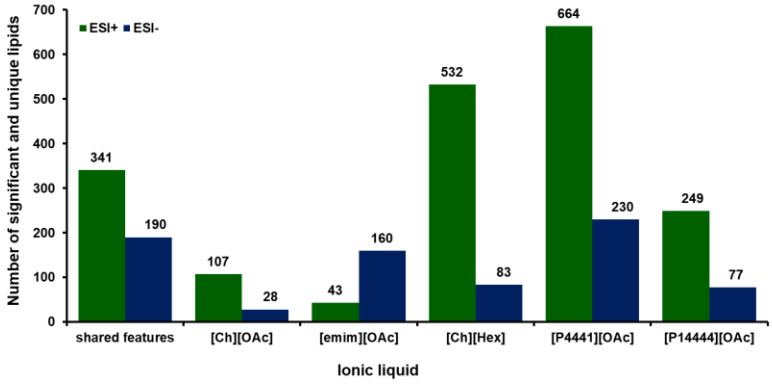

Figure 94: Numbers of shared and unique Lipids: Comparison of significantly altered lipids caused by one IL independent of time

In total, all ILs have 341 shared altered lipids in ESI+ mode and 190 in ESI-. [Ch] [Hex] shows a relatively high number of lipids with significant fold-change, although choline based ILs are considered harmless [5,9,12,21,26,37,38,53,75]. However, this observation fits perfectly into the group affiliation, as [P_{4441}] [OAc] shows a similar number of altered lipids. This was expected for group II ILs, because, according to Ruokonen *et al.*, [P_{4441}] [OAc] and [Ch][Hex] affect both cell metabolism and partially disrupt the cell membrane [1]. Group I, as [Ch][OAc] and [emim][OAc], affect the lowest amounts of lipids, while group III as [P_{14444}][OAc] show intermediate results.

Overall, the differences are more visible in Venn-diagrams [493] of positive ionization mode compared to negative mode. Figure 95 shows a clear difference between group I and III compared to group II. Almost half of the significantly altered lipids in the positive mode and about 30% of the negative mode lipids are triggered by ILs in group II. Only around 9% in ESI+ and 18% in ESI- lipids are triggered by group I and around 9% and 7%, respectively, are triggered by group III. Therefore, group I has less over all effects (are relatively harmless) and group III kills the cells very fast, that there is no time for changes in the profile (less altered lipids). However, group II is more toxic than group I, as group II shows more effects on lipid profile, but is less toxic than group III, even though the number of altered lipids is higher. The Venn-diagram

in negative mode shows a slightly clearer difference between the groups. It is shown that the metabolism influenced by ILs of group I apparently produces significantly more altered lipids than the destruction of the membrane by ILs of group III, as the toxic reaction of group III is too fast to see alterations in lipid profile.

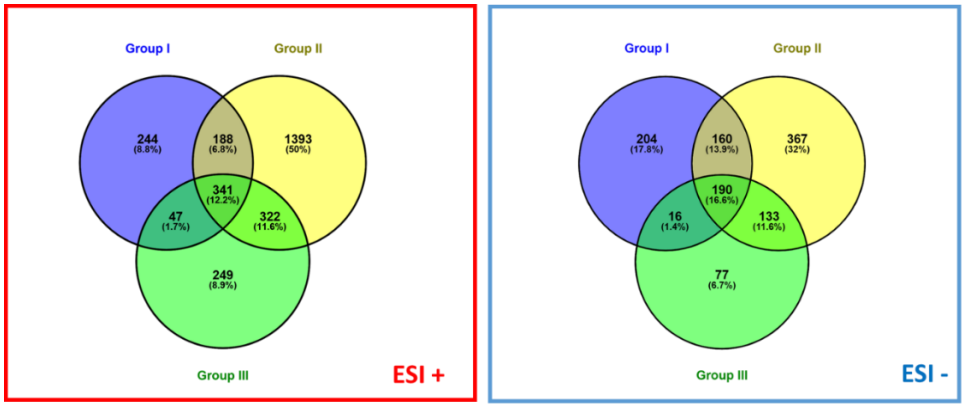

Figure 95: Venn diagram: Number of all altered Lipids after IL treatment within one group and compared to the other groups

Thus, with respect to the lipid profile, it is not of importance whether ILs affect metabolism or disrupt the membrane. However, the effect is intensified when both mechanisms are combined, as shown by a significantly increased number of lipids in group II.

A closer look at the individual groups (Figure 96) shows, that for group I, [Ch][OAc] and [emim][OAc], the number of significantly altered lipids is similar, suggesting similar pathways of toxicity.

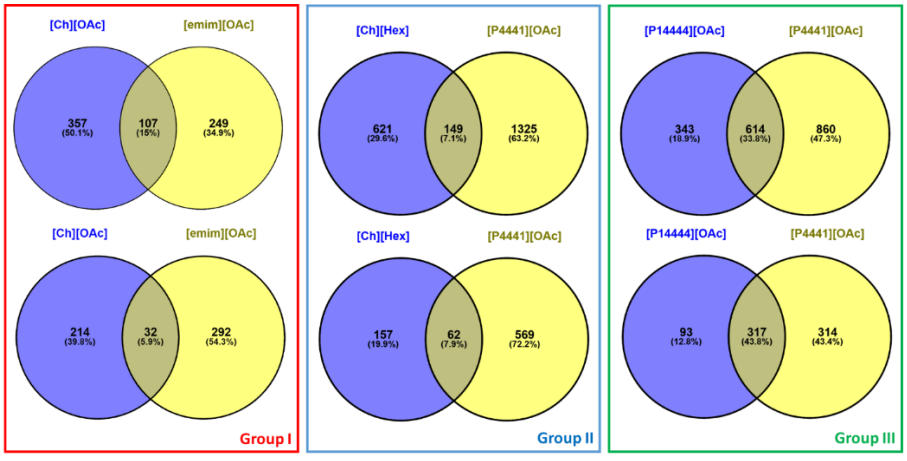

Figure 96: Venn diagram: Number of altered lipids only in a specific IL and shared lipids within the same group (top ESI+, bottom ESI-)

This hypothesis is shown more clearly in the Venn-diagram of the negative ionization mode. The effect of an imidazolium compared to a choline core on lipid metabolism is not significantly higher. In contrast, the comparison of the ILs from group II shows a clear difference between [Ch][Hex] and [P_{4441}][OAc], which has already been described in the previous chapter. Thus, [P_{4441}][OAc] causes significantly altered lipids of around 60% in positive mode and 70% in negative mode. Therefore, it is natural that [P_{4441}][OAc] is the pivotal factor in group II when comparing the groups with each other. This observation supports our previously published hypothesis that within the investigated IL classes, quaternary phosphonium ILs are by far the most toxic ILs [1,480]. In the case of [Ch][Hex], the toxicity is most likely sourced in the longer chain of the anion. Since it is able to interact with membranes and also induces metabolic changes [1], the number of affected lipid species is higher than with the corresponding choline-based IL having an acetate counterpart.

Because they are composed of the same cationic core and the same anion, [P_{4441}][OAc] and [P_{14444}][OAc] were compared in a Venn-diagram as group III (see Figure 96). Almost a third of significantly altered lipids in ESI+ and nearly a half in ESI- are common between the two ILs (Figure 96, Group III). Although [P_{14444}][OAc] is more cytotoxic by three orders of magnitude compared to [P_{4441}][OAc] (Figure 92), the number of affected lipids was not proportional. This can be expected from an IL that shows such strong interference with the organization of lipid membranes. The cell death is most likely fast and due to cell lysis complex metabolic changes do not have enough time to develop [10, 50]. But, Mikkola *et al.* demonstrated that compared to other ILs, [P_{14444}][OAc] does not induce the release of interleukin 8 (IL-8), which is an indicator for the activation of the cellular stress response, further suggesting a fast and uncontrolled cell death [22]. It seems likely that the long side chain of the phosphonium cation in [P_{14444}][OAc], would integrate in the lipid bilayer disturbing the cell membrane, and inducing cell lysis.

3.6.4.5. Toxicity

An overview of the identified, significantly altered lipid classes of the individual ILs, processed all together independent of time points, in the form of fold changes compared to untreated cells are visualized by heat maps (see Figure 97-Figure 103). A FC <1 indicates higher levels of the corresponding compound in the IL-treated

sample extract in comparison to the control sample and FC >1 indicates lower levels. They show clear differences between the 3 groups of ILs. ILs in group I exhibit a clear influence on metabolic processes, since in contrast to group II, significantly more lipids with signalling function (e.g. ceramide (Cer-NDS and Cer-NS), sphingomyelin (SM), phosphatidylethanolamine (PE), diacylglycerol (DAG) or lysophosphatidylcholine (LPC) are altered (Figure 97 – Figure 98 and Figure 101- Figure 102). However, there are also clear differences within the groups. For example, [emim][OAc] influences the metabolism mainly by activating the sphingolipid pathway (Figure 104) known to be involved in the cellular stress response [494–496]. The sphingolipid pathway is composed of the de-novo pathway, the sphingomyelin pathway and the salvage pathway [494,496–498]. During the de-novo pathway, palmitoyl CoA and L-Serine are metabolized in several steps to (Ceramide non-hydroxyfatty acid-) dihydrosphingosines (Cer-NDS) and finally to (Ceramide non-hydroxyfatty acid-) sphingosines (Cer-NS). Cer-NS are commonly known as ceramides, widely accepted as signalling lipids in the cellular stress response. The intracellular accumulation of ceramides is toxic and commonly associated with apoptosis [494,496,497,499]. In stress, the main source of ceramide is through sphingomyelins (SM) hydrolysis.

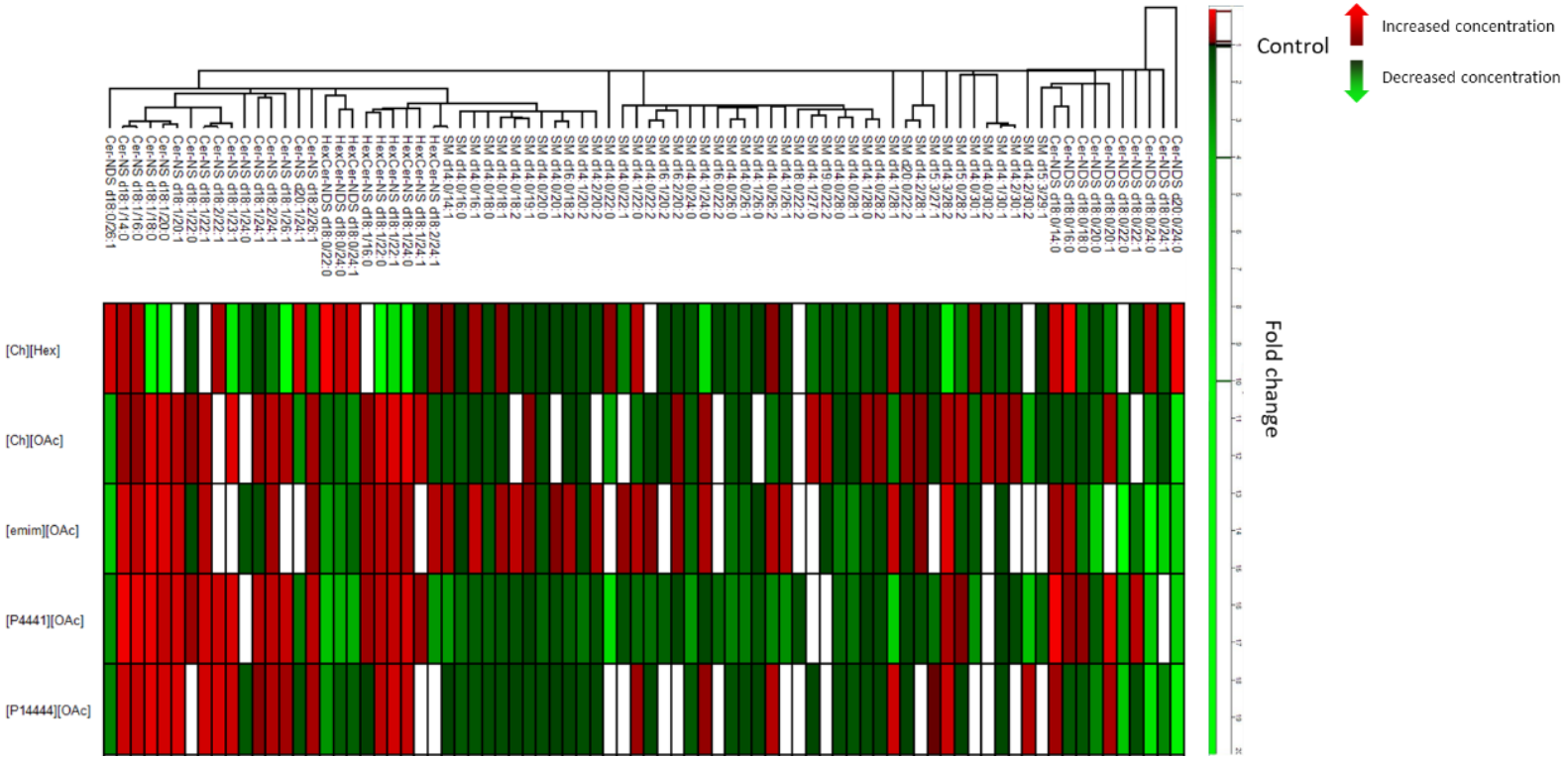

Figure 97: Heatmap: Showing all identified and significantly altered features, which belong to the stress pathway, analysed in ESI+ mode

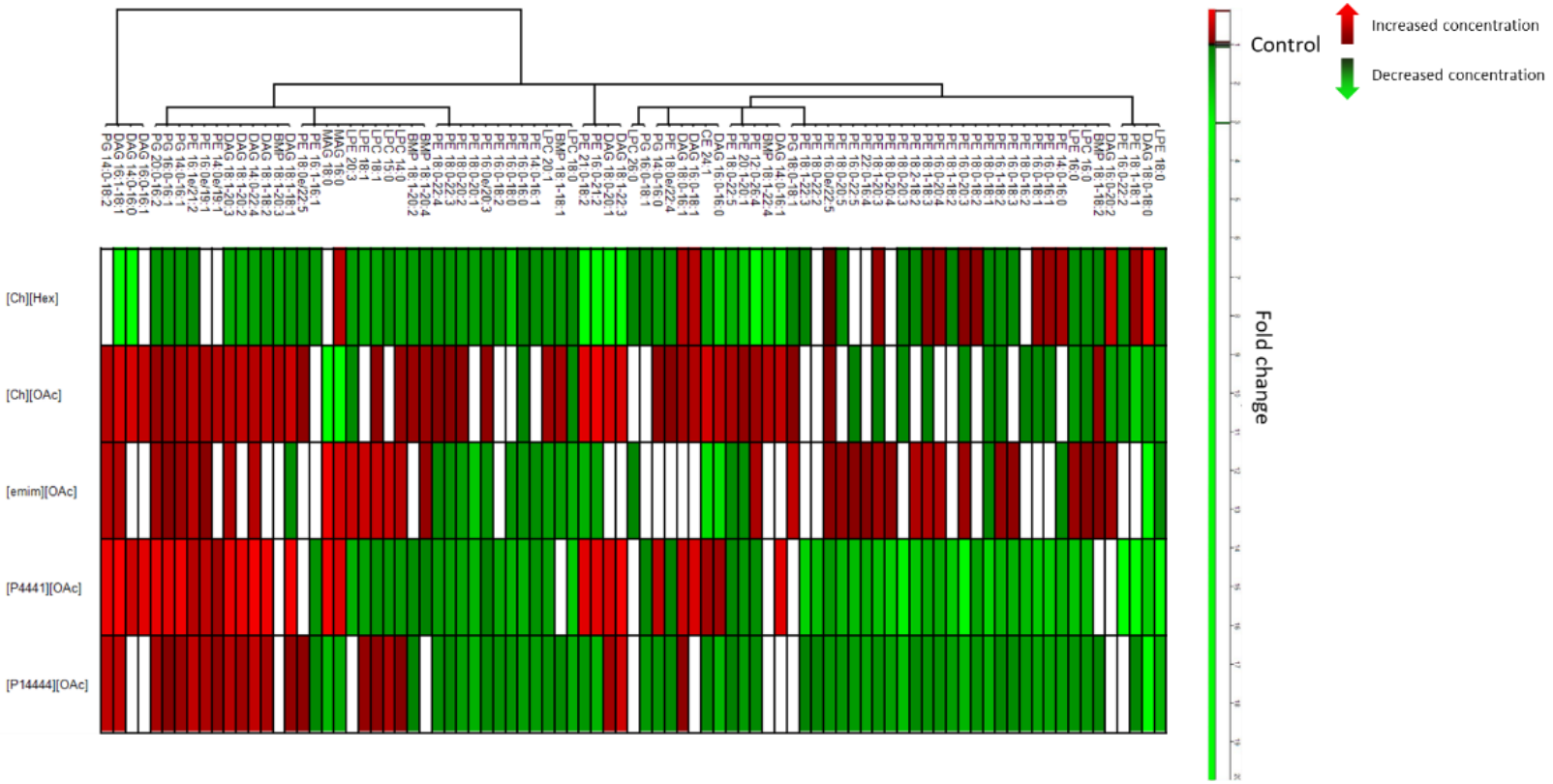

Figure 98: Heatmap: Showing all identified and significantly altered signalling features, analysed in ESI+ mode

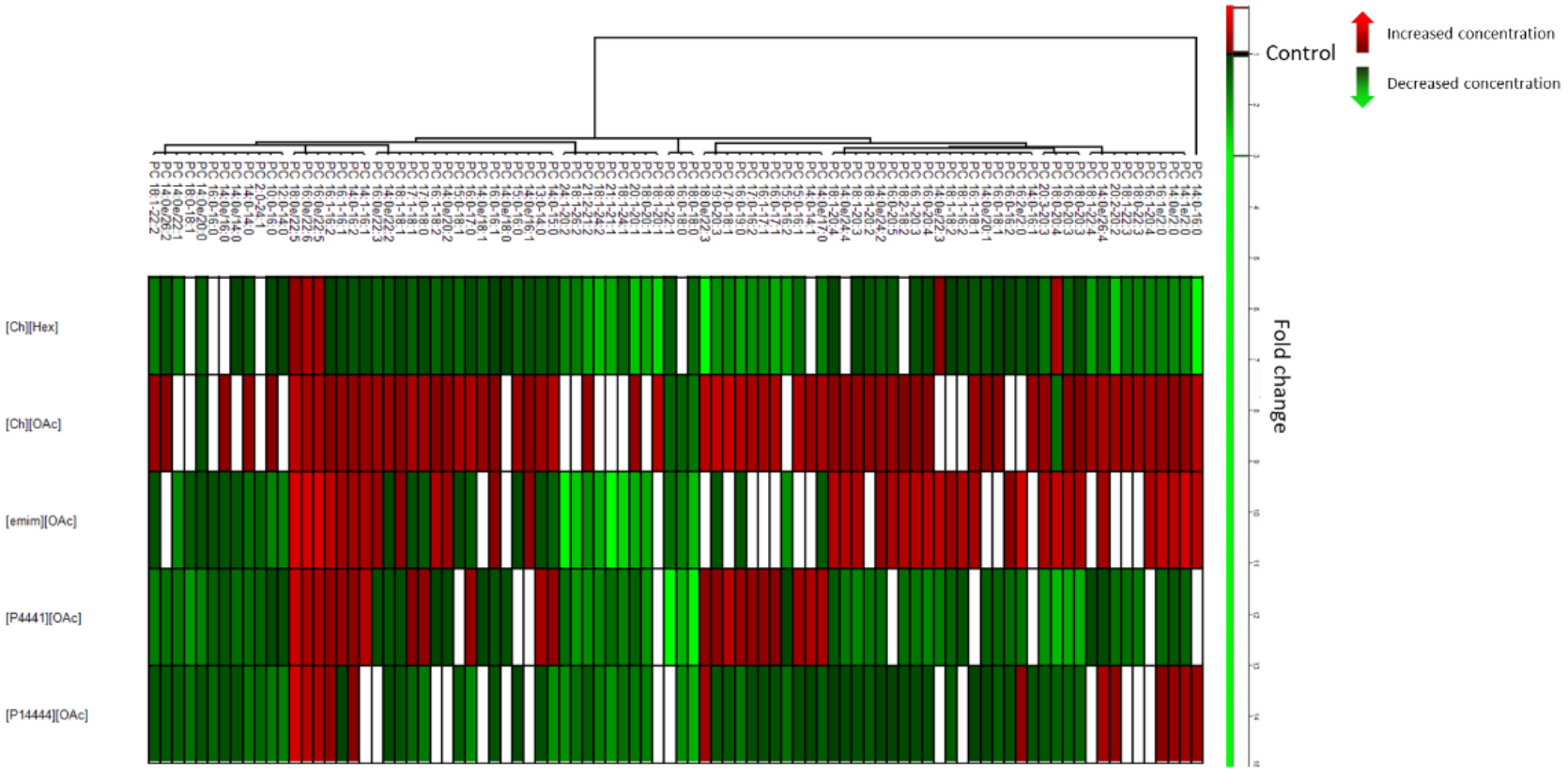

Figure 99: Heatmap: Showing all identified and significantly altered phosphocholine features, analysed in ESI+ mode

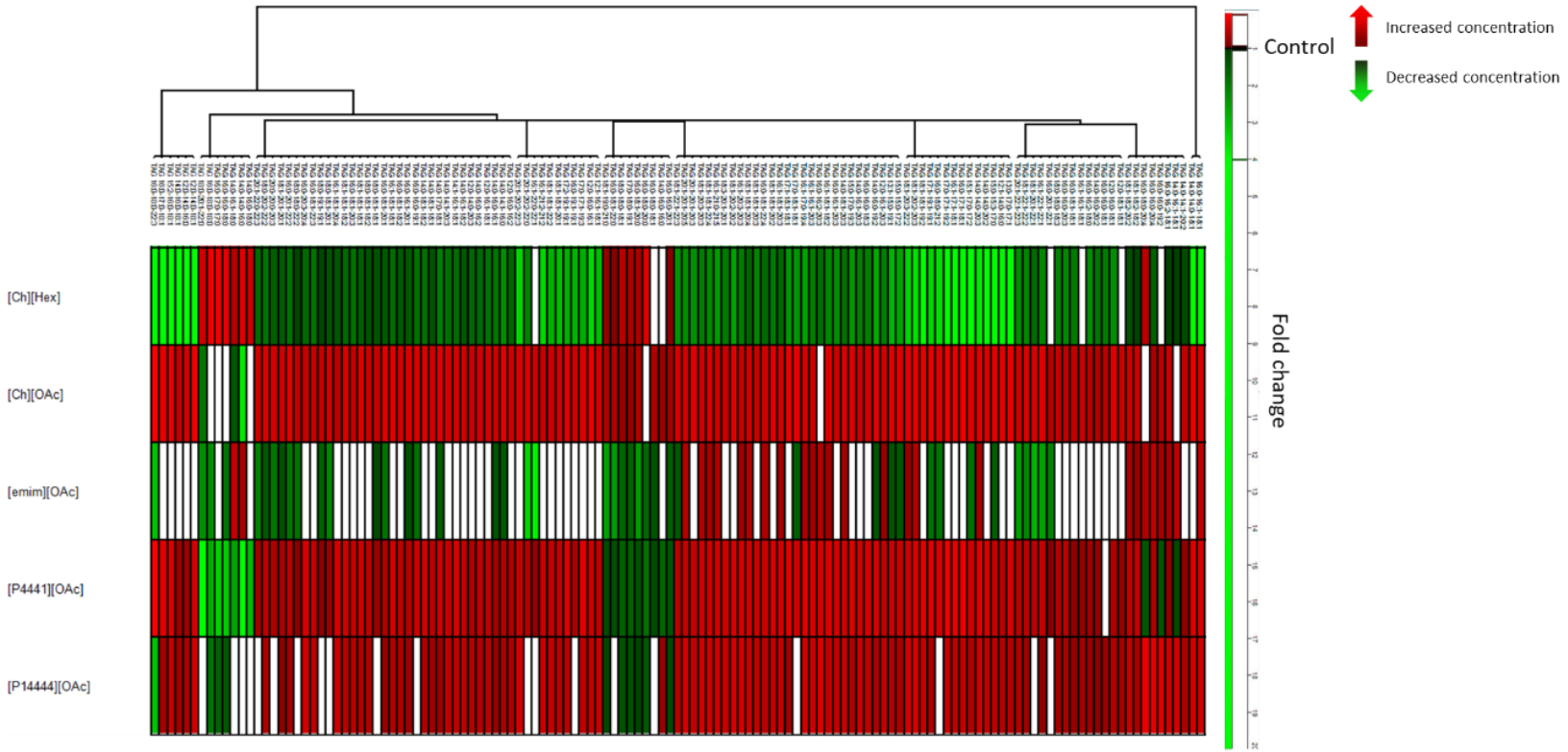

Figure 100: Heatmap: Showing all identified and significantly altered Triacylglyceride features, analysed in ESI+ mode

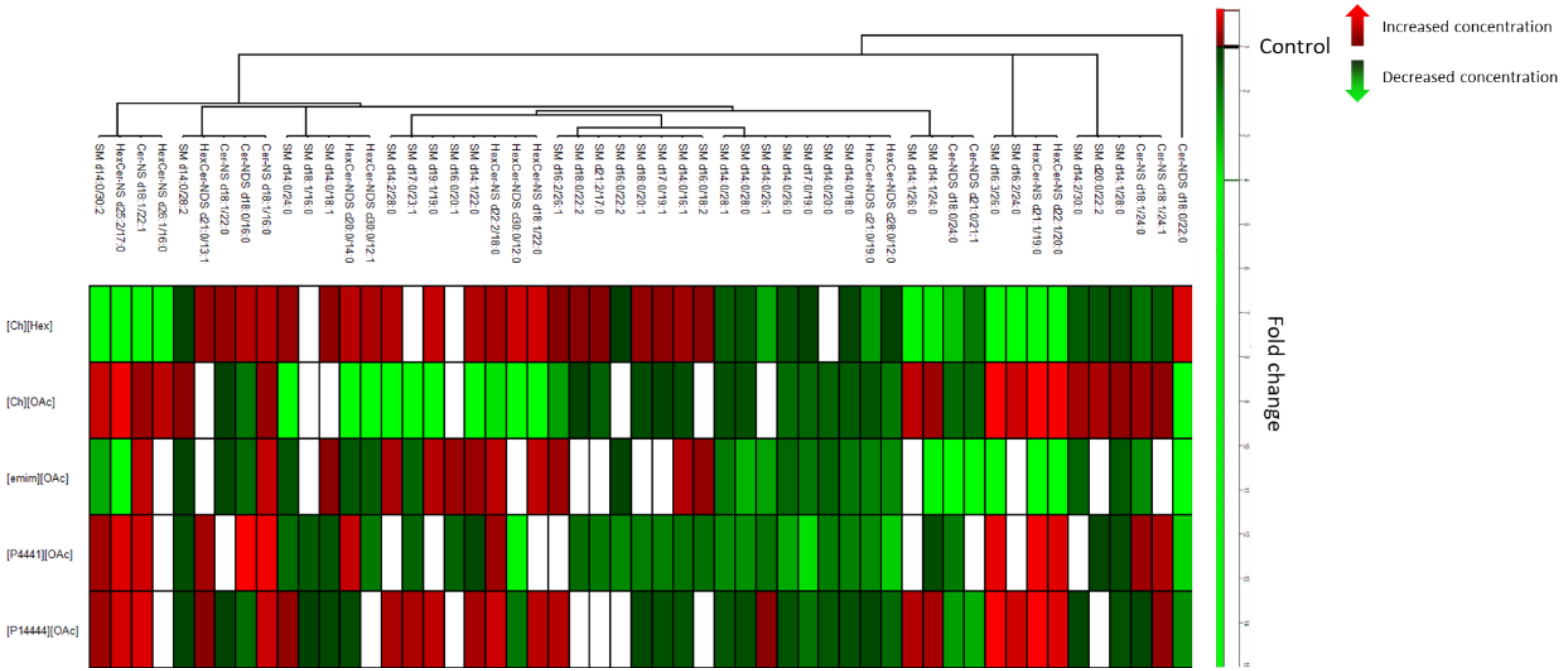

Figure 101: Heatmap: Showing all identified and significantly altered features, which belong to the stress pathway, analysed in ESI- mode

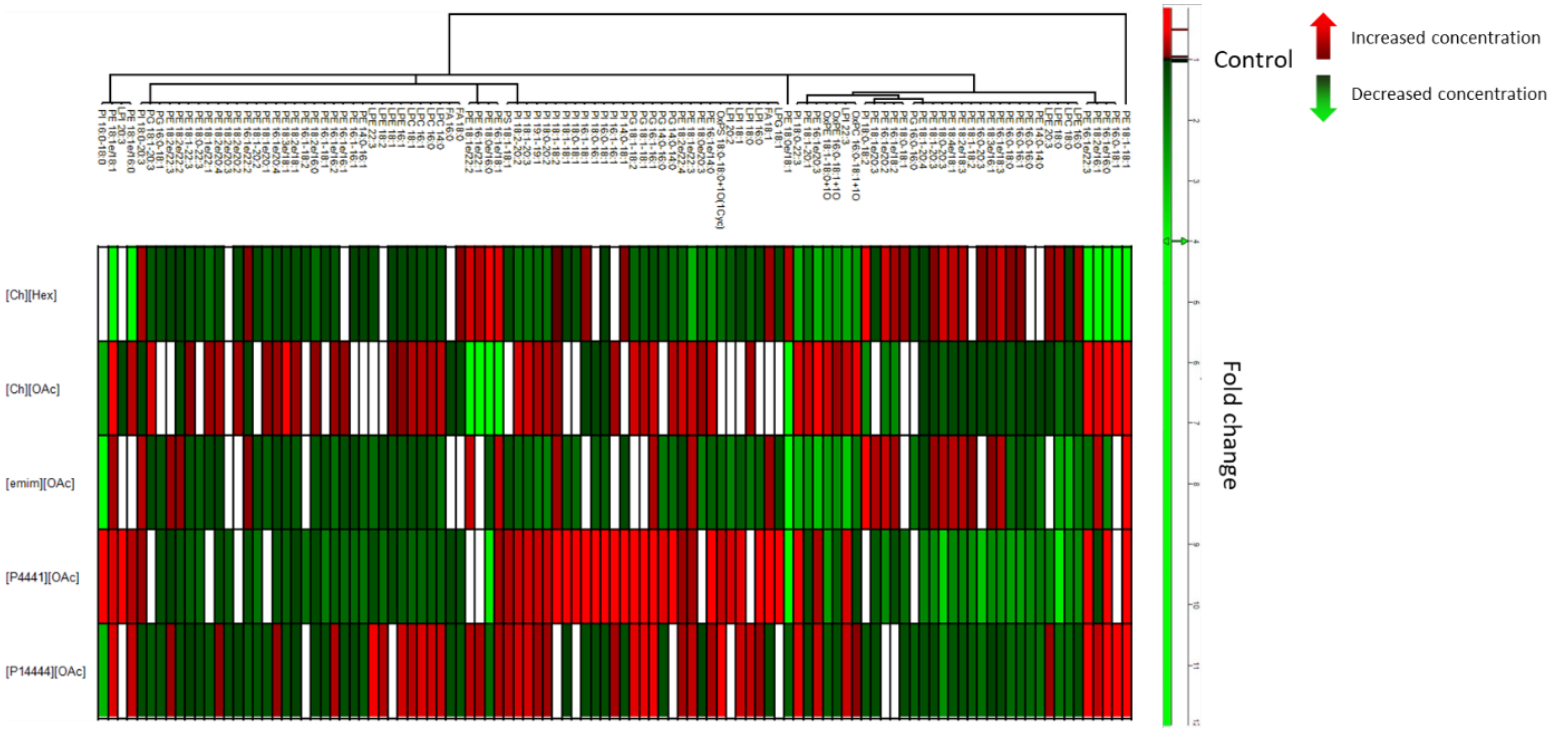

Figure 102: Heatmap: Showing all identified and significantly altered signalling features, analysed in ESI- mode

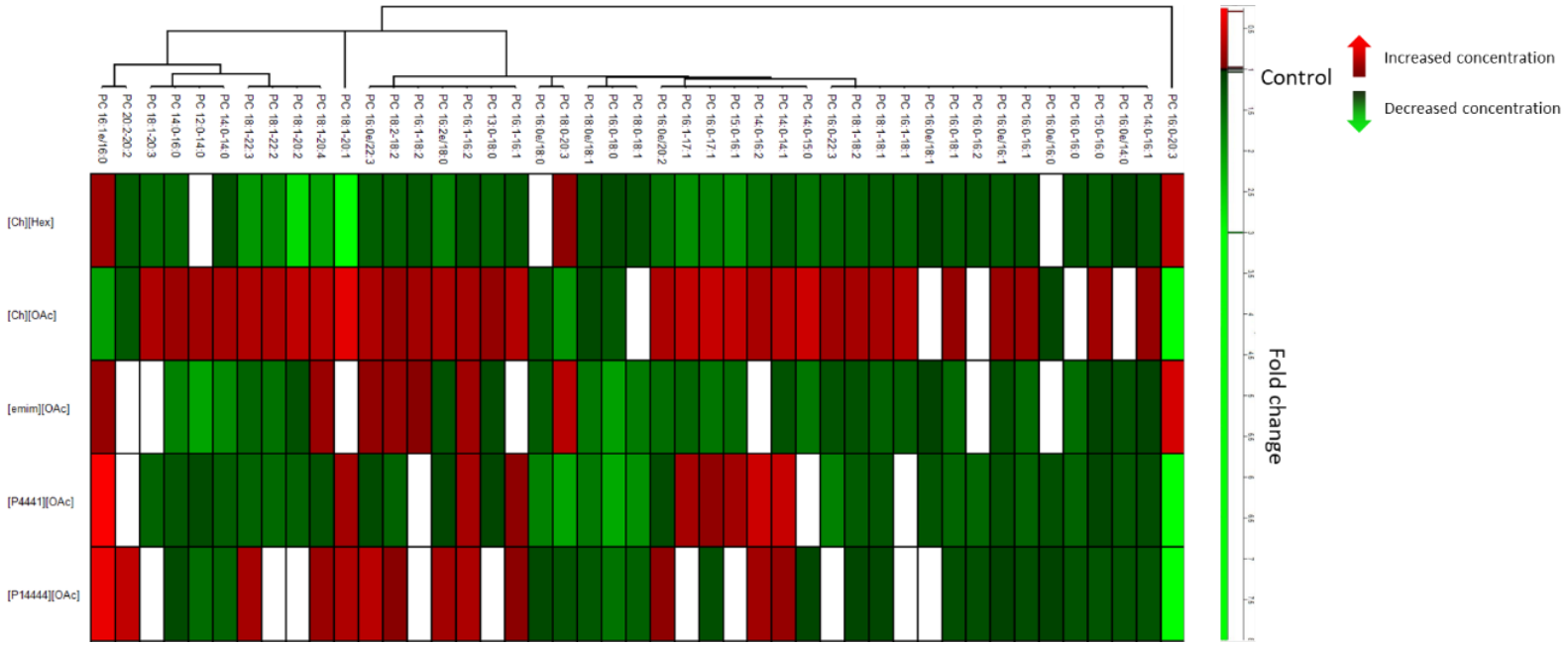

Figure 103: Heatmap: Showing all identified and significantly altered phosphocholine features, analysed in ESI- mode

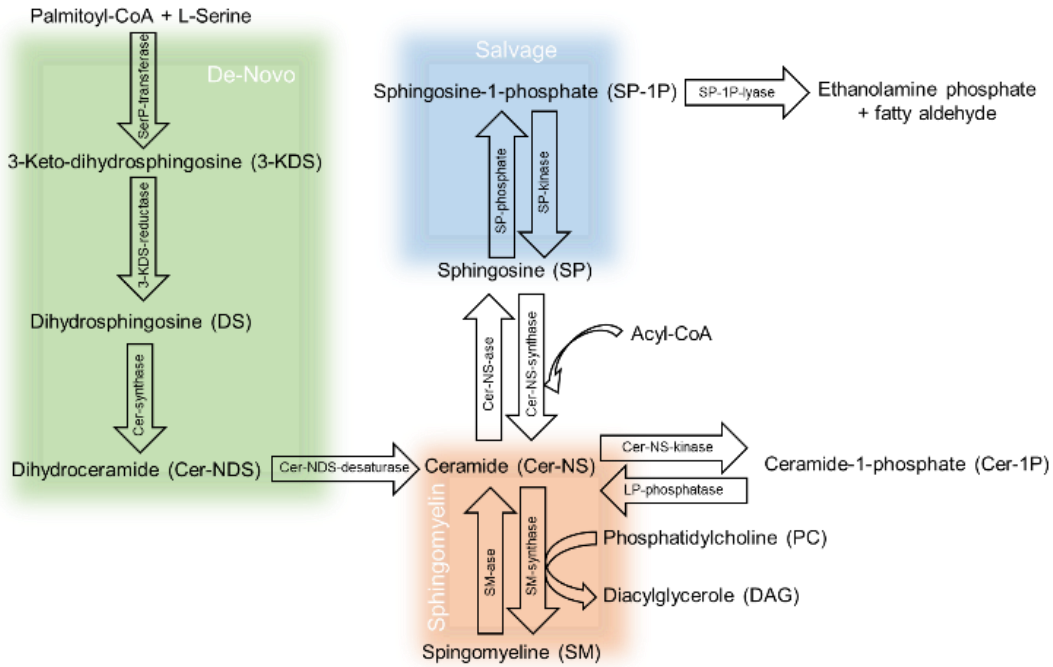

Figure 104: Sphingolipid metabolic pathway (stress pathway): This pathway contains of the de-novo synthesis of Ceramides (green), the Sphingomyelin pathway (red) and the salvage pathway (blue). SerP-transferase = Serine Palmitoyltransferase; 3KDS-reductase = 3-Keto-dihydrosphigosine reductase; Cer-synthase = Ceramide Synthase; Cer-NDS-desaturase = Dihydroceramide desaturase; Cer-NS-kinase = Ceramide kinase; LP-phosphatase = lipid phosphate phosphatase; SM-synthase = Sphingomyelin Synthase; SM-ase = Sphingomyelinase; Cer-NS-ase = Ceramidase; Cer-NS-synthase = Ceramide Synthase; SP-phosphate = Sphingosine phosphate; SP-kinase = Sphingosine Kinase; SP-1P-lyase = Sphingosine-1-phosphate lyase

All interconversions in the sphingolipid pathway are reversible with the exception of the de novo synthesis and the hydrolysis of sphingosine-1-phosphate. All sphingolipids possess specific biophysical activities and interaction partners; consequently, the outcome of the activation of the sphingolipid stress response pathway depends on the molecular species that accumulates in the cell membranes [500]. The increase in Cer-NS and the corresponding decrease in SM species and Cer-NDS measured in the present work suggests that this stress pathway is activated by the ILs (Figure 97 and Figure 101).

[Ch][OAc] on the other hand influences the metabolism by means of signal lipids (Figure 97- Figure 99). In particular, Figure 99 shows that [Ch][OAc] is the only one of the tested ILs with strongly increased levels of phosphatidylcholines (PC). The significant accumulation of triacyl-glycerides (TAGs) suggests that [Ch][OAc], and to a lesser extent [emim][OAc], induce the formation of intracellular lipid droplets known also as stress droplets (Figure 100) [501]. These droplets have both protective as well as detrimental functions, as they increase survival under stress, but also are reservoirs for eicosanoid production [499].

The difference between [Ch][Hex] and [P_{4441}][OAc] is even more pronounced: [P_{4441}][OAc] seems to activate the sphingolipid pathway (Figure 97 and as example SI Figure S29; A) and other signalling lipids, like diacylglycerols (DAG) (Figure 98 and as example SI Figure S29; B), phosphatidylinositols (PI) and lysophosphatidylinositoles (LPI) (Figure 102 and as example SI Figure S29; C and D), while [Ch][Hex] induce altogether different changes in the cells (Figure 97 – Figure 103). In group III, at first sight, the toxic effect can be described by activation of the sphingolipid pathway and signal lipids (Figure 97– Figure 98 and Figure 101 - Figure 102).

A closer look at only identified and significantly altered lipids at certain time points of single processed ILs compared to the control allows more detailed conclusions about different mechanisms of action, especially within group II (see fold changes, SI Table S32-Table S41). The treatment with [Ch][Hex] induces only a few significant changes in the identified lipids. After an exposure of 8h to [Ch][Hex], no significantly increased or decreased lipids were found in comparison with the control in ESI+ or ESI-. Only after 16h the first signs of an altered lipid metabolism appear as increased intensities of TAGs in ESI+ mode (SI Table S34). The TAGs accumulate in lipid

droplets as a direct reaction to the stress caused by the ILs and a potential source could be membrane phospholipids [499]. Damaged membrane is recycled and the excess phospholipids are stored as TAGs [499,502]. The number of significantly altered lipids increased dramatically after 24h treatment in ESI+ and ESI- measurements (SI Table S34 and Table S35). However, only TAG levels have increased compared to control. As mentioned before, TAG accumulation is favourable because it prevents the accumulation of more cytotoxic lipids, such as free fatty acids from phospholipid breakdown, but it can also have negative consequences. The EC_{50} value for [Ch][Hex] is comparable to $[P_{4441}]$[OAc] and belongs to the toxic ILs. This cannot be explained only by build-up of lipid droplets as reaction to stress. In a previous study [1], we have shown, that the long-chain anion of [Ch][Hex] can implement itself into the membrane and destabilize it, which could be the reason for an EC_{50} of 22.7 mM. Additionally, [Ch][Hex] showed a lot of unknown significantly altered features. Their identification might better explain the toxicity mechanism of [Ch][Hex].

According to the group classification, one could assume that $[P_{4441}]$[OAc] shows a similar behaviour as [Ch][Hex]. But already after 8h treatment a slight activation of the sphingolipid pathway of the cells in response to the toxic IL becomes noticeable, because the intensities of Cer-NDS and SM are decreased by increasing levels of Cer-NS compared to the control (SI Table S38) causing apoptosis. At the same time, only $[P_{4441}]$[OAc] showed increased levels of diacylglycerols (DAG), phosphatidylinositol (PI) and lysophosphatidylinositol (LPI) (SI Table S38 and Table S39), which can also be involved in the process of apoptosis [503]. For example, PI and LPI could be metabolized to phosphatidylinositol-4,5-bisphosphat (PIP_2), which serves as substrate for the phospholipase C (PLC) [503,504]. PIP_2 can be cleaved to DAG and inositol-1,4,5-trisphosphate (IP_3) by PLC. This is supported by the increase in DAGs compared to control. Downstream from IP_3 is protein kinase C, involved in several signalling pathways including apoptosis [503,505,506]. PLC activity is also supported by the reduced levels of phosphatidylcholines (PC) (SI Table S38 and Table S39). Therefore, already after 8h treatment a clear influence on metabolic processes leading to apoptosis can be observed. Longer incubation of 16h and 24h triggers TAGs accumulation (SI Table S38), which are synthesised to avoid the toxic accumulation

of DAG and Cer-NS in the cell [499]. Thus, $[P_{4441}][OAc]$, unlike [Ch][Hex], affects also signalling lipids along lipid droplet formation.

Comparing the two choline-based ILs, [Ch][OAc] and [Ch][Hex], neither seems to have rapid effects on lipid metabolism since there are no significant changes at the 8h time point. However, significant differences between the two ILs can already be seen after 16h (SI Table S32-Table S33 and Table S34-Table S35). For instance, in [Ch][OAc] everything points to the fact that metabolic processes are influenced, since signal molecules such as lysophosphatidylethanolamines (LPE), PC, PE and DAG are increased (see SI Table S32). In addition, the sphingolipid pathway (Figure 104) is also active, as Cer-NS shows increased intensities, but Cer-NDS and SM are decreased compared to the control (SI Table S32). Furthermore, after 16h treatment, increased levels of TAG and cholesteryl ester (Chol Ester) can be observed (SI Table S32). As mentioned above, the treatment with [Ch][OAc] shows increased PC levels. Ruokonen *et al*. have shown in a previous study, that [Ch][OAc] permeates the membrane without disturbance [1]. Therefore, it is possible, that [Ch][OAc] enters the cells causing an excess of choline used for the synthesis of different metabolites, like PC. This uptake and usage of choline could also be observed in a previous study by increased levels of acetylcholine [480]. High amounts of PC can be metabolized to DAG, which is visible in increased levels of DAG (SI Table S32) and further to TAGs [507], as described above (SI Table S32). Additionally, further signal lipids, such as Cer-NS are significantly increased with decreased levels of Cer-NDS and SM at the same time, indicating an active sphingolipid pathway (SI Table S32). [Ch][OAc] thus can efficiently influence metabolic processes but is generally rather harmless in comparison to the other ILs, since [Ch][OAc], besides [Ch][Hex], has the highest EC_{50} value. Similarly, [emim][OAc] can permeate the membrane [1] causing increased intensities of a few Cer-NS lipids after 16h together with decreased levels of Cer-NDS and SM (SI Table S36). Additionally, TAG levels are increased (SI Table S36), as the cells try to avoid accumulation of harmful lipids. However, only increased PC levels, but no increased DAG intensities could be observed (SI Table S36). After 24h only TAGs continue to accumulate, as well as Cer-NS (SI Table S36). Therefore, it seems that [emim][OAc] is also able to activate the sphingolipid pathway.

The most toxic IL within this project, [P_{14444}][OAc] is clearly confirmed by the lipid profile. Already after 8 hours the cells activate the sphingolipid pathway, whereby Cer-NS again shows increased intensities, and Cer-NDS as well as SM are detected in lower intensities (SI Table S40 and Table S41). After 16 hours the intensity of BMP has increased in addition to the sphingolipid pathway (SI Table S40). BMP promotes the fusion of membranes or the formation of internal vesicles [508] and indicates the intention of the cells to repair the membrane [509] destroyed by the treatment of [P_{14444}][OAc] [1]. Furthermore, the concentration of DAG also increases (SI Table S40). This shows that the cells are in the process of apoptosis. This results in a significant increase in the number of identified and increased TAG levels (SI Table S40). Similar changes are observed also after 24h.

3.6.5. Conclusion

An untargeted UHPLC-ESI-MS/MS method for lipidomic profiling in cells was adapted and applied to analyse toxicity of five different ILs belonging to three groups, based on changes in the lipid profile. An extraction method presented by Calderón *et al.*, using a 2-propanol/water (90:10; v/v) mixture as extraction agent, was successfully applied. Additionally, an experimental setup for EC_{50} evaluation of ILs on HeLa cells were developed.

The results show that the grouping of ILs already described by Ruokonen *et al*. could be confirmed by the analysis of the lipid profile. The toxicity increases for most of the ILs over time. An in-house developed VBA script made a comparison of the different ILs possible, which allowed the analysis of the similarities of the ILs as well as unique characteristics and further strengthened the group assignment. For example, it was shown that [Ch][OAc], in contrast to [emim][OAc], affects less sphingolipid species, but significantly influences metabolic processes that involve phospholipids. In group II, the differences between the two ILs [Ch][Hex] and [P_{4441}][OAc] are even more noticeable, since [Ch][Hex] showed only a few significant changes in lipids and therefore the toxicity must be related to the influence of other metabolic processes, which are not based on lipids. [P_{4441}][OAc], on the other hand, activates the sphingolipid pathway and other lipid metabolic pathways. Last but not least, the assignment of [P_{14444}][OAc] in group III was confirmed by a clear lipid profile showing

fast effects on the sphingolipid pathway, followed by membrane fusion as response to membrane destruction.

These results provide first insights into the so far unknown toxicity mechanisms, which has to be further investigated by analysis of e.g. individual enzymes, proteins, or by using targeted lipidomics assays to elucidate specific pathway routes in more detail.

3.6.6. Supporting information

HeLa cell lipid metabolism under ionic liquid stress

3.6.6.1. Experimental

Table S19: Internal standard: Information about internal standards of the SPLASH™ Lipidomix Mass Spec Standard (in MeOH) and corresponding concentrations in the mix before dilution

Mixture Components	Conc. in Lipidomix (µg/mL)
15:0-18:1(d7) PC	160
15:0-18:1(d7) PE	5
15:0-18:1(d7) PS	5
15:0-18:1(d7) PG	30
15:0-18:1(d7) PI	10
15:0-18:1(d7) PA	7
18:1(d7) LPC	25
18:1(d7) LPE	5
18:1(d7) Chol Ester	350
18:1(d7) MG	2
15:0-18:1(d7) DG	10
15:0-18:1(d7)-15:0 TG	55
18:1(d9) SM	30
Cholesterol (d7)	100

3.6.6.1.1. Determination of EC_{50}-values

3.6.6.1.1.1. Preparation of ionic liquid samples

All IL solutions were prepared by adding EX-CELL HeLa serum free media supplemented with 2 mM L-Glutamine to the respective IL, to reach the highest concentration listed below in Table S20. For the EC_{50} determinations the IL solutions were further diluted with media to the additional six concentrations in Table S20 below. All measurements were repeated in duplicates.

3.6.6.1.1.2. Cell culture conditions

The HeLa cell line (AC free, ECACC 08011102 from Sigma/Merck, Darmstadt, Germany) were cultivated in EX-CELL HeLa serum free media (Sigma/Merck, Darmstadt, Germany) supplemented with 2 mM L-Glutamine at 37 °C and 5 % CO_2 atmosphere incubator (Thermo Fisher Scientific, Waltham, MA). Cells ($8x10^4$ cells) were seeded in 48 well-plates.

3.6.6.1.1.3. Cytotoxicity assay

Cytotoxicity of the tested ILs was assessed using a metabolic activity detector, alamarBlue assay (Thermo Fisher Scientific). The non-fluorescent/blue reagent shifts to fluorescent/red state in the presence of intracellular reducing agents. Therefore, the number of live cells is directly proportional to the fluorescence/red shift of the alamarBlue reagent. For our study, we have monitored the increase in fluorescence using an EnSpire plate reader (PerkinElmer, Waltham, MA) with excitation/emission wavelengths of 570/590 nm.

To calculate the EC_{50} values for the ILs, a calibration curve was devised to correlate fluorescence units and number of cells. Therefore, a serial dilution of cells was prepared in EX-CELL media and mixed with alamarBlue. After 90 min of incubation fluorescence was measured in medium aliquots.

Appropriate concentrations of each IL were prepared and mixed with the EX-CELL medium to produce a two-fold serial dilution with 7 steps (SI Table S20). The IL-dilutions were then added on the seeded HeLa cells and incubated for 18h. Each well-plate included a no-cells blank and a control (no-ILs). Subsequently, the alamarBlue reagent was added (1:10, v:v) in all wells and after a 90min incubation the samples were centrifuged at 400g for 5 min to pellet cells. Aliquots from the supernatants were transferred to a 96 well-plate and fluorescence was measured.

The equation from the calibration curve, that correlated the cell number with the fluorescence unit, was used to calculate the number of cells in the treated samples and control and a survival rate was calculated. To calculate the EC_{50} values of the ILs, a mathematical equation (SI Equation S3) which best described the observed values was developed:

$$y = \frac{a_3}{(1 + e^{(a_2 * (x - a_1))})}$$

Equation S3: Calculation of EC_{50} value: With a_1 as the EC_{50} value, a_2 as the slope of the sigmoidal curve, a_3 as the saturation point which describes the first half of the sigmoidal curve, y as survival rate and x as the concentration of the IL

based on a model described before by Verschuuren *et al.* [93]. The equation contained a_2 as the slope of the sigmoidal curve, a_1 as the EC_{50} value, a_3 as the saturation point which describes the first half of the (not shown) sigmoidal curve, y as survival rate and x as the concentration of the IL (SI Figure S28).

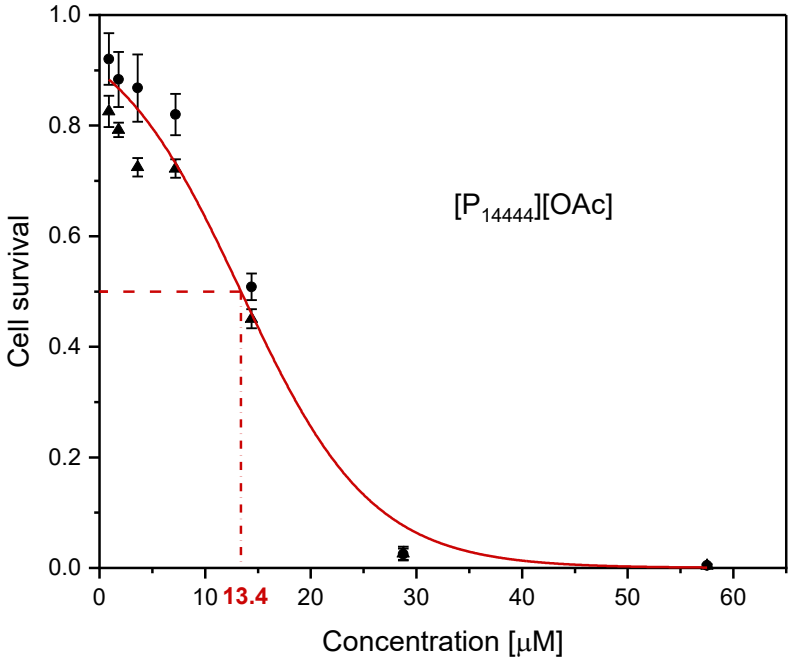

Figure S28: Graphical example of the observed and calculated EC_{50} values for $[P_{14444}][OAc]$: The observed values (round and triangles; black) represent the experimental data from two independent experiments; while predicted values (red curve) represent the curve point calculated based on the aforementioned equation

Table S20: The final IL concentrations: Dissolved in media, used for EC_{50} determination as well as corresponding **EC_{50} values ± STD**

Ionic liquid	**Concentration range [mM]**							**EC_{50} [mM]**
[Ch][OAc]	306.35	153.18	76.59	38.29	19.15	9.57	4.79	**139.5 ± 6.2**
[Ch][Hex]	228.00	114.00	57.00	28.50	14.25	7.13	3.56	**22.7 ± 1.5**
[emim][OAc]	293.75	146.88	73.44	36.72	18.36	9.18	4.59	**73.3 ± 3.9**
$[P_{4441}][OAc]$	45.25	22.63	11.31	5.56	2.83	1.41	0.70	**12.8 ± 1.1**
	Concentration range [μM]							
$[P_{14444}][OAc]$	57.50	28.75	14.40	7.20	3.60	1.80	0.90	**13.4 ± 0.8**

Table S21: The final IL concentrations: Dissolved in media, used for treatment of the cells before extraction for lipidomic profiling and corresponding molar masses (g/mol) and EC_{50} (mM)

IL	Final concentration [mM]	M (g/mol)	EC_{50} [mM]
[Ch][OAc]	35.26	163.21	139.5
[Ch][Hex]	5.05	219.32	22.7
[emim][OAc]	9.89	170.21	74.4
$[P_{4441}][OAc]$	5.05	276.39	12.8
$[P_{14444}][OAc]$	0.03	458.70	0.0134

Table S22: Injection sequence: Of the validation samples in negative and positive mode

	Positive mode	**Negative mode**		**Positive mode**	**Negative mode**
Injection order	**Sample name**		**Injection order**	**Sample name**	
1	QC-IDA-1	QC-IDA-1	23	QC-06	QC-06
2	QC-IDA-2	QC-IDA-2	24	Conc 2-Pre 4	Conc 1-Post 4
3	QC-01	QC-01	25	Conc 2-Pre 3	Conc 1-Post 2
4	Conc 1-Pre 1	Conc 2-Pre 4	26	Conc 1-Pre 2	Conc 3-Pre 5
5	Conc 2-Post 1	Conc 1-Pre 4	27	QC-07	QC-07
6	Conc 2-Post 5	Conc 3-Post 1	28	Conc 1-Pre 3	Conc 2-Pre 2
7	QC-02	QC-02	29	Conc 1-Post 1	Conc 3-Pre 4
8	Conc 1-Post 3	Conc 2-Pre 1	30	Conc 1-Post 4	Conc 3-Pre 1
9	Conc 3-Post 2	Conc 2-Post 1	31	QC-08	QC-08
10	Conc 3-Pre 3	Conc 1-Post 3	32	Conc 2-Post 3	Conc 2-Pre 5
11	QC-03	QC-03	33	Conc 3-Pre 5	Conc 2-Post 3
12	Conc 2-Post 2	Conc 1-Pre 2	34	Conc 3-Post 1	Conc 1-Pre 3
13	Conc 2-Post 4	Conc 1-Post 1	35	QC-09	QC-09
14	Conc 2-Pre 5	Conc 3-Post 4	36	Conc 3-Post 3	Conc 1-Pre 5
15	QC-04	QC-04	37	Conc 1-Pre 4	Conc 3-Post 5
16	Conc 3-Post 5	Conc 2-Post 4	38	Conc 3-Post 4	Conc 1-Post 5
17	Conc 2-Pre 2	Conc 2-Post 2	39	QC-10	QC-10
18	Conc 1-Post 5	Conc 3-Pre 2	40	Conc 1-Pre 5	Conc 1-Pre 1
19	QC-05	QC-05	41	Conc 1-Post 2	Conc 3-Post 3
20	Conc 2-Pre 1	Conc 2-Post 5	42	Conc 3-Pre 4	Conc 2-Pre 3
21	Conc 3-Pre 1	Conc 3-Pre 3	43	QC-11	QC-11
22	Conc 3-Pre 2	Conc 3-Post 2	44	QC-12	QC-12

Table S23: Injection sequence: Of the samples treated with [Ch][OAc] in negative and positive mode

	Positive mode	Negative mode		Positive mode	Negative mode
Injection order	**Sample name**		**Injection order**	**Sample name**	
1	QC-01	QC-01	26	[Ch][OAc] 5 8h	Ctr 3 [Ch][OAc] 16h
2	Ctr 3 [Ch][OAc] 24h	[Ch][OAc] 4 8h	27	Ctr 4 [Ch][OAc] 24h	Ctr 2 [Ch][OAc] 8h
3	Ctr 2 [Ch][OAc] 16h	Ctr 1 [Ch][OAc] 24h	28	[Ch][OAc] 4 16h	Ctr 4 [Ch][OAc] 24h
4	Ctr 6 [Ch][OAc] 24h	Ctr 2 [Ch][OAc] 16h	29	QC-08	QC-08
5	QC-02	QC-02	30	Ctr 4 [Ch][OAc] 8h	[Ch][OAc] 2 16h
6	[Ch][OAc] 5 16h	Ctr 3 [Ch][OAc] 24h	31	[Ch][OAc] 2 8h	[Ch][OAc] 3 24h
7	Ctr 2 [Ch][OAc] 8h	[Ch][OAc] 3 8h	32	Ctr 5 [Ch][OAc] 24h	Ctr 1 [Ch][OAc] 8h
8	Ctr 6 [Ch][OAc] 16h	Ctr 2 [Ch][OAc] 24h	33	QC-09	QC-09
9	QC-03	QC-03	34	Ctr 5 [Ch][OAc] 8h	Ctr 4 [Ch][OAc] 8h
10	[Ch][OAc] 1 24h	[Ch][OAc] 3 16h	35	[Ch][OAc] 3 8h	[Ch][OAc] 5 8h
11	[Ch][OAc] 2 24h	Ctr 6 [Ch][OAc] 8h	36	Ctr 1 [Ch][OAc] 24h	[Ch][OAc] 5 16h
12	Ctr 1 [Ch][OAc] 16h	[Ch][OAc] 6 8h	37	QC-10	QC-10
13	QC-04	QC-04	38	Ctr 1 [Ch][OAc] 8h	Ctr 5 [Ch][OAc] 16h
14	[Ch][OAc] 2 16h	[Ch][OAc] 1 8h	39	[Ch][OAc] 4 8h	[Ch][OAc] 5 24h
15	Ctr 3 [Ch][OAc] 8h	[Ch][OAc] 2 8h	40	Ctr 4 [Ch][OAc] 16h	Ctr 6 [Ch][OAc] 24h
16	Ctr 5 [Ch][OAc] 16h	Ctr 5 [Ch][OAc] 8h	41	QC-11	QC-11
17	QC-05	QC-05	42	[Ch][OAc] 5 24h	[Ch][OAc] 1 24h
18	[Ch][OAc] 6 24h	[Ch][OAc] 6 24h	43	[Ch][OAc] 4 24h	[Ch][OAc] 4 24h
19	[Ch][OAc] 1 16h	[Ch][OAc] 6 16h	44	[Ch][OAc] 3 24h	Ctr 6 [Ch][OAc] 16h
20	[Ch][OAc] 6 8h	Ctr 4 [Ch][OAc] 16h	45	QC-12	QC-12
21	QC-06	QC-06	46	[Ch][OAc] 3 16h	Ctr 5 [Ch][OAc] 24h
22	[Ch][OAc] 6 16h	[Ch][OAc] 4 16h	47	Ctr 3 [Ch][OAc] 16h	Ctr 1 [Ch][OAc] 16h
23	Ctr 2 [Ch][OAc] 24h	[Ch][OAc] 1 16h	48	Ctr 6 [Ch][OAc] 8h	[Ch][OAc] 2 24h
24	[Ch][OAc] 1 8h	Ctr 3 [Ch][OAc] 8h	49	QC-13	QC-13
25	QC-07	QC-07	50	QC-14	QC-14

Table S24: Injection sequence: Of the samples treated with [Ch][Hex] in negative and positive mode

	Positive mode	Negative mode		Positive mode	Negative mode
Injection order	**Sample name**		**Injection order**	**Sample name**	
1	QC-01	QC-01	26	[Ch][Hex] 1 16h	[Ch][Hex] 1 16h
2	Ctr 3 [Ch][Hex] 24h	[Ch][Hex] 6 8h	27	[Ch][Hex] 5 16h	Ctr 2 [Ch][Hex] 24h
3	Ctr 6 [Ch][Hex] 8h	Ctr 5 [Ch][Hex] 16h	28	Ctr 6 [Ch][Hex] 16h	Ctr 4 [Ch][Hex] 16h
4	[Ch][Hex] 3 24h	[Ch][Hex] 5 8h	29	QC-08	QC-08
5	QC-02	QC-02	30	[Ch][Hex] 2 24h	Ctr 2 [Ch][Hex] 16h
6	Ctr 2 [Ch][Hex] 8h	[Ch][Hex] 5 24h	31	Ctr 4 [Ch][Hex] 24h	Ctr 5 [Ch][Hex] 8h
7	[Ch][Hex] 4 16h	[Ch][Hex] 6 24h	32	Ctr 1 [Ch][Hex] 8h	[Ch][Hex] 2 8h
8	[Ch][Hex] 3 8h	Ctr 4 [Ch][Hex] 8h	33	QC-09	QC-09
9	QC-03	QC-03	34	Ctr 6 [Ch][Hex] 24h	[Ch][Hex] 1 8h
10	Ctr 5 [Ch][Hex] 16h	[Ch][Hex] 2 16h	35	[Ch][Hex] 5 8h	Ctr 4 [Ch][Hex] 24h
11	Ctr 2 [Ch][Hex] 16h	[Ch][Hex] 4 8h	36	Ctr 5 [Ch][Hex] 8h	Ctr 1 [Ch][Hex] 24h
12	[Ch][Hex] 6 16h	[Ch][Hex] 4 24h	37	QC-10	QC-10
13	QC-04	QC-04	38	[Ch][Hex] 3 16h	[Ch][Hex] 3 16h
14	Ctr 5 [Ch][Hex] 24h	[Ch][Hex] 4 16h	39	Ctr 3 [Ch][Hex] 8h	[Ch][Hex] 3 8h
15	[Ch][Hex] 2 8h	Ctr 6 [Ch][Hex] 8h	40	[Ch][Hex] 6 24h	[Ch][Hex] 2 24h
16	[Ch][Hex] 6 8h	[Ch][Hex] 6 16h	41	QC-11	QC-11
17	QC-05	QC-05	42	Ctr 2 [Ch][Hex] 24h	[Ch][Hex] 5 16h
18	[Ch][Hex] 4 8h	[Ch][Hex] 3 24h	43	[Ch][Hex] 1 24h	Ctr 5 [Ch][Hex] 24h
19	[Ch][Hex] 5 24h	Ctr 2 [Ch][Hex] 8h	44	[Ch][Hex] 1 8h	Ctr 1 [Ch][Hex] 8h
20	Ctr 4 [Ch][Hex] 8h	Ctr 3 [Ch][Hex] 24h	45	QC-12	QC-12
21	QC-06	QC-06	46	Ctr 3 [Ch][Hex] 16h	Ctr 1 [Ch][Hex] 16h
22	Ctr 1 [Ch][Hex] 24h	Ctr 3 [Ch][Hex] 16h	47	Ctr 4 [Ch][Hex] 16h	[Ch][Hex] 1 24h
23	[Ch][Hex] 4 24h	Ctr 6 [Ch][Hex] 16h	48	Ctr 1 [Ch][Hex] 16h	Ctr 6 [Ch][Hex] 24h
24	[Ch][Hex] 2 16h	Ctr 3 [Ch][Hex] 8h	49	QC-13	QC-13
25	QC-07	QC-07	50	QC-14	QC-14

Table S25: Injection sequence: Of the samples treated with [emim][OAc] in negative and positive mode

	Positive mode	Negative mode		Positive mode	Negative mode
Injection order	**Sample name**		**Injection order**	**Sample name**	
1	QC-01	QC-01	26	Ctr 4 [emim][OAc] 16h	[emim][OAc] 1 24h
2	[emim][OAc] 4 8h	Ctr 2 [emim][OAc] 16h	27	Ctr 4 [emim][OAc] 8h	[emim][OAc] 1 8h
3	[emim][OAc] 4 24h	[emim][OAc] 6 8h	28	Ctr 5 [emim][OAc] 8h	Ctr 1 [emim][OAc] 8h
4	[emim][OAc] 5 24h	[emim][OAc] 2 8h	29	QC-08	QC-08
5	QC-02	QC-02	30	[emim][OAc] 3 24h	Ctr 6 [emim][OAc] 16h
6	Ctr 5 [emim][OAc] 24h	[emim][OAc] 6 16h	31	[emim][OAc] 5 8h	Ctr 5 [emim][OAc] 8h
7	Ctr 2 [emim][OAc] 24h	Ctr 5 [emim][OAc] 24h	32	Ctr 2 [emim][OAc] 16h	[emim][OAc] 4 8h
8	Ctr 3 [emim][OAc] 8h	[emim][OAc] 5 24h	33	QC-09	QC-09
9	QC-03	QC-03	34	[emim][OAc] 3 16h	[emim][OAc] 4 24h
10	Ctr 4 [emim][OAc] 24h	Ctr 6 [emim][OAc] 24h	35	Ctr 6 [emim][OAc] 24h	[emim][OAc] 3 24h
11	Ctr 3 [emim][OAc] 16h	Ctr 6 [emim][OAc] 8h	36	[emim][OAc] 2 16h	Ctr 3 [emim][OAc] 8h
12	Ctr 5 [emim][OAc] 16h	[emim][OAc] 4 16h	37	QC-10	QC-10
13	QC-04	QC-04	38	[emim][OAc] 1 16h	Ctr 1 [emim][OAc] 16h
14	Ctr 1 [emim][OAc] 16h	[emim][OAc] 6 24h	39	[emim][OAc] 2 8h	Ctr 3 [emim][OAc] 16h
15	[emim][OAc] 2 24h	[emim][OAc] 5 16h	40	[emim][OAc] 5 16h	[emim][OAc] 5 8h
16	[emim][OAc] 1 24h	[emim][OAc] 3 16h	41	QC-11	QC-11
17	QC-05	QC-05	42	[emim][OAc] 6 24h	[emim][OAc] 2 24h
18	Ctr 1 [emim][OAc] 24h	Ctr 5 [emim][OAc] 16h	43	[emim][OAc] 3 8h	Ctr 2 [emim][OAc] 8h
19	[emim][OAc] 6 8h	Ctr 1 [emim][OAc] 24h	44	[emim][OAc] 1 8h	Ctr 4 [emim][OAc] 24h
20	Ctr 6 [emim][OAc] 8h	[emim][OAc] 3 8h	45	QC-12	QC-12
21	QC-06	QC-06	46	Ctr 6 [emim][OAc] 16h	Ctr 2 [emim][OAc] 24h
22	Ctr 3 [emim][OAc] 24h	Ctr 3 [emim][OAc] 24h	47	Ctr 2 [emim][OAc] 8h	[emim][OAc] 1 16h
23	Ctr 1 [emim][OAc] 8h	Ctr 4 [emim][OAc] 16h	48	[emim][OAc] 6 16h	Ctr 4 [emim][OAc] 8h
24	[emim][OAc] 4 16h	[emim][OAc] 2 16h	49	QC-13	QC-13
25	QC-07	QC-07	50	QC-14	QC-14

Table S26: Injection sequence: Of the samples treated with $[P_{4441}][OAc]$ in negative and positive mode

	Positive mode	Negative mode		Positive mode	Negative mode
Injection order	**Sample name**		**Injection order**	**Sample name**	
1	QC-01	QC-01	26	Ctr 2 $[P_{4441}][OAc]$ 16h	$[P_{4441}][OAc]$ 4 16h
2	$[P_{4441}][OAc]$ 5 8h	$[P_{4441}][OAc]$ 6 16h	27	$[P_{4441}][OAc]$ 4 8h	Ctr 5 $[P_{4441}][OAc]$ 8h
3	Ctr 5 $[P_{4441}][OAc]$ 24h	Ctr 3 $[P_{4441}][OAc]$ 24h	28	Ctr 5 $[P_{4441}][OAc]$ 8h	Ctr 4 $[P_{4441}][OAc]$ 24h
4	Ctr 3 $[P_{4441}][OAc]$ 8h	$[P_{4441}][OAc]$ 1 24h	29	QC-08	QC-08
5	QC-02	QC-02	30	$[P_{4441}][OAc]$ 4 16h	Ctr 6 $[P_{4441}][OAc]$ 24h
6	$[P_{4441}][OAc]$ 5 24h	$[P_{4441}][OAc]$ 6 8h	31	$[P_{4441}][OAc]$ 3 8h	$[P_{4441}][OAc]$ 4 24h
7	$[P_{4441}][OAc]$ 6 24h	Ctr 1 $[P_{4441}][OAc]$ 16h	32	Ctr 4 $[P_{4441}][OAc]$ 8h	$[P_{4441}][OAc]$ 5 16h
8	$[P_{4441}][OAc]$ 6 8h	$[P_{4441}][OAc]$ 6 24h	33	QC-09	QC-09
9	QC-03	QC-03	34	$[P_{4441}][OAc]$ 2 16h	Ctr 2 $[P_{4441}][OAc]$ 16h
10	Ctr 4 $[P_{4441}][OAc]$ 24h	Ctr 4 $[P_{4441}][OAc]$ 16h	35	$[P_{4441}][OAc]$ 4 24h	Ctr 3 $[P_{4441}][OAc]$ 8h
11	Ctr 1 $[P_{4441}][OAc]$ 24h	$[P_{4441}][OAc]$ 2 24h	36	Ctr 1 $[P_{4441}][OAc]$ 16h	$[P_{4441}][OAc]$ 4 8h
12	Ctr 6 $[P_{4441}][OAc]$ 16h	Ctr 2 $[P_{4441}][OAc]$ 8h	37	QC-10	QC-10
13	QC-04	QC-04	38	$[P_{4441}][OAc]$ 3 16h	$[P_{4441}][OAc]$ 1 16h
14	Ctr 2 $[P_{4441}][OAc]$ 8h	$[P_{4441}][OAc]$ 5 24h	39	Ctr 1 $[P_{4441}][OAc]$ 8h	Ctr 3 $[P_{4441}][OAc]$ 16h
15	Ctr 3 $[P_{4441}][OAc]$ 16h	$[P_{4441}][OAc]$ 2 16h	40	$[P_{4441}][OAc]$ 1 8h	$[P_{4441}][OAc]$ 2 8h
16	$[P_{4441}][OAc]$ 3 24h	$[P_{4441}][OAc]$ 3 24h	41	QC-11	QC-11
17	QC-05	QC-05	42	$[P_{4441}][OAc]$ 2 8h	Ctr 5 $[P_{4441}][OAc]$ 16h
18	Ctr 6 $[P_{4441}][OAc]$ 24h	$[P_{4441}][OAc]$ 1 8h	43	Ctr 5 $[P_{4441}][OAc]$ 16h	$[P_{4441}][OAc]$ 3 16h
19	$[P_{4441}][OAc]$ 1 24h	$[P_{4441}][OAc]$ 5 8h	44	Ctr 6 $[P_{4441}][OAc]$ 8h	$[P_{4441}][OAc]$ 3 8h
20	$[P_{4441}][OAc]$ 5 16h	Ctr 5 $[P_{4441}][OAc]$ 24h	45	QC-12	QC-12
21	QC-06	QC-06	46	Ctr 3 $[P_{4441}][OAc]$ 24h	Ctr 6 $[P_{4441}][OAc]$ 8h
22	$[P_{4441}][OAc]$ 6 16h	Ctr 6 $[P_{4441}][OAc]$ 16h	47	$[P_{4441}][OAc]$ 2 24h	Ctr 2 $[P_{4441}][OAc]$ 24h
23	$[P_{4441}][OAc]$ 1 16h	Ctr 1 $[P_{4441}][OAc]$ 24h	48	Ctr 4 $[P_{4441}][OAc]$ 16h	Ctr 1 $[P_{4441}][OAc]$ 8h
24	Ctr 2 $[P_{4441}][OAc]$ 24h	Ctr 4 $[P_{4441}][OAc]$ 8h	49	QC-13	QC-13
25	QC-07	QC-07	50	QC-14	QC-14

Table S27: Injection sequence: Of the samples treated with $[P_{14444}][OAc]$ in negative and positive mode

	Positive mode	Negative mode		Positive mode	Negative mode
Injection order	**Sample name**		**Injection order**	**Sample name**	
1	QC-01	QC-01	26	$[P_{14444}][OAc]$ 6 8h	Ctr 2 $[P_{14444}][OAc]$ 16h
2	Ctr 3 $[P_{14444}][OAc]$ 16h	$[P_{14444}][OAc]$ 2 24h	27	Ctr 3 $[P_{14444}][OAc]$ 24h	$[P_{14444}][OAc]$ 6 24h
3	$[P_{14444}][OAc]$ 5 8h	Ctr 4 $[P_{14444}][OAc]$ 8h	28	$[P_{14444}][OAc]$ 5 24h	$[P_{14444}][OAc]$ 5 24h
4	$[P_{14444}][OAc]$ 5 16h	Ctr 6 $[P_{14444}][OAc]$ 24h	29	QC-08	QC-08
5	QC-02	QC-02	30	Ctr 6 $[P_{14444}][OAc]$ 8h	Ctr 2 $[P_{14444}][OAc]$ 24h
6	$[P_{14444}][OAc]$ 1 24h	$[P_{14444}][OAc]$ 3 16h	31	Ctr 5 $[P_{14444}][OAc]$ 16h	$[P_{14444}][OAc]$ 1 24h
7	Ctr 5 $[P_{14444}][OAc]$ 24h	Ctr 3 $[P_{14444}][OAc]$ 16h	32	$[P_{14444}][OAc]$ 4 24h	$[P_{14444}][OAc]$ 4 8h
8	$[P_{14444}][OAc]$ 2 8h	Ctr 5 $[P_{14444}][OAc]$ 16h	33	QC-09	QC-09
9	QC-03	QC-03	34	Ctr 6 $[P_{14444}][OAc]$ 16h	Ctr 5 $[P_{14444}][OAc]$ 8h
10	Ctr 1 $[P_{14444}][OAc]$ 8h	Ctr 1 $[P_{14444}][OAc]$ 8h	35	Ctr 6 $[P_{14444}][OAc]$ 24h	$[P_{14444}][OAc]$ 2 16h
11	$[P_{14444}][OAc]$ 1 8h	Ctr 2 $[P_{14444}][OAc]$ 8h	36	$[P_{14444}][OAc]$ 1 16h	Ctr 5 $[P_{14444}][OAc]$ 24h
12	$[P_{14444}][OAc]$ 2 16h	$[P_{14444}][OAc]$ 3 24h	37	QC-10	QC-10
13	QC-04	QC-04	38	Ctr 2 $[P_{14444}][OAc]$ 8h	$[P_{14444}][OAc]$ 5 16h
14	Ctr 3 $[P_{14444}][OAc]$ 8h	Ctr 4 $[P_{14444}][OAc]$ 24h	39	Ctr 2 $[P_{14444}][OAc]$ 16h	Ctr 4 $[P_{14444}][OAc]$ 16h
15	Ctr 1 $[P_{14444}][OAc]$ 16h	$[P_{14444}][OAc]$ 1 16h	40	Ctr 4 $[P_{14444}][OAc]$ 16h	$[P_{14444}][OAc]$ 4 16h
16	Ctr 5 $[P_{14444}][OAc]$ 8h	Ctr 6 $[P_{14444}][OAc]$ 16h	41	QC-11	QC-11
17	QC-05	QC-05	42	$[P_{14444}][OAc]$ 3 24h	$[P_{14444}][OAc]$ 6 8h
18	$[P_{14444}][OAc]$ 4 16h	$[P_{14444}][OAc]$ 3 8h	43	$[P_{14444}][OAc]$ 6 16h	Ctr 6 $[P_{14444}][OAc]$ 8h
19	$[P_{14444}][OAc]$ 4 8h	$[P_{14444}][OAc]$ 5 8h	44	Ctr 2 $[P_{14444}][OAc]$ 24h	Ctr 3 $[P_{14444}][OAc]$ 24h
20	$[P_{14444}][OAc]$ 6 24h	Ctr 3 $[P_{14444}][OAc]$ 8h	45	QC-12	QC-12
21	QC-06	QC-06	46	$[P_{14444}][OAc]$ 3 16h	Ctr 1 $[P_{14444}][OAc]$ 24h
22	Ctr 4 $[P_{14444}][OAc]$ 8h	$[P_{14444}][OAc]$ 2 8h	47	$[P_{14444}][OAc]$ 2 24h	Ctr 1 $[P_{14444}][OAc]$ 16h
23	Ctr 1 $[P_{14444}][OAc]$ 24h	$[P_{14444}][OAc]$ 6 16h	48	$[P_{14444}][OAc]$ 3 8h	$[P_{14444}][OAc]$ 1 8h
24	Ctr 4 $[P_{14444}][OAc]$ 24h	$[P_{14444}][OAc]$ 4 24h	49	QC-13	QC-13
25	QC-07	QC-07	50	QC-14	QC-14

Table S28: MS measurement windows: Information about design of MS experiments determined with SWATH Tuner software

Experiment	MS Type	Accumulation time (ms)	Pos mode		Neg mode	
			Min m/z	Max m/z	Min m/z	Max m/z
MS	SCAN	80	50	1250	50	1050
MS/MS	SWATH 1	31	50.0	214.6	50.0	342.2
MS/MS	SWATH 2	31	213.6	281.8	341.2	453.6
MS/MS	SWATH 3	31	280.8	390.7	452.6	480.8
MS/MS	SWATH 4	31	389.7	480.4	479.8	507.8
MS/MS	SWATH 5	31	479.4	509	506.8	532.3
MS/MS	SWATH 6	31	508	536.5	531.3	566.8
MS/MS	SWATH 7	31	535.5	610.6	565.8	617.4
MS/MS	SWATH 8	31	609.6	677.1	616.4	687.1
MS/MS	SWATH 9	31	676.1	709.0	686.1	715.0
MS/MS	SWATH 10	31	708.0	735.1	714.0	744.1
MS/MS	SWATH 11	31	734.1	759.1	743.1	755.1
MS/MS	SWATH 12	31	758.1	773.1	754.1	776.0
MS/MS	SWATH 13	31	772.1	790.2	775.0	794.6
MS/MS	SWATH 14	31	789.2	811.2	793.6	807.6
MS/MS	SWATH 15	31	810.2	827.2	806.6	830.3
MS/MS	SWATH 16	31	826.2	856.2	829.3	840.1
MS/MS	SWATH 17	31	855.2	884.3	839.1	859.2
MS/MS	SWATH 18	31	883.3	915.9	858.2	889.1
MS/MS	SWATH 19	31	914.9	983.7	888.1	924.6
MS/MS	SWATH 20	31	982.7	1250.0	923.6	1050.0

Table S29: MS-DIAL Parameters: Used for processing of data with MS-Dial in negative and positive mode

Mode	POSITIVE	NEGATIVE
Data collection parameters		
Retention time begin	0.5	0.5
Retention time end	13	13
Mass range begin	50	50
Mass range end	1250	1050
Centroid parameters		
MS1 tolerance	0.01	0.01
MS2 tolerance	0.025	0.025
Peak detection-based	TRUE	TRUE
Isotope recognition		
Maximum charged number	2	2
Data processing		
Number of threads	4	3
Peak detection parameters		
Smoothing method	Linear Weighted Moving Average	Linear Weighted Moving Average
Smoothing level	3	3
Minimum peak width	5	5
Minimum peak height	3000	1000
Peak spotting parameters		
Mass slice width	0.1	0.1
Exclusion mass list (mass & tolerance)		
Deconvolution parameters		
Peak consideration	Both	Both
Sigma window value	0.5	0.5
Exclude after precursor	TRUE	TRUE
MSP file and MS/MS identification setting		
MSP file	MSDIAL-LipidDBs-VS35-FiehnO.lbm	MSDIAL-LipidDBs-VS35-FiehnO.lbm
Retention time tolerance	0.5	0.5
Accurate mass tolerance (MS1)	0.01	0.01
Accurate mass tolerance (MS2)	0.05	0.05
Identification score cut off	80	80
Text file and post identification (retention time and accurate mass based) setting		
Text file	IS_PostIdentification_Pos.txt	IS_PostIdentification_Neg.txt
Retention time tolerance	0.1	0.1
Accurate mass tolerance	0.01	0.01
Identification score cut off	85	85
Advanced setting for identification		
Relative abundance cut off	0	0
Top candidate report	TRUE	TRUE
Adduct ion setting		
	$[M+H]^+$, $[M+NH4]^+$, $[M+Na]^+$	$[M-H]^-$, $[M-H2O-H]^-$, $[M+Cl]^-$, $[M+FA-H]^-$
Alignment parameters setting		
Reference file	QC-5.abf	QC-05.abf
Retention time tolerance	0.05	0.05
MS1 tolerance	0.015	0.015
Retention time factor	0.5	0.5
MS1 factor	0.5	0.5
Peak count filter	0	0
N% detected in at least one group	51	51
QC at least filter	FALSE	FALSE
Tracking of isotope labels		
Tracking of isotopic labels	FALSE	FALSE

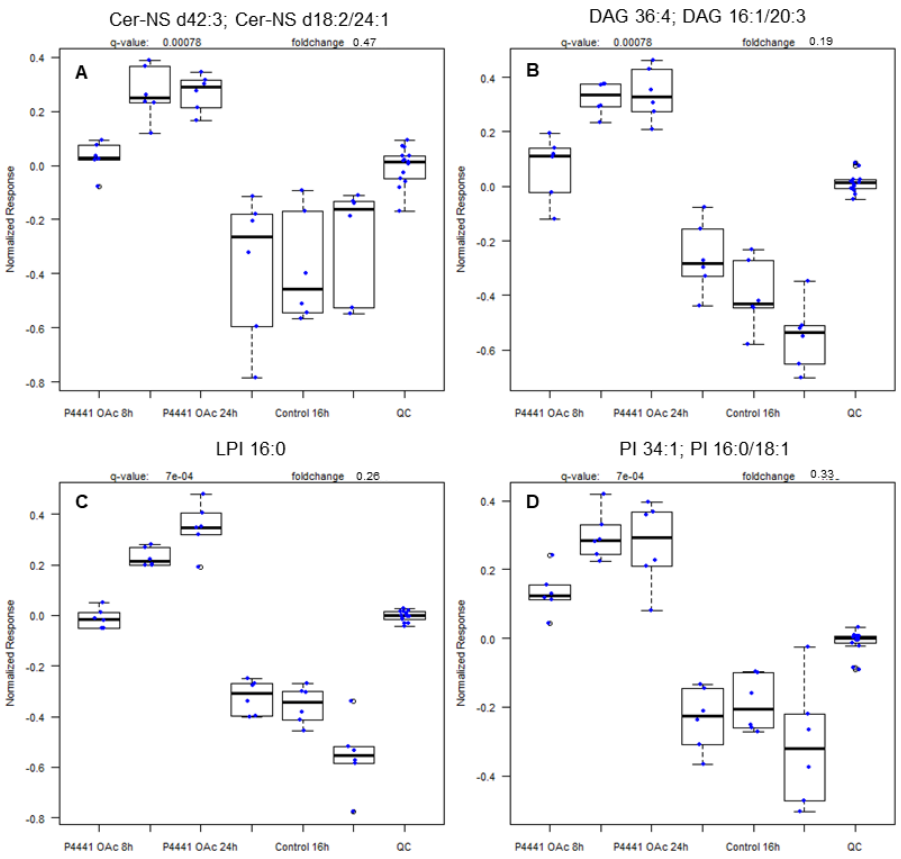

Figure S29: Boxplots: Exemplary boxplots after R script-based comparison of [P_{4441}][OAc] treated samples (16h treatment) with the corresponding control samples measured in ESI+ (A and B) and ESI– (C and D) mode

3.6.6.1.2. Between-batch feature alignment workflow

For the time-dependence evaluation, significantly altered features after 8h, 16h, and 24h of incubation, thus three tables, were used for alignment for each IL separately. As a result, a list of features for each IL was obtained structured by features present after all incubation periods, present after two periods, or only present after one incubation time (see SI Figure S30A). These lists were further used as reference tables for feature alignment between different ILs (see SI Figure S30B and C).

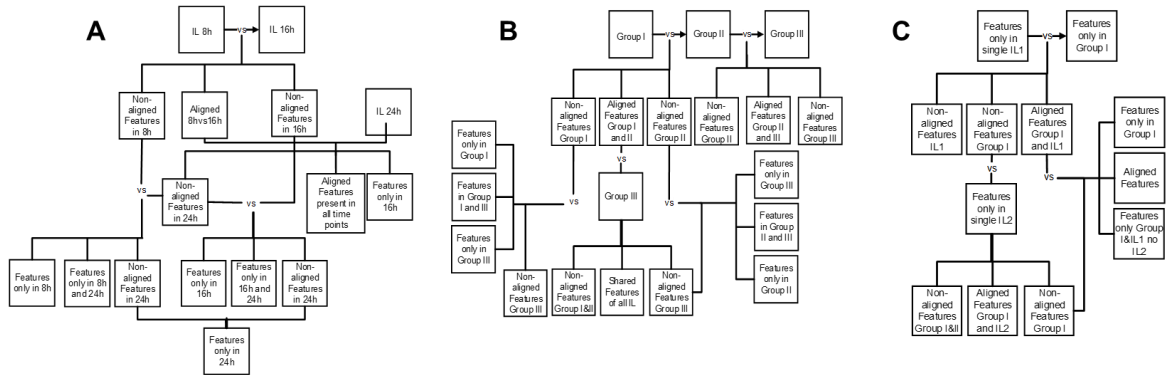

Figure S30: VBA feature alignment workflows: A) Between-batch VBA feature alignment workflow of single ILs and single time points; B) VBA feature alignment workflow with grouped ILs using combined reference tables from ILs in the specific groups prepared after workflow shown in A; C) VBA feature alignment workflow with grouped ILs and single IL (reference tables prepared after workflow A) to obtain features which are only present in one specific IL

Table S30: Validation Results (ESI+): Mean peak areas, precision and accuracy of isotopically labelled internal standards in pre- and post-spiked cell extracts as well as calculated recoveries

positive mode									
Compound	Concentration [µg/mL]	mean peak area		Precision %CV		Accuracy [%]		RE [%]	
		post-spike	pre-spike	post-spike	pre-spike	post-spike	pre-spike		mean
15:0-18:1(d7) DAG	0.22	1.09E+05	8.81E+04	3.91	3.98	100	101	80	79
	0.44	2.17E+05	1.70E+05	2.89	3.17	100	99	78	
	0.88	4.33E+05	3.40E+05	1.73	3.82	100	100	79	
15:0-18:1(d7) PC	3.77	5.55E+06	5.54E+06	2.88	6.67	98	101	100	100
	7.53	1.08E+07	1.06E+07	1.51	3.11	102	99	98	
	15.06	2.05E+07	2.09E+07	4.75	4.12	100	100	102	
15:0-18:1(d7) PE	0.13	3.82E+04	3.44E+04	4.07	6.80	104	103	90	92
	0.27	7.02E+04	6.55E+04	3.79	4.75	95	97	93	
	0.53	1.43E+05	1.31E+05	1.06	3.52	101	101	91	
15:0-18:1(d7) PI NH_4^+	0.21	2.00E+04	2.35E+04	3.23	2.65	102	98	118	109
	0.43	4.03E+04	4.44E+04	5.33	1.73	98	101	110	
	0.85	8.28E+04	8.18E+04	6.06	4.54	100	100	99	
15:0-18:1(d7)-15:0 TAG	1.32	1.60E+06	7.07E+05	1.97	7.14	102	113	44	41
	2.64	3.18E+06	1.21E+06	3.33	5.63	98	92	38	
	5.28	6.71E+06	2.81E+06	2.84	3.00	100	102	42	
18:1(d7) Chol Ester	8.23	1.73E+05	7.56E+04	5.52	9.23	96	92	44	41
	16.46	2.78E+05	1.15E+05	5.45	2.73	104	106	41	
	32.91	4.59E+05	1.76E+05	7.42	5.17	100	99	38	
18:1(d7) LPC	0.60	7.82E+05	7.85E+05	4.97	3.27	101	101	100	99
	1.19	1.54E+06	1.52E+06	2.54	3.67	99	99	99	
	2.38	3.13E+06	3.04E+06	3.32	5.74	100	100	97	
18:1(d7) LPE	0.12	2.79E+04	2.69E+04	4.18	1.51	99	101	97	93
	0.25	5.84E+04	5.31E+04	4.23	3.30	101	99	91	
	0.49	1.12E+05	1.03E+05	4.88	3.23	100	100	92	
18:1(d7) MAG	0.05	1.98E+03	1.92E+03	3.02	4.70	95	104	97	92
	0.09	3.86E+03	3.24E+03	6.2	5.73	104	96	84	
	0.18	7.34E+03	6.92E+03	2.46	3.44	99	101	94	
d18:1-18:1(d9) SM	0.74	4.87E+05	4.92E+05	3.87	5.23	101	98	101	97
	1.48	9.78E+05	9.63E+05	2.8	2.44	99	101	98	
	2.96	2.01E+06	1.84E+06	3.76	6.36	100	100	92	
d18:1-18:0(d7) Cer	0.19	5.95E+04	5.70E+04	2.1	2.93	100	99	96	98
	0.38	1.14E+05	1.14E+05	2.76	1.34	100	101	99	
	0.75	2.24E+05	2.19E+05	3.96	2.67	100	100	98	

Table S31: Validation results (ESI-): Mean peak areas, precision and accuracy of isotopically labelled internal standards in pre- and post-spiked cell extracts as well as calculated recoveries

negative mode									
Compound	Concentration [µg/mL]	mean peak area		Precision %CV		Accuracy [%]		RE [%]	
		post-spike	pre-spike	post-spike	pre-spike	post-spike	pre-spike		mean
15:0-18:1(d7) DAG	0.22	1.86E+03	1.55E+03	4.76	4.26	104	99	83	88
	0.44	3.02E+03	2.76E+03	7.68	2.76	98	101	91	
	0.88	5.68E+03	5.09E+03	3.3	4.81	101	100	90	
15:0-18:1(d7) PC	3.77	2.39E+05	2.36E+05	3.87	4.08	98	98	99	98
	7.53	4.74E+05	4.66E+05	3.1	2.73	102	102	98	
	15.06	9.05E+05	8.87E+05	2.67	1.82	100	100	98	
15:0-18:1(d7) PE	0.13	9.41E+03	9.17E+03	3.61	3.31	101	100	97	95
	0.27	1.91E+04	1.82E+04	2.04	1.49	99	100	95	
	0.53	3.77E+04	3.47E+04	2.05	4.26	100	100	92	
15:0-18:1(d7) PG Na^+	0.67	5.13E+04	5.07E+04	2.82	0.97	99	100	99	99
	1.34	9.92E+04	9.76E+04	3.15	1.35	101	100	98	
	2.67	1.91E+05	1.90E+05	3.3	2.17	100	100	99	
15:0-18:1(d7) PI $NH4^+$	0.21	2.44E+04	2.54E+04	4.6	2.10	100	100	104	102
	0.43	4.64E+04	4.71E+04	2.91	1.96	100	100	102	
	0.85	8.82E+04	8.79E+04	2.37	1.10	100	100	100	
18:1(d7) LPC	0.60	1.02E+05	1.03E+05	2.9	1.38	99	101	100	102
	1.19	2.04E+05	2.06E+05	2.48	1.97	101	99	101	
	2.38	4.02E+05	4.22E+05	3.78	2.30	100	100	105	
18:1(d7) LPE	0.12	2.47E+04	2.28E+04	2.12	2.63	101	102	93	94
	0.25	4.86E+04	4.56E+04	2.81	3.59	99	98	94	
	0.49	9.51E+04	9.04E+04	2.09	0.39	100	100	95	
18:1(d7) MAG	0.05	4.34E+02	3.99E+02	2.52	3.05	105	104	92	95
	0.09	9.41E+02	9.09E+02	7.04	9.11	95	95	97	
	0.18	2.42E+03	2.37E+03	5.99	2.93	101	101	98	
d18:1-18:1(d9) SM	0.74	2.48E+04	2.48E+04	4.3	1.12	98	99	100	100
	1.48	5.17E+04	5.08E+04	2.59	5.76	102	101	98	
	2.96	1.01E+05	1.01E+05	3	4.48	100	100	100	
20:4(d8)AA	0.06	3.79E+03	3.50E+03	4.92	6.35	102	102	92	94
	0.13	8.53E+03	7.99E+03	4.56	4.60	99	97	94	
	0.25	1.72E+04	1.67E+04	1.1	3.94	100	101	98	
d18:1-18:0(d7) Cer	0.19	2.92E+04	2.96E+04	2.07	1.40	101	100	101	102
	0.38	6.06E+04	6.19E+04	3.54	1.37	99	100	102	
	0.75	1.23E+05	1.25E+05	4.33	3.23	100	100	101	

Table S32: Fold change values: Of [Ch][OAc] treated cells after 8h, 16h and 24h, measured in ESI+

[Ch][OAc] ESI +	p-value			Fold change			[Ch][OAc] ESI +	p-value			Fold change		
Name	**8h**	**16h**	**24h**	**8h**	**16h**	**24h**	**Name**	**8h**	**16h**	**24h**	**8h**	**16h**	**24h**
CE 18:2	-	0.00154	-	-	0.61	-	TAG 47:3; TAG 14:0-16:0-17:3	-	0.00285	-	-	0.58	-
CE 22:2	-	0.01124	-	-	0.54	-	TAG 48:1; TAG 14:0-16:0-18:1	-	-	0.00434	-	-	0.80
CE 22:4	-	0.02652	-	-	0.57	-	TAG 48:2; TAG 12:0-16:0-20:2	-	0.00068	-	-	0.56	-
Cer-NDS d38:0; Cer-NDS d18:0/20:0	-	0.01368	0.00078	-	1.67	1.91	TAG 48:2; TAG 14:0-16:1-18:1	-	0.00185	-	-	0.50	-
Cer-NDS d38:2; Cer-NDS d18:0/20:2	-	0.00398	-	-	0.70	-	TAG 48:2; TAG 16:0-16:0-16:2	-	0.00234	-	-	0.65	-
Cer-NDS d40:0; Cer-NDS d18:0/22:0	-	0.00162	0.00035	-	2.42	3.53	TAG 48:3; TAG 12:0-16:1-20:2	-	0.00038	-	-	0.49	-
Cer-NDS d42:0; Cer-NDS d18:0/24:0	-	0.00779	0.00088	-	2.10	4.30	TAG 48:3; TAG 14:0-16:1-18:2	-	0.00026	-	-	0.48	-
Cer-NDS d42:1; Cer-NDS d18:0/24:1	-	0.01139	0.00220	-	1.71	2.04	TAG 49:1; TAG 15:0-17:0-17:1	-	0.01521	-	-	0.45	-
Cer-NDS d44:1; Cer-NDS d18:0/26:1	-	0.00220	0.00066	-	2.15	3.13	TAG 49:2; TAG 16:0-16:0-17:2	-	0.01645	-	-	0.70	-
Cer-NS d34:1; Cer-NS d18:1/16:0	-	0.00330	0.00002	-	0.71	0.69	TAG 49:3; TAG 15:1-17:0-17:2	-	0.00801	-	-	0.59	-
Cer-NS d36:1; Cer-NS d18:1/18:0	-	0.01576	-	-	0.65	-	TAG 49:3; TAG 15:2-17:0-17:1	-	0.00985	-	-	0.66	-
Cer-NS d40:3; Cer-NS d18:2/22:1	-	0.03189	0.00203	-	0.73	0.66	TAG 49:3; TAG 15:3-17:0-17:0	-	0.01314	-	-	0.65	-
Cer-NS d42:3; Cer-NS d18:2/24:1	-	0.00851	-	-	0.66	-	TAG 49:4; TAG 15:2-16:1-18:1	-	0.00475	-	-	0.61	-
DAG 30:0; DAG 14:0-16:0	0.00146	-	-	1.57	-	-	TAG 50:1; TAG 16:0-16:0-18:1	-	0.00884	-	-	0.45	-
DAG 32:0; DAG 16:0-16:0	0.00038	-	-	1.61	-	-	TAG 50:2; TAG 14:0-16:0-20:2	-	-	0.00218	-	-	0.73
DAG 32:1; DAG 16:0-16:1	-	-	0.00511	-	-	0.67	TAG 50:2; TAG 14:0-18:1-18:1	-	-	0.00201	-	-	0.75
DAG 34:2; DAG 16:1-18:1	-	0.00268	-	-	0.68	-	TAG 50:3; TAG 14:0-14:0-22:3	-	0.00664	-	-	0.69	-
DAG 36:2; DAG 18:1-18:1	-	0.00283	0.00368	-	0.63	0.80	TAG 50:3; TAG 14:0-18:0-18:3	-	0.00153	-	-	0.53	-
DAG 36:4; DAG 16:1-20:3	-	0.00164	-	-	0.62	-	TAG 50:3; TAG 14:0-18:1-18:2	-	0.00959	-	-	0.69	-
DAG 40:4; DAG 18:1-22:3	-	0.00724	-	-	0.69	-	TAG 50:4; TAG 14:0-14:0-22:4	-	0.01010	-	-	0.58	-
HexCer-NS d34:1; HexCer-NS d18:1/16:0	-	0.00022	0.00558	-	0.57	0.70	TAG 50:4; TAG 14:0-16:1-20:3	-	-	0.00447	-	-	0.74
HexCer-NS d42:1; HexCer-NS d18:1/24:0	-	0.00618	-	-	0.78	-	TAG 50:4; TAG 16:1-16:1-18:2	-	0.00072	-	-	0.57	-
LPC 14:0	-	0.00698	-	-	0.62	-	TAG 50:5; TAG 14:0-16:2-20:3	-	-	0.00207	-	-	0.59
LPC 18:1	-	0.00730	-	-	0.74	-	TAG 51:1; TAG 16:0-17:0-18:1	-	0.03220	-	-	0.75	-
LPC 20:1	-	0.02031	-	-	0.68	-	TAG 51:2; TAG 15:0-15:0-21:2	-	-	0.00188	-	-	0.61
LPE 18:1	-	0.02983	-	-	0.73	-	TAG 51:2; TAG 16:0-17:1-18:1	-	0.00113	-	-	0.61	-
PC 16:1e; PC 14:1e/2:0	-	0.00278	0.00228	-	0.65	0.76	TAG 51:2; TAG 16:1-17:0-18:1	-	0.00960	-	-	0.32	-
PC 18:1e; PC 16:1e/2:0	-	-	0.00014	-	-	0.72	TAG 51:3; TAG 15:0-17:0-19:3	-	0.00601	-	-	0.46	-
PC 30:2; PC 14:0-16:2	-	0.03233	-	-	0.71	-	TAG 51:4; TAG 15:0-17:2-19:2	-	0.01798	-	-	0.57	-
PC 32:2; PC 16:1-16:1	-	0.02261	-	-	0.75	-	TAG 52:1; TAG 16:0-16:0-20:1	-	0.00456	-	-	0.67	-
PC 32:3; PC 14:0-18:3	-	0.02990	-	-	0.74	-	TAG 52:1; TAG 16:0-18:0-18:1	-	0.00644	-	-	0.67	-
PC 34:0; PC 16:0-18:0	0.00328	-	0.00399	1.59	-	1.22	TAG 52:2; TAG 16:0-16:1-20:1	-	0.02646	0.00177	-	0.77	0.73
PC 36:0; PC 18:0-18:0	-	0.01157	0.00520	-	1.51	1.66	TAG 52:3; TAG 16:0-16:0-20:3	-	0.00216	-	-	0.73	-
PC 36:3e; PC 14:0e/22:3	-	0.00209	0.00008	-	0.64	0.64	TAG 52:3; TAG 16:0-18:1-18:2	-	0.00626	-	-	0.72	-
PC 36:5; PC 16:1-20:4	-	0.01940	0.00181	-	0.79	0.77	TAG 52:3; TAG 16:1-18:1-18:1	-	0.00227	-	-	0.73	-
PC 38:3e; PC 16:0e/22:3	-	0.02070	-	-	0.70	-	TAG 52:4; TAG 16:0-16:0-20:4	-	0.00453	-	-	0.56	-
PC 38:4e; PC 14:0e/24:4	-	0.01864	-	-	0.72	-	TAG 52:4; TAG 16:1-16:1-20:2	-	0.02930	-	-	0.61	-
PC 38:5; PC 18:1-20:4	-	0.02759	-	-	0.81	-	TAG 52:4; TAG 16:1-18:1-18:2	-	0.00400	-	-	0.48	-
PC 38:6e; PC 16:0e/22:6	0.00029	0.00073	0.00003	0.81	0.59	0.53	TAG 52:5; TAG 16:1-16:1-20:3	-	0.00518	-	-	0.49	-
PC 40:3e; PC 18:0e/22:3	-	0.00879	-	-	0.80	-	TAG 53:3; TAG 17:0-17:1-19:2	-	0.01134	-	-	0.49	-
PC 40:4e; PC 14:0e/26:4	-	0.02388	0.00222	-	0.69	0.76	TAG 53:3; TAG 17:1-18:1-18:1	-	0.02609	-	-	0.66	-

Table S32: Fold change values: Of [Ch][OAc] treated cells after 8h, 16h and 24h, measured in ESI+ (Continuation)

[Ch][OAc] ESI +	p-value			Fold change			[Ch][OAc] ESI +	p-value			Fold change		
Name	**8h**	**16h**	**24h**	**8h**	**16h**	**24h**	**Name**	**8h**	**16h**	**24h**	**8h**	**16h**	**24h**
PC 44:2; PC 22:1-22:1	0.00157	-	-	1.45	-	-	TAG 54:2; TAG 16:0-18:1-20:1	-	0.00639	-	-	0.66	-
PE 35:1e; PE 16:0e/19:1	-	0.01036	0.00203	-	0.72	0.73	TAG 54:2; TAG 16:0-19:1-19:1	-	0.01073	-	-	0.68	-
PE 36:1; PE 18:0-18:1	0.00222	-	0.00077	1.47	-	1.29	TAG 54:3; TAG 16:0-18:2-20:1	-	0.02140	-	-	0.57	-
PE 37:3e; PE 16:1e/21:2	-	0.00027	0.00595	-	0.61	0.67	TAG 54:3; TAG 18:1-18:1-18:1	-	0.02112	-	-	0.46	-
PE 38:1; PE 18:0-20:1	0.00123	-	0.00295	1.61	-	1.56	TAG 54:4; TAG 16:0-18:1-20:3	-	0.01144	-	-	0.44	-
PG 36:2; PG 20:0-16:2	-	0.03188	-	-	0.78	-	TAG 54:4; TAG 16:1-18:1-20:2	-	0.01951	-	-	0.48	-
PG 38:2; PG 18:0-20:2	-	0.00013	0.00042	-	0.50	0.57	TAG 54:4; TAG 18:1-18:1-18:2	-	0.01882	-	-	0.41	-
SM d34:0; SM d14:0/20:0	0.00321	-	-	1.57	-	-	TAG 54:5; TAG 16:0-18:4-20:1	-	-	0.00106	-	-	0.70
SM d40:0; SM d14:0/26:0	0.00381	-	0.00366	1.47	-	1.67	TAG 54:5; TAG 16:1-18:1-20:3	-	0.00039	-	-	0.63	-
SM d40:1; SM d14:0/26:1	0.00387	-	0.00403	1.64	-	1.35	TAG 54:6; TAG 16:1-18:1-20:4	-	0.00299	-	-	0.47	-
SM d42:0; SM d14:0/28:0	-	-	0.00354	-	-	1.73	TAG 55:4; TAG 15:0-18:1-22:3	-	0.01984	0.00480	-	0.69	0.71
SM d42:1; SM d14:0/28:1	0.00255	-	-	1.51	-	-	TAG 55:5; TAG 17:0-19:2-19:3	-	0.01387	-	-	0.56	-
SM d42:2; SM d20:0/22:2	0.00335	-	0.00143	1.66	-	1.47	TAG 56:2; TAG 18:0-18:1-20:1	-	0.02862	-	-	0.66	-
SM d44:4; SM d14:2/30:2	0.00299	-	-	1.54	-	-	TAG 56:3; TAG 18:1-18:1-20:1	-	0.01226	-	-	0.69	-
TAG 42:0; TAG 12:0-14:0-16:0	-	0.02141	-	-	0.57	-	TAG 56:4; TAG 16:3-19:1-21:0	-	0.00117	-	-	0.62	-
TAG 42:1; TAG 12:0-14:0-16:1	-	0.00165	-	-	0.58	-	TAG 56:4; TAG 18:1-18:1-20:2	-	0.02356	-	-	0.49	-
TAG 43:0; TAG 13:0-14:0-16:0	-	0.01847	-	-	0.64	-	TAG 56:5; TAG 16:0-18:3-22:2	-	0.00069	-	-	0.67	-
TAG 44:0; TAG 14:0-14:0-16:0	-	0.02613	-	-	0.51	-	TAG 56:5; TAG 18:1-18:1-20:3	-	0.00086	-	-	0.56	-
TAG 44:1; TAG 12:0-14:0-18:1	-	0.00248	-	-	0.57	-	TAG 56:6; TAG 16:0-20:3-20:3	-	0.01208	-	-	0.52	-
TAG 45:0; TAG 13:0-16:0-16:0	-	0.00850	-	-	0.52	-	TAG 56:7; TAG 16:1-20:3-20:3	-	0.00990	-	-	0.51	-
TAG 45:1; TAG 13:0-16:0-16:1	-	0.00919	-	-	0.57	-	TAG 58:3; TAG 16:0-20:1-22:2	-	0.02775	-	-	0.53	-
TAG 46:1; TAG 14:0-14:0-18:1	-	0.00367	-	-	0.51	-	TAG 58:5; TAG 18:1-18:2-22:2	-	0.01714	-	-	0.59	-
TAG 46:1; TAG 14:0-16:0-16:1	-	0.00149	-	-	0.57	-	TAG 58:6; TAG 18:1-20:2-20:3	-	0.00458	-	-	0.65	-
TAG 46:2; TAG 12:0-16:1-18:1	-	0.00092	-	-	0.52	-	TAG 58:6; TAG 18:4-20:0-20:2	-	0.01225	-	-	0.56	-
TAG 46:2; TAG 14:0-16:1-16:1	-	-	0.00172	-	-	0.63	TAG 58:7; TAG 18:1-20:3-20:3	-	0.01050	-	-	0.37	-
TAG 46:3; TAG 12:0-16:1-18:2	-	0.00074	-	-	0.55	-	TAG 60:6; TAG 18:2-20:2-22:2	-	0.02457	-	-	0.46	-
TAG 47:0; TAG 13:0-16:0-18:0	-	0.03135	-	-	0.75	-	TAG 60:7; TAG 18:1-21:3-21:3	-	0.01717	-	-	0.45	-
TAG 47:1; TAG 13:0-15:0-19:1	-	0.00206	-	-	0.57	-	TAG 60:8; TAG 18:1-20:1-22:6	-	0.00046	0.00171	-	0.61	0.63
TAG 47:2; TAG 14:0-16:0-17:2	-	0.00372	-	-	0.58	-	TAG 64:6; TAG 20:1-22:2-22:3	0.00031	-	-	1.61	-	-

Table S33: Fold change values*:* Of [Ch][OAc] treated cells after 8h, measured in ESI-

[Ch][OAc] ESI -	p-value	Fold change	[Ch][OAc] ESI -	p-value	Fold change
Name	**8h**	**8h**	**Name**	**8h**	**8h**
Cer-NDS d42:0; Cer-NDS d18:0/24:0	0.03456	2.32	PE 34:2e; PE 16:1e/18:1	0.04453	1.25
Cer-NS d42:2; Cer-NS d18:1/24:1	0.04771	1.25	PE 34:2e; PE 18:2e/16:0	0.00584	1.21
HexCer-NDS d40:0; HexCer-NDS d21:0/19:0	0.03319	1.75	PE 34:3e; PE 16:1e/18:2	0.00741	1.40
HexCer-NS d40:1; HexCer-NS d21:1/19:0	0.03077	1.22	PE 36:1; PE 18:0-18:1	0.03021	1.24
HexCer-NS d42:1; HexCer-NS d22:1/20:0	0.01648	1.33	PE 36:2; PE 18:1-18:1	0.01157	1.30
LPE 16:0	0.01021	1.29	PE 36:2e; PE 18:1e/18:1	0.02218	1.23
LPE 18:0	0.00385	1.40	PE 36:3e; PE 18:2e/18:1	0.03256	1.19
LPE 18:1	0.01424	1.19	PE 36:4e; PE 16:1e/20:3	0.00772	1.25
LPE 20:3	0.0018	1.29	PE 38:2; PE 18:1-20:1	0.00878	1.28
LPE 22:3	0.01159	1.37	PE 38:3; PE 18:0-20:3	0.01535	1.30
LPG 18:1	0.03144	1.25	PE 38:3; PE 18:1-20:2	0.02147	1.52
LPI 18:1	0.0017	1.66	PE 38:3e; PE 16:1e/22:2	0.02053	1.22
OxPE 34:1+1O; OxPE 16:0-18:1+1O	0.00056	1.37	PE 38:4; PE 18:1-20:3	0.02978	1.23
PC 26:0; PC 12:0-14:0	0.02189	1.23	PE 38:4e; PE 18:1e/20:3	0.03249	1.18
PC 28:0; PC 14:0-14:0	0.01936	1.37	PE 38:4e; PE 18:2e/20:2	0.00808	1.26
PC 29:0; PC 14:0-15:0	0.00181	1.37	PE 38:5; PE 18:1-20:4	0.03782	1.27
PC 30:0; PC 14:0-16:0	0.01227	1.23	PE 40:3; PE 18:0-22:3	0.03174	1.40
PC 30:0e; PC 16:0e/14:0	0.02012	1.24	PE 40:3e; PE 18:1e/22:2	0.02456	1.38
PC 30:1; PC 14:0-16:1	0.03271	1.24	PE 40:4; PE 18:1-22:3	0.01583	1.39
PC 31:0; PC 15:0-16:0	0.00183	1.32	PE 40:4e; PE 18:1e/22:3	0.02116	1.27
PC 32:0; PC 16:0-16:0	0.0225	1.34	PE 40:5e; PE 18:2e/22:3	0.03757	1.19
PC 32:1; PC 16:0-16:1	0.02094	1.16	PE 40:6e; PE 18:2e/22:4	0.04870	1.21
PC 32:1e; PC 16:0e/16:1	0.02647	1.21	PI 34:2; PI 16:1-18:1	0.02239	1.28
PC 32:2; PC 16:1-16:1	0.03313	1.24	PI 36:1; PI 18:0-18:1	0.02520	1.23
PC 34:0; PC 16:0-18:0	0.01163	1.49	PI 36:2; PI 18:1-18:1	0.00896	1.26
PC 34:1; PC 16:0-18:1	0.01444	1.23	PI 38:3; PI 18:0-20:3	0.03462	1.19
PC 36:1; PC 18:0-18:1	0.00325	1.22	SM d32:0; SM d14:0/18:0	0.01954	1.40
PC 36:1e; PC 18:0e/18:1	0.02895	1.20	SM d34:0; SM d14:0/20:0	0.00383	1.43
PC 38:2; PC 18:1-20:1	0.01054	1.25	SM d34:1; SM d14:0/20:1	0.01954	1.19
PE 30:1; PE 14:0-16:1	0.01500	1.45	SM d36:1; SM d17:0/19:1	0.04067	1.22
PE 32:0; PE 16:0-16:0	0.01043	1.42	SM d40:1; SM d14:0/26:1	0.00731	1.57
PE 32:3e; PE 16:1e/16:2	0.04768	1.31	SM d40:1; SM d14:1/26:0	0.01547	1.21
PE 34:0; PE 16:0-18:0	0.01116	1.61	SM d40:2; SM d18:0/22:2	0.03782	1.32
PE 34:1; PE 16:0-18:1	0.01735	1.32	SM d42:1; SM d14:0/28:1	0.01203	1.44
PE 34:1e; PE 18:1e/16:0	0.02266	1.34	SM d42:2; SM d20:0/22:2	0.02007	1.22
PE 34:2; PE 16:1-18:1	0.00734	1.29	SM d42:3; SM d16:3/26:0	0.03593	1.20

Table S34: Fold change values: Of [Ch][Hex] treated cells after 16h and 24h, measured in ESI+

[Ch][Hex] ESI +	p-value		Fold change		[Ch][Hex] ESI +	p-value		Fold change	
Name	**16h**	**24h**	**16h**	**24h**	**Name**	**16h**	**24h**	**16h**	**24h**
BMP 38:3; BMP 18:1-20:2	-	0.01441	-	1.53	SM d30:0; SM d14:0/16:0	-	0.02382	-	1.48
BMP 38:4; BMP 18:1-20:3	-	0.00552	-	1.62	SM d32:0; SM d14:0/18:0	-	0.00155	-	1.43
Cer-NDS d32:0; Cer-NDS d18:0/14:0	-	0.0039	-	0.73	SM d32:1; SM d14:0/18:1	-	0.03189	-	1.12
Cer-NDS d38:0; Cer-NDS d18:0/20:0	-	0.00327	-	1.70	SM d32:2; SM d14:0/18:2	-	0.00375	-	1.63
Cer-NDS d40:0; Cer-NDS d18:0/22:0	-	0.00028	-	1.72	SM d34:0; SM d14:0/20:0	-	0.02548	-	1.40
Cer-NDS d42:0; Cer-NDS d18:0/24:0	-	0.00325	-	1.42	SM d34:2; SM d16:0/18:2	-	0.00085	-	1.50
Cer-NS d40:1; Cer-NS d18:1/22:0	-	0.00485	-	1.40	SM d36:0; SM d14:0/22:0	-	0.00132	-	1.85
Cer-NS d40:3; Cer-NS d18:2/22:1	-	0.00459	-	1.68	SM d38:0; SM d14:0/24:0	-	0.00002	-	1.84
Cer-NS d41:2; Cer-NS d18:1/23:1	-	0.00934	-	1.31	SM d40:0; SM d14:0/26:0	-	0.00073	-	1.71
Cer-NS d42:1; Cer-NS d18:1/24:0	-	0.02986	-	1.25	SM d40:1; SM d14:0/26:1	-	0.00214	-	1.66
Cer-NS d42:3; Cer-NS d18:2/24:1	-	0.00562	-	1.50	SM d41:1; SM d14:1/27:0	-	0.02587	-	1.27
Cer-NS d42:4; Cer-NS d18:2/24:2	-	0.00957	-	1.37	SM d42:0; SM d14:0/28:0	-	0.01842	-	1.45
Cer-NS d44:2; Cer-NS d20:1/24:1	-	0.03911	-	1.30	SM d42:1; SM d14:0/28:1	-	0.00223	-	1.60
Cer-NS d44:3; Cer-NS d18:1/26:2	-	0.00731	-	1.44	SM d42:2; SM d14:1/28:1	-	0.0379	-	1.24
DAG 34:0; DAG 16:0-18:0	-	0.03107	-	1.32	SM d42:2; SM d20:0/22:2	-	0.00052	-	1.61
DAG 34:2; DAG 16:1-18:1	-	0.01468	-	1.46	SM d42:3; SM d14:2/28:1	-	0.00456	-	1.35
HexCer-NDS d40:0; HexCer-NDS d18:0/22:0	-	0.00248	-	1.79	SM d44:1; SM d14:0/30:1	-	0.00334	-	1.59
HexCer-NDS d42:0; HexCer-NDS d18:0/24:0	-	0.04005	-	1.46	SM d44:2; SM d14:1/30:1	-	0.03595	-	1.25
HexCer-NS d42:3; HexCer-NS d18:2/24:1	-	0.00768	-	1.49	SM d44:3; SM d14:2/30:1	-	0.03663	-	1.26
LPC 16:0	-	0.00069	-	1.48	SM d44:4; SM d15:3/29:1	-	0.01812	-	1.25
LPC 18:0	-	0.00043	-	1.69	SM d44:5; SM d22:3/22:2	-	0.01652	-	1.48
LPC 18:1	-	0.0116	-	1.24	TAG 44:0; TAG 14:0-14:0-16:0	-	0.00101	-	0.48
LPC 20:0	-	0.00174	-	1.91	TAG 44:1; TAG 12:0-14:0-18:1	-	0.00666	-	0.63
LPC 24:0	-	0.00856	-	1.55	TAG 44:2; TAG 12:0-14:0-18:2	0.00045	0.00009	0.48	0.41
LPE 16:0	-	0.00709	-	1.40	TAG 46:0; TAG 14:0-16:0-16:0	-	0.03353	-	0.74
LPE 18:0	-	0.0013	-	1.55	TAG 46:1; TAG 14:0-14:0-18:1	0.00143	0.00138	0.58	0.58
LPE 18:1	-	0.00669	-	1.39	TAG 46:2; TAG 14:0-14:0-18:2	-	0.00109	-	0.60
LPE 22:3	-	0.0434	-	1.29	TAG 46:2; TAG 14:0-16:0-16:2	0.00436	0.00466	0.68	0.63
MAG 18:0	0.00001	-	0.05	-	TAG 46:2; TAG 14:1-16:0-16:1	-	0.00947	-	0.60
PC 16:1e; PC 14:1e/2:0	-	0.04019	-	1.14	TAG 46:3; TAG 12:1-16:1-18:1	-	0.00377	-	0.64
PC 18:0e; PC 16:0e/2:0	-	0.00023	-	1.83	TAG 47:1; TAG 13:0-15:1-19:0	-	0.00603	-	0.56
PC 20:1e; PC 18:1e/2:0	-	0.01991	-	1.34	TAG 47:1; TAG 15:0-15:1-17:0	-	0.00501	-	0.60
PC 20:2e; PC 18:2e/2:0	-	0.01251	-	1.59	TAG 48:1; TAG 14:0-16:0-18:1	0.00014	0.00025	0.58	0.52
PC 26:1; PC 2:0-24:1	-	0.00019	-	1.91	TAG 48:1; TAG 16:0-16:0-16:1	-	0.00561	-	0.62
PC 28:0e; PC 14:0e/14:0	-	0.00951	-	1.25	TAG 48:2; TAG 12:0-18:1-18:1	0.00069	0.00103	0.64	0.65
PC 28:1; PC 14:0-14:1	-	0.03645	-	1.22	TAG 48:2; TAG 14:0-16:1-18:1	0.00094	0.0013	0.65	0.57
PC 30:0e; PC 14:0e/16:0	-	0.04337	-	1.29	TAG 48:2; TAG 16:0-16:1-16:1	-	0.00009	-	0.62
PC 30:2; PC 14:1-16:1	-	0.0353	-	1.30	TAG 48:3; TAG 14:1-16:1-18:1	-	0.00018	-	0.62
PC 31:2; PC 15:0-16:2	-	0.00036	-	1.95	TAG 48:4; TAG 12:0-16:1-20:3	-	0.03601	-	0.73
PC 32:0e; PC 14:0e/18:0	-	0.01299	-	1.29	TAG 48:4; TAG 14:1-16:1-18:2	-	0.04494	-	0.67
PC 32:1; PC 16:0-16:1	-	0.02104	-	1.25	TAG 49:3; TAG 15:2-17:0-17:1	-	0.01625	-	0.70

Table S34: Fold change values: Of [Ch][Hex] treated cells after 16h and 24h, measured in ESI+ (Continuation)

[Ch][Hex] ESI +	p-value		Fold change		[Ch][Hex] ESI +	p-value		Fold change	
Name	**16h**	**24h**	**16h**	**24h**	**Name**	**16h**	**24h**	**16h**	**24h**
PC 32:1e; PC 14:0e/18:1	-	0.01324	-	1.55	TAG 50:1; TAG 16:0-16:0-18:1	0.0031	0.00624	0.59	0.63
PC 32:2; PC 16:0-16:2	-	0.02681	-	1.23	TAG 50:2; TAG 14:0-16:0-20:2	0.00032	0.00025	0.57	0.52
PC 32:2; PC 16:1-16:1	-	0.0208	-	1.24	TAG 50:2; TAG 14:0-18:1-18:1	0.00255	-	0.69	-
PC 33:2; PC 17:0-16:2	-	0.00248	-	1.67	TAG 50:3; TAG 14:0-16:0-20:3	-	0.00819	-	0.64
PC 34:0; PC 16:0-18:0	-	0.00686	-	1.34	TAG 50:3; TAG 14:0-18:1-18:2	0.00335		0.72	-
PC 34:0e; PC 14:0e/20:0	-	0.00318	-	1.42	TAG 50:3; TAG 16:1-16:1-18:1	0.00005	0.00753	0.65	0.65
PC 34:1e; PC 14:0e/20:1	-	0.00152	-	1.44	TAG 50:4; TAG 12:0-18:1-20:3	-	0.0315	-	0.71
PC 34:2e; PC 14:0e/20:2	-	0.0254	-	1.29	TAG 50:4; TAG 14:0-14:0-22:4	-	0.0158	-	0.65
PC 34:3; PC 16:1-18:2	-	0.00372	-	1.30	TAG 50:5; TAG 14:0-16:1-20:4	-	0.02521	-	0.75
PC 34:4; PC 16:1-18:3	-	0.00255	-	1.27	TAG 51:1; TAG 16:0-17:0-18:1	0.00399	0.00663	0.67	0.63
PC 35:0; PC 17:0-18:0	-	0.01077	-	1.41	TAG 51:2; TAG 16:0-17:1-18:1	-	0.00009	-	0.59
PC 36:0; PC 18:0-18:0	-	0.00072	-	1.62	TAG 51:4; TAG 15:0-17:1-19:3	-	0.00431	-	0.64
PC 36:1; PC 18:0-18:1	-	0.0131	-	1.46	TAG 52:1; TAG 16:0-18:0-18:1	-	0.00153	-	0.53
PC 36:1e; PC 14:0e/22:1	-	0.00476	-	1.62	TAG 52:2; TAG 16:0-18:1-18:1	0.00221	0.00313	0.58	0.61
PC 36:2e; PC 14:0e/22:2	-	0.00658	-	1.52	TAG 52:3; TAG 16:0-16:0-20:3	-	0.04443	-	0.74
PC 36:3; PC 16:0-20:3	-	0.02327	-	1.26	TAG 52:3; TAG 16:0-18:1-18:2	-	0.01219	-	0.69
PC 36:4; PC 16:0-20:4	-	0.0292	-	0.82	TAG 52:3; TAG 16:1-18:1-18:1	0.00014	0.027	0.59	0.54
PC 36:4; PC 18:2-18:2	-	0.0187	-	1.23	TAG 52:4; TAG 16:0-16:0-20:4	-	0.00122	-	0.69
PC 38:1; PC 18:0-20:1	-	0.00957	-	1.73	TAG 52:4; TAG 16:1-18:1-18:2	-	0.01994	-	0.67
PC 38:2; PC 18:1-20:1	-	0.02026	-	1.27	TAG 52:5; TAG 16:1-16:1-20:3	-	0.0067	-	0.71
PC 38:2e; PC 14:0e/24:2	-	0.00695	-	1.44	TAG 53:2; TAG 16:0-16:0-21:2	-	0.00526	-	0.58
PC 38:3; PC 18:1-20:2	-	0.0366	-	1.68	TAG 53:2; TAG 16:1-17:0-20:1	-	0.00207	-	0.57
PC 38:3e; PC 16:0e/22:3	-	0.00277	-	1.32	TAG 53:3; TAG 16:0-18:1-19:2	-	0.00104	-	0.63
PC 38:4; PC 18:1-20:3	-	0.03225	-	1.25	TAG 54:1; TAG 16:0-18:1-20:0	-	0.00164	-	0.67
PC 38:4e; PC 14:0e/24:4	-	0.01545	-	1.27	TAG 54:1; TAG 18:0-18:0-18:1	-	0.01956	-	0.73
PC 38:5; PC 18:1-20:4	-	0.02862	-	1.32	TAG 54:2; TAG 16:0-18:1-20:1	0.00192	0.01778	0.5	0.47
PC 38:6e; PC 16:0e/22:6	-	0.01752	-	0.78	TAG 54:2; TAG 16:0-19:1-19:1	-	0.00018	-	0.73
PC 40:2; PC 18:1-22:1	-	0.00638	-	1.47	TAG 54:2; TAG 18:0-18:1-18:1	-	0.00286	-	0.72
PC 40:2e; PC 14:0e/26:2	-	0.00592	-	1.66	TAG 54:3; TAG 16:0-18:0-20:3	0.0037	0.00189	0.66	0.76
PC 40:3; PC 18:1-22:2	-	0.0031	-	1.45	TAG 54:3; TAG 18:0-18:1-18:2	0.00102	-	0.66	-
PC 40:4; PC 20:1-20:3	-	0.03478	-	2.22	TAG 54:3; TAG 18:1-18:1-18:1	0.00047	0.00199	0.57	0.65
PC 40:4e; PC 14:0e/26:4	-	0.00195	-	1.42	TAG 54:4; TAG 16:0-18:0-20:4	-	0.01021	-	0.62
PC 40:6; PC 20:3-20:3	-	0.00159	-	1.54	TAG 54:4; TAG 16:0-18:1-20:3	-	0.03554	-	0.76
PC 42:2; PC 18:1-24:1	-	0.01817	-	1.54	TAG 54:4; TAG 18:1-18:1-18:2	0.00096	0.00105	0.69	0.57
PC 42:2e; PC 16:0e/26:2	-	0.00215	-	1.67	TAG 54:5; TAG 16:1-18:1-20:3	-	0.00938	-	0.64
PC 42:3; PC 18:1-24:2	-	0.00534	-	1.51	TAG 56:1; TAG 17:0-19:1-20:0	0.00357	-	0.75	-
PC 42:4; PC 21:2-21:2	-	0.00011	-	1.57	TAG 56:2; TAG 16:0-20:1-20:1	-	0.03499	-	0.72
PC 44:3; PC 18:1-26:2	-	0.00075	-	1.68	TAG 56:2; TAG 18:0-18:1-20:1	-	0.00333	-	0.57
PC 44:4; PC 22:2-22:2	-	0.02999	-	1.57	TAG 56:2; TAG 18:0-18:2-20:0	-	0.02579	-	0.67
PE 28:1; PE 14:0-14:1	0.00127	-	0.65	-	TAG 56:3; TAG 18:1-18:1-20:1	-	0.00261	-	0.56
PE 30:0; PE 14:0-16:0	0.00235	-	0.65	-	TAG 56:4; TAG 18:1-18:1-20:2	-	0.00629	-	0.68
PE 30:1; PE 14:0-16:1	-	0.02366	-	1.24	TAG 56:5; TAG 16:0-18:1-22:4	-	0.03462	-	0.78

Table S34: Fold change values: Of [Ch][Hex] treated cells after 16h and 24h, measured in ESI+ (Continuation)

[Ch][Hex] ESI +	p-value		Fold change		[Ch][Hex] ESI +	p-value		Fold change	
Name	**16h**	**24h**	**16h**	**24h**	**Name**	**16h**	**24h**	**16h**	**24h**
PE 32:2; PE 16:1-16:1	-	0.01779	-	1.41	TAG 56:5; TAG 18:1-18:1-20:3	0.00191	0.04128	0.69	0.68
PE 34:0; PE 16:0-18:0	-	0.02188	-	1.16	TAG 56:6; TAG 16:0-20:3-20:3	-	0.01626	-	0.74
PE 34:2; PE 16:0-18:2	-	0.03238	-	1.27	TAG 58:1; TAG 18:1-19:0-21:0	-	0.01017	-	0.71
PE 34:3; PE 16:1-18:2	-	0.02487	-	1.33	TAG 58:2; TAG 16:0-20:1-22:1	-	0.01835	-	0.66
PE 35:1e; PE 14:0e/21:1	-	0.01679	-	0.73	TAG 58:2; TAG 16:0-21:1-21:1	-	0.03722	-	0.71
PE 36:0; PE 18:0-18:0	-	0.00182	-	1.54	TAG 58:3; TAG 16:0-20:1-22:2	-	0.00334	-	0.60
PE 36:1e; PE 16:0e/20:1	-	0.00034	-	2.42	TAG 58:3; TAG 18:1-20:1-20:1	0.00367	-	0.61	-
PE 36:2; PE 18:1-18:1	-	0.01547	-	1.33	TAG 58:4; TAG 18:1-18:1-22:2	-	0.01575	-	0.68
PE 36:3; PE 18:0-18:3	-	0.04004	-	1.34	TAG 58:5; TAG 18:1-20:2-20:2	-	0.00438	-	0.62
PE 38:1; PE 18:0-20:1	-	0.03549	-	1.30	TAG 60:2; TAG 16:2-22:0-22:0	-	0.03216	-	0.67
PE 38:2; PE 18:0-20:2	-	0.00772	-	1.39	TAG 60:2; TAG 18:2-20:0-22:0	-	0.01501	-	0.66
PE 38:3; PE 18:0-20:3	-	0.01281	-	1.24	TAG 60:3; TAG 20:0-20:1-20:2	-	0.02976	-	0.72
PE 38:4; PE 22:0-16:4	-	0.01822	-	1.40	TAG 60:3; TAG 20:1-20:1-20:1	-	0.00525	-	0.50
PE 38:5; PE 18:0-20:5	-	0.03654	-	1.30	TAG 60:4; TAG 16:0-22:1-22:3	-	0.00037	-	0.57
PE 40:2; PE 18:0-22:2	-	0.00351	-	1.35	TAG 60:6; TAG 20:1-20:2-20:3	-	0.02597	-	0.76
PE 40:4; PE 18:1-22:3	-	0.00609	-	1.36	TAG 62:2; TAG 20:1-20:1-22:0	0.00296	0.04263	0.61	0.75
SM d28:0; SM d14:0/14:0	-	0.02881	-	1.32	TAG 64:3; TAG 21:0-21:0-22:3	-	0.03711	-	0.69
					TAG 64:4; TAG 20:1-22:1-22:2	-	0.01211	-	0.68

Table S35: Fold change values*:* Of [Ch][Hex] treated cells after 16h and 24h, measured in ESI-

[Ch][Hex] ESI -	p-value		Fold change		[Ch][Hex] ESI -	p-value		Fold change	
Name	**16h**	**24h**	**16h**	**24h**	**Name**	**16h**	**24h**	**16h**	**24h**
FA 18:0	-	0.04561	-	1.21	PE 36:2e; PE 18:1e/18:1	-	0.00082	-	1.41
HexCer-NDS d34:0; HexCer-NDS d20:0/14:0	-	0.00058	-	1.46	PE 36:3e; PE 16:1e/20:2	-	0.01276	-	1.33
HexCer-NDS d40:0; HexCer-NDS d28:0/12:0	-	0.0021	-	1.59	PE 36:3e; PE 18:2e/18:1	-	0.04105	-	1.22
LPC 16:0	-	0.00856	-	1.37	PE 36:4e; PE 16:1e/20:3	-	0.03534	-	1.23
LPC 18:0	-	0.00198	-	1.71	PE 36:4e; PE 18:3e/18:1	-	0.04163	-	1.26
LPE 16:0	-	0.03868	-	1.29	PE 38:3e; PE 16:1e/22:2	-	0.04363	-	1.23
LPE 18:0	-	0.00124	-	1.57	PE 38:3e; PE 18:2e/20:1	0.00312	0.00017	1.31	1.79
LPE 18:1	-	0.03677	-	1.22	PE 38:4; PE 18:1-20:3	-	0.04069	-	1.25
LPI 18:0	-	0.01215	-	1.23	PE 38:4e; PE 18:1e/20:3	-	0.01066	-	1.27
OxPE 36:1+1O; OxPE 18:1-18:0+1O	-	0.00017	-	1.61	PE 38:4e; PE 18:2e/20:2	-	0.0328	-	1.22
PC 28:0; PC 14:0-14:0	-	0.03302	-	1.33	PE 40:3e; PE 18:0e/22:3	-	0.00108	-	1.79
PC 28:1; PC 14:0-14:1	-	0.03513	-	1.29	PE 40:3e; PE 18:1e/22:2	-	0.00687	-	1.29
PC 30:0e; PC 16:0e/14:0	-	0.01618	-	1.33	PE 40:4e; PE 18:1e/22:3	-	0.00979	-	1.25
PC 30:1; PC 14:0-16:1	-	0.01844	-	1.29	PE 40:5e; PE 18:2e/22:3	-	0.03589	-	1.25
PC 30:2; PC 14:0-16:2	-	0.01371	-	1.27	PG 32:0; PG 16:0-16:0	-	0.01028	-	1.41
PC 32:1e; PC 16:0e/16:1	-	0.04181	-	1.34	PG 34:1; PG 16:0-18:1	-	0.04504	-	1.29
PC 32:2; PC 16:1-16:1	-	0.01342	-	1.28	PI 32:1; PI 16:0-16:1	-	0.03876	-	1.23
PC 34:1e; PC 16:0e/18:1	-	0.00735	-	1.38	PI 36:1; PI 18:0-18:1	-	0.01233	-	1.19
PC 34:2; PC 16:1-18:1	-	0.03347	-	1.23	SM d32:0; SM d14:0/18:0	-	0.00348	-	1.53
PC 34:2e; PC 16:2e/18:0	-	0.01774	-	1.36	SM d34:0; SM d14:0/20:0	-	0.01579	-	1.35
PC 34:3; PC 16:1-18:2	-	0.01867	-	1.34	SM d34:2; SM d16:0/18:2	-	0.002	-	1.57
PC 36:1; PC 18:0-18:1	-	0.03041	-	1.28	SM d36:0; SM d17:0/19:0	-	0.00125	-	1.59
PC 36:3; PC 16:0-20:3	-	0.03097	-	1.24	SM d38:0; SM d14:0/24:0	-	0.00042	-	1.76
PC 36:4; PC 18:2-18:2	-	0.03639	-	1.25	SM d38:2; SM d16:0/22:2	-	0.01972	-	1.35
PC 38:3; PC 20:1-18:2	-	0.01136	-	1.32	SM d40:0; SM d14:0/26:0	-	0.00123	-	1.63
PC 38:4; PC 18:1-20:3	-	0.03225	-	1.25	SM d40:1; SM d17:0/23:1	-	0.02487	-	1.56
PE 34:2e; PE 16:1e/18:1	-	0.03648	-	1.24	SM d42:1; SM d17:1/25:0	-	0.0028	-	1.53
PE 34:3e; PE 16:1e/18:2	-	0.02986	-	1.25	SM d42:2; SM d16:2/26:0	-	0.01806	-	1.51
PE 36:1e; PE 18:0e/18:1	0.00322	0.00031	1.53	2.33	SM d42:3; SM d14:2/28:1	-	0.00766	-	1.42
PE 36:2; PE 18:1-18:1	-	0.0447	-	1.22					

Table S36: Fold change values: Of [emim][OAc] treated cells after 8h, 16h and 24h, measured in ESI+

[emim][OAc] ESI +	p-value			Fold change			[emim][OAc] ESI +	p-value			Fold change		
Name	**8h**	**16h**	**24h**	**8h**	**16h**	**24h**	**Name**	**8h**	**16h**	**24h**	**8h**	**16h**	**24h**
Cer-NDS d34:0; Cer-NDS d18:0/16:0	-	0.00226	0.00017	-	2.23	2.31	PC 38:4; PC 18:1-20:3	-	0.00276	0.00068	-	0.68	0.68
Cer-NDS d36:0; Cer-NDS d18:0/18:0	0.00179	0.00341	0.0003	4.17	6.09	5.65	PC 38:4; PC 19:2-19:2	-	0.00267	0.00186	-	0.68	0.69
Cer-NDS d38:0; Cer-NDS d18:0/20:0	-	0.00944	0.01772	-	4.11	4.50	PC 38:4e; PC 14:0e/24:4	0.00196	0	0	0.54	0.42	0.35
Cer-NDS d40:0; Cer-NDS d18:0/22:0	0.00000	0	0.00008	13.17	13.36	11.11	PC 38:5; PC 18:1-20:4	-	0.00009	0.00363	-	0.61	0.61
Cer-NDS d40:1; Cer-NDS d18:0/22:1	0.0006	-	-	2.66	-	-	PC 38:5e; PC 16:0e/22:5	-	0.00001	0.00002	-	0.44	0.36
Cer-NDS d42:0; Cer-NDS d18:0/24:0	0	0.00002	0.00031	13.16	19.61	23.71	PC 40:2; PC 16:0-24:2	-	0.00002	0.00002	-	2.01	2.51
Cer-NDS d42:1; Cer-NDS d18:0/24:1	0.00027	0.00037	0.00001	6.32	10.26	8.98	PC 40:3e; PC 18:0e/22:3	-	0.00528	0.01923	-	1.85	1.49
Cer-NS d32:1; Cer-NS d18:1/14:0	-	0.00021	0.00005	-	0.47	0.42	PC 40:4; PC 18:1-22:3	-	0.01	0.00188	-	0.80	0.72
Cer-NS d34:1; Cer-NS d18:1/16:0	-	0.00024	0.00006	-	0.57	0.53	PC 40:4e; PC 14:0e/26:4	-	0.00002	0.01328	-	0.57	0.61
Cer-NS d36:1; Cer-NS d18:1/18:0	-	-	0.00683	-	-	0.54	PC 40:5; PC 18:1-22:4	-	0.00661	0.00916	-	0.68	0.72
Cer-NS d38:1; Cer-NS d18:1/20:0	-	-	0.01444	-	-	0.63	PC 40:6; PC 20:3-20:3	-	0.00433	0.00244	-	0.64	0.69
Cer-NS d38:2; Cer-NS d18:1/20:1	-	0.00021	0.00002	-	0.52	0.48	PC 42:2; PC 21:1-21:1	-	0	0	-	3.25	4.37
Cer-NS d40:2; Cer-NS d18:1/22:1	-	0.00041	0.0004	-	0.52	0.52	PC 44:2; PC 22:1-22:1	-	0.00003	0.00001	-	5.03	7.23
Cer-NS d40:3; Cer-NS d18:2/22:1	-	0.00002	0.00001	-	0.51	0.37	PE 30:1; PE 14:0-16:1	-	0.01275		-	1.40	-
Cer-NS d42:2; Cer-NS d18:1/24:1	-	-	0.01057	-	-	1.86	PE 32:0; PE 16:0-16:0	-	-	0.00756	-	-	1.98
Cer-NS d42:3; Cer-NS d18:2/24:1	-	0.00481	-	-	1.62	-	PE 32:1; PE 16:0-16:1	-	-	0.00702	-	-	1.52
DAG 32:1; DAG 16:0-16:1	-	0.00011	0.01964	-	2.12	1.49	PE 34:1; PE 16:0-18:1	-	-	0.01686	-	-	1.37
DAG 34:1; DAG 16:0-18:1	-	-	0.001	-	-	0.57	PE 35:1e; PE 16:0e/19:1	-	-	0.01725	-	-	0.75
DAG 36:2; DAG 18:1-18:1	-	0.00162	-	-	1.88	-	PE 38:1; PE 17:0-21:1	-	-	0.0164	-	-	2.04
LPC 16:0	-	0.01232	0.0009	-	1.37	1.84	PG 32:2; PG 16:1-16:1	0.00085	0.0009	0.01032	0.55	0.58	0.55
LPC 18:0	-	0	0	-	2.40	3.60	SM d28:0; SM d14:0/14:0	-	0.00023	0.00007	-	2.22	2.08
LPC 20:0	-	0.0005	0.00005	-	3.19	4.90	SM d30:0; SM d14:0/16:0	-	0.00421	0.00264	-	1.78	1.84
LPC 26:0	-	-	0.01204	-	-	1.22	SM d32:0; SM d14:0/18:0	-	0	0.00032	-	2.61	2.27
LPE 16:0	-	-	0.00019	-	-	1.88	SM d34:0; SM d14:0/20:0	-	0.00017	0.00008	-	1.86	2.07
LPE 18:1	-	-	0.0039	-	-	1.39	SM d34:3; SM d14:1/20:2	-	0.00067	0.00103	-	1.96	2.12
PC 20:3e; PC 18:3e/2:0	-	0.00036	0.01308	-	0.60	0.66	SM d36:0; SM d14:0/22:0	-	0.00003	0.00002	-	2.34	2.61
PC 26:0; PC 13:0-13:0	-	0.00005	0.00052	-	1.91	2.21	SM d36:1; SM d14:1/22:0	-	0.00411	0	-	1.32	1.33
PC 28:0; PC 14:0-14:0	-	0.00857	0.00085	-	1.48	1.77	SM d38:0; SM d14:0/24:0	-	0.00132	0.01077	-	2.56	2.76
PC 28:0e; PC 14:0e/14:0	-	-	0.0213	-	-	1.68	SM d40:0; SM d14:0/26:0	-	0.00077	0	-	2.97	3.26
PC 30:0; PC 14:0-16:0	-	-	0.00442	-	-	1.36	SM d40:1; SM d14:0/26:1	-	0.0001	0.00038	-	2.02	2.33
PC 30:0e; PC 14:0e/16:0	-	0.0078	0.00327	-	1.29	1.41	SM d40:1; SM d14:1/26:0	-	-	0.00029	-	-	1.35
PC 30:2; PC 14:0-16:2	-	0.0037	0.01053	-	0.73	0.73	SM d42:0; SM d14:0/28:0	-	0.00126	0.02065	-	5.07	6.81
PC 30:2; PC 15:1-15:1	-	0.01108	-	-	0.67	-	SM d42:1; SM d14:0/28:1	-	0.00074	0.00031	-	2.65	2.97
PC 32:2; PC 16:1-16:1	-	0.00881	-	-	0.74	-	SM d42:4; SM d15:3/27:1	-	-	0.00007	-	-	1.40
PC 32:3; PC 14:0-18:3	-	0.00117	0.00107	-	0.64	0.64	SM d44:1; SM d14:0/30:1	-	0.00041	0.00668	-	2.92	3.07
PC 32:3; PC 16:1-16:2	-	0.00025	0.00292	-	0.60	0.65	SM d44:5; SM d22:3/22:2	-	0.00041	0.00001	-	2.16	2.58
PC 33:0; PC 16:0-17:0	-	-	0.01585	-	-	1.36	TAG 48:1; TAG 14:0-16:0-18:1	-	-	0.00138	-	-	0.59
PC 34:0; PC 16:0-18:0	-	0	0.00001	-	1.87	2.20	TAG 48:3; TAG 14:0-16:1-18:2	-	-	0.00871	-	-	0.29
PC 34:0e; PC 14:0e/20:0	-	0.00001	0.00003	-	3.17	3.12	TAG 48:3; TAG 14:1-16:1-18:1	-	-	0.0207	-	-	0.3
PC 34:3; PC 18:1-16:2	-	0.00465	-	-	0.72	-	TAG 50:4; TAG 14:0-16:1-20:3	-	-	0.01582	-	-	0.27
PC 36:0; PC 18:0-18:0	-	0.00002	0.00027	-	3.82	6.88	TAG 52:2; TAG 16:0-18:1-18:1	-	0.0026	0.00012	-	0.58	0.47

Table S36: Fold change values: Of [emim][OAc] treated cells after 8h, 16h and 24h, measured in ESI+ (Continuation)

[emim][OAc] ESI +	p-value			Fold change			[emim][OAc] ESI +	p-value			Fold change		
Name	**8h**	**16h**	**24h**	**8h**	**16h**	**24h**	**Name**	**8h**	**16h**	**24h**	**8h**	**16h**	**24h**
PC 36:1; PC 18:0-18:1	-	0.00009	0.00016	-	1.63	2.03	TAG 52:4; TAG 16:0-16:0-20:4	-	-	0.00091	-	-	0.38
PC 36:1e; PC 14:0e/22:1	-	0.00002	0.00002	-	1.96	2.65	TAG 53:3; TAG 17:1-18:1-18:1	-	-	0.00475	-	-	0.36
PC 36:3e; PC 14:0e/22:3	-	0.00038	0.0002	-	0.66	0.61	TAG 54:3; TAG 18:1-18:1-18:1	-	0.00215	0.00002	-	0.43	0.30
PC 36:4; PC 16:0-20:4	-	0.00278	-	-	0.67	-	TAG 56:3; TAG 16:1-18:1-22:1	-	-	0.00187	-	-	0.36
PC 36:4; PC 18:2-18:2	-	0.00285	0.00255	-	0.61	0.65	TAG 56:3; TAG 16:1-20:1-20:1	-	0.00023	0.00046	-	0.41	0.31
PC 38:1; PC 18:0-20:1	-	0	0	-	2.49	3.03	TAG 56:4; TAG 18:1-18:1-20:2	-	0.00147	0.00001	-	0.40	0.24
PC 38:2; PC 18:1-20:1	-	0.00531	0.00159	-	1.34	1.43	TAG 56:5; TAG 18:1-18:1-20:3	0.00007	0.00038	0	0.48	0.34	0.21
PC 38:2; PC 19:1-19:1	-	0.00551	0.00348	-	1.31	1.42	TAG 56:5; TAG 18:1-18:2-20:2	-	-	0.00592	-	-	0.23
PC 38:2e; PC 14:0e/24:2	-	0.00009	0.00008	-	1.95	2.09	TAG 58:6; TAG 18:1-18:2-22:3	-	-	0.00794	-	-	0.21
PC 38:3; PC 18:0-20:3	-	0.00617	-	-	0.78	-	TAG 60:6; TAG 18:2-20:2-22:2	-	-	0.00744	-	-	0.18
PC 38:3e; PC 16:0e/22:3	-	0.00005	0.00894	-	0.64	0.70	TAG 60:7; TAG 18:1-20:4-22:2	-	-	0.01336	-	-	0.21

Table S37: Fold change values: Of [emim][OAc] treated cells after 8h, 16h and 24h, measured in ESI-

[emim][OAc] ESI-	p-value			Fold change			[emim][OAc] ESI-	p-value			Fold change		
Name	**8h**	**16h**	**24h**	**8h**	**16h**	**24h**	**Name**	**8h**	**16h**	**24h**	**8h**	**16h**	**24h**
Cer-NDS d40:0; Cer-NDS d18:0/22:0	0.00001	0	0	10.78	18.51	20.00	PE 34:0e; PE 18:0e/16:0	0.00001	0	0.00001	3.08	3.18	3.14
Cer-NDS d42:0; Cer-NDS d18:0/24:0	0.00017	0	0	10.98	30.78	39.48	PE 34:1; PE 16:0-18:1	-	0.00368	0.01254	-	1.24	1.45
Cer-NS d40:1; Cer-NS d18:1/22:0	-	0.00211	0.02284	-	1.55	1.34	PE 34:1e; PE 18:1e/16:0	-	0.01079	-	-	1.27	-
Cer-NS d40:2; Cer-NS d18:1/22:1	0.00415	0.00018	0.00061	0.61	0.64	0.62	PE 34:2; PE 16:1-18:1	-	0.01575	0.0297	-	1.21	1.29
Cer-NS d42:1; Cer-NS d18:1/24:0	-	0.00067	0.00004	-	2.09	2.63	PE 34:2e; PE 16:1e/18:1	-	-	0.04505	-	-	1.26
GlcADG 28:0; GlcADG 14:0-14:0	-	-	0.00985	-	-	1.34	PE 34:3e; PE 16:1e/18:2	-	0.04239	-	-	1.23	-
HexCer-NDS d40:0; HexCer-NDS d21:0/19:0	-	0	0	-	3.57	4.40	PE 34:3e; PE 18:2e/16:1	-	0.02896	-	-	1.25	-
HexCer-NDS d42:1; HexCer-NDS d30:0/12:1	-	0.00004	0.00001	-	2.48	2.84	PE 36:1; PE 18:0-18:1	-		0.00303	-	-	1.53
HexCer-NS d40:2; HexCer-NS d22:2/18:0	-	0.03826	0.00167	-	0.78	0.69	PE 36:1e; PE 18:0e/18:1	-	0.00351	0.00102	-	5.41	8.49
HexCer-NS d42:1; HexCer-NS d22:1/20:0	-	-	0.03485	-	-	1.31	PE 36:2e; PE 18:1e/18:1	-	-	0.01694	-	-	1.47
LPC 14:0	-	0.00177	0.00077	-	1.50	1.74	PE 36:3; PE 16:0-20:3	-	-	0.03615	-	-	1.34
LPC 16:0	-	0.0001	0	-	2.15	2.98	PE 38:2e; PE 16:1e/22:1	-	0.026	0.00879	-	1.31	1.44
LPC 18:0	-	0	0	-	3.11	5.01	PE 38:3; PE 18:1-20:2	-	0.02882	0.02846	-	1.18	1.28
LPC 18:1	-	0.00098	0.01093	-	1.45	1.45	PE 38:3e; PE 16:1e/22:2	-	0.01439	0.0444	-	1.23	1.23
LPE 16:0	-	0.00005	0.00001	-	2.21	3.12	PE 38:3e; PE 18:0e/20:3	-	0.02884	0.00002	-	1.41	2.11
LPE 18:0	0.01122	0	0	1.6	3.88	5.87	PE 38:4e; PE 18:1e/20:3	-	0.01629	-	-	1.24	-
LPE 18:1	-	0.03185	0.00098	-	1.17	1.58	PE 38:6e; PE 18:2e/20:4	-	0.02255	-	-	0.77	-
LPE 20:3	-	0.01441	0.00449	-	1.13	1.38	PE 40:2e; PE 18:1e/22:1	-	0.00676	0.00982	-	1.52	1.42
LPI 18:0	-	0.01937	-	-	1.34	-	PE 40:3; PE 18:0-22:3	-	0.04916	-	-	1.11	-
LPI 18:1	-	0.00018	0.00036	-	1.70	1.92	PE 40:3e; PE 18:1e/22:2	-	0.00136	0.01603	-	1.36	1.34
OxPE 36:1+1O; OxPE 18:1-18:0+1O	-	-	0.00295	-	-	1.46	PE 40:5e; PE 18:2e/22:3	-	0.00448	0.02589	-	0.70	0.75
PC 26:0; PC 12:0-14:0	-	0.00067	0.00003	-	1.68	2.42	PG 32:0; PG 16:0-16:0	-	0.0022	0.00039	-	1.77	2.13

Table S37: Fold change values: Of [emim][OAc] treated cells after 8h, 16h and 24h, measured in ESI- (Continuation)

[emim][OAc] ESI-	p-value			Fold change			[emim][OAc] ESI-	p-value			Fold change		
Name	**8h**	**16h**	**24h**	**8h**	**16h**	**24h**	**Name**	**8h**	**16h**	**24h**	**8h**	**16h**	**24h**
PC 28:0; PC 14:0-14:0	-	0.00837	0.00172	-	1.47	1.57	PG 34:1; PG 16:0-18:1	-	-	0.02374	-	-	1.35
PC 30:0; PC 14:0-16:0	-	0.00474	-	-	1.33	-	PG 36:2; PG 18:1-18:1	0.01106	0.0003	0.00249	0.57	0.57	0.61
PC 30:2; PC 14:0-16:2	0.0025	0.00146	0.03823	0.59	0.65	0.77	PI 32:1; PI 14:0-18:1	-	0.0003	0.00247	-	1.51	1.59
PC 32:0; PC 16:0-16:0	-	0.01277	0.01611	-	1.21	1.35	PI 34:0; PI 16:0-18:0	0.00026	0	0	2.90	9.60	9.44
PC 32:1e; PC 16:0e/16:1	-	0.01666	0.00822	-	1.28	1.26	PI 34:1; PI 18:0-16:1	-	0.00006	0.01189	-	1.68	1.60
PC 32:1e; PC 16:1e/16:0	-	-	0.00138	-	-	0.64	PI 36:1; PI 18:0-18:1	-	0.00005	0.00008	-	1.58	1.90
PC 32:2; PC 16:1-16:1	0.01269	0.00656	-	0.63	0.73	-	PI 36:2; PI 18:1-18:1	-	0.00374	0.00498	-	1.34	1.42
PC 32:3; PC 16:1-16:2	0.00606	0.00031	0.00481	0.56	0.59	0.64	PI 36:3; PI 18:1-18:2	-	0.03692	-	-	0.81	-
PC 34:0; PC 16:0-18:0	-	0.00188	0.0002	-	1.48	1.91	PI 38:2; PI 19:1-19:1	-	0.00385	0.00194	-	1.29	1.51
PC 34:1; PC 16:0-18:1	-	0.04647	0.01178	-	1.21	1.33	SM d32:0; SM d14:0/18:0	0.00871	0.00003	0.00012	1.69	2.19	2.27
PC 34:3; PC 16:1-18:2	0.00399	0.0033	-	0.58	0.70	-	SM d34:0; SM d14:0/20:0	-	0.00001	0.00043	-	2.12	2.12
PC 36:1; PC 18:0-18:1	-	0.02917	0.00066	-	1.26	1.64	SM d36:0; SM d17:0/19:0	0.00911	0.00002	0.00035	1.66	2.59	2.52
PC 36:3; PC 16:0-20:3	-	0.01364	0.02818	-	0.72	0.75	SM d38:1; SM d19:1/19:0	-	0.02749	-	-	1.19	-
PC 36:4; PC 16:0-20:4	-	0.00173	0.00617	-	0.62	0.63	SM d38:2; SM d21:2/17:0	-	0.04691	0.03243	-	1.20	1.27
PC 36:4; PC 18:2-18:2	0.00365	0.00595	0.02152	0.62	0.73	0.73	SM d40:0; SM d14:0/26:0	-	0.00061	0.00001	-	2.28	2.85
PC 38:3; PC 18:0-20:3	-	0.00654	-	-	0.72	-	SM d40:1; SM d14:0/26:1	-	0.00009	0.00001	-	2.22	2.22
PC 38:4; PC 18:1-20:3	-	0.00401	0.00717	-	0.62	0.67	SM d40:1; SM d14:1/26:0	-	0.00292	-	-	1.23	-
PC 38:5; PC 18:1-20:4	0.00683	0.0018	0.00349	0.67	0.68	0.62	SM d42:0; SM d14:0/28:0	-	0.00082	0	-	2.50	3.47
PC 40:4; PC 18:1-22:3	-	-	0.03209	-	-	0.83	SM d42:1; SM d14:0/28:1	-	0.00104	0.00005	-	2.07	2.25
PE 30:1e; PE 16:1e/14:0	-	0.02032	0.04387	-	1.28	1.27	SM d42:1; SM d14:1/28:0	-	-	0.01067	-	-	1.37
PE 32:1; PE 16:0-16:1	-	-	0.02828	-	-	1.33	SM d42:3; SM d16:2/26:1	-	0.0279	-	-	0.74	-
PE 32:2e; PE 16:1e/16:1	-	0.01047	0.02962	-	1.35	1.35	SM d44:2; SM d14:2/30:0	-	0.00559	-	-	1.12	-
PE 32:3e; PE 16:1e/16:2	-	0.00153	-	-	1.27	-							

Table S38: Fold change values: Of [P_{4441}][OAc] treated cells after 8h, 16h and 24h, measured in ESI+

[P_{4441}][OAc] ESI +	p-value			Fold change			[P_{4441}][OAc] ESI +	p-value			Fold change		
Name	**8h**	**16h**	**24h**	**8h**	**16h**	**24h**	**Name**	**8h**	**16h**	**24h**	**8h**	**16h**	**24h**
BMP 36:2; BMP 18:1-18:1	0.00114	-	-	1.52	-	-	PG 30:0; PG 14:0-16:0	0.0007	0.00013	0.00004	0.54	0.53	0.52
BMP 36:3; BMP 18:1-18:2	-	0.02971	0.04987	-	0.83	0.87	PG 30:1; PG 14:0-16:1	0.00096	0	0	0.51	0.20	0.25
BMP 38:3; BMP 18:1-20:2	0.00112	0.04086	0.0309	1.54	1.28	1.45	PG 32:1; PG 14:0-18:1	0.00019	0.00218	0.00029	0.49	0.28	0.40
BMP 38:4; BMP 18:1-20:3	0.00112	-	-	1.56	-	-	PG 32:1; PG 16:0-16:1	0	0	0.0001	0.47	0.32	0.40
BMP 38:5; BMP 18:1-20:4	0.0239	-	-	1.48	-	-	PG 32:2; PG 16:1-16:1	0.00004	0	0.00011	0.40	0.18	0.28
CE 18:1	0.00255	0.00043	-	1.79	1.94	-	PG 34:1; PG 16:0-18:1	-	0.00543	0.01017	-	1.25	1.38
CE 20:1	0.00167	0.0065	0.0419	1.78	1.92	1.49	PG 36:1; PG 18:0-18:1	0.00064	-	-	1.32	-	-
CE 20:3	0.00215	0.03803	0.01262	1.70	1.68	1.56	PG 36:2; PG 18:1-18:1	0	0	0.00004	0.36	0.20	0.29
CE 22:1	0.02216	-	0.04813	1.41	-	1.40	PG 38:2; PG 18:0-20:2	0.01953	0.01181	0.00129	0.69	0.65	0.52
CE 22:2	0.03778	-	-	1.65	-	-	SM d30:1; SM d14:0/16:1	0.00185	0.02084	-	1.47	1.42	-
CE 22:4	0.00245	0.04655	-	1.87	1.87	-	SM d32:1; SM d14:0/18:1	0.01565	-	-	1.30	-	-
Cer-NDS d32:0; Cer-NDS d18:0/14:0	0	0	0	0.23	0.07	0.05	SM d34:0; SM d14:0/20:0	0.00003	0	0.00247	1.76	1.74	1.45
Cer-NDS d34:0; Cer-NDS d18:0/16:0	0.00053	0	0	0.44	0.12	0.08	SM d34:1; SM d14:0/20:1	0.00052	0.00252	0.01567	1.44	1.29	1.35
Cer-NDS d36:0; Cer-NDS d18:0/18:0	0.00005	0.01209	0.00001	3.01	0.68	0.31	SM d34:2; SM d16:0/18:2	0.00174	-	-	1.63	-	-
Cer-NDS d36:1; Cer-NDS d18:0/18:1	0.00005	0	0	0.32	0.06	0.04	SM d34:3; SM d14:1/20:2	0.00015	0.00081	0.02489	2.74	2.53	1.59
Cer-NDS d38:0; Cer-NDS d18:0/20:0	0.00037	0.00386	-	3.96	1.47		SM d34:4; SM d14:2/20:2	0.00323	-	-	1.72	-	-
Cer-NDS d38:1; Cer-NDS d18:0/20:1	0.00069	0	0	1.76	0.28	0.23	SM d36:0; SM d14:0/22:0	0.00011	0	0.00012	2.89	2.92	2.57
Cer-NDS d38:2; Cer-NDS d18:0/20:2	-	0.00015	0	-	0.4	0.24	SM d36:1; SM d14:0/22:1	0.00002	0	0.00365	1.70	1.62	1.60
Cer-NDS d40:0; Cer-NDS d18:0/22:0	0.0001	0	0.00185	4.86	3.41	2.07	SM d36:2; SM d14:0/22:2	0.00112	0	0.0041	2.26	1.67	1.55
Cer-NDS d40:1; Cer-NDS d18:0/22:1	0.00133	0.00047	0.00006	1.97	0.52	0.37	SM d36:3; SM d16:1/20:2	-	0.00165	-	-	2.10	-
Cer-NDS d42:0; Cer-NDS d18:0/24:0	0.00008	0.00007	0.00003	3.55	5.87	4.62	SM d38:0; SM d14:0/24:0	0.00079	0.00462	0.00006	3.13	2.97	3.18
Cer-NDS d42:1; Cer-NDS d18:0/24:1	0.00017	0.02599	-	2.42	1.24	-	SM d38:1; SM d14:1/24:0	0.00017	0.00044	0.00159	1.68	1.41	1.47
Cer-NS d32:1; Cer-NS d18:1/14:0	0	0.00001	0	0.32	0.13	0.07	SM d38:2; SM d16:0/22:2	0.00015	0.00011	0.00444	1.74	1.74	1.43
Cer-NS d34:1; Cer-NS d18:1/16:0	0	0	0	0.38	0.18	0.14	SM d40:0; SM d14:0/26:0	0.0002	0.00014	0.00008	1.97	1.92	2.32
Cer-NS d36:1; Cer-NS d18:1/18:0	-	0	0	-	0.34	0.26	SM d40:1; SM d14:0/26:1	0.00001	0	0.00022	2.61	2.50	2.25
Cer-NS d36:2; Cer-NS d18:1/18:1	0.00358	0.00024	0	0.66	0.26	0.20	SM d40:1; SM d14:1/26:0	0.00207	0.00057	0.00059	1.57	1.35	1.48
Cer-NS d38:1; Cer-NS d18:1/20:0	0.01305	0.00005	0.00004	1.52	0.56	0.47	SM d40:2; SM d14:0/26:2	0.00009	0.00011	0.01648	1.61	1.56	1.47
Cer-NS d38:3; Cer-NS d18:1/20:2	0.00002	0.00837	0.00004	2.52	0.68	0.31	SM d40:2; SM d18:0/22:2	0.00011	0.00019	0.00747	1.50	1.38	1.39
Cer-NS d40:1; Cer-NS d18:1/22:0	-	0.03797	0.02297	-	0.8	0.77	SM d41:1; SM d14:1/27:0	0.00799	-	0.00968	1.49	-	1.44
Cer-NS d40:2; Cer-NS d18:1/22:1	-	0.00005	0.00002	-	0.43	0.39	SM d41:2; SM d19:0/22:2	0.00008	0.01393	0.00703	1.59	1.30	1.48
Cer-NS d40:3; Cer-NS d18:2/22:1	0.004	0.00019	0.0005	0.60	0.38	0.19	SM d42:0; SM d14:0/28:0	0.002	0.00015	0.00062	1.61	1.68	2.05
Cer-NS d42:1; Cer-NS d18:1/24:0	-	-	0.03754	-	-	1.50	SM d42:1; SM d14:0/28:1	0.00008	0	0.00007	2.01	2.15	2.31
Cer-NS d42:2; Cer-NS d18:1/24:1	-	0.00011	0.00357	-	0.62	0.62	SM d42:1; SM d14:1/28:0	0.00081	0.0058	0.00204	1.61	1.25	1.48
Cer-NS d42:3; Cer-NS d18:2/24:1	0.01537	0	0.00007	0.78	0.47	0.48	SM d42:2; SM d14:1/28:1	0.00105	0.00536	0.00289	1.52	1.27	1.44
Cer-NS d44:2; Cer-NS d20:1/24:1	-	0.04247	-	-	0.81	-	SM d42:2; SM d20:0/22:2	0.00008	0.00009	0.01223	1.50	1.44	1.36
Cer-NS d44:3; Cer-NS d18:2/26:1	-	0.00011	0.00301	-	0.54	0.55	SM d42:3; SM d14:2/28:1	0.00001	0.00317	0.01814	1.63	1.30	1.36
DAG 30:1; DAG 14:0-16:1	0.00542	0.00001	0.00032	0.53	0.28	0.29	SM d42:4; SM d15:3/27:1	0.00161	0.00017	0.00011	2.08	2.30	2.37
DAG 32:1; DAG 16:0-16:1	0.00079	0	0	0.67	0.36	0.25	SM d42:5; SM d14:3/28:2	0.0084	-	-	1.61	-	-
DAG 34:1; DAG 16:0-18:1	0.00089	0	0	0.65	0.39	0.35	SM d43:2; SM d15:0/28:2	0.00016	-	0.0248	2.06	-	1.60
DAG 34:2; DAG 16:1-18:1	0.00001	0	0	0.50	0.21	0.15	SM d44:2; SM d14:1/30:1	0.00081	-	0.02252	1.61	-	1.52
DAG 34:3; DAG 16:1-18:2	0.00346	0.00002	0	0.58	0.24	0.22	SM d44:3; SM d14:2/30:1	0.00211	0.00034	0.02676	1.50	1.34	1.33

Table S38: Fold change values: Of [P_{4441}][OAc] treated cells after 8h, 16h and 24h, measured in ESI+ (Continuation)

[P_{4441}][OAc] ESI +	p-value			Fold change			[P_{4441}][OAc] ESI +	p-value			Fold change		
Name	**8h**	**16h**	**24h**	**8h**	**16h**	**24h**	**Name**	**8h**	**16h**	**24h**	**8h**	**16h**	**24h**
DAG 36:2; DAG 18:1-18:1	0.00016	0	0	0.51	0.23	0.19	SM d44:4; SM d15:3/29:1	0.00037	0.00144	0.0015	1.82	1.88	1.80
DAG 36:3; DAG 18:1-18:2	0.02716	0.00001	0	0.60	0.24	0.20	SM d44:5; SM d22:3/22:2	0.00083	0.01614	0.00097	2.41	1.81	1.97
DAG 36:4; DAG 16:1-20:3	0.00093	0	0	0.47	0.19	0.13	TAG 42:0; TAG 12:0-14:0-16:0	0.00003	0.00078	-	2.57	2.41	-
DAG 38:1; DAG 18:0-20:1	0.01896	-	0.00805	1.40	-	0.54	TAG 42:1; TAG 12:0-14:0-16:1	0.00002	0.04462	0.01008	2.52	1.58	1.80
DAG 38:3; DAG 20:1-18:2	0.00724	0.00001	0	0.72	0.31	0.24	TAG 44:0; TAG 14:0-14:0-16:0	0.00063	-	0.00462	1.94	-	1.52
DAG 38:4; DAG 18:1-20:3	-	0.00007	0	-	0.29	0.23	TAG 44:1; TAG 12:0-14:0-18:1	0.0001	0.00787	0.03116	2.26	1.72	1.51
DAG 40:3; DAG 18:0-22:3	0.00005	-	-	2.47	-	-	TAG 44:1; TAG 12:0-16:0-16:1	0.00006	0.00546	-	2.13	1.55	-
DAG 40:4; DAG 18:1-22:3	0.00373	0	0	0.69	0.28	0.24	TAG 44:2; TAG 12:1-14:0-18:1	0.00228	-	-	1.72	-	-
DAG 40:5; DAG 18:1-22:4	0.01107	0.00053	0	0.68	0.29	0.25	TAG 45:0; TAG 14:0-15:0-16:0	0.00031	0.03884	0.01835	2.24	2.01	1.73
HexCer-NS d34:1; HexCer-NS d18:1/16:0	-	0.01339	0.01614	-	0.43	0.52	TAG 45:1; TAG 13:0-14:0-18:1	0.00141	0.01644	-	1.98	1.79	-
HexCer-NS d40:1; HexCer-NS d18:1/22:0	0.0009	-	0.00764	1.90	-	1.76	TAG 46:1; TAG 14:0-14:0-18:1	0.00003	0.00424	-	2.41	1.57	-
HexCer-NS d40:2; HexCer-NS d18:1/22:1	0.00398	-	-	1.89	-	-	TAG 46:1; TAG 14:0-16:0-16:1	0.0031	0.02869	-	1.79	1.58	-
HexCer-NS d42:1; HexCer-NS d18:1/24:0	0.01532	-	-	1.38	-	-	TAG 46:2; TAG 12:0-16:1-18:1	0.00485	-	-	1.83	-	-
HexCer-NS d42:2; HexCer-NS d18:1/24:1	0.01325	-	-	1.40	-	-	TAG 46:2; TAG 14:0-16:0-16:2	0.00528	-	-	1.37	-	-
LPC 14:0	0.0022	-	-	1.74	-	-	TAG 46:3; TAG 12:2-16:0-18:1	0.00122	-	-	1.81	-	-
LPC 15:0	0.00406	-	-	2.15	-	-	TAG 47:1; TAG 13:0-16:0-18:1	0.00122	-	-	1.88	-	-
LPC 18:0	-	0.00106	0.00126	-	1.69	1.80	TAG 47:1; TAG 13:0-17:0-17:1	0.01156	-	-	1.79	-	-
LPC 18:1	0.00033	0.02311		1.54	1.13	-	TAG 47:2; TAG 14:0-16:0-17:2	0.01287	-	-	1.66	-	-
LPC 20:1	0.00806	0.00639	0.00536	1.75	2.00	1.75	TAG 47:2; TAG 15:2-16:0-16:0	0.00727	-	-	1.78	-	-
LPC 26:0	0.01168	0.01892	-	1.45	0.78	-	TAG 48:1; TAG 14:0-16:0-18:1	0.00001	0.00671	0.00457	1.92	1.66	1.78
LPE 18:0	0.002	0.0049	0.00041	2.06	2.72	3.09	TAG 48:2; TAG 12:0-18:1-18:1	0.00115	-	-	1.86	-	-
LPE 18:1	0.00099	-	-	1.46	-	-	TAG 48:2; TAG 14:0-16:1-18:1	0.00275	-	-	1.77	-	-
LPE 20:3	0.00093	0.0235	-	1.86	1.27	-	TAG 48:2; TAG 16:0-16:1-16:1	0.00163	-	-	1.70	-	-
PC 16:0e; PC 14:0e/2:0	0.00003	0	-	1.97	1.86	-	TAG 48:3; TAG 14:0-14:0-20:3	0.00729	-	0.04306	1.56	-	0.66
PC 16:1e; PC 14:1e/2:0	0.0005	-	0.04146	2.10	-	0.70	TAG 48:3; TAG 14:0-16:2-18:1	0.01028	-	-	1.47	-	-
PC 18:1e; PC 16:1e/2:0	0.00002	-	-	2.07	-	-	TAG 48:4; TAG 14:1-16:1-18:2	0.0201	-	-	1.57	-	-
PC 18:2e; PC 16:2e/2:0	0.00237	-	-	1.84	-	-	TAG 49:1; TAG 15:0-15:0-19:1	0.00026	-	0.03284	1.86	-	1.25
PC 20:1e; PC 18:1e/2:0	-	0.01036	0.00804	-	2.02	1.67	TAG 49:1; TAG 15:0-17:0-17:1	0.00122	-	-	1.75	-	-
PC 20:3e; PC 18:3e/2:0	0.00059	-	-	2.27	-	-	TAG 49:1; TAG 16:0-16:0-17:1	0.00502	-	-	1.73	-	-
PC 26:0; PC 12:0-14:0	0.01113	0.04216	0.00513	1.45	1.30	1.72	TAG 49:2; TAG 14:0-16:0-19:2	0.00338	-	-	1.56	-	-
PC 28:0; PC 14:0-14:0	0.00002	0.00024	0.0001	1.75	1.68	2.00	TAG 49:3; TAG 15:0-15:0-19:3	0.04677	-	-	1.33	-	-
PC 28:0e; PC 14:0e/14:0	0.02991	0.02035	0.00248	1.41	1.40	1.75	TAG 49:3; TAG 15:2-17:0-17:1	0.01446	-	-	1.76	-	-
PC 28:1; PC 14:0-14:1	-	0.00001	0.01404	-	0.51	0.69	TAG 49:4; TAG 15:2-17:0-17:2	0.01345	-	-	1.43	-	-
PC 29:0; PC 13:0-16:0	0.00178	-	-	1.61	-	-	TAG 50:0; TAG 16:0-16:0-18:0	0.00807	-	0.00227	3.17	-	5.55
PC 29:0; PC 14:0-15:0	0.00362	0.00018	0.03446	1.48	1.53	1.47	TAG 50:1; TAG 16:0-16:0-18:1	0.00033	0.03292	-	1.80	2.61	-
PC 30:0; PC 14:0-16:0	0.00012	0.00012	0.00009	1.61	1.72	1.93	TAG 50:1; TAG 16:0-17:0-17:1	0.00013	0.00201	0.01122	2.08	1.82	1.67
PC 30:0e; PC 14:0e/16:0	0.00306	0.0031	0.01107	1.29	1.23	1.31	TAG 50:2; TAG 14:0-16:0-20:2	0.00039	-	-	1.78	-	-
PC 30:1; PC 14:0-16:1	0.00016	0.01531	-	1.41	0.89	-	TAG 50:2; TAG 14:0-18:1-18:1	0.02817	-	-	2.22	-	-
PC 30:1e; PC 14:0e/16:1	0.00191	-	-	1.63	-	-	TAG 50:2; TAG 16:0-16:2-18:0	0.00207	0.01492	-	1.58	1.35	-
PC 30:2; PC 14:0-16:2	-	0.00031	0.00627	-	0.64	0.66	TAG 50:2; TAG 16:1-16:1-18:0	0.01005	-	-	1.44	-	-
PC 30:2; PC 14:1-16:1	0.01226	0	0.00025	0.82	0.47	0.54	TAG 50:3; TAG 16:0-16:0-18:3	0.02653	-	0.04108	1.26	-	0.81
PC 31:0; PC 15:0-16:0	0.00012	0.02786	0.03157	1.57	1.29	1.37	TAG 50:3; TAG 16:0-16:1-18:2	-	-	0.01887	-	-	0.70

Table S38: Fold change values: Of [P_{4441}][OAc] treated cells after 8h, 16h and 24h, measured in ESI+ (Continuation)

[P_{4441}][OAc] ESI +	p-value			Fold change			[P_{4441}][OAc] ESI +	p-value			Fold change		
Name	**8h**	**16h**	**24h**	**8h**	**16h**	**24h**	**Name**	**8h**	**16h**	**24h**	**8h**	**16h**	**24h**
PC 31:1; PC 15:0-16:1	0.04153	0.00474	-	1.25	0.82	-	TAG 50:3; TAG 16:1-16:1-18:1	0.03766	-	0.01387	1.41	-	0.65
PC 32:0; PC 16:0-16:0	0.00248	0.00013	0.02402	1.32	1.41	1.31	TAG 50:4; TAG 14:0-16:0-20:4	-	0.02059	0.00101	-	0.67	0.51
PC 32:0e; PC 14:0e/18:0	0.01974	0.01348	-	1.22	1.17	-	TAG 50:4; TAG 16:1-16:1-18:2	-	-	0.00196	-	-	0.59
PC 32:1; PC 16:0-16:1	0.00017	0.00212	0.02042	1.64	1.31	1.37	TAG 50:5; TAG 14:1-16:1-20:3	-	0.01043	0.0006	-	0.58	0.55
PC 32:1e; PC 14:0e/18:1	0.00029	-	-	1.35	-	-	TAG 51:1; TAG 16:0-16:0-19:1	0.00085	-	-	1.77	-	-
PC 32:2; PC 16:0-16:2	0.00001	0.00643	-	1.71	1.25	-	TAG 51:2; TAG 15:0-18:1-18:1	0.00023	-	-	1.71	-	-
PC 32:2; PC 16:1-16:1	0.01203	0.00007	0.01024	1.27	0.78	0.73	TAG 51:2; TAG 16:0-17:1-18:1	0.00991	-	-	1.61	-	-
PC 32:3; PC 16:1-16:2	-	0.00063	0.00124	-	0.63	0.65	TAG 51:2; TAG 16:1-17:0-18:1	0.00593	-	-	1.64	-	-
PC 33:0; PC 16:0-17:0	0.00634	-	-	1.28	-	-	TAG 51:3; TAG 15:0-17:0-19:3	0.02697	-	-	1.49	-	-
PC 33:1; PC 15:0-18:1	0.00167	-	-	1.57	-	-	TAG 51:4; TAG 15:0-17:2-19:2	0.01116	-	-	1.78	-	-
PC 33:2; PC 17:0-16:2	0.02326	-	-	1.29	-	-	TAG 52:0; TAG 16:0-18:0-18:0	0.01731	-	0.01497	2.92	-	4.74
PC 34:0; PC 16:0-18:0	0.00043	0	0.00005	1.61	2.35	2.18	TAG 52:1; TAG 16:0-16:0-20:1	0.00125	0.01627	0.00087	1.87	1.67	1.99
PC 34:0e; PC 14:0e/20:0	0.01944	0.00581	0.00003	1.31	1.35	1.82	TAG 52:1; TAG 16:0-18:0-18:1	0.00005	0.00125	0.0062	2.27	1.75	1.92
PC 34:1; PC 16:0-18:1	0	0.00076	0.00692	1.70	1.31	1.43	TAG 52:1; TAG 17:0-17:0-18:1	0.00015	0.01702	0.00073	1.90	1.74	1.99
PC 34:1e; PC 14:0e/20:1	0.00005	0.00067	0.00548	1.56	1.20	1.32	TAG 52:2; TAG 16:0-16:1-20:1	0.00396	-	-	1.54	-	-
PC 34:2; PC 16:1-18:1	0.00022	-	-	1.44	-	-	TAG 52:2; TAG 16:0-18:1-18:1	0.00027	0.00623	-	1.77	1.40	-
PC 34:2e; PC 14:0e/20:2	0.0002	-	-	1.39	-	-	TAG 52:3; TAG 16:0-16:0-20:3	0.01355	-	-	1.64	-	-
PC 34:3; PC 16:1-18:2	0.01602	0.00551		1.26	0.79	-	TAG 52:3; TAG 16:1-16:1-20:1	0.04186	0.0229	0.01271	1.31	0.78	0.65
PC 34:3; PC 18:1-16:2	0.00009	-	-	1.49	-	-	TAG 52:3; TAG 16:1-18:1-18:1	0.02035	-	0.04505	1.36	-	0.68
PC 34:3e; PC 14:0e/20:3	-	0.00008	0.0053	-	0.69	0.68	TAG 52:4; TAG 16:0-16:0-20:4	-	-	0.00065	-	-	0.58
PC 35:0; PC 16:0-19:0	0.0016	0.00094	-	1.64	1.44	-	TAG 52:4; TAG 16:1-16:1-20:2	0.02799	0.01786	0.02079	1.25	0.76	0.66
PC 35:1; PC 16:0-19:1	-	0.0322	0.03808	-	2.12	1.87	TAG 52:4; TAG 16:1-18:1-18:2	-	0.03556	0.00093	-	0.72	0.58
PC 35:1; PC 17:0-18:1	0.01638	-	-	1.40	-	-	TAG 52:5; TAG 16:1-16:1-20:3	-	0.01266	0.00011	-	0.61	0.45
PC 35:2; PC 17:1-18:1	0.00067	-	-	1.61	-	-	TAG 52:6; TAG 16:0-16:2-20:4	-	0.00089	0.00333	-	0.62	0.53
PC 36:1; PC 18:0-18:1	0	0	0.00001	1.84	1.97	2.28	TAG 53:2; TAG 17:0-17:0-19:2	0.00975	-	-	1.47	-	-
PC 36:1e; PC 14:0e/22:1	0.00349	0.00186	0.00119	1.64	1.30	1.81	TAG 53:2; TAG 17:0-18:1-18:1	0.0023	0.03165		1.86	1.38	-
PC 36:2; PC 18:1-18:1	0.00043	-	-	1.57	-	-	TAG 53:3; TAG 17:1-18:1-18:1	0.01168	-	0.02053	1.58	-	0.66
PC 36:2e; PC 14:0e/22:2	0.00001	0.00014	0.02983	1.68	1.33	1.31	TAG 53:4; TAG 17:0-17:1-19:3	0.02264	-	-	1.41	-	-
PC 36:3; PC 16:0-20:3	0.00632	0.00262	0.03687	3.26	4.02	1.98	TAG 54:0; TAG 18:0-18:0-18:0	0.00094	-	-	3.79	-	-
PC 36:3; PC 18:1-18:2	0.00001	0.00632	-	1.59	1.19	-	TAG 54:1; TAG 16:0-18:1-20:0	0.00061	0.02652	0.00471	2.31	1.61	2.17
PC 36:3; PC 20:1-16:2	0.00001	0.00281	-	1.64	1.21	-	TAG 54:1; TAG 17:0-17:0-20:1	0.00036	-	-	1.94	-	-
PC 36:3e; PC 14:0e/22:3	-	0.00199	0.01122	-	0.72	0.71	TAG 54:2; TAG 16:0-18:0-20:2	0.00009	-	-	2.01	-	-
PC 36:4; PC 16:0-20:4	0	0.02056	0.02315	1.94	1.59	1.43	TAG 54:2; TAG 16:0-18:1-20:1	0.00009	0.0075	0.01203	2.05	1.75	1.55
PC 36:4; PC 18:2-18:2	0.00011	-	-	1.76	-	-	TAG 54:2; TAG 16:0-19:1-19:1	0.0001	0.02042	0.004	1.72	1.71	1.51
PC 36:4e; PC 14:0e/22:4	0.00001	-	-	1.39	-	-	TAG 54:3; TAG 16:1-18:1-20:1	0.04877	-	-	1.27	-	-
PC 36:5; PC 16:1-20:4	0.01005	-	-	1.34	-	-	TAG 54:3; TAG 18:0-18:1-18:2	0.007	-	-	1.38	-	-
PC 37:1; PC 17:0-20:1	0.00001	0.01606	-	1.57	1.34	-	TAG 54:3; TAG 18:1-18:1-18:1	0.00011	-	-	1.71	-	-
PC 38:1; PC 18:0-20:1	0.00006	0.00001	0.00001	1.75	2.02	2.8	TAG 54:4; TAG 16:0-18:1-20:3	0.04894	-	0.0145	1.31	-	0.54
PC 38:2; PC 18:1-20:1	0	0	0.00104	1.74	1.60	1.68	TAG 54:4; TAG 18:0-18:1-18:3	0.00639	-	-	1.36	-	-
PC 38:2; PC 19:1-19:1	0.02097	-	-	2.46	-	-	TAG 54:4; TAG 18:1-18:1-18:2	-	-	0.00309	-	-	0.59
PC 38:2e; PC 14:0e/24:2	0.00061	0.00029	0.00688	1.56	1.43	1.54	TAG 54:5; TAG 16:1-18:1-20:3	-	0.00693	0.00002	-	0.60	0.47
PC 38:3; PC 18:0-20:3	0	0	0.00013	2.56	2.02	2.03	TAG 54:6; TAG 16:1-18:1-20:4	-	0.00332	0.00011	-	0.54	0.38

Table S38: Fold change values: Of [P_{4441}][OAc] treated cells after 8h, 16h and 24h, measured in ESI+ (Continuation)

[P_{4441}][OAc] ESI +	p-value			Fold change			[P_{4441}][OAc] ESI +	p-value			Fold change		
Name	**8h**	**16h**	**24h**	**8h**	**16h**	**24h**	**Name**	**8h**	**16h**	**24h**	**8h**	**16h**	**24h**
PC 38:3; PC 18:1-20:2	0.00131	0.00763	0	3.42	2.55	3.99	TAG 55:2; TAG 16:0-18:0-21:2	0.00009	0.03478	-	2.09	1.45	-
PC 38:3e; PC 16:0e/22:3	0.00002	0.0022	-	1.84	1.32	-	TAG 55:3; TAG 17:1-19:1-19:1	0.00445	-	-	1.79	-	-
PC 38:4; PC 18:1-20:3	0.00008	0.00034	0.01085	2.02	1.49	1.48	TAG 55:4; TAG 17:0-17:2-21:2	0.01518	-	0.00851	1.49	-	0.67
PC 38:4e; PC 14:0e/24:4	0	0.00003	0.03792	2.08	1.45	1.37	TAG 55:4; TAG 17:2-19:1-19:1	0.00645	-	0.00726	1.41	-	0.72
PC 38:5; PC 18:1-20:4	0.00005	-	-	1.71	-	-	TAG 55:5; TAG 17:2-19:0-19:3	0.03445	-	0.00783	1.41	-	0.49
PC 38:5e; PC 16:0e/22:5	0.00259	0.00007	0.00001	0.83	0.55	0.50	TAG 56:1; TAG 16:0-18:1-22:0	0.00107	-	0.0101	1.71	-	2.27
PC 38:6e; PC 16:0e/22:6	0.00189	0.00002	0.00006	0.75	0.42	0.43	TAG 56:2; TAG 16:0-18:0-22:2	0.01745	-	-	1.66	-	-
PC 40:2; PC 20:1-20:1	0.00049	0	0.00037	1.54	1.69	2.14	TAG 56:2; TAG 16:0-20:1-20:1	0.03445	-	-	1.59	-	-
PC 40:3; PC 18:0-22:3	0	0.00001	0.00057	2.23	2.26	2.17	TAG 56:2; TAG 18:0-18:1-20:1	0.0005	0.00913	0.02109	2.27	1.74	1.73
PC 40:3; PC 18:1-22:2	0	0	0.00008	1.91	1.95	2.00	TAG 56:3; TAG 17:1-18:0-21:2	0.00005	-	-	1.9	-	-
PC 40:4; PC 18:1-22:3	0	0.00003	0.00003	2.05	1.95	1.87	TAG 56:3; TAG 18:1-18:1-20:1	0.00059	-	-	1.79	-	-
PC 40:4; PC 20:2-20:2	0	0.00001	0.00331	2.59	2.29	1.85	TAG 56:4; TAG 16:0-18:1-22:3	0.00624	-	-	1.47	-	-
PC 40:4e; PC 14:0e/26:4	0.00001	-	-	1.54	-	-	TAG 56:4; TAG 16:1-18:1-22:2	0.01686	-	-	1.88	-	-
PC 40:5; PC 18:1-22:4	0.00069	0.00128	0.02147	1.72	1.49	1.40	TAG 56:4; TAG 16:1-20:1-20:2	0.01525	-	0.0298	1.66	-	0.77
PC 40:5e; PC 18:0e/22:5	0.0008	0.00001	0.00001	0.68	0.45	0.36	TAG 56:5; TAG 16:0-18:3-22:2	-	0.00473	0.00233	-	0.65	0.55
PC 40:6; PC 20:3-20:3	0.00009	0.00302	0.00015	2.19	1.46	1.79	TAG 56:5; TAG 18:1-18:1-20:3	-	0.04319	0.00067	-	0.73	0.54
PC 42:2; PC 18:1-24:1	0.0006	0	0	1.48	1.87	2.47	TAG 56:6; TAG 18:1-18:1-20:4	-	0.00028	0.00059	-	0.62	0.50
PC 42:3; PC 18:1-24:2	0.00083	0.00003	0	1.50	1.80	2.41	TAG 56:6; TAG 18:1-18:2-20:3	-	0.00007	0.00009	-	0.62	0.49
PC 42:4; PC 21:2-21:2	0.00001	0	0.00017	2.24	2.20	2.37	TAG 56:7; TAG 16:1-20:3-20:3	-	0.00266	0.0001	-	0.57	0.44
PE 30:0; PE 14:0-16:0	0.01912	0.00659	0.01508	1.52	1.73	1.44	TAG 58:1; TAG 18:1-19:0-21:0	0.00557	-	0.02721	1.68	-	1.81
PE 30:1; PE 14:0-16:1	0.00426	0.00031	-	1.71	1.50	-	TAG 58:2; TAG 16:0-20:1-22:1	0.0111	-	-	1.62	-	-
PE 32:0; PE 16:0-16:0	0.00198	0.00001	0.0005	1.62	1.79	1.72	TAG 58:2; TAG 16:0-20:2-22:0	0.00459	-	-	1.83	-	-
PE 32:1; PE 16:0-16:1	0.00001	0.00001	0.00024	1.93	1.97	2.01	TAG 58:3; TAG 16:0-20:1-22:2	0.00314	-	0.04164	1.97	-	1.45
PE 32:2; PE 16:1-16:1	0.00038	-	-	1.63	-	-	TAG 58:3; TAG 18:0-20:1-20:2	0.01682	-	-	1.41	-	-
PE 34:0; PE 16:0-18:0	0.00018	0	0.00146	2.26	2.20	2.61	TAG 58:3; TAG 18:1-20:1-20:1	0.00483	-	-	1.57	-	-
PE 34:1; PE 16:0-18:1	0	0	0.00022	1.85	1.94	1.84	TAG 58:4; TAG 18:1-18:1-22:2	0.0044	-	0.01205	1.37	-	1.35
PE 34:2; PE 14:0-20:2	0.00007	0.00001	0.00034	2.03	1.49	1.78	TAG 58:5; TAG 16:1-21:2-21:2	-	-	0.02239	-	-	0.71
PE 34:2; PE 16:1-18:1	0	0.00001	0.00128	2.01	1.75	1.66	TAG 58:5; TAG 18:1-18:1-22:3	0.04107	-	0.00285	1.36	-	0.66
PE 34:3; PE 16:1-18:2	0.00126	0.00064	0.00007	2.13	1.64	1.73	TAG 58:6; TAG 18:1-20:2-20:3	-	-	0.00656	-	-	0.66
PE 35:1e; PE 16:0e/19:1	0.00489	0.00001	0.00017	0.75	0.56	0.57	TAG 58:7; TAG 18:0-18:3-22:4	-	0.0006	0.00041	-	0.70	0.49
PE 36:1; PE 18:0-18:1	-	-	0.00893	-	-	3.32	TAG 59:3; TAG 17:1-21:0-21:2	0.009	-	-	1.81	-	-
PE 36:1; PE 21:0-15:1	0	0	0.00001	2.25	2.72	2.72	TAG 60:2; TAG 16:1-22:0-22:1	0.01421	-	-	1.88	-	-
PE 36:2; PE 18:0-18:2	0.00001	0	0.00076	1.71	1.65	1.61	TAG 60:3; TAG 18:2-20:0-22:1	0.01186	-	-	1.85	-	-
PE 36:2; PE 18:1-18:1	0.00001	0	0.00103	1.71	1.63	1.61	TAG 60:4; TAG 16:0-22:2-22:2	0.00056	-	-	1.57	-	-
PE 36:3; PE 16:0-20:3	0	0	0.00001	2.32	2.33	2.1	TAG 60:4; TAG 16:1-22:1-22:2	0.00105	-	-	1.83	-	-
PE 36:3; PE 18:1-18:2	0.00026	0.00073	0.00105	1.83	1.51	1.81	TAG 60:5; TAG 18:0-20:2-22:3	0.00035	-	-	1.71	-	-
PE 36:3e; PE 16:0e/20:3	0.00062	0.04743	-	1.36	1.12	-	TAG 60:5; TAG 18:1-20:2-22:2	0.00195	-	-	1.65	-	-
PE 36:4; PE 16:0-20:4	0.03351	-	-	1.34	-	-	TAG 60:6; TAG 18:1-20:3-22:2	0.00049	-	-	1.59	-	-
PE 38:1; PE 18:0-20:1	0.00044	0	0	1.81	2.27	2.44	TAG 60:6; TAG 18:2-20:2-22:2	0.00048	-	-	1.45	-	-
PE 38:2; PE 18:0-20:2	0.00019	0.00001	0.00027	1.88	1.88	2.07	TAG 60:7; TAG 18:1-20:3-22:3	-	-	0.00634	-	-	0.63
PE 38:3; PE 18:0-20:3	0	0	0.00003	2.53	3.01	2.76	TAG 60:7; TAG 20:1-20:3-20:3	-	-	0.01056	-	-	0.59
PE 38:4; PE 18:0-20:4	0.00486	0.00004	0.00014	2.57	1.70	1.85	TAG 60:8; TAG 18:2-20:5-22:1	-	-	0.02183	-	-	0.67

Table S38: Fold change values: Of [P_{4441}][OAc] treated cells after 8h, 16h and 24h, measured in ESI+ (Continuation)

[P_{4441}][OAc] ESI +	p-value			Fold change			[P_{4441}][OAc] ESI +	p-value			Fold change		
Name	**8h**	**16h**	**24h**	**8h**	**16h**	**24h**	**Name**	**8h**	**16h**	**24h**	**8h**	**16h**	**24h**
PE 38:4; PE 18:1-20:3	0.00001	0.00042	0.00806	1.73	1.51	1.46	TAG 62:3; TAG 18:1-22:1-22:1	0.04844	-	-	1.45	-	-
PE 38:5; PE 16:0-22:5	0.00003	0	0.00147	1.73	1.64	1.68	TAG 62:3; TAG 20:1-20:2-22:0	0.03253	-	-	1.73	-	-
PE 39:2; PE 21:0-18:2	0.00001	0.0032	-	1.66	1.34	-	TAG 62:4; TAG 20:0-20:0-22:4	0.04287	-	-	1.60	-	-
PE 40:2; PE 18:1-22:1	0.0002	0.04776	0.00105	2.00	1.85	2.19	TAG 62:4; TAG 20:1-20:2-22:1	0.02658	-	-	1.70	-	-
PE 40:3; PE 18:0-22:3	0.00045	0	0.01345	1.78	2.00	1.86	TAG 62:5; TAG 18:1-22:2-22:2	0.018	0.02883	-	1.58	1.63	-
PE 40:4; PE 18:1-22:3	0.00132	0.00001	0.00045	1.63	1.67	1.67	TAG 62:6; TAG 18:1-22:2-22:3	0.00011	-	-	1.89	-	-
PE 40:4e; PE 18:0e/22:4	0.04081	-	-	1.21	-	-	TAG 64:5; TAG 20:1-22:1-22:3	0.01002	-	-	2.03	-	-
PE 40:5; PE 18:0-22:5	0.0016	0.0257	0.02693	1.56	1.25	1.41	TAG 64:6; TAG 20:1-22:1-22:4	-	-	0.02738	-	-	1.55

Table S39: Fold change values: Of [P_{4441}][OAc] treated cells after 8h,16h and 24h, measured in ESI-

[P_{4441}][OAc] ESI -	p-value			Fold change			[P_{4441}][OAc] ESI -	p-value			Fold change		
Name	**8h**	**16h**	**24h**	**8h**	**16h**	**24h**	**Name**	**8h**	**16h**	**24h**	**8h**	**16h**	**24h**
Cer-NDS d34:0; Cer-NDS d18:0/16:0	0.00001	0	0	0.37	0.11	0.06	PE 32:1e; PE 16:1e/16:0	0.00129	0.00082	0.03611	0.72	0.71	0.79
Cer-NDS d42:0; Cer-NDS d18:0/24:0	0.00063	0	0.00001	2.97	4.69	4.12	PE 32:2; PE 16:1-16:1	0.00003	0.00005	0.00532	1.77	1.38	1.41
Cer-NDS d42:1; Cer-NDS d21:0/21:1	0.00017	0.0464	-	2.17	1.29	-	PE 32:2e; PE 16:1e/16:1	0.0001	0.00125	-	1.69	1.33	-
Cer-NS d34:1; Cer-NS d18:1/16:0	0	0	0	0.34	0.16	0.12	PE 32:3e; PE 16:1e/16:2	0.00253	-	-	1.69	-	-
Cer-NS d40:2; Cer-NS d18:1/22:1	-	0.00013	0.00001	-	0.54	0.43	PE 34:0; PE 16:0-18:0	0.00088	0	0.00196	1.77	2.02	1.82
Cer-NS d42:1; Cer-NS d18:1/24:0	-		0.02593	-	-	1.27	PE 34:1; PE 16:0-18:1	0.00226	0.0001	-	1.65	1.66	-
Cer-NS d42:2; Cer-NS d18:1/24:1	-	0.00248	0.02538	-	0.76	0.78	PE 34:1e; PE 18:1e/16:0	-	0.00473	0.00518	-	1.22	1.41
FA 16:0	0.0131	-	0.03529	1.15	-	0.77	PE 34:2; PE 16:1-18:1	0.00013	0.00001	0.03481	1.77	1.50	1.45
FA 18:0	0.00047	-	-	1.33	-	-	PE 34:2e; PE 16:1e/18:1	0.00003	0.04037	0.00969	1.37	1.19	1.28
FA 18:1	0.00001	0	0	0.40	0.20	0.10	PE 34:3; PE 16:1-18:2	0.00002	0.00018	0.00325	1.74	1.48	1.56
HexCer-NDS d40:0; HexCer-NDS d28:0/12:0	0.0002	0.00003	0	2.52	3.09	3.04	PE 34:3e; PE 16:1e/18:2	-	0.00012	-	-	1.33	-
HexCer-NS d40:1; HexCer-NS d21:1/19:0	0.00012	0.01909	0.00479	1.53	1.31	1.37	PE 34:3e; PE 18:2e/16:1	0.00013	0.00007	0.00027	1.96	1.65	1.60
HexCer-NS d42:1; HexCer-NS d26:1/16:0	0.00205	-	0.03616	1.67	-	1.49	PE 34:4e; PE 18:3e/16:1	0.00015	0.00019	-	1.82	1.38	-
HexCer-NS d42:2; HexCer-NS d25:2/17:0	0.00935	-	-	1.46	-	-	PE 36:1; PE 18:0-18:1	0	0.00001	0.00001	1.97	2.17	2.11
LPC 14:0	0.00022	0.00403	-	1.82	1.49	-	PE 36:2; PE 18:1-18:1	0.00002	0	0.0005	1.75	1.60	1.58
LPC 16:0	0.00212	0.03596	0.03619	1.85	1.14	0.76	PE 36:2e; PE 18:1e/18:1	0	-	0.02582	1.37	-	1.24
LPC 16:1	0.00001	0.02492	-	2.03	1.21	-	PE 36:3; PE 16:0-20:3	0.00115	0.00003	0.00072	1.97	2.20	2.20
LPC 18:0	0.02264	0	0.00025	1.21	1.91	1.84	PE 36:3; PE 18:1-18:2	0.00006	0.00003	0.00914	1.80	1.60	1.56
LPC 18:1	0.00007	0.01209	-	1.60	1.28	-	PE 36:3e; PE 18:2e/18:1	0.02167	-	-	1.32	-	-
LPE 16:0	0.01504	0.00039	0.02445	1.40	1.69	1.41	PE 36:4e; PE 16:1e/20:3	0	0.00003	0.00561	1.68	1.46	1.36
LPE 16:1	0.00004	0.00017	-	1.83	1.40	-	PE 36:5e; PE 16:1e/20:4	0.01203	0.03279	-	1.45	1.19	-
LPE 18:0	0.00106	0.00004	0.00014	1.90	3.43	3.82	PE 38:2; PE 18:1-20:1	0.00012	0.00001	0.00007	1.63	1.80	1.83
LPE 18:1	0.00011	0.00045	-	1.67	1.40	-	PE 38:2e; PE 18:1e/20:1	0.02011	-	0.00136	1.23	-	1.53
LPE 20:3	0.00042	0.00004	0.01131	1.81	1.56	1.37	PE 38:3; PE 18:0-20:3	0.00007	0.00002	0.00203	2.25	2.14	1.92
LPE 22:3	0.00796	0.04585	-	1.37	1.12	-	PE 38:3; PE 18:1-20:2	0.00013	0.0001	0.03319	1.73	1.63	1.44
LPG 18:1	0.00001	0	0	0.64	0.34	0.30	PE 38:3e; PE 16:1e/22:2	0.00065	-	-	1.27	-	-
LPI 16:0	0.00001	0	0	0.49	0.26	0.12	PE 38:4; PE 18:1-20:3	0.0012	0.00094	-	1.54	1.48	-
LPI 16:1	0.00043	0	0	0.58	0.24	0.11	PE 38:4e; PE 16:1e/22:3	0.00392	-	0.04397	1.20	-	0.82

Table S39: Fold change values: Of [P_{4441}][OAc] treated cells after 8h,16h and 24h, measured in ESI- (Continuation)

[P_{4441}][OAc] ESI -	p-value			Fold change			[P_{4441}][OAc] ESI -	p-value			Fold change		
Name	**8h**	**16h**	**24h**	**8h**	**16h**	**24h**	**Name**	**8h**	**16h**	**24h**	**8h**	**16h**	**24h**
LPI 18:0	0.01025	-	0.00093	1.41	-	0.67	PE 38:4e; PE 18:1e/20:3	0	0.00155	0.0054	1.58	1.28	1.33
LPI 18:1	-	0	0	-	0.40	0.18	PE 38:4e; PE 18:2e/20:2	0.00177	-	-	1.31	-	-
LPI 20:2	0.00013	0.00001	0	1.55	0.55	0.26	PE 38:5e; PE 18:2e/20:3	0.00008	0.00125	-	1.55	1.24	-
LPI 20:3	0.03165	0.00002	0	1.28	0.38	0.12	PE 40:2e; PE 18:1e/22:1	0.0374	-	-	1.22	-	-
LPI 22:3	0.00061	0.00172	0.00002	1.51	0.73	0.45	PE 40:3; PE 18:0-22:3	0.00064	0.00001	-	1.63	1.54	-
OxPE 34:1+1O; OxPE 16:0-18:1+1O	0.00028	0.00001	0.00002	1.59	1.67	1.95	PE 40:3e; PE 18:1e/22:2	0.01274	-	-	1.29	-	-
OxPE 36:1+1O; OxPE 18:1-18:0+1O	0.00001	0	0	3.08	4.16	4.01	PE 40:4; PE 18:1-22:3	0.00139	0.00285	-	1.63	1.27	-
PC 26:0; PC 12:0-14:0	0.02352	0.02238	0.00331	1.35	1.28	1.57	PE 40:4e; PE 18:1e/22:3	0.00259	0.0483	-	1.40	1.22	-
PC 28:0; PC 14:0-14:0	0.00014	0.00025	0.0002	1.77	1.77	1.96	PE 40:4e; PE 18:2e/22:2	0.01122	-	-	1.28	-	-
PC 28:1; PC 14:0-14:1	-	0	0.00162	-	0.53	0.65	PE 40:6e; PE 18:2e/22:4	-	0.04041	0.00745	-	0.83	0.61
PC 29:0; PC 14:0-15:0	0.00142	0.00106	0.00456	1.54	1.44	1.60	PG 28:0; PG 14:0-14:0	0.00195	0.00003	0.00698	0.57	0.51	0.66
PC 30:0; PC 14:0-16:0	-	0.01518	-	-	1.26	-	PG 32:2; PG 16:1-16:1	0	0	0.00007	0.39	0.24	0.33
PC 30:0; PC 15:0-15:0	0.04941	0.02102	-	1.27	1.24	-	PG 34:1; PG 16:0-18:1	-	0.00133	0.00115	-	1.36	1.55
PC 30:0e; PC 16:0e/14:0	0.02914	0.04354	0.00798	1.21	1.19	1.35	PG 36:2; PG 18:1-18:1	0.00101	0.03895	0.00674	1.28	1.11	1.31
PC 30:1; PC 14:0-16:1	0.00004	0.01051	-	1.63	1.20	-	PG 36:3; PG 18:1-18:2	0.00001	0	0.00038	0.60	0.51	0.59
PC 30:2; PC 14:0-16:2	0.01165	0	0.00005	0.86	0.50	0.49	PI 32:1; PI 14:0-18:1	0	0	0	0.34	0.27	0.26
PC 31:0; PC 15:0-16:0	0.03262	-	-	1.24	-	-	PI 32:2; PI 16:1-16:1	0	0	0	0.31	0.21	0.21
PC 31:1; PC 15:0-16:1	0.00011	-	-	1.43	-	-	PI 34:1; PI 16:0-18:1	0.00002	0	0.00011	0.43	0.33	0.26
PC 32:0; PC 16:0-16:0	0.00164	0.00027	0.00073	1.31	1.52	1.55	PI 34:2; PI 16:1-18:1	0	0	0.00002	0.47	0.39	0.38
PC 32:1; PC 16:0-16:1	0	0	0.00693	1.69	1.30	1.36	PI 36:1; PI 18:0-18:1	0.00031	0.00005	0.00002	0.71	0.52	0.46
PC 32:1e; PC 16:0e/16:1	0.0001	0.00989	-	1.44	1.18	-	PI 36:2; PI 18:1-18:1	0.00002	0	0.00001	0.60	0.44	0.50
PC 32:2; PC 16:1-16:1	0.00011	0.00761	0.02053	1.36	0.87	0.77	PI 36:3; PI 18:1-18:2	0.00002	0	0.00002	0.63	0.49	0.46
PC 33:1; PC 16:0-17:1	0.01954	-	-	1.39	-	-	PI 38:2; PI 18:0-20:2	-	0.02074	0.02293	-	0.82	0.63
PC 34:0; PC 16:0-18:0	0.00253	0.00002	0	1.56	2.36	2.44	PI 38:3; PI 18:0-20:3	-	0.00101	0.00041	-	0.66	0.61
PC 34:0e; PC 16:0e/18:0	-	0.00425	0.00129	-	1.41	1.69	PS 36:2; PS 18:1-18:1	-	0.00016	0.00962	-	0.69	0.60
PC 34:1; PC 16:0-18:1	0	0	0.00133	1.62	1.44	1.42	SM d32:0; SM d14:0/18:0	0.00013	0.00004	0.00551	2.08	1.96	1.42
PC 34:2; PC 16:1-18:1	0.00469	-	-	1.74	-	-	SM d32:1; SM d14:0/18:1	0.0007	-	-	1.40	-	-
PC 34:3; PC 16:1-18:2	0.00001	-	-	1.46	-	-	SM d34:0; SM d14:0/20:0	0.0028	0.00235	-	1.70	1.43	-
PC 36:1; PC 18:0-18:1	0.00195	0.00001	0.01918	1.57	1.58	1.68	SM d34:2; SM d16:0/18:2	0.00657	0.04035	-	1.57	1.34	-
PC 36:2; PC 18:1-18:1	0.00023	0.00343	-	1.57	1.24	-	SM d36:0; SM d17:0/19:0	0.00002	0	0.00247	2.67	2.56	2.23
PC 36:3; PC 16:0-20:3	0	0	0	7.64	6.85	4.74	SM d36:1; SM d16:0/20:1	0.00005	0.00025	0.00023	1.69	1.72	1.79
PC 36:3; PC 18:1-18:2	0.00083	-	-	1.60	-	-	SM d38:1; SM d19:1/19:0	0.00013	0.00219	0.00286	1.56	1.53	1.42
PC 38:2; PC 18:1-20:1	0.0002	0.00269	-	1.64	1.43	-	SM d40:0; SM d14:0/26:0	0.00003	0.00016	0	1.93	2.12	2.17
PC 38:3; PC 18:1-20:2	0.00001	0.0003	0.00346	2.22	1.77	1.70	SM d40:1; SM d14:0/26:1	0.00002	0	0.00001	2.16	2.28	1.88
PC 38:4; PC 18:1-20:3	0.00044	-	-	1.90	-	-	SM d40:1; SM d14:1/26:0	0.01676	-	-	1.33	-	-
PC 38:5; PC 18:1-20:4	0.00003	0.021	-	1.95	1.14	-	SM d40:2; SM d18:0/22:2	0.0009	0.00207	0.0064	1.48	1.44	1.39
PC 40:3; PC 18:1-22:2	0.00013	0.00005	0.00001	1.90	2.02	2.23	SM d42:1; SM d14:0/28:1	0.00003	0.00001	0.00001	1.91	2.41	2.23
PC 40:4; PC 18:1-22:3	0.00001	0.00051	-	1.84	1.58	-	SM d42:1; SM d14:1/28:0	0.00018	0.01331	0.00092	1.53	1.37	1.60
PE 28:0; PE 14:0-14:0	0.00012	0.00013	0.00088	1.99	2.30	1.83	SM d42:2; SM d14:0/28:2	0.0001	-	0.01395	1.47	-	1.28
PE 30:1e; PE 16:1e/14:0	0.00003	0.00013	0.00071	0.63	0.62	0.70	SM d42:3; SM d16:3/26:0	0.00098	-	-	1.41	-	-
PE 32:1; PE 16:0-16:1	0.0004	0.00002	0.01671	1.92	1.91	1.69	SM d44:2; SM d14:2/30:0	0.00307	-	0.0086	1.41	-	1.40

Table S40: Fold change values: Of $[P_{14444}][OAc]$ treated cells after 8h, 16 and 24h, measured in ESI+

$[P_{14444}][OAc]$ ESI +	p-value			Fold change			$[P_{14444}][OAc]$ ESI +	p-value			Fold change		
Name	**8h**	**16h**	**24h**	**8h**	**16h**	**24h**	**Name**	**8h**	**16h**	**24h**	**8h**	**16h**	**24h**
BMP 38:3; BMP 18:1-20:2	-	0.03465	0.00201	-	0.67	0.51	PE 40:3; PE 18:0-22:3	-	0.00281	0.00068	-	1.48	1.43
BMP 40:5; BMP 18:1-22:4	-	0.00998	0.02	-	0.61	0.59	PE 40:4; PE 18:1-22:3	-	0.00103	0.00015	-	1.38	1.74
Cer-NDS d34:0; Cer-NDS d18:0/16:0	-	0.00026	-	-	1.63	-	PE 40:4e; PE 18:0e/22:4	-	-	0.02124	-	-	1.42
Cer-NDS d36:0; Cer-NDS d18:0/18:0	0.00036	0.00004	-	2.47	2.27	-	PE 40:5; PE 18:0-22:5	-	0.01409	0.00914	-	1.32	1.49
Cer-NDS d38:0; Cer-NDS d18:0/20:0	0.00044	0.00005	0.00002	3.10	3.89	2.44	PG 30:0; PG 14:0-16:0	-	0.02019	0.01116	-	1.41	1.50
Cer-NDS d40:0; Cer-NDS d18:0/22:0	0.00014	0	0	2.98	7.98	4.14	PG 34:1; PG 16:0-18:1	-	0.00869	0.00465	-	1.36	1.53
Cer-NDS d40:1; Cer-NDS d18:0/22:1	-	0.00076	-	-	1.68	-	PG 36:1; PG 18:0-18:1	-	-	0.01408	-	-	1.30
Cer-NDS d42:0; Cer-NDS d18:0/24:0	-	0	0	-	11.28	8.22	PG 36:2; PG 20:0-16:2	-	0.00434	0.00987	-	0.59	0.50
Cer-NDS d42:1; Cer-NDS d18:0/24:1	-	0	0	-	4.95	2.70	SM d28:1; SM d14:0/14:1	-	0.00383	-	-	1.23	-
Cer-NDS d44:0; Cer-NDS d18:0/26:0	-	0.00014	0.00021	-	4.78	6.91	SM d32:0; SM d14:0/18:0	-	0.00004	0.00058	-	1.71	1.36
Cer-NS d32:1; Cer-NS d18:1/14:0	0.00002	0	0.00018	0.52	0.25	0.31	SM d32:1; SM d14:0/18:1	-	-	0.00676	-	-	1.41
Cer-NS d34:1; Cer-NS d18:1/16:0	0.00005	0	0	0.54	0.33	0.37	SM d34:0; SM d14:0/20:0	-	0.00037	0.00032	-	1.46	1.59
Cer-NS d36:1; Cer-NS d18:1/18:0	-	0.00002	0.00008	-	0.42	0.40	SM d34:1; SM d14:0/20:1	-	-	0.00393	-	-	1.37
Cer-NS d38:1; Cer-NS d18:1/20:0	-	0.00064	0.00049	-	0.55	0.51	SM d34:2; SM d16:0/18:2	-	-	0.02001	-	-	1.24
Cer-NS d38:2; Cer-NS d18:1/20:1	-	0.00005	0.00014	-	0.41	0.33	SM d34:3; SM d14:1/20:2	-	0.01467	0.00019	-	1.46	1.56
Cer-NS d40:2; Cer-NS d18:1/22:1	-	0	0.00011	-	0.4	0.43	SM d34:4; SM d14:2/20:2	-	-	0.01177	-	-	1.36
Cer-NS d40:3; Cer-NS d18:2/22:1	-	0.00025	0.00354	-	0.28	0.29	SM d36:0; SM d14:0/22:0	-	0.00002	0.00004	-	1.97	1.92
Cer-NS d41:2; Cer-NS d18:1/23:1	-	0.00199	0.03686	-	0.41	0.56	SM d36:1; SM d14:0/22:1	-	0.01644	0.02446	-	1.24	1.29
Cer-NS d42:1; Cer-NS d18:1/24:0	-	0.00009	0.00844	-	1.57	1.50	SM d36:1; SM d14:1/22:0	-	-	0.00022	-	-	1.49
Cer-NS d42:2; Cer-NS d18:1/24:1	-	0.00232	-	-	0.74	-	SM d36:3; SM d16:1/20:2	-	-	0.02176	-	-	0.55
Cer-NS d42:3; Cer-NS d18:2/24:1	0.00023	0.01102	0.00082	0.21	0.29	0.25	SM d36:4; SM d16:2/20:2	-	-	0.00657	-	-	0.64
Cer-NS d44:1; Cer-NS d18:1/26:0	-	-	0.00184	-	-	2.17	SM d38:0; SM d14:0/24:0	-	0.00001	0.00107	-	1.82	2.06
Cer-NS d44:3; Cer-NS d18:2/26:1	-	-	0.04378	-	-	0.76	SM d38:1; SM d14:1/24:0	-	-	0.00477	-	-	1.32
DAG 30:0; DAG 14:0-16:0	-	0.00074	-	-	1.82	-	SM d38:2; SM d16:0/22:2	-	-	0.02136	-	-	1.39
DAG 32:0; DAG 16:0-16:0	0.0001	0.00001	0.00388	2.32	2.83	1.94	SM d40:0; SM d14:0/26:0	-	0.00003	0.00026	-	1.74	1.80
DAG 32:1; DAG 16:0-16:1	0.00088	-	-	1.41	-	-	SM d40:1; SM d14:0/26:1	-	0.00001	0.00066	-	1.66	1.85
DAG 34:2; DAG 16:1-18:1	-	0.002	0.02411	-	0.69	0.64	SM d40:1; SM d14:1/26:0	-	-	0.03329	-	-	1.33
DAG 36:2; DAG 18:1-18:1	-	0.00097	0.0039	-	0.63	0.57	SM d40:2; SM d14:0/26:2	-	-	0.01839	-	-	1.30
DAG 36:3; DAG 18:1-18:2	-	0.00013	0.01294	-	0.58	0.60	SM d41:2; SM d19:0/22:2	-	-	0.02856	-	-	1.34
DAG 36:4; DAG 16:2-20:2	-	0.00026	0.00157	-	0.48	0.33	SM d42:0; SM d14:0/28:0	-	0.0027	0.00002	-	1.37	2.16
DAG 38:4; DAG 18:1-20:3	-	0.00121	0.00048	-	0.40	0.31	SM d42:1; SM d14:0/28:1	-	0.00013	0.00177	-	1.74	1.81
DAG 38:4; DAG 18:2-20:2	-	0.01289	0.01214	-	0.64	0.52	SM d42:1; SM d14:1/28:0	-	0.01743	0.01687	-	1.20	1.27
DAG 40:4; DAG 18:1-22:3	-	0.00405	0.01222	-	0.59	0.50	SM d42:2; SM d20:0/22:2	0.00068	0	0.00123	1.51	1.65	1.90
HexCer-NS d34:1; HexCer-NS d18:1/16:0	-	0.00984	-	-	0.70	-	SM d42:3; SM d14:2/28:1	-	-	0.02989	-	-	1.20
HexCer-NS d40:2; HexCer-NS d18:1/22:1	-	-	0.03197	-	-	0.74	SM d42:4; SM d15:3/27:1	-	-	0.02763	-	-	1.48
LPC 15:0	-	0.01939	0.00332	-	0.61	0.54	SM d42:5; SM d14:3/28:2	-	-	0.00102	-	-	0.47
LPC 16:0	-	0.00001	0.04571	-	1.69	1.32	SM d44:0; SM d14:0/30:0	-	-	0.00213	-	-	2.37
LPC 18:0	-	0	0.00478	-	2.18	1.65	SM d44:1; SM d14:0/30:1	-	0.00257	0.00036	-	1.53	2.37
LPC 20:1	-	0.00007	-	-	1.64	-	SM d44:3; SM d14:2/30:1	-	-	0.02569	-	-	1.30
LPC 24:0	-	-	0.01093	-	-	1.93	SM d44:5; SM d22:3/22:2	-	0.01207	0.03732	-	1.49	1.58
LPE 16:0	-	0.00043	0.00379	-	1.66	1.47	TAG 44:1; TAG 12:0-14:0-18:1	-	0.00622	0.00001	-	0.67	0.59

Table S40: Fold change values: Of [P_{14444}][OAc] treated cells after 8h, 16 and 24h, measured in ESI+ (Continuation)

[P_{14444}][OAc] ESI +	p-value			Fold change			[P_{14444}][OAc] ESI +	p-value			Fold change		
Name	**8h**	**16h**	**24h**	**8h**	**16h**	**24h**	**Name**	**8h**	**16h**	**24h**	**8h**	**16h**	**24h**
LPE 18:0	0.00053	0	0.00025	1.57	2.35	2.09	TAG 44:1; TAG 14:0-14:0-16:1	-	0.00821	0.00003	-	0.65	0.46
LPE 20:2	-	0.01784	-	-	1.32	-	TAG 44:1; TAG 14:0-14:1-16:0	-	0.00199	0.00008	-	0.60	0.55
PC 16:1e; PC 14:1e/2:0	-	0.0169	0.01968	-	0.79	0.56	TAG 46:1; TAG 12:0-16:0-18:1	-	0.00398	0.00566	-	0.62	0.61
PC 20:1e; PC 18:1e/2:0	-	0.0004	-	-	1.58	-	TAG 46:1; TAG 14:0-14:0-18:1	-	0.0158	0.00181	-	0.71	0.68
PC 20:3e; PC 18:3e/2:0	-	-	0.02864	-	-	0.63	TAG 46:2; TAG 14:0-16:0-16:2	-	0.0007	0.00006	-	0.54	0.51
PC 26:0; PC 13:0-13:0	-	0.01251	0.00186	-	1.46	1.82	TAG 46:2; TAG 14:0-16:1-16:1	-	0.00084	0.00016	-	0.53	0.49
PC 28:0; PC 14:0-14:0	-	0.00087	0.00071	-	1.32	1.87	TAG 46:3; TAG 12:0-14:0-20:3	-	0.00845	0.00341	-	0.51	0.61
PC 28:1; PC 14:0-14:1	-	-	0.0081	-	-	1.36	TAG 46:3; TAG 15:0-15:0-16:3	-	0.00043	0	-	0.45	0.43
PC 29:0; PC 14:0-15:0	-	-	0.01983	-	-	1.48	TAG 47:1; TAG 13:0-16:0-18:1	-	0.00318	0.00062	-	0.66	0.54
PC 30:0; PC 14:0-16:0	-	0.00054	0.00248	-	1.32	1.70	TAG 47:2; TAG 14:0-16:0-17:2	-	0.01113	0.00024	-	0.63	0.52
PC 30:0e; PC 14:0e/16:0	-	-	0.02738	-	-	1.29	TAG 48:1; TAG 14:0-16:0-18:1	-	0.01624	0.00652	-	0.74	0.71
PC 30:1; PC 14:0-16:1	-	-	0.02471	-	-	1.33	TAG 48:2; TAG 12:0-18:1-18:1	-	0.00188	0.00165	-	0.60	0.64
PC 30:2; PC 14:1-16:1	-	0.00117	0.00936	-	0.75	1.29	TAG 48:2; TAG 14:0-16:1-18:1	-	0.00087	0.0001	-	0.57	0.54
PC 31:0; PC 15:0-16:0	-	-	0.02087	-	-	1.33	TAG 48:2; TAG 16:0-16:0-16:2	-	0.00669	0.00526	-	0.59	0.54
PC 31:1; PC 15:0-16:1	-	-	0.03868	-	-	1.33	TAG 48:3; TAG 14:0-16:1-18:2	-	0.00015	0.0002	-	0.49	0.54
PC 32:0; PC 16:0-16:0	-	0.00061	0.0004	-	1.42	1.58	TAG 48:4; TAG 12:0-16:1-20:3	-	0.00052	0.00001	-	0.42	0.47
PC 32:1; PC 16:0-16:1	-	-	0.02526	-	-	1.28	TAG 49:1; TAG 14:0-17:0-18:1	-	0.01073	0.00375	-	0.69	0.62
PC 32:2; PC 16:0-16:2	-	-	0.00706	-	-	1.57	TAG 49:3; TAG 15:1-17:0-17:2	-	0.0105	0.00196	-	0.55	0.60
PC 32:2; PC 16:1-16:1	-	-	0.03112	-	-	1.31	TAG 49:4; TAG 15:0-15:2-19:2	-	0.00078	0.00313	-	0.53	0.47
PC 32:3; PC 16:1-16:2	-	0.01063	-	-	0.81	-	TAG 50:2; TAG 14:0-16:0-20:2	-	0.0022	0.001	-	0.62	0.57
PC 33:1; PC 15:0-18:1	-	-	0.0143	-	-	1.35	TAG 50:2; TAG 14:0-18:1-18:1	-	0.00229	0.0001	-	0.62	0.62
PC 34:0; PC 16:0-18:0	-	0.00001	0.00015	-	1.84	1.86	TAG 50:2; TAG 16:0-16:0-18:2	-	0.03362	0.0123	-	0.71	0.60
PC 34:0e; PC 14:0e/20:0	-	0.0048	-	-	1.30	-	TAG 50:2; TAG 16:0-16:1-18:1	-	0.00161	0.00254	-	0.62	0.60
PC 34:1e; PC 14:0e/20:1	-	-	0.02117	-	-	1.25	TAG 50:3; TAG 14:0-18:0-18:3	-	0.00222	0.00606	-	0.59	0.61
PC 34:2; PC 16:1-18:1	-	-	0.00061	-	-	1.43	TAG 50:3; TAG 16:0-16:0-18:3	-	0.001	0.00094	-	0.56	0.50
PC 34:3; PC 16:1-18:2	-	-	0.00989	-	-	1.46	TAG 50:3; TAG 16:0-16:1-18:2	-	0.00005	0.00045	-	0.49	0.49
PC 35:1; PC 17:0-18:1	-	-	0.02061	-	-	1.36	TAG 50:3; TAG 16:1-16:1-18:1	-	0.00002	0.00043	-	0.47	0.52
PC 35:2; PC 16:0-19:2	-	-	0.0252	-	-	1.38	TAG 50:4; TAG 14:0-14:0-22:4	-	0.0005	0.00014	-	0.40	0.39
PC 36:0; PC 18:0-18:0	-	0	0.00048	-	2.53	2.64	TAG 50:4; TAG 14:0-16:1-20:3	-	0.00012	0.00001	-	0.41	0.39
PC 36:1; PC 18:0-18:1	-	0.00021	0.00286	-	1.35	1.77	TAG 50:4; TAG 16:1-16:1-18:2	-	0.00026	0.00627	-	0.41	0.48
PC 36:1e; PC 14:0e/22:1	-	0.00242	0.0094	-	1.33	1.40	TAG 50:5; TAG 14:0-16:0-20:5	-	0.00026	0.00052	-	0.46	0.39
PC 36:2; PC 18:1-18:1	-	-	0.03543	-	-	1.28	TAG 50:5; TAG 14:0-16:2-20:3	-	0.00001	0	-	0.42	0.38
PC 36:3; PC 16:0-20:3	-	-	0.00016	-	-	1.66	TAG 51:1; TAG 15:0-17:0-19:1	-	0.02233	-	-	0.69	-
PC 36:3; PC 18:1-18:2	-	0.02684	0.00155	-	1.15	1.49	TAG 51:2; TAG 16:0-17:1-18:1	-	0.00288	0.03086	-	0.54	0.65
PC 36:3; PC 20:1-16:2	-	-	0.00081	-	-	1.59	TAG 51:3; TAG 15:1-17:0-19:2	-	0.00371	0.00095	-	0.51	0.53
PC 36:3e; PC 14:0e/22:3	-	0	0.00011	-	0.46	0.50	TAG 51:4; TAG 15:2-18:1-18:1	-	0.02457	0.00447	-	0.59	0.6
PC 36:4; PC 16:0-20:4	-	-	0.04261	-	-	1.27	TAG 52:2; TAG 16:0-18:1-18:1	-	-	0.02974	-	-	0.68
PC 36:4e; PC 14:0e/22:4	-	0.00009	0.00004	-	0.55	0.55	TAG 52:3; TAG 14:3-19:0-19:0	-	0.02388	0.00614	-	0.67	0.54
PC 36:5; PC 16:1-20:4	-	0.01109	-	-	0.81	-	TAG 52:3; TAG 16:0-18:1-18:2	-	0.00066	0.00318	-	0.55	0.55
PC 38:1; PC 18:0-20:1	-	0.00026	0.00377	-	1.77	2.19	TAG 52:3; TAG 16:1-18:1-18:1	-	0.00313	0.00044	-	0.58	0.54
PC 38:2; PC 18:1-20:1	-	0.00139	0.00023	-	1.36	1.71	TAG 52:4; TAG 14:0-16:0-22:4	-	0.00003	0.00017	-	0.40	0.41
PC 38:2; PC 19:1-19:1	-	0.00119	0.00036	-	1.34	1.67	TAG 52:4; TAG 16:0-16:0-20:4	-	0.00053	0.00342	-	0.47	0.47

Table S40: Fold change values: Of [P_{14444}][OAc] treated cells after 8h, 16 and 24h, measured in ESI+ (Continuation)

[P_{14444}][OAc] ESI +	p-value			Fold change			[P_{14444}][OAc] ESI +	p-value			Fold change		
Name	**8h**	**16h**	**24h**	**8h**	**16h**	**24h**	**Name**	**8h**	**16h**	**24h**	**8h**	**16h**	**24h**
PC 38:3; PC 18:0-20:3	-	0.03401	0.00069	-	1.14	1.38	TAG 52:4; TAG 16:1-18:1-18:2	-	0.0001	0.00015	-	0.43	0.45
PC 38:3; PC 18:1-20:2	-	0.00682	0.01164	-	1.20	1.35	TAG 52:4; TAG 16:2-18:1-18:1	-	0.00102	0.00041	-	0.53	0.40
PC 38:3e; PC 16:0e/22:3	-	0.00904	0.00154	-	0.82	0.73	TAG 52:5; TAG 16:1-16:1-20:3	-	0.00011	0.00003	-	0.38	0.38
PC 38:4; PC 18:1-20:3	-	-	0.00798	-	-	1.40	TAG 52:6; TAG 16:1-16:1-20:4	-	0.00003	0.00042	-	0.43	0.51
PC 38:4e; PC 14:0e/24:4	-	0.00587	0.01787	-	0.85	0.83	TAG 53:3; TAG 17:1-18:1-18:1	-	0.00134	0.00082	-	0.53	0.55
PC 40:2; PC 20:1-20:1	-	0.00005	0.00364	-	1.72	1.86	TAG 54:1; TAG 16:0-18:0-20:1	-	-	0.04075	-	-	1.62
PC 40:3; PC 18:0-22:3	-	-	0.00247	-	-	1.39	TAG 54:3; TAG 16:3-19:0-19:0	-	0.02211	0.00736	-	0.65	0.53
PC 40:3; PC 18:1-22:2	-	0.01538	0.01093	-	1.28	1.51	TAG 54:3; TAG 18:0-18:1-18:2	-	0.00246	0.00069	-	0.60	0.51
PC 40:4; PC 18:1-22:3	-	-	0.0407	-	-	1.27	TAG 54:3; TAG 18:1-18:1-18:1	-	0.00154	0.0021	-	0.60	0.58
PC 40:4e; PC 14:0e/26:4	-	0.00025	0.00136	-	0.65	0.68	TAG 54:4; TAG 16:0-16:0-22:4	-	0.00109	-	-	0.62	-
PC 40:5; PC 18:1-22:4	-	-	0.02133	-	-	1.32	TAG 54:4; TAG 16:0-18:1-20:3	-	0.00023	0.03537	-	0.41	0.50
PC 40:6; PC 20:3-20:3	-	-	0.01663	-	-	1.63	TAG 54:4; TAG 18:1-18:1-18:2	-	0.00006	0.00064	-	0.45	0.44
PC 42:2; PC 21:1-21:1	-	0.00062	0.00172	-	1.89	2.80	TAG 54:5; TAG 16:1-18:1-20:3	-	0.00008	0.00001	-	0.36	0.38
PC 42:2e; PC 16:0e/26:2	-	0.02413	-	-	1.33	-	TAG 54:6; TAG 16:1-18:1-20:4	-	0.00001	0.00004	-	0.38	0.40
PC 42:3; PC 18:1-24:2	-	0.00003	0.00199	-	1.67	2.40	TAG 54:7; TAG 14:0-20:3-20:4	-	-	0.0202	-	-	0.77
PC 42:4; PC 21:2-21:2	-	0.00045	0.00006	-	1.58	1.57	TAG 55:3; TAG 17:1-18:1-20:1	-	0.01791	0.01623	-	0.63	0.62
PC 44:2; PC 22:1-22:1	-	0.00188	0.00006	-	2.36	4.67	TAG 55:5; TAG 17:2-19:0-19:3	-	0.00095	0.0337	-	0.41	0.61
PE 30:0; PE 14:0-16:0	-	0.00807	0.00022	-	1.60	1.77	TAG 56:3; TAG 18:1-18:1-20:1	-	0.00098	0.04993	-	0.63	0.69
PE 30:1; PE 14:0-16:1	-	0.02229	0.00426	-	1.53	1.92	TAG 56:4; TAG 18:1-18:1-20:2	-	0.00066	0.00162	-	0.50	0.47
PE 32:0; PE 16:0-16:0	-	0.00002	0.00012	-	1.92	1.71	TAG 56:5; TAG 18:0-18:4-20:1	-	0.00031	0.00023	-	0.40	0.43
PE 32:1; PE 14:0-18:1	-	0.00007	0.00003	-	1.56	1.89	TAG 56:5; TAG 18:1-18:1-20:3	-	0.0001	0.00034	-	0.36	0.38
PE 32:1; PE 16:0-16:1	-	0	0	-	1.64	1.97	TAG 56:6; TAG 18:1-18:1-20:4	-	0.00002	0.00008	-	0.39	0.43
PE 32:2; PE 16:1-16:1	-	-	0.01465	-	-	1.67	TAG 56:7; TAG 16:1-18:1-22:5	-	0.00006	0.00007	-	0.37	0.40
PE 34:0; PE 16:0-18:0	-	0.00065	0.00001	-	1.67	2.16	TAG 56:7; TAG 16:1-20:3-20:3	-	0.00024	0.00093	-	0.36	0.44
PE 34:1; PE 16:0-18:1	-	0.00036	0.00011	-	1.51	1.91	TAG 58:3; TAG 18:1-20:1-20:1	-	0.01181	-	-	0.65	-
PE 34:2; PE 16:0-18:2	-	0.00206	0.00056	-	1.34	1.78	TAG 58:4; TAG 18:1-18:1-22:2	-	0.00184	0.04501	-	0.52	0.59
PE 34:2; PE 16:1-18:1	-	0.00072	0.00112	-	1.43	1.85	TAG 58:5; TAG 18:1-18:1-22:3	-	0.00005	0.00038	-	0.41	0.46
PE 34:3; PE 16:1-18:2	-	-	0.00019	-	-	1.68	TAG 58:5; TAG 18:3-20:1-20:1	-	0.00056	0.03714	-	0.42	0.53
PE 35:1e; PE 16:0e/19:1	-	0.00003	0.00011	-	0.60	0.49	TAG 58:6; TAG 18:1-20:2-20:3	-	0.00002	0.00045	-	0.40	0.38
PE 36:1; PE 18:0-18:1	-	0.0001	0.00001	-	1.81	2.07	TAG 58:6; TAG 18:2-20:2-20:2	-	0.0026	0.00794	-	0.48	0.48
PE 36:2; PE 18:0-18:2	-	0.00014	0.00009	-	1.43	1.71	TAG 58:7; TAG 18:1-18:2-22:4	-	0.00002	0.00023	-	0.35	0.36
PE 36:2; PE 18:1-18:1	-	0.00077	0.00009	-	1.39	1.76	TAG 58:7; TAG 18:1-20:3-20:3	-	0.00002	0.00005	-	0.35	0.33
PE 36:3; PE 16:0-20:3	-	0.00002	0	-	1.65	2.09	TAG 58:8; TAG 18:1-20:3-20:4	-	0.00044	0.00012	-	0.38	0.38
PE 36:3; PE 18:1-18:2	-	0.00178	0.00001	-	1.40	2.18	TAG 58:8; TAG 18:3-20:0-20:5	-	0.00017	0.00017	-	0.36	0.40
PE 36:4; PE 16:1-20:3	-	-	0.00377	-	-	1.90	TAG 60:4; TAG 18:0-20:1-22:3	-	0.01558	-	-	0.66	-
PE 36:4; PE 18:2-18:2	-	-	0.00325	-	-	1.48	TAG 60:4; TAG 18:0-20:2-22:2	-	0.0315	-	-	0.67	-
PE 38:1; PE 17:0-21:1	-	0.00007	0.0001	-	1.71	2.10	TAG 60:5; TAG 18:2-20:1-22:2	-	0.00844	0.03854	-	0.46	0.56
PE 38:2; PE 18:0-20:2	-	0.00032	0.00002	-	1.47	2.10	TAG 60:6; TAG 18:1-20:3-22:2	-	0.00074	0.02746	-	0.41	0.50
PE 38:3; PE 18:0-20:3	0.00123	0	0	1.63	2.04	2.42	TAG 60:7; TAG 20:2-20:2-20:3	-	0.00023	0.03767	-	0.42	0.51
PE 38:4; PE 18:0-20:4	-	0.00239	0.00073	-	1.54	1.64	TAG 60:8; TAG 20:2-20:2-20:4	-	0.00324	0.03512	-	0.45	0.46
PE 38:4; PE 22:0-16:4	-	0.00088	0.00001	-	1.49	1.80	TAG 62:5; TAG 18:1-22:1-22:3	-	0.00879	-	-	0.49	-
PE 38:5; PE 16:0-22:5	-	0.00131	0.00058	-	1.51	1.69	TAG 62:7; TAG 20:2-20:3-22:2	-	0.00021	0.00383	-	0.43	0.41

Table S40: Fold change values: Of [P_{14444}][OAc] treated cells after 8h, 16 and 24h, measured in ESI+ (Continuation)

[P_{14444}][OAc] ESI +	p-value			Fold change			[P_{14444}][OAc] ESI +	p-value			Fold change		
Name	**8h**	**16h**	**24h**	**8h**	**16h**	**24h**	**Name**	**8h**	**16h**	**24h**	**8h**	**16h**	**24h**
PE 40:2; PE 18:1-22:1	-	0.00002	0.00218	-	1.56	1.74	TAG 64:7; TAG 20:2-22:2-22:3	-	0.00165	0.02377	-	0.46	0.51

Table S41: Fold change values: Of [P_{14444}][OAc] treated cells after 8h, 16h and 24h, measured in ESI-

[P_{14444}][OAc] ESI -	p-value			Fold change			[P_{14444}][OAc] ESI -	p-value			Fold change		
Name	**8h**	**16h**	**24h**	**8h**	**16h**	**24h**	**Name**	**8h**	**16h**	**24h**	**8h**	**16h**	**24h**
Cer-NS d34:1; Cer-NS d18:1/16:0	0.0007	0	0	0.57	0.39	0.43	PE 32:3e; PE 16:1e/16:2	-	-	0.00069	-	-	1.38
Cer-NS d40:2; Cer-NS d18:1/22:1	-	0.00002	0.00001	-	0.44	0.41	PE 34:0e; PE 18:0e/16:0	0.00399	0.00001	0.00004	1.88	3.07	2.45
Cer-NS d42:1; Cer-NS d18:1/24:0	-	0.00299	0.01217	-	1.42	1.63	PE 34:1; PE 16:0-18:1	0.0122	0.00026	0	1.33	1.53	1.75
FA 18:0	-	-	0.0207	-	-	1.29	PE 34:1e; PE 18:1e/16:0	-	0.00794	0.00009	-	1.34	1.58
HexCer-NDS d40:0; HexCer-NDS d28:0/12:0	0.00448	0.00003	0	1.52	2.26	2.53	PE 34:2; PE 16:1-18:1	0.00733	0.00214	0.00004	1.25	1.31	1.70
HexCer-NS d42:1; HexCer-NS d26:1/16:0	-	-	0.0236	-	-	1.34	PE 34:2e; PE 16:1e/18:1	-	0.0351	0.00174	-	1.15	1.27
LPC 14:0	-	-	0.00944	-	-	0.70	PE 34:3; PE 16:1-18:2	-	0.00393	0.0002	-	1.36	1.71
LPC 16:0	0.00104	0.00356	-	1.32	1.41	-	PE 34:3e; PE 18:2e/16:1	-	-	0.02146	-	-	1.25
LPC 18:0	0.03078	0.00018	0.02854	1.43	2.32	1.52	PE 34:4e; PE 18:2e/16:2	-	-	0.00126	-	-	1.34
LPC 18:1	-	0.0264	0.04503	-	0.83	0.72	PE 36:1; PE 18:0-18:1	0.00235	0.00013	0	1.43	1.65	1.87
LPE 16:0	0.00636	0.0006	0.00141	1.38	1.51	1.42	PE 36:1e; PE 16:0e/20:1	-	0.00001	0.00419	-	2.33	2.83
LPE 18:0	0.00292	0.00005	0.00084	1.57	2.20	1.60	PE 36:2; PE 18:1-18:1	-	0.00033	0.00002	-	1.43	1.71
LPE 20:3	0.02083	0.00329	0.00103	1.34	1.59	1.54	PE 36:2e; PE 18:1e/18:1	-	0.00207	0.00007	-	1.23	1.46
LPE 22:3	-	0.01769	0.0068	-	1.45	1.44	PE 36:3; PE 18:1-18:2	-	0.00601	0.00025	-	1.27	1.72
LPI 18:0	-	0.00137	0.00013	-	0.78	0.65	PE 36:4e; PE 16:1e/20:3	-	0.0336	0.00012	-	1.16	1.47
LPI 18:1	0.0034	0.00026	0.00886	1.32	1.59	1.44	PE 36:5e; PE 18:4e/18:1	-	-	0.03999	-	-	1.26
LPI 20:2	0.01608	0.00038	0.00236	1.33	1.35	1.38	PE 38:2; PE 18:1-20:1	0.01261	0.00002	0	1.34	1.56	1.86
LPI 20:3	0.00376	-	-	1.38	-	-	PE 38:2e; PE 18:1e/20:1	-	0.00319	0.00296	-	1.45	1.62
LPI 22:3	-	0.0366	-	-	1.17	-	PE 38:3; PE 18:0-20:3	0.00015	0.00008	0	1.75	1.95	2.16
OxPE 34:1+1O; OxPE 16:0-18:1+1O	-	0.0011	0.0012	-	1.70	2.04	PE 38:3; PE 18:1-20:2	0.00956	0.0017	0.00001	1.28	1.48	1.92
OxPE 36:1+1O; OxPE 18:1-18:0+1O	0.00004	0.00175	0	1.85	2.04	2.58	PE 38:3e; PE 16:1e/22:2	-	0.01018	0.00025	-	1.27	1.37
PC 26:0; PC 12:0-14:0	-	0.00024	0.0022	-	1.38	1.61	PE 38:3e; PE 18:2e/20:1	-	0.00018	0.02682	-	1.54	1.61
PC 28:0; PC 14:0-14:0	0.01235	0.0227	0.00061	1.32	1.22	1.49	PE 38:4; PE 18:1-20:3	0.00037	0.00018	0	1.44	1.55	1.93
PC 28:1; PC 14:0-14:1	-	0.00405	-	-	0.81	-	PE 38:4e; PE 18:1e/20:3	-	0.0274	0.00161	-	1.19	1.37
PC 30:0; PC 14:0-16:0	-	0.00073	0.00179	-	1.30	1.61	PE 38:5e; PE 18:2e/20:3	0.02527	0.0303	0.00086	1.22	1.14	1.34
PC 30:1; PC 14:0-16:1	0.03505	0.04418	0.00449	1.21	1.20	1.38	PE 40:3; PE 18:0-22:3	0.02578	0.00121	0.00102	1.39	1.39	1.55
PC 30:2; PC 14:1-16:1	-	0.00044	-	-	0.78	-	PE 40:3e; PE 18:1e/22:2	-	0.00503	0.01288	-	1.37	1.46
PC 32:0; PC 16:0-16:0	-	0.00131	0.00007	-	1.39	1.58	PE 40:4; PE 18:1-22:3	0.00472	0.00288	0.00055	1.26	1.39	1.59
PC 32:0e; PC 16:0e/16:0	-	-	0.03782	-	-	1.15	PE 40:4e; PE 18:1e/22:3	-	0.023	0.00326	-	1.22	1.21
PC 32:1; PC 16:0-16:1	0.01364	0.00685	0.00006	1.29	1.26	1.50	PE 40:4e; PE 18:2e/22:2	-	0.00891	0.01012	-	1.22	1.28
PC 32:2; PC 16:0-16:2	0.00056	-	-	1.32	-	-	PE 40:6e; PE 18:2e/22:4	0.00503	-	-	1.18	-	-
PC 32:2; PC 16:1-16:1	-	-	0.02224	-	-	1.32	PG 30:0; PG 14:0-16:0	-	-	0.02228	-	-	1.42

Table S41: Fold change values: Of $[P_{14444}][OAc]$ treated cells after 8h, 16h and 24h, measured in ESI- (Continuation)

$[P_{14444}][OAc]$ ESI -	p-value			Fold change			$[P_{14444}][OAc]$ ESI -	p-value			Fold change		
Name	**8h**	**16h**	**24h**	**8h**	**16h**	**24h**	**Name**	**8h**	**16h**	**24h**	**8h**	**16h**	**24h**
PC 33:1; PC 15:0-18:1	-	0.02113	0.00085	-	1.18	1.46	PG 34:1; PG 16:0-18:1	-	0.00046	0.00138	-	1.50	1.76
PC 34:0; PC 16:0-18:0	0.03564	0.00016	0.00071	1.25	1.94	1.72	PG 36:2; PG 18:1-18:1	-	0.00573	0.00086	-	1.33	1.59
PC 34:1; PC 16:0-18:1	0.02403	0.00405	0.00036	1.24	1.33	1.48	PI 34:2; PI 16:1-18:1	-	0.01385	0.0025	-	1.27	1.59
PC 34:1e; PC 16:0e/18:1	-	-	0.0308	-	-	1.16	PI 36:2; PI 18:1-18:1	-	-	0.04752	-	-	1.26
PC 34:2; PC 16:1-18:1	0.01291	0.03316	0.00879	1.21	1.22	1.36	SHexCer d33:0	-	-	0.00306	-	-	1.55
PC 34:3; PC 16:1-18:2	-	-	0.00417	-	-	1.45	SM d32:0; SM d14:0/18:0	0.0022	0.00001	0.00045	1.45	1.58	1.64
PC 36:1; PC 18:0-18:1	0.02394	0.00128	0.0003	1.22	1.37	1.65	SM d32:1; SM d14:0/18:1	-	-	0.01162	-	-	1.25
PC 36:2; PC 18:1-18:1	-	-	0.02209	-	-	1.45	SM d34:0; SM d14:0/20:0	0.00222	0.00003	0.00039	1.55	1.55	1.57
PC 36:3; PC 18:1-18:2	0.00576	0.02758	0.0016	1.30	1.21	1.45	SM d34:1; SM d18:1/16:0	-	-	0.00007	-	-	1.39
PC 36:4; PC 18:2-18:2	0.02116	-	-	1.22	-	-	SM d36:0; SM d17:0/19:0	0.00493	0.00024	0.00141	1.87	1.85	2.12
PC 38:2; PC 18:1-20:1	0.01135	0.00117	0.00042	1.33	1.34	1.60	SM d36:1; SM d17:0/19:1	0.03512	0.01505	0	1.24	1.19	1.46
PC 38:3; PC 16:0-22:3	-	0.0303	0.01511	-	1.19	1.32	SM d38:2; SM d16:0/22:2	0.03343	-	0.01206	1.20	-	1.33
PC 38:3; PC 18:1-20:2	-	-	0.0325	-	-	1.36	SM d40:0; SM d14:0/26:0	0.02942	0.00002	0.00005	1.28	1.63	2.07
PC 38:3e; PC 16:0e/22:3	-	0.0161	0.02119	-	0.73	0.73	SM d40:1; SM d14:0/26:1	0.01012	0.00025	0.00157	1.62	1.60	1.61
PC 38:4; PC 18:1-20:3	0.03608	-	0.03919	1.26	-	1.41	SM d40:1; SM d14:1/26:0	-	-	0.00504	-	-	1.26
PC 40:4; PC 18:1-22:3	0.01737	-	-	1.19	-	-	SM d40:2; SM d18:0/22:2	-	-	0.00063	-	-	1.28
PE 28:0; PE 14:0-14:0	0.00153	0.00004	0.00024	1.64	2.12	1.94	SM d42:0; SM d14:0/28:0	-	0.00882	0	-	1.44	2.41
PE 30:1; PE 14:0-16:1	0.00387	0.00472	0.00048	1.41	1.45	1.63	SM d42:1; SM d14:0/28:1	0.03151	0.0001	0.00065	1.40	1.64	2.03
PE 32:1; PE 16:0-16:1	0.01535	0.00047	0	1.32	1.60	1.92	SM d42:1; SM d21:0/21:1	-	-	0.01604	-	-	1.30
PE 32:1e; PE 16:1e/16:0	0.01984	0.00504	0.0004	1.29	1.32	1.50	SM d42:2; SM d14:0/28:2	-	-	0.00432	-	-	1.24
PE 32:2; PE 16:1-16:1	-	0.00105	0.00004	-	1.41	1.98	SM d44:2; SM d14:2/30:0	-	0.04688	0.0072	-	1.29	1.34
PE 32:2e; PE 16:1e/16:1	-	-	0.00145	-	-	1.37	SM d44:3; SM d14:2/30:1	-	-	0.00829	-	-	1.23

References

[1] S.-K. Ruokonen, C. Sanwald, A. Robciuc, S. Hietala, A.H. Rantamäki, J. Witos, A.W.T. King, M. Lämmerhofer, S.K. Wiedmer, Correlation between ionic liquid cytotoxicity and liposome-ionic liquid interactions, Chem. - A Eur. J. 24 (2017) 2669–2680. doi:10.1002/chem.201704924.

[2] Y. Wang, M. Tian, W. Bi, K.H. Row, Application of Ionic Liquids in High Performance Reversed-Phase Chromatography, Int. J. Mol. Sci. 10 (2009) 2591–2610. doi:10.3390/ijms10062591.

[3] K.S. Egorova, V.P. Ananikov, Ionic liquids in whole-cell biocatalysis : a compromise between toxicity and efficiency, Biophys. Rev. 10 (2018) 881–900. doi:10.1007/s12551-017-0389-9.

[4] P. Sun, D.W. Armstrong, Ionic liquids in analytical chemistry, Anal. Chim. Acta. 661 (2010) 1–16. doi:10.1016/j.aca.2009.12.007.

[5] X. Wang, C.A. Ohlin, Q. Lu, Z. Fei, J. Hu, P.J. Dyson, Cytotoxicity of ionic liquids and precursor compounds towards human cell line HeLa, Green Chem. 9 (2007) 1191. doi:10.1039/b704503d.

[6] S. Pandey, Analytical applications of room-temperature ionic liquids: A review of recent efforts, Anal. Chim. Acta. 556 (2006) 38–45. doi:10.1016/j.aca.2005.06.038.

[7] P. Stepnowski, A.C. Skladanowski, A. Ludwiczak, E. Laczyńska, Evaluating the cytotoxicity of ionic liquids using human cell line HeLa, Hum. Exp. Toxicol. 23 (2004) 513–517. doi:10.1191/0960327104ht480oa.

[8] A. Romero, A. Santos, J. Tojo, A. Rodríguez, Toxicity and biodegradability of imidazolium ionic liquids, J. Hazard. Mater. 151 (2008) 268–273. doi:10.1016/j.jhazmat.2007.10.079.

[9] M. Cvjetko Bubalo, K. Radošević, I. Radojčić Redovniković, J. Halambek, V. Gaurina Srček, A brief overview of the potential environmental hazards of ionic liquids, Ecotoxicol. Environ. Saf. 99 (2014) 1–12. doi:10.1016/j.ecoenv.2013.10.019.

[10] A. Sosnowska, M. Barycki, M. Zaborowska, A. Rybinska, T. Puzyn, Towards designing environmentally safe ionic liquids: The influence of the cation structure, Green Chem. 16 (2014) 4749–4757. doi:10.1039/c4gc00526k.

[11] C. Pretti, C. Chiappe, I. Baldetti, S. Brunini, G. Monni, L. Intorre, Acute toxicity of ionic liquids for three freshwater organisms: Pseudokirchneriella subcapitata, Daphnia magna and Danio rerio, Ecotoxicol. Environ. Saf. 72 (2009) 1170–1176. doi:10.1016/j.ecoenv.2008.09.010.

[12] M. Petkovic, K.R. Seddon, L.P.N. Rebelo, C.S. Pereira, Ionic liquids: A pathway to environmental acceptability, Chem. Soc. Rev. 40 (2011) 1383–1403. doi:10.1039/c004968a.

[13] K.S. Egorova, V.P. Ananikov, Toxicity of Ionic Liquids : Eco (cyto) activity as Complicated , but Unavoidable Parameter for Task-Specific Optimization, 7 (2014) 336–360. doi:10.1002/cssc.201300459.

[14] R.F.M. Frade, C.A.M. Afonso, Impact of ionic liquids in environment and humans: An overview, Hum. Exp. Toxicol. 29 (2010) 1038–1054. doi:10.1177/0960327110371259.

[15] M. Matzke, J. Arning, J. Ranke, B. Jastorff, S. Stolte, Design of Inherently Safer Ionic Liquids: Toxicology and Biodegradation, in: Handb. Green Chem., 2010: pp. 225–290.

[16] S. Stolte, M. Matzke, J. Arning, A. Böschen, W.R. Pitner, U. Welz-Biermann, B. Jastorff, J. Ranke, Effects of different head groups and functionalised side chains on the aquatic toxicity of ionic liquids, Green Chem. 9 (2007) 1170–1179. doi:10.1039/b711119c.

[17] A.S. Wells, V.T. Coombe, On the freshwater ecotoxicity and biodegradation properties of some common ionic liquids, Org. Process Res. Dev. 10 (2006) 794–798. doi:10.1021/op060048i.

[18] J. Pernak, K. Sobaszkiewicz, I. Mirska, Anti-microbial activities of ionic liquids, Green Chem. 5 (2003) 52–56. doi:10.1039/b207543c.

[19] S.P.M. Ventura, C.S. Marques, A.A. Rosatella, C.A.M. Afonso, F. Gonçalves, J.A.P. Coutinho, Toxicity assessment of various ionic liquid families towards Vibrio fischeri marine bacteria, Ecotoxicol. Environ. Saf. 76 (2012) 162–168. doi:10.1016/j.ecoenv.2011.10.006.

[20] S.P.M. Ventura, R.L.F. de Barros, T. Sintra, C.M.F. Soares, Á.S. Lima, J.A.P. Coutinho, Simple screening method to identify toxic/non-toxic ionic liquids: Agar diffusion test adaptation, Ecotoxicol. Environ. Saf. 83 (2012) 55–62. doi:10.1016/j.ecoenv.2012.06.002.

[21] D.O. Hartmann, K. Shimizu, F. Siopa, M.C. Leitão, C.A.M. Afonso, J.N. Canongia Lopes, C. Silva Pereira, Plasma membrane permeabilisation by ionic liquids: a matter of charge, Green Chem. 17 (2015) 4587–4598. doi:10.1039/c5gc01472g.

[22] S. Mikkola, A. Robciuc, J. Lokajova, A.J. Holding, M. Lämmerhofer, I. Kilpeläinen, J.M. Holopainen, A.W.T. King, S.K. Wiedmer, Impact of Amphiphilic Biomass-Dissolving Ionic Liquids on Biological Cells and Liposomes, Env. Sci Technol. 49 (2015) 1870–1878. doi:10.1021/es505725g.

[23] M.C. Bubalo, K. Radošević, I.R. Redovniković, I. Slivac, V.G. Srček, Toxicity mechanisms of ionic liquids, Arh Hig Rada Toksikol. 68 (2017) 171–179. doi:10.1515/aiht-2017-68-2979.

[24] G.S. Lim, J. Zidar, D.W. Cheong, S. Jaenicke, M. Klähn, Impact of Ionic Liquids in Aqueous Solution on Bacterial Plasma Membranes Studied with Molecular Dynamics Simulations, J. Phys. Chem. B. 118 (2014) 10444–10459. doi:10.1021/jp5060952.

[25] A. Benedetto, Room-temperature ionic liquids meet bio-membranes: the state-of-the-art, Biophys. Rev. 9 (2017) 309–320. doi:10.1007/s12551-017-0279-1.

[26] J.I. Santos, A.M.M. Gonçalves, J.L. Pereira, B.F.H.T. Figueiredo, F.A. Silva, J.A.P. Coutinho, S.P.M. Ventura, F. Gonçalves, Environmental safety of cholinium-based ionic liquids: assessing structure–ecotoxicity relationships, Green Chem. 17 (2015) 4657–4668. doi:10.1039/c5gc01129a.

[27] B. Yoo, J.K. Shah, Y. Zhu, E.J. Maginn, Amphiphilic interactions of ionic liquids with lipid biomembranes: a molecular simulation study, Soft Matter. 10 (2014) 8641–8651. doi:10.1039/c4sm01528b.

[28] L. Rakers, F. Glorius, Flexible design of ionic liquids for membrane interactions, Biophys. Rev. 10 (2018) 747–750. doi:10.1007/s12551-018-0412-9.

[29] R.J. Bernot, M.A. Brueseke, M.A. Evans-White, G.A. Lamberti, Acute and chronic toxicity of imidazolium-based ionic liquids on Daphnia magna, Environ. Toxicol. Chem. 24 (2005) 87–92. doi:10.1897/03-635.1.

[30] X.Y. Li, C.Q. Jing, W.L. Lei, J. Li, J.J. Wang, Apoptosis caused by imidazolium-based ionic liquids in PC12 cells, Ecotoxicol. Environ. Saf. 83 (2012) 102–107. doi:10.1016/j.ecoenv.2012.06.013.

[31] Z. Du, L. Zhu, M. Dong, J. Wang, J. Wang, H. Xie, S. Zhu, Effects of the ionic liquid [Omim]PF6 on antioxidant enzyme systems, ROS and DNA damage in zebrafish (Danio rerio), Aquat. Toxicol. 124–125 (2012) 91–93. doi:10.1016/j.aquatox.2012.08.002.

[32] B. Bachowska, J. Kazmierczak-Baranska, M. Cieslak, B. Nawrot, D. Szczęsna, J. Skalik, P. Bałczewski, High Cytotoxic Activity of Phosphonium Salts and Their Complementary Selectivity towards HeLa and K562 Cancer Cells: Identification of Tri- n -butyl- n -hexadecylphosphonium bromide as a Highly Potent Anti-HeLa Phosphonium Salt, ChemistryOpen. 1 (2012) 33–38. doi:10.1002/open.201100003.

[33] W.A. Cooper, W.A. Bartier, D.C. Rideout, E.J. Delikatny, 1H NMR visible lipids are induced by phosphonium salts and 5-fluorouracil in human breast cancer cells, Magn. Reson. Med. 45 (2001) 1001–1010. doi:10.1002/mrm.1133.

[34] B. Jing, N. Lan, J. Qiu, Y. Zhu, Interaction of Ionic Liquids with a Lipid Bilayer: A Biophysical Study of Ionic Liquid Cytotoxicity, J. Phys. Chem. B. 120 (2016) 2781–2789. doi:10.1021/acs.jpcb.6b00362.

[35] B. Yoo, B. Jing, S.E. Jones, G.A. Lamberti, Y. Zhu, J.K. Shah, E.J. Maginn, Molecular mechanisms of ionic liquid cytotoxicity probed by an integrated experimental and computational approach, Sci. Rep. 6 (2016) 1–8. doi:10.1038/srep19889.

[36] A. Benedetto, P. Ballone, Room-Temperature Ionic Liquids and Biomembranes: Setting the Stage for Applications in Pharmacology, Biomedicine, and Bionanotechnology, Langmuir. 34 (2018) 9579–9597. doi:10.1021/acs.langmuir.7b04361.

[37] M. Amde, J.F. Liu, L. Pang, Environmental Application, Fate, Effects, and Concerns of Ionic Liquids: A Review, Environ. Sci. Technol. 49 (2015) 12611–12627. doi:10.1021/acs.est.5b03123.

[38] N. Muhammad, M.I. Hossain, Z. Man, M. El-Harbawi, M.A. Bustam, Y.A. Noaman, N.B. Mohamed Alitheen, M.K. Ng, G. Hefter, C.Y. Yin, Synthesis and physical properties of choline carboxylate ionic liquids, J. Chem. Eng. Data. 57 (2012) 2191–2196. doi:10.1021/je300086w.

[39] R.J. Cornmell, C.L. Winder, G.J.T. Tiddy, R. Goodacre, G. Stephens, Accumulation of ionic liquids in Escherichia coli cells, Green Chem. 10 (2008) 836–841. doi:10.1039/b807214k.

[40] N. Kundu, S. Roy, D. Mukherjee, T.K. Maiti, N. Sarkar, Unveiling the Interaction between Fatty-Acid-Modified Membrane and Hydrophilic Imidazolium-Based Ionic Liquid: Understanding the Mechanism of Ionic Liquid Cytotoxicity, J. Phys. Chem. B. 121 (2017) 8162–8170. doi:10.1021/acs.jpcb.7b06231.

[41] A. Bado-nilles, A. Diallo, G. Marlair, P. Pandard, L. Chabot, A. Geffard, C. Len, J. Porcher, W. Sanchez, Coupling of OECD standardized test and immunomarkers to select the most environmentally benign ionic liquids option — Towards an innovative “ safety by design ” approach, J. Hazard. Mater. 283 (2015) 202–210. doi:10.1016/j.jhazmat.2014.09.023.

[42] V. Kumar, S. V. Malhotra, Study on the potential anti-cancer activity of phosphonium and ammonium-based ionic liquids, Bioorganic Med. Chem. Lett. 19 (2009) 4643–4646. doi:10.1016/j.bmcl.2009.06.086.

[43] Ionic liquids, (n.d.). http://oasys2.confex.com/acs/231nm/techprogram/P947344.HTM%0A.

[44] R. Pezoa-Conte, A. Leyton, I. Anugwom, S. von Schoultz, J. Paranko, P. Mäki-Arvela, S. Willför, M. Muszyński, J. Nowicki, M.E. Lienqueo, J.P. Mikkola, Deconstruction of the green alga Ulva rigida in ionic liquids: Closing the mass balance, Algal Res. 12 (2015) 262–273. doi:10.1016/j.algal.2015.09.011.

[45] A.X. Zeng, S.T. Chin, Y. Nolvachai, C. Kulsing, L.M. Sidisky, P.J. Marriott, Characterisation of capillary ionic liquid columns for gas chromatography-mass spectrometry analysis of fatty acid methyl esters, Anal. Chim. Acta. 803 (2013) 166–173. doi:10.1016/j.aca.2013.07.002.

[46] M.C. García-Alvarez-Coque, M.J. Ruiz-Angel, A. Berthod, S. Carda-Broch, On the use of ionic liquids as mobile phase additives in high-performance liquid chromatography. A review, Anal. Chim. Acta. 883 (2015) 1–21. doi:10.1016/j.aca.2015.03.042.

[47] U. Holzgrabe, J. Wahl, Ionic Liquids in Capillary Electrophoresis, Capill. Electrophor. Methods Protoc. Methods Mol. Biol. 1483 (2016) 471–507. doi:10.1007/978-1-4939-6403-1.

[48] I.D. Souza, L.W. Hantao, M.E.C. Queiroz, Polymeric ionic liquid open tubular capillary column for on-line in-tube SPME coupled with UHPLC-MS/MS to determine endocannabinoids in plasma samples, Anal. Chim. Acta. 1045 (2019) 108–116. doi:10.1016/j.aca.2018.08.062.

[49] S. Kazemiabnavi, Z. Zhang, K. Thornton, S. Banerjee, Electrochemical Stability Window of Imidazolium-Based Ionic Liquids as Electrolytes for Lithium Batteries, J. Phys. Chem. B. 120 (2016) 5691–5702. doi:10.1021/acs.jpcb.6b03433.

[50] X. Yu, Y. Chen, L. Chang, L. Zhou, F. Tang, X. Wu, β-cyclodextrin non-covalently modified ionic liquid-based carbon paste electrode as a novel voltammetric sensor for specific detection of bisphenol A, Sensors Actuators B. 186 (2013) 648–656. doi:10.1016/j.snb.2013.06.089.

[51] B. Kudłak, K. Owczarek, J. Namieśnik, Selected issues related to the toxicity of ionic liquids and deep eutectic solvents — a review, Env. Sci Pollut Res. 22 (2015) 11975–11992. doi:10.1007/s11356-015-4794-y.

[52] X. Li, J. Ma, J. Wang, Cytotoxicity, oxidative stress, and apoptosis in HepG2 cells induced by ionic liquid 1-methyl-3-octylimidazolium bromide, Ecotoxicol. Environ. Saf. 120 (2015) 342–348. doi:10.1016/j.ecoenv.2015.06.018.

[53] S.P.M. Ventura, F.A. e Silva, A.M.M. Gonçalves, J.L. Pereira, F. Gonçalves, J.A.P. Coutinho, Ecotoxicity analysis of cholinium-based ionic liquids to Vibrio fischeri marine bacteria, Ecotoxicol. Environ. Saf. 102 (2014) 48–54. doi:10.1016/j.ecoenv.2014.01.003.

[54] R.F.M. Frade, A. Matias, L.C. Branco, C.A.M. Afonso, C.M.M. Duarte, Effect of ionic liquids on human colon carcinoma HT-29 and CaCo-2 cell lines, Green Chem. 9 (2007) 873–877. doi:10.1039/b617526k.

[55] N. Byrne, L.M. Wang, J.P. Belieres, C.A. Angell, Reversible folding-unfolding, aggregation protection, and multi-year stabilization, in high concentration protein solutions, using ionic liquids, Chem. Commun. (2007) 2714–2716. doi:10.1039/b618943a.

[56] N. Byrne, C.A. Angell, Protein Unfolding, and the “Tuning In” of Reversible Intermediate States, in Protic Ionic Liquid Media, J. Mol. Biol. 378 (2008) 707–714. doi:10.1016/j.jmb.2008.02.050.

[57] N. Byrne, C.A. Angell, Formation and dissolution of hen egg white lysozyme amyloid fibrils in protic ionic liquids, Chem. Commun. (2009) 1046–1048. doi:10.1039/b817590j.

[58] G.A. O’Toole, M. Wathier, M.E. Zegans, R.M.Q. Shanks, R. Kowalski, M.W. Grinstaff, Diphosphonium Ionic Liquids as Broad Spectrum Antimicrobial Agents, Cornea. 31 (2012) 810–816. doi:10.1097/ICO.0b013e31823f0a86.

[59] K.D. Clark, O. Nacham, H. Yu, T. Li, M.M. Yamsek, D.R. Ronning, J.L. Anderson, Extraction of DNA by magnetic ionic liquids: Tunable solvents for rapid and selective DNA analysis, Anal. Chem. 87 (2015) 1552–1559. doi:10.1021/ac504260t.

[60] K.D. Clark, M. Sorensen, O. Nacham, J.L. Anderson, Preservation of DNA in nuclease-rich samples using magnetic ionic liquids, RSC Adv. 6 (2016) 39846–39851. doi:10.1039/c6ra05932e.

[61] A. Kumar, P. Venkatesu, A comparative study of myoglobin stability in the presence of Hofmeister anions of ionic liquids and ionic salts, Process Biochem. 49 (2014) 2158–2169. doi:10.1016/j.procbio.2014.09.014.

[62] A. Kumar, M. Bisht, P. Venkatesu, Biocompatibility of ionic liquids towards protein stability: A comprehensive overview on the current understanding and their implications, Int. J. Biol. Macromol. 96 (2017) 611–651. doi:10.1016/j.ijbiomac.2016.12.005.

[63] G. Bhattacharya, R.P. Giri, H. Saxena, V. V. Agrawal, A. Gupta, M.K. Mukhopadhyay, S.K. Ghosh, X-ray Reflectivity Study of the Interaction of an Imidazolium-Based Ionic Liquid with a Soft Supported Lipid Membrane, Langmuir. 33 (2017) 1295–1304. doi:10.1021/acs.langmuir.6b03192.

[64] A. Benedetto, R.J. Bingham, P. Ballone, Structure and dynamics of POPC bilayers in water solutions of room temperature ionic liquids, J. Chem. Phys. 142 (2015). doi:10.1063/1.4915918.

[65] A. Benedetto, E. Bodo, L. Gontrani, P. Ballone, R. Caminiti, Amino acid anions in organic ionic compounds. An ab initio study of selected ion pairs, J. Phys. Chem. B. 118 (2014) 2471–2486. doi:10.1021/jp412281n.

[66] P. Drücker, A. Rühling, D. Grill, D. Wang, A. Draeger, V. Gerke, F. Glorius, H.J. Galla, Imidazolium Salts Mimicking the Structure of Natural Lipids Exploit Remarkable Properties Forming Lamellar Phases and Giant Vesicles, Langmuir. 33 (2017) 1333–1342. doi:10.1021/acs.langmuir.6b03182.

[67] B. Yoo, Y. Zhu, E.J. Maginn, Molecular Mechanism of Ionic-Liquid-Induced Membrane Disruption: Morphological Changes to Bilayers, Multilayers, and Vesicles, Langmuir. 32 (2016) 5403–5411. doi:10.1021/acs.langmuir.6b00768.

[68] A. Rühling, D. Wang, J.B. Ernst, S. Wulff, R. Honeker, C. Richter, A. Ferry, H.J. Galla, F. Glorius, Influence of the Headgroup of Azolium-Based Lipids on Their Biophysical Properties and Cytotoxicity, Chem. - A Eur. J. 23 (2017) 5920–5924. doi:10.1002/chem.201604182.

[69] K.O. Evans, Supported phospholipid membrane interactions with 1-butyl-3-methylimidazolium chloride, J. Phys. Chem. B. 112 (2008) 8558–8562. doi:10.1021/jp7116592.

[70] Y. Li, X. Liu, S. Zhang, Y. Yao, X. Yao, J. Xu, X. Lu, Dissolving process of a cellulose bunch in ionic liquids: A molecular dynamics study, Phys. Chem. Chem. Phys. 17 (2015) 17894–17905. doi:10.1039/c5cp02009c.

[71] H. Liu, K.L. Sale, B.M. Holmes, B.A. Simmons, S. Singh, Understanding the interactions of cellulose with ionic liquids: a molecular dynamics study, J. Phys. Chem. B. 114 (2010) 4293–4301. doi:10.1021/jp9117437.

[72] J. Zhang, J. Wu, J. Yu, X. Zhang, J. He, J. Zhang, Application of ionic liquids for dissolving cellulose and fabricating cellulose-based materials: State of the art and future trends, Mater. Chem. Front. 1 (2017) 1273–1290. doi:10.1039/c6qm00348f.

[73] T.G.A. Youngs, J.D. Holbrey, C.L. Mullan, S.E. Norman, M.C. Lagunas, C. D'Agostino, M.D. Mantle, L.F. Gladden, D.T. Bowron, C. Hardacre, Neutron diffraction, NMR and molecular dynamics study of glucose dissolved in the ionic liquid 1-ethyl-3-methylimidazolium acetate, Chem. Sci. 2 (2011) 1594–1605. doi:10.1039/c1sc00241d.

[74] G. Cheng, P. Varanasi, C. Li, H. Liu, Y.B. Melnichenko, B.A. Simmons, M.S. Kent, S. Singh, Transition of cellulose crystalline structure and surface morphology of biomass as a function of ionic liquid pretreatment and its relation to enzymatic hydrolysis, Biomacromolecules. 12 (2011) 933–941. doi:10.1021/bm101240z.

[75] A. Benedetto, P. Ballone, Room Temperature Ionic Liquids Meet Biomolecules: A Microscopic View of Structure and Dynamics, ACS Sustain. Chem. Eng. 4 (2016) 392–412. doi:10.1021/acssuschemeng.5b01385.

[76] A. Benedetto, H.-J. Galla, Overview of the "Ionic Liquids meet Biomolecules" session at the 19th international IUPAB and 11th EBSA congress, Biophys. Rev. 9 (2017) 279–281. doi:10.1007/s12551-017-0309-z.

[77] N. V. Plechkova, K.R. Seddon, Applications of ionic liquids in the chemical industry, Chem. Soc. Rev. 37 (2008) 123–150. doi:10.1039/b006677j.

[78] C.R. Goodlett, K.H. Horn, Mechanisms of alcohol-induced damage to the developing nervous system, Alcohol Res. Heal. 25 (2001) 175–184.

[79] M. Klähn, M. Zacharias, Transformations in plasma membranes of cancerous cells and resulting consequences for cation insertion studied with molecular dynamics, Phys. Chem. Chem. Phys. 15 (2013) 14427–14441. doi:10.1039/c3cp52085d.

[80] R.J. Bingham, P. Ballone, Computational study of room-temperature ionic liquids interacting with a POPC phospholipid bilayer, J. Phys. Chem. B. 116 (2012) 11205–11216. doi:10.1021/jp306126q.

[81] A. Cornellas, L. Perez, F. Comelles, I. Ribosa, A. Manresa, T.T. Garcia, Self-aggregation and antimicrobial activity of imidazolium and pyridinium based ionic liquids in aqueous solution, J. Colloid Interface Sci. 355 (2011) 164–171. doi:10.1016/j.jcis.2010.11.063.

[82] X.D. Hou, N. Li, M.H. Zong, Renewable bio ionic liquids-water mixtures-mediated selective removal of lignin from rice straw: Visualization of changes in composition and cell wall structure, Biotechnol. Bioeng. 110 (2013) 1895–1902. doi:10.1002/bit.24862.

[83] X.D. Hou, Q.P. Liu, T.J. Smith, N. Li, M.H. Zong, Evaluation of Toxicity and Biodegradability of Cholinium Amino Acids Ionic Liquids, PLoS One. 8 (2013). doi:10.1371/journal.pone.0059145.

[84] M. Petkovic, J.L. Ferguson, H.Q.N. Gunaratne, R. Ferreira, M.C. Leitão, K.R. Seddon, L.P.N. Rebelo, C.S. Pereira, Novel biocompatible cholinium-based ionic liquids - Toxicity and biodegradability, Green Chem. 12 (2010) 643–649. doi:10.1039/b922247b.

[85] K.D. Weaver, H.J. Kim, J. Sun, D.R. MacFarlane, G.D. Elliott, Cyto-toxicity and biocompatibility of a family of choline phosphate ionic liquids designed for pharmaceutical applications, Green Chem. 12 (2010) 507–51. doi:10.1039/b918726j.

[86] M.G. Freire, L.M.N.B.F. Santos, A.M. Fernandes, J.A.P. Coutinho, I.M. Marrucho, An overview of the mutual solubilities of water-imidazolium-based ionic liquids systems, Fluid Phase Equilib. 261 (2007) 449–454. doi:10.1016/j.fluid.2007.07.033.

[87] J.L. Anthony, E.J. Maginn, J.F. Brennecke, Solution thermodynamics of imidazolium-based ionic liquids and water, J. Phys. Chem. B. 105 (2001) 10942–10949. doi:10.1021/jp0112368.

[88] M. Petkovic, D.O. Hartmann, G. Adamová, K.R. Seddon, L.P.N. Rebelo, C.S. Pereira, Unravelling the mechanism of toxicity of alkyltributylphosphonium chlorides in Aspergillus nidulans conidia, New J. Chem. 36 (2012) 56–63. doi:10.1039/c1nj20470j.

[89] J.L. Sebaugh, Guidelines for accurate EC50/IC50 estimation, Pharm. Stat. 10 (2011) 128–134. doi:10.1002/pst.426.

[90] EC50 Definition, (n.d.). https://www.definitions.net/definition/The+term+half+maximal+effective+concentration+refers+to+the+concentration+of+a+drug+antibody+or+toxicant+which+induces+a+response+halfway+between+the+baseline+and+maximum+after+a+specified+exposure+time+It+is+commonl.

[91] Z. Chen, R. Bertin, G. Froldi, EC50 estimation of antioxidant activity in DPPH assay using several statistical programs, Food Chem. 138 (2013) 414–420. doi:10.1016/j.foodchem.2012.11.001.

[92] A. De Lean, P.J. Munson, D. Rodbard, Simultaneous analysis of families of sigmoidal curves: application to bioassay, radioligand assay, and physiological dose-response curves, Am. J. Physiol. Endocrinol. Metab. Gastrointest. Physiol. 4 (1978). doi:10.1152/ajpendo.1978.235.2.e97.

[93] G.M. Dr. Verschuuren, Excel 2007 for Scientists, 2008.

[94] Invitrogen, alamarBlue ™ Cell Viability Reagent PIS, (2019) 1–2.

[95] S.-K. Ruokonen, C. Sanwald, M. Sundvik, S. Polnick, K. Vyavaharkar, F. Duša, A.J. Holding, A.W.T. King, I. Kilpeläinen, M. Lämmerhofer, P. Panula, S.K. Wiedmer, Effect of Ionic Liquids on Zebrafish (Danio rerio) Viability, Behavior, and Histology; Correlation between Toxicity and Ionic Liquid Aggregation, Env. Sci Technol. 50 (2016) 7116–7125. doi:10.1021/acs.est.5b06107.

[96] Q. Fu, D. Lyu, L. Zhang, Z. Qin, Q. Tang, H. Yin, X. Lou, Z. Chen, K. Yao, Airborne particulate matter (PM2.5) triggers autophagy in human corneal epithelial cell line, Environ. Pollut. 227 (2017) 314–322. doi:10.1016/j.envpol.2017.04.078.

[97] J.-H. Park, J.-Y. Kim, D.J. Kim, M. Kim, M. Chang, R.S. Chuck, C.Y. Park, Effect of Nitric Oxide on Human Corneal Epithelial Cell Viability and Corneal Wound Healing, Sci. Rep. 7 (2017) 1–10. doi:10.1038/s41598-017-08576-9.

[98] A. Robciuc, Environmental Stress and the corneal epithelium, 2017.

[99] G. Pellegrini, C.E. Traverso, A.T. Franzi, M. Zingirian, R. Cancedda, M. De Luca, Long-term restoration of damaged corneal surfaces with autologous cultivated corneal epithelium, Lancet. 349 (1997) 990–993. doi:10.1016/S0140-6736(96)11188-0.

[100] K. Araki-sasaki, Y. Ohashi, T. Sasabe, K. Hayashi, H. Watanabe, Y. Tano, H. Handa, An SV40-Immortalized Human Corneal Epithelial Cell Line and Its Characterization, Invest. Ophthalmol. Vis. Sci. 36 (1995) 614–621.

[101] C.R. Kahn, E. Young, I.H. Lee, S. Rhim, Human Corneal Epithelial Primary Cultures and Cell Lines With Extended Life Span: In Vitro Model for Ocular Studies, Invest. Ophthalmol. Vis. Sci. 34 (1993) 3429–3441.

[102] S. Hainsworth, Modified Culture Method for Human Corneal Epithelial Cells, J. Tiss. Cult. Meth. 13 (1991) 45–48.

[103] J.J.M. Landry, P.T. Pyl, T. Rausch, T. Zichner, M.M. Tekkedil, A.M. Stütz, A. Jauch, R.S. Aiyar, G. Pau, N. Delhomme, J. Gagneur, J.O. Korbel, W. Huber, L.M. Steinmetz, The Genomic and Transcriptomic Landscape of a HeLa Cell Line, G3. 3 (2013) 1213–1224. doi:10.1534/g3.113.005777.

[104] R. Rhabari, T. Sheahan, V. Modes, P. Collier, C. Macfarlane, R.M. Badge, A novel L1 retrotransposon marker for HeLa cell line identification, Biotechniques. 46 (209AD) 277–284. doi:10.2144/000113089.A.

[105] M.D. Hongbao, HeLa cells and Immortality, Cancer Biol. 7 (2017) 71–78. doi:10.7537/marscbj070317.11.Key.

[106] P.F. Ambros, H.I. Karlic, HeLa cells: Origin of this important cell line in life science research, Hum. Genet. 77 (1987) 251–254. doi:10.1007/BF00284479.

[107] B.P. Lucey, W.A. Nelson-Rees, G.M. Hutchins, Henrietta Lacks, HeLa Cells, and Cell Culture Contamination, Arch Pathol Lab Med. 133 (2009) 1463–1467. doi:10.1043/1543-2165-133.9.1463.

[108] H.J. Phillips, H.L. McCarthy, Oxygen Uptake and Lactate Formation of HeLa Cells, Proc Soc Exp Biol Med. 93 (1956) 573–576.

[109] T.T. Puck, H.W. Fisher, Genetics of somatic mammalian cells: I. Demonstration of the existence of mutants with different growth requirements in a human cancer cell strain (HeLa), J. Exp. Med. 104 (1956) 427–434.

[110] M. Carter, J. Shieh, Cell Culture Techniques, in: Guid. to Res. Tech. Neurosci., 2015: pp. 295–310. doi:10.1016/B978-0-12-800511-8.00014-9.

[111] W.W. Franke, U. Scheer, Some structural differentiations in the Hela cell : heavy bodies , annulate lamellae , and coUe de maillet endoplasmic reticulum, Cytobiologie. 4 (1971) 317–329.

[112] R.A. Erlandson, E. De Harven, The Ultrastructure of Synchronized HeLa cells, J. Cell Sci. 8 (1971) 353–397.

[113] T.T. Puck, P.I. Marcus, S.J. Cieciura, Clonal Growth of Mammalian Cells in vitro, J Exp Med. 103 (1956) 273–284.

[114] M.A. Epstein, Some Unusual Features of Fine Structure Observed in HeLa Cells, J Biophys Biochem Cytol. 10 (1961) 153–162.

[115] S. Zielinski, Cracking the Code of the Human Genome, 2010.

[116] G. Stolfa, M.T. Smonskey, R. Boniface, A. Hachmann, P. Gulde, A.D. Joshi, A.P. Pierce, S.J. Jacobia, A. Campbell, CHO-Omics Review : The Impact of Current and Emerging Technologies on Chinese Hamster Ovary Based Bioproduction, Biotechnol. J. 13 (2017) 1–14. doi:10.1002/biot.201700227.

[117] T.T. Puck, The genetics of somatic mammalian cells, Adv. Biol. Med. Phys. 5 (1957) 75–101. doi:10.1016/B978-1-4832-3111-2.50006-7.

[118] S. Fischer, R. Handrick, K. Otte, The art of CHO cell engineering: A comprehensive retrospect and future perspectives, Biotechnol. Adv. 33 (2015) 1878–1896. doi:10.1016/j.biotechadv.2015.10.015.

[119] B.C. Mulukutla, J. Kale, T. Kalomeris, M. Jacobs, G.W. Hiller, Identification and Control of Novel Growth Inhibitors in Fed-batch Cultures of Chinese Hamster Ovary Cells, Biotechnol. Bioeng. 114 (2017) 1779–1790. doi:10.1002/bit.26313.

[120] R.P. Nolan, K. Lee, Dynamic model of CHO cell metabolism, Metab. Eng. 13 (2011) 108–124. doi:http://dx.doi.org/10.1016/j.ymben.2010.09.003.

[121] D. Chee Furng Wong, K. Tin Kam Wong, L. Tang Goh, C. Kiat Heng, M. Gek Sim Yap, Impact of dynamic online fed-batch strategies on metabolism, productivity and N-glycosylation quality in CHO cell cultures, Biotechnol. Bioeng. 89 (2005) 164–177. doi:10.1002/bit.20317.

[122] A. Nicolae, J. Wahrheit, J. Bahnemann, A.-P. Zeng, E. Heinzle, Non-stationary 13C metabolic flux analysis of Chinese hamster ovary cells in batch culture using extracellular labeling highlights metabolic reversibility and compartmentation, BMC Syst. Biol. 8 (2014) 1–15. doi:10.1186/1752-0509-8-50.

[123] H.J. Cruz, C.M. Freitas, P.M. Alves, J.L. Moreira, M.J.T. Carrondo, Effects of ammonia and lactate on growth, metabolism, and productivity of BHK cells, Enzyme Microb. Technol. 27 (2000) 43–52. doi:10.1016/S0141-0229(00)00151-4.

[124] M.S. Lao, D. Toth, Effects of ammonium and lactate on growth and metabolism of a recombinant Chinese hamster ovary cell culture, Biotechnol. Prog. 13 (1997) 688–691. doi:10.1021/bp9602360.

[125] Z. León, J.C. García-Cañaveras, M.T. Donato, A. Lahoz, Mammalian cell metabolomics: Experimental design and sample preparation, Electrophoresis. 34 (2013) 2762–2775. doi:10.1002/elps.201200605.

[126] A. Zhang, H. Sun, P. Wang, Y. Han, X. Wang, Modern analytical techniques in metabolomics analysis, Analyst. 137 (2012) 293–300. doi:10.1039/C1AN15605E.

[127] F. Courant, J.-P. Antignac, G. Dervilly-Pinel, B. Le Bizec, Basics of mass spectrometry based metabolomics, Proteomics. 14 (2014) 2369–2388. doi:10.1002/pmic.201400255.

[128] I. Kohler, A. Verhoeven, R.J. Derks, M. Giera, Analytical pitfalls and challenges in clinical metabolomics, Bioanalysis. 8 (2016) 1509–32. doi:10.4155/bio-2016-0090.

[129] P. Yin, G. Xu, Current state-of-the-art of nontargeted metabolomics based on liquid chromatography-mass spectrometry with special emphasis in clinical applications, J. Chromatogr. A. 1374 (2014) 1–13. doi:10.1016/j.chroma.2014.11.050.

[130] S. Dietmair, N.E. Timmins, P.P. Gray, L.K. Nielsen, J.O. Krömer, Towards quantitative metabolomics of mammalian cells: Development of a metabolite extraction protocol, Anal. Biochem. 404 (2010) 155–164. doi:10.1016/j.ab.2010.04.031.

[131] K. Dettmer, N. Nürnberger, H. Kaspar, M.A. Gruber, M.F. Almstetter, P.J. Oefner, Metabolite extraction from adherently growing mammalian cells for metabolomics studies: Optimization of harvesting and extraction protocols, Anal. Bioanal. Chem. 399 (2011) 1127–1139. doi:10.1007/s00216-010-4425-x.

[132] A. Hutschenreuther, A. Kiontke, G. Birkenmeier, C. Birkemeyer, Comparison of extraction conditions and normalization approaches for cellular metabolomics of adherent growing cells with GC-MS, Anal. Methods. 4 (2012) 1953–1963. doi:10.1039/c2ay25046b.

[133] Q. Teng, W. Huang, T.W. Collette, D.R. Ekman, C. Tan, A direct cell quenching method for cell-culture based metabolomics, Metabolomics. 5 (2009) 199–208. doi:10.1007/s11306-008-0137-z.

[134] Y. Wu, L. Li, Sample normalization methods in quantitative metabolomics, J. Chromatogr. A. 1430 (2016) 80–95. doi:10.1016/j.chroma.2015.12.007.

[135] A.B. Canelas, A. Ten Pierick, C. Ras, R.M. Seifar, J.C. Van Dam, W.M. Van Gulik, J.J. Heijnen, Quantitative evaluation of intracellular metabolite extraction techniques for yeast metabolomics, Anal. Chem. 81 (2009) 7379–7389. doi:10.1021/ac900999t.

[136] A.P.H. Danielsson, T. Moritz, H. Mulder, P. Spégel, Development and optimization of a metabolomic method for analysis of adherent cell cultures, Anal. Biochem. 404 (2010) 30–39. doi:10.1016/j.ab.2010.04.013.

[137] J.B. Ritter, Y. Genzel, U. Reichl, Simultaneous extraction of several metabolites of energy metabolism and related substances in mammalian cells: Optimization using experimental design, Anal. Biochem. 373 (2008) 349–369. doi:10.1016/j.ab.2007.10.037.

[138] R.J. Raterink, P.W. Lindenburg, R.J. Vreeken, R. Ramautar, T. Hankemeier, Recent developments in sample-pretreatment techniques for mass spectrometry-based metabolomics, Trends Anal. Chem. 61 (2014) 157–167. doi:10.1016/j.trac.2014.06.003.

[139] E.J. Want, G. O'Maille, C.A. Smith, T.R. Brandon, W. Uritboonthai, C. Qin, S.A. Trauger, G. Siuzdak, Solvent-dependent metabolite distribution, clustering, and protein extraction for serum profiling with mass spectrometry, Anal. Chem. 78 (2006) 743–752. doi:10.1021/ac051312t.

[140] A. Agin, D. Heintz, E. Ruhland, J.M. Chao de la Barca, J. Zumsteg, V. Moal, A.S. Gauchez, I.J. Namer, Metabolomics - an overview. From basic principles to potential biomarkers (part 1), Med. Nucl. 40 (2016) 4–10. doi:10.1016/j.mednuc.2015.12.006.

[141] N. Vinayavekhin, A. Saghatelian, Untargeted Metabolomics, in: Curr. Protoc. Mol. Biol., 2010. doi:10.1002/0471142727.mb3001s90.

[142] M. Schwaiger, H. Schoeny, Y. El Abiead, G. Hermann, E. Rampler, G. Koellensperger, Merging metabolomics and lipidomics into one analytical run, Analyst. 144 (2019) 220–229. doi:10.1039/c8an01219a.

[143] A. Wojakowska, M. Chekan, P. Widlak, M. Pietrowska, Application of metabolomics in thyroid cancer research, Int. J. Endocrinol. 2015 (2015). doi:10.1155/2015/258763.

[144] Z. Lei, D. V. Huhman, L.W. Sumner, Mass spectrometry strategies in metabolomics, J. Biol. Chem. 286 (2011) 25435–25442. doi:10.1074/jbc.R111.238691.

[145] C. Junot, F. Fenaille, B. Colsch, F. Bécher, High resolution mass spectrometry based techniques at the crossroads of metabolic pathways, Mass Spectrom. Rev. 33 (2014) 471–500. doi:10.1002/mas.21401.

[146] D.B. Liesenfeld, N. Habermann, R.W. Owen, A. Scalbert, C.M. Ulrich, Review of mass spectrometry-based metabolomics in cancer research, Cancer Epidemiol. Biomarkers Prev. 22 (2013) 2182–2201. doi:10.1158/1055-9965.EPI-13-0584.

[147] K. Jurowski, K. Kochan, J. Walczak, M. Barańska, W. Piekoszewski, B. Buszewski, Analytical techniques in lipidomics : state of the art, Crit. Rev. Anal. Chem. 47 (2017) 418–437. doi:10.1080/10408347.2017.1310613.

[148] A.C. Schrimpe-Rutledge, S.G. Codreanu, S.D. Sherrod, J.A. McLean, Untargeted Metabolomics Strategies-Challenges and Emerging Directions, J. Am. Soc. Mass Spectrom. 27 (2016) 1897–1905. doi:10.1007/s13361-016-1469-y.

[149] E. Siminska, M. Koba, Amino acid profiling as a method of discovering biomarkers for early diagnosis of cancer, Amino Acids. 48 (2016) 1339–1345. doi:10.1007/s00726-016-2215-2.

[150] M.D. Luque de Castro, F. Priego-Capote, The analytical process to search for metabolomics biomarkers, J. Pharm. Biomed. Anal. 147 (2018) 341–349. doi:10.1016/j.jpba.2017.06.073.

[151] O.A. Aboud, R.H. Weiss, New opportunities from the cancer metabolome, Clin. Chem. 59 (2013) 138–146. doi:10.1373/clinchem.2012.184598.

[152] Y.Y. Zhao, R.C. Lin, UPLC-MSE application in disease biomarker discovery: The discoveries in proteomics to metabolomics, Chem. Biol. Interact. 215 (2014) 7–16. doi:10.1016/j.cbi.2014.02.014.

[153] S. Collino, F.P.J. Martin, S. Rezzi, Clinical metabolomics paves the way towards future healthcare strategies, Br. J. Clin. Pharmacol. 75 (2012) 619–629. doi:10.1111/j.1365-2125.2012.04216.x.

[154] H.G. Gika, G.A. Theodoridis, R.S. Plumb, I.D. Wilson, Current practice of liquid chromatography-mass spectrometry in metabolomics and metabonomics, J. Pharm. Biomed. Anal. 87 (2014) 12–25. doi:10.1016/j.jpba.2013.06.032.

[155] A. Scalbert, L. Brennan, O. Fiehn, T. Hankemeier, B.S. Kristal, B. van Ommen, E. Pujos-Guillot, E. Verheij, D. Wishart, S. Wopereis, Mass-spectrometry-based metabolomics: limitations and recommendations for future progress with particular focus on nutrition research, Metabolomics. 5 (2009) 435–458. doi:10.1007/s11306-009-0168-0.

[156] J. Zhou, Y. Yin, Strategies for large-scale targeted metabolomics quantification by liquid chromatography-mass spectrometry, Analyst. 141 (2016) 6362–6373. doi:10.1039/C6AN01753C.

[157] S. Cacciatore, M. Loda, Innovation in metabolomics to improve personalized healthcare, Ann. N. Y. Acad. Sci. 1346 (2015) 57–62. doi:10.1111/nyas.12775.

[158] S.G. Villas-Bôas, S. Mas, M. Åkesson, J. Smedsgaard, J. Nielsen, Mass spectrometry in metabolome analysis, Mass Spectrom. Rev. 24 (2005) 613–646. doi:10.1002/mas.20032.

[159] L.D. Roberts, R.E. Gerszten, Toward new biomarkers of cardiometabolic diseases, Cell Metab. 18 (2013) 43–50. doi:10.1016/j.cmet.2013.05.009.

[160] C.J. Clarke, J.N. Haselden, Metabolic Profiling as a Tool for Understanding Mechanisms of Toxicity, Toxicol. Pathol. 36 (2008) 140–147. doi:10.1177/0192623307310947.

[161] O. Begou, H.G. Gika, I.D. Wilson, G. Theodoridis, Hyphenated MS-based targeted approaches in metabolomics, Analyst. 142 (2017) 3079–3100. doi:10.1039/c7an00812k.

[162] H.F.N. Kvitvang, T. Andreassen, T. Adam, S.G. Villas-Bôas, P. Bruheim, Highly sensitive GC/MS/MS method for quantitation of amino and nonamino organic acids, Anal. Chem. 83 (2011) 2705–2711. doi:10.1021/ac103245b.

[163] K.K. Pasikanti, P.C. Ho, E.C.Y. Chan, Gas chromatography/mass spectrometry in metabolic profiling of biological fluids, J. Chromatogr. B. 871 (2008) 202–211. doi:10.1016/j.jchromb.2008.04.033.

[164] A.R. Fernie, R.N. Trethewey, A.J. Krotzky, Metabolite profiling: from diagnostics to systems biology, Nat. Rev. Mol. Cell Biol. 5 (2004) 1–7.

[165] J. Gullberg, P. Jonsson, A. Nordström, M. Sjöström, T. Moritz, Design of experiments: An efficient strategy to identify factors influencing extraction and derivatization of Arabidopsis thaliana samples in metabolomic studies with gas chromatography/mass spectrometry, Anal. Biochem. 331 (2004) 283–295. doi:10.1016/j.ab.2004.04.037.

[166] G.A. Theodoridis, H.G. Gika, E.J. Want, I.D. Wilson, Liquid chromatography-mass spectrometry based global metabolite profiling: A review, Anal. Chim. Acta. 711 (2012) 7–16. doi:10.1016/j.aca.2011.09.042.

[167] S. Hendrickx, E. Adams, D. Cabooter, Recent advances in the application of hydrophilic interaction chromatography for the analysis of biological matrices., Bioanalysis. 7 (2015) 2927–2945. doi:10.4155/bio.15.200.

[168] G. Marrubini, P. Appelblad, M. Maietta, A. Papetti, Hydrophilic interaction chromatography in food matrices analysis: An updated review, Food Chem. 257 (2018) 53–66. doi:10.1016/j.foodchem.2018.03.008.

[169] G. Greco, T. Letzel, Main interactions and influences of the chromatographic parameters in HILIC separations, J. Chromatogr. Sci. 51 (2013) 684–693. doi:10.1093/chromsci/bmt015.

[170] D. V. McCalley, Hydrophilic Interaction Chromatography, LCGC North Am. Suppl. 26 (2008) 53–58. doi:10.1002/9781118495247.

[171] B. Buszewski, S. Noga, Hydrophilic interaction liquid chromatography (HILIC)-a powerful separation technique, Anal. Bioanal. Chem. 402 (2012) 231–247. doi:10.1007/s00216-011-5308-5.

[172] Y. Guo, Recent progress in the fundamental understanding of hydrophilic interaction chromatography (HILIC), Analyst. 140 (2015) 6452–6466. doi:10.1039/c5an00670h.

[173] D. V. McCalley, Understanding and manipulating the separation in hydrophilic interaction liquid chromatography, J. Chromatogr. A. 1523 (2017) 49–71. doi:10.1016/j.chroma.2017.06.026.

[174] A.J. Alpert, Hydrophilic-interaction chromatography for the separation of peptides, nucleic acids and other polar compounds, J. Chromatogr. 499 (1990) 177–196. doi:10.1016/S0021-9673(00)96972-3.

[175] P. Jandera, Stationary and mobile phases in hydrophilic interaction chromatography: a review, Anal. Chim. Acta. 692 (2011) 1–25. doi:http://dx.doi.org/10.1016/j.aca.2011.02.047.

[176] Z. Li, J. Han, S. Sun, K. Chen, D. Tang, Hydrophilic Interaction Liquid Chromatography Tandem Mass Spectrometry: An Attractive and Prospective Method for Quantitative Bioanalysis in Drug Metabolism, Curr. Drug Metab. 17 (2016) 386–400. doi:10.2174/1389200217666151210141757.

[177] K. Spagou, H. Tsoukali, N. Raikos, H. Gika, I.D. Wilson, G. Theodoridis, Hydrophilic interaction chromatography coupled to MS for metabonomic/metabolomic studies, J. Sep. Sci. 33 (2010) 716–727. doi:10.1002/jssc.200900803.

[178] L. Qiao, X. Shi, G. Xu, Recent advances in development and characterization of stationary phases for hydrophilic interaction chromatography, Trends Anal. Chem. 81 (2016) 23–33. doi:http://dx.doi.org/10.1016/j.trac.2016.03.021.

[179] P. Hemström, K. Irgum, Hydrophilic interaction chromatography, J. Sep. Sci. 29 (2006) 1784–1821. doi:10.1002/jssc.200600199.

[180] J. Pesek, M.T. Matyska, A Comparison of Two Separation Modes: HILIC and Aqueous Normal Phase Chromatography, LCGC North Am. 25 (2007).

[181] Atlantis HILIC, (n.d.). http://www.waters.com/webassets/cms/category/media/detail_page_images/atlantis_hilic_detail_1.gif?locale=en_US.

[182] D.S. Bell, Retention and Selectivity of Stationary Phases Used in HILIC, LCGC North Am. 33 (2015) 90–101. http://www.chromatographyonline.com/retention-and-selectivity-stationary-phases-used-hilic.

[183] P. Jandera, T. Hájek, Mobile phase effects on the retention on polar columns with special attention to the dual hydrophilic interaction–reversed-phase liquid chromatography mechanism, a review, J. Sep. Sci. 41 (2018) 145–162. doi:10.1002/jssc.201701010.

[184] P. Jandera, P. Janás, Recent advances in stationary phases and understanding of retention in hydrophilic interaction chromatography. A review, Anal. Chim. Acta. 967 (2017) 12–32. doi:10.1016/j.aca.2017.01.060.

[185] S. Cubbon, C. Antonio, J. Wilson, J. Thomas-Oates, Metabolomic applications of HILIC-LC-MS, Mass Spectrom Rev. 29 (2010) 671–684. doi:10.1002/mas.20252.

[186] W. Jiang, G. Fischer, Y. Girmay, K. Irgum, Zwitterionic stationary phase with covalently bonded phosphorylcholine type polymer grafts and its applicability to separation of peptides in the hydrophilic interaction liquid chromatography mode, J. Chromatogr. A. 1127 (2006) 82–91. doi:10.1016/j.chroma.2006.05.080.

[187] Hochleistungsflüssigchromatographische Verfahren zur Bestimmung organischer Substanzen in biologischem Material, in: n.d.

[188] F. Gritti, G. Guiochon, The van Deemter equation: Assumptions, limits, and adjustment to modern high performance liquid chromatography, J. Chromatogr. A. 1302 (2013) 1–13. doi:10.1016/j.chroma.2013.06.032.

[189] G. Weber, N. von Wirén, H. Hayen, Hydrophilic interaction chromatography of small metal species in plants using sulfobetaine- and phosphorylcholine-type zwitterionic stationary phases, J. Sep. Sci. 31 (2008) 1615–1622. doi:10.1002/jssc.200800060.

[190] H. Luo, Y.K. Cheng, A comparative study of void volume markers in immobilized-artificial- membrane and reversed-phase liquid chromatography, J. Chromatogr. A. 1103 (2006) 356–361. doi:10.1016/j.chroma.2005.12.036.

[191] Y. Chen, Z. Zhou, W. Yang, N. Bi, J. Xu, J. He, R. Zhang, L. Wang, Z. Abliz, Development of a Data-Independent Targeted Metabolomics Method for Relative Quantification Using Liquid Chromatography Coupled with Tandem Mass Spectrometry, Anal. Chem. 89 (2017) 6954–6962. doi:10.1021/acs.analchem.6b04727.

[192] R. Bonner, G. Hopfgartner, SWATH data independent acquisition mass spectrometry for metabolomics, TrAC - Trends Anal. Chem. 120 (2019). doi:10.1016/j.trac.2018.10.014.

[193] J.H. Gross, Massenspektrometrie, Springer Spectrum, 2011. doi:10.1007/978-3-8274-2981-0.

[194] M. Dell'mour, L. Jaitz, E. Oburger, M. Puschenreiter, G. Koellensperger, S. Hann, Hydrophilic interaction LC combined with electrospray MS for highly sensitive analysis of underivatized amino acids in rhizosphere research, J Sep Sci. 33 (2010) 911–922. doi:10.1002/jssc.200900743.

[195] S.J. Lehotay, Y. Sapozhnikova, H.G.J. Mol, Current issues involving screening and identification of chemical contaminants in foods by mass spectrometry, TrAC - Trends Anal. Chem. 69 (2015) 62–75. doi:10.1016/j.trac.2015.02.012.

[196] T.J. De Koning, Amino acid synthesis deficiencies, J Inherit Metab Dis. 40 (2017) 609–620. doi:10.1007/s10545-017-0063-1.

[197] G. Wu, Amino acids: Metabolism, functions, and nutrition, Amino Acids. 37 (2009) 1–17. doi:10.1007/s00726-009-0269-0.

[198] M. Häggström, Amino acid catabolism, (2014). doi:10.15347/wjm/2014.008.

[199] R.O. Esquivel, M. Molina-Espiritu, F. Salas, C. Soriano, C. Barrientos, J.S. Dehesa, J.A. Dobado, Decoding the Building Blocks of Life from the Perspective of Quantum Information, in: Adv. Quantum Mech., 2013. doi:10.5772/55160.

[200] D. Nelson, M. Cox, Aminosäuren, Peptide und Proteine, in: Lehninger Biochem., Springer Berlin Heidelberg, 2001.

[201] Z. Yang, M. Morar, S.E. Ealick, Structural Biology of the Purine Biosynthetic Pathway, Cell Mol Life Sci. 23 (2008) 3699–3724. doi:10.1038/jid.2014.371.

[202] R.C. Geck, A. Toker, Nonessential amino acid metabolism in breast cancer, Adv. Biol. Regul. 62 (2016) 11–17. doi:10.1016/j.jbior.2016.01.001.

[203] B.H. Choi, J.L. Coloff, The diverse functions of non-essential amino acids in cancer, Cancers (Basel). 11 (2019). doi:10.3390/cancers11050675.

[204] H.D. McIntyre, P. Catalano, C. Zhang, G. Desoye, E.R. Mathiesen, P. Damm, Gestational diabetes mellitus, Nat. Rev. Dis. Prim. 5 (2019). doi:10.1038/s41572-019-0098-8.

[205] S. Chen, S. Akter, K. Kuwahara, Y. Matsushita, T. Nakagawa, M. Konishi, T. Honda, S. Yamamoto, T. Hayashi, M. Noda, T. Mizoue, Serum amino acid profiles and risk of type 2 diabetes among Japanese adults in the Hitachi Health Study, Sci. Rep. 9 (2019) 1–9. doi:10.1038/s41598-019-43431-z.

[206] B. Blaus, Coronary Artery Disease, (n.d.). doi:10.15347/wjm/2014.010.

[207] I. Nakagawa, T. Takahashi, T. Suzuki, K. Kobayashi, Amino Acid Requirements of Children: Nitrogen Balance At the Minimal Level of Essential Amino Acids, J. Nutr. 83 (1964) 115–118. doi:10.1093/jn/83.2.115.

[208] H. Eagle, V.I. Oyama, M. Levy, Amino Acid Requirements of Normal and Malignant Human Cells in Tissue Culture, Arch. Biochem. Biophys. 67 (1957) 432–446.

[209] J. Maeda, M. Higashiyama, A. Imaizumi, T. Nakayama, H. Yamamoto, T. Daimon, M. Yamakado, F. Imamura, K. Kodama, Possibility of multivariate function composed of plasma amino acid profiles as a novel screening index for non-small cell lung cancer: A case control study, BMC Cancer. 10 (2010). doi:10.1186/1471-2407-10-690.

[210] Y. Miyagi, M. Higashiyama, A. Gochi, M. Akaike, T. Ishikawa, T. Miura, N. Saruki, E. Bando, H. Kimura, F. Imamura, M. Moriyama, I. Ikeda, A. Chiba, F. Oshita, A. Imaizumi, H. Yamamoto, H. Miyano, K. Horimoto, O. Tochikubo, T. Mitsushima, M. Yamakado, N. Okamoto, Plasma free amino acid profiling of five types of cancer patients and its application for early detection, PLoS One. 6 (2011). doi:10.1371/journal.pone.0024143.

[211] H.J. Kim, S.H. Jang, J.S. Ryu, J.E. Lee, Y.C. Kim, M.K. Lee, T.W. Jang, S.Y. Lee, H. Nakamura, N. Nishikata, M. Mori, Y. Noguchi, H. Miyano, K.Y. Lee, The performance of a novel amino acid multivariate index for detecting lung cancer: A case control study in Korea, Lung Cancer. 90 (2015) 522–527. doi:10.1016/j.lungcan.2015.10.006.

[212] A.B. Leichtle, J.M. Nuoffer, U. Ceglarek, J. Kase, T. Conrad, H. Witzigmann, J. Thiery, G.M. Fiedler, Serum amino acid profiles and their alterations in colorectal cancer, Metabolomics. 8 (2012) 643–653. doi:10.1007/s11306-011-0357-5.

[213] P.J. Stover, A.J. MacFarlane, Mouse models to elucidate mechanisms of folate-related cancer pathologies, Nutr. Rev. 66 (2008) 54–58. doi:10.1111/j.1753-4887.2008.00069.x.

[214] Y. Qiu, G. Cai, M. Su, T. Chen, X. Zheng, Y. Xu, Y. Ni, A. Zhao, L.X. Xu, S. Cai, W. Jia, Serum metabolite profiling of human colorectal cancer using GC-TOFMS and UPLC-QTOFMS, J. Proteome Res. 8 (2009) 4844–4850. doi:10.1021/pr9004162.

[215] J. Budczies, C. Denkert, B.M. Müller, S.F. Brockmöller, F. Klauschen, B. Györffy, M. Dietel, C. Richter-Ehrenstein, U. Marten, R.M. Salek, J.L. Griffin, M. Hilvo, M. Orešič, G. Wohlgemuth, O. Fiehn, Remodeling of central metabolism in invasive breast cancer compared to normal breast tissue - a GC-TOFMS based metabolomics study, BMC Genomics. 13 (2012). doi:10.1186/1471-2164-13-334.

[216] Y. Gu, T. Chen, S. Fu, X. Sun, L. Wang, J. Wang, Y. Lu, S. Ding, G. Ruan, L. Teng, M. Wang, Perioperative dynamics and significance of amino acid profiles in patients with cancer, J. Transl. Med. 13 (2015) 1–14. doi:10.1186/s12967-015-0408-1.

[217] M. Shingyoji, T. Iizasa, M. Higashiyama, F. Imamura, N. Saruki, A. Imaizumi, H. Yamamoto, T. Daimon, O. Tochikubo, T. Mitsushima, M. Yamakado, H. Kimura, The significance and robustness of a plasma free amino acid (PFAA) profile-based multiplex function for detecting lung cancer, BMC Cancer. 13 (2013). doi:10.1186/1471-2407-13-77.

[218] J.W. Locasale, Serine, Glycine and the one-carbon cycle: cancer metabolism in full circle, Nat. Rev Cancer. 13 (2013) 572–583. doi:10.1038/nrc3557.Serine.

[219] P. Luo, P. Yin, W. Zhang, L. Zhou, X. Lu, X. Lin, G. Xu, Optimization of large-scale pseudotargeted metabolomics method based on liquid chromatography-mass spectrometry, J. Chromatogr. A. 1437 (2016) 127–136. doi:10.1016/j.chroma.2016.01.078.

[220] R. Wang, Y. Yin, Z.J. Zhu, Advancing untargeted metabolomics using data-independent acquisition mass spectrometry technology, Anal. Bioanal. Chem. 411 (2019) 4349–4357. doi:10.1007/s00216-019-01709-1.

[221] R. Bonner, G. Hopfgartner, SWATH acquisition mode for drug metabolism and metabolomics investigations, Bioanalysis. 8 (2016) 1735–1750. doi:10.4155/bio-2016-0141.

[222] B. Drotleff, Development and Optimization of Targeted / Untargeted Lipidomic Screening Methodologies in Pharmaceutical and Clinical Bioanalysis by Liquid Chromatography-High Resolution-Mass Spectrometry, 2019.

[223] R.E. Ardrey, Liquid Chromatography– Mass Spectrometry: An Introduction, John Wiley & Sons, Ltd, 2003.

[224] D.T. Rossi, M.W. Sinz, M. Dekker, Mass Spectrometry in Drug Discovery, J. Med. Chem. 45 (2002) 4375–4376. doi:10.1021/jm020305j.

[225] F. Lottspeich, J.W. Engels, Bioanalytik, Springer Berlin Heidelberg, 2012.

[226] B.A. Mamyrin, Laser assisted reflectron time-of-flight mass spectrometry, Int. J. Mass Spectrom. Ion Process. 131 (1994) 1–19. doi:10.1016/0168-1176(93)03891-O.

[227] M. Wilm, Principles of electrospray ionization, Mol. Cell. Proteomics. 10 (2011) 1–8. doi:10.1074/mcp.M111.009407.

[228] A.J.R. Heck, R.H.H. Van Den Heuvel, Investigation of intact protein complexes by mass spectrometry, Mass Spectrom. Rev. 23 (2004) 368–389. doi:10.1002/mas.10081.

[229] S. Cristoni, L.R. Bernardi, Development of new methodologies for the mass spectrometry study of bioorganic macromolecules, Mass Spectrom. Rev. 22 (2003) 369–406. doi:10.1002/mas.10062.

[230] C.A. Schalley, Supramolecular chemistry goes gas phase: The mass spectrometric examination of noncovalent interactions in host-guest chemistry and molecular recognition, Int. J. Mass Spectrom. 194 (2000) 11–39. doi:10.1016/S1387-3806(99)00243-2.

[231] M.H. Amad, N.B. Cech, G.S. Jackson, C.G. Enke, Importance of gas-phase proton affinities in determining the electrospray ionization response for analytes and solvents, J. Mass Spectrom. 35 (2000) 784–789. doi:10.1002/1096-9888(200007)35:7<784::AID-JMS17>3.0.CO;2-Q.

[232] J. Zeleny, Instability of electrified liquid surfaces, Phys. Rev. 10 (1917) 175–176. doi:10.1038/131175a0.

[233] G. Taylor, Desintegration of water drops in an electric field, Proc. R. Soc. Lond. A. 280 (1964) 383–397. doi:10.1098/rspa.1964.0151.

[234] J.B. Fenn, M. Mann, C.K. Meng, S.F. Wong, C.M. Whitehouse, Electrospray ionization for mass spectrometry of large biomolecules, Science (80-.). 246 (1989) 64–71. doi:10.1126/science.2675315.

[235] J.B. Fenn, Electrospray wings for molecular elephants (Nobel lecture), Angew. Chemie - Int. Ed. 42 (2003) 3871–3894. doi:10.1002/anie.200300605.

[236] M. Yamashita, J.B. Fenn, Electrospray ion source. Another variation on the free-jet theme, J. Phys. Chem. 88 (1984) 4451–4459. doi:10.1021/j150664a002.

[237] M. Yamashita, J.B. Fenn, Negative ion production with the electrospray ion source, J. Phys. Chem. 88 (1984) 4671–4675. doi:10.1021/j150664a046.

[238] C.M. Whitehouse, R.N. Dreyer, M. Yamashita, J.B. Fenn, Electrospray Interface for Liquid Chromatographs and Mass Spectrometers, Anal. Chem. 57 (1985) 675–679. doi:10.1021/ac00280a023.

[239] M.S. Wilm, M. Mann, Electrospray and Taylor-Cone theory, Dole's beam of macromolecules at last?, Int. J. Mass Spectrom. Ion Process. 136 (1994) 167–180. doi:10.1016/0168-1176(94)04024-9.

[240] I. Marginean, P. Nemes, L. Parvin, A. Vertes, How much charge is there on a pulsating Taylor cone?, Appl. Phys. Lett. 89 (2006) 10–13. doi:10.1063/1.2266889.

[241] M.G. Ikonomou, A.T. Blades, P. Kebarle, Electrospray-Ion Spray: A Comparison of Mechanisms and Performance, Anal. Chem. 63 (1991) 1989–1998. doi:10.1021/ac00018a017.

[242] P. Nemes, I. Marginean, A. Vertes, Spraying mode effect on droplet formation and ion chemistry in electrosprays, Anal. Chem. 79 (2007) 3105–3116. doi:10.1021/ac062382i.

[243] A. Dahlin, ESI positive mode, (n.d.). https://de.wikipedia.org/wiki/Elektrospray-Ionisation#/media/Datei:ESI_positive_mode_(21589986840).jpg.

[244] A.P. Bruins, J.D. Henion, T.R. Covey, Ion Spray Interface for Combined Liquid Chromatography/Atmospheric Pressure Ionization Mass Spectrometry, Anal. Chem. 59 (1987) 2642–2646. doi:10.1021/ac00149a003.

[245] T.R. Covey, A.P. Bruins, J.D. Henion, Comparison of thermospray and ion spray mass spectrometry in an atmospheric pressure ion source, Org. Mass Spectrom. 23 (1988) 178–186. doi:10.1002/oms.1210230305.

[246] M. Karas, U. Bahr, T. Dülcks, Nano-electrospray ionization mass spectrometry: Addressing analytical problems beyond routine, Fresenius. J. Anal. Chem. 366 (2000) 669–676. doi:10.1007/s002160051561.

[247] Lord Rayleigh, On the equilibrium of liquid conducting masses charged with electricity, London, Edinburgh, Dublin Philos. Mag. J. Sci. 14 (1882) 184–186. doi:10.1080/14786448208628425.

[248] P. Kebarle, L. Tang, From Ions in Solution to Ions in the Gas Phase: The Mechanism of Electrospray Mass Spectrometry, Anal. Chem. 65 (1993). doi:10.1021/ac00070a001.

[249] R.B. Cole, Some tenets pertaining to electrospray ionization mass spectrometry, J. Mass Spectrom. 35 (2000) 763–772. doi:10.1002/1096-9888(200007)35:7<763::aid-jms16>3.0.co;2-%23.

[250] A. Gomez, K. Tang, Charge and fission of droplets in electrostatic sprays, Phys. Fluids. 6 (1994) 404–414. doi:10.1063/1.868037.

[251] N. Felitsyn, M. Peschke, P. Kebarle, Origin and number of charges observed on multiply-protonated native proteins produced by ESI, Int. J. Mass Spectrom. 219 (2002) 39–62. doi:10.1016/S1387-3806(02)00588-2.

[252] M. Dole, L.L. Mack, R.L. Hines, R.C. Mobley, L.D. Ferguson, M.B. Alice, Molecular beams of macroions, J. Chem. Phys. 49 (1968) 2240–2249. doi:10.1063/1.1672733.

[253] J. V. Iribarne, B.A. Thomson, On the evaporation of small ions from charged droplets, J. Chem. Phys. 64 (1976) 2287–2294. doi:10.1063/1.432536.

[254] B.A. Thomson, J. V. Iribarne, Field induced ion evaporation from liquid surfaces at atmospheric pressure, J. Chem. Phys. 71 (1979) 4451–4463. doi:10.1063/1.438198.

[255] M. Labowsky, J.B. Fenn, J. La Fernandez Mora, A continuum model for ion evaporation from a drop: effect of curvature and charge on ion solvation energy, Anal. Chim. Acta. 406 (2000) 105–118.

[256] E. de Hoffmann, V. Stroobant, Mass Spectrometry: Principles and Applications, 3rd Edition, 3rd Editio, Wiley, 2007.

[257] F. Fenaille, P. Barbier Saint-Hilaire, K. Rousseau, C. Junot, Data acquisition workflows in liquid chromatography coupled to high resolution mass spectrometry-based metabolomics: Where do we stand?, J. Chromatogr. A. 1526 (2017) 1–12. doi:10.1016/j.chroma.2017.10.043.

[258] J. Schlotterbeck, Data-Independent Acquisition of Targeted and Untargeted Lipidomics for Pharmaceutical and Clinical Applications Using Ultra-High-Performance Liquid Chromatography Coupled to an Electrospray Ionization Quadrupole Time-Of-Flight Mass Spectrometer, 2018.

[259] B. Güssregen, Isotopenmuster. In: Gressner A.M., Arndt T (eds) Lexikon der Medizinischen Laboratoriumsdiagnostic, Springer Berlin Heidelberg, 2019. doi:10.1007/978-3-662-48986-4_1642.

[260] L. Sleno, The use of mass defect in modern mass spectrometry, J. Mass Spectrom. 47 (2012). doi:10.1002/jms.2978.

[261] M. Raetz, R. Bonner, G. Hopfgartner, SWATH-MS for Metabolomics and Lipidomics: Critical Aspects of Qualitative and Quantitative Analysis, Metabolomics. 16 (2020) 1–14. doi:10.1007/s11306-020-01692-0.

[262] Y. Zhang, A. Bilbao, T. Bruderer, J. Luban, C. Strambio-De-Castillia, F. Lisacek, G. Hopfgartner, E. Varesio, The Use of Variable Q1 Isolation Windows Improves Selectivity in LC-SWATH-MS Acquisition, J. Proteome Res. 14 (2015) 4359–4371. doi:10.1021/acs.jproteome.5b00543.

[263] I. Nikolskiy, N.G. Mahieu, Y.J. Chen, R. Tautenhahn, G.J. Patti, An untargeted metabolomic workflow to improve structural characterization of metabolites, Anal. Chem. 85 (2013) 7713–7719. doi:10.1021/ac400751j.

[264] G. Theodoridis, H.G. Gika, I.D. Wilson, Mass spectrometry-based holistic analytical approaches for metabolite profiling in systems biology studies, Mass Spectrom. Rev. 30 (2011) 884–906. doi:10.1002/mas.20306.

[265] H. Tsugawa, T. Cajka, T. Kind, Y. Ma, B. Higgins, K. Ikeda, M. Kanazawa, J. Vandergheynst, O. Fiehn, M. Arita, MS-DIAL: Data-independent MS/MS deconvolution for comprehensive metabolome analysis, Nat. Methods. 12 (2015) 523–526. doi:10.1038/nmeth.3393.

[266] H. Li, Y. Cai, Y. Guo, F. Chen, Z.J. Zhu, MetDIA: Targeted Metabolite Extraction of Multiplexed MS/MS Spectra Generated by Data-Independent Acquisition, Anal. Chem. 88 (2016) 8757–8764. doi:10.1021/acs.analchem.6b02122.

[267] E. Fahy, M. Sud, D. Cotter, S. Subramaniam, LIPID MAPS online tools for lipid research, Nucleic Acids Res. 35 (2007) 606–612. doi:10.1093/nar/gkm324.

[268] T. Kind, K.H. Liu, D.Y. Lee, B. Defelice, J.K. Meissen, O. Fiehn, LipidBlast in silico tandem mass spectrometry database for lipid identification, Nat. Methods. 10 (2013) 755–758. doi:10.1038/nmeth.2551.

[269] J. Wang, C. Wang, X. Han, Tutorial on lipidomics, Anal. Chim. Acta. 1061 (2019) 28–41. doi:10.1016/j.aca.2019.01.043.

[270] T. Züllig, H.C. Köfeler, High Resolution Mass Spectrometry in Lipidomics, Mass Spectrom. Rev. 00 (2020) 1–15. doi:10.1002/mas.21627.

[271] E. Fahy, S. Subramaniam, R.C. Murphy, M. Nishijima, C.R.H. Raetz, T. Shimizu, F. Spener, G. Van Meer, M.J.O. Wakelam, E.A. Dennis, Update of the LIPID MAPS comprehensive classification system for lipids, J. Lipid Res. 50 (2009) 9–14. doi:10.1194/jlr.R800095-JLR200.

[272] E. Fahy, S. Subramaniam, H.A. Brown, C.K. Glass, A.H. Merrill, R.C. Murphy, C.R.H. Raetz, D.W. Russell, Y. Seyama, W. Shaw, T. Shimizu, F. Spener, G. Van Meer, M.S. VanNieuwenhze, S.H. White, J.L. Witztum, E.A. Dennis, A comprehensive classification system for lipids, J. Lipid Res. 46 (2005) 839–861. doi:10.1194/jlr.E400004-JLR200.

[273] LIPID MAPS, (n.d.). https://www.lipidmaps.org.

[274] X. Han, Neurolipidomics: challenges and developments, Front. Biosci. 12 (2007) 2601–2615.

[275] A. Shevchenko, K. Simons, Lipidomics: Coming to grips with lipid diversity, Nat. Rev. Mol. Cell Biol. 11 (2010) 593–598. doi:10.1038/nrm2934.

[276] R.W. Gross, X. Han, Lipidomics at the interface of structure and function in systems biology, Chem. Biol. 18 (2011) 284–291. doi:10.1016/j.chembiol.2011.01.014.

[277] G. Van Meer, D.R. Voelker, G.W. Feigenson, Membrane lipids: Where they are and how they behave, Nat. Rev. Mol. Cell Biol. 9 (2008) 112–124. doi:10.1038/nrm2330.

[278] T. Züllig, M. Trötzmüller, H.C. Köfeler, Lipidomics from sample preparation to data analysis: a primer, Anal. Bioanal. Chem. 412 (2020) 2191–2209. doi:10.1007/s00216-019-02241-y.

[279] X. Han, R.W. Gross, Electrospray ionization mass spectroscopic analysis of human erythrocyte plasma membrane phospholipids, Proc. Natl. Acad. Sci. U. S. A. 91 (1994) 10635–10639. doi:10.1073/pnas.91.22.10635.

[280] S.M. Lam, H. Tian, G. Shui, Lipidomics, en route to accurate quantitation, Biochim. Biophys. Acta. 1862 (2017) 752–761. doi:10.1016/j.bbalip.2017.02.008.

[281] H.C. Lee, T. Yokomizo, Applications of mass spectrometry-based targeted and non-targeted lipidomics, Biochem. Biophys. Res. Commun. 504 (2018) 576–581. doi:10.1016/j.bbrc.2018.03.081.

[282] K. Yang, X. Han, Lipidomics: Techniques, applications, and outcomes related to biomedical sciences, Trends Biochem. Sci. 41 (2016) 954–969. doi:10.1016/j.tibs.2016.08.010.

[283] X. Han, S. Rozen, S.H. Boyle, C. Hellegers, H. Cheng, J.R. Burke, K.A. Welsh-Bohmer, P.M. Doraiswamy, R. Kaddurah-Daouk, Metabolomics in early Alzheimer's disease: Identification of altered plasma sphingolipidome using shotgun lipidomics, PLoS One. 6 (2011). doi:10.1371/journal.pone.0021643.

[284] E.G. Bligh, W.J. Dyer, A rapid method of total lipid extraction and purification, Can. J. Biochem. Physiol. 37 (1959) 911–917.

[285] F.N. Lebaron, J. Folch, The effect of pH and salt concentration on aqueous extraction of brain proteins and lipoproteins, J. Neurochem. 4 (1959) 1–8. doi:10.1111/j.1471-4159.1959.tb13168.x.

[286] J. Folch, M. Lees, G.. Sloane Stanley, A simple method for the isolation and purification of total lipides from animal tissues, J. Biol. Chem. 226 (1957) 497–509.

[287] V. Matyash, G. Liebisch, T. V. Kurzchalia, A. Shevchenko, D. Schwudke, Lipid extraction by methyl- tert -butyl ether for high-throughput lipidomics, J. Lipid Res. 49 (2008) 1137–1146. doi:10.1194/jlr.D700041-JLR200.

[288] M. Cruz, M. Wang, J. Frisch-Daiello, X. Han, Improved Butanol–Methanol (BUME) Method by Replacing Acetic Acid for Lipid Extraction of Biological Samples, Lipids. 51 (2016) 887–896. doi:10.1007/s11745-016-4164-7.

[289] L. Löfgren, G.B. Forsberg, M. Ståhlman, The BUME method: A new rapid and simple chloroform-free method for total lipid extraction of animal tissue, Sci. Rep. 6 (2016) 1–11. doi:10.1038/srep27688.

[290] L. Löfgren, M. Ståhlman, G.B. Forsberg, S. Saarinen, R. Nilsson, G.I. Hansson, The BUME method: A novel automated chloroform-free 96-well total lipid extraction method for blood plasma, J. Lipid Res. 53 (2012) 1690–1700. doi:10.1194/jlr.D023036.

[291] C. Calderón, C. Sanwald, J. Schlotterbeck, B. Drotleff, M. Lämmerhofer, Comparison of simple monophasic versus classical biphasic extraction protocols for comprehensive UHPLC-MS/MS lipidomic analysis of Hela cells, Anal. Chim. Acta. 1048 (2019) 66–74. doi:10.1016/j.aca.2018.10.035.

[292] B. Brügger, G. Erben, R. Sandhoff, F.T. Wieland, W.D. Lehmann, Quantitative analysis of biological membrane lipids at the low picomole level by nano-electrospray ionization tandem mass spectrometry, Proc. Natl. Acad. Sci. U.S.A. 94 (1997) 2339–2344.

[293] X. Han, K. Yang, J. Yang, K.N. Fikes, H. Cheng, R.W. Gross, Factors influencing the electrospray intrasource separation and selective ionization of glycerophospholipids, J. Am. Soc. Mass Spectrom. 17 (2006) 264–274. doi:10.1016/j.jasms.2005.11.003.

[294] M. Wang, R.H. Han, X. Han, Fatty acidomics: Global analysis of lipid species containing a carboxyl group with a charge-remote fragmentation-assisted approach, Anal. Chem. 85 (2013) 9312–9320. doi:10.1021/ac402078p.

[295] C. Wang, M. Wang, X. Han, Comprehensive and quantitative analysis of lysophospholipid molecular species present in obese mouse liver by shotgun lipidomics, Anal Chem. 87 (2015) 4879–4887. doi:10.1021/acs.analchem.5b00410.

[296] C. Wang, J.P. Palavicini, M. Wang, L. Chen, K. Yang, P.A. Crawford, X. Han, Comprehensive and quantitative analysis of polyphosphoinositide species by shotgun lipidomics revealed their alterations in db/db mouse brain, Anal. Chem. 88 (2016) 12137–12144. doi:10.1021/acs.analchem.6b02947.

[297] S.J. Blanksby, T.W. Mitchell, Advances in Mass Spectrometry for Lipidomics, Annu. Rev. Anal. Chem. 3 (2010) 433–465. doi:10.1146/annurev.anchem.111808.073705.

[298] M. Holčapek, G. Liebisch, K. Ekroos, Lipidomic Analysis, Anal. Chem. 90 (2018) 4249–4257. doi:10.1021/acs.analchem.7b05395.

[299] T. Cajka, O. Fiehn, Comprehensive analysis of lipids in biological systems by liquid chromatography-mass spectrometry, TrAC - Trends Anal. Chem. 61 (2014) 192–206. doi:10.1016/j.trac.2014.04.017.

[300] V.B. O'Donnell, K. Ekroos, G. Liebisch, M. Wakelam, Lipidomics: Current state of the art in a fast moving field, Wiley Interdiscip. Rev. Syst. Biol. Med. 12 (2020) 1–6. doi:10.1002/wsbm.1466.

[301] Y.H. Rustam, G.E. Reid, Analytical Challenges and Recent Advances in Mass Spectrometry Based Lipidomics, Anal. Chem. 90 (2018) 374–397. doi:10.1021/acs.analchem.7b04836.

[302] E. Rampler, A. Criscuolo, M. Zeller, Y. El Abiead, H. Schoeny, G. Hermann, E. Sokol, K. Cook, D.A. Peake, B. Delanghe, G. Koellensperger, A Novel Lipidomics Workflow for Improved Human Plasma Identification and Quantification Using RPLC-MSn Methods and Isotope Dilution Strategies, Anal. Chem. 90 (2018) 6494–6501. doi:10.1021/acs.analchem.7b05382.

[303] B. Worley, R. Powers, Multivariate Analysis in Metabolomics, Curr. Metabolomics. 1 (2013) 92–107. doi:10.2174/2213235x11301010092.

[304] W. Hoffmann, G. von Helden, K. Pagel, Ion mobility-mass spectrometry and orthogonal gas-phase techniques to study amyloid formation and inhibition, Curr. Opin. Struct. Biol. 46 (2017) 7–15. doi:10.1016/j.sbi.2017.03.002.

[305] G. Paglia, M. Kliman, E. Claude, S. Geromanos, G. Astarita, Applications of ion-mobility mass spectrometry for lipid analysis, Anal. Bioanal. Chem. 407 (2015) 4995–5007. doi:10.1007/s00216-015-8664-8.

[306] B. et al (Clemmer), Biomolecule Analysis by Ion Mobility Mass Spectrometry, 100 (2012) 130–134. doi:10.1016/j.pestbp.2011.02.012.Investigations.

[307] A.B. Kanu, P. Dwivedi, M. Tam, L. Matz, H.H. Hill, Ion mobility-mass spectrometry, J. Mass Spectrom. 43 (2008) 1–22. doi:10.1002/jms.1383.

[308] Z.S. Qureshi, K.M. Deshmukh, B.M. Bhanage, Applications of ionic liquids in organic synthesis and catalysis, Clean Technol. Environ. Policy. 16 (2014) 1487–1513. doi:10.1007/s10098-013-0660-0.

[309] J. Park, Y. Jung, P. Kusumah, J. Lee, K. Kwon, C.K. Lee, Application of ionic liquids in hydrometallurgy, Int. J. Mol. Sci. 15 (2014) 15320–15343. doi:10.3390/ijms150915320.

[310] A.J. Holding, M. Heikkilä, I. Kilpeläinen, A.W.T. King, Amphiphilic and phase-separable ionic liquids for biomass processing, ChemSusChem. 7 (2014) 1422–1434. doi:10.1002/cssc.201301261.

[311] N. Gal, D. Malferarri, S. Kolusheva, P. Galletti, E. Tagliavini, R. Jelinek, Membrane interactions of ionic liquids: Possible determinants for biological activity and toxicity, Biochim. Biophys. Acta - Biomembr. 1818 (2012) 2967–2974. doi:10.1016/j.bbamem.2012.07.025.

[312] A.W.T. King, J. Asikkala, I. Mutikainen, P. Järvi, I. Kilpeläinen, Distillable acid-base conjugate ionic liquids for cellulose dissolution and processing, Angew. Chemie - Int. Ed. 50 (2011) 6301–6305. doi:10.1002/anie.201100274.

[313] A.M. Stepan, A.W.T. King, T. Kakko, G. Toriz, I. Kilpeläinen, P. Gatenholm, Fast and highly efficient acetylation of xylans in ionic liquid systems, Cellulose. 20 (2013) 2813–2824. doi:10.1007/s10570-013-0028-y.

[314] A. Parviainen, A.W.T. King, I. Mutikainen, M. Hummel, C. Selg, L.K.J. Hauru, H. Sixta, I. Kilpeläinen, Predicting cellulose solvating capabilities of acid-base conjugate ionic liquids, ChemSusChem. 6 (2013) 2161–2169. doi:10.1002/cssc.201300143.

[315] Q. Yang, D. Xu, J. Zhang, Y. Zhu, Z. Zhang, C. Qian, Q. Ren, H. Xing, Long-chain fatty acid-based phosphonium ionic liquids with strong hydrogen-bond basicity and good lipophilicity: Synthesis, characterization, and application in extraction, ACS Sustain. Chem. Eng. 3 (2015) 309–316. doi:10.1021/sc5006796.

[316] M. Abe, K. Kuroda, D. Sato, H. Kunimura, H. Ohno, Effects of polarity, hydrophobicity, and density of ionic liquids on cellulose solubility, Phys. Chem. Chem. Phys. 17 (2015) 32276–32282. doi:10.1039/c5cp05808b.

[317] C. Pretti, C. Chiappe, D. Pieraccini, M. Gregori, F. Abramo, G. Monni, L. Intorre, Acute toxicity of ionic liquids to the zebrafish (Danio rerio), Green Chem. 8 (2006) 238–240. doi:10.1039/b511554j.

[318] G. Dumitrescu, L. Petculescu-Ciochină, I. Bencsik, D. Dronca, L. Boca, Evaluation on acute toxicity of tetrabuthylammonium bromide ionic liquid at histological structure of some organs in zebrafish (Danio rerio), AACL Bioflux. 3 (2010) 404–414.

[319] M. Dong, L. Zhu, S. Zhu, J. Wang, J. Wang, H. Xie, Z. Du, Toxic effects of 1-decyl-3-methylimidazolium bromide ionic liquid on the antioxidant enzyme system and DNA in zebrafish (Danio rerio) livers, Chemosphere. 91 (2013) 1107–1112. doi:http://dx.doi.org/10.1016/j.chemosphere.2013.01.013.

[320] M. El-Harbawi, Y.S.B. Yusri, M. Ismail Hossain, Toxicity assessment of phosphonium based ionic liquids towards female guppy fish, Am. J. Environ. Sci. 9 (2014) 511–517. doi:10.3844/ajessp.2013.511.517.

[321] T. Omasa, M. Onitsuka, W.-D. Kim, Cell Engineering and Cultivation of Chinese Hamster Ovary (CHO) Cells, Curr. Pharm. Biotechnol. 11 (2010) 233–240. doi:10.2174/138920110791111960.

[322] J. Kaslin, P. Panula, Comparative anatomy of the histaminergic and other aminergic systems in zebrafish (Danio rerio), J. Comp. Neurol. 440 (2001) 342–377. doi:10.1002/cne.1390.

[323] N. Peitsaro, M. Sundvik, O. V. Anichtchik, J. Kaslin, P. Panula, Identification of zebrafish histamine H1, H2 and H3 receptors and effects of histaminergic ligands on behavior, Biochem. Pharmacol. 73 (2007) 1205–1214. doi:10.1016/j.bcp.2007.01.014.

[324] M. Sundvik, H. Kudo, P. Toivonen, S. Rozov, Y. Chen, P. Panula, The histaminergic system regulates wakefulness and orexin/hypocretin neuron development via histamine receptor H1 in zebrafish, FASEB J. 25 (2011) 4338–4347. doi:10.1096/fj.11-188268.

[325] M. Westerfield, The Zebrafish Book: A Guide for the Laboratory Use of Zebrafish (Danio rerio), University of Oregon Press, 2000.

[326] U.N.E.C. f. E. Secretariat, Globally harmonized system of classification and labelling of chemicals (GHS) and its implementation in Japan, 2010. doi:10.1265/jjh.65.5.

[327] M. Panula, P.; Sallinen, V. Sundvik, J. Kolehmainen, T. V., A. Tiittula, M. Moshnyakov, P. Podlasz, Modulatory neurotransmitter systems and behavior: towards zebrafish models of neurodegenerative diseases, Zebrafish. 3 (2006) 235–247. doi:10.1089/zeb.2006.3.235.

[328] F. Duša, S.K. Ruokonen, J. Petrovaj, T. Viitala, S.K. Wiedmer, Ionic liquids affect the adsorption of liposomes onto cationic polyelectrolyte coated silica evidenced by quartz crystal microbalance, Colloids Surfaces B Biointerfaces. 136 (2015) 496–505. doi:10.1016/j.colsurfb.2015.09.059.

[329] C.B. Kimmel, W.W. Ballard, S.R. Kimmel, B. Ullmann, T.F. Schilling, Stages of embryonic development of the zebrafish, Dev. Dyn. 203 (1995) 253–310. doi:10.1002/aja.1002030302.

[330] K. Henn, T. Braunbeck, Dechorionation as a tool to improve the fish embryo toxicity test (FET) with the zebrafish (Danio rerio), Comp. Biochem. Physiol. - C Toxicol. Pharmacol. 153 (2011) 91–98. doi:10.1016/j.cbpc.2010.09.003.

[331] A. Sih, A. Bell, J.C. Johnson, Behavioral syndromes: An ecological and evolutionary overview, Trends Ecol. Evol. 19 (2004) 372–378. doi:10.1016/j.tree.2004.04.009.

[332] R.F. Benus, B. Bohus, J.M. Koolhaas, G.A. van Oortmerssen, Heritable variation for aggression as a reflection of individual coping strategies, Experientia. 47 (1991) 1008–1019. doi:10.1007/BF01923336.

[333] N.J. Dingemanse, C. Both, A.J. Van Noordwijk, A.L. Rutten, P.J. Drent, Natal dispersal and personalities in great tits (Parus major), Proc. R. Soc. B Biol. Sci. 270 (2003) 741–747. doi:10.1098/rspb.2002.2300.

[334] N.J. Dingemanse, J. Wright, A.J.N. Kazem, D.K. Thomas, R. Hickling, N. Dawnay, Behavioural syndromes differ predictably between 12 populations of three-spined stickleback, J. Anim. Ecol. 76 (2007) 1128–1138. doi:10.1111/j.1365-2656.2007.01284.x.

[335] W.H.J. Norton, K. Stumpenhorst, T. Faus-Kessler, A. Folchert, N. Rohner, M.P. Harris, J. Callebert, L. Bally-Cuif, Modulation of Fgfr1a Signaling in Zebrafish Reveals a Genetic Basis for the Aggression-Boldness Syndrome, J. Neurosci. 31 (2011) 13796–13807. doi:10.1523/JNEUROSCI.2892-11.2011.

[336] F.A. Huntingford, The Relationship between Anti-Predator Behaviour and Aggression among Conspecifics in the Three-Spined Stickleback , Gasterosteus Aculeatus, Anim. Behav. 24 (1976) 245–260.

[337] J.A. Moretz, E.P. Martins, B.D. Robison, Behavioral syndromes and the evolution of correlated behavior in zebrafish, Behav. Ecol. 18 (2007) 556–562. doi:10.1093/beheco/arm011.

[338] H. Sixta, A. Michud, L. Hauru, S. Asaadi, Y. Ma, A.W.T. King, I. Kilpeläinen, M. Hummel, Ioncell-F: A high-strength regenerated cellulose fibre, Nord. Pulp Pap. Res. J. 30 (2015) 43–57. doi:10.3183/npprj-2015-30-01-p043-057.

[339] M. Hummel, A. Michud, M. Tanttu, S. Asaadi, Y. Ma, L.K.J. Hauru, A. Parviainen, A.W.T. King, I. Kilpeläinen, H. Sixta, Ionic Liquids for the Production of Man-Made Cellulosic Fibers: Opportunities and Challenges, in: Advances in Polymer Science, 2015: pp. 1–36.

[340] D. Glas, C. Van Doorslaer, D. Depuydt, F. Liebner, T. Rosenau, K. Binnemans, D.E. De Vos, Lignin solubility in non-imidazolium ionic liquids, J. Chem. Technol. Biotechnol. 90 (2015) 1821–1826. doi:10.1002/jctb.4492.

[341] D. Wright, L.B. Rimmer, V.L. Pritchard, J. Krause, R.K. Butlin, Inter and intra-population variation in shoaling and boldness in the zebrafish (Danio rerio), Naturwissenschaften. 90 (2003) 374–377. doi:10.1007/s00114-003-0443-2.

[342] R. Gerlai, M. Lahav, S. Guo, A. Rosenthal, Drinks like a fish: Zebra fish (Danio rerio) as a behavior genetic model to study alcohol effects, Pharmacol. Biochem. Behav. 67 (2000) 773–782. doi:10.1016/S0091-3057(00)00422-6.

[343] W.J. Rowland, Studying visual cues in fish behavior, a review of ethological techniques, Environ. Biol. Fishes. 56 (1999) 285–305.

[344] X.Y. Li, S.H. Zeng, X.Y. Dong, J.G. Ma, J.J. Wang, Acute toxicity and responses of antioxidant systems to 1-methyl-3- octylimidazolium bromide at different developmental stages of goldfish, Ecotoxicology. 21 (2012) 253–259. doi:10.1007/s10646-011-0785-z.

[345] X.-Y. Li, S.-H. Zeng, W.-H. Thang, L. Liu, S. Ma, J.-J. Wang, Acute Toxicity and Superficial Damage to Goldfish from the Ionic Liquid 1-Methyl-3-Octylimidazolium Bromide, Environ. Toxicol. 28 (2013) 207–214. doi:10.1002/tox.

[346] D.N. Lebard, B.G. Levine, R. DeVane, W. Shinoda, M.L. Klein, Premicelles and monomer exchange in aqueous surfactant solutions above and below the critical micelle concentration, Chem. Phys. Lett. 522 (2012) 38–42. doi:10.1016/j.cplett.2011.11.075.

[347] B. Dong, N. Li, L. Zheng, L. Yu, T. Inoue, Surface adsorption and micelle formation of surface active ionic liquids in aqueous solution, Langmuir. 23 (2007) 4178–4182. doi:10.1021/la0633029.

[348] E. Ghasemian, M. Najafi, A.A. Rafati, Z. Felegari, Effect of electrolytes on surface tension and surface adsorption of 1-hexyl-3-methylimidazolium chloride ionic liquid in aqueous solution, J. Chem. Thermodyn. 42 (2010) 962–966. doi:10.1016/j.jct.2010.03.007.

[349] N.J. Turro, A. Yekta, Luminescent Probes for Detergent Solutions. A Simple Procedure for Determination of the Mean Aggregation Number of Micelles, J. Am. Chem. Soc. 100 (1978) 5951–5952. doi:10.1021/ja00486a062.

[350] J.N. Phillips, The energetics of micelle formation, Trans. Faraday Soc. 51 (1955) 561–569. doi:10.1039/tf9555100561.

[351] J. Łuczak, J. Hupka, J. Thöming, C. Jungnickel, Self-organization of imidazolium ionic liquids in aqueous solution, Colloids Surfaces A Physicochem. Eng. Asp. 329 (2008) 125–133. doi:10.1016/j.colsurfa.2008.07.012.

[352] J. Lin, A. Alexander-Katz, Cell membranes open “doors” for cationic nanoparticles/ biomolecules: Insights into uptake kinetics, ACS Nano. 7 (2013) 10799–10808. doi:10.1021/nn4040553.

[353] E.H. Hill, K. Stratton, D.G. Whitten, D.G. Evans, Molecular dynamics simulation study of the interaction of cationic biocides with lipid bilayers: Aggregation effects and bilayer damage, Langmuir. 28 (2012) 14849–14854. doi:10.1021/la303158c.

[354] R.D. Groot, K.L. Rabone, Mesoscopic simulation of cell membrane damage, morphology change and rupture by nonionic surfactants, Biophys. J. 81 (2001) 725–736. doi:10.1016/S0006-3495(01)75737-2.

[355] J. Lokajová, V. Hruška, E. Tesařová, B. Gaš, System peaks in micellar electrophoresis: I. Utilization of system peaks for determination of critical micelle concentration, Electrophoresis. 29 (2008) 1189–1195. doi:10.1002/elps.200700780.

[356] M. Tariq, M.G. Freire, B. Saramago, J.A.P. Coutinho, J.N.C. Lopes, L.P.N. Rebelo, Surface tension of ionic liquids and ionic liquid solutions, Chem. Soc. Rev. 41 (2012) 829–868. doi:10.1039/c1cs15146k.

[357] T. Křížek, Z.S. Breitbach, D.W. Armstrong, E. Tesařová, P. Coufal, Separation of inorganic and small organic anions by CE using phosphonium-based mono- and dicationic reagents, Electrophoresis. 30 (2009) 3955–3963. doi:10.1002/elps.200900416.

[358] S.K. Wiedmer, A.W.T. King, M.L. Riekkola, Phosphonium-based ionic liquids in electrokinetic capillary chromatography for the separation of neutral analytes, J. Chromatogr. A. 1253 (2012) 171–176. doi:10.1016/j.chroma.2012.06.084.

[359] A. Mendes, L.C. Branco, C. Morais, A.L. Simplício, Electroosmotic flow modulation in capillary electrophoresis by organic cations from ionic liquids, Electrophoresis. 33 (2012) 1182–1190. doi:10.1002/elps.201100486.

[360] S.-K. Ruokonen, F. Duša, J. Lokajová, I. Kilpeläinen, A.W.T. King, S.K. Wiedmer, Effect of ionic liquids on the interaction between liposomes and common wastewater pollutants investigated by capillary electrophoresis, J. Chromatogr. A. 1405 (2015) 178–187. doi:http://dx.doi.org/10.1016/j.chroma.2015.05.064.

[361] K.S. Egorova, E.G. Gordeev, V.P. Ananikov, Biological Activity of Ionic Liquids and Their Application in Pharmaceutics and Medicine, Chem. Rev. 117 (2017) 7132–7189. doi:10.1021/acs.chemrev.6b00562.

[362] A.A.C. Toledo Hijo, G.J. Maximo, M.C. Costa, E.A.C. Batista, A.J.A. Meirelles, Applications of Ionic Liquids in the Food and Bioproducts Industries, ACS Sustain. Chem. & Eng. 4 (2016) 5347–5369. doi:10.1021/acssuschemeng.6b00560.

[363] T.P. Thuy Pham, C.W. Cho, Y.S. Yun, Environmental fate and toxicity of ionic liquids: A review, Water Res. 44 (2010) 352–372. doi:10.1016/j.watres.2009.09.030.

[364] D. Zhao, Y. Liao, Z.D. Zhang, Toxicity of ionic liquids, Clean - Soil, Air, Water. 35 (2007) 42–48. doi:10.1002/clen.200600015.

[365] S.P.F. Costa, A.M.O. Azevedo, P.C.A.G. Pinto, M.L.M.F.S. Saraiva, Environmental Impact of Ionic Liquids: Recent Advances in (Eco)toxicology and (Bio)degradability, ChemSusChem. 10 (2017) 2321–2347. doi:10.1002/cssc.201700261.

[366] P. Galletti, D. Malferrari, C. Samorì, G. Sartor, E. Tagliavini, Effects of ionic liquids on membrane fusion and lipid aggregation of egg-PC liposomes, Colloids Surfaces B Biointerfaces. 125 (2015) 142–150. doi:10.1016/j.colsurfb.2014.11.021.

[367] A.H. Rantamäki, S.K. Ruokonen, E. Sklavounos, L. Kyllönen, A.W.T. King, S.K. Wiedmer, Impact of surface- active guanidinium-, tetramethylguanidinium-, and cholinium-based ionic liquids on vibrio Fischeri cells and dipalmitoylphosphatidylcholine liposomes, Sci. Rep. 7 (2017) 1–12. doi:10.1038/srep46673.

[368] K.O. Evans, Room-temperature ionic liquid cations act as short-chain surfactants and disintegrate a phospholipid bilayer, Colloids Surfaces A Physicochem. Eng. Asp. 274 (2006) 11–17. doi:10.1016/j.colsurfa.2005.10.007.

[369] J. Ranke, A. Müller, U. Bottin-Weber, F. Stock, S. Stolte, J. Arning, R. Störmann, B. Jastorff, Lipophilicity parameters for ionic liquid cations and their correlation to in vitro cytotoxicity, Ecotoxicol. Environ. Saf. 67 (2006) 430–438. doi:10.1016/j.ecoenv.2006.08.008.

[370] M. Galluzzi, S. Zhang, S. Mohamadi, A. Vakurov, A. Podestà, A. Nelson, Interaction of imidazolium-based room-temperature ionic liquids with DOPC phospholipid monolayers: Electrochemical study, Langmuir. 29 (2013) 6573–6581. doi:10.1021/la400923d.

[371] O. López, A. De La Maza, L. Coderch, C. López-Iglesias, E. Wehrli, J.L. Parra, Direct formation of mixed micelles in the solubilization of phospholipid liposomes by Triton X-100, FEBS Lett. 426 (1998) 314–318. doi:10.1016/S0014-5793(98)00363-9.

[372] E.H. Hayakawa, E. Mochizuki, T. Tsuda, K. Akiyoshi, H. Matsuoka, S. Kuwabata, The effect of hydrophilic ionic liquids 1-ethyl-3-methylimidazolium lactate and choline lactate on lipid vesicle fusion, PLoS One. 8 (2013) 1–9. doi:10.1371/journal.pone.0085467.

[373] B. Lachance, P.Y. Robidoux, J. Hawari, G. Ampleman, S. Thiboutot, G.I. Sunahara, Cytotoxic and genotoxic effects of energetic compounds on bacterial and mammalian cells in vitro, Mutat. Res. - Genet. Toxicol. Environ. Mutagen. 444 (1999) 25–39. doi:10.1016/S1383-5718(99)00073-X.

[374] N.S. Kudryasheva, Bioluminescence and exogenous compounds: Physico-chemical basis for bioluminescent assay, J. Photochem. Photobiol. B Biol. 83 (2006) 77–86. doi:10.1016/j.jphotobiol.2005.10.003.

[375] A. Mariscal, M.T. Peinado, M. Carnero-Varo, J. Fernández-Crehuet, Influence of organic solvents on the sensitivity of a bioluminescence toxicity test with Vibrio harveyi, Chemosphere. 50 (2003) 349–354. doi:10.1016/S0045-6535(02)00312-0.

[376] P.C. Burcham, An Introduction to Toxicology, Springer, 2013.

[377] A.P. Li, In Vitro Approaches to Evaluate ADMET Drug Properties, Curr. Top. Med. Chem. 4 (2004) 701–706. doi:10.2174/1568026043451050.

[378] D.C. Liebler, F.P. Guengerich, Elucidating mechanisms of drug-induced toxicity, Nat. Rev. Drug Discov. 4 (2005) 410–420. doi:10.1038/nrd1720.

[379] R.M. LoPachin, T. Gavin, A. DeCaprio, D.S. Barber, Application of the Hard and Soft, Acids and Bases (HSAB) theory to toxicant - Target interactions, Chem. Res. Toxicol. 25 (2012) 239–251. doi:10.1021/tx2003257.

[380] Y. Fan, X. Dong, L. Yan, D. Li, S. Hua, C. Hu, C. Pan, Evaluation of the toxicity of ionic liquids on trypsin: A mechanism study, Chemosphere. 148 (2016) 241–247. doi:10.1016/j.chemosphere.2016.01.033.

[381] F. Stock, J. Hoffmann, J. Ranke, R. Störmann, B. Ondruschka, B. Jastorff, Effects of ionic liquids on the acetylcholinesterase - A structure-activity relationship consideration, Green Chem. 6 (2004) 286–290. doi:10.1039/b402348j.

[382] A.C. Składanowski, P. Stepnowski, K. Kleszczyński, B. Dmochowska, AMP deaminase in vitro inhibition by xenobiotics: A potential molecular method for risk assessment of synthetic nitro- and polycyclic musks, imidazolium ionic liquids and N-glucopyranosyl ammonium salts, Environ. Toxicol. Pharmacol. 19 (2005) 291–296. doi:10.1016/j.etap.2004.08.005.

[383] I. Kontro, K. Svedström, F. Duša, P. Ahvenainen, S.K. Ruokonen, J. Witos, S.K. Wiedmer, Effects of phosphonium-based ionic liquids on phospholipid membranes studied by small-angle X-ray scattering, Chem. Phys. Lipids. 201 (2016) 59–66. doi:10.1016/j.chemphyslip.2016.11.003.

[384] D. Lichtenberg, H. Ahyayauch, A. Alonso, F.M. Goñi, Detergent solubilization of lipid bilayers: A balance of driving forces, Trends Biochem. Sci. 38 (2013) 85–93. doi:10.1016/j.tibs.2012.11.005.

[385] H. Heerklotz, Interactions of surfactants with lipid membranes, Q. Rev. Biophys. 41 (2008) 205–264. doi:10.1017/S0033583508004721.

[386] P.R. Majhi, A. Blume, Temperature-induced micelle-vesicle transitions in DMPC-SDS and DMPC-DTAB mixtures studied by calorimetry and dynamic light scattering, J. Phys. Chem. B. 106 (2002) 10753–10763. doi:10.1021/jp025849b.

[387] J. Witos, G. Russo, S.K. Ruokonen, S.K. Wiedmer, Unraveling interactions between ionic liquids and phospholipid vesicles using nanoplasmonic sensing, Langmuir. 33 (2017) 1066–1076. doi:10.1021/acs.langmuir.6b04359.

[388] M. Figueira-González, V. Francisco, L. García-Río, E.F. Marques, M. Parajó, P. Rodríguez-Dafonte, Self-aggregation properties of ionic liquid 1,3-didecyl-2-methylimidazolium chloride in aqueous solution: From spheres to cylinders to bilayers, J. Phys. Chem. B. 117 (2013) 2926–2937. doi:10.1021/jp3117962.

[389] M.H. Chiu, E.J. Prenner, Differential scanning calorimetry: An invaluable tool for a detailed thermodynamic characterization of macromolecules and their interactions, J Pharm Bioall Sci. 3 (2011) 39–59. doi:10.4103/0975-7406.76463.

[390] A. Rahman, Studies in Natural Products Chemistry, Elsevier Science Pakistan, 2008.

[391] O. Reer, T.K. Bock, B.W. Müller, In vitro corneal permeability of diclofenac sodium in formulations containing cyclodextrins compared to the commercial product voltaren ophtha, J. Pharm. Sci. 83 (1994) 1345–1349. doi:10.1002/jps.2600830928.

[392] C.H. Huang, J.P. Sipe, S.T. Chow, R.B. Martin, Differential interaction of cholesterol with phosphatidylcholine on the inner and outer surfaces of lipid bilayer vesicles, Proc. Natl. Acad. Sci. U. S. A. 71 (1974) 359–362. doi:10.1073/pnas.71.2.359.

[393] S.E. Feller, R.M. Venable, R.W. Pastor, Computer simulation of a DPPC phospholipid bilayer: Structural Changes as a function of molecular surface area, Langmuir. 13 (1997) 6555–6561. doi:10.1021/la970746j.

[394] L.J. Lis, M. McAlister, N. Fuller, R.P. Rand, V.A. Parsegian, Interactions between neutral phospholipid bilayer membranes, Biophys. J. 37 (1982) 657–666.

[395] K. Mitra, I. Ubarretxena-Belandia, T. Taguchi, G. Warren, D.M. Engelman, Modulation of the bilayer thickness of exocytic pathway membranes by membrane proteins rather than cholesterol, Proc. Natl. Acad. Sci. U. S. A. 101 (2004) 4083–4088. doi:10.1073/pnas.0307332101.

[396] C.R. Peterson, M. Gorbet, D. Cira, C. Amos, C.A. Woods, F. Desmond, Non-Invasive Collection and Examination of Human Corneal Epithelial Cells, Optom. Vis. Sci. 88 (2011) 1317–1325. doi:10.1097/OPX.0b013e31822c095d.

[397] G. Zauner, A.M. Deelder, M. Wuhrer, Recent advances in hydrophilic interaction liquid chromatography (HILIC) for structural glycomics, Electrophoresis. 32 (2011) 3456–3466. doi:10.1002/elps.201100247.

[398] G. Kahsay, H. Song, A. Van Schepdael, D. Cabooter, E. Adams, Hydrophilic interaction chromatography (HILIC) in the analysis of antibiotics, J. Pharm. Biomed. Anal. 87 (2014) 142–154. doi:10.1016/j.jpba.2013.04.015.

[399] D.Q. Tang, L. Zou, X.X. Yin, C.N. Ong, HILIC-MS for metabolomics: An attractive and complementary approach to RPLC-MS, Mass Spectrom. Rev. 35 (2016) 574–600. doi:10.1002/mas.21445.

[400] B. Dejaegher, Y. Vander Heyden, HILIC methods in pharmaceutical analysis, J. Sep. Sci. 33 (2010) 698–715. doi:10.1002/jssc.200900742.

[401] P. Jiang, D. Wu, C.A. Lucy, Determination of void volume in normal phase liquid chromatography, J. Chromatogr. A. 1324 (2014) 63–70. doi:10.1016/j.chroma.2013.11.019.

[402] R.E. Majors, P.W. Carr, Glossary of Liquid-Phase Watch, LCGC North Am. 19 (2001) 124–162.

[403] F. Tsopelas, M. Ochsenkühn-Petropoulou, A. Tsantili-Kakoulidou, Void volume markers in reversed-phase and biomimetic liquid chromatography, J. Chromatogr. A. 1217 (2010) 2847–2854. doi:10.1016/j.chroma.2010.02.062.

[404] W.H. Pirkle, C.J. Welch, A convenient void volume marker for several chiral hplc columns, J. Liq. Chromatogr. 14 (1991) 1–8. doi:10.1080/01483919108049593.

[405] C.A. Rimmer, C.R. Simmons, J.G. Dorsey, The measurement and meaning of void volumes in reversed-phase liquid chromatography, J. Chromatogr. A. 965 (2002) 219–232. doi:10.1016/S0021-9673(02)00730-6.

[406] M. Liu, M. Ronk, D. Ren, J. Ostovic, N. Cauchon, Z.S. Zhou, J. Cheetham, Structure elucidation of highly polar basic degradants by on-line hydrogen/deuterium exchange hydrophilic interaction chromatography coupled to tandem mass spectrometry, J. Chromatogr. A. 1217 (2010) 3598–3611. doi:10.1016/j.chroma.2010.03.040.

[407] M. Lämmerhofer, M. Richter, J. Wu, R. Nogueira, W. Bicker, W. Lindner, Mixed-mode ion-exchangers and their comparative chromatographic characterization in reversed-phase and hydrophilic interaction chromatography elution modes, J. Sep. Sci. 31 (2008) 2572–2588. doi:10.1002/jssc.200800178.

[408] P. Appelblad, T. Jonsson, W. Jiang, K. Irgum, Fast hydrophilic interaction liquid chromatographic separations on bonded zwitterionic stationary phase, J. Sep. Sci. 31 (2008) 1529–1536. doi:10.1002/jssc.200800080.

[409] A. Yanagida, H. Murao, M. Ohnishi-Kameyama, Y. Yamakawa, A. Shoji, M. Tagashira, T. Kanda, H. Shindo, Y. Shibusawa, Retention behavior of oligomeric proanthocyanidins in hydrophilic interaction chromatography, J. Chromatogr. A. 1143 (2007) 153–161. doi:10.1016/j.chroma.2007.01.004.

[410] F.C. Normand, D.M. Goodall, S.B. Duckett, M.F.H. van Tol, J.-J.H. Nusselder, Separation and characterisation of caprolactam-formaldehyde reaction products, Analyst. 127 (2002) 1312–1317. doi:10.1039/b205438h.

[411] K.J. Fountain, J. Xu, D.M. Dieh, D. Morrison, Influence of stationary phase chemistry and mobile-phase composition on retention, selectivity, and MS response in hydrophilic interaction chromatography, J. Sep. Sci. 33 (2010) 740–751. doi:10.1002/jssc.200900660.

[412] L. Buchholz, C.-H. Cai, L. Andress, A. Cleton, J. Brodfuehrer, L. Cohen, Evaluation of the human serum albumin column as a discovery screening tool for plasma protein binding, Eur. J. Pharm. Sci. 15 (2002) 209–215. doi:10.1016/S0928-0987(01)00219-6.

[413] T. Kubo, K. Kuroda, Y. Tominaga, T. Naito, K. Sueyoshi, K. Hosoya, K. Otsuka, Effective determination of a pharmaceutical, sulpiride, in river water by online SPE-LC-MS using a molecularly imprinted polymer as a preconcentration medium, J. Pharm. Biomed. Anal. 89 (2014) 111–117. doi:10.1016/j.jpba.2013.10.040.

[414] J. Soukup, P. Jandera, Adsorption of water from aqueous acetonitrile on silica-based stationary phases in aqueous normal-phase liquid chromatography, J Chromatogr A. 1374 (2014) 102–111. doi:10.1016/j.chroma.2014.11.028.

[415] MarvinSketch version 14.12.15.0, calculation module developed by ChemAxon, (2016). http:www.chemaxon.com/products/marvin/marvinsketch/.

[416] Column Manual -Nucleoshell HILIC, (n.d.) 80.

[417] ZIC - c HILIC HPLC Column Analytical PEEK coated Columns General Instructions for Care and Use, 49 (2015) 75205.

[418] A. D'Attoma, S. Heinisch, On-line comprehensive two dimensional separations of charged compounds using reversed-phase high performance liquid chromatography and hydrophilic interaction chromatography. Part II: Application to the separation of peptides, J. Chromatogr. A. 1306 (2013) 27–36. doi:10.1016/j.chroma.2013.07.048.

[419] U. Lindner, J. Lingott, S. Richter, W. Jiang, N. Jakubowski, U. Panne, Analysis of Gadolinium-based contrast agents in tap water with a new hydrophilic interaction chromatography (ZIC-cHILIC) hyphenated with inductively coupled plasma mass spectrometry, Anal. Bioanal. Chem. 407 (2015) 2415–2422. doi:10.1007/s00216-014-8368-5.

[420] S. Tufi, M. Lamoree, J. de Boer, P. Leonards, Simultaneous analysis of multiple neurotransmitters by hydrophilic interaction liquid chromatography coupled to tandem mass spectrometry, J. Chromatogr. A. 1395 (2015) 79–87. doi:10.1016/j.chroma.2015.03.056.

[421] S. Di Palma, S. Mohammed, A.J.R. Heck, ZIC-cHILIC as a fractionation method for sensitive and powerful shotgun proteomics, Nat. Protoc. 7 (2012) 2041–2055. doi:http://www.nature.com/nprot/journal/v7/n11/abs/nprot.2012.124.html#supplementary-information.

[422] S. Di Palma, P.J. Boersema, A.J.R. Heck, S. Mohammed, Zwitterionic Hydrophilic Interaction Liquid Chromatography (ZIC-HILIC and ZIC-cHILIC) Provide High Resolution Separation and Increase Sensitivity in Proteome Analysis, Anal. Chem. 83 (2011) 3440–3447. doi:10.1021/ac103312e.

[423] J. Zhou, Y. Qi, J. Ritho, L. Duan, L. Wu, Q. Diao, Y. Li, J. Zhao, Analysis of maltooligosaccharides in honey samples by ultra-performance liquid chromatography coupled with evaporative light scattering detection, Food Res. Int. 56 (2014) 260–265. doi:10.1016/j.foodres.2014.01.014.

[424] M. van der Ham, M. Albersen, T.J. de Koning, G. Visser, A. Middendorp, M. Bosma, N.M. Verhoeven-Duif, M.G.M. De Sain-van der Velden, Quantification of vitamin B6 vitamers in human cerebrospinal fluid by ultra performance liquid chromatography-tandem mass spectrometry, Anal. Chim. Acta. 712 (2012) 108–114. doi:10.1016/j.aca.2011.11.018.

[425] H.G. Gika, G.A. Theodoridis, U. Vrhovsek, F. Mattivi, Quantitative profiling of polar primary metabolites using hydrophilic interaction ultrahigh performance liquid chromatography-tandem mass spectrometry, J. Chromatogr. A. 1259 (2012) 121–127. doi:10.1016/j.chroma.2012.02.010.

[426] D. Kotoni, A. Ciogli, C. Villani, D.S. Bell, F. Gasparrini, Separation of complex sugar mixtures on a hydrolytically stable bidentate urea-type stationary phase for hydrophilic interaction near ultra high performance liquid chromatography, J. Sep. Sci. 37 (2014) 527–535. doi:10.1002/jssc.201301008.

[427] B. Zhu, F. Liu, X. Li, Y. Wang, X. Gu, J. Dai, G. Wang, Y. Cheng, C. Yan, Fast quantification of endogenous carbohydrates in plasma using hydrophilic interaction liquid chromatography coupled with tandem mass spectrometry, J. Sep. Sci. 38 (2015) 34–41. doi:10.1002/jssc.201400899.

[428] A.G.M. Leijdekkers, M.G. Sanders, H.A. Schols, H. Gruppen, Characterizing plant cell wall derived oligosaccharides using hydrophilic interaction chromatography with mass spectrometry detection, J. Chromatogr. A. 1218 (2011) 9227–9235. doi:10.1016/j.chroma.2011.10.068.

[429] J.S. Wilkes, A short history of ionic liquids—from molten salts to neoteric solvents, Green Chem. 4 (2002) 73–80. doi:10.1039/b110838g.

[430] N. Muhammad, Z. Man, M.A.B. Khalil, Ionic liquid-a future solvent for the enhanced uses of wood biomass, Eur. J. Wood Wood Prod. 70 (2012) 125–133. doi:10.1007/s00107-011-0526-2.

[431] P.C. Alves, D.O. Hartmann, O. Núñez, I. Martins, T.L. Gomes, H. Garcia, M.T. Galceran, R. Hampson, J.D. Becker, C.S. Pereira, Transcriptomic and metabolomic profiling of ionic liquid stimuli unveils enhanced secondary metabolism in Aspergillus nidulans, BMC Genomics. 17 (2016) 1–18. doi:10.1186/s12864-016-2577-6.

[432] M.S.P. Boyles, C. Ranninger, R. Reischl, M. Rurik, R. Tessadri, O. Kohlbacher, A. Duschl, C.G. Huber, Copper oxide nanoparticle toxicity profiling using untargeted metabolomics, Part. Fibre Toxicol. 13 (2016) 1–20. doi:10.1186/s12989-016-0160-6.

[433] G. Hopfgartner, D. Tonoli, E. Varesio, High-resolution mass spectrometry for integrated qualitative and quantitative analysis of pharmaceuticals in biological matrices, Anal. Bioanal. Chem. 402 (2012) 2587–2596. doi:10.1007/s00216-011-5641-8.

[434] B. Grund, L. Marvin, B. Rochat, Quantitative performance of a quadrupole-orbitrap-MS in targeted LC-MS determinations of small molecules, J. Pharm. Biomed. Anal. 124 (2016) 48–56. doi:10.1016/j.jpba.2016.02.025.

[435] A.T. Roemmelt, A.E. Steuer, T. Kraemer, Liquid Chromatography, In Combination with a Quadrupole Time-of-Flight Instrument, with Sequential Window Acquisition of All Theoretical Fragment-Ion Spectra Acquisition: Validated Quantification of 39 Antidepressants in Whole Blood As Part of a Simultane, Anal Chem. 87 (2015) 9294–9301. doi:10.1021/acs.analchem.5b02031.

[436] D. Siegel, A.C. Meinema, H. Permentier, G. Hopfgartner, R. Bischoff, Integrated quantification and identification of aldehydes and ketones in biological samples, Anal. Chem. 86 (2014) 5089–5100. doi:10.1021/ac500810r.

[437] B. Drotleff, M. Hallschmid, M. Lämmerhofer, Quantification of steroid hormones in plasma using a surrogate calibrant approach and UHPLC-ESI-QTOF-MS/MS with SWATH-acquisition combined with untargeted profiling, Anal. Chim. Acta. 1022 (2018) 70–80. doi:10.1016/j.aca.2018.03.040.

[438] M. Schwaiger, E. Rampler, G. Hermann, W. Miklos, W. Berger, G. Koellensperger, Anion-Exchange Chromatography Coupled to High-Resolution Mass Spectrometry: A Powerful Tool for Merging Targeted and Non-targeted Metabolomics, Anal. Chem. 89 (2017) 7667–7674. doi:10.1021/acs.analchem.7b01624.

[439] A.T. Roemmelt, A.E. Steuer, M. Poetzsch, T. Kraemer, Liquid chromatography, in combination with a quadrupole time-of-flight instrument (LC QTOF), with sequential window acquisition of all theoretical fragment-ion spectra (SWATH) acquisition: systematic studies on its use for screenings in clinical and foren, Anal Chem. 86 (2014) 11742–11749. doi:10.1021/ac503144p.

[440] N.S. Greenspan, A.K. Sheth, V. Desai, HIV vaccine development and broadly neutralizing antibodies, Evol. Med. Public Heal. 2015 (2015) 75–75. doi:10.1021/acs.analchem.8b02377.

[441] J. Zhou, Y. Li, X. Chen, L. Zhong, Y. Yin, Development of data-independent acquisition workflows for metabolomic analysis on a quadrupole-orbitrap platform, Talanta. 164 (2017) 128–136. doi:10.1016/j.talanta.2016.11.048.

[442] J.D. Venable, M.-Q. Dong, J. Wohlschlegel, A. Dillin, J.R. Yates, Automated approach for quantitative analysis of complex peptide mixtures from tandem mass spectra, Nat. Methods. 1 (2004) 39–45. doi:10.1038/nmeth705.

[443] J. Ji, P. Zhu, F. Cui, F. Pi, Y. Zhang, X. Sun, The disorder metabolic profiling in kidney and spleen of mice induced by mycotoxins deoxynivalenol through gas chromatography mass spectrometry, Chemosphere. 180 (2017) 267–274. doi:10.1016/j.chemosphere.2017.03.129.

[444] S. Salihovic, T. Fall, A. Ganna, C.D. Broeckling, J.E. Prenni, T. Hyötyläinen, A. Kärrman, P.M. Lind, E. Ingelsson, L. Lind, Identification of metabolic profiles associated with human exposure to perfluoroalkyl substances, J. Expo. Sci. Environ. Epidemiol. 29 (2018) 196–205. doi:10.1038/s41370-018-0060-y.

[445] S. Guo, J.A. Duan, D. Qian, Y. Tang, Y. Qian, D. Wu, S. Su, E. Shang, Rapid determination of amino acids in fruits of Ziziphus jujuba by hydrophilic interaction ultra-high-performance liquid chromatography coupled with triple-quadrupole mass spectrometry, J Agric Food Chem. 61 (2013) 2709–2719. doi:10.1021/jf305497r.

[446] M.A. Alterman, P. Hunziker, Amino Acid Analysis : Methods and Protocols, Humana Press, Totowa, NJ, 2012. doi:10.1007/978-1-61779-445-2.

[447] G. Sharma, S.V. Attri, B. Behra, S. Bhisikar, P. Kumar, M. Tageja, S. Sharda, P. Singhi, S. Singhi, Analysis of 26 amino acids in human plasma by HPLC using AQC as derivatizing agent and its application in metabolic laboratory, Amino Acids. 46 (2014) 1253–1263. doi:10.1007/s00726-014-1682-6.

[448] W. Li, L.H. Cohen, Quantitation of Endogenous Analytes in Biofluid without a True Blank Matrix, Anal. Chem. 75 (2003) 5854–5859. doi:10.1021/ac034505u.

[449] S. Schiesel, M. Lämmerhofer, W. Lindner, Multitarget quantitative metabolic profiling of hydrophilic metabolites in fermentation broths of β-lactam antibiotics production by HILIC–ESI–MS/MS, Anal. Bioanal. Chem. 396 (2010) 1655–1679. doi:10.1007/s00216-009-3432-2.

[450] X. Han, Lipidomics for studying metabolism, Nat. Publ. Gr. 12 (2016) 668–679. doi:10.1038/nrendo.2016.98.

[451] M. Wang, C. Wang, R.H. Han, X. Han, Novel advances in shotgun lipidomics for biology and medicine, Prog. Lipid Res. 61 (2016) 83–108. doi:10.1016/j.plipres.2015.12.002.

[452] S.K. Bhattacharya, Lipidomics, Humana Press, 2017. doi:10.1007/978-1-4939-6996-8.

[453] S. Tumanov, J.J. Kamphorst, Recent advances in expanding the coverage of the lipidome, Curr. Opin. Biotechnol. 43 (2017) 127–133. doi:10.1016/j.copbio.2016.11.008.

[454] C. Breil, M. Abert Vian, T. Zemb, W. Kunz, F. Chemat, “Bligh and Dyer” and Folch methods for solid–liquid–liquid extraction of lipids from microorganisms. Comprehension of solvatation mechanisms and towards substitution with alternative solvents, Int. J. Mol. Sci. 18 (2017) 1–21. doi:10.3390/ijms18040708.

[455] T. a Lydic, J. V Busik, G.E. Reid, A monophasic extraction strategy for the simultaneous lipidome analysis of polar and nonpolar retina lipids., J. Lipid Res. 55 (2014) 1797–1809. doi:10.1194/jlr.D050302.

[456] R.E. Patterson, A.J. Ducrocq, D.J. McDougall, T.J. Garrett, R.A. Yost, Comparison of blood plasma sample preparation methods for combined LC–MS lipidomics and metabolomics, J Chromatogr B Anal. Technol Biomed Life Sci. 1002 (2015) 260–266. doi:10.1016/j.jchromb.2015.08.018.

[457] C.Z. Ulmer, R.A. Yost, T.J. Garrett, Global UHPLC/HRMS Lipidomics Workflow for the Analysis of Lymphocyte Suspension Cultures, in: Lipidomics, 2017. doi:10.1007/978-1-4939-6946-3_13.

[458] H. Zhang, Y. Gao, J. Sun, S. Fan, X. Yao, X. Ran, C. Zheng, M. Huang, H. Bi, Optimization of lipid extraction and analytical protocols for UHPLC-ESI-HRMS-based lipidomic analysis of adherent mammalian cancer cells, Anal. Bioanal. Chem. 409 (2017) 5349–5358. doi:10.1007/s00216-017-0483-7.

[459] A. Hara, N.S. Radin, Lipid extraction of tissues with a low-toxicity solvent, Anal. Biochem. 90 (1978) 420–426. doi:10.1016/0003-2697(78)90046-5.

[460] T.W.T. Rupasinghe, Lipidomics: Extraction Protocols for Biological Matrices, in: Metabolomics Tools Nat. Prod. Discov., 2013: pp. 71–80. doi:10.1007/978-1-62703-577-4_6.

[461] A. Reis, A. Rudnitskaya, G.J. Blackburn, N.M. Fauzi, A.R. Pitt, C.M. Spickett, A comparison of five lipid extraction solvent systems for lipidomic studies of human LDL, J. Lipid Res. 54 (2013) 1812–1824. doi:10.1194/jlr.M034330.

[462] J. Sheng, R. Vannela, B.E. Rittmann, Evaluation of methods to extract and quantify lipids from Synechocystis PCC 6803, Bioresour. Technol. 102 (2011) 1697–1703. doi:10.1016/j.biortech.2010.08.007.

[463] K. Jurowski, K. Kochan, J. Walczak, M. Barańska, W. Piekoszewski, B. Buszewski, Comprehensive review of trends and analytical strategies applied for biological samples preparation and storage in modern medical lipidomics: State of the art, TrAC Trends Anal. Chem. 86 (2017) 276–289. doi:10.1016/j.trac.2016.10.014.

[464] J.M. Weir, G. Wong, C.K. Barlow, M.A. Greeve, A. Kowalczyk, L. Almasy, A.G. Comuzzie, M.C. Mahaney, J.B. Jowett, J. Shaw, J.E. Curran, J. Blangero, P.J. Meikle, Plasma lipid profiling in a large population-based cohort, J Lipid Res. 54 (2013) 2898–2908. doi:10.1194/jlr.P035808.

[465] P.J. Meikle, G. Wong, D. Tsorotes, C.K. Barlow, J.M. Weir, M.J. Christopher, G.L. MacIntosh, B. Goudey, L. Stern, A. Kowalczyk, I. Haviv, A.J. White, A.M. Dart, S.J. Duffy, G.L. Jennings, B.A. Kingwell, Plasma lipidomic analysis of stable and unstable coronary artery disease, Arterioscler. Thromb. Vasc. Biol. 31 (2011) 2723–2732. doi:10.1161/ATVBAHA.111.234096.

[466] Z.H. Alshehry, C.K. Barlow, J.M. Weir, Y. Zhou, M.J. McConville, P.J. Meikle, An efficient single phase method for the extraction of plasma lipids, Metabolites. 5 (2015) 389–403. doi:10.3390/metabo5020389.

[467] R.L. Shaner, J.C. Allegood, H. Park, E. Wang, S. Kelly, C.A. Haynes, M.C. Sullards, A.H. Merrill, Quantitative analysis of sphingolipids for lipidomics using triple quadrupole and quadrupole linear ion trap mass spectrometers, J. Lipid Res. 50 (2009) 1692–1707. doi:10.1194/jlr.d800051-jlr200.

[468] M.C. Sullards, Y. Liu, Y. Chen, A.H. Merrill, Analysis of mammalian sphingolipids by liquid chromatography tandem mass spectrometry (LC-MS/MS) and tissue imaging mass spectrometry (TIMS), Biochim. Biophys. Acta. 1811 (2011) 838–853. doi:10.1016/j.bbalip.2011.06.027.

[469] L. Yao, S.L. Lee, T. Wang, J.A. Gerde, Comparison of lipid extraction from microalgae and soybeans with aqueous isopropanol, J. Am. Oil Chem. Soc. 90 (2013) 571–578. doi:10.1007/s11746-012-2197-5.

[470] M.H. Sarafian, M. Gaudin, M.R. Lewis, F.P. Martin, E. Holmes, J.K. Nicholson, M.E. Dumas, Objective set of criteria for optimization of sample preparation procedures for ultra-high throughput untargeted blood plasma lipid profiling by ultra performance liquid chromatography-mass spectrometry, Anal. Chem. 86 (2014) 5766–5774. doi:10.1021/ac500317c.

[471] J. Sostare, R. Di Guida, J. Kirwan, K. Chalal, E. Palmer, W.B. Dunn, M.R. Viant, Comparison of modified Matyash method to conventional solvent systems for polar metabolite and lipid extractions, Anal. Chim. Acta. 1037 (2018) 302–315. doi:10.1016/j.aca.2018.03.019.

[472] C. Pizarro, I. Arenzana-Rámila, N. Pérez-Del-Notario, P. Pérez-Matute, J.M. González-Sáiz, Plasma lipidomic profiling method based on ultrasound extraction and liquid chromatography mass spectrometry, Anal. Chem. 85 (2013) 12085–12092. doi:10.1021/ac403181c.

[473] S.K. Jensen, Improved Bligh and Dyer extraction procedure, Lipid Technol. 20 (2008) 280–281. doi:10.1002/lite.200800074.

[474] M.L. Dória, Z. Cotrim, B. MacEdo, C. Simões, P. Domingues, L. Helguero, M.R. Domingues, Lipidomic approach to identify patterns in phospholipid profiles and define class differences in mammary epithelial and breast cancer cells, Breast Cancer Res. Treat. 133 (2012) 635–648. doi:10.1007/s10549-011-1823-5.

[475] L.C. Gillet, P. Navarro, S. Tate, H. Rost, N. Selevsek, L. Reiter, R. Bonner, R. Aebersold, Targeted data extraction of the MS/MS spectra generated by data-independent acquisition: a new concept for consistent and accurate proteome analysis, Mol. Cell. Proteomics. 11 (2012). doi:10.1074/mcp.O111.016717.

[476] J.S. Wilkes, J.A. Levisky, R.A. Wilson, C.L. Hussey, Dialkylimidazolium Chloroaluminate Melts: A New Class of Room-Temperature Ionic Liquids for Electrochemistry, Spectroscopy, and Synthesis, Inorg. Chem. 21 (1982) 1263–1264. doi:10.1021/ic00133a078.

[477] A. Benedetto, H.-J. Galla, Editorial of the “ionic liquids and biomolecules” special issue, Biophys. Rev. 10 (2018) 687–690. doi:10.1007/s12551-018-0426-3.

[478] S. V. Malhotra, V. Kumar, A profile of the in vitro anti-tumor activity of imidazolium-based ionic liquids, Bioorganic Med. Chem. Lett. 20 (2010) 581–585. doi:10.1016/j.bmcl.2009.11.085.

[479] C. Jing, X. Li, J. Zhang, J. Wang, Responses of the Antioxidant System in QGY-7701 Cells to the Cytotoxicity and Apoptosis Induced by 1-Octyl-3-methylimidazolium Chloride, J. Biochem Mol. Toxicol. 27 (2013) 246–255. doi:10.1002/jbt.

[480] C. Sanwald, A. Robciuc, S.-K. Ruokonen, S.K. Wiedmer, M. Lämmerhofer, A combined targeted/untargeted LC-MS/MS-based screening approach for mammalian cell lines treated with ionic liquids: Toxicity correlates with metabolic profile, Talanta. 197 (2019) 472–481. doi:10.1016/J.TALANTA.2019.01.054.

[481] J. Schlotterbeck, M. Chatterjee, M. Gawaz, M. Lämmerhofer, Comprehensive MS/MS Profiling by UHPLC-ESI-QTOF-MS/MS using SWATH Data-independent Acquisition for the Study of Platelet Lipidomes in Coronary Artery Disease, Anal. Chim. Acta. 1046 (2019) 1–15. doi:10.1016/j.aca.2018.08.060.

[482] B. Drotleff, M. Lämmerhofer, Guidelines for selection of internal standard-based normalization strategies in untargeted lipidomic profiling by LC-HR-MS/MS, Anal. Chem. 91 (2019) 9836–9843. doi:10.1021/acs.analchem.9b01505.

[483] J.D. Storey, A.J. Bass, Bioconductor's qvalue package, (n.d.).

[484] B.K. Matuszewski, M.L. Constanzer, C.M. Chavez-Eng, Strategies for the Assessment of Matrix Effect in Quantitative Bioanalytical Methods Based on HPLC−MS/MS, Anal. Chem. 75 (2003) 3019–3030. doi:10.1021/ac020361s.

[485] F. Endres, Physical chemistry of ionic liquids, Phys. Chem. Chem. Phys. 12 (2010) 1648–1648. doi:10.1039/c001176m.

[486] J.S. Torrecilla, J. Palomar, J. Lemus, F. Rodríguez, A quantum-chemical-based guide to analyze/quantify the cytotoxicity of ionic liquids, Green Chem. 12 (2010) 123–134. doi:10.1039/b919806g.

[487] H.L. Chen, H.F. Kao, J.Y. Wang, G.T. Wei, Cytotoxicity of imidazole ionic liquids in human lung carcinoma A549 cell line, J. Chinese Chem. Soc. 61 (2014) 763–769. doi:10.1002/jccs.201300632.

[488] A. Latała, M. Ndzi, P. Stepnowski, Toxicity of imidazolium and pyridinium based ionic liquids towards algae. Chlorella vulgaris, Oocystis submarina (green algae) and Cyclotella meneghiniana, Skeletonema marinoi (diatoms), Green Chem. 11 (2009) 580–588. doi:10.1039/b821140j.

[489] T. Schaffran, E. Justus, M. Elfert, T. Chen, D. Gabel, Toxicity of N, N, N-trialkylammoniododecaborates as new anions of ionic liquids in cellular , liposomal and enzymatic test systems, Green Chem. 11 (2009) 1458–1464. doi:10.1039/b906165g.

[490] S. Stolte, J. Arning, U. Bottin-Weber, M. Matzke, F. Stock, K. Thiele, M. Uerdingen, U. Welz-Biermann, B. Jastorff, J. Ranke, Anion effects on the cytotoxicity of ionic liquids, Green Chem. 8 (2006) 621–629. doi:10.1039/b602161a.

[491] T.L. Cover, S.A. Halter, M.J. Blaser, Characterization of Hela cell vacuoles induced by Helicobacter pylori broth culture supernatant, Hum. Pathol. 23 (1992) 1004–1010. doi:10.1016/0046-8177(92)90261-Z.

[492] B. Ekwall, Screening of Toxic Compounds in Mammalian Cell Cultures, Ann. N. Y. Acad. Sci. 407 (1983) 64–77. doi:10.1111/j.1749-6632.1983.tb47814.x.

[493] J.C. Oliveros (Centro Nacional de Biotecnologia), Venny. An interactive tool for comparing lists with Venn's diagrams, (n.d.). https://bioinfogp.cnb.csic.es/tools/venny/index.html.

[494] M. Rahmaniyan, A. Qudeimat, J.M. Kraveka, Bioactive Sphingolipids in Neuroblastoma, in: Neuroblastoma - Present Futur., 2012. doi:10.5772/27830.

[495] K. Kitatani, J. Idkowiak-Baldys, Y.A. Hannun, The sphingolipid salvage pathway in ceramide metabolism and signaling, Cell. Signal. 20 (2008) 1010–1018. doi:10.1016/j.cellsig.2007.12.006.

[496] A. Robciuc, A.H. Rantaṁaki, M. Jauhiainen, J.M. Holopainen, Lipid-modifying enzymes in human tear fluid and corneal epithelial stress response, Investig. Ophthalmol. Vis. Sci. 55 (2014) 16–24. doi:10.1167/iovs.13-12577.

[497] A.C. Lewis, C.T. Wallington-Beddoe, J.A. Powell, S.M. Pitson, Targeting sphingolipid metabolism as an approach for combination therapies in haematological malignancies, Cell Death Discov. 4 (2018). doi:10.1038/s41420-018-0075-0.

[498] R.I. Castillo, L.E. Rojo, M. Henriquez-Henriquez, H. Silva, A. Maturana, M.J. Villar, M. Fuentes, P.A. Gaspar, From molecules to the clinic: Linking schizophrenia and metabolic syndrome through sphingolipids metabolism, Front. Neurosci. 10 (2016). doi:10.3389/fnins.2016.00488.

[499] A. Robciuc, T. Hyötyläinen, M. Jauhiainen, J.M. Holopainen, Hyperosmolarity-induced lipid droplet formation depends on ceramide production by neutral sphingomyelinase 2, J. Lipid Res. 53 (2012) 2286–2295. doi:10.1194/jlr.M026732.

[500] Y.A. Hannun, L.M. Obeid, Principles of bioactive lipid signalling: Lessons from sphingolipids, Nat. Rev. Mol. Cell Biol. 9 (2008) 139–150. doi:10.1038/nrm2329.

[501] M.R. Quintero, M.E. Cabañas, C. Arús, A possible cellular explanation for the NMR-visible mobile lipid (ML) changes in cultured C6 glioma cells with growth, Biochim. Biophys. Acta. 1771 (2007) 31–44. doi:10.1016/j.bbalip.2006.10.003.

[502] C. Tam, V. Idone, C. Devlin, M.C. Fernandes, A. Flannery, X. He, E. Schuchman, I. Tabas, N.W. Andrews, Exocytosis of acid sphingomyelinase by wounded cells promotes endocytosis and plasma membrane repair, J. Cell Biol. 189 (2010) 1027–1038. doi:10.1083/jcb.201003053.

[503] I. Mérida, J. Arranz-Nicolás, C. Rodríguez-Rodríguez, A. Ávila-Flores, Diacylglycerol kinase control of protein kinase C, Biochem. J. 476 (2019) 1205–1219. doi:10.1042/BCJ20180620.

[504] G. Kadamur, E.M. Ross, Mammalian phospholipase C, Annu. Rev. Physiol. 75 (2013) 127–154. doi:10.1146/annurev-physiol-030212-183750.

[505] F. Sekiya, Phospholipase C, in: Encycl. Biol. Chem. Second Ed., 2013: pp. 467–471. doi:10.1016/B978-0-12-378630-2.00346-7.

[506] B.U. Wilke, M. Lindner, L. Greifenberg, A. Albus, Y. Kronimus, M. Bünemann, M.G. Leitner, D. Oliver, Diacylglycerol mediates regulation of TASK potassium channels by Gq-coupled receptors, Nat. Commun. 5 (2014). doi:10.1038/ncomms6540.

[507] J.N. van der Veen, J.P. Kennelly, S. Wan, J.E. Vance, D.E. Vance, R.L. Jacobs, The critical role of phosphatidylcholine and phosphatidylethanolamine metabolism in health and disease, Biochim. Biophys. Acta. 1859 (2017) 1558–1572. doi:10.1016/j.bbamem.2017.04.006.

[508] T.E. Frederick, J.N. Chebukati, C.E. Mair, P.C. Goff, G.E. Fanucci, Bis(monoacylglycero)phosphate forms stable small lamellar vesicle structures: Insights into vesicular body formation in endosomes, Biophys. J. 96 (2009) 1847–1855. doi:10.1016/j.bpj.2008.12.3892.

[509] F. Hullin-Matsuda, C. Luquain-Costaz, J. Bouvier, I. Delton-Vandenbroucke, Bis(monoacylglycero)phosphate, a peculiar phospholipid to control the fate of cholesterol: Implications in pathology, Prostaglandins Leukot. Essent. Fat. Acids. 81 (2009) 313–324. doi:10.1016/j.plefa.2009.09.006.

List of Figures

List of Supporting information Figures

List of Tables

List of Supporting information Tables

List of Equations

List of Supporting information Equations